

2009

## Subaqueous, hurricane-initiated shelf failure morphodynamics along the Mississippi River Delta Front, north-central Gulf of Mexico

Walter Scott Guidroz

*Louisiana State University and Agricultural and Mechanical College*

Follow this and additional works at: [https://digitalcommons.lsu.edu/gradschool\\_dissertations](https://digitalcommons.lsu.edu/gradschool_dissertations)



Part of the [Oceanography and Atmospheric Sciences and Meteorology Commons](#)

---

### Recommended Citation

Guidroz, Walter Scott, "Subaqueous, hurricane-initiated shelf failure morphodynamics along the Mississippi River Delta Front, north-central Gulf of Mexico" (2009). *LSU Doctoral Dissertations*. 1416.  
[https://digitalcommons.lsu.edu/gradschool\\_dissertations/1416](https://digitalcommons.lsu.edu/gradschool_dissertations/1416)

This Dissertation is brought to you for free and open access by the Graduate School at LSU Digital Commons. It has been accepted for inclusion in LSU Doctoral Dissertations by an authorized graduate school editor of LSU Digital Commons. For more information, please contact [gradetd@lsu.edu](mailto:gradetd@lsu.edu).

**SUBAQUEOUS, HURRICANE-INITIATED SHELF FAILURE  
MORPHODYNAMICS ALONG THE MISSISSIPPI RIVER DELTA FRONT,  
NORTH-CENTRAL GULF OF MEXICO**

A Dissertation

Submitted to the Graduate Faculty of the  
Louisiana State University and  
Agricultural and Mechanical College  
in partial fulfillment of the  
requirements for the degree of  
Doctor of Philosophy

in

The Department of Oceanography and Coastal Sciences

by

Walter Scott Guidroz  
B.S., Nicholls State University, 1979  
M.S., University of Mississippi, 1981  
M.B.A., The University of Texas at Austin, 2000

December 2009

## **ACKNOWLEDGMENTS**

I begin by thanking my major professor and advisor, Dr. Gregory Stone, for his guidance and support during my time at LSU. My committee included several early pioneers in submarine mudslide research – Dr. James Coleman and Dr. Harry Roberts of LSU, and Dr. Robert Bea of the University of California, Berkeley – and I thank them for their valuable input. This dissertation also benefited from guidance and suggestions from additional committee members Dr. Michael Blum, Dr. Jaye Cable, Dr. Felix Jose and Dean’s Representative Dr. Marc Levitan. In addition to my committee members, Dr. Donald Davis has been a source of support and help since I was an undergraduate at Nicholls State University.

My degree program was carried out while simultaneously working for BP in Houston, Texas. BP management provided continual support, and in particular my thanks go to Dr. Mike Bowman, Paul Carragher, Michelle Judson, Herlinde Mannaerts-Drew and Todd Stephenson for their encouragement.

BP geohazards specialists Bernie Care, Andy Hill, Craig Scherschel, Michael Taylor, James Thomson and Dr. Richard Weiland all greatly helped ease my transition into site investigation after spending most of my career as a traditional subsurface geologist. In addition, K.C. Gan and James Hooper of Fugro GeoServices, Inc. provided helpful suggestions in my research, and Dr. Bob Gilbert and Dr. Stephen Wright of the University of Texas at Austin provided insight into the engineering implications of seafloor movement.

Data were obtained from multiple sources. BP allowed access to its site investigation archive over the Mississippi River Delta Front (MRDF), much of it collected by its heritage companies Amoco, Vastar and Standard Oil Company of Ohio (Sohio). Mike Garrett of BP Pipelines facilitated permissions to use these data. Several additional geohazard datasets were acquired externally – Enterprise Products LLC provided data over their South Pass and Viosca Knoll pipeline route and I thank Dennis Jahde for permission to work with these data. Plains Resources provided data over South Pass 18 and I thank Wayne McBride for permission to work

with these data. I also thank Hallie Graves and Bruce Samuel from C&C Technologies who facilitated data transfer from Enterprise and Plains, respectively.

Digitized versions of regional MRDF bathymetry were provided by Chris Hitchcock of William Lettis and Associates. Wind field hindcast data for Hurricanes Camille and Andrew were provided by Dr. Vince Cardone of Oceanweather, Inc. Geotechnical borehole data were made available by the Coastal Studies Institute at LSU, and I appreciate Dr. James Coleman for providing the raw data. Dr. Skip Ward of the Offshore Technology Resource Center provided a digital catalog of additional borehole information that had been catalogued by Texas A&M University under contract to the U.S. Minerals Management Service.

Staff from the Wave-Current-Surge Information System (WAVCIS) Laboratory at LSU provided invaluable help with numerical wave modeling efforts. Dr. Felix Jose provided support for MIKE 21 modeling efforts along with Yuliang Chen and Yixin Luo. Seyed Mostafa Siadatmousavi provided help with ArcGIS and data loading issues.

Lastly, I thank friends and family who provided invaluable support and encouragement. David and Caren Jones, Don Griffin and Mary Cubanski, David and Cindy Chastain, Darryl and Susan Hutchinson, and Dr. Julie Dean Rosati, my fellow work-while-going-to-graduate-school compatriot, all stood by me as I pursued the Ph.D. paper chase. And as always, my mother, Olive Guidroz, and late father, Scott Guidroz, were ever supportive as I pursued my goals.



## TABLE OF CONTENTS

ACKNOWLEDGMENTS .....	ii
LIST OF TABLES .....	viii
LIST OF FIGURES .....	x
ABSTRACT .....	xx
CHAPTER 1. FUNDAMENTAL OBJECTIVES .....	1
CHAPTER 2. CONCEPTUAL FRAMEWORK AND STATEMENT OF PROBLEM .....	4
2.1 Observations to Date .....	7
2.2 Meteorological and Sea-State Controls .....	9
2.3 Lithologic and Geotechnical Controls .....	14
2.4 Morphologic Controls .....	15
2.5 Infrastructure Controls and Statistical Analyses .....	17
2.6 Numerical Modeling Integration and Proposed Contribution .....	17
CHAPTER 3. PREVIOUS STUDIES .....	19
3.1 Causation and Mechanics of Subaqueous Sediment Flow .....	19
3.1.1 Differential Loading and Slope Steepening .....	19
3.1.2 Gas and Gas Hydrate Effects .....	22
3.1.3 Wave- and Current-Induced Failure .....	23
3.2 Morphology and Classification of Submarine Sediment Flow .....	26
3.3 Selected MRDF Hurricanes – Synoptic History and Sea-State Conditions .....	28
3.3.1 Hurricane Betsy (1965) .....	29
3.3.2 Hurricane Camille (1969) .....	31
3.3.3 Hurricane Andrew (1992) .....	35
3.3.4 Hurricane Ivan (2004) .....	39
3.3.5 Hurricane Katrina (2005) .....	40
3.3.6 Additional GOM Hurricanes .....	41
3.4 Non-Hurricane GOM Events .....	44
CHAPTER 4. RESEARCH STRATEGY AND METHODOLOGY .....	45
4.1 Study Area .....	45
4.1.1 MRDF Bathymetric Data .....	48
4.1.2 Recent, Hurricane-Induced Seafloor Failures, MRDF Vicinity .....	53
4.1.3 Regional Lithologic and Geotechnical Data .....	53
4.1.4 Meteorological and Metocean Data .....	55
4.2 Research Objectives and Tactics .....	56
4.2.1 Metocean Screening .....	56
4.2.2 Seafloor Morphology Screening .....	57
4.2.3 Modeling and Integration .....	58
4.2.4 Application of Results .....	59
CHAPTER 5. METEOROLOGICAL AND SEA-STATE CONTROLS .....	60
5.1 General Hurricane History, North-Central Gulf of Mexico .....	60
5.1.1 MRDF Tropical Cyclone History, 1851-2008 .....	60
5.1.2 MRDF Tropical Cyclone History, 1718-1851 .....	63

5.2	Modeled Response of Hurricane Metocean Conditions.....	65
5.2.1	Model Calibration to Metocean Conditions during Recent Hurricanes .....	66
5.2.2	Hindcast Model Application to Prior Hurricanes.....	75
5.3	Directional Wave Spectra Applications .....	77
CHAPTER 6. LITHOLOGIC AND GEOTECHNICAL CONTROLS .....		89
6.1	MRDF Seafloor Characterization .....	89
6.1.1	Sedimentologic History and Depositional Parameters.....	89
6.1.2	Lithologic Characterization.....	91
6.2	MRDF Geotechnical Framework.....	92
6.3	Geotechnical Characterization, MRDF Seafloor and Shallow Sediments .....	116
6.3.1	Shear Strength Characterization.....	116
6.3.2	Safety Factor Characterization.....	119
6.4	Shelf Failure Modeling .....	130
6.4.1	1D Sediment Failure Modeling Program (BING).....	130
6.4.2	1D Sediment Failure Modeling, Prior MRDF Mudslides .....	132
6.4.3	1D Sediment Failure Modeling, Potential MRDF Mudslides.....	137
CHAPTER 7. MORPHOLOGIC CONTROLS .....		140
7.1	Regional Bathymetric Changes in Study Area, 1874-1977 .....	140
7.2	Case Studies of Localized Bathymetric Changes in Study Area, 1964-2008 .....	144
7.2.1	Case Studies in Seafloor Failure – Validation Test Area One .....	144
7.2.2	Case Studies in Seafloor Failure – Validation Test Area Two .....	148
7.2.3	Case Studies in Seafloor Failure – Validation Test Area Three .....	151
7.2.4	Case Studies in Seafloor Failure – Validation Test Area Four .....	165
7.3	Mississippi Canyon Morphologic Effects .....	172
7.3.1	MIKE 21 Modeling Trial .....	173
7.3.2	Trial Ramifications .....	179
7.4	Climate Change and Anthropogenic Effects.....	182
CHAPTER 8. INFRASTRUCTURE CONTROLS AND STATISTICAL ANALYSIS .....		184
8.1	Historical Offshore Infrastructure Development, 1937-2008 .....	184
8.2	Time-Sequenced Offshore Infrastructure Distribution .....	185
8.3	Infrastructure Damage and Loss, Major GOM Hurricanes .....	193
8.3.1	Hurricane Betsy (1965).....	194
8.3.2	Hurricane Camille (1969) .....	196
8.3.3	Hurricane Andrew (1992) .....	198
8.3.4	Hurricane Ivan (2004).....	199
8.3.5	Hurricane Katrina (2005).....	200
CHAPTER 9. RESULTS AND VULNERABILITY MATRIX .....		202
9.1	Common Hazard Framework .....	202
9.1.1	Hazard and Vulnerability Assessment History .....	202
9.1.2	MRDF Hazard Application and Vulnerability Framework .....	204
9.2	MRDF Risk Synthesis.....	206
9.2.1	Danger Characterization .....	206
9.2.1.1	Triggering Factors .....	206
9.2.1.2	Revealing Factors .....	210
9.2.1.3	Predisposition Factors.....	212
9.2.2	Magnitude Characterization.....	222
9.2.3	Hazard Characterization.....	224

9.2.4	Risk Characterization .....	232
9.2.5	Total MRDF Risk .....	240
9.3	Risk Results Testing.....	245
9.4	Risk Results Application Guidelines .....	248
CHAPTER 10. CONCLUSIONS .....		250
10.1	Key Project Conclusions .....	250
10.2	Recommendations for Future Study.....	254
REFERENCES.....		256
APPENDIX A: COMMON TYPES OF OFFSHORE INDUSTRY INFRASTRUCTURE .....		278
APPENDIX B: KEY HURRICANE ROUTES AND STORM INTENSITY HISTORY .....		281
APPENDIX C: INFRASTRUCTURE DAMAGE AND LOSS, HURRICANE IVAN (2004) .....		286
APPENDIX D: MRDF HURRICANE PATHS, 1947-2005 .....		291
APPENDIX E: RISK ASSESSMENT FOR SUBMARINE SLOPE FAILURES, HOUSTON FORUM 2002.....		292
APPENDIX F: OFFSHORE LOUISIANA BATHYMETRIC DATASETS, 1868-2007 .....		293
APPENDIX G: METOCEAN CONDITIONS, HURRICANE CAMILLE (1969) .....		296
APPENDIX H: NATIONAL DATA BUOY CENTER GULF OF MEXICO BUOYS .....		297
APPENDIX I: SUMMARY OF OFFSHORE INFRASTRUCTURE DAMAGE, HURRICANE ANDREW (1992).....		299
APPENDIX J: SEA-STATE CONDITIONS DURING HURRICANE IVAN (2004) AS RECORDED BY U.S. NAVAL RESEARCH LABORATORY MOORINGS.....		300
APPENDIX K: LOCAL BATHYMETRY DATASETS AND ACQUISITION PARAMETERS (ARRANGED IN TIME-CHRONOLOGICAL ORDER) .....		301
APPENDIX L: MRDF GEOTECHNICAL BOREHOLE DATABASE .....		314
APPENDIX M: MIKE 21 NUMERICAL MODELING .....		320
APPENDIX N: SHEAR STRENGTH SAMPLE COLLECTION METHODS .....		325
APPENDIX O: MIKE 21 WAVE MODELING RESULTS, HURRICANE ANDREW (1992) .....		336
APPENDIX P: STUDY AREA PLATFORM HISTORY (SORTED BY PROTRACTION AREA).....		338

APPENDIX Q: DAILY MRDF PRODUCTION RATES AND MONETARY VALUE.....	354
VITA .....	355

## LIST OF TABLES

Table 1: MRDF Category 3 Hurricane History within 300 km of the Mississippi River Delta, 1851-2008.....	11
Table 2: Validation Test Area boundaries, north-central Gulf of Mexico .....	46
Table 3: Operator-reported, hurricane-induced seafloor failure, Hurricanes Ivan and Katrina ....	54
Table 4: Recurrence intervals, MRDF hurricanes (Category 3+), 1851-2008 .....	62
Table 5: MRDF Hurricane History near New Orleans, 1718-1851.....	64
Table 6: Modeled parameters for GOM-wide and Study Area MIKE 21 wave models .....	66
Table 7: Correlation coefficients, observed vs. modeled metocean parameters, Hurricane Katrina.....	71
Table 8: Correlation coefficients, observed vs. modeled metocean parameters, Hurricane Ivan..	75
Table 9: Regional BING model sensitivities, Cross Section B-B' .....	133
Table 10: BING model match, South Pass 70 failure.....	134
Table 11: BING model results, Cross section D-D' .....	135
Table 12: BING model results, South Pass 38, Cross section F-F' .....	137
Table 13: BING model results, South Pass 70 failure (future case).....	138
Table 14: BING model results, Cross Section D-D' (future case) .....	139
Table 15: BING model results, South Pass 38, Cross section F-F' (future case).....	139
Table 16: Modeling stations, Mississippi Canyon Infilling Exercise.....	174
Table 17: Summary of flow line and transfer line breaks, South Pass Block 27 Field Area.....	195
Table 18: Platform failures from all causes in hurricanes prior to Hurricane Andrew .....	197
Table 19: Reported pipeline damage due to natural hazards.....	199
Table 20: Reported platform damage due to natural hazards .....	199
Table 21: Significant wave height matrix, MRDF study area .....	208
Table 22: Wave period (T-02) matrix, MRDF study area .....	209
Table 23: Temporal exposure matrix, MRDF study area .....	211
Table 24: Morphology type matrix, MRDF study area .....	211

Table 25: MRDF vulnerability matrix – slope steepness .....	218
Table 26: MRDF vulnerability matrix – rate of seafloor change .....	219
Table 27: Submarine mudslide susceptibility, seafloor sediment characteristics.....	222
Table 28: Hazard scoring matrix, prior MRDF Hurricanes.....	231
Table 29: Sample scoring matrix, projected MRDF Hurricanes .....	233
Table 30: Total risk calculations, VTA 1, 3 and 4 (shelf environment).....	242
Table 31: Total risk calculations, VTA 2 (outer shelf environment) .....	243
Table 32: Total risk calculations, VTA 3 (deep water environment) .....	244

## LIST OF FIGURES

Figure 1: Location map and recent hurricane paths, north-central Gulf of Mexico, USA .....	5
Figure 2: Location map of Mississippi River Delta Front study area within the north-central Gulf of Mexico, USA .....	5
Figure 3: Damage to platforms and pipelines from Hurricanes Ivan and Katrina, 2004-2005 .....	8
Figure 4: Key metocean parameters from Hurricane Ivan, 2004 based on readings from NDBC Buoy 42040 .....	12
Figure 5: Key wave parameters from Hurricane Ivan, 2004 based on readings from U.S. Naval Research Laboratory.....	13
Figure 6: Key metocean parameters from Hurricane Katrina, 2005 based on readings from NDBC Buoy 42040 .....	13
Figure 7: Approximate locations of study area boreholes relative to platform and pipeline damage reported during either Hurricanes Ivan or Katrina .....	16
Figure 8: Mississippi River Delta Front .....	20
Figure 9: Model for wave loading of submarine sediments .....	25
Figure 10: Schematic distribution and morphology of subaqueous landslides in the vicinity of a distributary and offshore, Mississippi River delta.....	27
Figure 11: Schematic diagram illustrating the major sediment instability facies off major river deltas.....	27
Figure 12: Ocean Data Gathering Stations relative to track of Hurricane Camille (1969), north-central Gulf of Mexico .....	33
Figure 13: Time variation of wave height parameters during Hurricane Camille.....	33
Figure 14: Time variation of wave period parameters during Hurricane Camille.....	33
Figure 15: Changes in bottom topography at SP 70 after Hurricane Camille (block outline in blue; location of SP 70 “B” platform highlighted with red circle .....	36
Figure 16: Pre- and post-Hurricane Camille cross-sectional profile, South Pass 70.....	36
Figure 17: Comparison of pre- and post-Camille soil borings, South Pass Block 70 .....	36
Figure 18: Key metocean parameters from Hurricane Andrew, 1992 based on readings from NDBC Buoy 42001 .....	38
Figure 19: Key metocean parameters from Hurricane Andrew, 1992 based on readings from NDBC Buoy 42003 .....	38
Figure 20: Theoretical wave height decay model.....	44

Figure 21: Extent of MRDF mudslides, circa 1980.....	46
Figure 22: Location of localized geohazard surveys and validation test areas relative to general MRDF study area .....	47
Figure 23: 1874 MRDF bathymetry, U.S. Coast and Geodetic Survey .....	49
Figure 24: 1940 MRDF bathymetry, U.S. Coast and Geodetic Survey .....	50
Figure 25: 1977 MRDF bathymetry, U.S. Coast and Geodetic Survey .....	51
Figure 26: Coarse-resolution MRDF bathymetry, National Oceanographic and Atmospheric Administration.....	52
Figure 27: Geotechnical borehole distribution and operator-reported seafloor failure during Hurricanes Ivan and Katrina.....	54
Figure 28: MRDF tropical cyclone frequency by decade, 1851-2008 .....	61
Figure 29: MRDF tropical cyclone angle of approach, Category 3+ hurricanes, 1851-2008 .....	63
Figure 30: Time sensitivity to MRDF hurricane intensity, Category 3+ hurricanes, 1851-2008..	64
Figure 31: MRDF Tropical cyclone frequency, 1718-1851 .....	65
Figure 32: Measured vs. hindcast significant wave heights at GOM NDBC buoys, Hurricanes Lili, Ivan, Katrina and Rita.....	68
Figure 33: Comparison of observed metocean conditions to MIKE 21 modeled response at NDBC Buoy 42040 during Hurricane Katrina .....	68
Figure 34: Significant wave height comparison, NCBC Buoy 42040, Hurricane Katrina approach (August 2005).....	70
Figure 35: Significant wave height comparison, NCBC Buoy 42040, Hurricane Katrina post-storm recovery (August 2005).....	70
Figure 36: Wave period comparison, NCBC Buoy 42040, Hurricane Katrina approach (August 2005).....	70
Figure 37: Wave period comparison, NCBC Buoy 42040, Hurricane Katrina post-storm recovery (August 2005).....	70
Figure 38: $H_{s_{max}}$ , Hurricane Katrina, August 29, 2005 0900Z as modeled through MIKE 21 numerical wave model.....	72
Figure 39: Wave period T02, Hurricane Katrina, August 29, 2005 0900 Z as modeled through MIKE 21 numerical wave model .....	72
Figure 40: Comparison of observed metocean conditions to MIKE 21 modeled response at NDBC Buoy 42040 during Hurricane Ivan.....	73



Figure 41: Significant wave height comparison, NCBC Buoy 42040, Hurricane Ivan approach (September 2004) .....	73
Figure 42: Wave period comparison, NCBC Buoy 42040, Hurricane Ivan approach (September 2004).....	73
Figure 43: $H_{s_{max}}$ , Hurricane Ivan, September 15, 2004 2100 Z as modeled through MIKE 21 numerical wave model.....	74
Figure 44: Wave period T02, Hurricane Ivan, September 15, 2004 2100 Z as modeled through MIKE 21 numerical wave model .....	74
Figure 45: $H_{s_{max}}$ , Hurricane Camille, August 17, 1969 1800 Z as modeled through MIKE 21 numerical wave model.....	76
Figure 46: $H_{s_{max}}$ , Hurricane Camille, August 17, 1969 2100 Z as modeled through MIKE 21 numerical wave model.....	76
Figure 47: Wave period T02 (zero-crossing), Hurricane Camille, August 17, 1969 1800Z as modeled through MIKE 21 numerical wave model .....	78
Figure 48: Wave period T02 (zero-crossing), Hurricane Camille, August 17, 1969 2100Z as modeled through MIKE 21 numerical wave model .....	78
Figure 49: $H_{s_{max}}$ , Hurricane Betsy, September 10, 1965 0000Z as modeled through MIKE 21 numerical wave model.....	79
Figure 50: $H_{s_{max}}$ , Hurricane Betsy, September 10, 1965 0600Z as modeled through MIKE 21 numerical wave model.....	79
Figure 51: Wave period T02 (zero-crossing), Hurricane Betsy, September 10, 1965 0000Z as modeled through MIKE 21 numerical wave model .....	80
Figure 52: Wave period T02 (zero-crossing), Hurricane Betsy, September 10, 1965 0000Z as modeled through MIKE 21 numerical wave model .....	80
Figure 53: Directional wave spectra, NDBC Buoy 42040, August 27, 2005, 0900 Z .....	82
Figure 54: Directional wave spectra, NDBC Buoy 42040, August 29, 2005, 0900 Z .....	82
Figure 55: Directional wave spectra, NDBC Buoy 42007, August 27, 2005, 0900 Z .....	82
Figure 56: Directional wave spectra, NDBC Buoy 42007, August 29, 2005, 0800 Z .....	82
Figure 57: Directional wave spectra, NDBC Buoy 42001, August 27, 2005, 0600 Z .....	82
Figure 58: Directional wave spectra, NDBC Buoy 42001, August 28, 2005, 1500 Z .....	82
Figure 59: Spectral evolution, NDBC Buoy 42001, Hurricanes Katrina and Ophelia, 2005 .....	84
Figure 60: Spectral evolution, NDBC Buoy 42040, Hurricane Katrina and Ophelia, 2005 .....	84

Figure 61: Directional wave spectra, NDBC Buoy 42040, September 14, 2004, 0000 Z.....	85
Figure 62: Directional wave spectra, NDBC Buoy 42040, September 15, 2004, 1400 Z.....	85
Figure 63: Directional wave spectra, NDBC Buoy 42007, September 14, 2004, 0000 Z.....	85
Figure 64: Directional wave spectra, NDBC Buoy 42007, September 16, 2004, 0000 Z.....	85
Figure 65: Directional wave spectra, NDBC Buoy 42001, September 14, 2004, 0100 Z.....	85
Figure 66: Directional wave spectra, NDBC Buoy 42001, September 15, 2004, 0700 Z.....	85
Figure 67: Spectral evolution, NDBC Buoy 42001, Hurricane Ivan, September 1-30, 2004 .....	88
Figure 68: Spectral evolution, NDBC Buoy 42040, Hurricane Ivan, September 1-16, 2004 .....	88
Figure 69: Location of shelf-edge deltas in proximity to MRDF study area.....	91
Figure 70: usSEABED grain-size data distribution, north-central Gulf of Mexico .....	92
Figure 71: Surficial sands, north-central GOM coast.....	93
Figure 72: MRDF geotechnical borehole grid.....	93
Figure 73: Bathymetry image along cross section A-A', Main Pass Area .....	94
Figure 74: Geotechnical borehole cross section A-A', Main Pass Area, north-central Gulf of Mexico.....	95
Figure 75: Bathymetry image along cross section B-B', Main Pass Area .....	96
Figure 76: Geotechnical borehole cross section B-B', Main Pass Area, north-central Gulf of Mexico.....	97
Figure 77: Bathymetry image along cross section C-C', South Pass Area .....	98
Figure 78: Geotechnical borehole cross section C-C', South Pass Area, north-central Gulf of Mexico.....	99
Figure 79: Bathymetry image along cross section D-D', South Pass Area .....	100
Figure 80: Geotechnical borehole cross section D-D', South Pass Area, north-central Gulf of Mexico.....	101
Figure 81: Bathymetry image along cross section E-E', South Pass Area.....	102
Figure 82: Geotechnical borehole cross section E-E', South Pass Area, north-central Gulf of Mexico.....	103
Figure 83: Bathymetry image along cross section F-F', South Pass Area .....	104

Figure 84: Geotechnical borehole cross section F-F', South Pass Area, north-central Gulf of Mexico.....	105
Figure 85: Bathymetry image along cross section G-G', West Delta Area.....	106
Figure 86: Geotechnical borehole cross section G-G', South Pass Area, north-central Gulf of Mexico.....	107
Figure 87: Geotechnical borehole cross section H-H', West Delta, South Pass and Main Pass Areas, north-central Gulf of Mexico .....	108
Figure 88: Geotechnical borehole cross section H-H', West Delta, South Pass and Main Pass Areas, north-central Gulf of Mexico .....	109
Figure 89: Geotechnical borehole cross section I-I', West Delta, South Pass and Main Pass Areas, north-central Gulf of Mexico.....	110
Figure 90: Geotechnical borehole cross section I-I', West Delta, South Pass and Main Pass Areas, north-central Gulf of Mexico.....	111
Figure 91: Typical shear strength profile through a crustal zone .....	118
Figure 92: GOM shear strength distribution.....	119
Figure 93: Bottom shear stress, Hurricane Katrina, 0900 UTC, August 29, 2005 .....	120
Figure 94: Bottom shear stress, Hurricane Ivan, 2100 UTC, September 15, 2004 .....	120
Figure 95: Example of safety factor calculation, Main Pass 290 .....	122
Figure 96: Factors of safety calculated along Cross Section A-A', Hurricanes Betsy through Katrina .....	123
Figure 97: Factors of safety calculated along Cross Section B-B', Hurricanes Betsy through Katrina .....	123
Figure 98: Factors of safety calculated along Cross Section C-C', Hurricanes Betsy through Katrina .....	124
Figure 99: Factors of safety calculated along Cross Section D-D', Hurricanes Betsy through Katrina .....	124
Figure 100: Factors of safety calculated along Cross Section E-E', Hurricanes Betsy through Katrina .....	125
Figure 101: Factors of safety calculated along Cross Section F-F', Hurricanes Betsy through Katrina .....	125
Figure 102: Factors of safety calculated along Cross Section G-G', Hurricanes Betsy through Katrina .....	126
Figure 103: Input panel for the BING 1D numerical simulation failure model .....	131

Figure 104: Shape of potential MC 20 seafloor failure and resulting mudflow nose during Hurricane Ivan as modeled in BING .....	136
Figure 105: Net change in MRDF seafloor bathymetry, 1874-1940.....	141
Figure 106: Regional MRDF bathymetry profiles, 1874-1977 .....	142
Figure 107: Net change in MRDF seafloor bathymetry, 1940-1977.....	143
Figure 108: Post-Ivan (2004) bathymetry, Main Pass Oil Gathering System .....	146
Figure 109: Slope steepness generated from post-Ivan (2004) bathymetry, Main Pass Oil Gathering System .....	146
Figure 110: Post-Katrina (2005) bathymetry, Main Pass Oil Gathering System .....	147
Figure 111: Net seafloor change, 2004-05, Main Pass Oil Gathering System .....	147
Figure 112: Bathymetric profile through time, Main Pass Oil Gathering System .....	148
Figure 113: Seafloor bathymetry and prior mudflow morphology, Main Pass Blocks 294 and 295 .....	150
Figure 114: Line 6 (10 inch <sup>3</sup> sleeve gun; interpreted and non-interpreted), Main Pass Blocks 294 and 295 .....	150
Figure 115: Seafloor bathymetry profile A-A', Main Pass Blocks 294 and 295.....	152
Figure 116: Side-scan sonar Line 111, Main Pass 308 and Viosca Knoll 914/915 survey .....	152
Figure 117: Semi-regional bathymetry data, South Pass Area .....	153
Figure 118: Net seafloor bathymetry change, 1977-1997, South Pass Protraction Area .....	153
Figure 119: Cross-sectional grid and net seafloor bathymetry change, Validation Area 3 .....	154
Figure 120: High-resolution bathymetry, Viosca Knoll and Mississippi Canyon Protraction Areas .....	155
Figure 121: Net seafloor bathymetry change, Viosca Knoll Block 985 (Validation Area 3).....	155
Figure 122: Generational mudflow history, Viosca Knoll Block 985.....	156
Figure 123: Comparison of high-resolution bathymetry survey acquired in 2005.....	157
Figure 124: Surface difference, VK 985 vicinity, 1983-2005 .....	158
Figure 125: Mudflow nose topography, Viosca Knoll 985 and vicinity .....	160
Figure 126: Terminus of elongated sediment flow (C-C') and downdip extent and confining boundary of elongated sediment flow (D-D' and E-E'), VK 985 .....	161

Figure 127: Generational mudflow history, northwest Mississippi Canyon .....	162
Figure 128: Mudflow nose topography, northwest Mississippi Canyon Protraction Area .....	163
Figure 129: Mudflow lobes and internal pressure ridges as inferred from slope steepness, northwest Mississippi Canyon Protraction Area .....	164
Figure 130: Bathymetric profiles through time, 1874-1997, South Pass Blocks 60 and 70 .....	164
Figure 131: Seafloor bathymetry, South Pass Block 28, 1962 (pre-Hurricane Hilda) .....	167
Figure 132: Seafloor bathymetry, South Pass Block 28, 1964 (post- Hilda/pre-Hurricane Betsy) .....	167
Figure 133: Seafloor bathymetry, South Pass Block 28, 1965 (post-Hurricane Betsy) .....	167
Figure 134: Net seafloor bathymetry change, 1962-1964, South Pass Block 28 (pre- and post- Hilda).....	167
Figure 135: Slope map, South Pass Block 28, 1964 (post-Hilda/pre-Betsy).....	167
Figure 136: Net seafloor bathymetry change, 1964-1965, South Pass Block 28 (post-Hilda/post- Betsy) .....	167
Figure 137: Time-series cross-sectional profile A-A', 1962-1965, South Pass Block 28 (pre- Hilda through post-Betsy) .....	168
Figure 138: Time-series cross-sectional profile B-B', 1962-1965, South Pass Block 28 (pre-Hilda through post-Betsy) .....	168
Figure 139: Seafloor bathymetry, South Pass Blocks 50 and 51, 1981.....	169
Figure 140: Seafloor bathymetry, South Pass Blocks 50 and 51, 1988.....	169
Figure 141: Seafloor bathymetry, South Pass Blocks 50 and 51, 1990.....	169
Figure 142: Net seafloor bathymetry change, 1981-1990, South Pass Blocks 50 and 51 .....	169
Figure 143: Seafloor and near-surface sediment change, 1977-1985, South Pass Block 52.....	170
Figure 144: Seafloor rendering, MRDF and adjacent GOM continental shelf including Mississippi Canyon.....	174
Figure 145: Significant wave height comparison between existing and modeled infilled Mississippi Canyon .....	175
Figure 146: Maximum significant wave height difference between existing and modeled infilled canyon .....	176
Figure 147: Comparison of significant wave height, wave period and horizontal particle velocity (seafloor) for canyon infill modeling exercise, Stations D, E, F and G, Mississippi Canyon transect.....	177

Figure 148: Wave period comparison between existing and modeled infilled Mississippi Canyon.....	178
Figure 149: Maximum wave period difference between existing and modeled infilled canyon.	178
Figure 150: Horizontal bottom orbital velocity comparison between existing and modeled infilled Mississippi Canyon .....	180
Figure 151: Horizontal bottom orbital velocity difference between existing and modeled infilled canyon .....	180
Figure 152: North-central GOM platform and pipeline infrastructure in place through end of 1965 .....	186
Figure 153: North-central GOM platform and pipeline infrastructure in place through end of 1969 .....	187
Figure 154: North-central GOM platform and pipeline infrastructure in place through Hurricane Andrew (August 1992).....	188
Figure 155: North-central GOM platform infrastructure in place through Hurricane Ivan (September 2004) .....	189
Figure 156: North-central GOM platform and pipeline infrastructure in place through Hurricane Katrina (August 2005).....	190
Figure 157: Historical water depth limits for installed Gulf of Mexico platforms, 1947-2008 .	191
Figure 158: Landslide hazard and risk analysis.....	205
Figure 159: Conceptual relationship between hazard, elements at risk, vulnerability and risk .	205
Figure 160: Risk management procedure for submarine landslides.....	207
Figure 161: Morphology scaling map, MRDF .....	213
Figure 162: High-resolution bathymetry superimposed on regional NOAA bathymetry grid, Validation Area 1 .....	214
Figure 163: Slope steepness computed from high-resolution bathymetry, Validation Area 1 ....	214
Figure 164: High-resolution bathymetry superimposed on regional NOAA bathymetry grid, Validation Area 2 .....	215
Figure 165: Slope steepness computed from high-resolution bathymetry, Validation Area 2 ....	215
Figure 166: High-resolution bathymetry superimposed on regional NOAA bathymetry grid, Validation Area 3 .....	216
Figure 167: Slope steepness computed from high-resolution bathymetry, Validation Area 3 ....	216

Figure 168: High-resolution bathymetry superimposed on regional NOAA bathymetry grid, Validation Area 4 .....	217
Figure 169: Slope steepness computed from high-resolution bathymetry, Validation Area 4....	217
Figure 170: Shear strength vs. bottom shear stresses, Hurricane Katrina 29 August 2005, 0900 Z.....	221
Figure 171: Shear strength vs. bottom shear stresses, Hurricane Ivan 15 September 2004, 2100 Z.....	221
Figure 172: Shear strength, bottom shear stresses and sediment grain size, Hurricane Katrina, 29 August 2005, 0900 Z .....	221
Figure 173: Shear strength, bottom shear stresses and sediment grain size, Hurricane Ivan, 15 September 2004, 2100 Z.....	221
Figure 174: Morphology type hazard map, Validation Test Area 1 .....	227
Figure 175: Morphology type hazard map, Validation Test Area 2.....	227
Figure 176: Morphology type hazard map, Validation Test Area 3 .....	227
Figure 177: Morphology type hazard map, Validation Test Area 4.....	227
Figure 178: Slope steepness hazard map, Validation Test Area 1 .....	228
Figure 179: Slope steepness hazard map, Validation Test Area 2 .....	228
Figure 180: Slope steepness hazard map, Validation Test Area 3 .....	228
Figure 181: Slope steepness hazard map, Validation Test Area 4 .....	228
Figure 182: Seafloor change, NOAA to local, Validation Test Area 1 .....	229
Figure 183: Seafloor change, NOAA to local, Validation Test Area 2.....	229
Figure 184: Seafloor change, NOAA to 1977, Validation Test Area 3.....	229
Figure 185: Seafloor change, NOAA to 1977, Validation Test Area 4.....	229
Figure 186: Seafloor sediment susceptibility, Validation Test Area 1 .....	230
Figure 187: Seafloor sediment susceptibility, Validation Test Area 2 .....	230
Figure 188: Seafloor sediment susceptibility, Validation Test Area 3 .....	230
Figure 189: Seafloor sediment susceptibility, Validation Test Area 4.....	230
Figure 190: Infrastructure and elements at risk, Validation Test Area 1.....	235
Figure 191: Infrastructure and elements at risk, Validation Test Area 2.....	236

Figure 192: Infrastructure and elements at risk, Validation Test Area 3.....	237
Figure 193: Infrastructure and elements at risk, Validation Test Area 4.....	238
Figure 194: MRDF morphology type vs. composite hazard score .....	246
Figure 195: MRDF hurricane temporal exposure vs. composite hazard score.....	247
Figure 196: MRDF slope steepness vs. composite hazard score.....	247



## **ABSTRACT**

Seafloor instability along the Mississippi River Delta Front (MRDF) gained renewed attention with the landfall of Hurricanes Ivan (2004) and Katrina (2005). Traditional root causes for MRDF shelf failure were exacerbated by sea-state conditions associated with these severe tropical cyclones and their interaction with the seafloor. These conditions were characterized by large waves, long wave periods and wave-induced turbulence in the bottom boundary layer and throughout the water column.

An evaluation of local and regional MRDF bathymetry data revealed substantial changes in seafloor elevation and the immediate subsurface sediment profile, hypothesized as the end result of cyclic wave-seafloor interaction, seafloor scour and failure, and the re-initiation of antecedent seafloor slides and subsequent sediment re-deposition. Observed bulk wave and bottom layer conditions during Hurricanes Ivan and Katrina, during which significant wave height and wave period exceeded 15 m and 12 sec, respectively, were used to calibrate a series of MIKE 21 numerical wave models. Once calibrated, hindcasts were generated for earlier MRDF hurricanes dating from 1965. Spectral frequency data indicated long-period, often bimodal MRDF wave effects up to 48 hours prior to storm arrival. Lithologic and geotechnical parameters revealed widely varying shear strengths and safety factors, with higher shear stresses coincident with the 25-m isobath. Safety factors decreased in tandem with hurricane approach both prior to and after peak conditions. One-dimensional sediment failure modeling, calibrated to past seafloor failures, indicated variable ranges of mudslide length, ranging up to several kilometers.

A composite risk framework was constructed that employed various triggering, revealing and predisposition danger factors, a statistical analysis of elements at risk, and a vulnerability assessment to identify likely scenarios for future hurricane-initiated seafloor failure. A top tier of historical storms, including Hurricanes Ivan, Camille and the 1856 Last Island Hurricane, was risked as most prone to failure; a secondary tier included Hurricanes Katrina, Opal, Carmen and the 1915 New Orleans Hurricane. Five hypothetical future hurricanes of varying intensity were

then used to help characterize potential MRDF seafloor response. Areas at highest risk included those characterized by steep slopes, rapid sedimentation rates, and lengthened temporal exposure to severe hurricane conditions.

## **CHAPTER 1. FUNDAMENTAL OBJECTIVES**

Ocean-bottom sediment re-distribution caused by subaqueous mudslides along the continental shelf and slope of the Gulf of Mexico (GOM) during severe hurricanes has gained renewed attention with the passage of Hurricane Ivan in 2004 and Hurricane Katrina in 2005. Both storms were classified as Category 5 hurricanes on the Saffir-Simpson Scale prior to landfall and rank among the most intense cyclones to impact the north-central Gulf in decades (Stewart, 2005; National Hurricane Center, 2009).

Several cases of subaqueous sediment failure were noted during these storms, particularly in the Mississippi Canyon, Viosca Knoll, South Pass and Main Pass protraction areas adjacent to the Mississippi River Delta Front (MRDF). The central and western GOM hosts a significant petroleum drilling and production network consisting of numerous production platforms and pipelines (see Appendix A for descriptions of common offshore infrastructure types). Catastrophic loss and severe damage within this network occurred during both Ivan and Katrina and can in some cases be traced to subaqueous seafloor movement and failure (MMS, 2005a, 2005b, 2006a, 2006b, and 2009).

A better understanding of submarine mass transport mechanics and the risk posed by future, hurricane-generated sediment failures is therefore a significant issue facing the offshore oil and gas industry. This dissertation examines various controls on submarine mudslide behavior adjacent to the MRDF during severe hurricanes. These controls, which include various metocean, lithological, geotechnical and morphological parameters, govern the potential for and severity of subaqueous seafloor failure. The impact of these controls is reflected on the seafloor through substantial changes in ocean-bottom bathymetry and the immediate subsurface sediment profile as the end result of (1) cyclic wave-seafloor interaction, (2) seafloor scour and failure, (3) the re-initiation of antecedent seafloor slides, and (4) sediment re-deposition. Previous scientific and engineering studies have concentrated only on investigating these parameters on a singular basis; a proposed, substantial contribution to both geological oceanographic science and

oceanographic engineering gleaned from this dissertation pertains to quantifying the relationships between all of these controls and seafloor morphodynamics. In that case, the maxim “the present is the key to the past” can be applied to help identify and elucidate seafloor response to process conditions associated with *past* hurricanes. Once the historical process condition/response cycle is established, hypotheses governing seafloor response can then be extrapolated for conditions that may reasonably be expected in *future* hurricanes.

Therefore, the fundamental purpose of this dissertation tests the following hypotheses:

- Observed bulk wave and bottom boundary layer conditions during recent MRDF hurricanes can be used to calibrate a series of numerical wave models that simulate these conditions during earlier MRDF hurricanes for which no direct or reliable observations exist. In addition to hurricane intensity, major factors in the incidence of MRDF shelf failure may include forward speed and temporal exposure to severe hurricane conditions.
- Lithological and geotechnical parameters comprise only part of the triggering mechanism required to initiate MRDF shelf failure during severe hurricanes. Variation in differential pressure along the seafloor due to bulk wave impact contributes to a full set of physical process conditions that govern hurricane-initiated subaqueous shelf failure.
- Integrated oceanographic, lithological and geotechnical conditions define past MRDF hurricane response and can be used to help build predictive models governing the morphological response of the MRDF seafloor to hurricane-initiated conditions. Prior changes in seafloor morphology can be quantified by examining regional and local bathymetric data acquired over time (some of which were repeated over the same area) and a series of one-dimensional sediment failure models given certain assumptions of initial conditions, material parameters, and elevation data. Once

these models are calibrated, predictions of future changes in seafloor morphology for a particular area can be estimated.

These hypotheses can then be tested through a statistical hindcast examination of past infrastructure damage and loss trends, in particular in four Validation Test Areas (VTAs) selected on the basis of data availability, proximity to recent hurricane tracks, and the level of infrastructure damage sustained during recent hurricanes. Risk matrices generated from this research can then be applied to quantify, and therefore better mitigate, future hurricane-induced risk to offshore infrastructure within the MRDF. The net result of this work is the compilation of a vulnerability matrix and total risk assessment that can be used to quantify future MRDF submarine shelf failure.

## **CHAPTER 2. CONCEPTUAL FRAMEWORK AND STATEMENT OF PROBLEM**

Offshore infrastructure damage induced by Hurricanes Ivan (2004) and Katrina (2005) spawned renewed efforts to better understand the phenomenon of subaqueous shelf failure during severe hurricanes. In addition to destruction and wide-spread damage caused by these storms on land, numerous cases of catastrophic loss and severe damage occurred offshore in the GOM, most notably among fixed production platforms, mobile drilling rigs and pipelines. While much of this damage was directly caused by winds and waves at the surface, several cases of subaqueous sediment failure were also noted, particularly in the Mississippi Canyon, Viosca Knoll, South Pass and Main Pass protraction areas adjacent to the MRDF (Figures 1 and 2; see Appendix B for maps of precise hurricane routes and storm histories).

Massive sediment flow due to shelf failure along the MRDF occurs during normal sea-state conditions in response to several fundamental processes. First, rapid sediment loading from the fluvial discharge of the Mississippi River results in the deposition of localized, relatively coarse-grained material near the river distributary mouths. These sediments overlie finer-grained prodelta muds and clays containing excessively high water content (Coleman and Prior, 1980a). The resulting temporal and spatial differential loading can lead to gravitational stress, soil instability and, ultimately, slope failure (Coleman and Prior, 1978; De Blasio et al., 2004). Secondly, pore water and methane gas, formed from the biochemical degradation of organic debris, builds up within these undercompacted sediments and results in the liquefaction of overlying sediments and subsequent slope failure (Grozic, 2003). Third, wave-induced processes, particularly during hurricanes, can impact the seafloor and result in catastrophic slope failure (Coleman and Prior, 1978; Bea, 1971; Bea and Bernard, 1973; Bea et al., 1975; Suhayda, 1977).

However, the risk and incidence of submarine shelf failure increased dramatically during extreme sea-state conditions during a series of severe hurricanes that impacted the MRDF from 1965-2005 (Arnold, 1967; Bea and Bernard, 1973; Sterling and Strohbeck, 1973; Daniels, 1994;

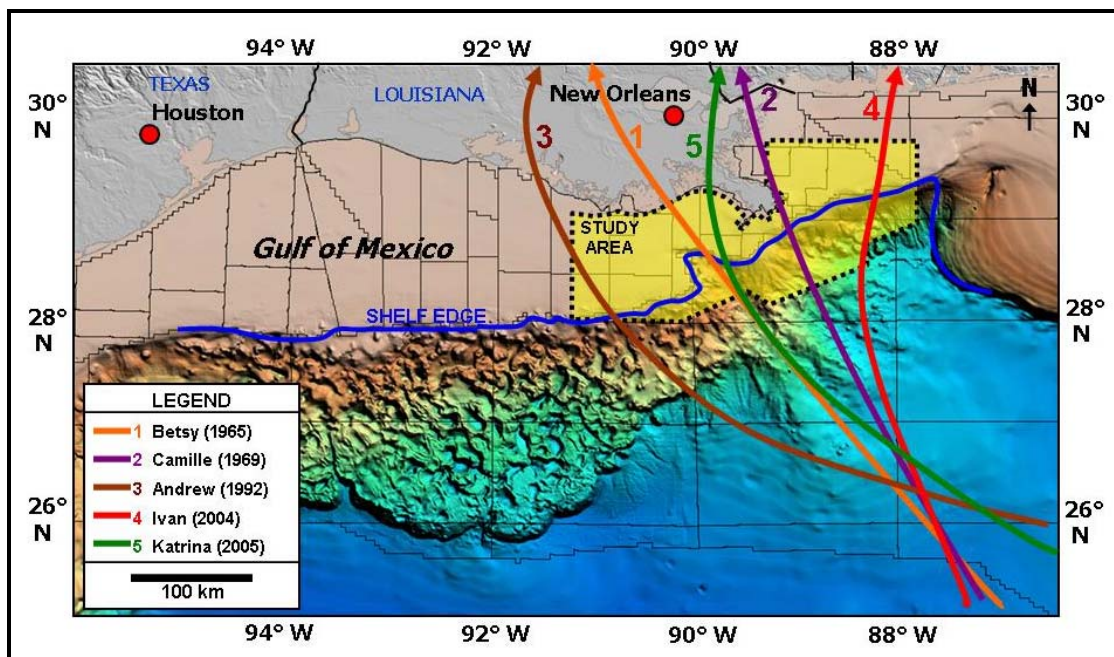


Figure 1: Location map and recent hurricane paths, north-central Gulf of Mexico, USA (modified imagery from Geoscience Earth & Marine Services, Inc., 2006)

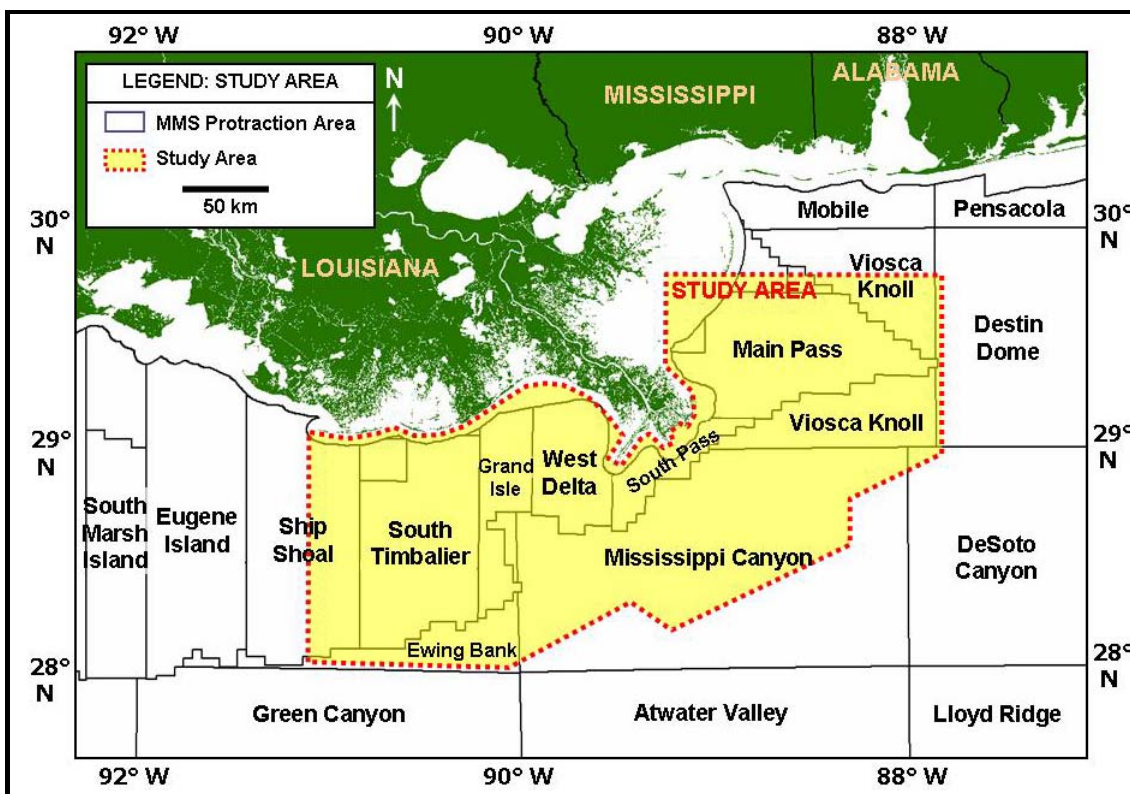


Figure 2: Location map of Mississippi River Delta Front study area within the north-central Gulf of Mexico, USA

Minerals Management Service (MMS), 2005a, 2005b, 2006a; Gilbert et al., 2007). Although 37 hurricanes approached the MRDF since weather observations began in 1851 (NHC, 2009), five major GOM hurricanes are notable for the offshore damage they caused – Hurricane Betsy (1965), Hurricane Camille (1969), Hurricane Andrew (1992), Hurricane Ivan (2004) and Hurricane Katrina (2005). The intensity of each of these hurricanes as they crossed over the MRDF prior to landfall was at least Category 3 on the Saffir-Simpson Scale (Stewart, 2005; NHC, 2009).

Submarine mudslide and shelf failure studies in the northern GOM began concurrent with initial oil and gas exploration activity offshore Louisiana in the 1950s (Prior and Coleman, 1978a; 1978b). The production of offshore oil and gas reserves required fixed platforms and pipelines to be installed on the ocean floor, and soil foundation borings and hydrographic data were used to ensure platform safety and reduce the risk of pipeline failure. In the 1950s and 1960s these data were incorporated into a broader geological framework relative to sedimentary patterns and processes active along the MRDF (Fisk and McClelland, 1959; Arnold, 1967). These studies were enhanced by research on the effects of Hurricane Camille, a powerful hurricane that made landfall in Mississippi in 1969 (Murray, 1970; Earle, 1975). This severe Category 5 storm induced several massive submarine mudslides adjacent to the MRDF resulting in the failure of two offshore platforms and severe damage to another in the South Pass Protraction Area (Bea, 1971; Bea and Bernard, 1973; Bea et al., 1975; Sterling and Strohbeck, 1973).

Little research was compiled on storm phenomena throughout the 1980s and early 1990s, mainly because fewer storms passed through the region. However, in September 2004 Hurricane Ivan induced several massive mudslides within the MRDF and numerous platforms and pipelines were either damaged or destroyed (MMS, 2005a). In 2005, the passage of Hurricane Katrina in waters adjacent southeastern Louisiana and Hurricane Rita adjacent to southwestern Louisiana caused additional offshore damage, warranting increased focus on better understanding and predicting the potential of future mudslides, which is a key objective of this research.



Wave-induced sediment failure profoundly impacted oil and gas industry infrastructure in the northern GOM during Hurricanes Ivan and Katrina. Seven production platforms were destroyed during Ivan and many others were significantly damaged (MMS, 2005a; Figure 3; also Appendix C, Table C-1, Figure C-1). An additional 46 platforms were destroyed during Katrina and many others were damaged (MMS, 2006; Figure 3; also Appendix C, Table C-2). Significant losses were also incurred during Hurricanes Betsy, Camille and Andrew although the magnitude of these losses was much less, in part due to the state of infrastructure development at the time (i.e., fewer platforms and pipelines existed then).

In addition to fixed platforms on the seabed, many drilling rigs and production pipelines also were either damaged or destroyed during Hurricane Katrina (Appendix C, Table C-3). Significant oil and gas production remained shut-in months after these storms occurred and compounded the economic loss of repairing or decommissioning damaged infrastructure. Economics were further degraded by production delays from blocks far away from direct storm paths and/or mudslide events since many pipelines that transport hydrocarbons to shore were damaged or destroyed (MMS, 2005b and 2005c). Thus, the advancement of scientific and engineering concepts governing submarine mass transport mechanics and the risk posed by future sediment failure appears a void in the literature. From an applied perspective, this is a significant issue facing the offshore oil and gas industry and thus is the primary driver in this research.

## **2.1 Observations to Date**

Following a period of heightened GOM hurricane activity in the 1950s and 1960s, a period of relatively lower activity emerged from the early 1970s through the mid-1990s (Landsea et. al., 1999; Muller and Stone, 2001, Keim et. al., 2004). However, beginning in 1995 with Hurricane Opal, a renewed period of increased hurricane activity began. This activity culminated with the passage of Hurricanes Ivan (2004) and Katrina (2005) and the resulting seafloor failure that occurred as manifested through damage and loss to offshore infrastructure.

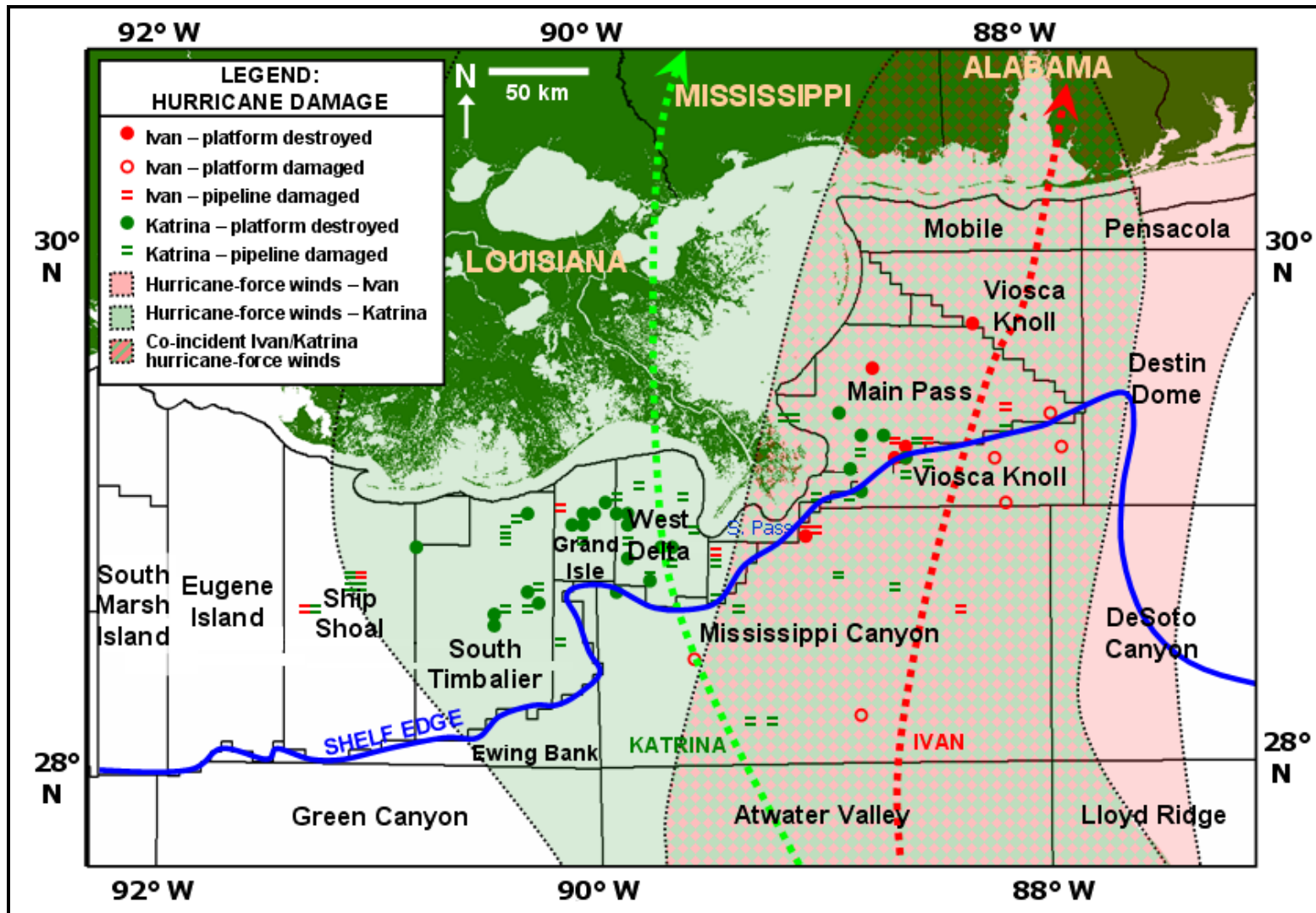


Figure 3: Damage to platforms and pipelines from Hurricanes Ivan and Katrina, 2004-2005 (some blocks have multiple cases of platform and/or pipeline damage; MMS; 2005a, 2005b)

The impact from these mudslides can cause substantial changes to the seafloor and immediate subsurface sediment profile through cyclic processes of differential pressure changes along the seafloor, seafloor scour, sediment re-deposition, and the re-initiation of antecedent seafloor slides. A set of unique factors control the potential for and severity of submarine mudslides and forms the basis for numerical modeling input as well as a comprehensive MRDF risk profile that are described in later chapters.

## **2.2 Meteorological and Sea-State Controls**

A scoping analysis of GOM hurricane activity reveals that 29 hurricanes with an intensity of Category 3 or higher passed within 300 km of the Mississippi River Delta since record-keeping began in 1851 (NHC, 2009, Keim et al., 2007; Table 1). Despite the varied and sporadic nature of reported data, particularly from earlier storms, these hurricanes varied considerably in size, forward speed, intensity, and associated oceanographic conditions. The data also reinforce the cyclic nature of GOM hurricane activity.

Offshore oil and gas exploration in the Gulf of Mexico began in 1947 (Hart Publications, 1997; Austin et al., 2004). Since then, 14 hurricanes (minimum Category 3) have passed through the MRDF (Appendix D; Figure D-1; National Hurricane Center, 2006; Stone et al., 1997; Stone et al., 1999; Muller and Stone, 2001), causing significant infrastructure damage at times together with several additional hurricanes that passed *near* the study area (MMS, 2005a, 2005b, 2009).

As an example, excessive wave action associated with Hurricane Camille in 1969 likely contributed to the loss of a Shell Oil Company production platform at South Pass Block 70 (SP 70) in a water depth of 105 m (Sterling and Strohbeck, 1973). Prior research on highly energetic surface gravity waves indicates that they can induce pressure anomalies with 300 m wavelengths in water depths of 60 m (Watkins and Kraft, 1976). However, the influence of storm waves (and therefore the resulting pressure amplitudes) decreases as water depth increases (Wiegel, 1964), and surface waves likely do not affect sea floor stability in water depths greater than 150 m (Watkins and Kraft, 1976). The damage to the SP 70 platform during Camille, and

the mudslide that caused it, was likely explained by wave activity that imposed oscillatory motion and wave loading on loose sediment (Henkel, 1970).

Extreme sea-state conditions existed during these storms and have been measured by several means. As an example, a series of offshore data buoys deployed by the National Data Buoy Center (NDBC) measured metocean conditions during both Ivan and Katrina that included significant wave height ( $H_{s_{max}}$ ), average wave period, wind speed and barometric pressure (NDBC, 2009). NDBC Data Buoy 42040, situated 118 km south of Dauphin Island, Alabama in a water depth of 444 m was in close proximity to the track of Hurricane Ivan. The buoy recorded sea conditions every hour until it broke loose from its mooring at approximately 0500 UTC on September 16, 2004 (NDBC, 2009). These data reveal a maximum  $H_{s_{max}}$  of 15.96 m, an average wave period of 12 sec, and a maximum wind speed of  $14.5 \text{ m sec}^{-1}$  prior to buoy failure (Figure 4). A more complete range of sea-state conditions was captured by a series of shelf and slope moorings maintained by the United States Naval Research Laboratory (USNRL) near the vicinity of Buoy 42040. Ivan moved directly over these moorings and yielded an  $H_{s_{max}}$  of 17.9 m with maximum crest-to-trough individual wave heights of 27.7 m (Figure 5; Wang et al., 2005; Teague et al., 2007).

The eye of Hurricane Katrina passed approximately 135 km west of NDBC Buoy 42040 and therefore the buoy failed to capture the full magnitude of the storm's severity (NDBC, 2009).  $H_{s_{max}}$  as measured by this buoy during Hurricane Katrina was at 16.91 m and the average wave period was measured at 14.3 sec (Figure 6). Because of the distance between Buoy 42040 and the track of Hurricane Katrina, a more accurate estimate of maximum wave height can be made using an alternate method relative to the minimum sea-level barometric pressure measured during a given hurricane (Equation 1; Hsu, 2006):

$$H_{s_{max}} = 0.2 (1013 - P_0) \quad (1)$$

where:  $H_{s_{max}}$  = maximum  $H_{s_{max}}$  (in meters)  
 $P_0$  = lowest sea-level pressure (in millibars)

Table 1: MRDF Category 3 Hurricane History within 300 km of the Mississippi River Delta, 1851-2008 (including MRDF bathymetry datasets when collected; hurricane data from National Hurricane Center, 2009)

	<u>Hurricane Name</u> * <sup>1</sup>	<u>Year</u>	<u>Maximum GOM</u> <u>Wind Speed</u> <u>(m sec<sup>-1</sup>)</u>	<u>Minimum Study Area</u> <u>Barometric Pressure</u> <u>(mb)</u>	<u>Estimated</u> <u>Hs<sub>max</sub> (m)*<sup>2</sup></u>	<u>Point of GOM Landfall</u> <u>(State: County/Parish)</u>
1	Gustav	2008	51.41	954	11.80	Louisiana: Terrebonne
2	Katrina	2005	78.23	902	22.20	Louisiana: Plaquemines
3	Ivan	2004	71.53	928	17.00	Alabama: Baldwin
4	Lili	2002	64.82	940	14.60	Louisiana: Vermilion
5	Opal	1995	67.06	919	18.80	Florida: Santa Rosa
6	Andrew	1992	67.06	937	15.20	Louisiana: St. Mary
7	Elena	1985	55.88	953	12.00	Mississippi: Harrison
8	Frederic	1979	60.35	943	14.00	Alabama: Mobile
Regional MRDF bathymetry survey, 1977						
9	Eloise	1975	55.88	955	11.60	Florida: Walton/Bay
10	Carmen	1974	67.06	937	15.20	Louisiana: Vermilion/Iberia
11	Camille	1969	84.94	905	21.60	Mississippi: Hancock
12	Betsy	1965	69.29	941	14.40	Louisiana: Lafourche/Jefferson
13	Hilda	1964	67.06	941	14.40	Louisiana: St. Mary
Regional MRDF bathymetry survey, 1940						
14	Great Miami	1926	55.88	N/A	N/A	Mississippi: Hancock
15	1917	1917	53.64	N/A	N/A	Florida: Santa Rosa
16	1916	1916	53.64	N/A	N/A	Mississippi: Harrison
17	New Orleans	1915	60.35	935	15.60	Louisiana: Plaquemines
18	Grand Isle	1909	53.64	952	12.20	Louisiana: Terrebonne/Lafourche
19	1906	1906	53.64	953	12.00	Mississippi: Jackson
20	1894	1894	53.64	N/A	N/A	Florida: Santa Rosa
21	Chenier Caminada	1893	60.35	948	13.00	Louisiana: Plaquemines
22	1886	1886	53.64	N/A	N/A	Louisiana: Cameron
23	1882	1882	51.41	949	12.80	Florida: Santa Rosa
Regional MRDF bathymetry survey, 1874						
24	1879	1879	55.88	N/A	N/A	Louisiana: Terrebonne
25	1860	1860	55.88	N/A	N/A	Louisiana: Jefferson/Plaquemines
26	Last Island	1856	67.06	934	15.80	Louisiana: St. Mary
27	Southeastern States	1856	51.41	N/A	N/A	Florida: Bay

--- continued on following page ---

	<u>Hurricane Name</u>	<u>Year</u>	<u>Maximum Study Area Wind Speed</u> (m sec <sup>-1</sup> )	<u>Minimum Study Area Barometric Pressure</u> (mb)	<u>Estimated H<sub>smax</sub> (m)*<sup>1</sup></u>	<u>Point of GOM Landfall</u> (State: County/Parish)
28	Middle Gulf Shore	1855	55.88	N/A	N/A	Louisiana: Plaquemines
29	Great Mobile	1852	51.41	961	10.40	Alabama: Mobile

\*1 Official names not assigned to hurricanes prior to 1950

\*2 Calculated via methods derived by Hsu (2006)

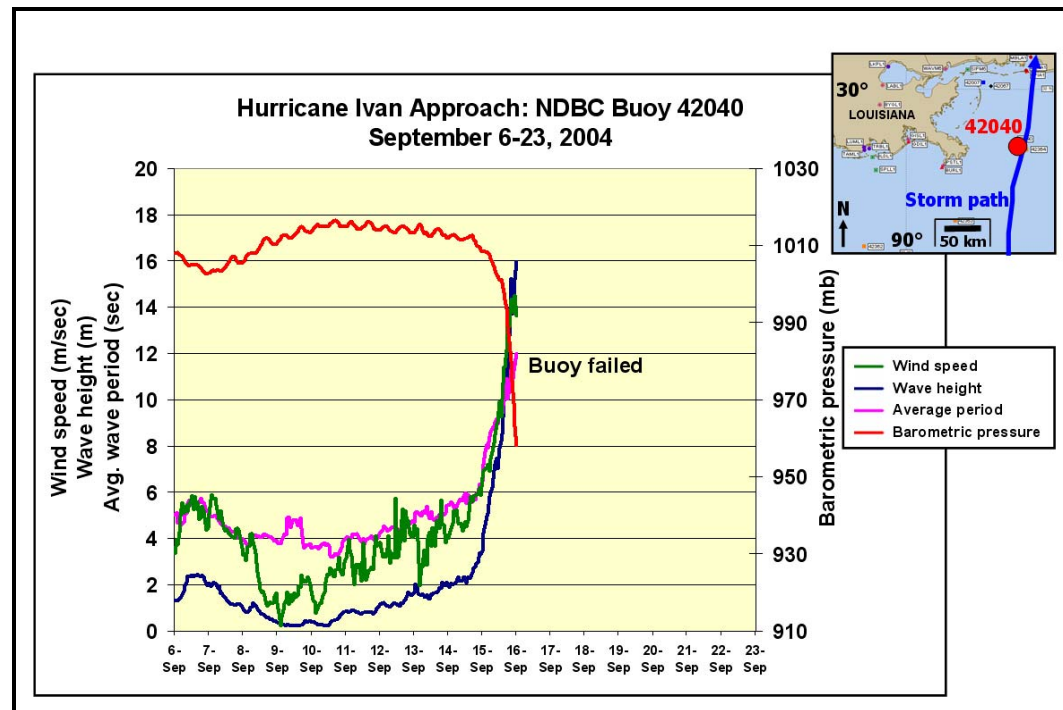


Figure 4: Key metocean parameters from Hurricane Ivan, 2004 based on readings from NDBC Buoy 42040 (data retrieved from archives available at NDBC, 2009)

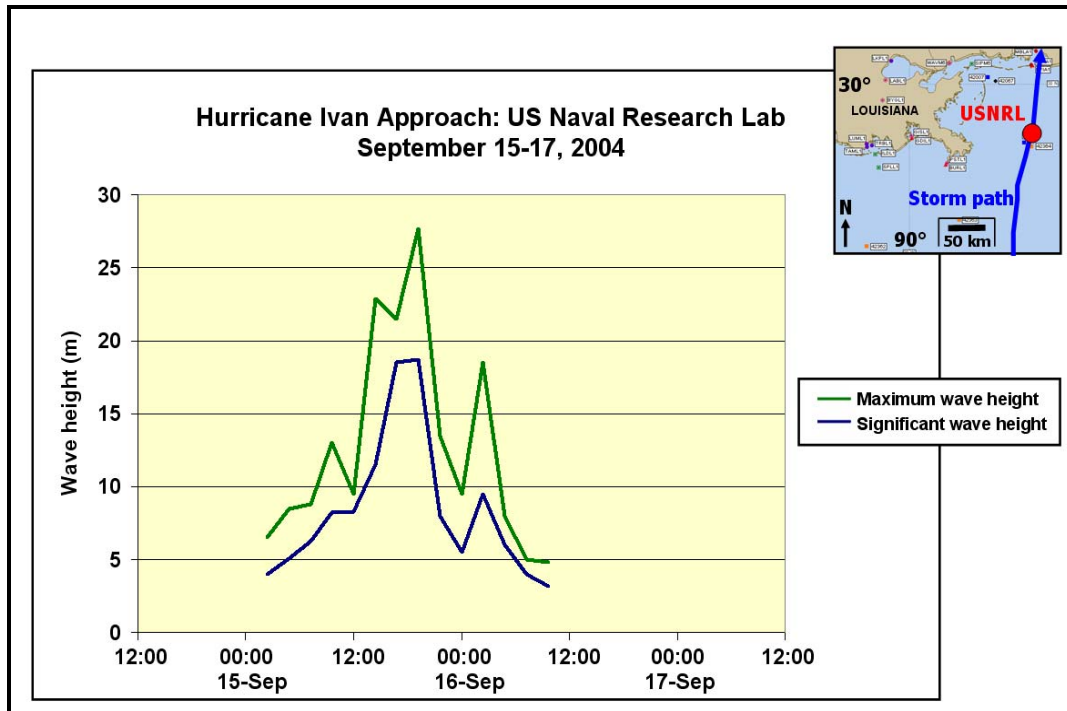


Figure 5: Key wave parameters from Hurricane Ivan, 2004 based on readings from U.S. Naval Research Laboratory (data retrieved from Wang et al., 2005)

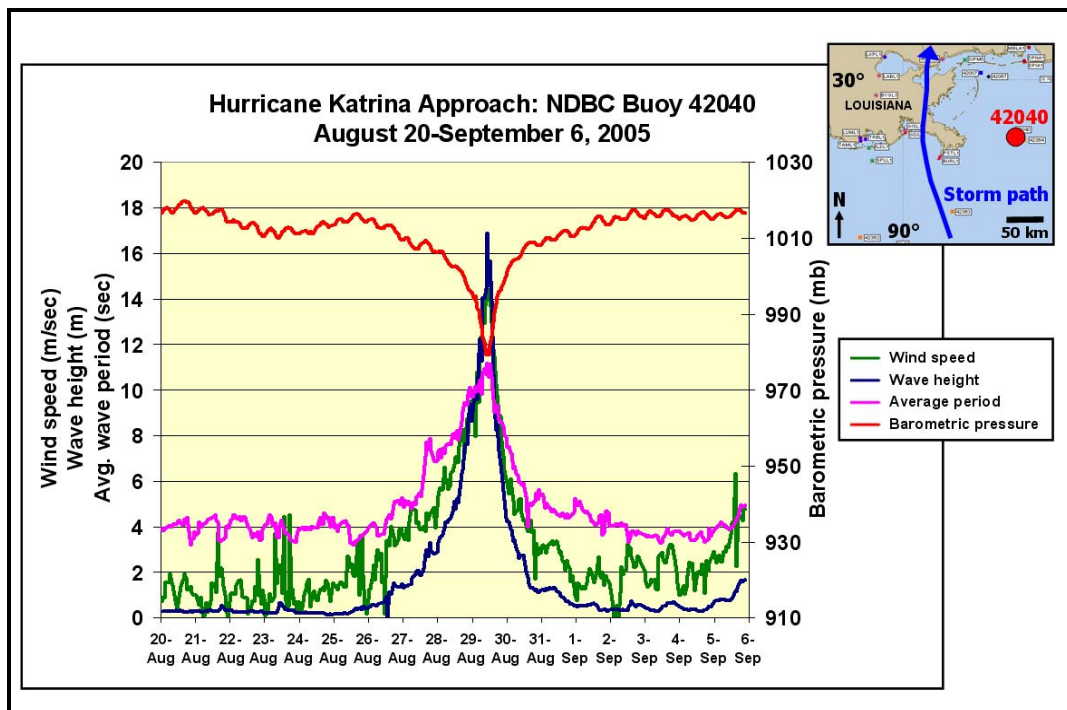


Figure 6: Key metocean parameters from Hurricane Katrina, 2005 based on readings from NDBC Buoy 42040 (data retrieved from archives available at NDBC, 2009)

Based on Equation 1 and the minimum barometric pressure observed during Katrina of 902 mb, the maximum  $H_{s_{max}}$  near the eye of the storm is estimated at 22.2 m. This equation is utilized when calculating estimated wave heights as input to numerical models and when bulk wave data, particularly from earlier storms, are incomplete.

Additional metocean data were recorded throughout the GOM during recent hurricanes. In addition to the NDBC buoys, data are also available through the Wave-Current Information System (WAVCIS) of Louisiana State University's Coastal Studies Institute as well as MMS-mandated Acoustic Doppler Current Profiler (ADCP) stations mounted on numerous production platforms offshore (WAVCIS, 2009; further discussed in Chapter 5). With these data, metocean conditions at given points of time can be compared to and calibrated against documented production losses, platform failures and pipeline damage reported to MMS by the industry. Once these conditions are known, hindcast modeling can then be applied to forecast the conditions prevalent in new mudslides or the re-initiation of older mudslides spawned by previous storms.

### **2.3 Lithologic and Geotechnical Controls**

Wave-induced action (primarily through storms such as winter cold front passages and hurricanes) is a major factor in subaqueous mass sediment transport (Coleman and Prior, 1980a; Suhayda, 1977). Under extreme wave action, wave-induced bottom pressure loads bottom sediments with forces not present under fair-weather conditions (Henkel, 1970). These additional forces can cause stresses within the sediment that exceed shear strength, eventually resulting in new equilibrium conditions (i.e., failure).

In order to correlate metocean conditions with known geologic events, this research utilizes a series of GOM geotechnical boreholes collected over time since 1956. These data, maintained by the Coastal Studies Institute (CSI) at LSU, extend across the GOM Shelf from the Ship Shoal to Viosca Knoll Protraction Areas and are comprised of nearly 250 boreholes from 166 offshore blocks (further discussed in Chapters 4 and 6). Although the data vary from borehole to borehole, basic information such as lithology, undrained shear strength, water content



and submerged unit weight is generally included. An additional borehole dataset used in this research consists of a series of geotechnical borehole information and resulting Gulf of Mexico shear strength maps (Dunlap et al., 2004). These data indicate broad areas of varying shear strengths based on a series of 748 soil borings collected throughout the GOM (further discussed in Chapter 6). Near the MRDF, data indicate that shear strengths are relatively high within early Holocene deltaic sediments near the head of Mississippi Canyon but are lower on the shelf near the active Mississippi River Delta both east and west of the river mouth.

In several cases, both the CSI and MMS/Texas A&M borehole locations are coincident with significant platform and/or pipeline failures during Hurricanes Ivan and Katrina (MMS, 2005b and 2009; Dunlap et al., 2004; Figure 7) and served as the initial focal points for this research. Data from these boreholes were used to help validate hydrodynamic modeling results and help determine the extent of lithologic and/or geotechnical controls on seafloor behavior.

Additional detail on lithologic and geotechnical controls is provided in Chapter 6.

## **2.4 Morphologic Controls**

Several classic studies previously outlined the submarine mudslide morphology along the MRDF (Coleman and Prior, 1978; 1980a and 1980b) and are discussed in detail in Chapter 3. In addition, micro-scale studies evaluated the internal sediment characteristics of stable and non-stable (i.e., mudslide) areas through a series of geotechnical boreholes to determine the effective depth of sediment movement (Roberts et al., 1976).

However, with the passage of Hurricanes Ivan and Katrina, more recent studies address metocean conditions and resulting seafloor changes during severe storms (Hooper and Suhayda, 2005a; 2005b; Stone et al., 2005; Thomson et al., 2005; Wang et al., 2005; Gilbert et al., 2007; Teague et al., 2007). In many cases these studies already outlined the known areal and vertical extent of submarine mudslides that occurred as a result of recent storm activity. These morphologic controls, which are discussed in more detail in Chapter 7, were then integrated with lithologic and geotechnical information as well as with morphological changes through time to

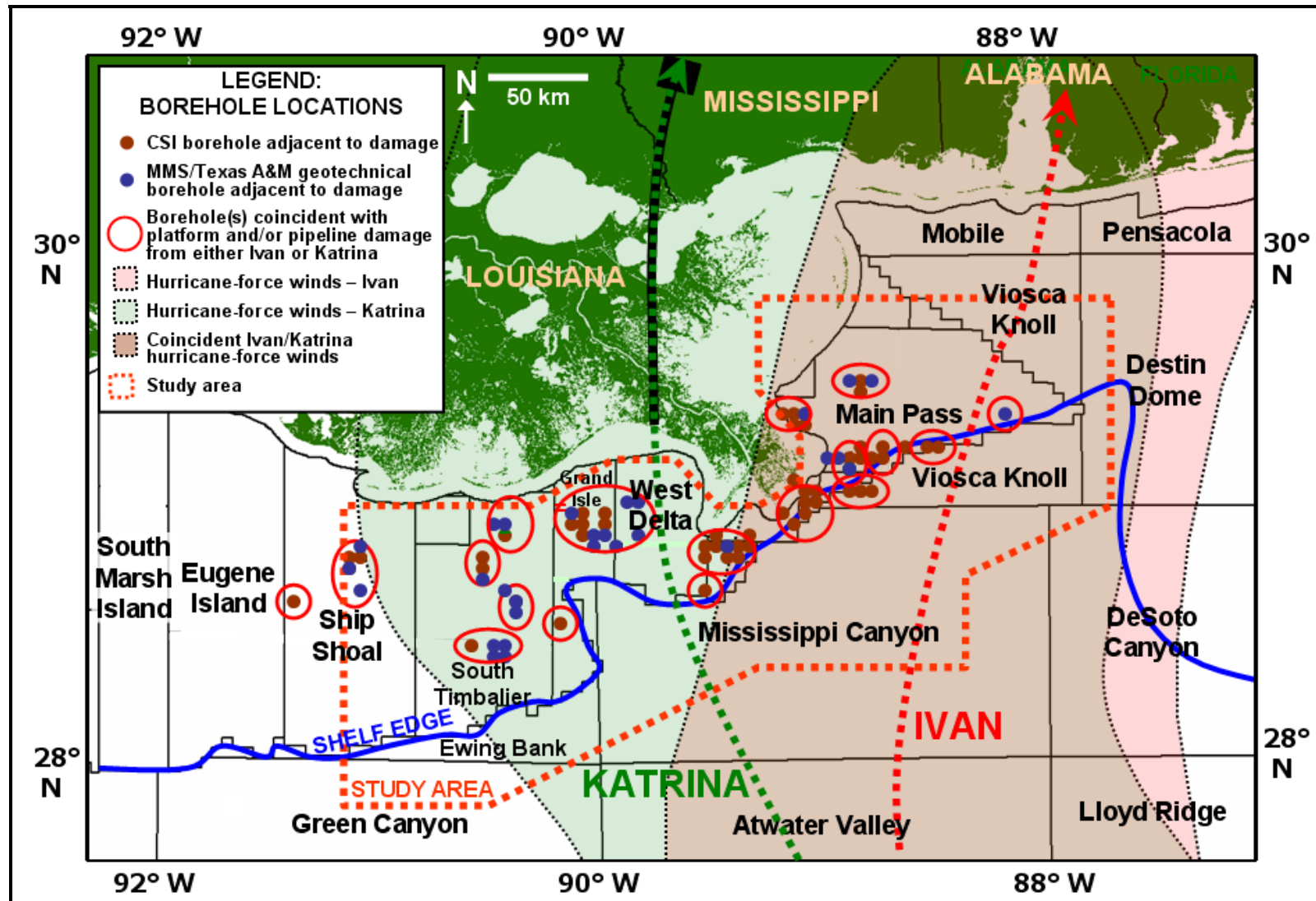


Figure 7: Approximate locations of study area boreholes relative to platform and pipeline damage reported during either Hurricanes Ivan or Katrina (damage reports from MMS, 2005b and 2006; MMS/Texas A&M geotechnical boreholes from Dunlap et al., 2004)

demonstrate the ephemeral nature of the shelf/slope environment and better determine possible geological controls on downslope sediment movement.

## **2.5 Infrastructure Controls and Statistical Analyses**

Submarine mudslides and shelf failure during hurricanes were recognized as a possible factor in pipeline and platform failures early in the production history of the Gulf of Mexico. Since then, significant damage has occurred to offshore infrastructure during many storms including Betsy (1965), Camille (1969) and Andrew (1992) as well as Ivan and Katrina (MMS, 2005a; 2005b). Hurricane damage and a statistical analysis of industry infrastructure controls are discussed in detail in Chapter 8. These two most recent storms provide the most complete (and most destructive) data record of offshore losses.

However, when examining precisely where this damage occurred, several trends are readily apparent (MMS, 2005a; 2005b; Figure 3). First, platform and pipeline damage *east* of the Mississippi River Delta appears concentrated to a relatively narrow, 30-km band coincident with the modern-day shelf edge. However, damage *west* of the delta is more sporadic and widespread across the entire shelf. Several hypotheses may explain this phenomenon, which include infrastructure age, seafloor lithology, and/or bathymetric controls on wave energy. These hypotheses were examined to develop methods by which the magnitude and extent of potential mudslides are controlled as a function of storm forcing, mudslide history, and regional geologic controls.

## **2.6 Numerical Modeling Integration and Proposed Contribution**

Previous studies across the MRDF have concentrated specifically on either the metocean, geotechnical or lithological studies involving submarine mudslides but none have involved successfully integrating the results into a comprehensive product. Therefore, a series of numerical wave models were run utilizing the MIKE 21 software package developed by the Danish Hydraulic Institute (DHI, 2005) to simulate the growth, decay and transformation of wind-generated waves and swell associated with the five hurricanes evaluated in this research.

Results from the wave models were compared to and calibrated against metocean data obtained from the NDBC buoy array as well as to directional spectra data obtained during Ivan and Katrina (the only storms for which these data are available) from a series of real-time observational stations operated by the WAVCIS Program. Model results were correlated to lithologic and geotechnical trends depicted from the borehole dataset described earlier. The integration of these results, combined with past failure history, provided a means to hindcast MRDF shelf failure as well as to develop a regionally applicable model to better assess the risk of future submarine mudslides.

These risks have been periodically examined by several consortia whose primary objectives, best identified at a forum in 2002, were to (a) identify the contributing elements, (b) clarify the implications to offshore facility design, (c) agree on the current state of knowledge within academia and industry, and (d) compile a “wish list” of knowledge needs to address critical issues (Wright, 2002; Appendix E). Given the dense infrastructure network along the MRDF and losses incurred during the 2004 and 2005 hurricane seasons, this dissertation not only addresses Parts (c) and (d) above but also provides a contribution towards better quantifying the fundamental relationships between various metocean, lithological and geotechnical controls that govern the risks inherent with submarine shelf failure described in Chapter 1.

The net deliverable, therefore, should help mitigate offshore losses due to platform and pipeline failures given various oceanographic conditions during future storms.

## **CHAPTER 3. PREVIOUS STUDIES**

### **3.1 Causation and Mechanics of Subaqueous Sediment Flow**

The phenomenon of subaqueous slope failure was first quantified nearly 80 years ago during the 1929 Grand Banks earthquake when submarine communications cables failed with progressive distance from the earthquake epicenter (Lee et al., 1991; Fine et al., 2005). Other early investigations of submarine slope failure took place adjacent to the mouth of the Magdalena River in Colombia, where oversteepening of the slope due to rapid deposition of sediment was suggested as the primary cause (Lee et al., 1991). Pioneering work in slope failure also sought to differentiate mass failure from better understood turbid and viscous fluid flow (Dott, 1963). Additional investigations have focused on size; the largest subaqueous slope failure noted to date is the Agulhas feature offshore South Africa in which  $2.03 \times 10^4 \text{ km}^3$  of sediment was moved in one event (Dingle, 1977).

In addition, past research has focused on two other well-known submarine sediment failures. First, the Storegga slide off Norway's west coast occurred approximately 8.2 MA as a retrogressive slide that set in motion a series of successively smaller slides characterized by varying sediment volume and sediment type (from hemipelagic marine to increasingly compacted and overconsolidated glacially derived sediments; Bryn et. al., 2002; Haflidason et. al., 2002; De Blasio et. al., 2005; Gauer et al., 2005). Secondly, shelf failure adjacent to the present-day Mississippi River delta has been extensively studied over the past several decades given its proximity to major industrial and population centers along the north-central Gulf coast. The remainder of this section includes the context behind many of these studies.

#### **3.1.1 Differential Loading and Slope Steepening**

The depositional environment offshore of the MRDF provides a classic example of how rapid fluvial sediment deposition onto a gently sloping delta platform can act as a catalyst for future mass sediment failure. The Mississippi River system is the largest river system in the United States and delivers approximately  $2.1 \times 10^8$  tons of sediment annually (Milliman and

Meade, 1983; Meade, 1996). The river's bedload consists of 90% fine sand; suspended load is comprised of 65% clay and 35% silt and very fine sand. Coarser material is deposited at or near the distributary mouths because of rapid deceleration and saltwater entrainment as river flow escapes the distributary and enters open water. Finer-grained material remains in suspension longer and is distributed farther offshore and laterally across the delta, building a platform fronting the delta consisting of clay-sized material (Fisk and McClelland, 1959; Coleman et al., 1998; Figure 8).

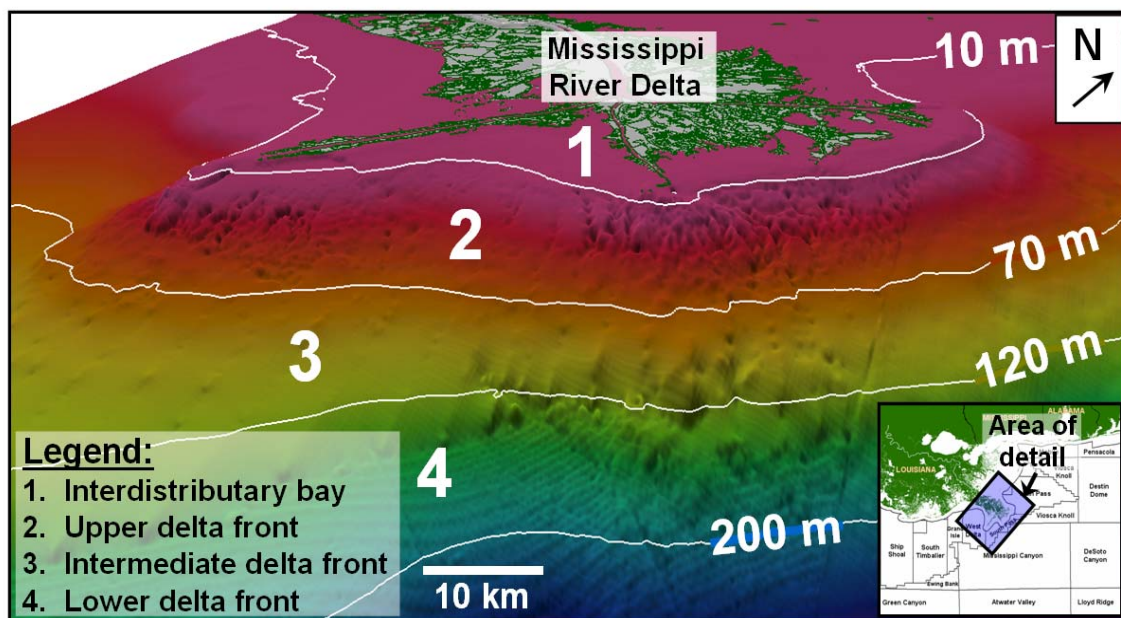


Figure 8: Mississippi River Delta Front (delta front classification from Coleman et al. (1998) superimposed on top of raw data extracted from NOAA, 2009; vertical exaggeration 40:1)

As a result, several primary topographic forms develop (Bea and Bernard, 1973; Coleman et al., 1998). The delta top generally lies at approximately the 5-8 m isobath and is comprised of a very flat plain crossed by a complex system of distributary channels. The sediment comprising this delta top displaces underlying, finer-grained plastic clays and can reach thicknesses of 250 m. The delta front, which can be segregated into upper, intermediate and lower sequences, lies at approximately the 5-200 m isobath and is comprised of progressively finer-grained material with increased distance from the sediment source (Figure 8; Coleman et al., 1998). Because of rapid

deposition, these deltaic deposits display high water contents, low strengths, and are usually underconsolidated (Walker and Messingill, 1970; Coleman and Garrison, 1977; Coleman and Prior, 1978; Coleman and Prior, 1988; Prior and Coleman, 1982). In addition, large quantities of *in situ* gases (primarily methane and carbon dioxide) can form as a result of rapid biochemical degradation of organic material contained in the deposits (Whelan et al., 1975).

Mass sediment failure can occur on relatively gentle slopes on the continental shelf. The MRDF contains slopes as low as  $0.5^{\circ}$  that become oversteepened through increased and rapid depositional loading (Prior and Coleman, 1978a; 1978b; McGregor, 1981). As an example, the bar associated with South Pass of the Mississippi River has advanced seaward approximately 1.6 km between 1867 and 1953. Nearly half of the sediment deposited on this bar was moved into deeper water by submarine sediment flow (Lindsay et al., 1984). Other instances of this phenomenon have been noted, particularly on the upper continental slope east of New Zealand, where surface sediment 10-50 m thick has slumped down bedding planes at slopes of  $1^{\circ}$ - $4^{\circ}$  (Lewis, 1971). Interestingly, an inverse relationship exists between slope steepness adjacent to failure versus slide runout length (McAdoo et al., 2000). On the continental shelves of California and Oregon, slope failure tends to steepen the local slope whereas failure in the Gulf of Mexico and offshore New Jersey tends to make local slopes less steep.

Slope steepness was also a primary factor in mass failure adjacent to the Huanghe (Yellow) River offshore China. Numerous cases of slope failure accompanied bottom sediment collapse and gullied sediment flow involving sandy and clayey silts eroded from inland loess deposits (Prior et al., 1986; 1989). As in the Gulf of Mexico, large areas of the Huanghe delta front were affected by collapse processes on initial shelf slopes of  $0.1^{\circ}$ - $0.4^{\circ}$ . Flow mechanics within subaqueous failures can vary greatly, as demonstrated by analyses of the Storegga slide in the Ormen Lange region of the Norwegian Sea. Modeling of this major debris flow indicates that the top layer of the slide was entirely preserved during failure and that flow occurred at high shear rates contained in a lubricated mud layer partly derived from the disintegration of the

overlying failed block (De Blasio et al., 2004). Other studies have demonstrated that failure occurs when shear stress surpasses abnormally low shear strength resulting from massive depositional loading taking place adjacent to major rivers, ultimately resulting in slope failure (Booth, 1979).

Slumping and other mass sediment failure processes can also lead to massive retrogressive scars and canyons or trenches that form at the shelf edge (Coleman et al., 1983). The resulting canyons attain widths of 10-20 km, depths of 800 m, and lengths of 80-100 km. Coleman et al. (1983) suggest that Mississippi Canyon formed in such a manner; shelf edge instability resulted in large volumes of shallow-water sediment that eventually resulted in the formation of massive submarine fans in deeper basins. Since deltaic progradation was rapid, large foreset deposits were formed near the canyon heads, and the low strength of rapidly deposited, underconsolidated sediments caused downslope creep and resulted in multiple filling and evacuation episodes (Coleman et al., 1983). Beyond the shelf edge, subaqueous flows can be altered by seafloor relief associated with recent salt tectonics (Tripsanas et al., 2004).

### **3.1.2 Gas and Gas Hydrate Effects**

Fine-grained sediments that accumulate through rapid depositional loading along the MRDF may contain abundant gas volumes. This gas can affect sediment stability either *directly* by entrapment of gas bubbles in unconsolidated sediment or by dissolved gases in the pore water, or *indirectly* by the upward migration of these gases resulting from bottom pressure perturbations, such as from storm waves (Coleman et al., 1974; Cooper and Hart, 2003).

Methane concentrations in shallow lower-delta sediment range from 0.047-150 ml l<sup>-1</sup> in offshore marine sediments; however in surface waters near the Mississippi Delta the concentration is 2-3 orders of magnitude higher (Brooks and Sackett, 1973). Competition for hydrogen exists in marine sediments between sulfate-reducing and methane-producing bacteria; if methane production begins as sulfate reduction diminishes, areas of low sulfate and high dissolved organic matter in sediment pore water can produce methane (Coleman et al., 1974;



Whelan et al., 1975). The high seasonal freshwater discharge of the Mississippi delta lowers sulphate concentration in nearshore waters that contain high organic concentrations. Through a series of combinations, dissolved carbon dioxide reacts with molecular hydrogen to form methane. The high gas content, combined with storm wave impact, can cause sediment instability quicker than in sediments with lower gas concentrations. This can happen on a massive scale during hurricanes as ambient pressure (and the pressure the gas is subject to) varies with wave frequency. These pressure changes allow gas to alternately contract and expand, resulting in a large expansion of gas that separates sediment grains and releases large amounts of gas at a time (Coleman, et al., 1974). Bottom sediment shear strengths then become greatly reduced, resulting in instantaneous downslope gravity movement.

Massive sediment failure can also occur through the melting of gas hydrate (Sultan et al., 2004). First discovered in the Green Canyon Protraction Area in 1984, gas hydrate is often associated with shallow chaotic sequences or faults suggesting formation through mud diapirism or volcanism (Neurauter and Bryant, 1989). Gas hydrate acts to cement sediment; any negative change in equilibrium parameters (e.g., temperature, pore pressure, gas chemistry, or porewater salinity) can cause sediment weakness and initiate failure as a result of converting hydrate to gas plus water (which weakens the sediment and generates increased pore pressure). Since the ratio of methane to water in the hydrate phase is about 150 times that in the aqueous phase, hydrate can generate huge quantities of methane when melted and contribute significantly to massive slope failure. In addition to the Gulf of Mexico, cases of slope failure initiated through interactions with gas hydrate have also been documented offshore Norway within the Finneidfjord slide in the Norwegian Sea (Best et al., 2003).

### **3.1.3 Wave- and Current-Induced Failure**

Wave-induced action (primarily through storms such as hurricanes and wintertime cold front passages) is a major factor in subaqueous mass sediment transport (Coleman et al., 1974; Suhayda, 1977). Under extreme wave action, wave-induced bottom pressure loads bottom

sediments with forces not present under normal conditions (Henkel, 1970). These additional forces can cause stresses within the sediment that exceed sediment shear strength, resulting in new bottom sediment equilibrium conditions. In these cases, the resulting equilibrium bottom slopes are less steep than those determined by gravity forces alone. An example from South Pass near the mouth of the Mississippi River shows a change in bottom topography from 1948-1950 in which slopes changed from about 1% to 0.5% (Coleman et al., 1974). The steepness of these slopes is much less than critical for these sediments (which was about 3%-5%); however, slope failure still occurred and can likely be attributed to wave action.

The same process can extend into deeper water. Seafloor slope at South Pass Block 70 (the location of Shell's platform failure during Hurricane Camille, in a water depth of 105 m) average about 1%, and sediment movement as a result of the storm extended to a depth of 21 m based on the depth at which the platform pilings failed (Sterling and Strohbeck, 1973). Here as in shallower water, since slope steepness is much less than critical, wave forces must be an important factor in slope failure.

Prior research on the role played by large surface water waves indicates that they can induce pressure anomalies with 300 m wavelengths in water depths of 60 m (Watkins and Kraft, 1976). However, the influence of storm waves (and therefore the resulting pressure amplitudes) decreases in progressively deeper water (Wiegel, 1964), and surface wave effects likely do not affect sea floor stability in water depths greater than 150 m (Watkins and Kraft, 1976). The damage to the SP 70 platform during Camille, and the mudslide that caused it, were likely explained by wave activity that imposed oscillatory motion and wave loading on loose sediment (Henkel, 1970). A graphical representation of wave motion effects on seafloor sediments can be reduced to calculating the magnitude of the disturbing moments ( $M_d$ ) relative to the resisting moments ( $M_r$ ) as noted in Equations 2 and 3 as well as in Figure 9. Sediment movement and failure occur when  $M_d > M_r$  (Henkel, 1970).

$$M_d = \frac{2}{3} \chi^3 \beta \gamma' + \frac{L^2 \Delta p}{2 \pi^2} (\sin \alpha - \alpha \cos \alpha) \quad (2)$$

$$M_r = 2 \chi^3 \frac{C\mu}{\gamma' z} \gamma' \left( \frac{\sin \Theta - \Theta \cos \Theta}{\sin^3 \Theta} \right) \quad (3)$$

Where:

$\chi$	= half-length of the slide	$\alpha$	= angular portion of sinusoidal load on slide length
$\beta$	= slope angle	$C\mu$	= undrained strength of slide material
$d$	= depth		
$\gamma'$	= buoyant unit weight		
$2\theta$	= angle of arc sliding		

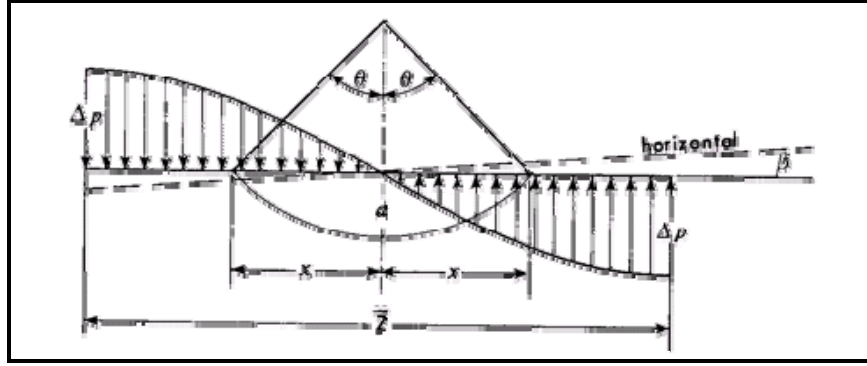


Figure 9: Model for wave loading of submarine sediments (from Henkel, 1970)

Additional studies along the MRDF have concentrated on net changes in water depth that were presumably due to subaqueous sediment failure. Bathymetry readings were first collected along the MRDF in 1868 and were updated thereafter by the U.S. Coast and Geodetic Survey (Appendix F). The ephemeral nature of the MRDF can be noted on distinct morphologic and bathymetric changes in increments from 1874 to 1940 and again from 1940 to 1977 (discussed further in Chapter 7). Comparisons between these bathymetric datasets clearly demonstrate net elevation changes along the seafloor, which range within a band of approximately  $\pm 0.75 \text{ m year}^{-1}$  ( $\pm 2.5 \text{ feet year}^{-1}$ ). From 1940-1967, changes in locally measured sediment accumulation and loss occurred were measured up to 15 m (49 feet) in South Pass Block 70 (discussed in Chapter 7).

Much of these GOM bathymetry data were gathered immediately after severe hurricanes to indicate the extent of topographic seafloor change through hurricane-induced wave action (Bea et al., 1975). Although the localized slope steepening by currents and creep associated with

steep, prograding mud fronts can lead to slope movement, failure as a result of storm waves is the predominant mechanism for sediment movement along the MRDF (Bea and Bernard, 1973).

### **3.2 Morphology and Classification of Submarine Sediment Flow**

Much of the pioneering work in MRDF submarine sediment flow morphology was carried out by LSU's Coastal Studies Institute. The classic morphologic scheme devised through this work includes five major instability types (Coleman and Garrison, 1977; Coleman and Prior, 1978; Prior and Suhayda, 1979; Prior and Coleman, 1984; Prior et al., 1984). They include:

- Peripheral rotational slumps: located nearest to river mouths, these features consist of slump blocks rotated in an upslope direction, often producing a reverse slope (Figure 10).
- Collapse depressions: located in interdistributary bays and immediate offshore regions (Figure 10), these features consist of circular, hummocky areas that are bowl-shaped in appearance and bound by distinct scarps (Figure 11).
- Bottleneck slides: located within interdistributary areas (Figure 10), these features are morphologically similar to collapse depressions except that the bounding scarps do not form a totally closed perimeter around the instability (Figure 11).
- Elongate retrogressive slides and mudflow gullies: located adjacent to major distributaries and extending radially seaward (Figure 10), these features occur in water depths of about 10-100 m. They emerge from extremely disturbed areas of slump topography and have a recognizable area of rotational instability (or “head slump” as noted by Coleman and Prior, 1978; Prior and Coleman, 1979; Figure 11). A critical component of these features is that they move episodically with catastrophic pulses or surges that can damage underwater oil and gas pipelines.

- Depositional lobes and mudflow noses: located seaward of the elongate chutes previously described are broad, overlapping depositional lobes composed of debris discharged from the gullies (Figures 10 and 11).

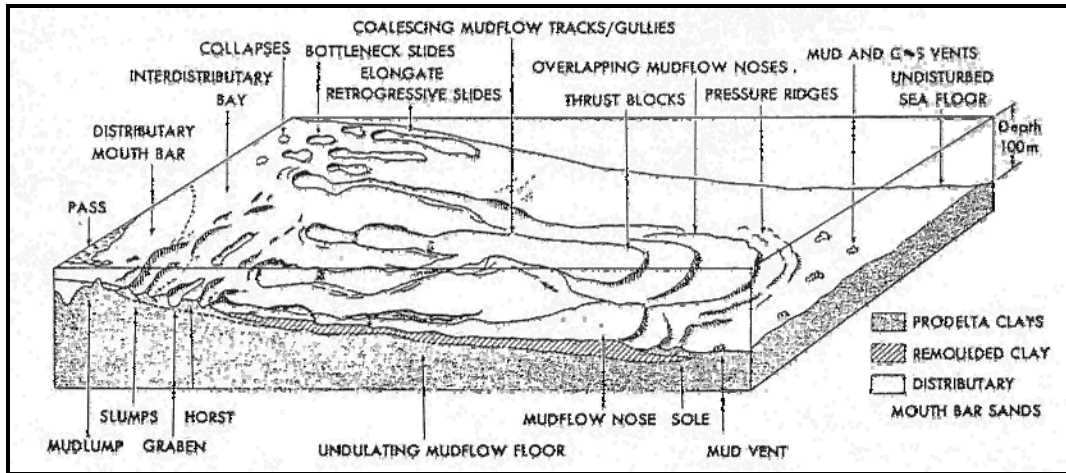


Figure 10: Schematic distribution and morphology of subaqueous landslides in the vicinity of a distributary and offshore, Mississippi River delta (from Coleman and Prior, 1978).

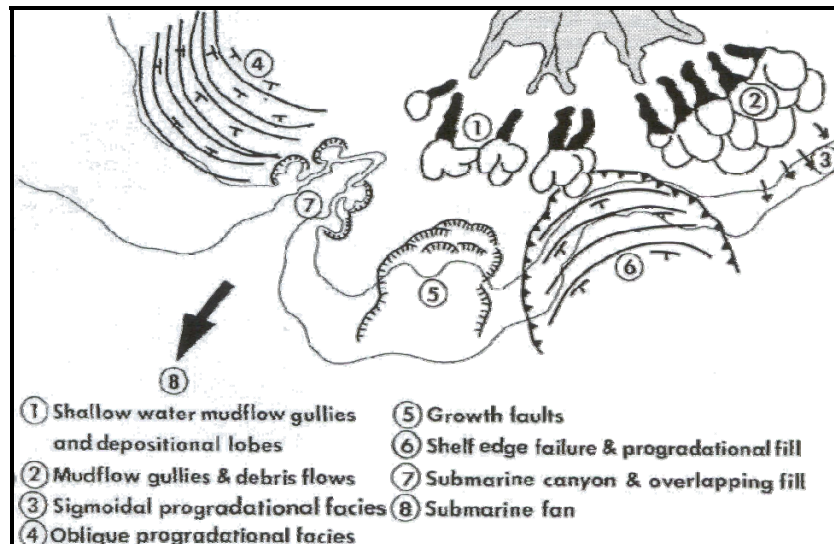


Figure 11: Schematic diagram illustrating the major sediment instability facies off major river deltas (from Coleman et al., 1983)

In addition to the scheme above, others more closely examine sediments comprising the sedimentary record and therefore account for changes that occurred between slide initiation and final deposition. As an example, a slide could change into a plastic flow and then into a turbidity current, resulting in changes in the shape of the flow as well as hydrodynamic parameters such as

speed, density and viscosity which become important in building accurate numerical models (Mulder and Cochonat, 1996).

Other classification schemes have been proposed based on rheology, where fluid and debris flows were distinguished by fluid and plastic behavior (Lowe, 1979; Suhayda and Prior, 1978). These flows were further subdivided into five types based on dominant coarse-particle support mechanisms and how they each influenced the texture and structure of flows and their deposits. Others modified this model by classifying failures based on the ultimate flow character *during flow* that will more likely be reflected in the ultimate failure deposit (Postma, 1986). Others have used the ratio of headscarp height to runout length as a measure of dynamic rheology for a given slope failure, thus providing a basis for classifying slides based on different sedimentary and tectonic environments (McAdoo et al., 2000).

### **3.3 Selected MRDF Hurricanes – Synoptic History and Sea-State Conditions**

The wave-induced mechanism for initiating mass sediment failure on continental shelves is particularly pronounced during intense events such as hurricanes. Most of the literature dwells on two unusually powerful hurricanes that struck the north-central Gulf coast within the past 40 years – Hurricane Camille in 1969 and Hurricane Ivan in 2004. However, mass movement associated with severe GOM hurricanes has been documented in three additional Category Four hurricanes that struck the north-central GOM coast. These storms include Hurricane Betsy, which struck the southeastern Louisiana coast in 1965, Hurricane Andrew, which struck the central Louisiana coast in 1992, and Hurricane Katrina, which struck the southeastern Louisiana and southern Mississippi coasts in 2005 (Figure 1). Additional hurricanes also occurred within the time span covered by MRDF-wide bathymetric data acquisition (Table 1; Appendix D). However, these storm events, for which neither metocean conditions nor damage reports were as severe, will only be used to help validate results from numerical modeling versus damage reports provided by the MMS.

Submarine sediment flow during hurricanes has also been documented in areas other than the GOM, most notably during Hurricane Iwa, a Category Two hurricane that passed just west of Hawaii in November 1982 (Normark et al., 1993). During that storm an array of current sensors recorded four successive episodes of downslope failure associated with nearbottom currents of up to  $200 \text{ cm s}^{-1}$ . Sensors from four moorings recorded an increase in water depth up to 220 m which implies downslope sediment transport approaching 2.4 km at a speed near  $300 \text{ cm s}^{-1}$  (Dengler et al., 1984).

### **3.3.1 Hurricane Betsy (1965)**

Hurricane Betsy, the second named storm system of the 1965 hurricane season, made two separate landfalls in the United States – the first over the Florida keys and the second several days later on September 9, 1965 in southeastern Louisiana near Grand Isle (Sugg et al., 1966; NHC, 2009). Betsy was first detected as a tropical disturbance in the eastern Atlantic and then moved steadily westward, crossing over the Lesser Antilles as a tropical depression. Betsy then strengthened into a hurricane and ultimately reached Category 4 status twice, first northeast of the Bahamas and a second time over the north-central GOM (Sugg et al., 1966). Estimates of GOM storm intensity include sustained winds of about  $67 \text{ m s}^{-1}$  (150 miles  $\text{hour}^{-1}$ ) and a minimum atmospheric pressure of 941 mb just prior to the Louisiana landfall (NHC, 2009). While these characteristics are typical for severe GOM storms, Betsy was notable for two parameters – its relatively fast forward movement of  $35 \text{ km hour}^{-1}$  (22 miles  $\text{hour}^{-1}$ ) as it passed through the north-central GOM (Figure 1) and its relatively large size, with hurricane-force winds extending 145 km (90 miles) away from the center and an eye diameter about 65 km (40 miles) wide at landfall (Appendix B, Figure B-1; Sugg et al., 1966).

The asymmetric wind field typical in most GOM hurricanes is evident as Hurricane Betsy moved through the GOM (Appendix B, Figure B-1). The strongest winds were indicated in the eastern half of the storm and in particular in the right front (i.e., northeastern) quadrant. This phenomenon is attributed to counter-clockwise hurricane wind circulation patterns and a common

south-to-north or southeast-to-northwest approach toward the coast in the GOM. This depiction of the wind field was derived as part of a surface wind pattern analysis known as the “H\*Wind Project” carried out by the Hurricane Research Division (HRD) of the Atlantic Oceanographic and Meteorological Laboratory, National Oceanographic and Atmospheric Administration (NOAA; Powell et. al., 1998, NOAA, 2007).

These time-series data, representing a blend of actual measurements and subsequent numerical modeling, were computed by HRD on a 12-km grid spacing for each hour that Hurricane Betsy moved through the GOM. Actual measurements were obtained from U.S. Air Force and NOAA aircraft, ships, buoys, C-MAN platforms and surface airways. These data were then processed to conform to a common framework for a height of 10 m, exposure (dependent on conditions that were either open marine or open terrain over land), and average maximum sustained wind speed for a period of one minute.

Maximum wind field measurements as Hurricane Betsy entered the study area were 124 knots (roughly  $64 \text{ m sec}^{-1}$ ; Powell et. al., 1998). Successive time series depictions indicate that Betsy’s maximum wind field in the study area ranged from 122-125 knots ( $63\text{-}64 \text{ m sec}^{-1}$ ). Central pressures during this time span (approximately the last four hours prior to landfall) ranged from 941 to 951 mb (NHC, 2009).  $H_{s_{\max}}$  wave height calculations, given these central pressures and the formula derived by Hsu (2006), indicate an  $H_{s_{\max}}$  wave range of 12.4-14.4 m.

Hurricane Betsy pre-dated the deployment of data buoys by NDBC; therefore real-time wave, wind and pressure data are unavailable. However, based on analyses of subsequent hurricanes where these data were available (e.g., Andrew, Ivan and Katrina) sea-state conditions likely remained unsettled several days after the storm before returning to calmer conditions, thus demonstrating wave energy transfer across the GOM in response to the storm (depicted in subsequent analyses of Hurricane Andrew; Grymes and Stone, 1995). By that time, the circulation center of the remnants of Hurricane Betsy was located over western Tennessee and Betsy had been downgraded to a tropical depression.



Time-series wind field data from the H\*Wind project were used as inputs into MIKE 21 wave modeling efforts, which are discussed in more detail in Chapter 5. A statistical evaluation of infrastructure damage and loss during Hurricane Betsy is discussed in Section 8.3.1.

### **3.3.2 Hurricane Camille (1969)**

Hurricane Camille began as a tropical disturbance over western Africa in August 1969 and then moved steadily westward across the Atlantic Ocean, attaining tropical storm status about 100 km (60 miles) west of Grand Cayman in the western Caribbean Sea. Camille rapidly gained intensity and moved over western Cuba as a minimal Category 3 hurricane. The storm continued on a northwesterly track through the central GOM, eventually attaining Category 5 status and striking the Gulf Coast near Waveland, Mississippi (Figure 1; also Appendix B, Figure B-2; Roberts, 1969; Wright et al., 1970; Simpson et al., 1970; Thom and Marshall, 1971). Camille ranks as one of the most intense storms to ever reach the United States. Only two other storms in the historical record, the Florida Keys Labor Day Hurricane (1935) and Hurricane Andrew (1992), made landfall as Category Five hurricanes (winds exceeding  $69.7 \text{ m sec}^{-1}$ , or 155 miles  $\text{hour}^{-1}$ ; NHC, 2009). Other recent Atlantic hurricanes reached Category Five status (e.g., Hurricanes Gilbert in 1988, Ivan in 2004, and Katrina, Rita and Wilma in 2005), but they either never struck the U.S. mainland or they lost intensity while still at sea (NHC, 2009).

Estimates of Camille's GOM storm intensity just prior to landfall in Mississippi include sustained winds of about  $85 \text{ m s}^{-1}$  (190 miles  $\text{hour}^{-1}$ ) and a minimum atmospheric pressure of 905 mb (Roberts, 1969; Simpson et al., 1970; NHC, 2009). The radius of hurricane-force wind was relatively small at 95 km (60 miles) as was the eye (7.2 km, or 4.5 miles) compared to Hurricane Betsy four years earlier (United States Weather Bureau, 1969). Precise parameter measurements for Hurricane Camille are spotty because (1) no recording instruments survived the storm at landfall, and (2) the hurricane's intensity and small eye diameter often precluded military reconnaissance aircraft from penetrating the eye of the storm as it passed through the central GOM (Simpson et al., 1970). A rare, key penetration was made by an Air Force reconnaissance

aircraft when the eye of Camille was located about 160 km (100 miles) from the mouth of the Mississippi River where surface winds were estimated at about  $92 \text{ m s}^{-1}$  (200 miles hour<sup>-1</sup>; Simpson et al., 1970). In addition, post-storm damage appraisal of structures within several hundred meters of the coastline and the way they splintered apart appeared consistent with wind velocities near  $92 \text{ m s}^{-1}$  (200 miles hour<sup>-1</sup>; Simpson et al., 1970).

A depiction of Camille's wind field pattern reveals the presence of a small, tightly knit storm as it made landfall on the Mississippi coast that began losing intensity after coastal impact (Appendix B; Figure B-2). Gridded wind field data were obtained for use in this dissertation from Oceanweather, Inc., a specialized oceanographic and meteorologic consulting and research firm that constructed a hindcast of Camille via techniques described in Oceanweather, Inc. (2003; 2007a; 2007b) and Cardone et al. (2004; 2007). Since Camille pre-dated the installation of most oceanographic observations stations in the GOM, hindcasts for subsequent storms (e.g. Lili, Ivan and Katrina) were carried out using all publicly available oceanographic and meteorologic data. These hindcasts were then calibrated against actual observations and measured data in order to validate results for earlier storms (Oceanweather, Inc., 2003; Cardone et al., 2004, 2007).

The few oceanographic observations available during Hurricane Camille consisted of a network of ocean data gathering stations deployed in the GOM from 1968-1971 by the Baylor Company (subsequently acquired by National Oilwell Varco). This program, consisting of an industry consortium of eight companies, is described in detail in Hamilton and Ward (1974) and Ward (1974). Camille passed between two of the stations, one located in South Pass Block 62 (26 km east of the eye path; water depth approximately 100 m) and the other located in West Delta Block 133 (76 km west of the eye path; water depth about 84 m; Figure 12; Patterson, 1974; Earle, 1975). Although the wave staffs at the two stations failed during the storm, the recorded data survived. Measurements were taken and later analyzed at 30-minute intervals for a ten-hour period as Camille moved over the area; they included significant wave period

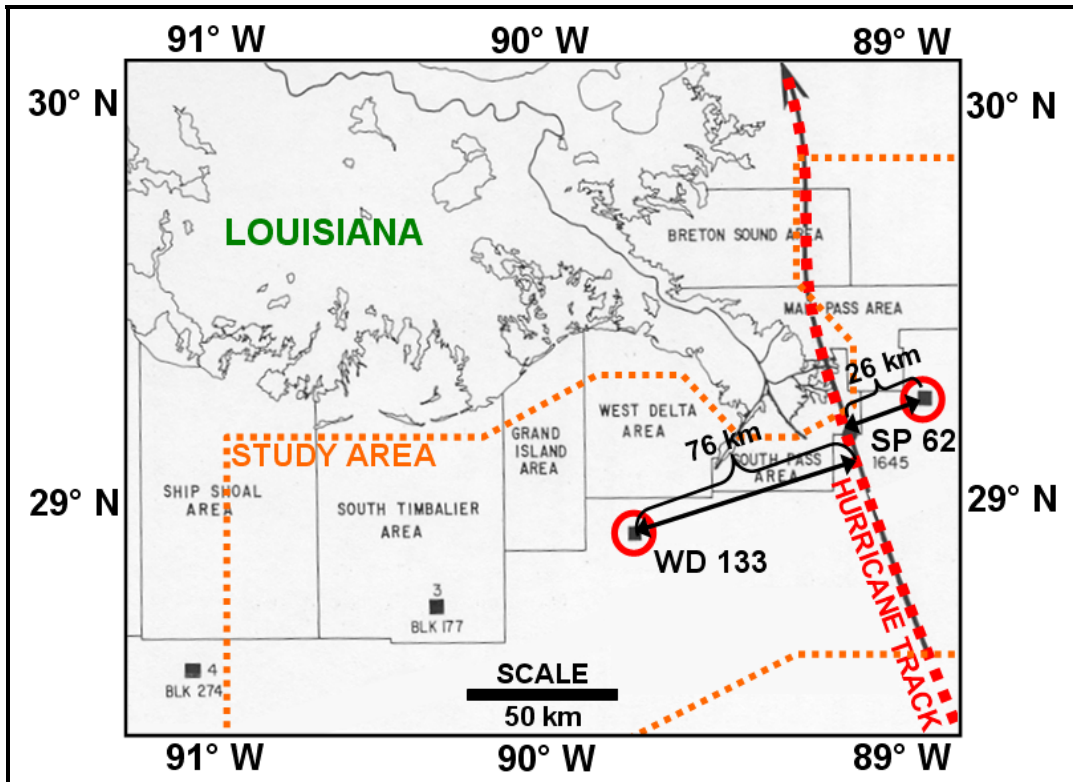


Figure 12: Ocean Data Gathering Stations relative to track of Hurricane Camille (1969), north-central Gulf of Mexico (modified from Patterson, 1974)

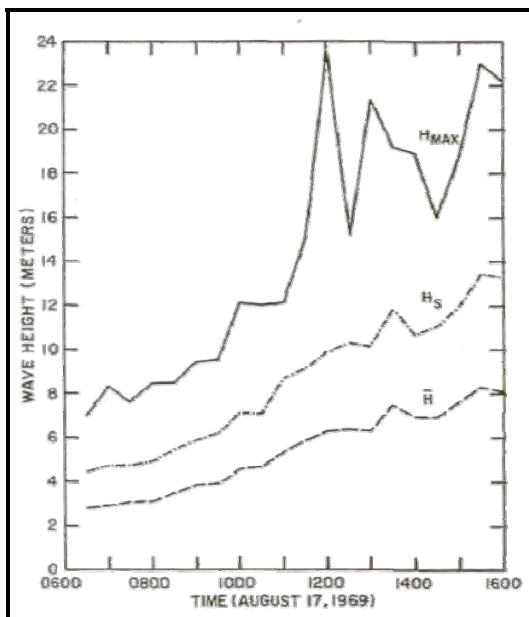


Figure 13: Time variation of wave height parameters during Hurricane Camille (from Earle, 1975)

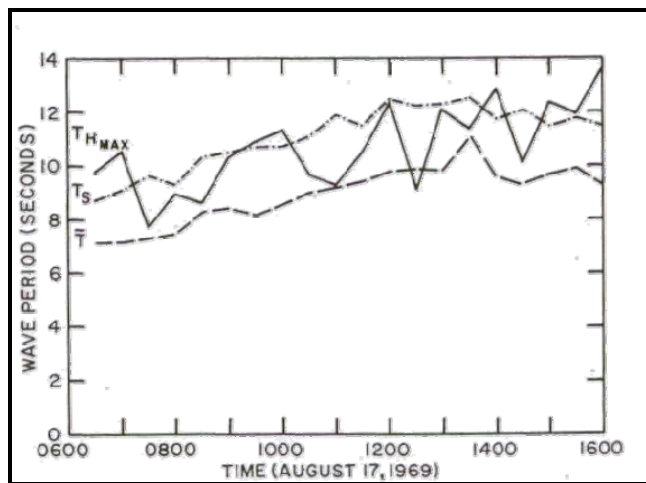


Figure 14: Time variation of wave period parameters during Hurricane Camille (from Earle, 1975)

approximately 11.1 sec) and significant wave height (21.6 m; Figures 13 and 14; Appendix G, Table G-1). However, wave heights were likely higher because the 21.6 m value equaled the maximum recording range of the wave staff. Also, significant wave period was much lower than that seen in other severe storms (12 sec; wave periods from Hurricane Ivan were timed at 17 sec). Observed maximum wave heights of 12.2 m and an associated average period of 14 sec were reported at the West Delta 133 location prior to failure. These lower values were likely because West Delta Block 133 was farther away from the eye path than South Pass Block 62 (Figure 12; Patterson, 1974). The discontinuous nature of reported data while Camille traversed the GOM leads to an incomplete record of  $H_{s_{max}}$  wave height. However, given the few central pressures recorded prior to landfall and the formula derived by Hsu (2006), it can be estimated that  $H_{s_{max}}$  ranged from 20.8-21.6 m in the 24 hours preceding landfall.

Wave spectra data from the Baylor data gathering system revealed that the frequency spectrum contained more than one peak of energy density (Shelton, 1977). One day prior to peak hurricane conditions, wave spectra contained an energy peak at about 0.2 Hz, which is associated with the dominant frequency in the GOM during normal conditions. However, peaks at frequencies of about 0.075 Hz and 0.125 to 0.15 Hz were also encountered. These lower frequency waves were produced by Camille and were among the first waves to be recorded by the Baylor system. As the hurricane approached the recording system, the peak in the spectra at about 0.075 Hz became more pronounced as peaks at higher frequencies apparently transferred their energy to lower frequency waves (Appendix G, Figure G-1). Once Camille passed the recording system, an abrupt change in the frequency spectrum was noted, as wave-generating winds suddenly reversed and generated waves in the opposite direction. Spectral energy developed at 0.125 Hz developed in addition to that at 0.075 Hz. As sea-state conditions returned to normal, a shift to higher frequencies (i.e., shorter periods) became evident as the peak at 0.075 Hz shifted to near 0.20 Hz (Shelton, 1977).

In addition, bottom current speeds were measured by a ducted current meter mounted on the seafloor in 6.3 m (20 feet) of water off the coast of the Florida panhandle 90 m (300 feet) seaward of the local outer bar (Murray, 1970; Earle, 1975). Three distinct temporal phases were detected during Hurricane Camille based on relationships between wind and current speed; the maximum bottom current speed was nearly  $160 \text{ cm sec}^{-1}$  (Appendix G, Figure G-1). Although this meter was located in the typically more intense upper right quadrant of the storm, it was still located over 100 km east of the hurricane's path and away from the most intense activity, therefore implying that maximum winds and currents were even more extreme closer to the hurricane's center.

As an example of the seafloor impact caused by Hurricane Camille, wave action was attributed as the cause of failure for Shell's South Pass Block 70 "B" production platform (Bea, 1971; Sterling and Strohbeck, 1973; Wright, 1976). This platform, in addition to a Gulf Oil platform in South Pass Block 61, was subjected to severe wave action and drastic changes in pre- and post-storm seafloor topography (Figure 15). The cross-sectional profile over South Pass Block 70 shows a clear change in slope, as the lowermost part of the profile thickened after the storm at the expense of sediments located farther upslope (Figure 16).

Soil borings were taken after the storm and compared to pre-storm borings used to site the platform. A definite reduction in shear strength appears at about 24 m (80 feet); pre- and post-storm shear strengths below that depth compare very closely and thus infer no storm-related soil movement (Sterling and Strohbeck, 1973; Figure 17). However, other nearby, similarly designed platforms withstood the storm and were presumably subjected to similar waves as those at SP 70, further reinforcing that pure wave-force overload unlikely caused the SP 70 platform failure and that massive sediment flow was responsible (Sterling and Strohbeck, 1973).

### **3.3.3 Hurricane Andrew (1992)**

Hurricane Andrew developed from a tropical wave that formed near the west coast of Africa in August 1992 (Mayfield et al., 1994, Grymes and Stone, 1995). Andrew moved

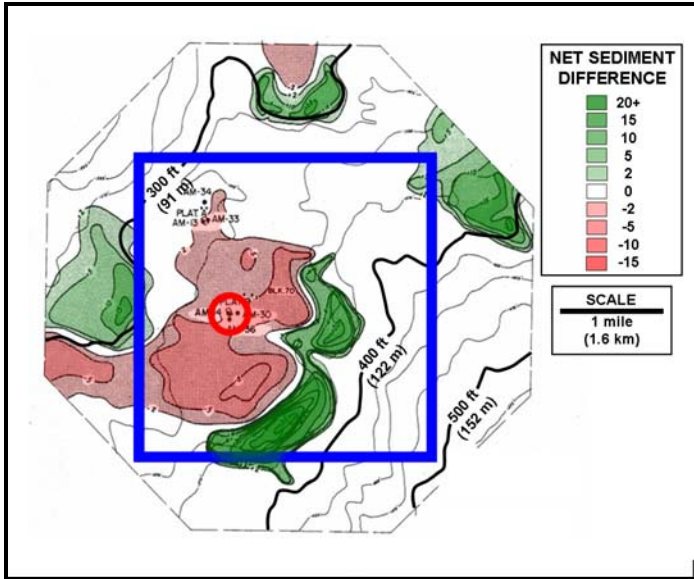


Figure 15: Changes in bottom topography at SP 70 after Hurricane Camille (block outline in blue; location of SP 70 "B" platform highlighted with red circle (modified from Sterling and Strohbeck, 1973)

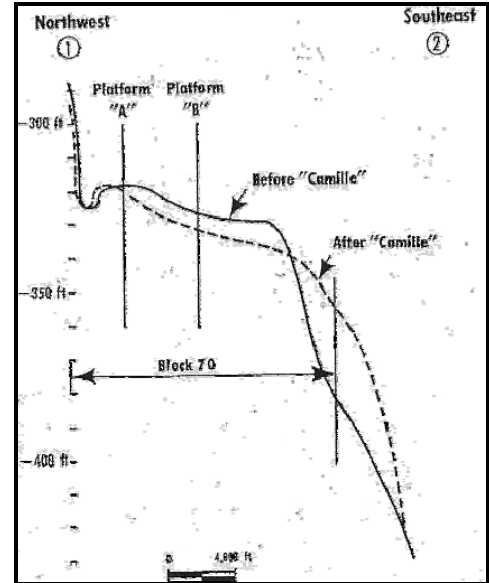


Figure 16: Pre- and post-Hurricane Camille cross-sectional profile, South Pass 70 (from Bea, 1971)

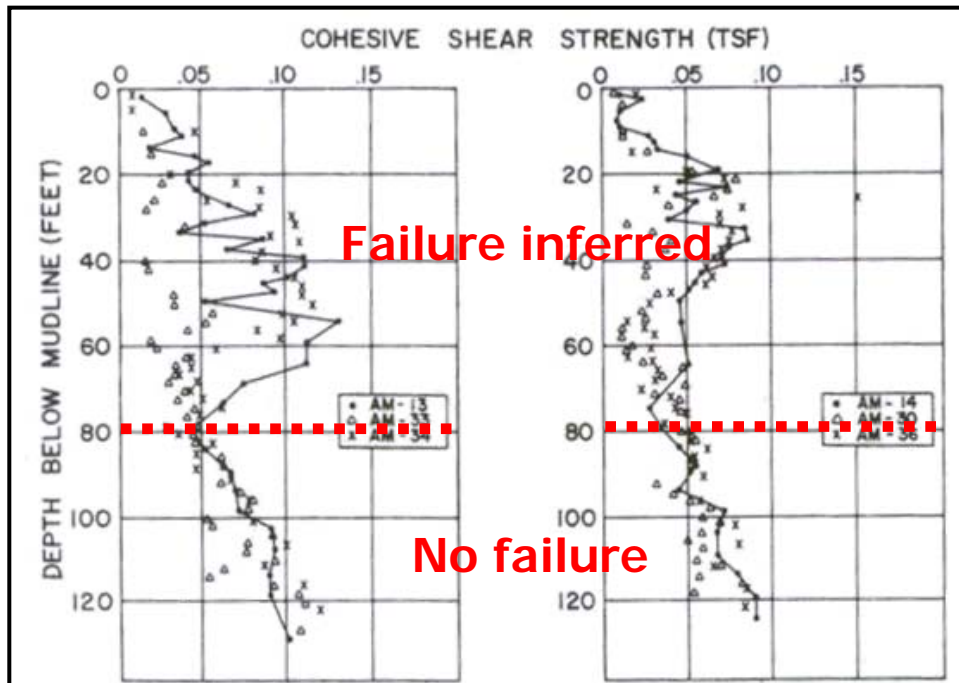


Figure 17: Comparison of pre- and post-Camille soil borings, South Pass Block 70 (from Sterling and Strohbeck, 1973)

westward, reaching the Bahamas as a Category 4 hurricane and weakening slightly after moving over the Great Bahama Bank. However, the hurricane intensified and made its first U.S. landfall in Dade County, Florida as a Category 5 hurricane (Mayfield et al., 1994; NHC, 2009). Andrew then crossed into the GOM and assumed a northwesterly course, eventually making its second U.S. landfall several days later as a Category 4 hurricane on the central Louisiana coast in St. Mary Parish (Figure 1; also Appendix B, Figure B-3). Prior to landfall, Andrew traversed the far western portion of the study area, with the eye passing about 150 km west of the MRDF (Figure 1).

Extreme meteorologic and metocean conditions were experienced during Hurricane Andrew even though the brunt of the storm passed far west of the MRDF. By 1992 an array of real-time meteorological, oceanographic and hydrological data gathering sites had been established offshore (Stone et al., 1995; NDBC, 2009; Appendix I). As a result, the reporting of these data is vastly improved relative to data from Hurricanes Betsy and Camille. The effects in the GOM from Andrew were first detected by NDBC buoys 42001 and 42003 on August 24, 1992 via long-period swells as the storm moved over Florida into the GOM (Figures 18 and 19).

These long-period swells, combined with overall decreasing wave frequencies, are often characteristic of storm-driven conditions (Grymes and Stone, 1995). The response from Buoy 42001 is significantly less pronounced than the response from Buoy 42003 because of the increased distance from Andrew's closest approach (240 km vs. 50 km). Peak conditions at Buoy 42003 included wind speeds of  $12 \text{ m sec}^{-1}$  and wave heights of 6.4 m on August 25 (Figure 19). Sea-state conditions remained at elevated levels for nearly 72 hours before returning to normal, implying wave-energy transfer across the GOM in response to the storm (Grymes and Stone, 1995). Despite the availability of these real-time data, true wave conditions were likely much higher as these two buoys were located away from the path of the eye and therefore did not capture the peak storm intensity.

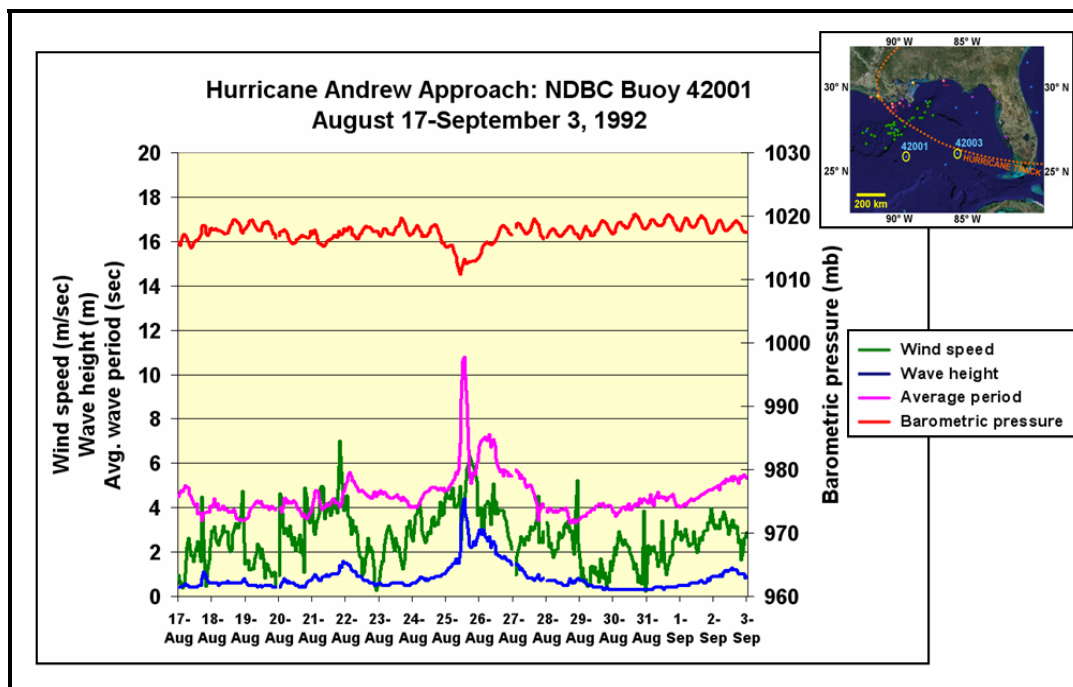


Figure 18: Key metocean parameters from Hurricane Andrew, 1992 based on readings from NDBC Buoy 42001 (data retrieved from archives available at NDBC, 2004)

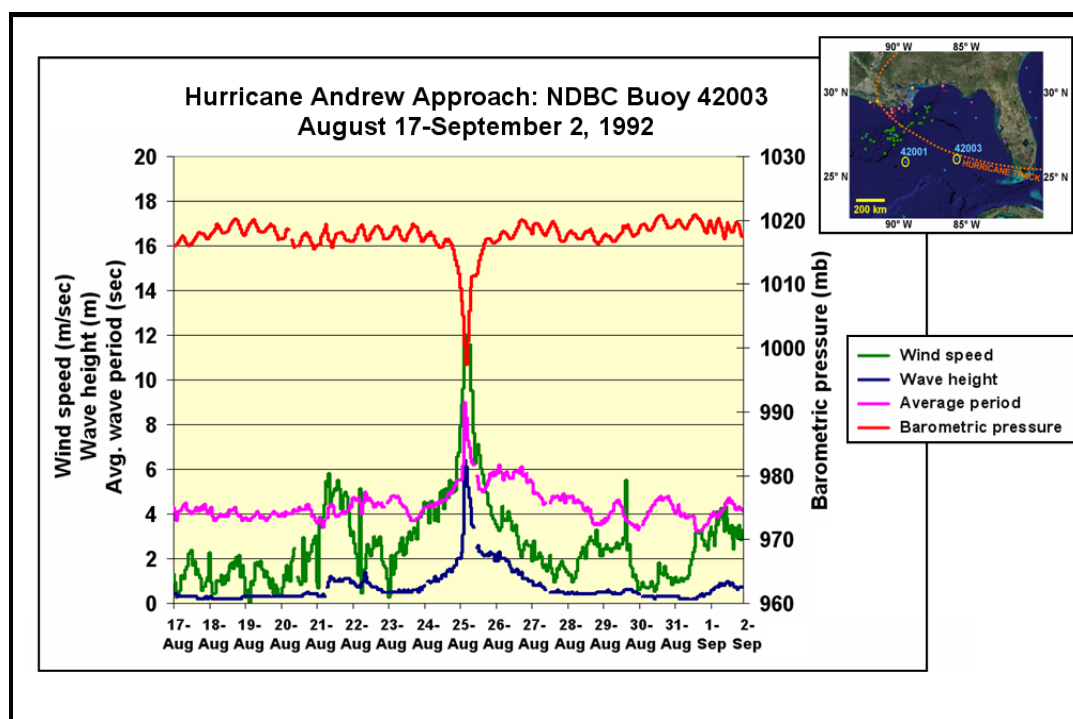


Figure 19: Key metocean parameters from Hurricane Andrew, 1992 based on readings from NDBC Buoy 42003 (data retrieved from archives available at NDBC, 2004)



Maximum wave height at the center can be estimated by applying the method advocated by Hsu (2006) based on minimum sea-level barometric pressure. This method yields an  $H_{s_{max}}$  of 15.2 m given an equivalent pressure of 937 mb as measured by hurricane reconnaissance aircraft at 0000Z on August 26, 1992. Values of  $H_{s_{max}}$  in the 24 hours preceding the Louisiana landfall ranged from 11.6-15.2 m, also using this method. In addition, post-storm hindcast work indicates  $H_{s_{max}}$  values of 13 m just off the Mississippi River Delta coincident with peak storm intensity (Oceanweather Inc., 1992). As a quality-control measure these results were compared to measurements from three sites in the GOM (NDBC Buoys 42001 and 42003, and Shell's Bullwinkle Platform in Green Canyon Block 155). The mean absolute difference between the two datasets was 0.38 m, thus providing additional assurance on wave height controls.

Gridded wind field data from Hurricane Andrew were also obtained from Oceanweather, Inc. These data were used to construct depictions of storm intensity as Andrew approached the Louisiana coast (Oceanweather, 2007b). Offshore damage reports for Hurricane Andrew are discussed further in Section 8.3.3 and in Appendix I, Tables I-1 and I-2.

#### **3.3.4 Hurricane Ivan (2004)**

Hurricane Ivan began as a tropical system in the middle Atlantic Ocean in mid-September 2004 and quickly gained Category Five status on the Saffir-Simpson scale while still in the Caribbean Sea. Ivan was unique in that it attained Category Five status three separate times while traversing the Caribbean Sea and GOM, mainly because of a series of eyewall replacement cycles (Stewart, 2005). As Ivan entered the GOM, storm intensity fluctuated and prior to landfall Ivan had weakened to a Category 3 hurricane with wind speeds of  $54 \text{ m sec}^{-1}$  (120 miles  $\text{hour}^{-1}$ ). However, while in the GOM Ivan spawned winds as strong as  $70 \text{ m sec}^{-1}$  (160 miles  $\text{hour}^{-1}$ ; NOAA, 2007). The eye made landfall on the north-central Gulf coast near Gulf Shores, Alabama on September 16, 2004 as a Category 3 hurricane (Stewart, 2005; Figure 1; also Appendix B, Figure B-4). Ivan weakened to a tropical disturbance before it re-emerged into the Atlantic Ocean, moved southward and looped across the southern tip of Florida back into the

GOM, and then struck the southwestern Louisiana coast as a tropical storm on September 23, 2004 (Stewart, 2005; NHC, 2009).

Compared to earlier GOM hurricanes, numerous oceanographic observation stations had been deployed and were operational by the time Ivan traversed through the study area. Combined with the extreme metocean conditions observed during Hurricane Ivan and the damage these conditions caused, this storm served as the catalyst for renewed study of offshore wave heights and extreme metocean conditions during GOM hurricanes. Significant wave heights during Ivan were the largest ever observed in the deployment history of the offshore GOM observing stations, with a maximum of 15.96 m at NDBC Buoy 42040 that translates to a maximum individual wave height in that sea state of about 29 m via statistical distribution methods described by Panchang and Gupta (1989). Significant wave heights measured by the USNRL program were even higher, with  $H_{s_{max}}$  of 17.9 m and maximum individual wave heights of 27.7 m (Appendix J). The highest  $H_{s_{max}}$  measurement in the GOM prior to Ivan was 10.88 m in 1988 (Panchang and Li, 2006). In a longer-term context these wave heights were exceeded only by  $H_{s_{max}}$  measurements of 16.32 m (NDBC Buoy 46006 in the Pacific Ocean offshore California/Oregon in 1999) and 16.9 m (NDBC Buoy 46003 in the Gulf of Alaska in 1991).

### **3.3.5 Hurricane Katrina (2005)**

Hurricane Katrina formed from the remnants of a dissipating tropical depression in the central Bahamas and, with an initial westward movement, struck the lower Florida peninsula as a Category One hurricane (NHC, 2009). After crossing into the GOM, Katrina turned to the northwest and underwent several phases of rapid intensification, attaining peak intensity and Category 5 status 275 km southeast of the mouth of the Mississippi River. The storm then turned northward but weakened as it made landfall first in Plaquemines Parish, Louisiana and later near the mouth of the Pearl River (the Louisiana/Mississippi boundary) as a Category 3 hurricane (Figure 1; also Appendix B, Figure B-5).

This rapid weakening prior to landfall appears to have been due to a combination of factors including internal structural changes (deterioration of the inner eyewall without the complete formation of a new outer eyewall), the entrainment of dry air, gradually increasing wind shear, slightly lower ocean temperatures, and land interaction (Knabb et al., 2005). In fact, during the past 20 years all 11 hurricanes in the northern Gulf of Mexico with a barometric pressure of less than 973 mb at least 12 hours before landfall weakened during those last 12 hours (NHC, 2009). However, Katrina remained very large as it weakened, and the extent of tropical storm-force and hurricane-force winds was nearly the same at final landfall as it had been while the storm was still 200 km offshore.

Hurricane Katrina was a highly asymmetrical storm as the most intense wind field was located in the eastern half of the storm and particularly in the northeastern quadrant (Cardone et al., 2007). This asymmetry places the maximum wind field (and likely the associated maximum significant wave height) within the center of the study area adjacent the MRDF. Details on metocean characteristics have been previously described in Section 2.2. These data are enhanced by the proximity of several NDBC buoys to the track of Hurricane Katrina as it moved through the study area, which is also discussed in Section 2.2 (also see Appendix J).

Several cases of sediment movement during Hurricane Katrina were detected through the use of data provided by several companies for this research. These areas included Main Pass Blocks 71 and 72 along the MPOG pipeline system in Validation Test Area (VTA) Number 1 (as was the case during Hurricane Ivan) and South Pass Block 19 just offshore from the Mississippi River Delta in VTA 3. VTA locations are contained in Section 4.1; additional detail on morphological changes in these areas is provided in Chapter 7.

### **3.3.6 Additional GOM Hurricanes**

In addition to the five hurricanes detailed in this chapter, nine other hurricanes traversed the study area between 1947 and 2007 (NHC, 2009; Table 1; also Appendix D, Figure D-1). These storms vary considerably in areal size, forward speed and intensity levels. Although they

impacted the study area they were not selected as a key hurricane for this research because they either (1) tracked along the periphery of the study area, (2) were relatively weaker storms, or (3) did not cause significant offshore infrastructure damage as they passed through the study area. Despite these criteria, evidence suggests that storms traveling through the GOM as far away as 400 km from the MRDF (e.g., Hurricane Carla in 1961) can still impact the seafloor (Bea and Audibert, 1980).

Among the more significant of the nearer storms was Hurricane Hilda, which struck the Louisiana coast in St. Mary Parish as a Category 3 storm in October 1964 (Dunn et al., 1965; NHC, 2009; Table 1; Appendix D, Figure D-1). Despite attaining strong Category 4 intensity while in the GOM, Hilda weakened as it moved over the south-central Louisiana offshore shelf. Hilda also passed well to the west of the primary MRDF focus within the study area.

Most platforms installed prior to Hilda were designed to accommodate wave heights of only 6-12 m (the air gap distance from the mean lower low water level to the base of the platform deck); wave heights during Hilda were estimated at the time as greater than 13 m (Lambert, 1964). The wave height method estimation method of Hsu (2006) yields a maximum wave height of 14.4 m while at sea in the central GOM. Despite Hilda's intensity, its westward track along the periphery of the study area likely contributed to a lack of major, reported platform failures. However, a large number of pipeline breaks were reported during the storm (Arnold, 1967).

Hurricane Carmen struck the Louisiana coast in Vermilion and Iberia Parishes as a Category 3 storm in September 1974 (NHC, 2009; Table 1; also Appendix D, Figure D-1). Like Hilda, Carmen attained strong Category 4 intensity while in the GOM but weakened as it moved over the south-central Louisiana offshore shelf and also passed well to the west of the primary MRDF focus within the study area. Offshore losses were minimal during this storm (The Oil and Gas Journal, 1974), likely because it passed even farther to the west than Hilda but also because it maintained Category 4 status only six hours compared to Hilda's 30 hours (NHC, 2009). The wave height method estimation method advocated by Hsu (2006) yields a maximum wave height

of 15.2 m while Carmen was at sea in the central GOM. However, this occurrence was a one-time peak; most estimated wave heights fall into a range of 9-12 m.

Hurricane Frederic moved through the eastern part of the study area, striking the Alabama coast in Mobile County as a Category 3 storm in September 1979 (NHC, 2009; Table 1; Appendix D, Figure D-1). Frederic also attained Category 4 intensity for about 12 hours while in the GOM but weakened as it moved over the shelf. The wave height method estimation method advocated by Hsu (2006) yields a maximum wave height of 14.0 m while at sea. Frederic made landfall at a point along the coastline similar to Hurricane Ivan but approached the coast from the southeast rather than from the south-southwest. As a result, offshore losses were minimal.

Additional significant hurricanes moved through the MRDF prior to 1947; these are discussed in more detail in Chapter 5. The absence of offshore infrastructure prior to 1947 precludes the use of offshore damage reports to provide insight to storm severity. These hurricanes, especially those further back in the historical record, contain meteorological data that are also less reliable. While they provide indications of historical storm cycles and anecdotal evidence of damage, they were therefore not used as key hurricanes in this dissertation.

However, as noted earlier, storms relatively far from the MRDF can impact the seafloor and cause potential changes in seafloor morphology. Hurricane Carla struck the Texas coast in Matagorda County in September 1961 as a Category 4 hurricane (NHC, 2009). Although Carla passed 400 km southwest of the MRDF at its closest approach, it did so as an intense Category 5 hurricane. The wave estimation method of Hsu (2006) yields significant wave heights of 15-16 m at the center of the storm when at maximum strength. Wave heights nearer the MRDF were reported as much lower, at 4-5 m, yet numerous “unexplained” pipeline failures occurred, particularly in water depths of 12 to 21 m, including over 30 failures in one producing field alone (Blumberg, 1974).

A hypothesis to explain the difference in wave heights is that the soft, muddy bottom nearer the coast acts like a high-frequency filter and essentially dampens shorter-period high

waves more quickly than longer-period low waves (Figure 20; Bea and Arnold, 1973; Bea and Audibert, 1980). This work has also been corroborated by additional studies across the relatively muddy, finer-grained Louisiana shelf (Kraft et al., 1990; Sheremet and Stone, 2003; Sheremet et al., 2005) and will be discussed in more detail in Chapter 6.

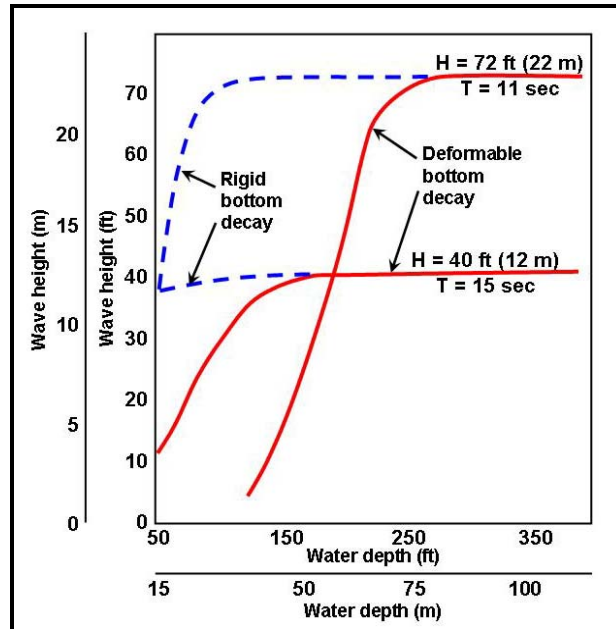


Figure 20: Theoretical wave height decay model (modified from Bea and Audibert, 1980)

### 3.4 Non-Hurricane GOM Events

In addition to hurricanes, other weather events may also impact the MRDF seafloor (Coleman and Prior, 1980a). Strong winter cold fronts, with strong northerly winds, can cause set-down conditions in shallow-water bays and inlets where heavier bar sands and silts have sunk into and displaced underlying plastic clays. When set-down conditions occur, these sediments become exposed and effectively become heavier (Bea and Audibert, 1980). A failure event in East Bay in December 1976 was likely caused by this phenomenon whereby water had been forced from the area by a strong cold front and new forces activated existing growth faults. Support piles on one side of a platform that straddled one of the faults were sheared off and subsequent investigation revealed vertical soil movement of up to 1 m (Bea and Audibert, 1980).

## **CHAPTER 4. RESEARCH STRATEGY AND METHODOLOGY**

### **4.1 Study Area**

The study area of this dissertation is located along the Mississippi River Delta Front (MRDF) offshore the southeastern Louisiana coast of the north-central Gulf of Mexico. The study area outline (Figures 1 and 2) was generated based on several key criteria that include:

- A natural environment conducive to submarine shelf sediment failure through both normal processes as well as extreme storm activity;
- A benchmark of early pioneering work on submarine shelf and slope failure within and adjacent to the MRDF (Figure 21);
- Recent hurricane history (1965-present) that includes five major hurricanes (i.e., Category 3+) and a number of less intense hurricanes, resulting in a wealth of observed and hindcast metocean storm data;
- Extensive infrastructure damage caused by these hurricanes (i.e., takes place within a dense infrastructure grid that supports a mature oil and gas producing area);
- Publicly available time-series bathymetric and oceanographic data;
- The existence of proprietary geohazard data along and adjacent to the MRDF acquired by BP and its heritage companies (Amoco, Arco, Sohio and Vastar), Plains Resources, and Enterprise Products LLC (survey details included in Appendix K).

In addition, four smaller-scale areas were outlined within the study area in which hypotheses and conclusions from this dissertation could be locally validated. These areas, referred to as Validation Test Areas (VTAs) 1-4, were chosen based on (1) the types and abundance of bathymetry and geohazard data available, especially if recorded repeatedly through time, (2) the proximity to hurricane-force wind fields and metocean conditions associated with recent storms, and (3) a documented history of hurricane-generated infrastructure damage (Table 2; Figure 22). Details on local bathymetric data are contained in the following section.

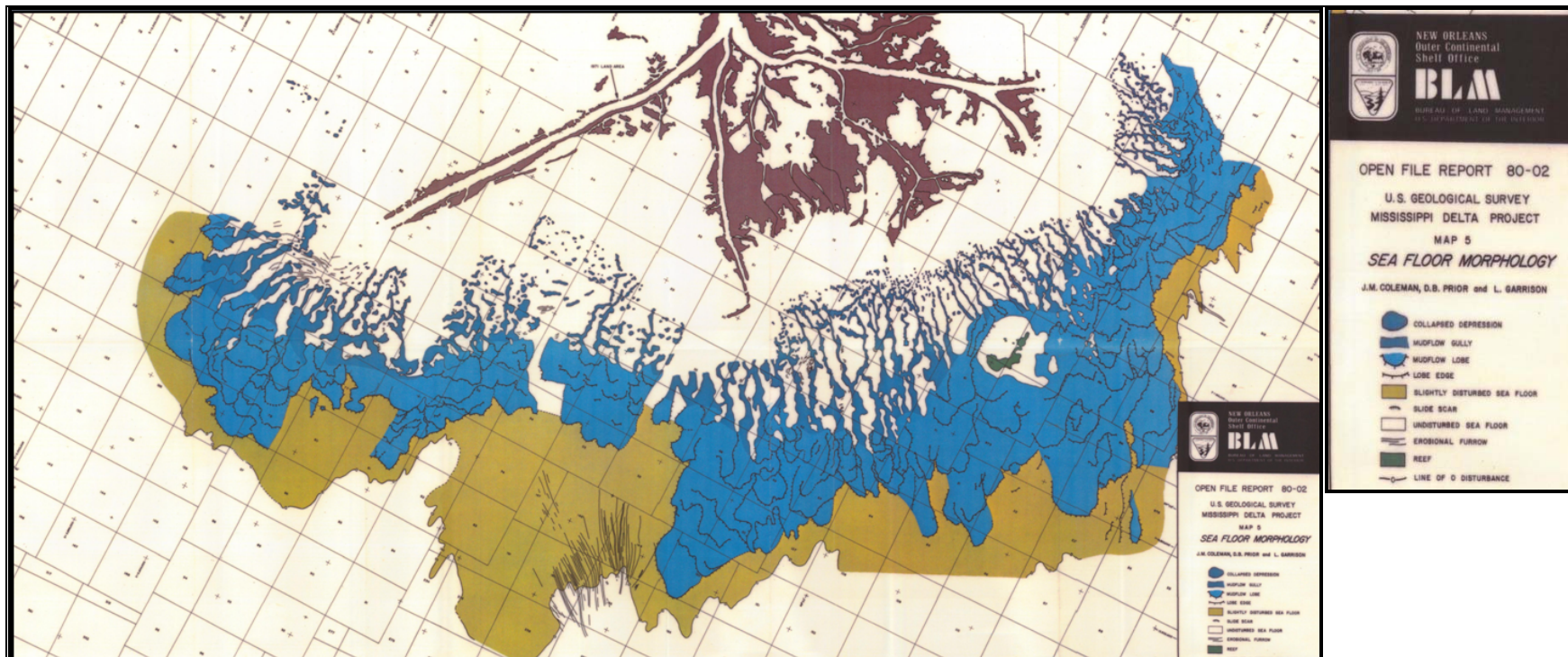


Figure 21: Extent of MRDF mudslides, circa 1980 (from Coleman and Prior, 1980b)

Table 2: Validation Test Area boundaries, north-central Gulf of Mexico

	<u>Northern boundary</u>	<u>Eastern boundary</u>	<u>Southern boundary</u>	<u>Western boundary</u>
Test Area 1	29.45° N	88.75° W	29.20° N	89.15° W
Test Area 2	29.35° N	88.50° W	29.15° N	88.70° W
Test Area 3	29.10° N	88.75° W	28.95° N	89.20° W
Test Area 4	28.90° N	89.10° W	28.75° N	89.45° W



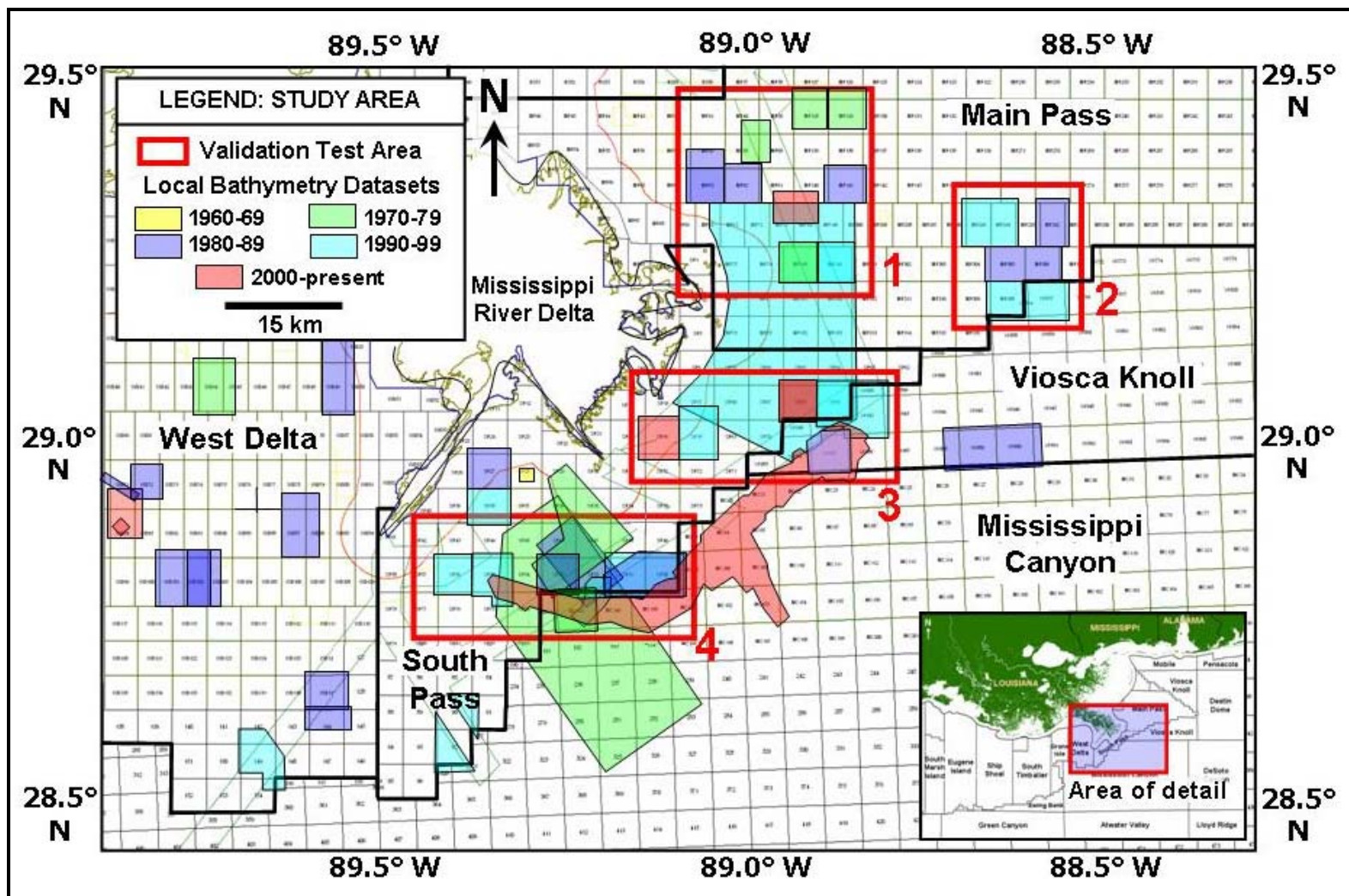


Figure 22: Location of localized geohazard surveys and validation test areas relative to general MRDF study area (see Appendix K for detailed descriptions of each survey)

#### **4.1.1 MRDF Bathymetric Data**

The first regional bathymetry surveys within the MRDF were conducted from 1872-1874 by the U.S. Coast and Geodetic Survey (Figure 23; also Appendix F; Coleman et al., 1980). The coverage and density of these early surveys vary greatly but overall they are considered of sufficient quality. These bathymetric data were used as an early benchmark for seafloor stability and relative rates of change.

Beginning in 1934 a series of bathymetry data was collected that is publicly available through the National Oceanic and Atmospheric Administration (NOAA; 2009). The coverage and density of these surveys, collected from 1934 through 1992, varies considerably (Appendix F). In addition, regional bathymetric datasets were acquired in 1940 and 1977 (Figures 24-25; Coleman et al., 1980b). For this dissertation, these data were digitized by RMSI, Inc. of Hyderabad, India and then imported into Fledermaus imaging software and an ArcGIS database to facilitate temporal comparisons of seafloor change. A regional grid available through NOAA, assumed to be mostly late 1980s vintage, is also available (Figure 26).

In addition to regional bathymetry data, a set of 46 locally acquired geohazard surveys were used to help validate local changes in seafloor topography and morphologic features (Figure 22; Appendix K). These surveys were collected by BP or its heritage companies (Amoco, Arco, Vastar or Sohio) from 1973 through 2006 (post-Katrina) and document seafloor investigation studies to support the emplacement of drilling rigs, production platforms, and/or pipeline routes. Although the coverage area of most of these surveys is relatively small (one or two offshore blocks, or approximately 25-45 km<sup>2</sup>) they provide locally higher seafloor resolution that can be used to help validate change resulting from physical process conditions. These studies typically contain the following types of survey data:

- Bathymetry surveys – either single-beam or multi-beam echo-sounder, which is used to record ocean depths;
- Side-scan sonar – an acoustically derived image of the seafloor;

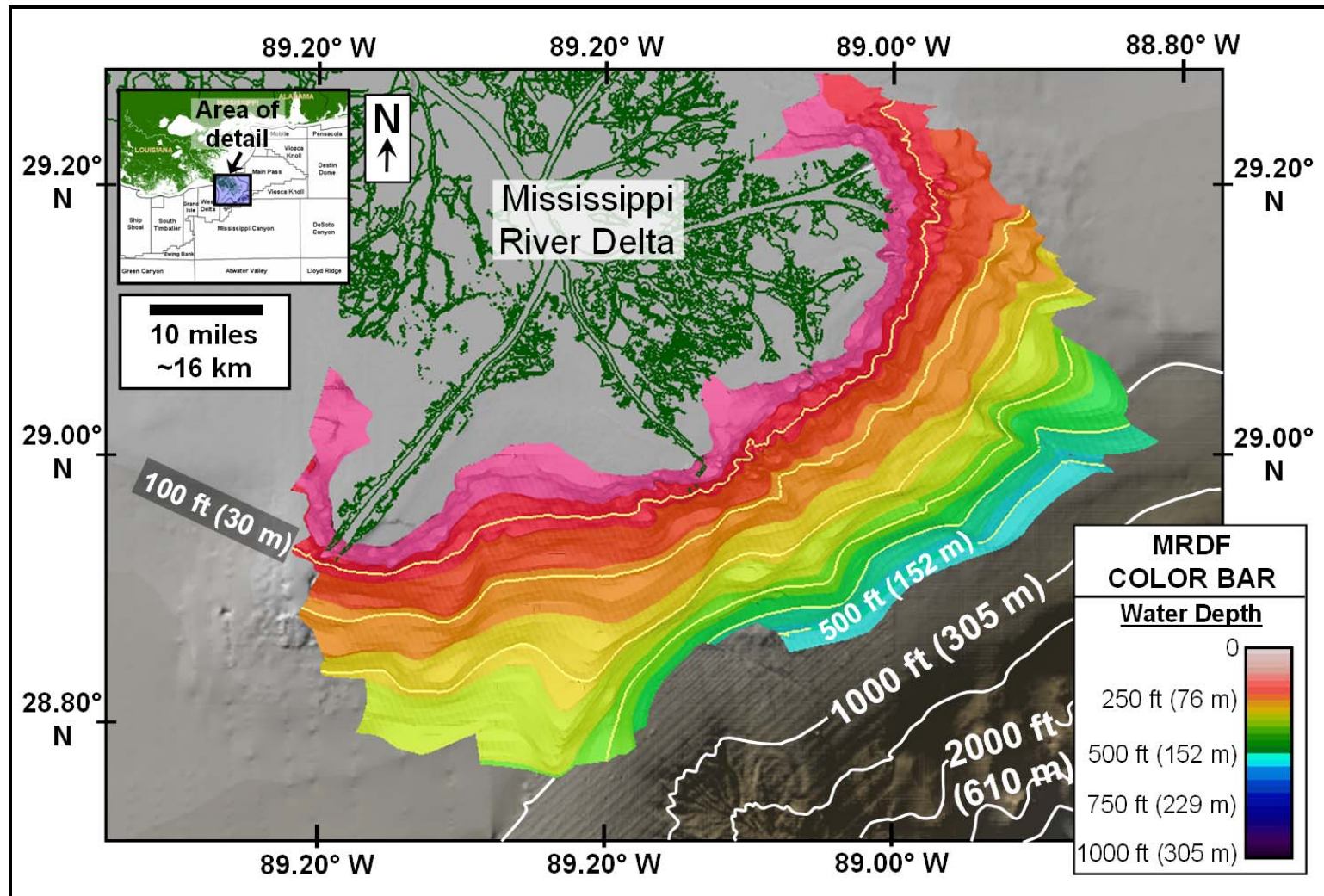


Figure 23: 1874 MRDF bathymetry, U.S. Coast and Geodetic Survey (raw data digitized from Coleman et al., 1980b and illustrated in spectrum color bar; underlying NOAA bathymetry displayed on brown-to-blue color bar; artificial shading applied from 330°)



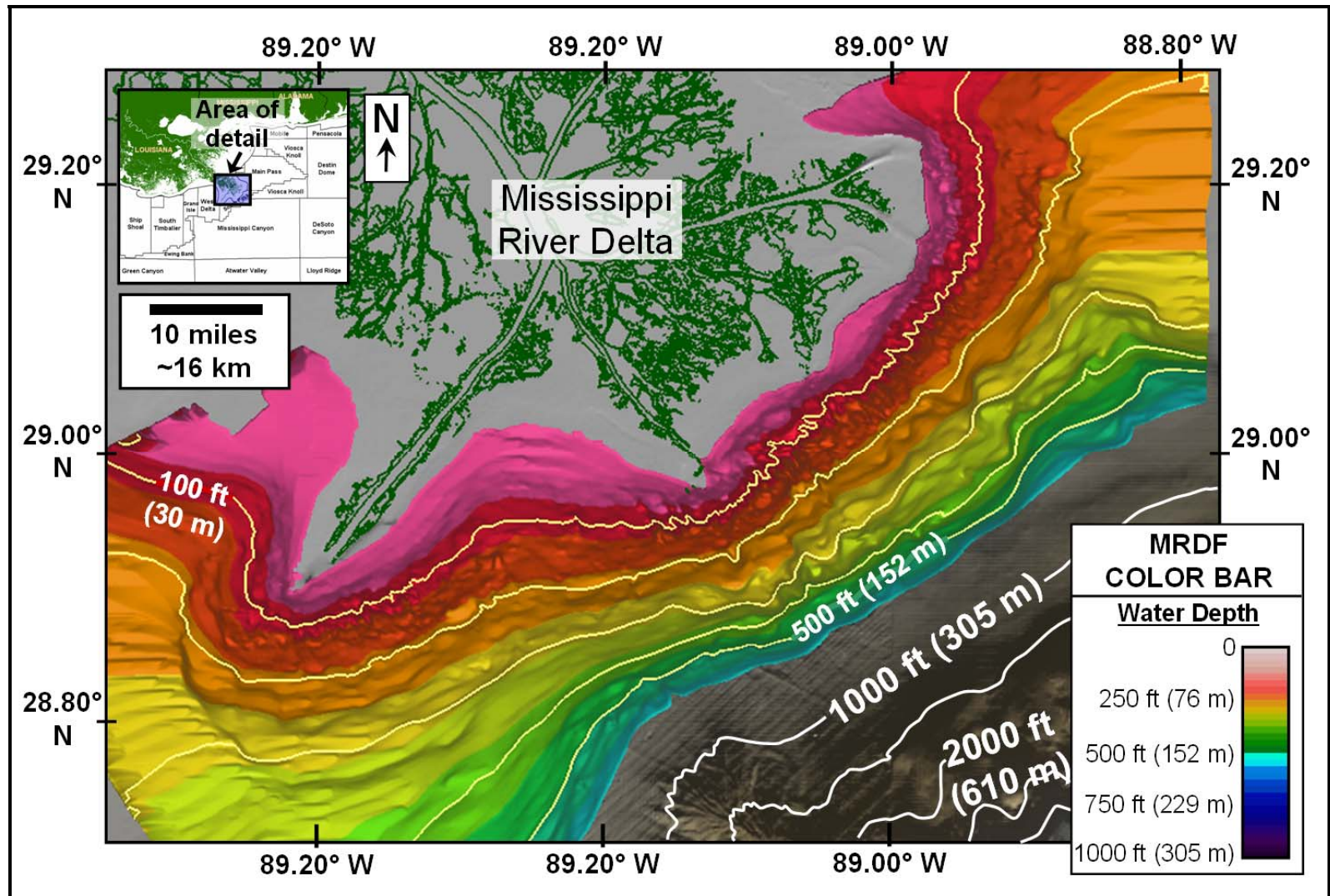


Figure 24: 1940 MRDF bathymetry, U.S. Coast and Geodetic Survey (raw data digitized from Coleman et al., 1980b and illustrated in spectrum color bar; underlying NOAA bathymetry displayed on brown-to-blue color bar; artificial shading applied from 330°)

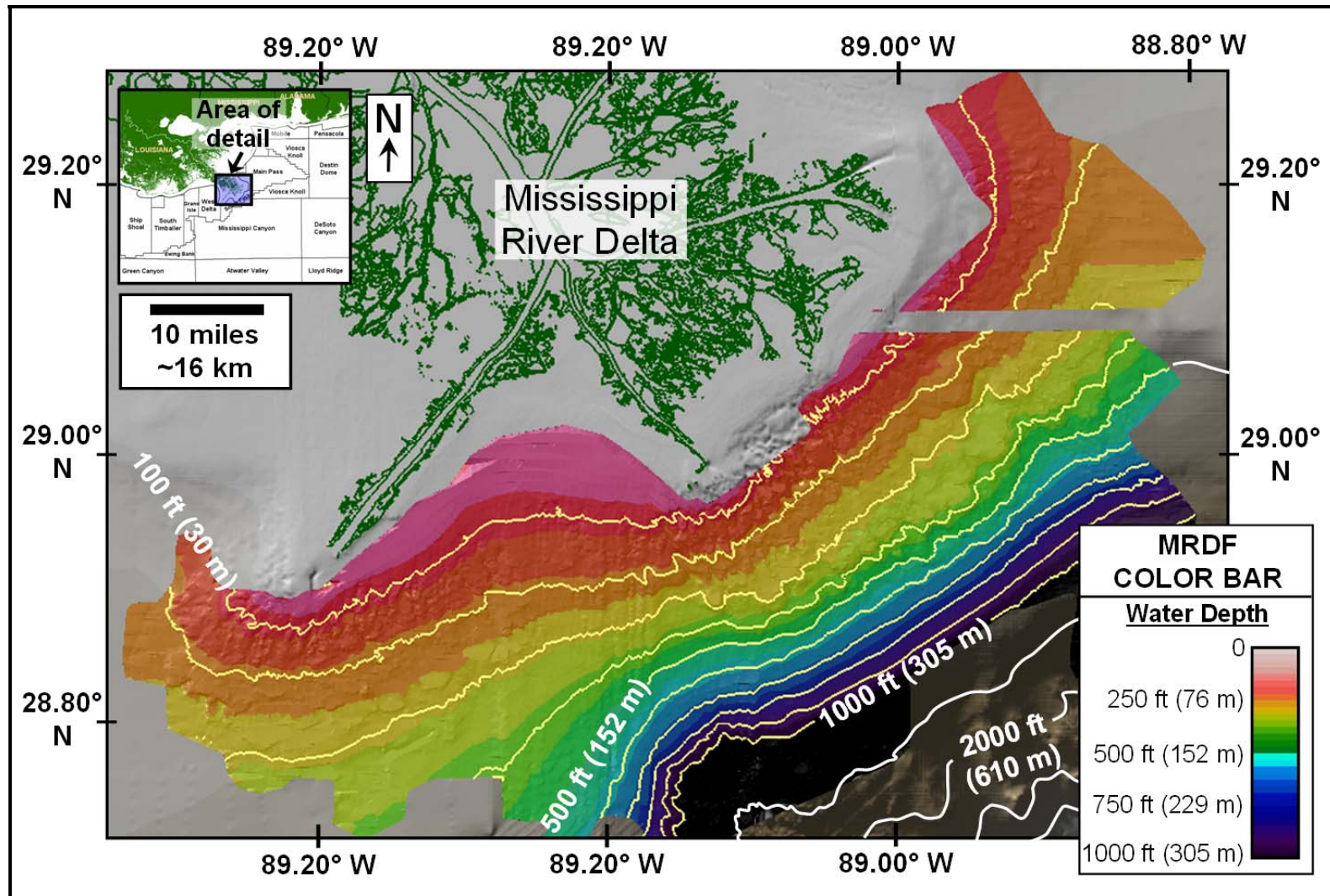


Figure 25: 1977 MRDF bathymetry, U.S. Coast and Geodetic Survey (raw data digitized from Coleman et al., 1980b and illustrated in spectrum color bar; underlying NOAA bathymetry displayed on brown-to-blue color bar; artificial shading applied from 330°)



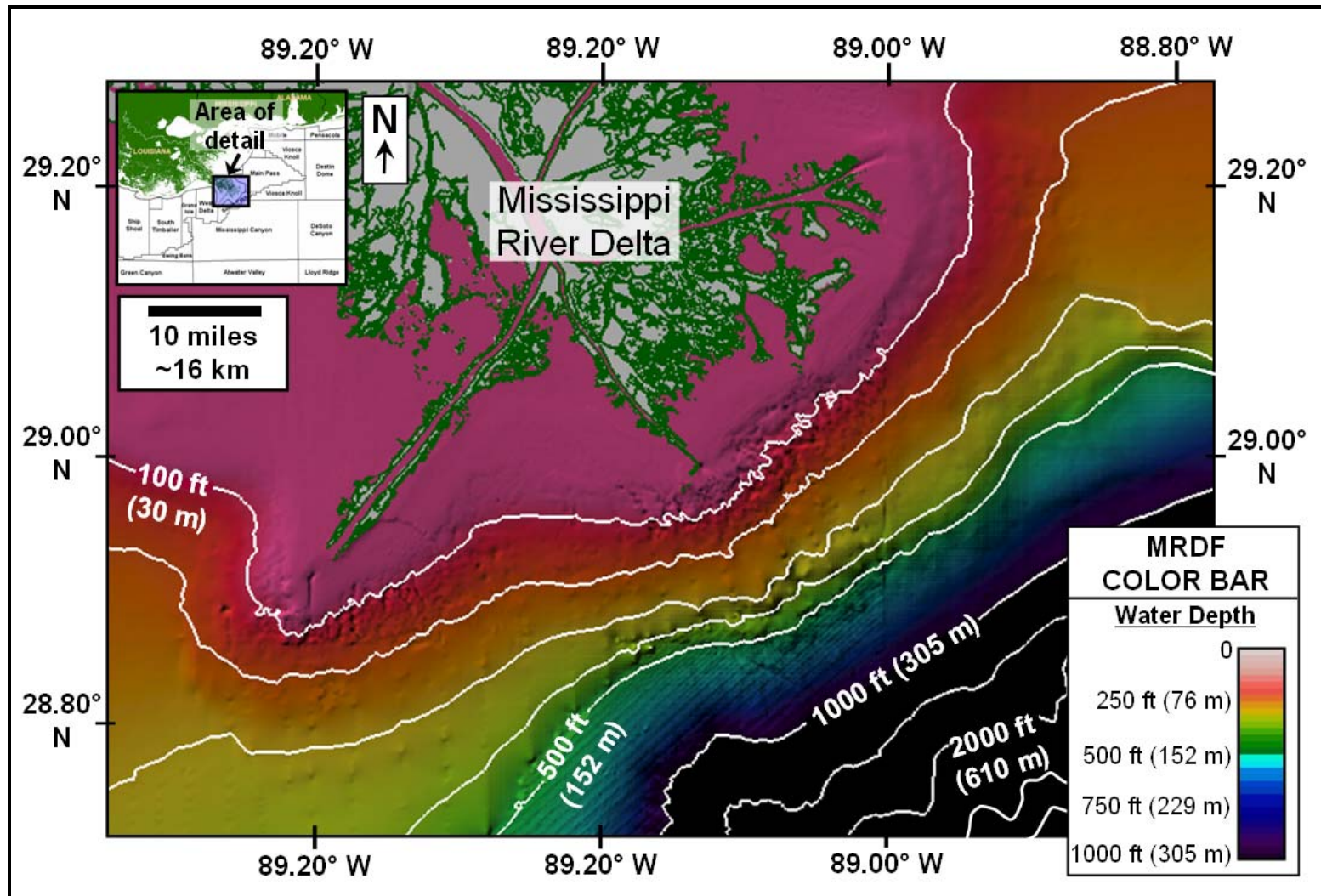


Figure 26: Coarse-resolution MRDF bathymetry, National Oceanographic and Atmospheric Administration (raw data from NOAA, 2009); illustrated in spectrum color bar; vintage assumed to be late 1980s; artificial shading applied from 330°)

- Shallow seismic data – sub-bottom profiler (pinger) occasionally with high-resolution 2D/3D seismic data that help delineate shallow horizons and stratigraphic relationships; and
- Geotechnical boreholes – taken at various depths depending on need to help delineate and quantify shallow stratigraphy and soil composition.

Acquisition details for each survey are contained in Appendix M.

In addition, several non-BP reports and data were also used to help validate models of seafloor bathymetry change before and after Hurricanes Ivan and Katrina. A shallow hazard dataset acquired over South Pass Block 19 in 2005 was provided by Plains Resources, LLP (Figure 22; also Appendix K). An additional bathymetry dataset acquired over a regional, southwest-northeast-trending pipeline route from South Pass Block 55 to Viosca Knoll Block 955 was provided by Enterprise Products Partners, LP (Figure 22; also Appendix K).

#### **4.1.2 Recent, Hurricane-Induced Seafloor Failures, MRDF Vicinity**

Reports by oil and gas operators to the MMS indicate multiple cases of seafloor failure during Hurricanes Ivan and Katrina (MMS, 2009; Nodine et al., 2006; 2007). These reports are based on the results of post-hurricane surveys in areas where platform and/or pipeline failure occurred (Table 3; Figure 27). While additional occurrences of seafloor failure may have taken place, the data are limited only to that reported to the MMS (MMS, 2009).

#### **4.1.3 Regional Lithologic and Geotechnical Data**

Geotechnical boreholes acquired during the planning stages of platform or drilling installation were used to help quantify lithologic controls on seafloor and near-surface sediments. An extensive grid of these boreholes now exists in the GOM and is catalogued via several databases below:

- Texas A&M University: This database was created under contract to MMS (Dunlap et al., 2004). A total of 748 boreholes were catalogued, of which 176 occur in the

Table 3: Operator-reported, hurricane-induced seafloor failure, Hurricanes Ivan and Katrina (MMS, 2009)

Protraction Area	Block	Hurricane Ivan	Hurricane Katrina
Mississippi Canyon	20	X	
South Pass	38		X
	49	X	
	55	X	
	60	X	X
	77	X	
Main Pass	70	X	X
	73	X	
	148	X	X
	151	X	
West Delta	108		X
	109	X	
	110		X

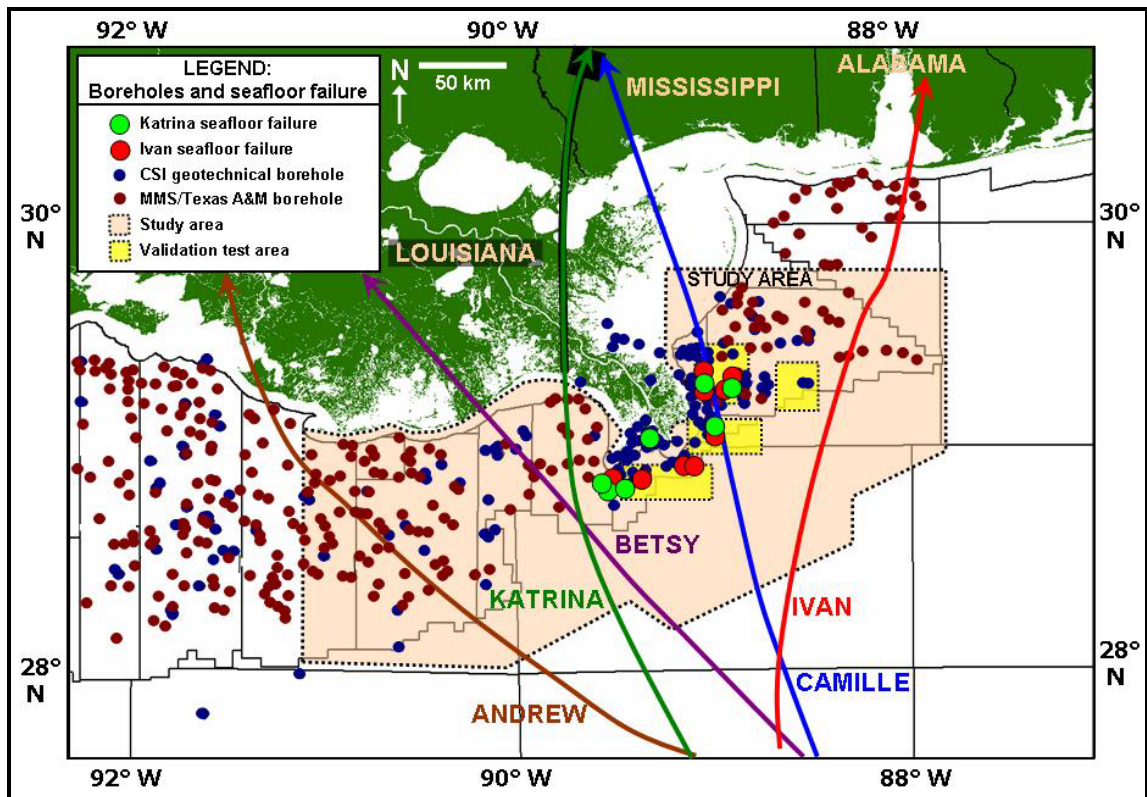


Figure 27: Geotechnical borehole distribution and operator-reported seafloor failure during Hurricanes Ivan and Katrina (Dunlap et al., 2004; MMS, 2009; Nodine et al., 2006; 2007)



study area and eight of which occur in one of the four VTAs described in Section 4.1 (Figure 27). Borehole details are contained in Appendix L, Table L-1.

- Coastal Studies Institute, Louisiana State University: This database, catalogued over time since 1956, contains 178 boreholes in the study area and 74 in one of the four VTAs (Figure 27; also Appendix L, Table L-2). These data provide critical coverage in the South Pass Area where the Texas A&M / MMS data are sparse.
- usSEABED: This publicly available database from the United States Geological Survey (USGS) contains grain size measurements, both published and unpublished, from federal, state, regional and local agencies and consortia as well as research institutions (Buczowski et al., 2006). These data include statistical measurements (i.e., mean grain size, sorting, skewness, kurtosis, etc.) as well as textural and benthic habitat information.

#### **4.1.4 Meteorological and Metocean Data**

Meteorological data for each hurricane evaluated were obtained from archives publicly available at the National Hurricane Center. These data typically include wind speed and direction, forward speed, barometric pressure, and estimates of hurricane- and tropical storm-force wind field.

Metocean data were compiled from offshore reporting stations emplaced during the more recent hurricanes evaluated, especially Hurricanes Ivan and Katrina. The primary data sources include the following:

- National Data Buoy Center (NDBC) buoy data: An array of offshore buoys is located throughout the GOM. Real-time oceanographic data are captured on an hourly basis and are publicly available on the NDBC website (NDBC, 2009). Data include significant wave height, wave period, wind speed and wind direction, barometric pressure, air and water temperature, and dew point.

- WAVCIS buoy data: An additional array of buoys, installed and operated by the WAVCIS Program at LSU's Coastal Studies Institute (CSI), is located throughout the GOM and state coastal waters. Data retrieved from these buoys are captured on an hourly basis. Although the data are freely available on the WAVCIS website they can be used (i.e. serve as the basis for research and publication) only with WAVCIS consent (WAVCIS, 2009). Data include significant wave height, wave period and direction, current speed and direction, wind speed and direction, barometric pressure, air temperature, and dew point.
- Acoustic Doppler Current Profiler (ADCP) data: An array of ADCP collecting stations are mounted on oil and gas production installations throughout the GOM as mandated by the MMS. Real-time ocean current data throughout the water column (mainly speed and direction) are captured from these stations. Data retrieved from these stations are available on the NDBC website (NDBC, 2009).
- Spectral wave density and direction data: These data are reported by the CSI stations on an hourly basis and identify the relative wave energy present at all frequencies and periods for a fixed location for a predefined length of time. Directional energy data are also provided.

## **4.2 Research Objectives and Tactics**

The major research objectives for this dissertation are broken out into four main phases. Specific tactics within each phase are described below.

### **4.2.1 Metocean Screening**

The purpose of this phase was to identify hurricane activity and associated metocean conditions within the study area. This effort chronicled hurricane history and characteristics within the study area since 1947 (Table 1) utilizing archived data from the National Hurricane Center. Emphasis was placed on five severe hurricanes to traverse the study area since 1965,

including Hurricanes Betsy (1965), Camille (1969), Andrew (1992), Ivan (2004) and Katrina (2005).

Metocean conditions during the most recent storms (i.e., Ivan and Katrina) were then quantified using NDBC and WAVCIS buoy data. Relationships between various parameters (e.g., significant wave height, wave period and wind speed) were then established, creating a metocean profile of each storm that could be used in subsequent numerical wave models. In addition, ADCP profiles for selected shallow-water sites on the GOM shelf during Hurricane Lili (2002) were used in constructing an analogy for ocean current downwelling during major storm events. This analogy was used to demonstrate that physical conditions other than turbidity may have been responsible for initiating major seafloor mudslides. Although the location of the ADCP sites was farther west along the central Louisiana coast, a hypothesis was assumed that process conditions in the study area would be similar and therefore valid for use.

#### **4.2.2 Seafloor Morphology Screening**

The purpose of this phase was to identify submarine mudslide parameters and characteristics within the study area. The four VTAs within the overall study area were used as a way of efficiently testing hypotheses and conclusions in this research. A series of local and regional bathymetric datasets, many of which were located in the VTAs, was used to help map seafloor topography. Many of these datasets overlie one another and, when combined with side-scan sonar and shallow seismic data, revealed the extent to which seafloor morphology changed shape and areal extent through time. Slope steepness was also estimated both local and regional scales, as steeper slope is a key factor governing the increased risk of future mudslides (Prior and Coleman, 1978a; Prior and Coleman, 1978b; McGregor, 1981; Prior et al., 1986; William Lettis & Associates Inc., 2005). Runout lengths for individual mudslides were also estimated for selected events within the four VTAs where possible given the extent of available data.

#### **4.2.3 Modeling and Integration**

The purpose of this phase was to conduct a series of numerical wave model simulations in which results from the first two research phases were integrated. First, a series of models were constructed for Hurricanes Ivan and Katrina using MIKE 21 modeling software to generate estimates of metocean parameters during each storm. These model runs were calibrated using actual metocean data measurements observed during Ivan and Katrina. Once the models were sufficiently calibrated, additional runs were then performed for Hurricanes Betsy, Camille and Andrew. Given that the models were calibrated against known metocean observations, model runs for these earlier storms have higher potential to accurately portray storm conditions for which limited to no observations are available. Detail on model parameters is included in Appendix M.

Results from the numerical wave models were then compared to areas of known mudslides as revealed by seafloor bathymetry surveys. Additional comparisons were made to geotechnical and lithological information gleaned from boreholes in the study area. These results yielded historical record of past mudslides and the metocean, morphologic, lithologic and geotechnical parameters that contributed to their occurrence. This subset of data was then used as the basis to compile the total risk assessment of potential mudslide response to future storms described in Section 9.3. This deliverable, in the form of vulnerability and hazard assessments, a risk procedure specific to the MRDF, and a set of risk maps across the study area, are based on the integration of the parameters described above and are the primary contributions of the dissertation.

An additional simulation was conducted to examine possible metocean effects as a result of seafloor morphology in the area of present-day Mississippi Canyon. A comparison to the MIKE 21 models was run by assuming that Mississippi Canyon was filled in and that seafloor bathymetry was constant with the surrounding shelf. This simulation was run because of the

concentration of infrastructure damage in the Grand Isle and West Delta Protraction Areas during Hurricane Katrina and is further described in Section 7.3.

#### **4.2.4 Application of Results**

The purpose of this phase was to apply results from the first three phases (and specifically, the risk assessment deliverable) into real-world utility within the offshore oil and gas industry. Risk assessments were compared to past and current networks of oil and gas platform locations and pipelines within the MRDF. A statistical analysis of infrastructure characteristics (e.g., platform design, construction type, age, etc.) and hurricane damage reports was then carried out to evaluate the impact of mudslide events linked to prior storms. Trends within those data were then evaluated to determine various scenarios under which the possible risk of future mudslides may become elevated during future storms. Based on the outcome of this statistical analysis, an assessment was then made as to which areas (and therefore which pipeline systems and platform locations) might contain the most risk for future mudslides. The outcome can be applied to future planning purposes when routing future pipelines across the MRDF or in selecting future platform locations.

## **CHAPTER 5. METEOROLOGICAL AND SEA-STATE CONTROLS**

### **5.1 General Hurricane History, North-Central Gulf of Mexico**

Meteorological records for Atlantic Basin tropical cyclones have been kept since 1851 (Tannehill, 1956; Neumann et al., 1987, 1993; Fernandez-Partagas and Diaz, 1996; NHC, 2009). During that time, 29 hurricanes with intensity levels of Category 3 or higher have traversed the study area adjacent to the Mississippi River Delta Front (MRDF; Table 1; Figure 28). Given the less precise information available for earlier storms and that their intensity cannot be accurately estimated, this dissertation concentrates only on five storms that attained at least Category 3 intensity across the MRDF study area (Betsy, 1965; Camille, 1969; Andrew, 1992; Ivan, 2004 and Katrina, 2005; Appendix B, Figures B-1 through B-5).

The historical record contains limited information for MRDF hurricanes prior to 1851 (Tannehill, 1956; Neumann et al., 1987; 1993). Precise meteorological conditions for these storms are unavailable beyond personal eye-witness accounts of damage at sea or at landfall.

#### **5.1.1 MRDF Tropical Cyclone History, 1851-2008**

MRDF historical hurricane frequency occurs in distinct patterns, often within a multi-decadal time scale (Stone et al., 1997, 1999; Muller and Stone, 2001; Keim et al., 2007; NHC, 2009; Figure 28). Causes for this frequency variation have often been attributed to fluctuation in El Nino or La Nina events, which are alternating cold and warm phases of ocean temperatures in the eastern and central Pacific Ocean off the coast of South America (Gray et al., 1993; Pielke and Landsea, 1999). These cycles, which are defined by variations in Pacific Ocean sea surface temperature of approximately 4° C, often affect tropical cyclone activity in the Atlantic Basin through corresponding changes in atmospheric circulation. Warmer cycles (El Nino) correlate with a reduction in hurricane frequency in the Atlantic; cooler cycles (La Nina) correlate with higher hurricane frequencies (Gray et al., 1993). Increased vertical shear during El Nino events due to westerly winds in the upper troposphere results in reduced Atlantic tropical activity; the opposite effect is true for La Nina events (Shapiro, 1987; Gray et al., 1993).

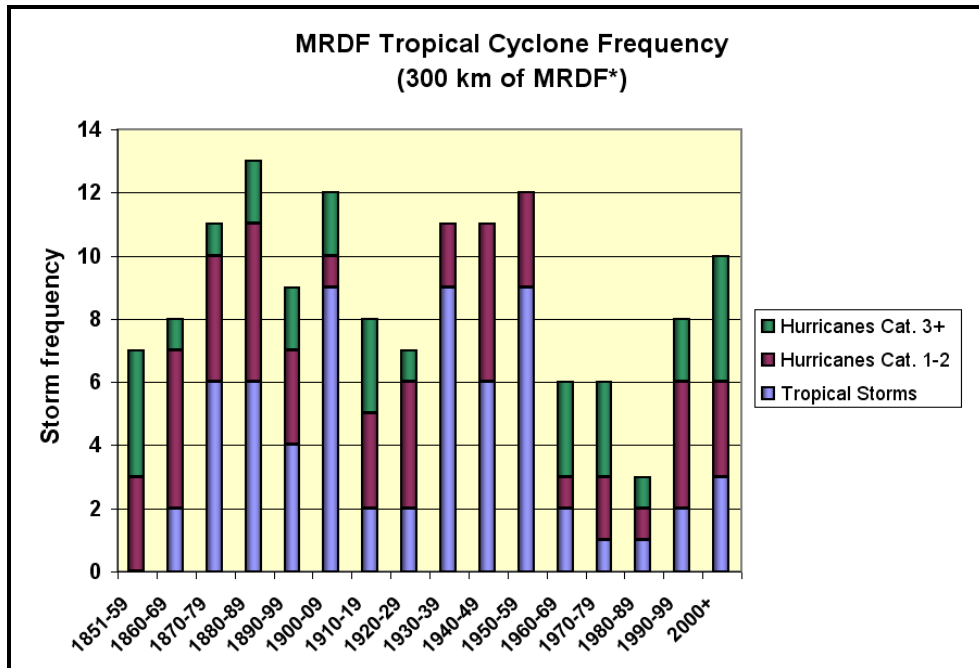


Figure 28: MRDF tropical cyclone frequency by decade, 1851-2008 (\*MRDF defined as 300 km from South Pass; raw data from NHC, 2009)

Three clusters of frequent hurricane activity occur from 1870-1909, 1930-1959 and 1990-2008 (Figure 28). Although the 1990s are reflected as active, the bulk of the frequency increase began only in 1995 (Stone et al., 1997). Lower hurricane frequency occurs from 1850-1869, 1910-1929 and 1960-1989 (although earlier periods could be reflect record quality). In addition, the period from 1930-1959 is notable for a lack of high-intensity hurricanes (i.e., Category 3+). Since 1960, intense hurricanes increased relative to the period from 1930-1959 and have continued through 2008.

The MRDF is a historically active hurricane area. Several statistical models suggest that hurricane distribution and severity vary as a function of location across the Gulf of Mexico (GOM), resulting in varying estimates of recurrence interval (RI; Chouinard and Liu, 1997; Chouinard et al., 1997). These models also suggest that the spatial variation of RI is statistically significant and that the highest hurricane frequency occurs offshore Louisiana west of New Orleans (Chouinard and Liu, 1997). These conclusions appear validated in hurricane counts

provided by Stone et al. (1997) that indicate increased storm distributions offshore southeastern and south-central Louisiana.

A simple calculation of the overall (RI) for Category 3+ hurricanes within 300 km of the mouth of the Mississippi River, as measured since 1851, is 5.4 years (Table 4). When decreasing distance from the MRDF is considered, the RI increases. The RI decreases when storms of lesser magnitude are included in the total.

Table 4: Recurrence intervals, MRDF hurricanes (Category 3+), 1851-2008

<u>Tropical Cyclone Criteria</u>	<u>Recurrence Interval (years)</u>	<u>Hurricane Count</u>
Category 3 RI (300 km)	5.4	29
Category 3 RI (200 km)	6.0	25
Category 3 RI (100 km)	13.6	11
All hurricanes (300 km)	2.0	78
All tropical cyclones (300 km)	1.1	142

Most hurricanes approach the MRDF from a southerly or southeasterly direction. A comparison of Category 3+ hurricanes from 1851-2008 reveals that hurricane approach ranges in arc from 110° (east-southeast) to 180° (south; Figure 29). Occasional hurricanes also approach from the southwest (through 225°) or from the east (through 100°). The five hurricanes evaluated in this dissertation all approached the MRDF from the southeast or south (Figure 29). All were major hurricanes and experienced the benefit of Caribbean or Atlantic storm origin prior to entering the GOM, where they continued to intensify over warm GOM waters. The forward speed of most tropical cyclones generally increases with northward progression after landfall, especially after re-curvature to a northerly or northeasterly direction (Ho et al., 1987).

Although older hurricane records are less reliable, several severe storms crossed the MRDF prior to Hurricane Betsy. These storms include the Last Island Hurricane (1856), the Chenier Caminada Hurricane (1893), the 1906 Hurricane, the New Orleans Hurricane (1915) and Hurricane Hilda (1964). The effects of these hurricanes reflect both their intensity and forward speed (i.e., the longer they linger in an area, the greater the impact). Hsu's (2006) method for estimating significant wave height based on central pressure was used as a proxy to estimate how



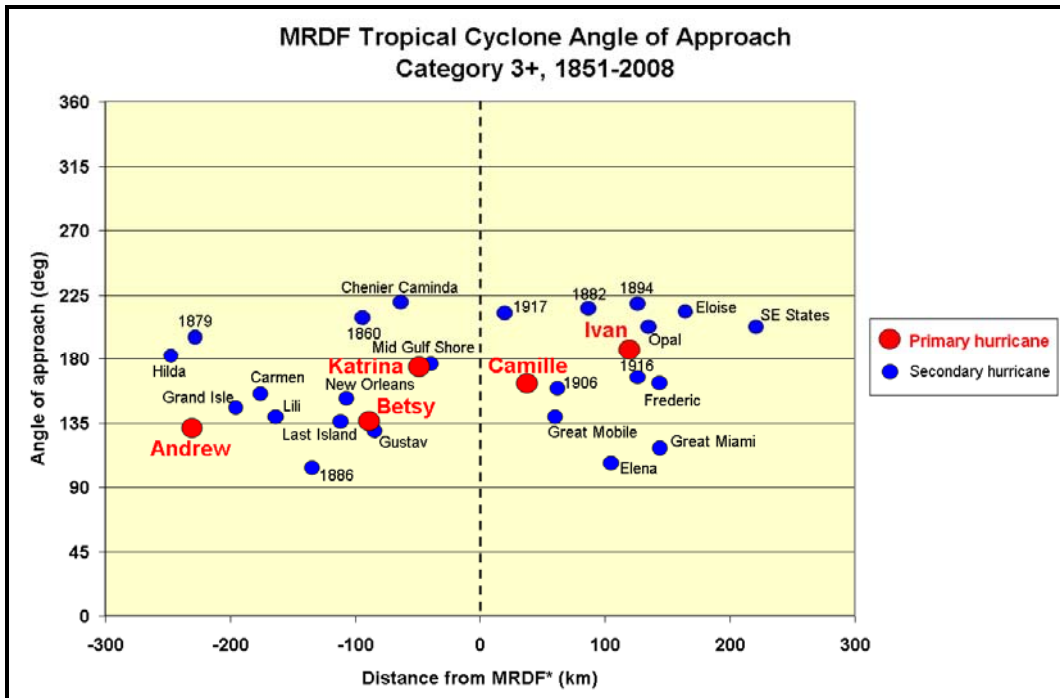


Figure 29: MRDF tropical cyclone angle of approach, Category 3+ hurricanes, 1851-2008  
(\*MRDF defined as 300 km from South Pass; raw data from NHC, 2009)

storm intensity affects seafloor conditions given the length of time hurricanes were present in the MRDF (Figure 30). Based on this analysis, Hurricanes Katrina, Ivan and the Last Island Hurricane most heavily impacted the area. The 1906 and New Orleans Hurricanes, along with Hurricane Hilda, followed closely behind. The matrix constructed in Figure 30 indicates that hurricanes in the upper right matrix box contain the highest potential for seafloor impact.

### 5.1.2 MRDF Tropical Cyclone History, 1718-1851

Fifteen hurricanes impacted the MRDF between 1718 (the founding of New Orleans) and 1851 (Tannehill, 1956; Table 5; Figure 31). Precise meteorological records for these storms are either unreliable or do not exist. However, these records help elucidate hurricane RI near New Orleans and, by extension, the MRDF.

Using these data, the RI for all storms is 8.9 years, which is lower than the 13.6-year RI for all hurricanes within 100 km of the MRDF since 1851. A complete set of records could yield additional, non-recorded hurricanes, thus increasing the RI. Also, decadal variation in hurricane

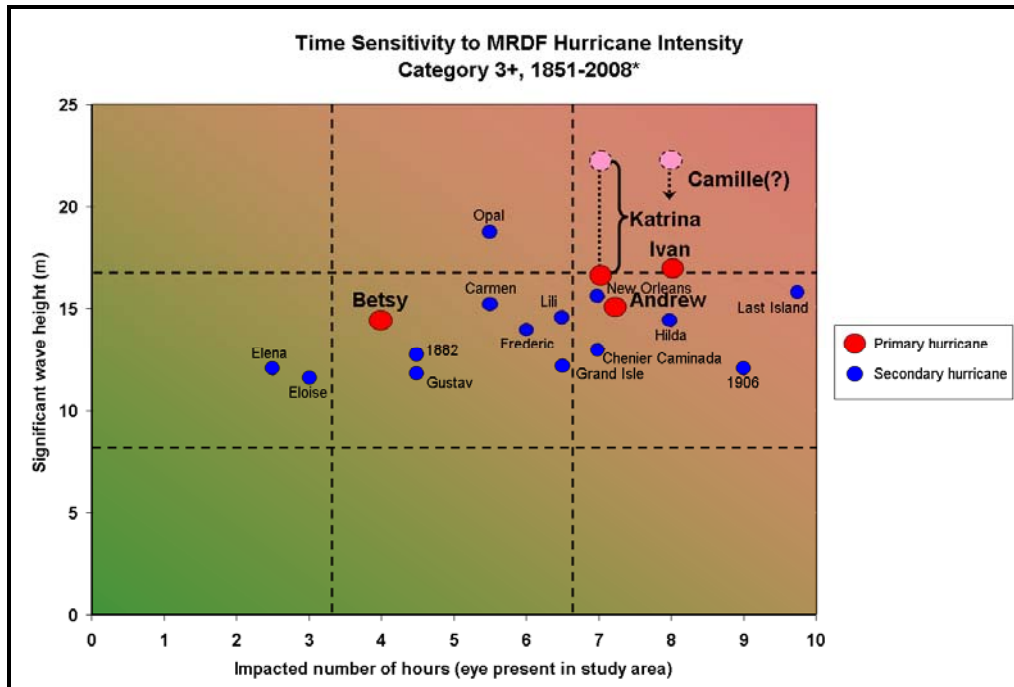


Figure 30: Time sensitivity to MRDF hurricane intensity, Category 3+ hurricanes, 1851-2008 (\*MRDF defined as 300 km from South Pass;  $H_{s,max}$  defined from Hsu's (2006) method; pink dots for Katrina and Camille from Hsu (2006); red dots for Katrina and Camille calibrated to NDBC and MIKE 21 modeled conditions (Katrina) or modeled conditions only (Camille))

Table 5: MRDF Hurricane History near New Orleans, 1718-1851 (from Tannehill, 1956)

	<u>Hurricane Name</u>	<u>Year</u>	<u>Point of GOM Landfall (State: County/Parish)</u>	<u>Historical Comments</u>
1	1846	1846	Louisiana: Orleans area	"New Orleans"
2	Racer's Storm	1837	Louisiana: Vermilion	"High storm surge, New Orleans"
3	1831	1831	Louisiana: Plaquemines	"Very destructive at mouth of Mississippi" (MRDF impact)
4	1821	1821	Louisiana: Orleans area	"New Orleans"
5	1819	1819	Louisiana: Orleans area	"Louisiana and Alabama" (likely MRDF impact)
6	1812	1812	Louisiana: Orleans area	"New Orleans"
7	1811	1811	Louisiana: Orleans area	"New Orleans"
8	1800	1800	Louisiana: Orleans area	"New Orleans"
9	1781	1781	Louisiana: Orleans area	"New Orleans"
10	1780	1780	Louisiana: Orleans area	"Destroyed crops, tore down buildings, sunk every vessel on the river"
11	1776	1776	Louisiana: Orleans area	"New Orleans"
12	1740	1740	Louisiana: Plaquemines	"Mouth of Mississippi and Pensacola" (likely MRDF impact)
13	1732	1732	Alabama: Mobile	"A destructive storm"
14	1723	1723	Louisiana: Orleans area	"Remarkable hurricane; nearly all buildings destroyed"
15	1722	1722	Louisiana: Orleans area	"Everything in the port lost"

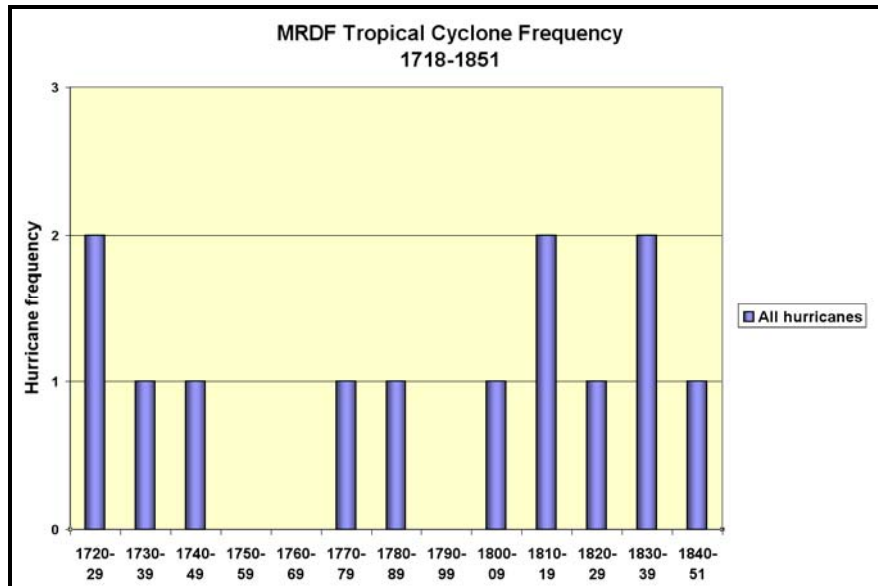


Figure 31: MRDF Tropical cyclone frequency, 1718-1851 (raw data from Tannehill, 1956)

frequency is evident in these records despite the lack of precise data, suggesting that frequency trends from 1851-2008 are not a statistical aberration.

## 5.2 Modeled Response of Hurricane Metocean Conditions

In order to quantify wave and bottom-boundary conditions during the five GOM hurricanes evaluated, a series of numerical wave models were applied using the MIKE 21 engineering software package, which is a two-dimensional numerical modeling suite developed by DHI Water & Environment, Inc. A wave model was performed using the MIKE 21 SW Module, which is a spectral wind-wave model based on an unstructured mesh that simulates the growth, decay and transformation of wind-generated waves and swell in offshore and coastal areas (DHI, 2005). This model has been previously implemented in the GOM (Jose and Stone, 2006; Jose et al., 2007; Jose et al., 2009) and specifically off the south-central Louisiana coast (Kobashi et al., 2009) to assess the impact of sand mining from Ship Shoal, one of the largest sand bodies found offshore Louisiana. Although other models such as SWAN are being utilized in the WAVCIS laboratory, MIKE 21 had been more scrutinized regarding skill assessment during this research. *In situ* and numerically derived data showed excellent agreement. Spaziani et al., (2009) implemented this same model for the coast offshore the Florida Panhandle to

quantify the impact of hurricanes on inner shelf sediment resuspension and transport, and have validated the results with MODIS imagery. Details on model parameterization, calibration parameters and other protocols used in the MIKE 21 model are discussed in Appendix M.

Several bulk wave and bottom boundary layer parameters were modeled for each hurricane as part of a time sequence prior to and after storm passage. The model was comprised of a more finely gridded domain over the MRDF study area nested within a relatively coarse-gridded GOM-wide domain (Appendix M). Jose et al. (2007), based on a similar nested modeling study, demonstrated the effectiveness of nesting in simulating the nearshore wave field along the northern GOM. In addition, the mesh used for the study area model was constrained even finer within the four Validation Test Areas (VTAs; Appendix M). Wave fields were computed using as inputs gridded wind field data for each storm as well as a combination of either regional bathymetry and/or localized bathymetric datasets where available.

The parameters modeled in MIKE 21 are listed in Table 6.

Table 6: Modeled parameters for GOM-wide and Study Area MIKE 21 wave models

1. Significant wave height (m)	10. Y-component of wave vector ( $\text{m sec}^{-1}$ )
2. Maximum wave height (m)	11. Radiation stress $S_{xx}$ ( $\text{m}^3 \text{sec}^{-2}$ )
3. Peak wave period (sec)	12. Radiation stress $S_{xy}$ ( $\text{m}^3 \text{sec}^{-2}$ )
4. Wave period T02 (sec)	13. Radiation stress $S_{yy}$ ( $\text{m}^3 \text{sec}^{-2}$ )
5. Wave period TM10 (sec)	14. Horizontal particle velocity, bed ( $\text{m sec}^{-1}$ )
6. Peak wave direction (degrees)	15. Horizontal particle velocity, surface ( $\text{m sec}^{-1}$ )
7. Mean wave direction (degrees)	16. Vertical particle velocity, surface ( $\text{m sec}^{-1}$ )
8. Dir. Standard deviation (degrees)	17. Horizontal particle velocity, Z-level ( $\text{m sec}^{-1}$ )
9. X-component of wave vector ( $\text{m sec}^{-1}$ )	18. Vertical particle velocity, Z-level ( $\text{m sec}^{-1}$ )

### 5.2.1 Model Calibration to Metocean Conditions during Recent Hurricanes

Reliable estimations of metocean conditions during MRDF hurricanes, such as wind intensity, forward speed, significant wave height, wave period and barometric pressure, are available only over the last several decades. Beginning around 1990, arrays of ocean-observing data collections sites were deployed offshore near the MRDF and adjoining coastal waters offshore Louisiana. Three severe hurricanes passed over or near the MRDF since then, including Andrew, Ivan and Katrina. Observations from the array of observing sites (mainly NDBC buoys,

LSU WAVCIS stations and permanently mounted stations on production platforms) were used as a means of calibrating the MIKE 21 simulated response for each storm.

Prior work hindcasting the metocean response during GOM hurricanes has been carried out since the mid-1990s (Cox et al., 2005; Cardone et al., 2004; 2007; Oceanweather, Inc., 1992; 2003; 2006; 2007a; 2007b). These hindcast studies are based on a proprietary hindcast product known as GOMOS (Gulf of Mexico Oceanographic Study) prepared by Oceanweather, Inc. of Cos Cob, CT. This product consists of a ten-year continuous wind and wave hindcast for the period 1990-1999 and is based on a wave model adapted to a grid  $1/8^{\text{th}}$  of a degree within the GOM (Oceanweather, Inc., 2007b). Once reliable hindcast studies were created, work focused on comparing observed vs. estimated conditions at specific offshore reporting stations during recent GOM hurricanes (Forristall, 2007a; 2007b).

Hindcasts of hurricane wind strength, significant wave height and current velocities were used in comparing conditions during Hurricanes Lili, Ivan, Katrina and Rita (Forristall, 2007a; 2007b). Observations from GOM NDBC stations during all four storms indicated good agreement between observed and hindcast bulk wave parameters (Figure 32). Using  $H_{s_{\text{max}}}$  as a proxy, measured vs. hindcast conditions agreed for wave heights below approximately 11 m. However, at wave heights exceeding 11 m the modeled values under-estimated observed conditions. These findings were consistent with those suggested by Cardone et al. (1996) who attribute the discrepancy to possible dynamic fetch associated with intense surface wind maxima that were not fully incorporated into their hindcast models or modeled in sufficient detail.

Hurricane Katrina moved across the MRDF in August 2005 (Figure 1; also Appendix B, Figure B-5). As part of the MIKE 21 Gulf-wide wave model, the precise coordinates of several recording stations located in the vicinity of Katrina's path were included as input coordinates such that various metocean outputs could be calculated for each location. An iterative process was then carried out to adjust the inputs and help ensure the closest match with observed conditions for each site (Figure 33).

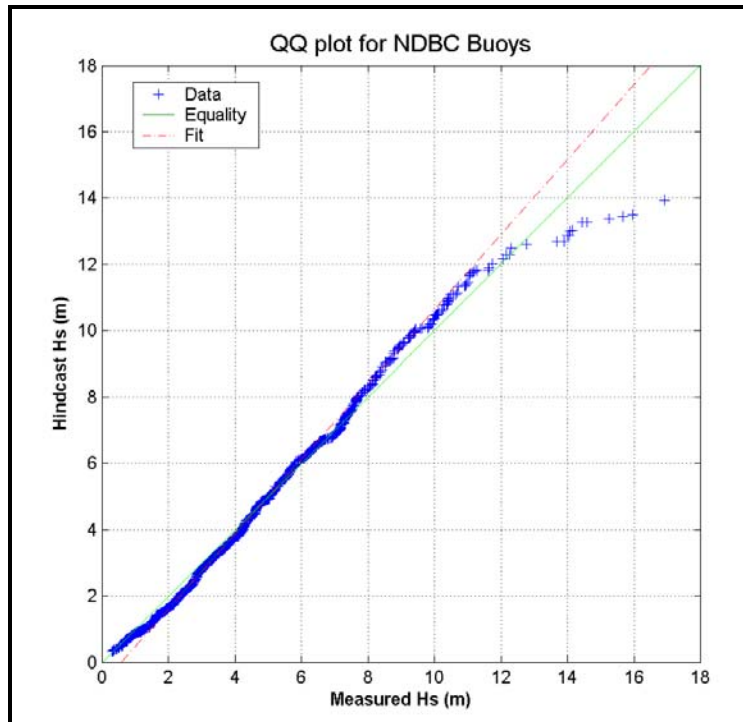


Figure 32: Measured vs. hindcast significant wave heights at GOM NDBC buoys, Hurricanes Lili, Ivan, Katrina and Rita (from Forristall, 2007)

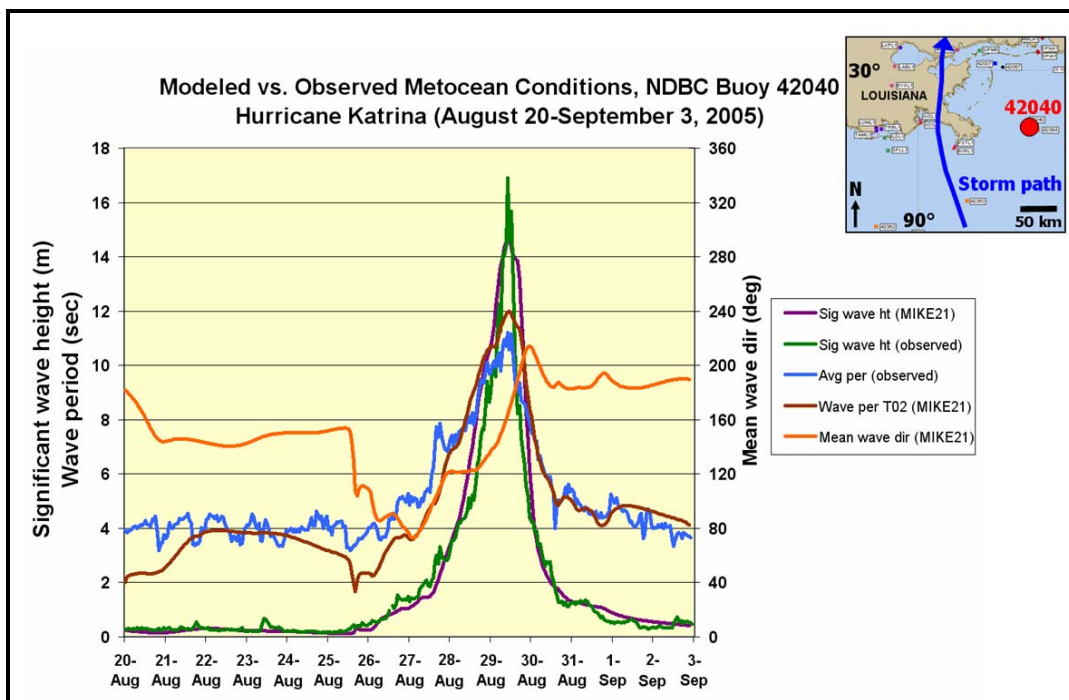


Figure 33: Comparison of observed metocean conditions to MIKE 21 modeled response at NDBC Buoy 42040 during Hurricane Katrina

As an example, a comparison of Hurricane Katrina's approach at the NDBC Buoy 42040 site (Figure 33) yielded a significant wave height ( $H_{s_{max}}$ ) correlation coefficient between observed and modeled conditions of  $R^2 = 0.992$  (Figure 34). The post-storm  $H_{s_{max}}$  correlation coefficient is also high, with an  $R^2 = 0.975$  (Figure 35). Comparisons between modeled and observed bulk wave parameters were evaluated using these methods (i.e., evaluating degree of fit through least squares regression) because they are more quantitative relative to relying solely on spectral data, which are more subjective.

A comparison of wave period was also performed by using the NDBC observed "Average Period" versus the MIKE 21 simulated parameter "Wave Period T02". Correlation coefficients between these data are also high; Katrina approach values display  $R^2 = 0.926$  whereas post-storm Katrina values display  $R^2 = 0.946$  (Figures 36 and 37). A distinct step appears in the wave period data at 1800 Z on August 25 in which both observed and modeled conditions decrease by about one meter (Figure 33). A shift in mean wave direction also occurs at that point, switching from about  $155^\circ$  to  $105^\circ$  (approximately SSE to ESE). An explanatory hypothesis is that Katrina's initial motion pushed waves from the south and southeast as it crossed southern Florida, but once it moved into the GOM on August 25 the counter-clockwise wind field had begun impacting the 42040 site by 1800 Z. Mean wave direction continued to switch with time, becoming ENE but eventually switching back to the south and WSW as Katrina passed 135 km to the west.

Additional sites used in model skill assessment during Katrina are catalogued in Table 7.

Once the GOM-wide and study area-wide models were sufficiently calibrated, the model runs generated map estimates of key bulk wave parameters. These time-series data were computed at three-hour intervals from August 20 through September 3, 2005 (a 14-day history that captures both pre-storm setup and post-storm recovery conditions) and reveal oceanographic conditions prevalent within the study area. Peak wave conditions for Hurricane Katrina as it moved over the MRDF are displayed in Figures 38 and 39.

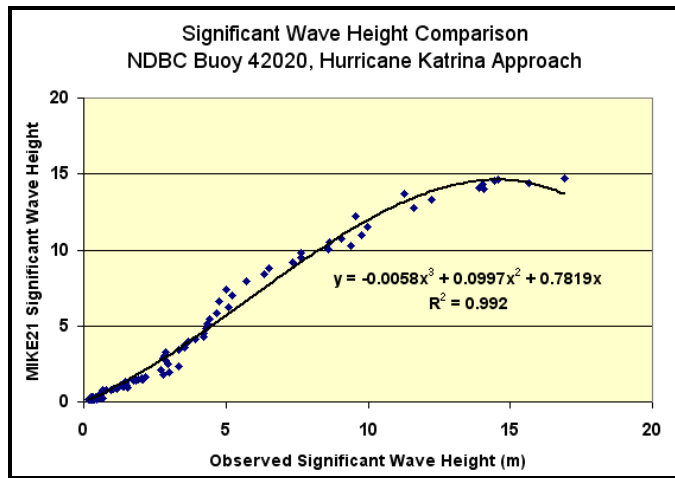


Figure 34: Significant wave height comparison, NCBC Buoy 42040, Hurricane Katrina approach (August 2005)

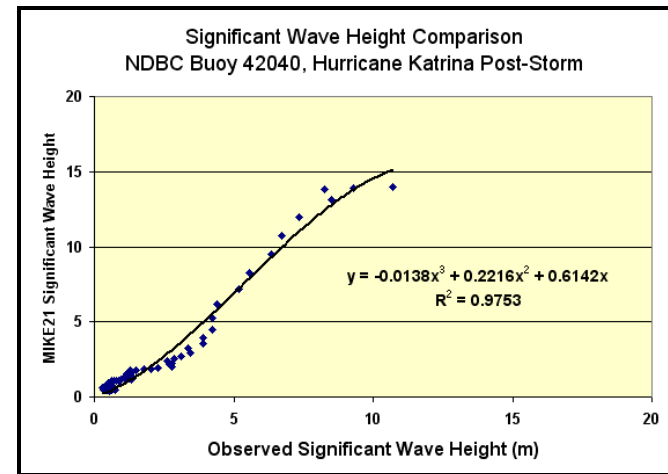


Figure 35: Significant wave height comparison, NCBC Buoy 42040, Hurricane Katrina post-storm recovery (August 2005)

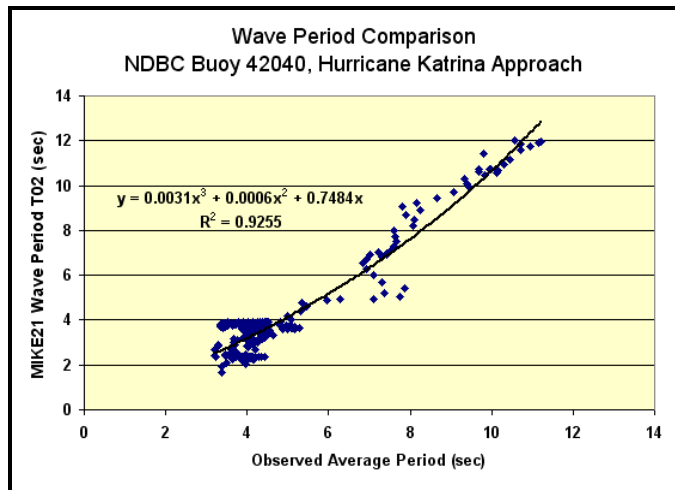


Figure 36: Wave period comparison, NCBC Buoy 42040, Hurricane Katrina approach (August 2005)

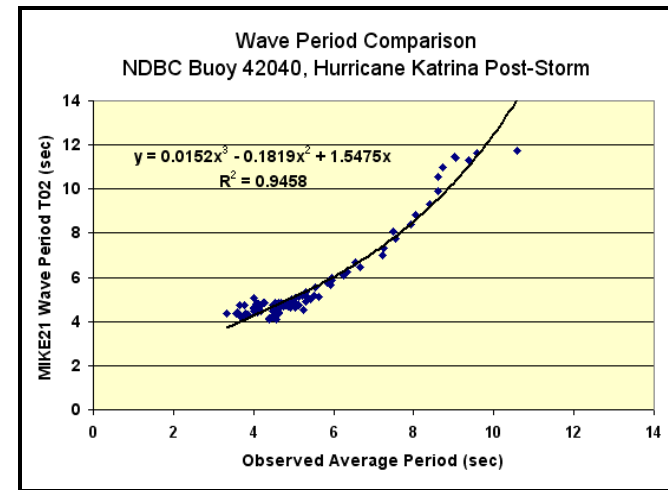


Figure 37: Wave period comparison, NCBC Buoy 42040, Hurricane Katrina post-storm recovery (August 2005)



Table 7: Correlation coefficients, observed vs. modeled metocean parameters, Hurricane Katrina

	<u>NDBC 42001</u>	<u>NDBC 42007*</u>	<u>NDBC 42040</u>
Proximity to eye (km/direction)	135 SW	70 E	135 ENE
Significant wave height (approach)	0.991	0.971	0.992
Significant wave height (recovery)	0.941	N/A; buoy failed	0.975
Wave period (approach)	0.913	0.922	0.926
Wave period (recovery)	0.874	N/A; buoy failed	0.946
* Not used as primary example due to (1) location in shallower water, (2) nearest proximity occurred after hurricane had made landfall, and (3) buoy failed during mid-hurricane			

Hurricane Ivan moved across the eastern periphery of the MRDF in August 2004 (Figure 1; also Appendix B, Figure B-4). The eye of Ivan passed 30 km east of NDBC Buoy 42040 at its closest point of approach. Although the buoy failed mid-storm, it was the closest NDBC buoy to the track of Ivan and was therefore used to help calibrate the Ivan MIKE 21 model (Figure 40). A comparison of  $H_{s_{max}}$  correlation coefficients between observed and modeled conditions during Ivan's approach yields a value of  $R^2 = 0.990$  using a third-order polynomial function (Figure 41). In addition, Hurricane Ivan moved directly over several buoys maintained by the United States Naval Research Laboratory (USNRL; Wang et al., 2005; Teague et al., 2007). However, detailed time-series data were not publicly available and therefore the data from Ivan's approach at Buoy 42040 were deemed the most useful. A comparison of wave period using the NDBC observed "Average Period" versus the MIKE 21 parameter "Wave Period T02" also yields high correlation coefficients for Ivan's approach ( $R^2 = 0.959$ ; Figure 42).

As with Hurricane Katrina, time-series data were computed at three-hour intervals for Hurricane Ivan over a 14-day period to capture both pre-storm setup and post-storm recovery conditions and illustrate oceanographic conditions prevalent within the study area. Peak wave conditions for Ivan as it moved over the MRDF are displayed in Figures 43 and 44.  $H_{s_{max}}$  values reached their maximum along the MRDF around date on September 15, 2004 at 2100 Z as wave heights exceeded 15 m in the northeast quadrant of the hurricane about ten hours prior to landfall.

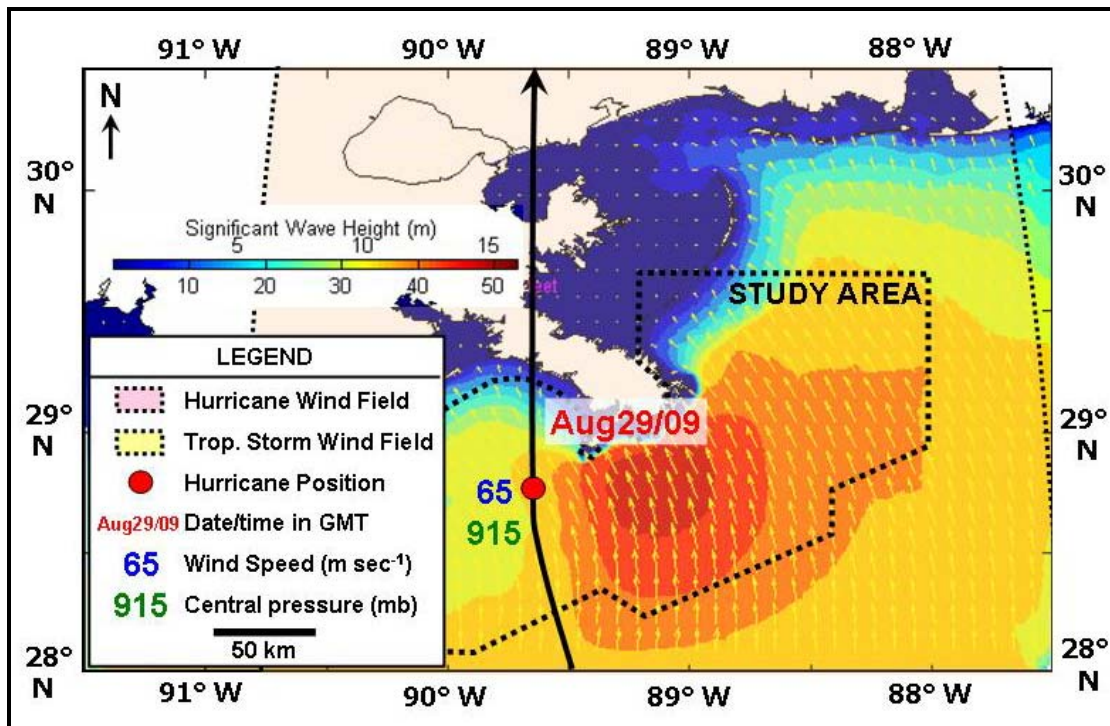


Figure 38:  $H_{s,max}$ , Hurricane Katrina, August 29, 2005 0900Z  
as modeled through MIKE 21 numerical wave model

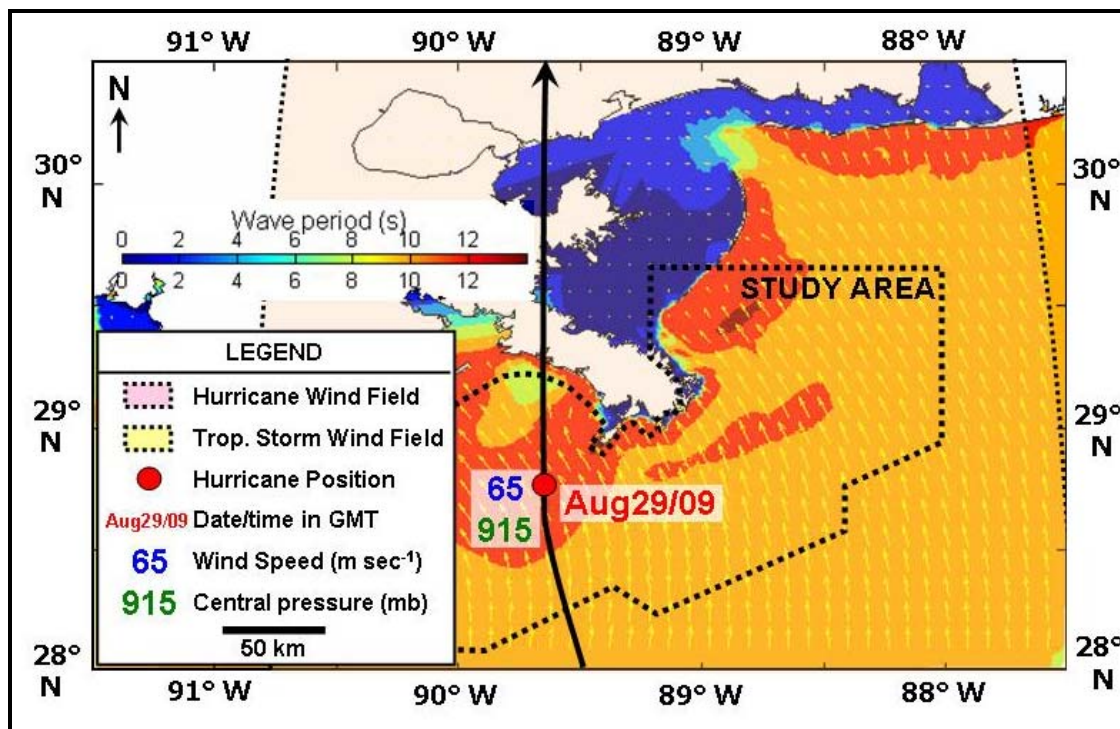


Figure 39: Wave period  $T_{02}$ , Hurricane Katrina, August 29, 2005 0900 Z  
as modeled through MIKE 21 numerical wave model

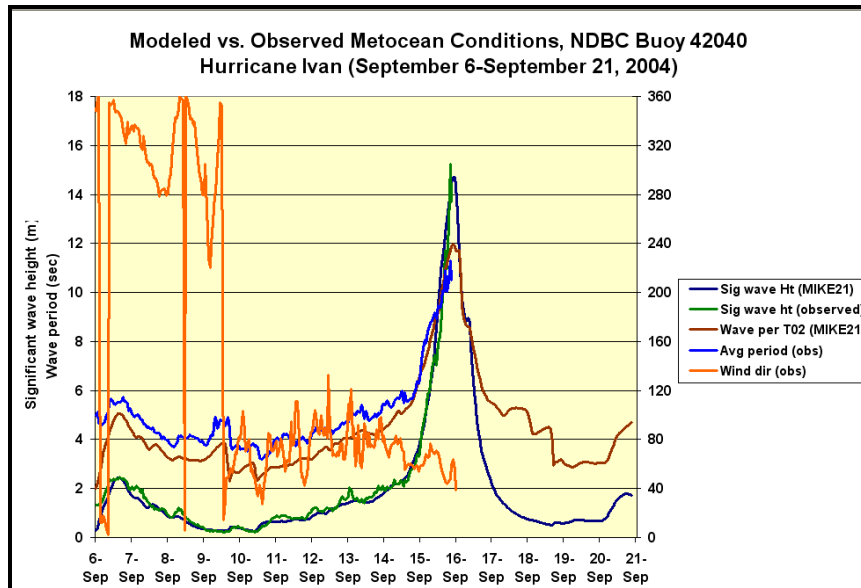


Figure 40: Comparison of observed metocean conditions to MIKE 21 modeled response at NDBC Buoy 42040 during Hurricane Ivan

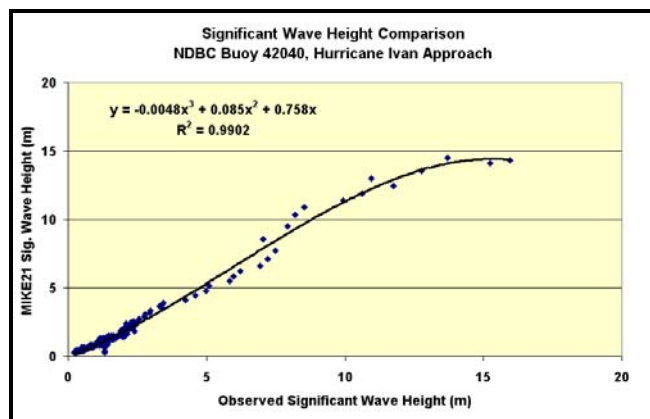


Figure 41: Significant wave height comparison, NCBC Buoy 42040, Hurricane Ivan approach (September 2004)

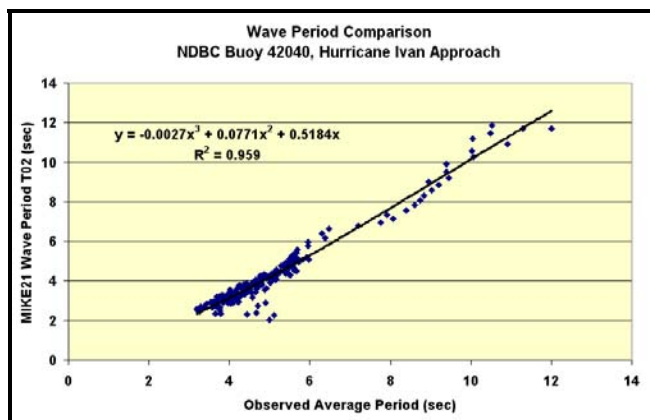


Figure 42: Wave period comparison, NCBC Buoy 42040, Hurricane Ivan approach (September 2004)

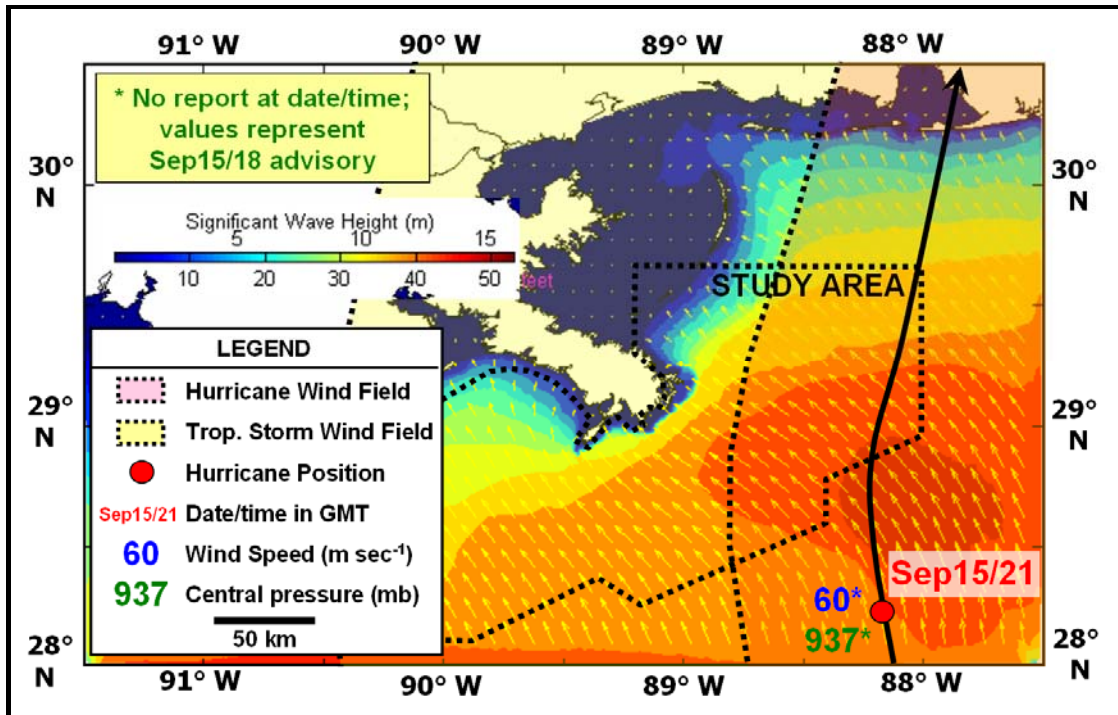


Figure 43:  $H_{s_{\max}}$ , Hurricane Ivan, September 15, 2004 2100 Z  
as modeled through MIKE 21 numerical wave model

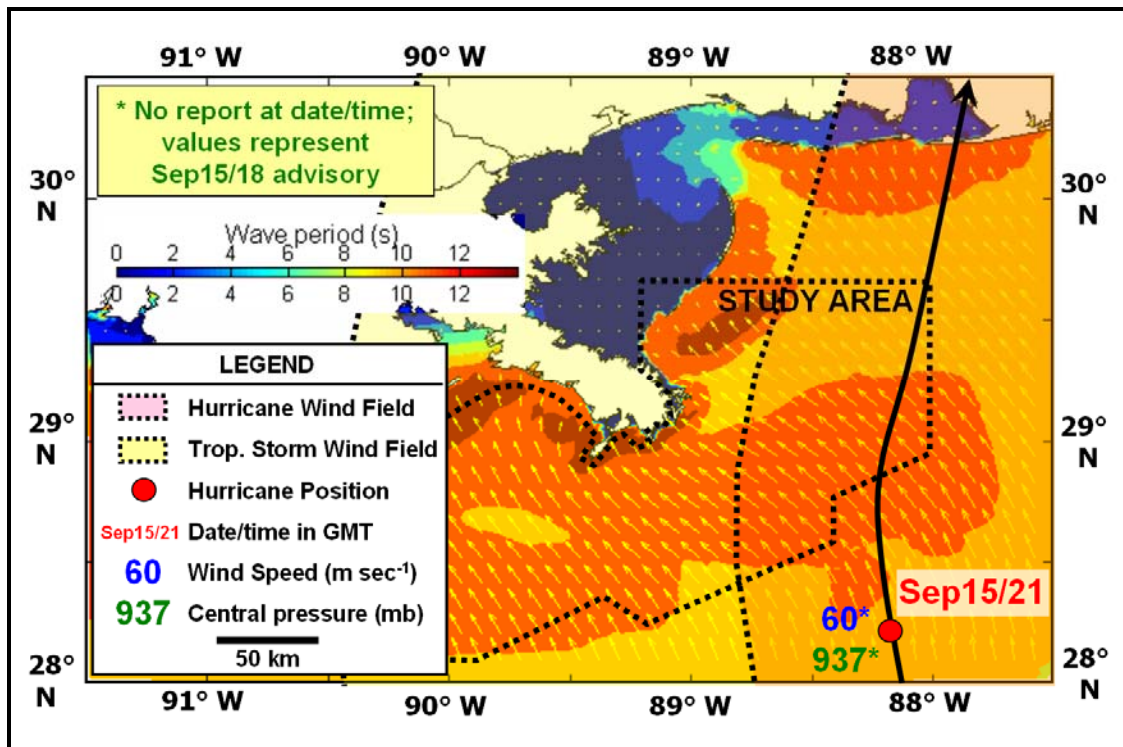


Figure 44: Wave period T02, Hurricane Ivan, September 15, 2004 2100 Z  
as modeled through MIKE 21 numerical wave model

Additional coordinate sites were used to help calibrate metocean conditions during Hurricane Ivan. These are catalogued, along with their corresponding  $R^2$  values, in Table 8.

Table 8: Correlation coefficients, observed vs. modeled metocean parameters, Hurricane Ivan

	<u>NDBC 42001</u>	<u>NDBC 42007</u>	<u>NDBC 42040</u>
Proximity to eye (km/direction)	255 W	75 W	30 W
Significant wave height (approach)	0.958	0.965	0.990
Significant wave height (recovery)	0.903	0.945	N/A; buoy failed
Wave period (approach)	0.825	0.856	0.959
Wave period (recovery)	0.788	0.800	N/A; buoy failed

Limited time-series data exist for Hurricane Andrew and therefore the MIKE 21 models used in this dissertation were calibrated primarily on observations from Hurricanes Ivan and Katrina. NDBC Buoy 42001 was active during Andrew but the storm passed approximately 240 km northwest of the buoy and metocean effects at this location were extremely limited (highest  $H_{s_{max}}$  was 4.4 m, longest average period was 10.8 sec, and lowest central pressure was 1012 mb). Station BUSL1 at Shell's Bullwinkle Platform (approximately 120 km SW of Andrew's path) and Station BURL1 at Southwest Pass of the Mississippi River (approximately 130 km NE of Andrew's path) were operational during Andrew but only wind data are available; no metocean data were recorded.

### 5.2.2 Hindcast Model Application to Prior Hurricanes

Once the MIKE 21 model was established and tested against known metocean conditions during recent hurricanes, a predictive hindcast model was run for the two earlier hurricanes evaluated (Camille and Betsy). The results of these models display expected hurricane-induced wave fields prevalent during each storm and lay the framework for how they impacted the seafloor in the study area despite the lack of reliable metocean observations.

The MIKE 21 model output for Hurricane Camille reveals excessive metocean conditions (i.e., abnormally large waves and long wave periods) prior to landfall (Figures 45 and 46).  $H_{s_{max}}$



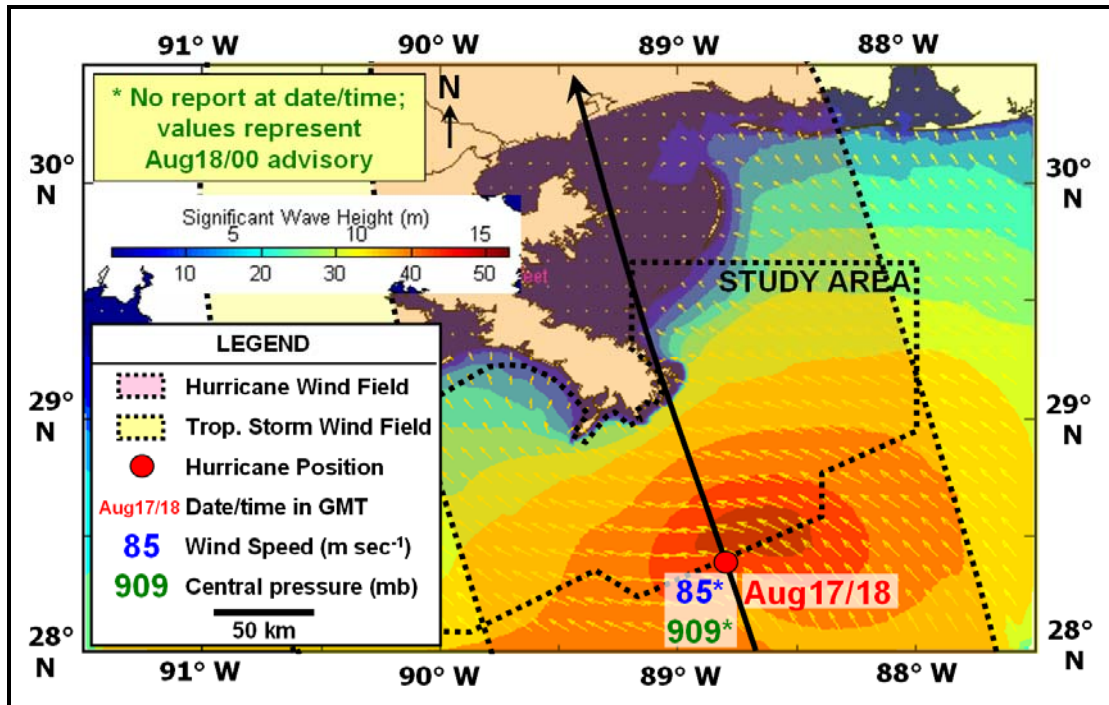


Figure 45:  $H_{s_{max}}$ , Hurricane Camille, August 17, 1969 1800 Z  
as modeled through MIKE 21 numerical wave model

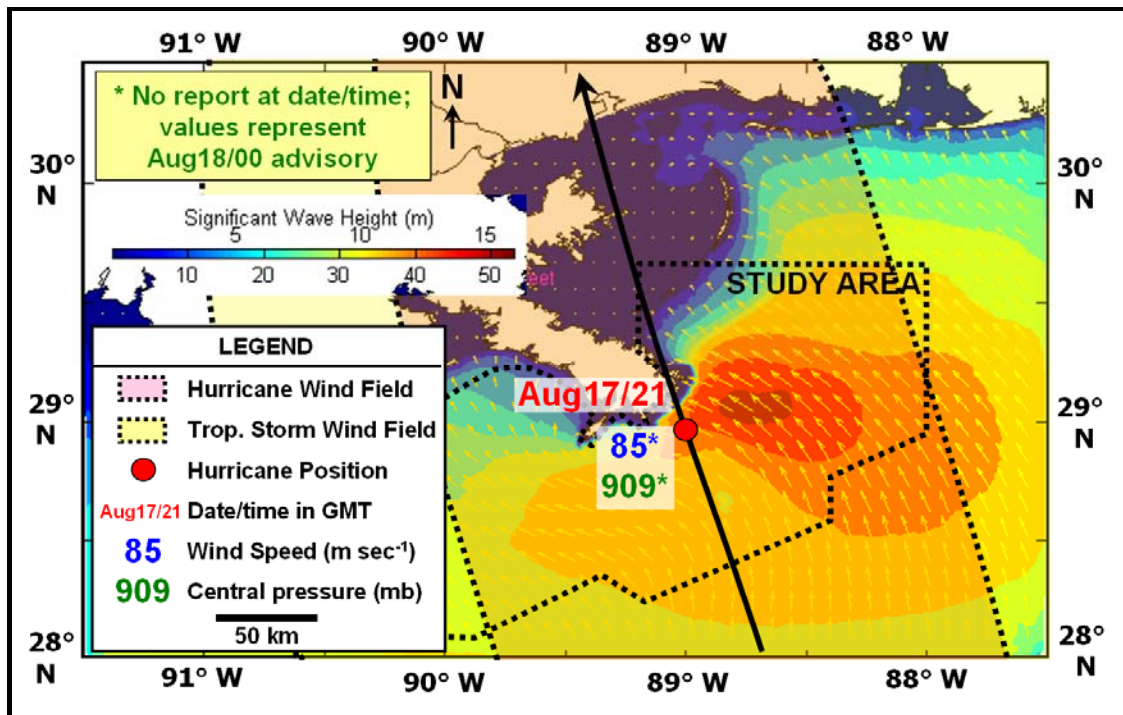


Figure 46:  $H_{s_{max}}$ , Hurricane Camille, August 17, 1969 2100 Z  
as modeled through MIKE 21 numerical wave model

values reached their maximum along the MRDF around August 17 at 2100 Z as wave heights exceeded 15 m in the northeast quadrant of the hurricane approximately nine hours prior to Mississippi landfall (Figure 46). However, wave conditions abated as Camille made landfall on the Mississippi coast, and modeled wave conditions receded to approximately 10-12 m by August 18 at 0300 Z. Likewise, the MIKE 21 model output generated for Hurricane Camille reveals excessive wave periods ( $T_{02}$ ; zero-crossing) within the MRDF (Figures 47 and 48), attaining values near 12 sec both east and west of the eye as Camille moved through the study area. Wave periods nearest the eye at this time were somewhat lower, approximating 9 sec.

The MIKE 21 model output for Hurricane Betsy also revealed high  $H_{s_{max}}$  prior to landfall, reaching heights exceeding 15 m in the northeast quadrant approximately four hours prior to Louisiana landfall (Figure 49). Over time,  $H_{s_{max}}$  decreased to about 10 m even though the center of circulation had already moved inland by this time (Figure 50). Despite these excessive conditions, Hurricane Betsy was a relatively fast-moving hurricane (forward speed of approximately 35 km hour<sup>-1</sup>; NHC, 2009) and these conditions did not remain long in the study area.

The MIKE 21 model-generated wave fields for Hurricane Betsy revealed long wave periods ( $T_{02}$ ; zero-crossing) within the MRDF study area (Figures 51 and 52). Periods exceeded 10 sec near the center as well as in shallower water both east and west of the MRDF about four hours prior to landfall (Figure 51). Wave periods receded after Betsy moved inland and averaged approximately 9 sec on 0600Z on September 10, 1965 (Figure 52).

### **5.3 Directional Wave Spectra Applications**

As ocean waves are irregular in time and space, the irregularity of an ocean surface can be modeled in either a time domain or a frequency domain (Daemrich et al., 2004). In the time domain, an irregular wave train consists of a sequence of individual waves characterized by wave measurements such as height and period. However, an irregular ocean surface is composed of a number of sinusoidal wave components with different frequencies. A time series can be

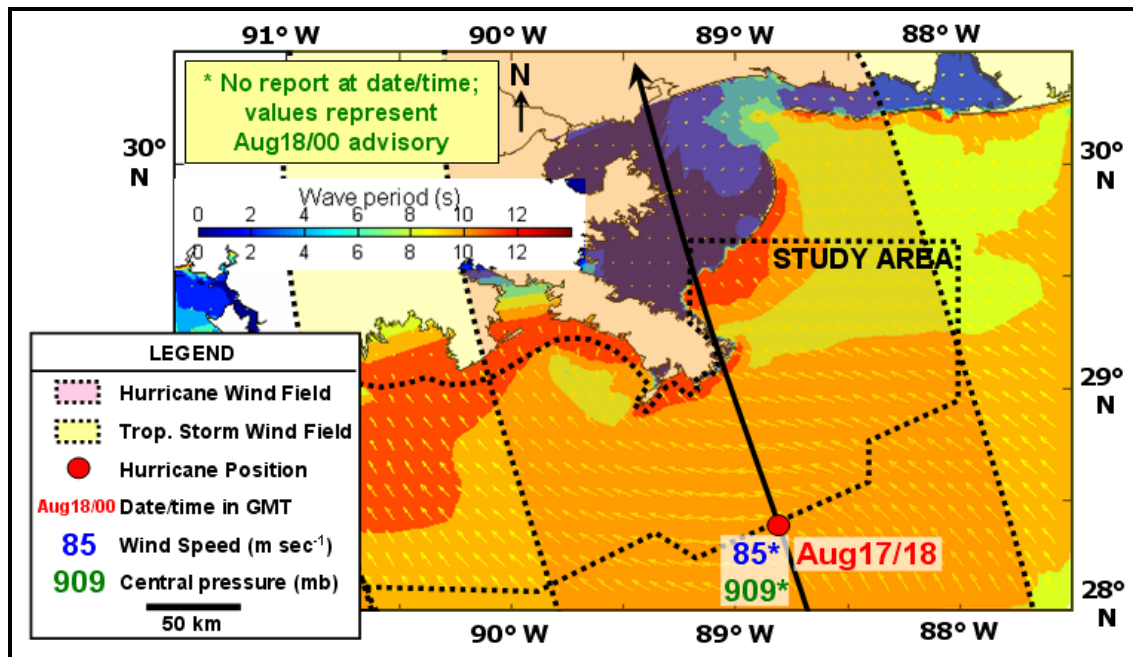


Figure 47: Wave period T02 (zero-crossing), Hurricane Camille, August 17, 1969 1800Z as modeled through MIKE 21 numerical wave model

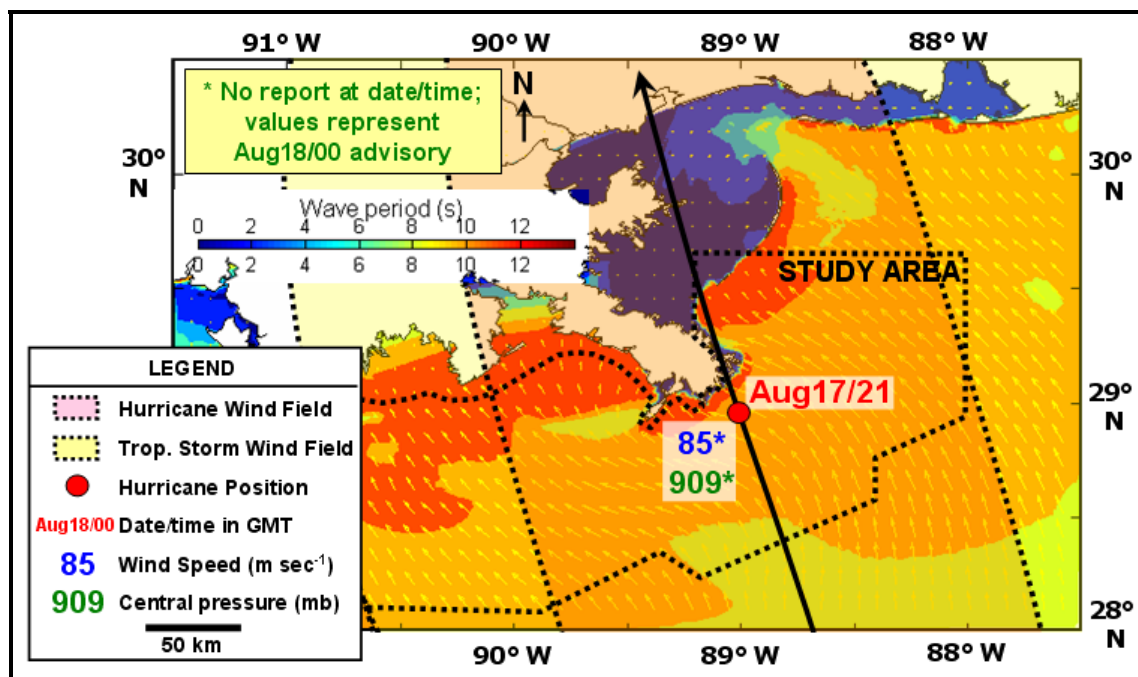


Figure 48: Wave period T02 (zero-crossing), Hurricane Camille, August 17, 1969 2100Z as modeled through MIKE 21 numerical wave model



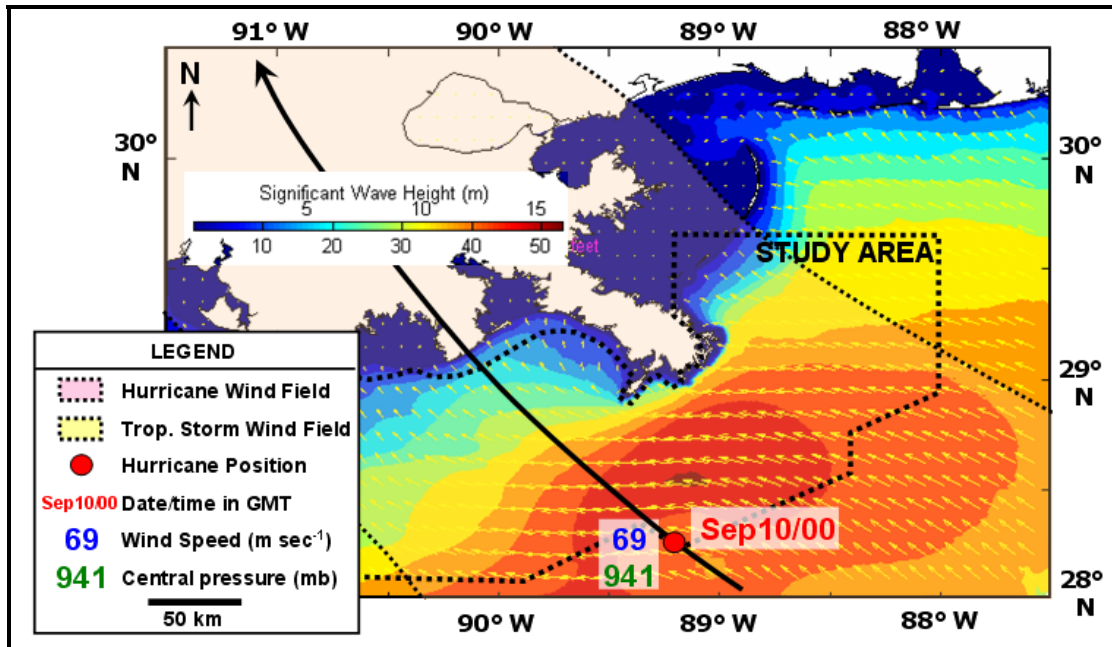


Figure 49:  $H_{s,max}$ , Hurricane Betsy, September 10, 1965 0000Z  
as modeled through MIKE 21 numerical wave model

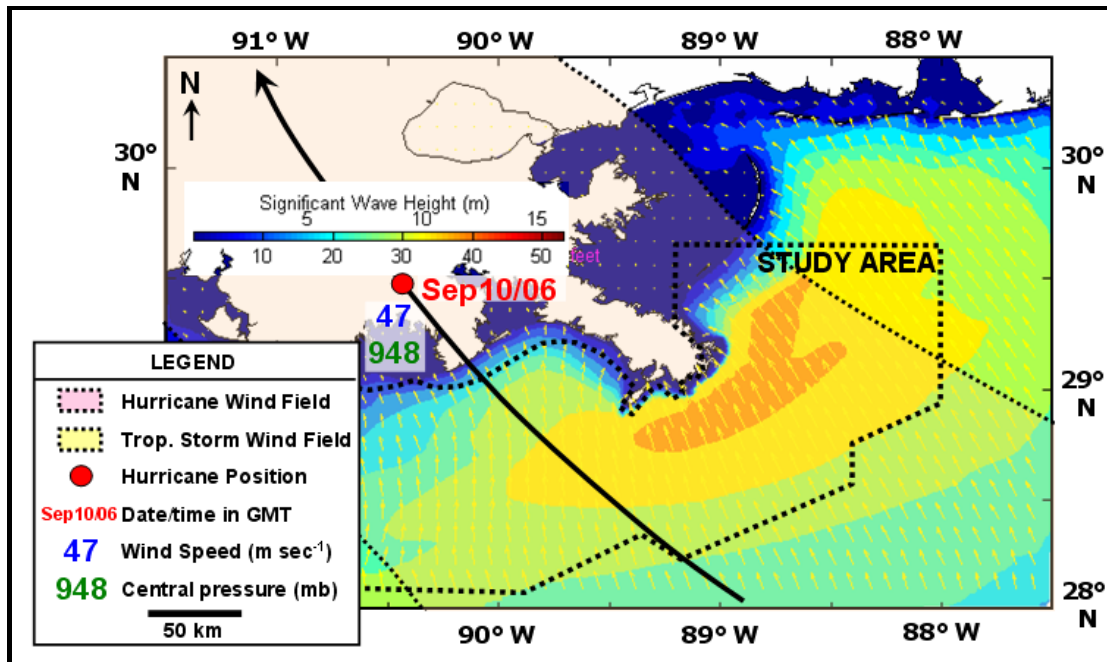


Figure 50:  $H_{s,max}$ , Hurricane Betsy, September 10, 1965 0600Z  
as modeled through MIKE 21 numerical wave model

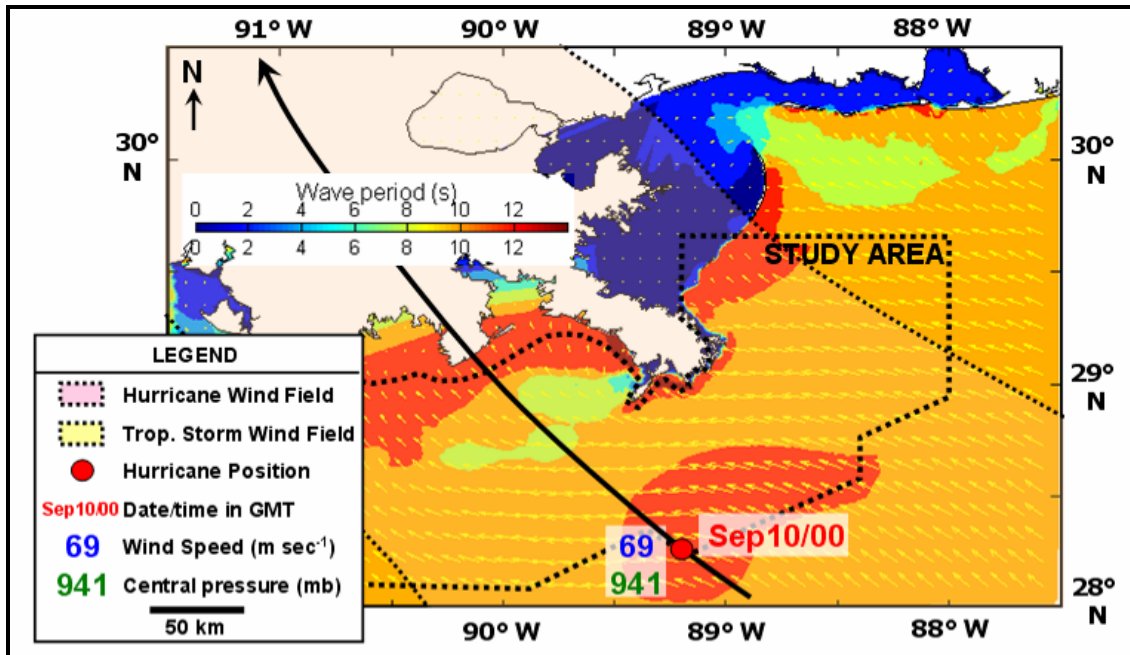


Figure 51: Wave period T02 (zero-crossing), Hurricane Betsy, September 10, 1965 0000Z as modeled through MIKE 21 numerical wave model

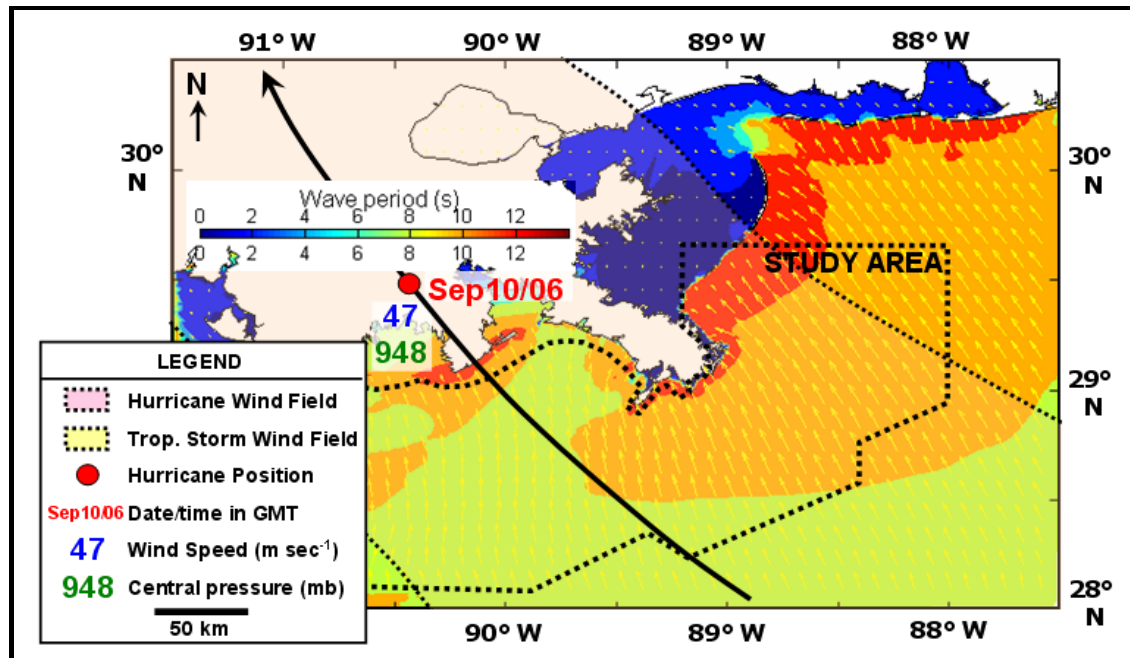
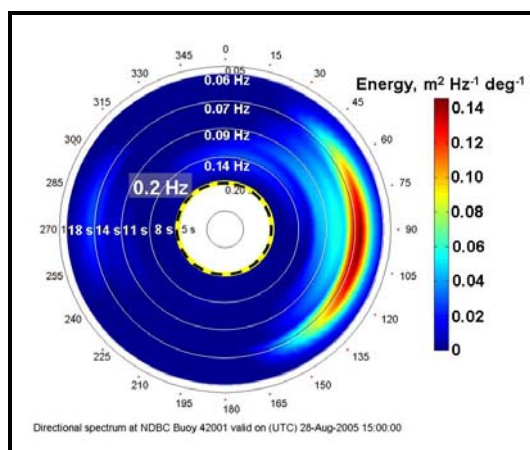
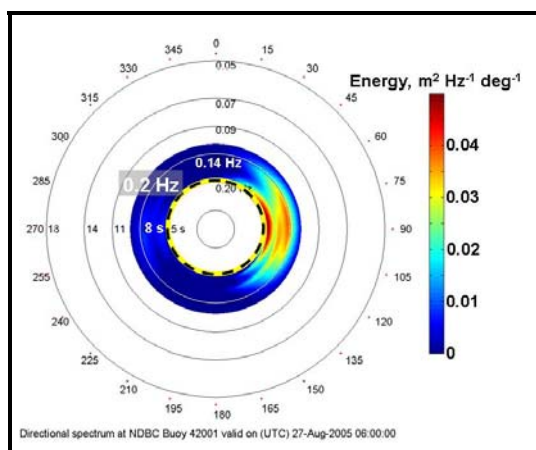
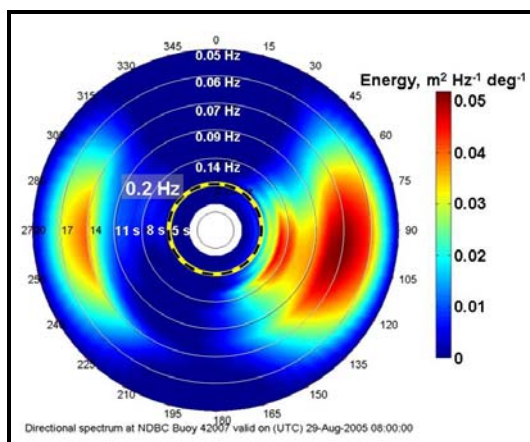
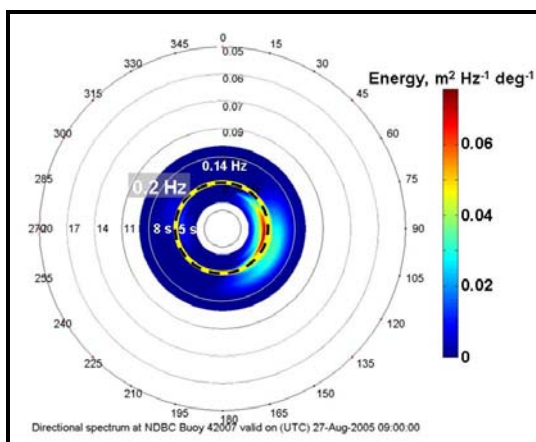
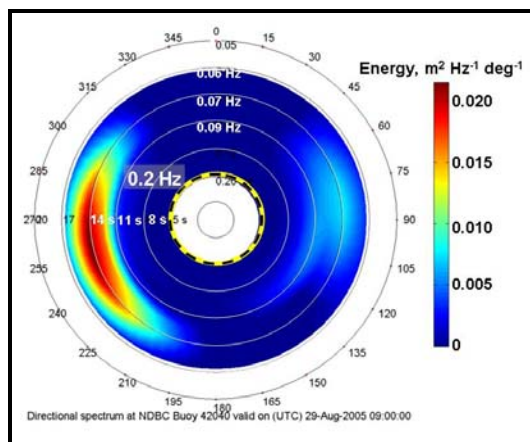
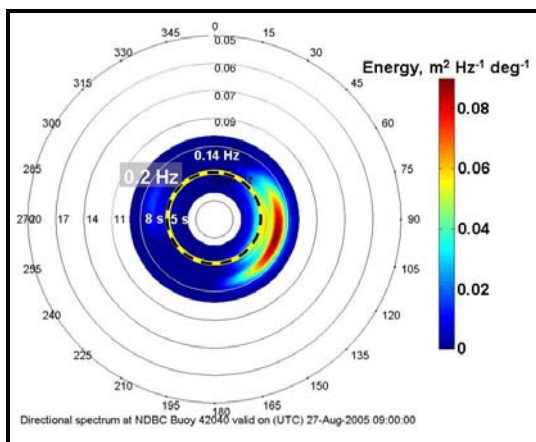


Figure 52: Wave period T02 (zero-crossing), Hurricane Betsy, September 10, 1965 0000Z as modeled through MIKE 21 numerical wave model

decomposed through a Fast-Fourier Transform and the resulting irregularity can be expressed as the frequency domain of wave spectra (Daemrich et al., 2004). Hurricanes produce complex and varying wave spectra in space and time, and these data provide valuable information regarding wave direction and frequency, such as that revealed during Hurricane Bonnie in 1998 (Moon et al., 2003).

Spectral wave density data were recorded at selected locations during Hurricanes Andrew, Ivan and Katrina (DiMarco et al., 1995; Jose and Stone, 2006) and complement the observed metocean conditions described earlier. The utility of these directional wave spectra was illustrated by Sheremet and Stone (2003) whereby low- and high-frequency waves were differentiated with respect to wave bottom interaction on a muddy shelf in Atchafalaya Bay off the Louisiana coast during winter storms. Frequency bands of less than 0.2 Hz (or 5 sec period) were considered low-frequency (i.e., longer period) waves whereas frequency bands higher than 0.2 Hz were considered high-frequency (i.e., shorter period) waves (Sheremet and Stone, 2003).

During Hurricane Katrina, spectral data were collected at NDBC Buoys 42001, 42007 (although the buoy failed mid-storm) and 42040 (Figures 53-58; see Table 8, Section 5.2.1, for the closest distance of each buoy relative to Katrina's path). A transition from higher-frequency to lower-frequency waves can be seen as Hurricane Katrina approached all three buoys. Frequencies from Buoys 42040 and 42007 some 48 hours before proximal passage indicate a range of slightly less than 0.20 Hz to 0.14 Hz from the east and southeast (Figures 53 and 55). Pre-storm spectra were not recorded at lower frequencies for these buoys during Katrina; however, they likely portray the available wave spectra accurately. At peak hurricane proximity to each buoy, frequencies decreased to nearly 0.06 Hz (Figures 54 and 56). These frequencies roughly correspond to wave periods of 16-17 sec and compare favorably to periods measured during Katrina (NDBC, 2008). The directional spectra measured from data recorded at these two buoys also shift from mostly easterly to both easterly and westerly as Katrina approached and then moved past the buoys (Figures 54 and 56). In addition, the easterly wave component from



Buoy 42007 displays a relatively wider frequency range at the point of closest hurricane approach, with values ranging from 0.14 Hz to 0.06 Hz. This buoy is located in relatively shallow water (13.7 m) close to the Mississippi coast (approximately 45 km; NDBC, 2009).

Data for Buoy 42001 at lower frequencies (i.e., less than 0.20 Hz) are not available; however the data suggest that frequencies some 24 hours prior to proximal hurricane passage ranged from 0.20 Hz to approximately 0.14 Hz from the east (Figure 57). At proximal hurricane passage, frequencies ranged from 0.65 Hz to 0.70 Hz from the east and east-southeast and likewise correspond to wave periods of about 16-17 sec (Figure 58).

The spectral evolution of wave energy during Hurricane Katrina is captured in measurements of the log of spectral wave density, in units of  $\text{m}^2 \text{Hz}^{-1} \text{deg}^{-1}$ , at Buoys 42040 and 42001 (Figures 59 and 60). The onset of the first high-frequency waves during Katrina occurred on August 25, four days prior to Katrina's eventual landfall. This wave energy persisted throughout and transitioned to lower-frequency wave energy by August 28-29, 2005 as the hurricane approached the Louisiana coast. Normal sea-state conditions were reestablished by September 3, about four days after landfall. Three days later, on September 6, 2005 a period of lower-frequency wave energy emanated from Hurricane Ophelia, a Category 1 hurricane that moved northward off the east coast of Florida (Figures 59 and 60). Normal sea-state conditions were again reestablished by September 9, 2005.

The spectral data that best illustrate wave frequency response during Hurricane Ivan were obtained from NDBC Buoys 42001, 42007 and, although it failed mid-storm, Buoy 42040 (Figures 61-66; see Table 8, Section 5.2.1, for the closest distance of each buoy relative to Ivan's path). As with Hurricane Katrina, a transition from higher-frequency to lower-frequency spectra can be seen as Hurricane Ivan approached Buoys 42040 and 42007. Frequencies about 36 hours before proximal passage indicate a range of less than 0.2 Hz to about 0.09 Hz from the southeast and south-southeast (Figures 61 and 63). At peak proximity to each respective buoy, frequencies decreased to nearly 0.06 Hz from the east and southeast (Figures 62 and 64). These frequencies



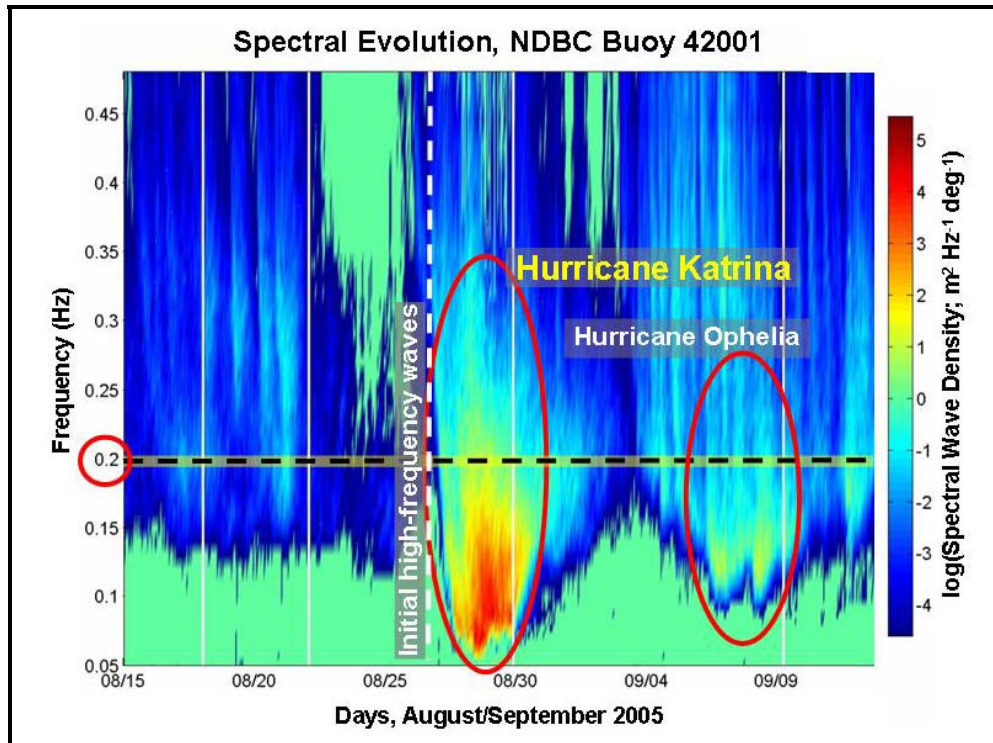


Figure 59: Spectral evolution, NDBC Buoy 42001, Hurricanes Katrina and Ophelia, 2005

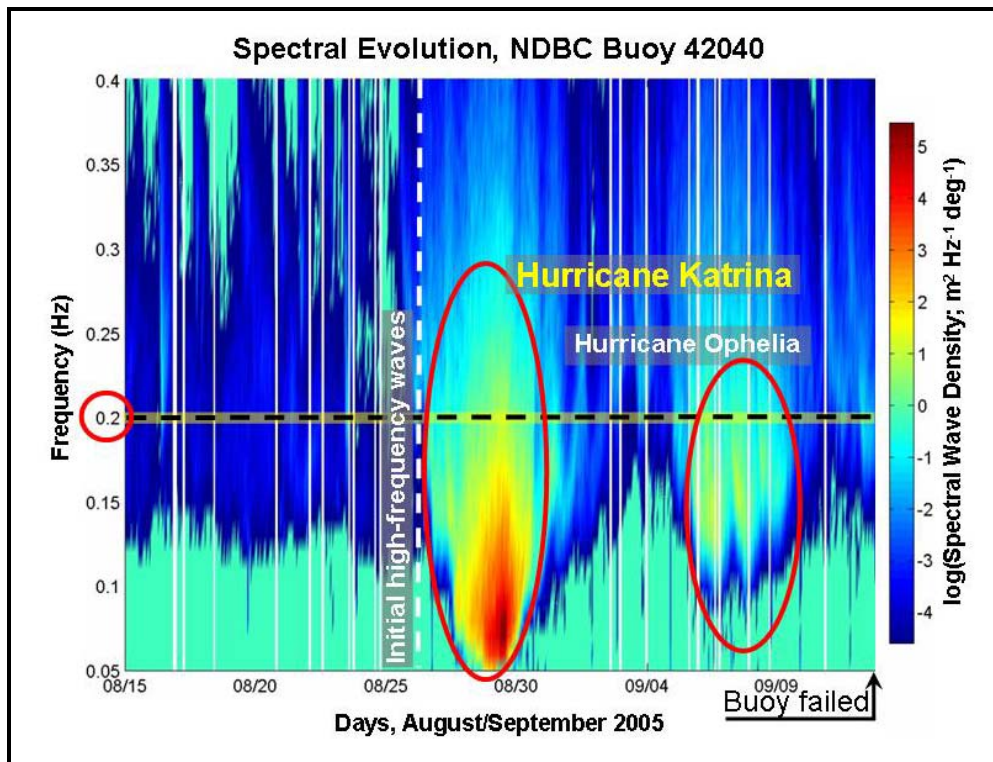


Figure 60: Spectral evolution, NDBC Buoy 42040, Hurricane Katrina and Ophelia, 2005

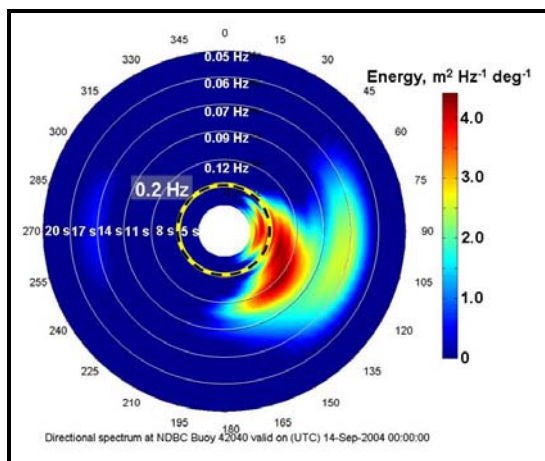


Figure 61: Directional wave spectra, NDBC Buoy 42040, September 14, 2004, 0000 Z

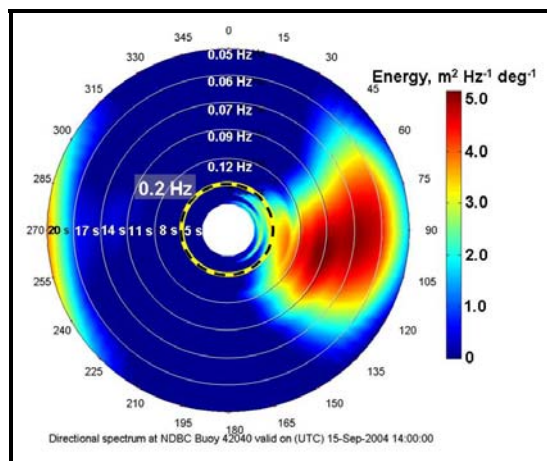


Figure 62: Directional wave spectra, NDBC Buoy 42040, September 15, 2004, 1400 Z

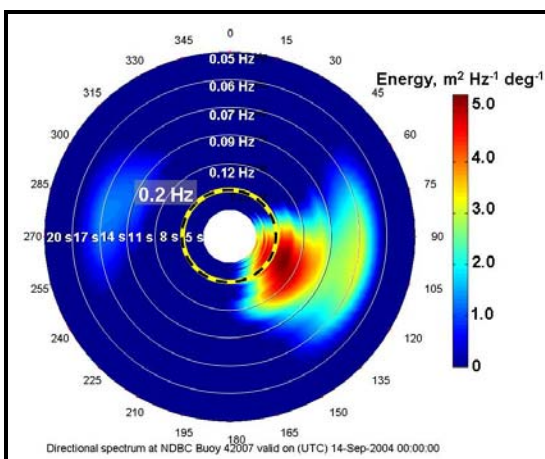


Figure 63: Directional wave spectra, NDBC Buoy 42007, September 14, 2004, 0000 Z

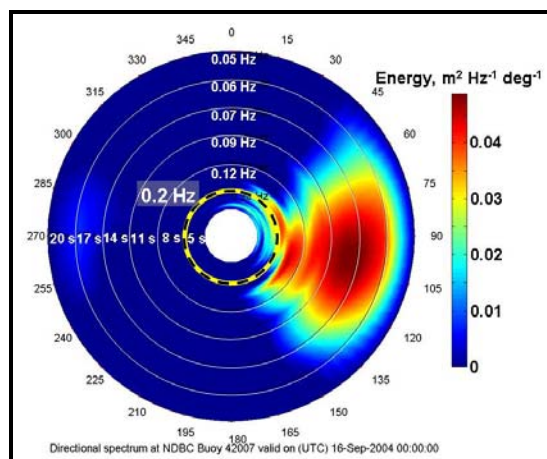


Figure 64: Directional wave spectra, NDBC Buoy 42007, September 16, 2004, 0000 Z

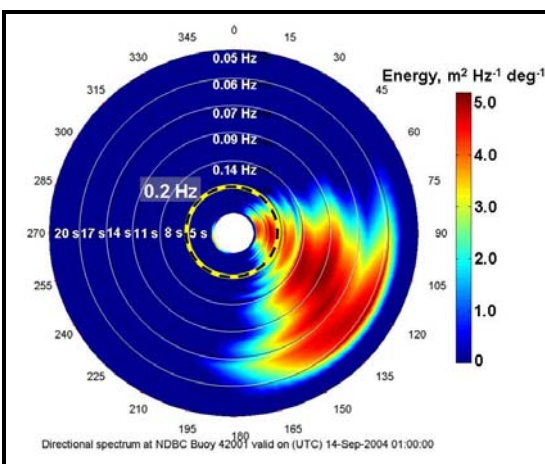


Figure 65: Directional wave spectra, NDBC Buoy 42001, September 14, 2004, 0100 Z

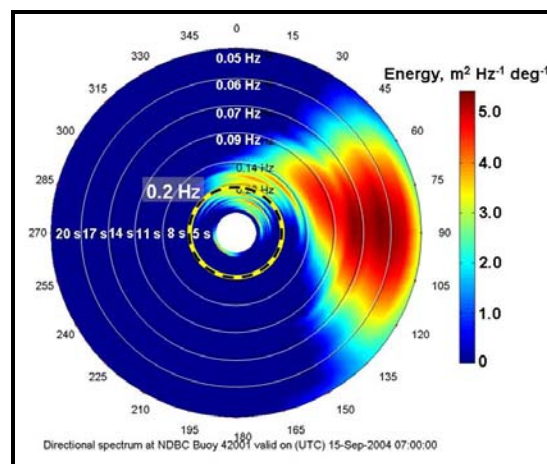


Figure 66: Directional wave spectra, NDBC Buoy 42001, September 15, 2004, 0700 Z

roughly correspond to wave periods of about 17 sec and compare favorably to wave periods measured during Ivan (NDBC, 2009).

Pre-storm spectra for Hurricane Ivan at Buoys 42040 and 42007 appear bimodal (Figures 61 and 63). Two foci of energy appear, one from about 0.12 Hz to 0.20 Hz, and another around 0.07 Hz. This may represent a combination of remotely generated swells and local wind-generated sea waves. Whalen and Ochi (1978) described how the distribution of wave spectra typically transitions from bimodal as hurricanes approach a recording site to unimodal as they move closer (i.e., during storms). These observations were affirmed by Young (1998; 2003) in a study of 16 hurricanes off the northwest coast of Australia whereby pre-storm and proximal conditions displayed bimodal and unimodal frequencies, respectively, in cases where the spectra were recorded within eight times the radius to maximum winds of the hurricane center. Pre-storm spectra for Buoy 42001 were not recorded far enough in advance to fully differentiate pre-storm and proximal storm effects and therefore a bimodal frequency distribution is not displayed (Figure 65).

In addition, the spectra display a wide spatial variation of wave frequencies at proximal hurricane passage relative to each buoy. Even at the height of the storm, wave spectra retain the high frequencies first encountered several days prior to Ivan's passage (Figures 62, 64 and 66). Wright et al. (2001) described how a wide spatial variation of wave components can be ascribed to primary, secondary and tertiary wave fields based on wave height using Hurricane Bonnie (1998) as an example. Hurricane Ivan traversed the GOM in only 42 hours (relative to Hurricane Katrina, which traversed the GOM in 75 hours with a more intense wind field). During that relatively short time period, multiple GOM wave fields may derive from pre-storm, remotely generated swell combined with local wind-generated waves could be present and remain active for the duration of the hurricane until the return to normal sea-state conditions.

Directional spectra measured at Buoy 42001 display similar trends as the other two buoys (i.e., higher-frequency wave spectra transitioning to lower-frequency spectra with hurricane



passage; Figures 65 and 66). However, in this case it appears that this is mainly due to the dissipation of high-frequency waves relative to those of lower frequencies, which are present throughout the observation period.

The spectral evolution of wave energy during Hurricane Ivan is best captured in measurements (log of spectral wave density, integrated over the directional domain and expressed in  $\text{m}^2 \text{Hz}^{-1}$ ) at Buoys 42040 and 42001 (Figures 67 and 68). The onset of the first high-frequency waves during Ivan occurred as early as September 10, six days prior to Ivan's eventual landfall and after Tropical Storm Frances moved through the northeastern GOM on September 5-6 as it crossed over Florida from the Atlantic. This wave energy persisted throughout and transitioned to lower-frequency wave energy by September 15-16 as the hurricane approached the Alabama coast. Normal sea-state conditions were reestablished by September 19, about three days after landfall. However, lower-frequency conditions returned by September 21 as Hurricane Ivan looped around the southeastern United States, crossed Florida back into the GOM, and made a secondary landfall in southwest Louisiana (Figure 67). Normal sea-state conditions then resumed by September 27, 2004.

As spectral data can be utilized to determine the relative timing and intensity of the sea-state in advance of and after the passage of severe hurricanes, any inference of hurricane severity based on the level of damage inflicted on land should be avoided. As has been shown in this chapter, the MRDF can be exposed to high-energy conditions several days in advance, yet hurricane intensity is often greatly reduced both within the 12-hour period prior to landfall (NHC, 2009; discussed in Section 3.3.5). In addition, hurricanes will be subject to surface friction once over land and they also no longer have access to warm ocean waters, both of which serve to reduce hurricane intensity. Conversely, if significant damage occurs on land, there may be many other factors that can influence whether submarine shelf failure occurs in the marine environment (e.g., hurricane approach angle and forward hurricane speed, both of which were discussed in Section 5.1.1).

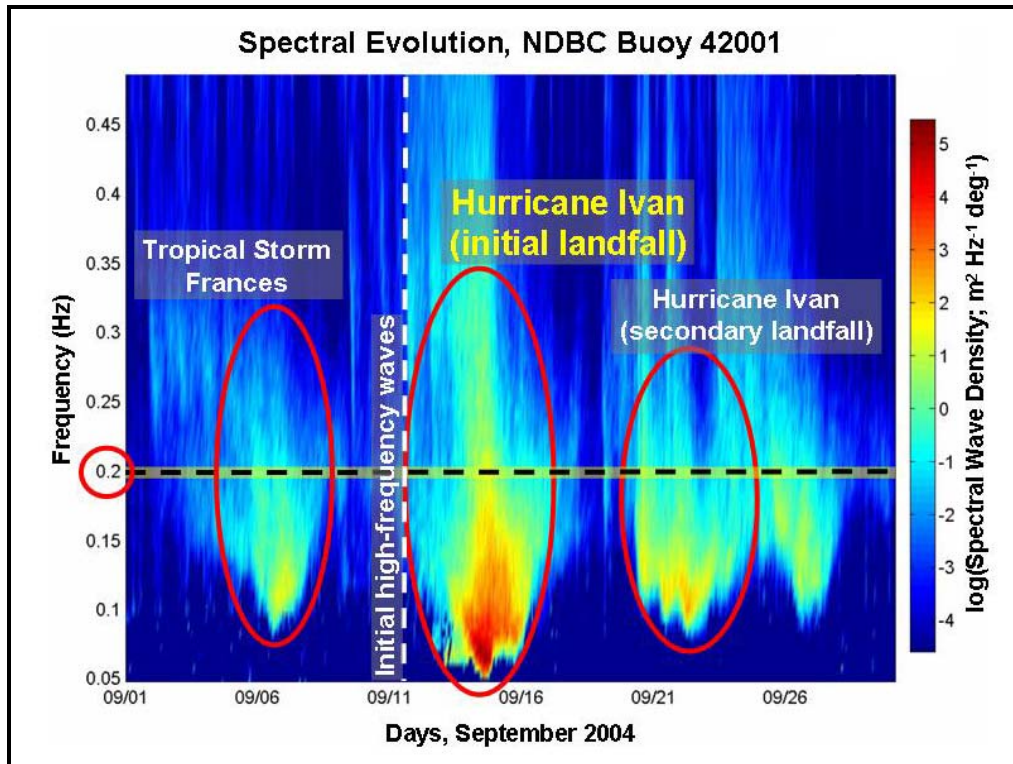


Figure 67: Spectral evolution, NDBC Buoy 42001, Hurricane Ivan, September 1-30, 2004

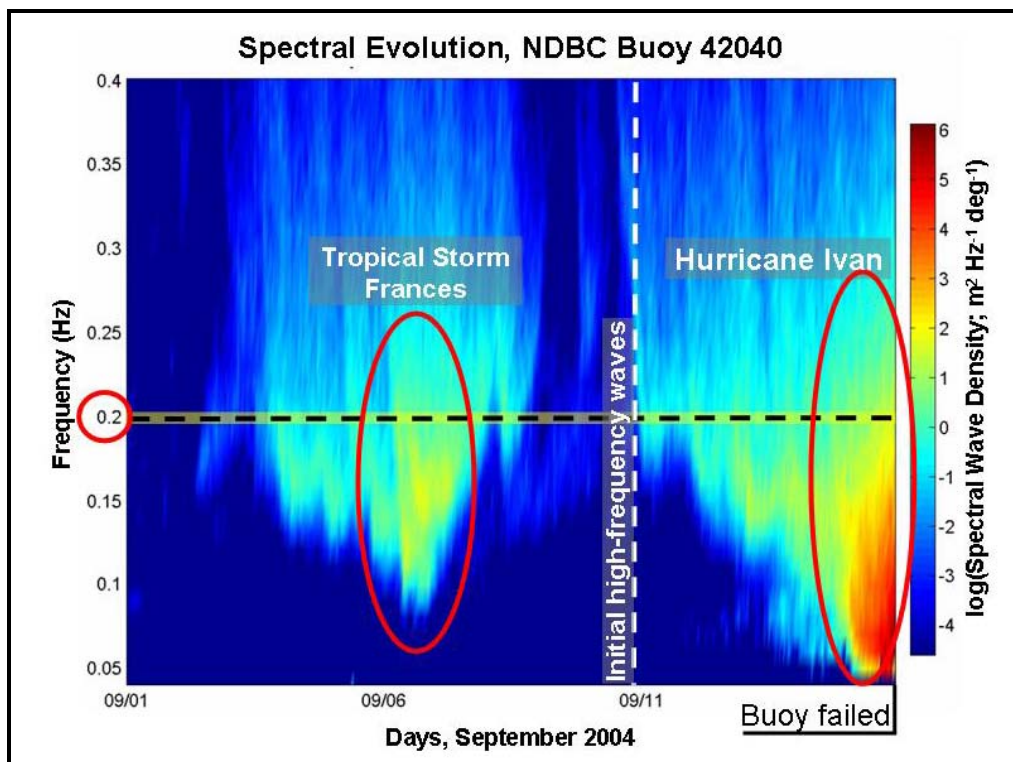


Figure 68: Spectral evolution, NDBC Buoy 42040, Hurricane Ivan, September 1-16, 2004

## **CHAPTER 6. LITHOLOGIC AND GEOTECHNICAL CONTROLS**

Seafloor lithology and surficial grain size vary across the Mississippi River Delta Front (MRDF) as evidenced in prior studies and in an array of geotechnical boreholes obtained since the 1950s (Dunlap et al., 2004). Grain size considerations have been examined across the Louisiana shelf in particular to evaluate the potential for wave dissipation across relatively finer-grained, muddy seafloors (Kraft et al., 1990; Sheremet and Stone, 2003; Sheremet et al., 2005). This dissertation addresses seafloor grain size variability as a possible control on wave dissipation during storm events and, therefore, on the potential for subsequent MRDF shelf failure.

Likewise, the complex stratigraphic history of the MRDF yields significant variability in subsurface geotechnical properties (Helwick and Bryant, 1978). Shear strengths, water content, and corresponding bulk density coupled to void space parameters can be used as indicators of MRDF depositional history and prior shelf failure, and can help delineate the extent to which the seafloor underwent morphological change. These combined properties govern controls on the extent to which subaqueous shelf failure occurs and can be demonstrated in a series of 1D sediment failure models.

### **6.1 MRDF Seafloor Characterization**

#### **6.1.1 Sedimentologic History and Depositional Parameters**

The MDRF is subject to excessive sedimentation rates, receiving approximately  $2.1 \times 10^8$  tons of sediment annually (Milliman and Meade, 1983; Meade, 1996). As a result, the shelf edge has prograded approximately 15 km in the last 15,000 years, and sediment deposited during the past 500 years covers an area of approximately  $1800 \text{ km}^2$  with a volume of approximately  $90 \text{ km}^3$  (Trabant et al., 1979).

Sediment accumulation varies considerably across the MRDF, especially nearest the distributary mouths. Sedimentation rates within interdistributary bays total only a few  $\text{cm yr}^{-1}$  yet point accumulation estimates near river mouths range from approximately 70 cm during seasonal flood events to more than 4 m during extreme floods (Coleman et al., 1980b). In addition,

progradation rates proximal to distributary mouths have been measured over  $100 \text{ m yr}^{-1}$ . These high sedimentation rates contribute significantly to the existence of underconsolidated sediments, relatively steep seafloor slopes and the formation of biogenic methane, all of which can lead to unstable morphologic conditions and ultimately to seafloor failure (Adams and Roberts, 1993). These conditions provide a catalyst for failure even in non-storm conditions. The aim of this research is to document the extent to which seafloor failure can be exacerbated during storm conditions.

The study area has been greatly influenced by cycles of subsidence and glacio-eustatic fluctuations in sea level that resulted in cyclic sea level rise and fall throughout the Quaternary (Ludwick, 1964; Frazier, 1974; Kindinger, 1988). The broader area nearer the MRDF is one of two distinct regions delineated by Mazzullo and Bates (1985) on the basis of surficial grain morphology and age. East of the MRDF the shelf is covered by a layer of relict fine-to-medium quartzose sand of late Pleistocene and early Holocene age that fines westward. These sediments were deposited by rivers of the southeastern United States that drain into the northeastern GOM and subsequently carried westward by net longshore transport along the coast (Stone and Stapor, 1996). Surficial sediments comprising this layer are typically composed of >90% sand, <2.7% mud and <2% granules (McBride and Byrnes, 1995). Farther westward and closer to the MRDF, the shelf is covered by Holocene sand, silt and clay associated with Mississippi River deposition (Ludwick, 1964; Mazzullo and Bates, 1985).

The depositional framework across the eastern part of the study area has also been impacted by a series of shelf-edge deltas active during periods of lower sea level (Suter and Berryhill, 1985; Coleman and Roberts, 1988a, 1988b; Sager et al., 1999). The existence of these shelf-edge deltas has been implied in previous studies by lobes in shelf break morphology (McBride and Byrnes, 1995). One of the more prominent of these deltas is the Lagniappe Delta, located east of the MRDF (Figure 69). This delta formed during a fall in sea level prior to the last glacial lowstand during the late Wisconsinan (Kindinger, 1988; 1989; Sydow and Roberts, 1994).

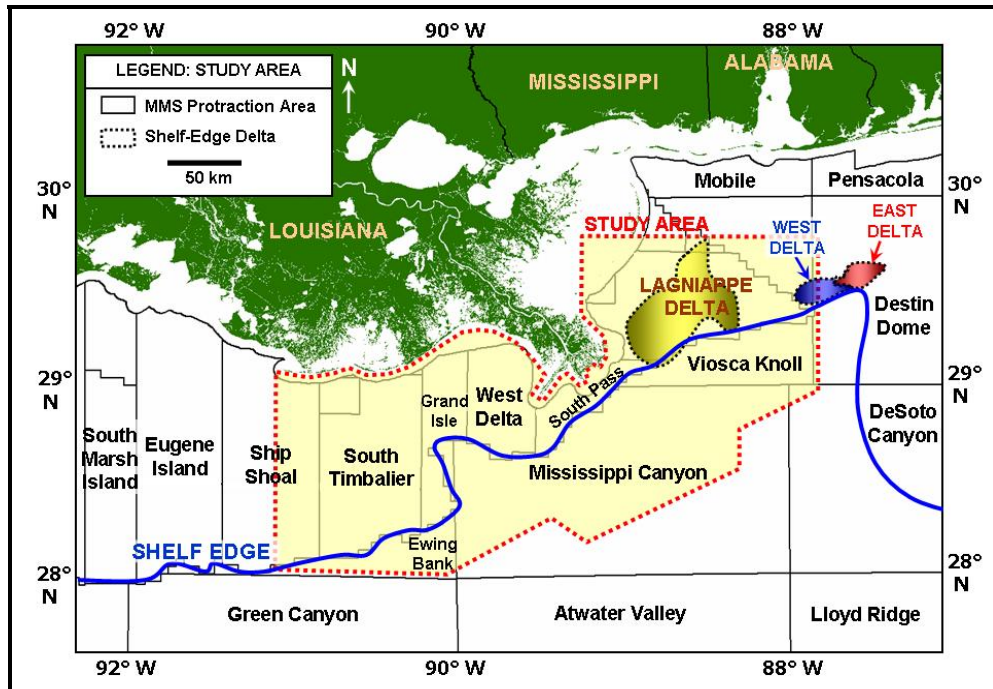


Figure 69: Location of shelf-edge deltas in proximity to MRDF study area (modified from Kindinger, 1989 and Sager et al., 1999)

A prominent shelf-wide erosional unconformity at the top of the Lagniappe Delta represents a boundary with overlying transgressive deposits and deltaic sediments of the St. Bernard Delta complex (Kindinger, 1988, 1989; Kindinger et al., 1989).

### 6.1.2 Lithologic Characterization

Surficial and near-surface sediment information in the north-central GOM was collected from several sources. The usSEABED database, maintained by the United States Geological Survey and described in Section 4.1.3, was one of two databases used to characterize surficial lithology in the study area (Buczkowski et al., 2006). Data within the study area are comprised of 1675 grain size data collection points and were subsequently mapped to illustrate grain size distribution (Figure 70). The raw data were also used to determine grain size and lithologic controls for the MIKE 21 numerical wave models described in Chapter 5.

In addition to the usSEABED database, sediment grain size data were previously collected and mapped based on data from an array of geotechnical boreholes archived by the MMS (Dunlap et al., 2004; described in Section 4.1.3). These results highlighted the lithological

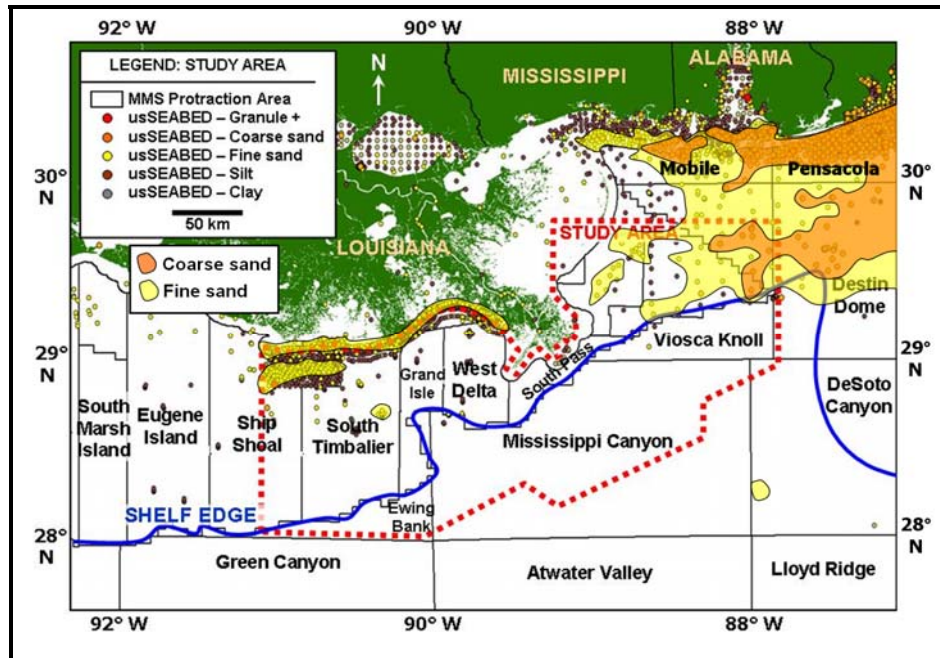


Figure 70: usSEABED grain-size data distribution, north-central Gulf of Mexico (raw grain-size data from Buczkowski et al., 2006)

variability that exists in the study area (Figure 71). Relatively coarser-grained, sandy material was found directly adjacent the Mississippi River Delta, in areas associated with several offshore shoals, and broadly across the shelf offshore Mississippi, Alabama and Florida. Sediment grain size data from these boreholes were used as inputs to the MIKE 21 numerical wave models described in Chapter 5.

## 6.2 MRDF Geotechnical Framework

A cross-sectional grid consisting of seven dip lines and two strike lines was created across the MRDF from available geotechnical borehole information (Figures 72-90). The orientation of these lines was chosen to best reflect a mix of available geotechnical borehole data, hurricane-induced seafloor failure from either Hurricanes Ivan or Katrina, and the availability of local and regional high-resolution bathymetry surveys of the seafloor archived through time. The lines were also laid out to illustrate varying morphologic factors that contribute to potential submarine mudslides, including proximity to higher sedimentation rates from the Mississippi River, position on the MRDF proper, and slope steepness (Figure 72).



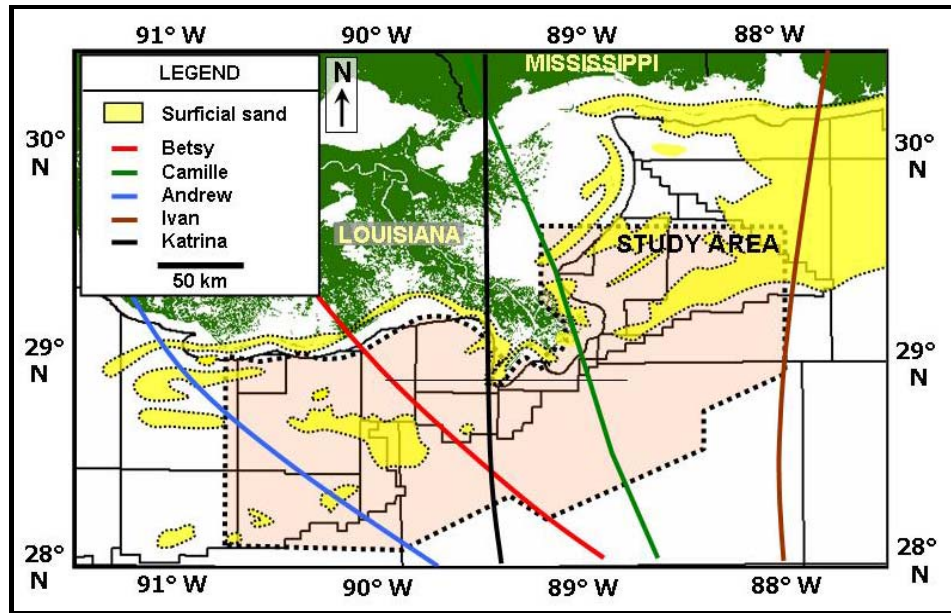


Figure 71: Surficial sands, north-central GOM coast (modified from Dunlap et al., 2004)

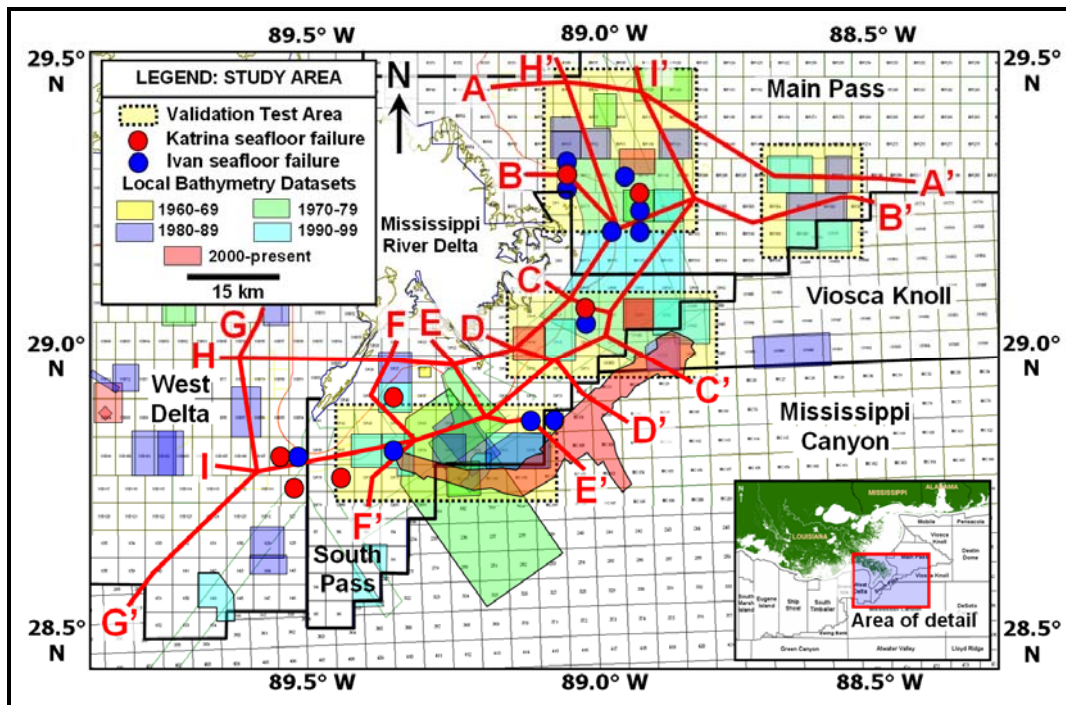


Figure 72: MRDF geotechnical borehole grid

Cross Section A-A' depicts a relatively stable platform area northeast of the present-day Mississippi River Delta (MRD; Figures 73 and 74). Although historical regional bathymetry data were not acquired this far north around the delta, regional bathymetry data (NOAA, 2009), together with local high-resolution (HR) data where available, indicate a broad apron punctuated

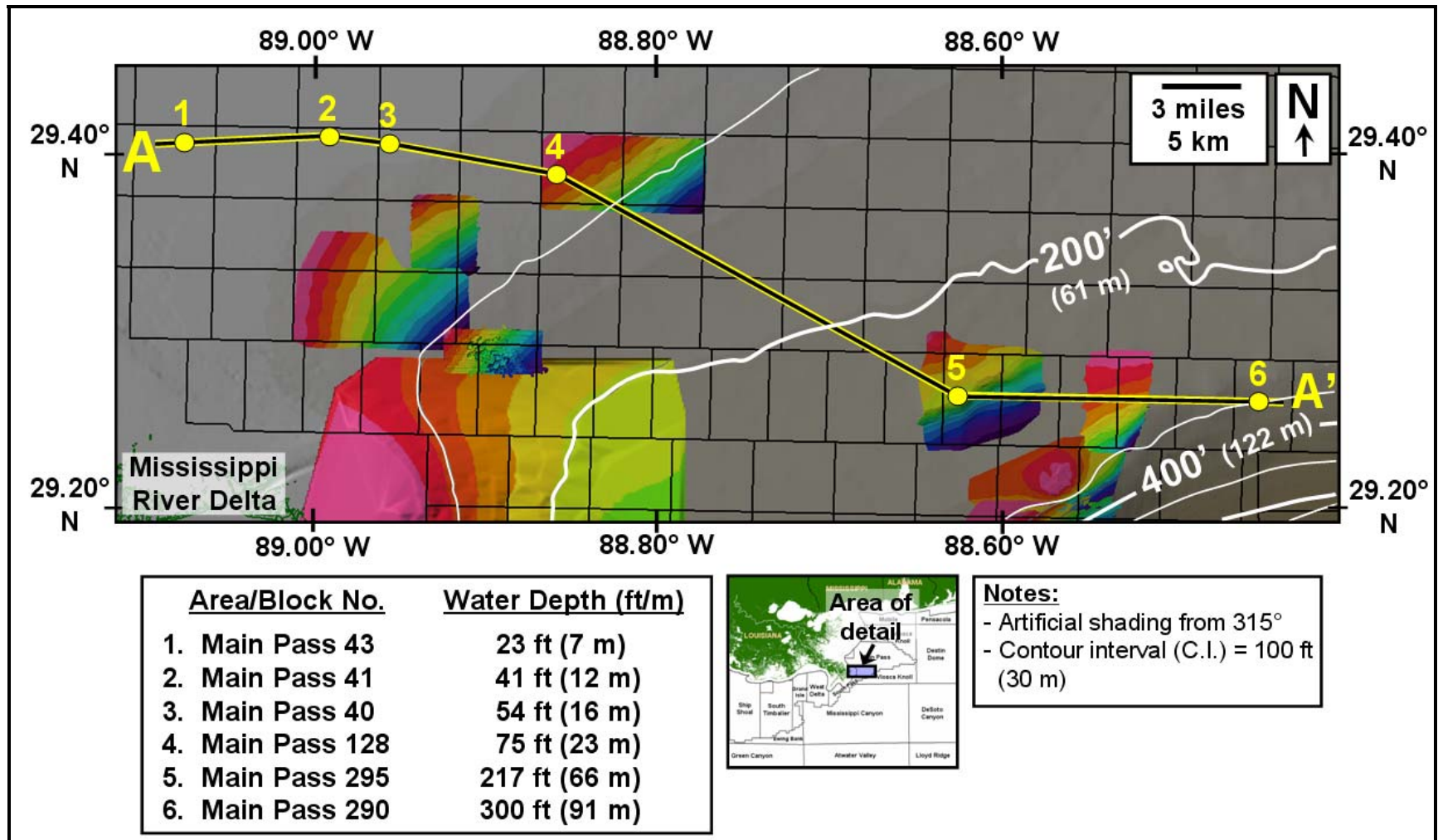


Figure 73: Bathymetry image along cross section A-A', Main Pass Area (high-resolution data from Vastar Resources, Inc., 1997a, John E. Chance & Associates, 1988a, 1989, 1994, and Fugro GeoServices, Inc., 2004 displayed on spectrum color bar; regional data from NOAA (2009) displayed on brown-to-blue color bar and fills gaps between high-resolution surveys)



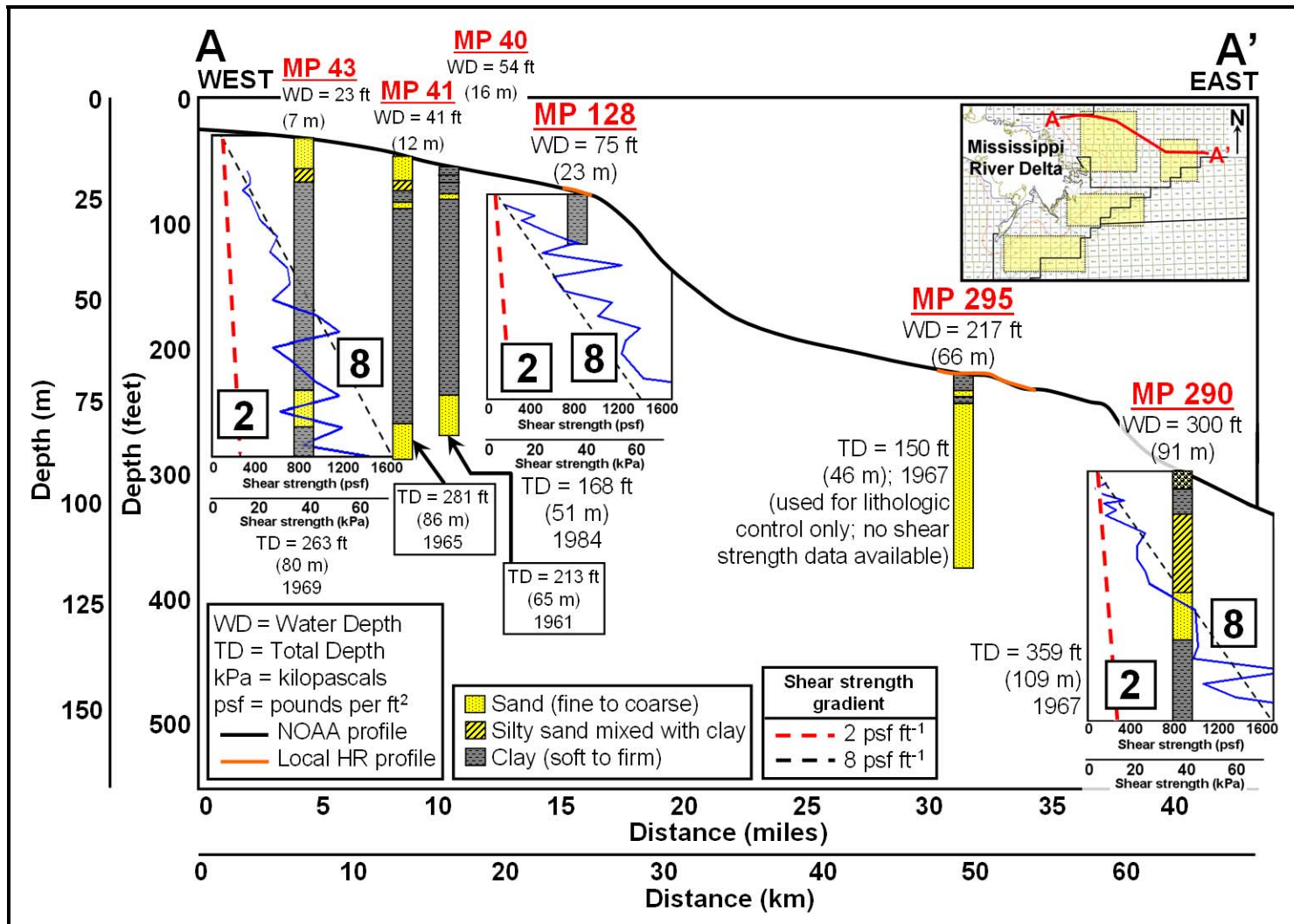


Figure 74: Geotechnical borehole cross section A-A', Main Pass Area, north-central Gulf of Mexico (vertical exaggeration ~400X; seafloor profiles derived from NOAA (2009) and local high-resolution (HR) bathymetry; 1874, 1940 and 1977 bathymetry not available in area)

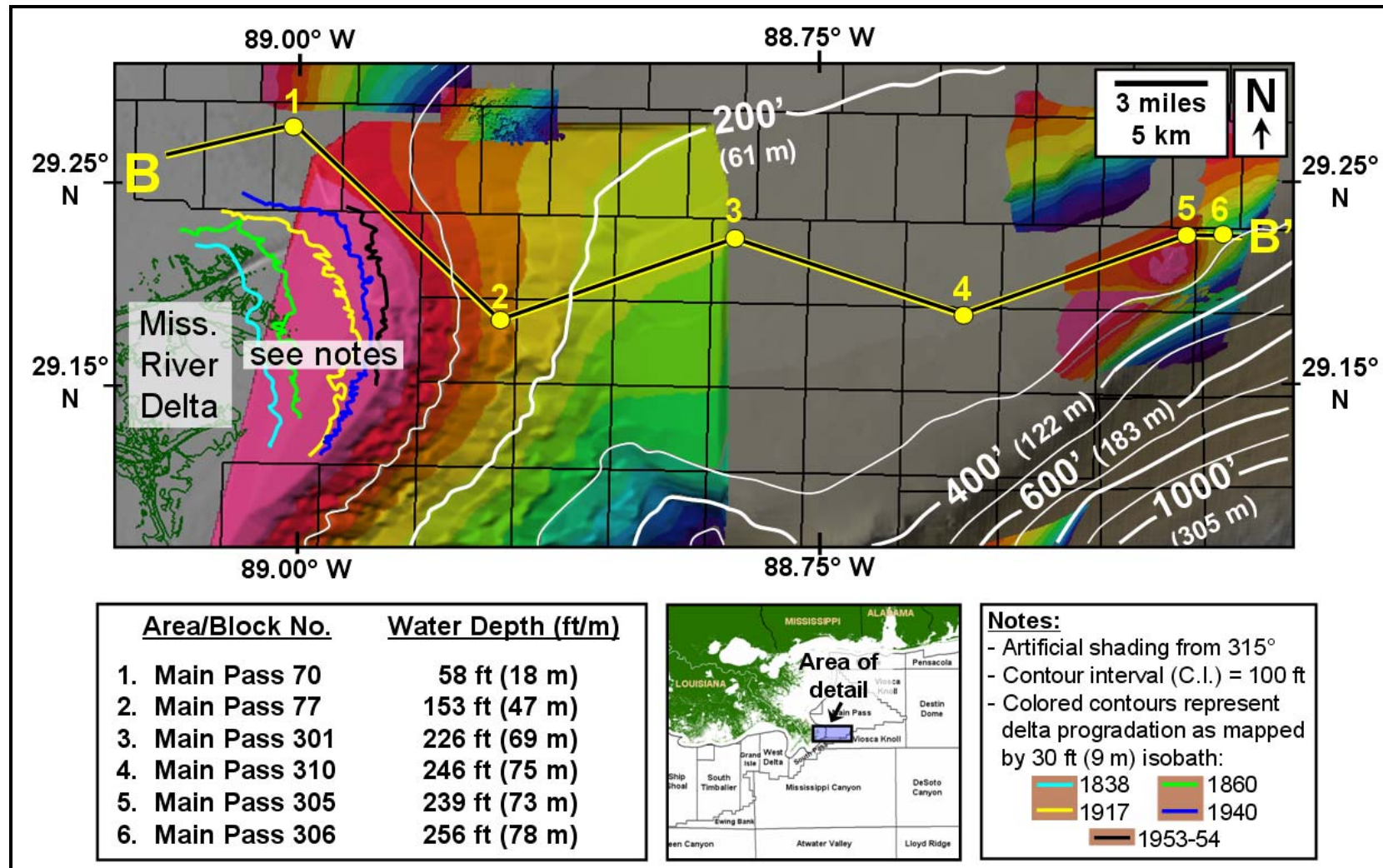


Figure 75: Bathymetry image along cross section B-B', Main Pass Area (high-resolution data from Vastar Resources, Inc., 1997a; John E. Chance & Associates, 1988a, 1989, 1994 displayed on spectrum color bar; regional data from NOAA (2009) displayed on brown-to-blue color bar and fills gaps between high-resolution surveys)

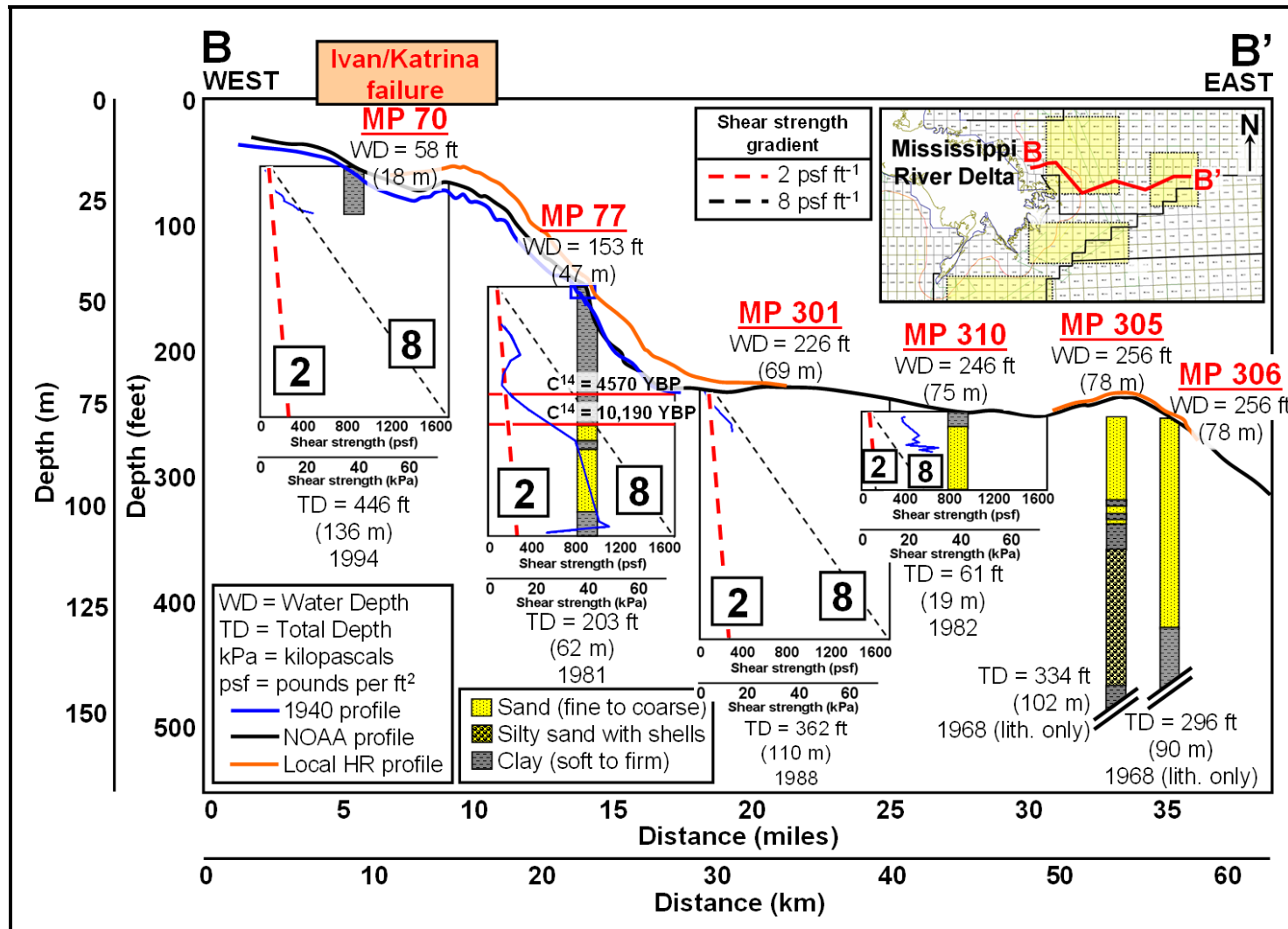


Figure 76: Geotechnical borehole cross section B-B', Main Pass Area, north-central Gulf of Mexico (seafloor profiles derived from Coleman et al., 1980, John E. Chance & Associates, 1988a, Vastar Resources, Inc., 1997a and NOAA, 2009)



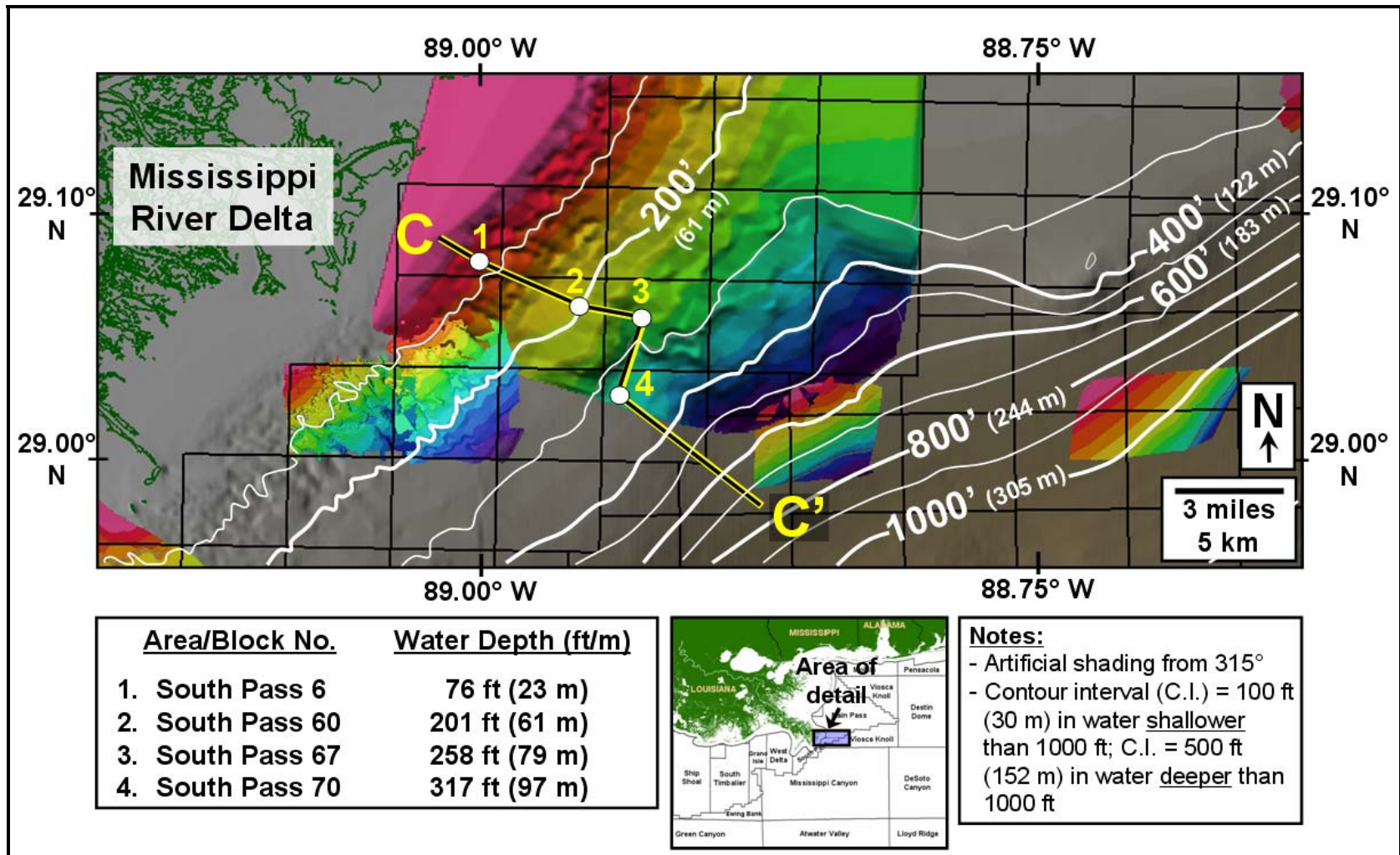


Figure 77: Bathymetry image along cross section C-C', South Pass Area (high-resolution data from John E. Chance & Associates, 1984a; Vastar Resources, Inc., 1995, 1997a, 1997b, Plains Resources, 2006 displayed on spectrum color bar; regional data from NOAA (2009) displayed on brown-to-blue color bar and fills gaps between high-resolution surveys)

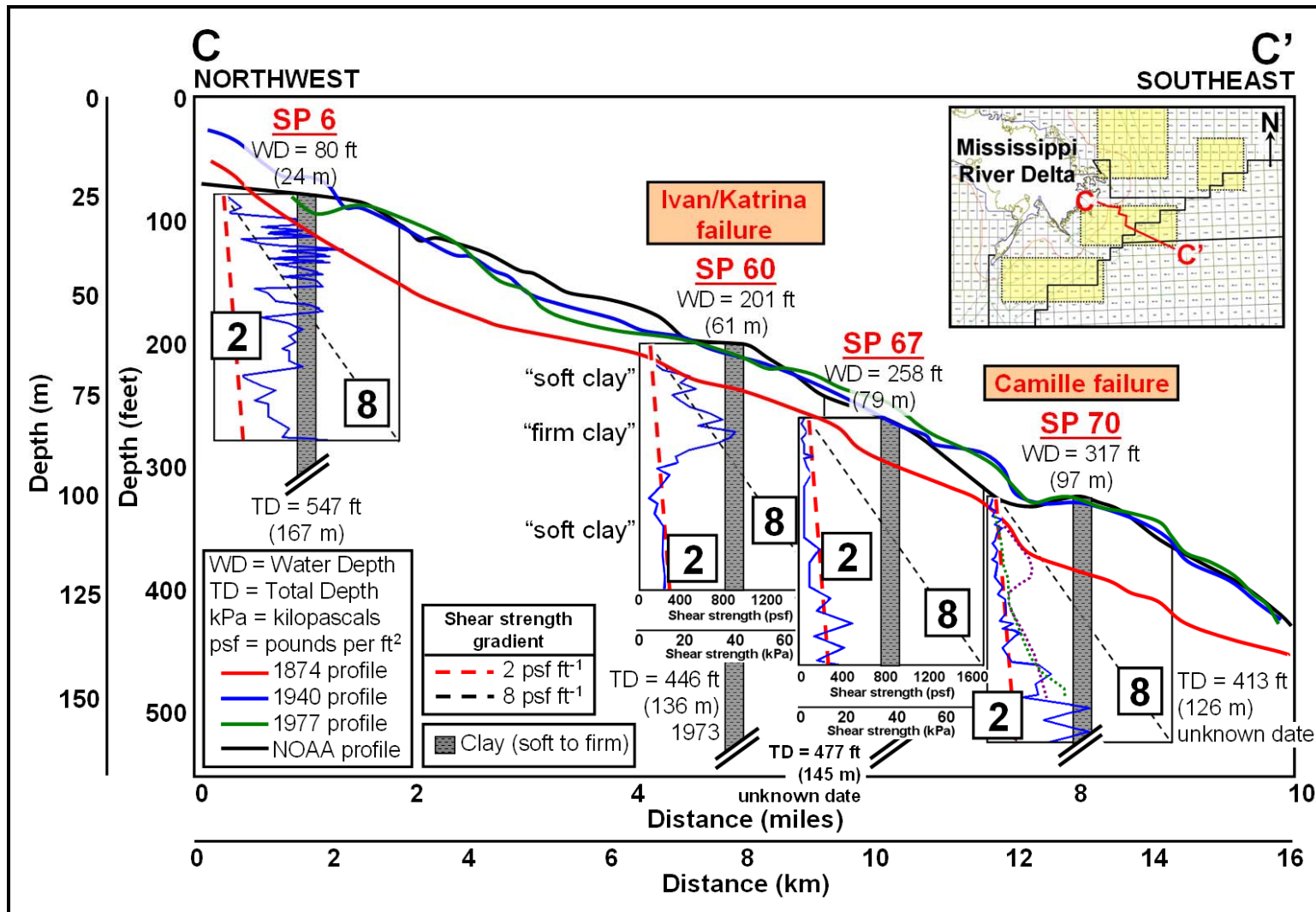


Figure 78: Geotechnical borehole cross section C-C', South Pass Area, north-central Gulf of Mexico (seafloor profiles derived from NOAA (2009) and 1874, 1940 and 1977 (Coleman et al., 1980) where available; dashed shear strengths on SP 70 profile from Bea et al., 1980)

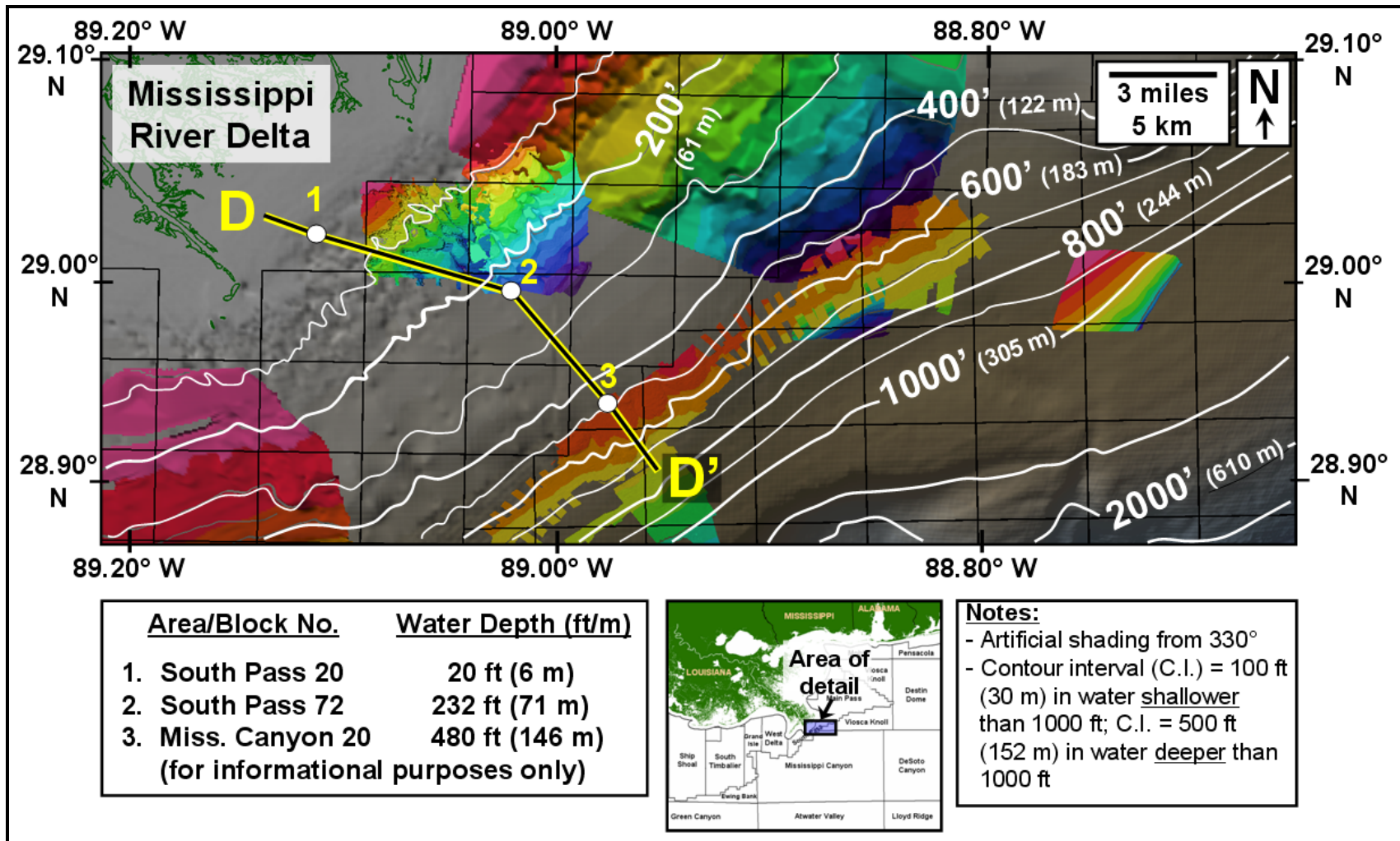


Figure 79: Bathymetry image along cross section D-D', South Pass Area (high-resolution data from John E. Chance & Associates, 1984a; Arco, 1990, 1991b; Vastar Resources, Inc., 1995, 1997a, 1997b, Enterprise Products Partners LLC, 2005; Plains Resources, 2006 displayed on spectrum color bar; regional data from NOAA (2009) displayed on brown-to-blue color bar and fills gaps between high-resolution surveys)



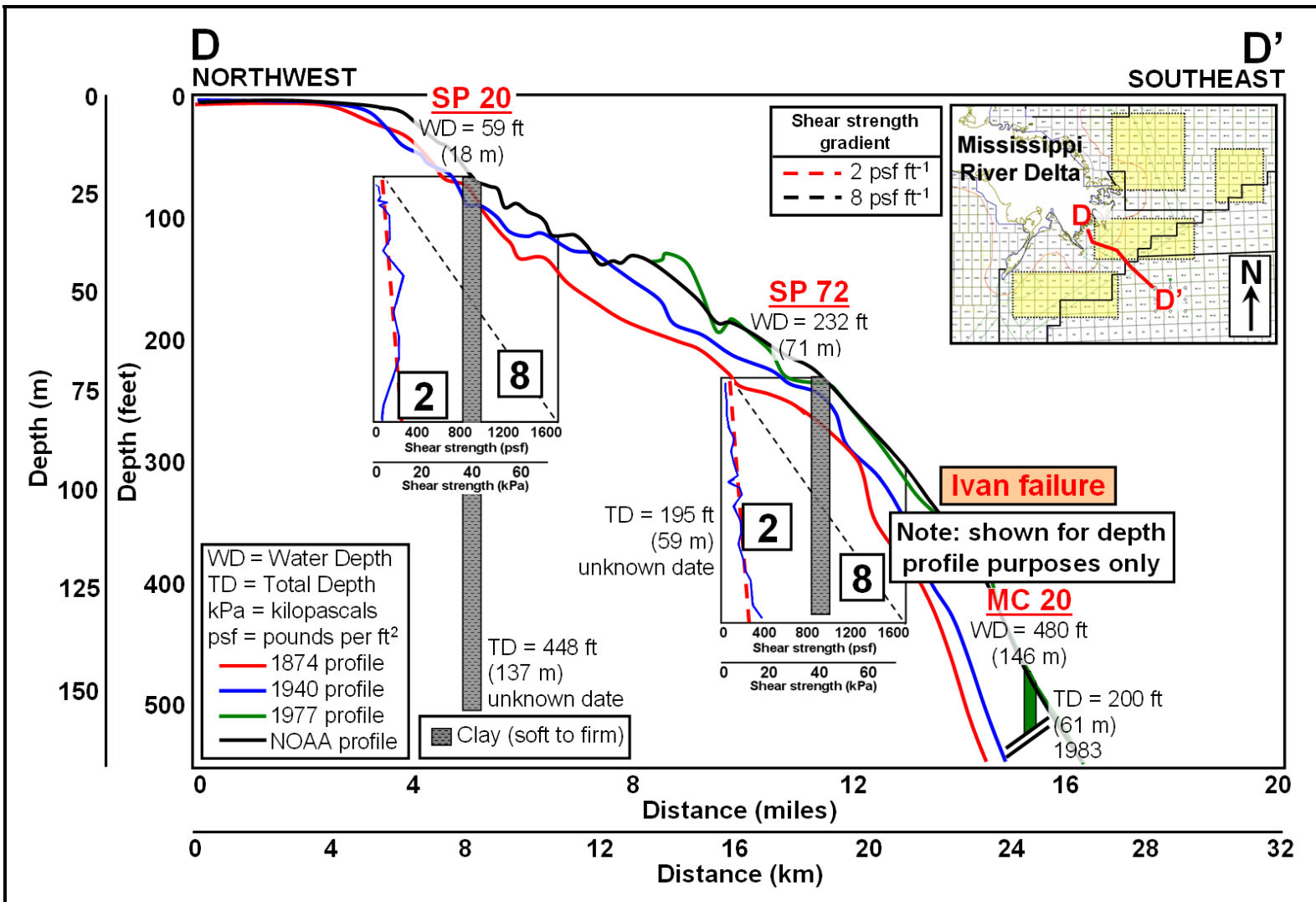


Figure 80: Geotechnical borehole cross section D-D', South Pass Area, north-central Gulf of Mexico (regional seafloor profiles derived from 1874, 1940 1977 (Coleman et al., 1980) and NOAA (2009) bathymetry data)

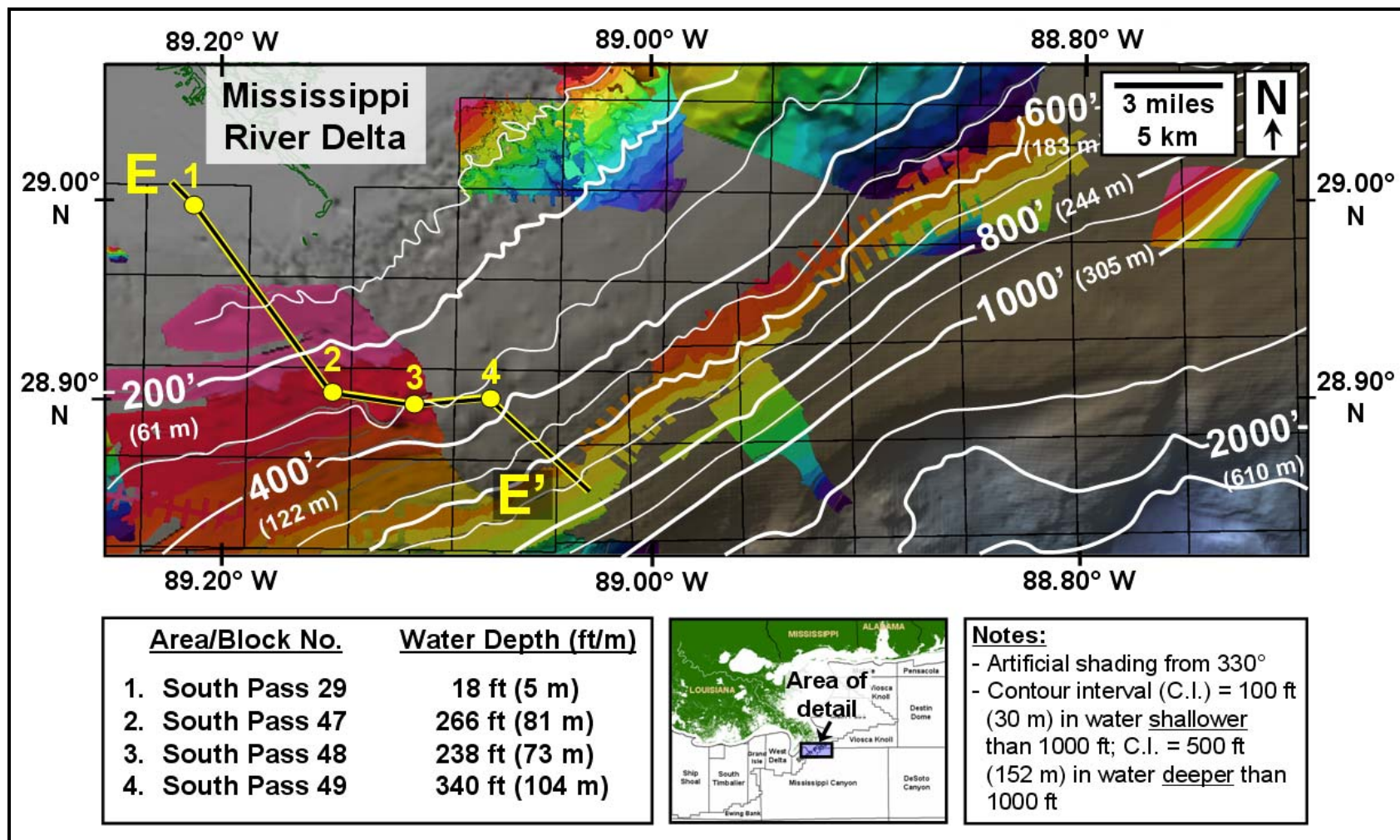


Figure 81: Bathymetry image along cross section E-E', South Pass Area (high-resolution data from John E. Chance & Associates, 1984a; Arco, 1990, 1991b; Vastar Resources, Inc., 1995, 1997a, 1997b, Enterprise Products Partners LLC, 2005; Plains Resources, 2006 displayed on spectrum color bar; regional data from NOAA (2009) displayed on brown-to-blue color bar and fills gaps between high-resolution surveys)



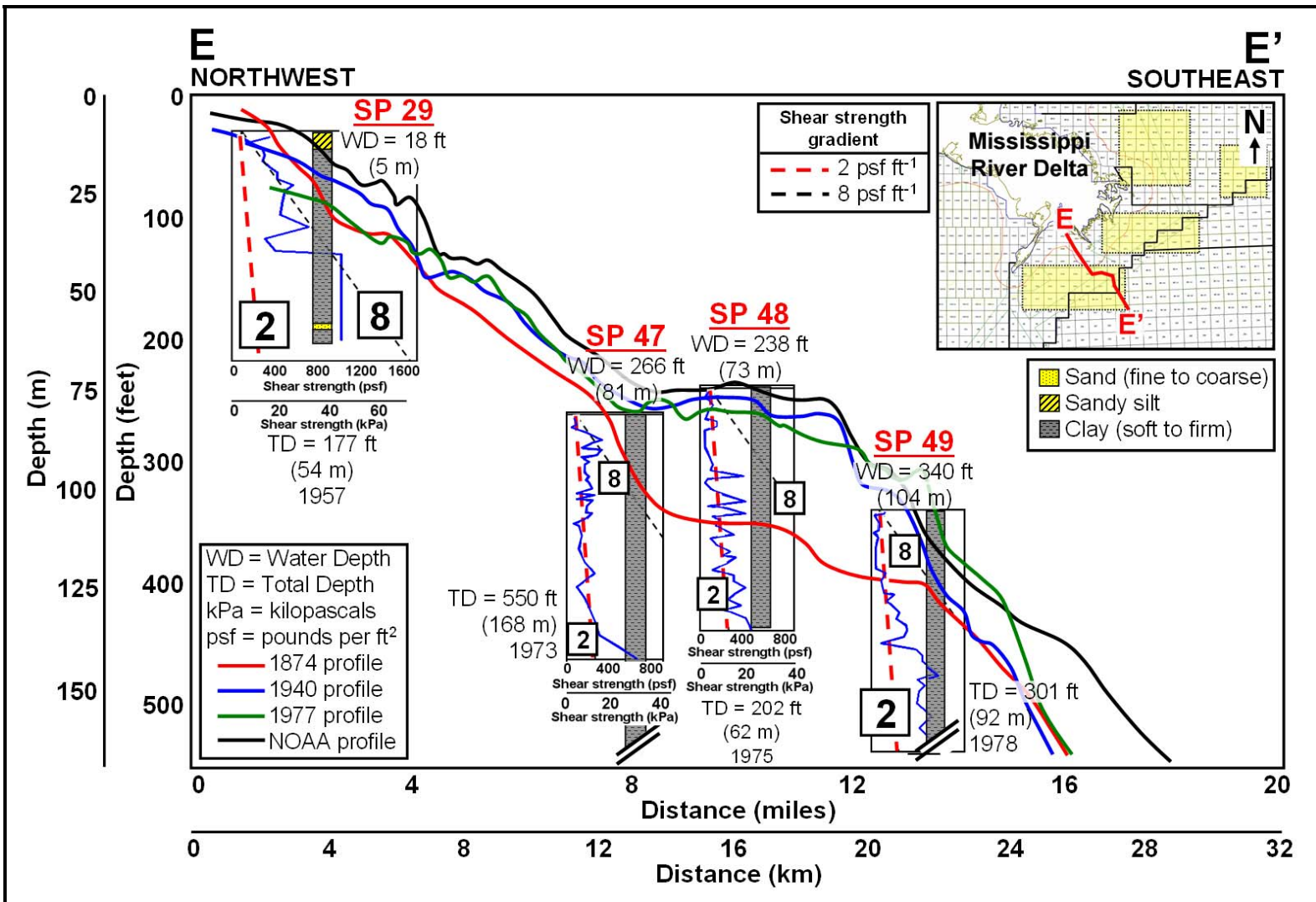


Figure 82: Geotechnical borehole cross section E-E', South Pass Area, north-central Gulf of Mexico (regional seafloor profiles derived from 1874, 1940 1977 (Coleman et al., 1980) and NOAA (2009) bathymetry data)

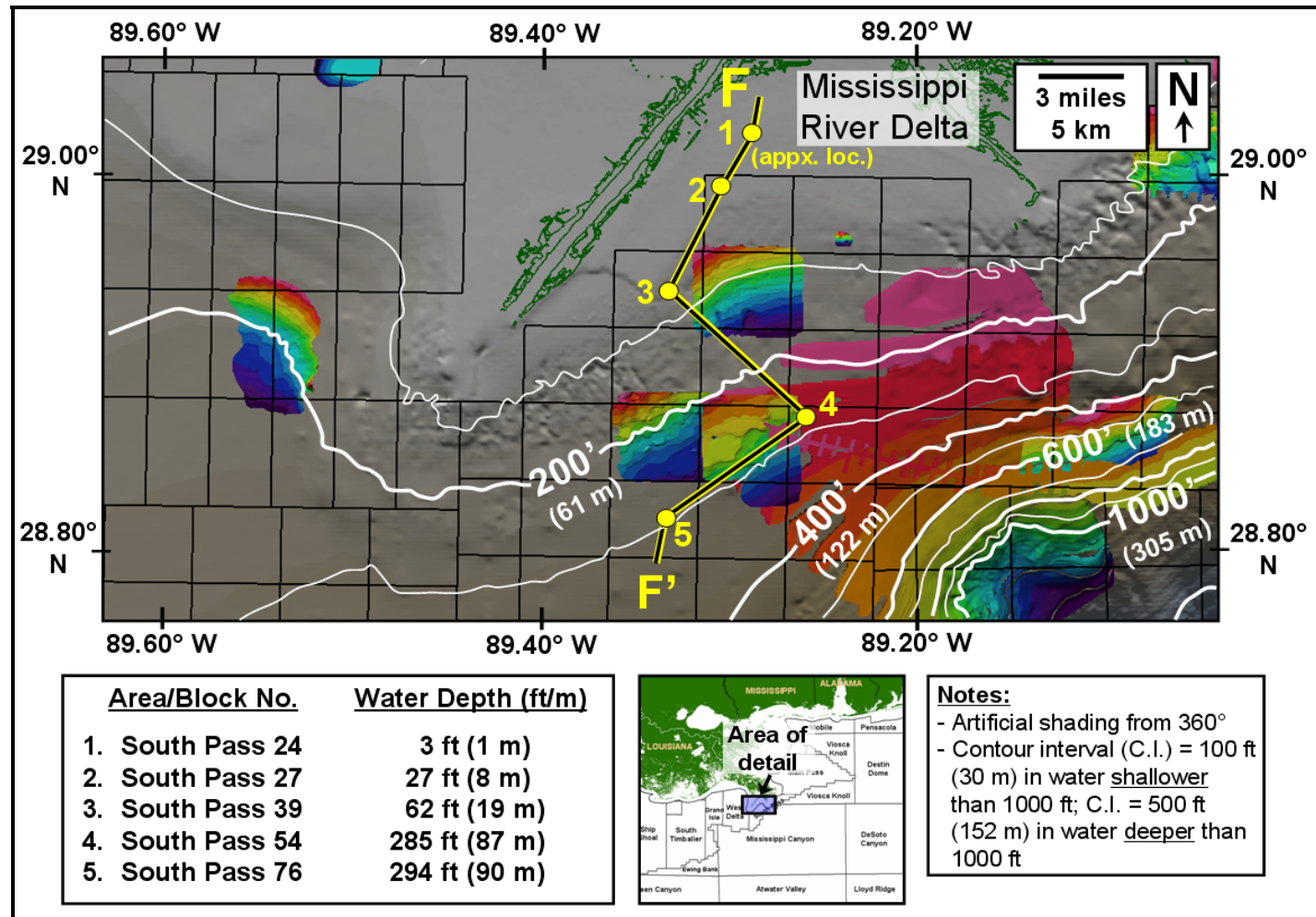


Figure 83: Bathymetry image along cross section F-F', South Pass Area (high-resolution data from John E. Chance & Associates, 1990a; Marine Technical Services, Inc., 1987; Arco, 1990, 1991b; Vastar Resources, Inc., 1995, 1997b, Enterprise Products Partners LLC, 2005; Plains Resources, 2006 displayed on spectrum color bar; regional data from NOAA (2009) displayed on brown-to-blue color bar and fills gaps between high-resolution surveys)

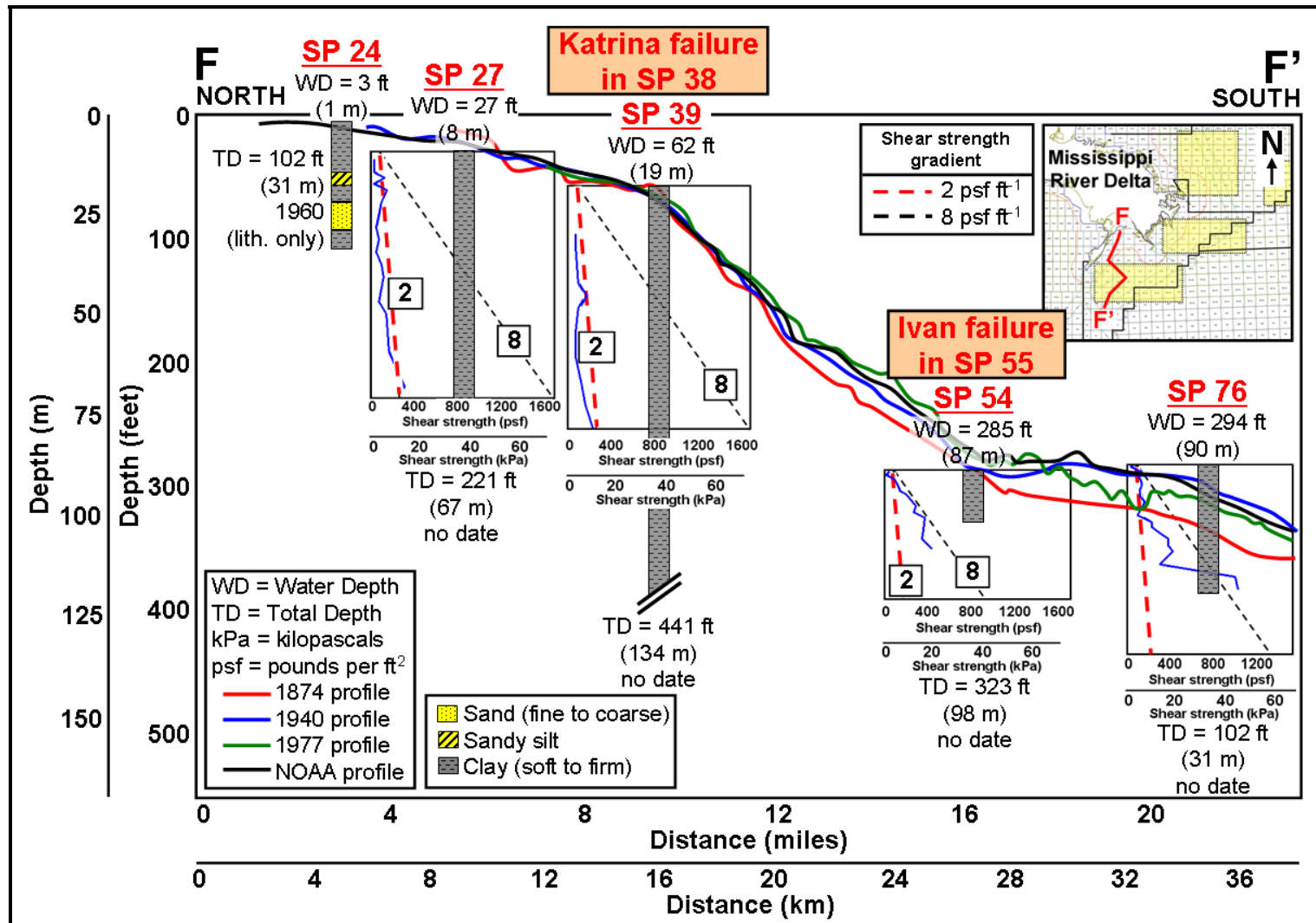


Figure 84: Geotechnical borehole cross section F-F', South Pass Area, north-central Gulf of Mexico (regional seafloor profiles derived from 1874, 1940 1977 (Coleman et al., 1980) and NOAA (2009) bathymetry data)

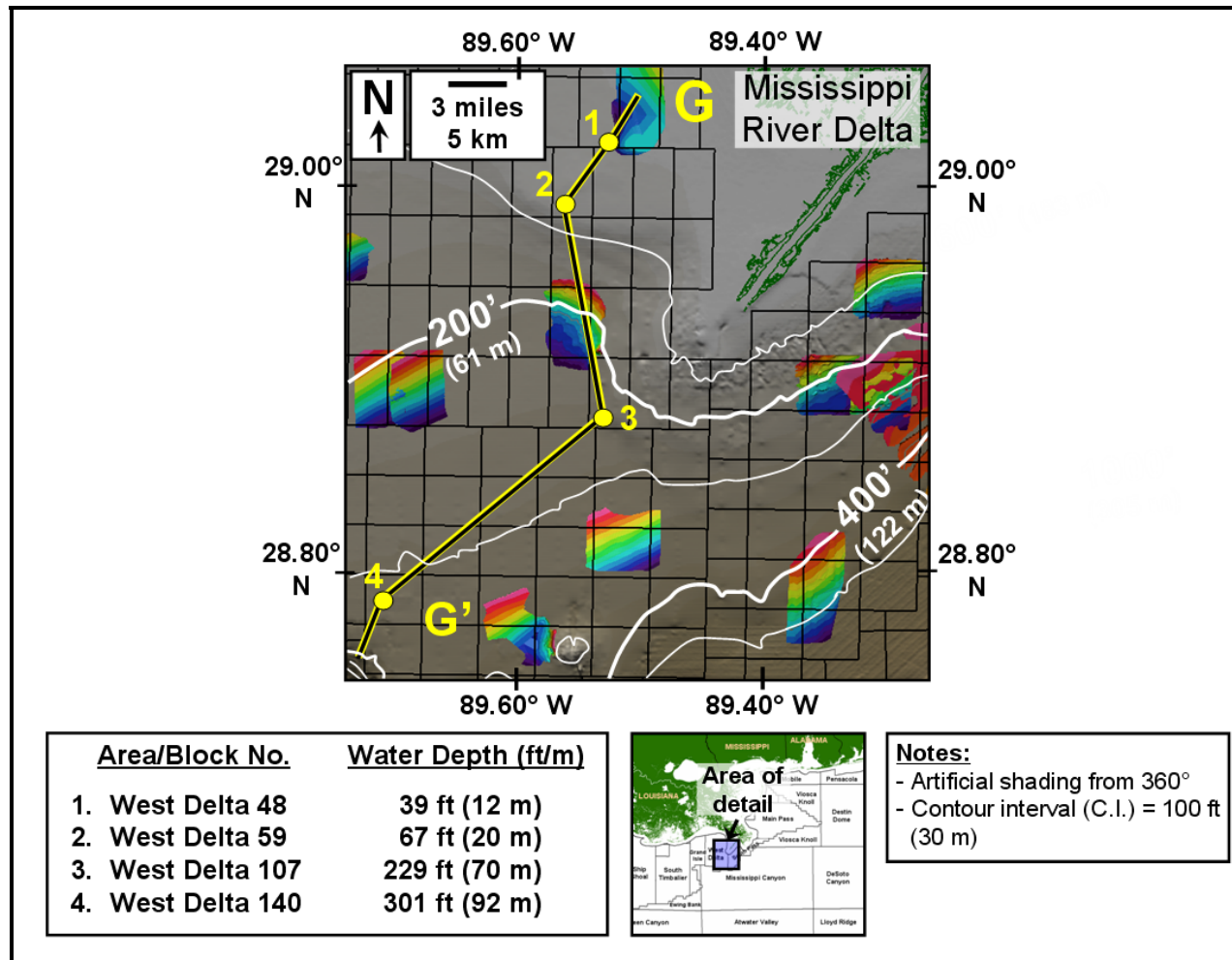


Figure 85: Bathymetry image along cross section G-G', West Delta Area (high-resolution data from Comap Geosurveys, Inc., 1984; Environmental Geosciences, 1987; Marine Technical Services, Inc., 1987; John E. Chance & Associates, 1988b; Arco, 1991c, 1992, 1993b, 1994; Vastar Resources, Inc., 1997a; displayed on spectrum color bar; regional data from NOAA (2009) displayed on brown-to-blue color bar and fills gaps between high-resolution surveys)



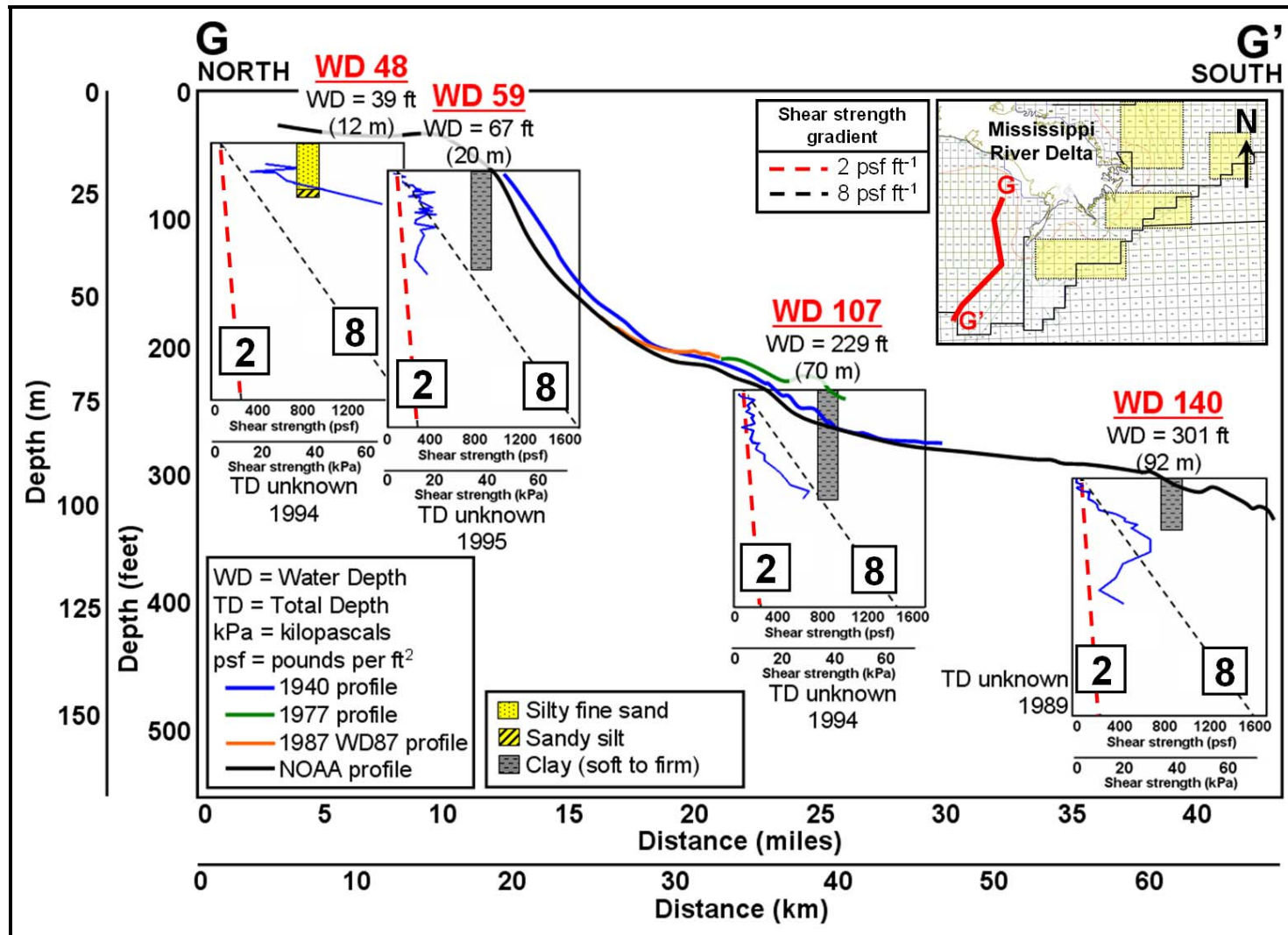


Figure 86: Geotechnical borehole cross section G-G', South Pass Area, north-central Gulf of Mexico (regional seafloor profiles derived from 1940 and 1977 (Coleman et al., 1980), WD87 (Marine Technical Services, Inc., 1987) and NOAA (2009) bathymetry data)

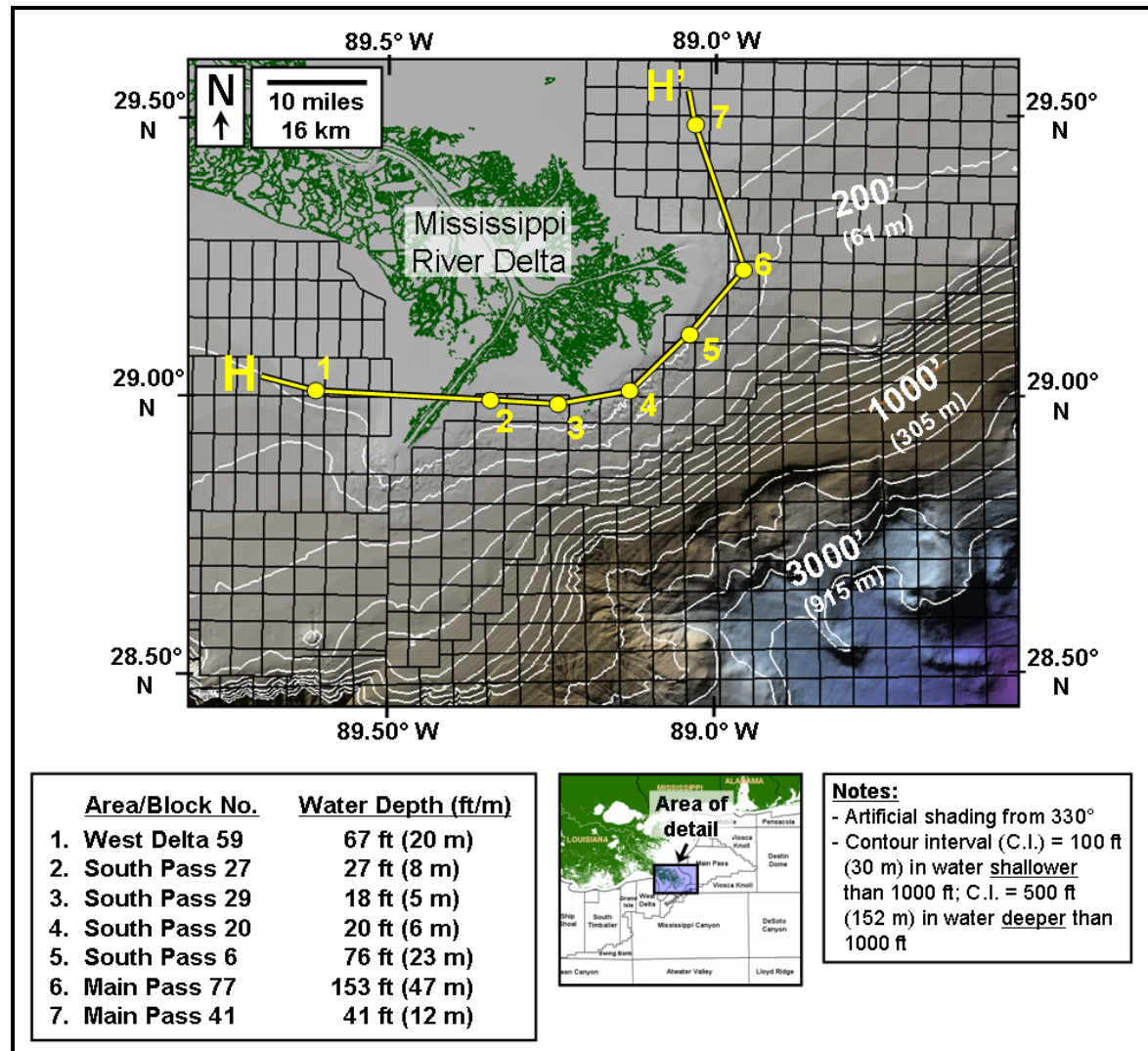


Figure 87: Geotechnical borehole cross section H-H', West Delta, South Pass and Main Pass Areas, north-central Gulf of Mexico (regional seafloor profiles derived from NOAA (2009) bathymetry data)

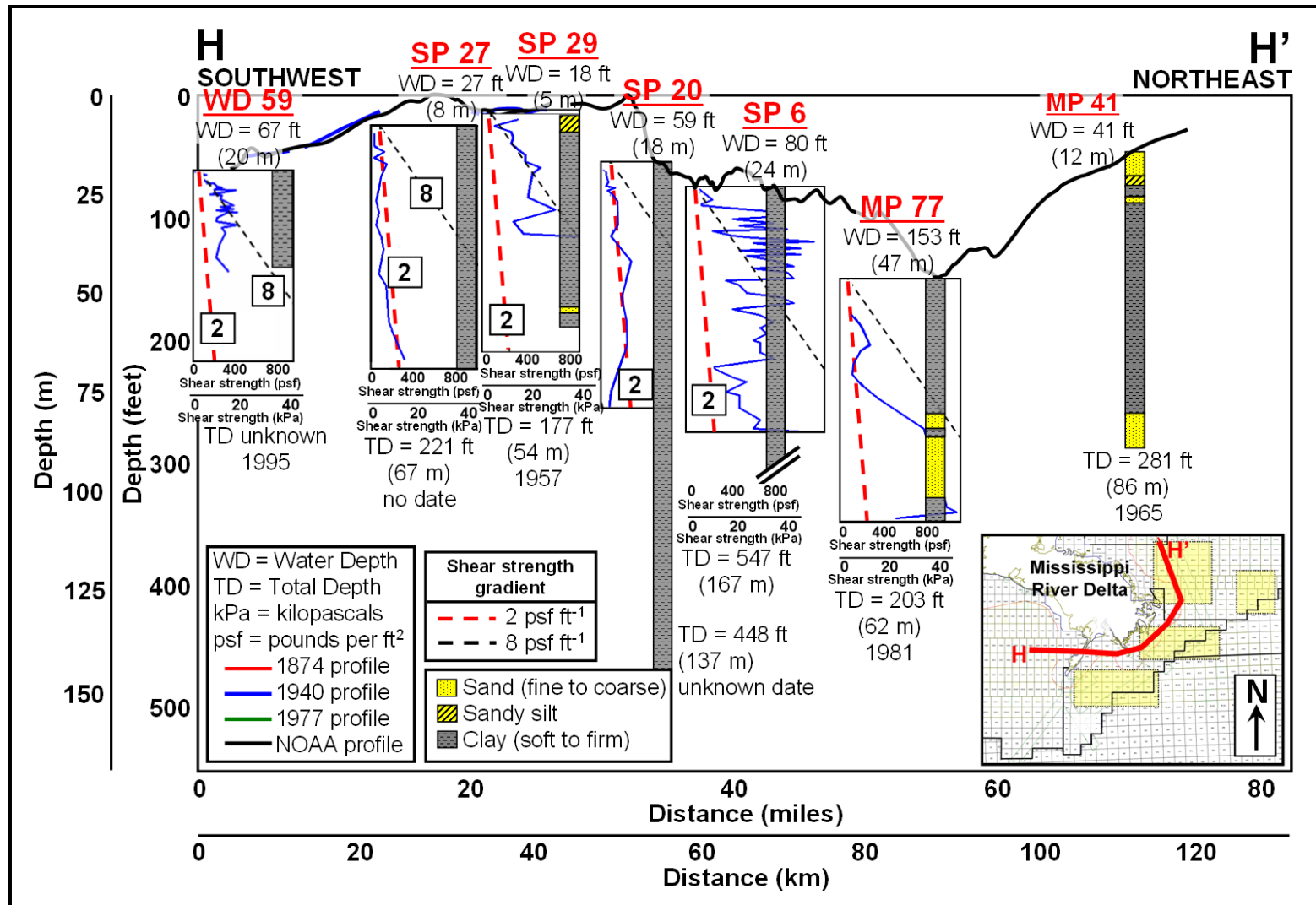


Figure 88: Geotechnical borehole cross section H-H', West Delta, South Pass and Main Pass Areas, north-central Gulf of Mexico (regional seafloor profiles derived from 1940 and 1977 (Coleman et al., 1980), and NOAA (2009) bathymetry data)

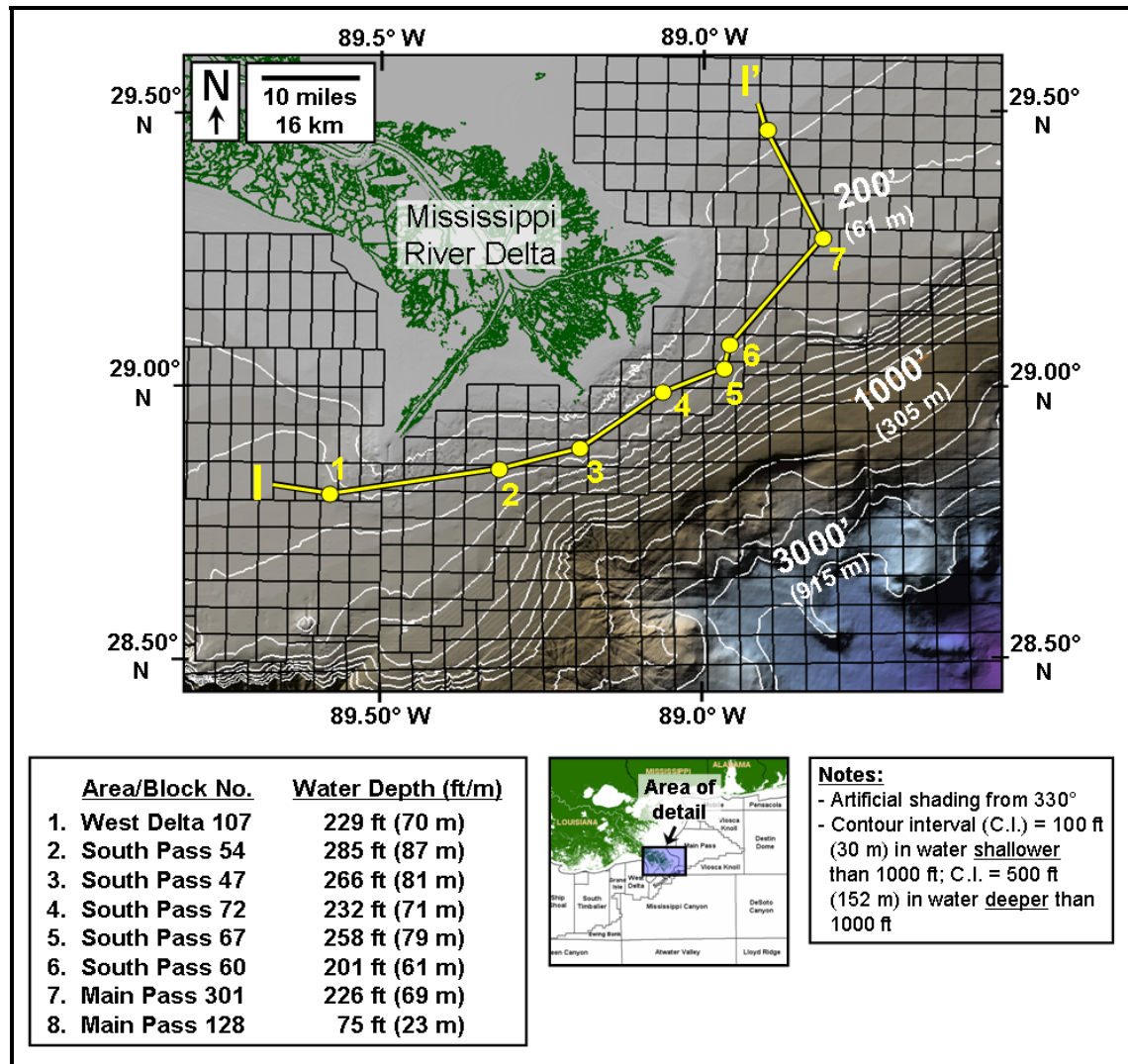


Figure 89: Geotechnical borehole cross section I-I', West Delta, South Pass and Main Pass Areas, north-central Gulf of Mexico (regional seafloor profiles derived from NOAA (2009) bathymetry data)



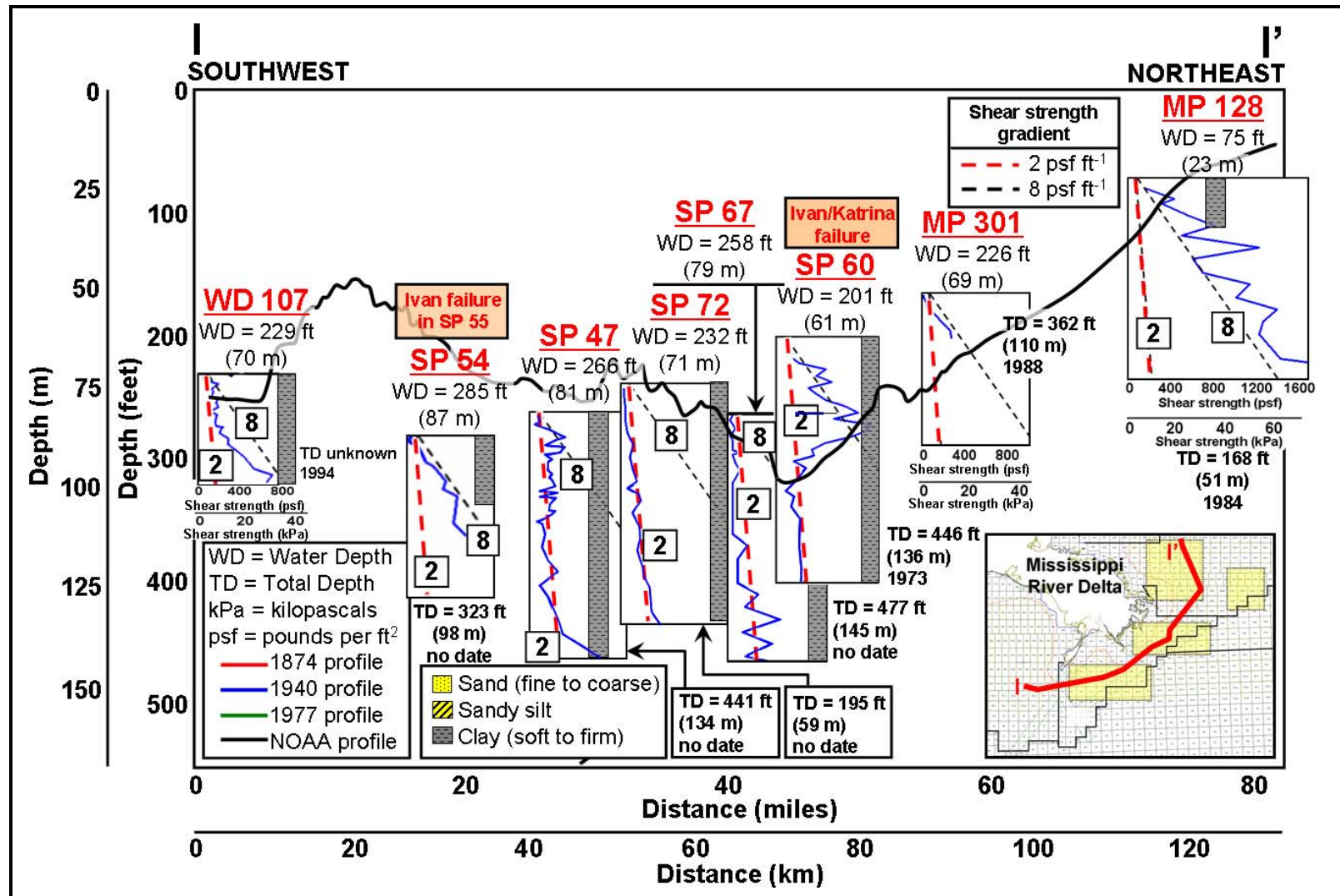


Figure 90: Geotechnical borehole cross section I-I', West Delta, South Pass and Main Pass Areas, north-central Gulf of Mexico (regional seafloor profiles derived from 1940 and 1977 (Coleman et al., 1980), and NOAA (2009) bathymetry data)

by occasional steeper slopes extending 10-15 km. Surficial and shallow subsurface lithology contains fine-to-coarse sand and silty sand, especially farther to the east in Main Pass Blocks 290 and 295. No submarine shelf failure was reported along this profile as the near-match between regional and local HR bathymetry data suggests.

Cross Section B-B' is located approximately 5-20 km south of and roughly parallel to Cross Section A-A'. This profile depicts a stable platform adjacent to the present-day MRD, a relatively steeper slope (approximately  $0.7^\circ$  vs.  $0.2^\circ$ ) through the middle of the profile, and then a relatively flat slope before reaching the shelf edge (Figures 75 and 76). The NOAA regional bathymetry on the western end of the profile reflects progradation that likely occurred since the 1940 data were acquired. The semi-regional bathymetry grid acquired in 1997 (Vastar Resources, Inc., 1997a) reflects sediment aggradation that took place since the NOAA data were acquired. Since the exact acquisition date of the NOAA data is unknown, it is impossible to ascribe the sediment addition to hurricane occurrence. Local HR bathymetric data from Main Pass Blocks 305 and 306 are similar to the NOAA data. However, the two boreholes from these blocks suggest deeper bathymetric values. These boreholes were acquired in 1968, one year prior to Hurricane Camille, leading to the hypothesis that net sediment addition reflected in the Vastar and NOAA bathymetry data may be due to local sediment failures along the northern face of a seafloor feature that overlies a deeper-seated salt dome (Block 305 in particular; Figure 75).

Surficial and near-surface lithology contains fine-to-coarse sand towards the east and predominantly fine-grained cohesive clays toward the west. Shelf failure was reported at Main Pass Block 70 during both Hurricanes Ivan and Katrina. However, lithology and shear strength data from this borehole extend only 11 m (37 feet) below the surface and therefore do not illustrate a clear trend indicating possible seafloor failure.

The Main Pass 77 borehole contains two  $C^{14}$  radiometric age estimates, one from 34 m (111 feet) and another at 27 m (89 feet) dated at 10,190 and 4570 years before present (McClelland Engineers, Inc., 1982). However, the age result from the shallower sample may be

inaccurate as the sampled material may have been contaminated by the presence of older organic remains transported to the site (McClelland Engineers, Inc., 1982). If so, then the interval could possibly be younger.

The origin of Cross Section C-C' is located approximately 15 km south of Section B-B' and extends southeastward across the South Pass and Viosca Knoll Protraction Areas in a nearly true dip profile seaward from the MRD (Figures 77 and 78). Each successive regional bathymetry survey after 1874 indicates net sediment aggradation of 5-15 m (15-50 feet). Surveys from 1940 through 1977 indicate local sediment failure and subsequent deposition. Along this section, sediment failure occurred at South Pass Block 60 during both Hurricanes Ivan and Katrina as well as at South Pass Block 70 during Hurricane Camille (Section 3.3.2).

Evidence of prior failures can be seen in the shear strength profiles in South Pass Blocks 60, 67 and 70. Normally consolidated clay in the Gulf of Mexico contains an undrained shear strength that increases at or above a gradient that increases at approximately 8 psf foot<sup>-1</sup> (1.26 kPa m<sup>-1</sup>; Quiros et al., 1983; shear strength significance is discussed in more detail in Section 6.2). Rapid sediment deposition can lead to underconsolidated sediment that is aligned more closely to a shear strength gradient of 2 psf foot<sup>-1</sup> ( $3.14 \times 10^{-1}$  kPa m<sup>-1</sup>). The highly variable nature of MRDF sediments translates into shear strength profiles that can vary from block to block or even within the same mudflow (Hooper, 1980). The borehole from SP 60 was acquired in 1973, four years after Hurricane Camille. Although no seafloor failures were officially reported at SP 60, a failure occurred in South Pass Block 61, approximately 5 km south of SP 60. Shear strength data follow a gradient of approximately 8 psf foot<sup>-1</sup> (1.26 kPa m<sup>-1</sup>) to a depth of about 24 m (80 feet), suggesting that "firm clay" as denoted on the borehole log reflects a stiffer crust that overlies relatively underconsolidated sediment when the borehole was taken. The date of the primary SP 70 borehole is unknown; however, the shear strength profile from this borehole as well as that from one of two other boreholes on the block follows the 2 psf foot<sup>-1</sup> ( $3.14 \times 10^{-1}$  kPa m<sup>-1</sup>) gradient, implying underconsolidated material. A third borehole from SP 70

reflects a stronger upper crust overlying weaker material down to a depth of approximately 80 feet (24 m; Bea et al., 1980), which is consistent with data supplied by Sterling and Stroheck (1973; see Section 3.3.2, Figure 17). Surficial and near-surface lithology reflects the cohesive nature of the clayey soil found in this area.

Cross Section D-D' is located approximately 10 km southwest of and parallel to Cross Section C-C' in a nearly true dip profile seaward from the MRD (Figures 79 and 80). Bathymetry data toward the northwest reflect a shallow, relatively flat apron that steepens nearer the shelf edge (approximately  $0.15^\circ$  vs.  $0.35^\circ$ ) and significantly once past the shelf edge near Mississippi Canyon (MC) Block 20 (approximately  $1.2^\circ$ ). Changes in regional bathymetry since 1874 reflect a highly ephemeral seafloor with high sedimentation rates and multiple failures through time. A significant seafloor failure occurred during Hurricane Ivan at MC 20, resulting in the loss of a major production platform (MMS, 2005a; Hooper and Suhayda, 2005a, 2005b; Nodine et al., 2006). Bathymetry data obtained over southern MC 20 confirm significant seafloor movement. Shear strength profiles in the two available boreholes reflect relatively high sedimentation rates adjacent the MRD as they follow a gradient of approximately  $2 \text{ psf foot}^{-1}$  ( $3.14 \times 10^{-1} \text{ kPa m}^{-1}$ ) and thus indicate the presence of highly underconsolidated material. Surficial and near-surface lithology reflects clayey, cohesive soils similar to those observed in Cross Section C-C'.

Cross Section E-E' is located approximately 15 km west of and parallel to Cross Section D-D; in a nearly true dip profile seaward from the MRD (Figures 81 and 82). Successive bathymetry surveys since 1874 indicate significant seafloor alteration, especially near South Pass Block 48 where approximately 30 m (100 feet) of sediment have accumulated since 1874. No seafloor failures were reported along this profile; however seafloor failure occurred during Hurricanes Hilda and Betsy at South Pass Block 28, 5 km west of SP 29 (Arnold, 1967; discussed in more detail in Section 7.2.4). Shear strength data from the SP 29 borehole, which is located in East Bay in an interdistributary between South Pass and Southwest Pass, follow a normally consolidated gradient of  $8 \text{ psf foot}^{-1}$  ( $1.26 \text{ kPa m}^{-1}$ ), suggesting relative seafloor stability. The

remainder of the boreholes, however, more closely follow an underconsolidated gradient which can be inferred from the highly variable seafloor profiles at South Pass Blocks 47, 48 and 49. Additional shear strength data from additional boreholes at SP 47 indicate the existence of crustal sediments approximately 18 m (60 feet) thick becoming increasingly underconsolidated with depth below that point (Hooper, 1996). Surficial and near-surface sediments along Cross Section E-E' are clayey except for a thin (3 m) zone of sandy silt in the uppermost section of the SP 29 borehole. A six-meter sand interval exists in the SP 47 boreholes at a depth of 136 m (445 feet) beneath the interval portrayed on Figure 82.

Cross Section F-F' consists of a north-south dip profile adjacent to the MRD in the South Pass Protraction Area (Figures 83 and 84). Time-series bathymetry data are more closely grouped together, inferring less vertical variability through time at least in shallower water toward the north. Toward the south, greater bathymetric variability exists, up to a maximum of 12 m between 1874 and 1977. Seafloor failures occurred during Hurricane Katrina at SP 38 (5 km east of SP 39 on Section F-F') as well as at SP 55 (4 km west of SP 54 on the section).

The widely variable nature of MRDF sediments is evident on Cross Section F-F'. Shear strength gradients in shallower water adhere to a  $2 \text{ psf foot}^{-1}$  ( $3.14 \times 10^{-1} \text{ kPa m}^{-1}$ ) gradient, including those near SP 39 which is only 5 km from the SP 38 failure during Katrina. Gradients follow a more consolidated gradient at SP 54, yet this borehole is located only 4 km from the Ivan failure at SP55. Shear data at SP 76 reflect variable gradients, with underconsolidated material overlying more normally consolidated material beginning at approximately 27 m (90 feet). The dates that any of the boreholes were acquired are unknown. Surficial and near-surface lithology is mostly clayey except for several zones of sand and sandy silt at depths of approximately 15-27 m (50-90 feet).

Cross Section G-G' is located approximately 25 km west of Section F-F' in the West Delta (WD) Protraction Area (Figures 85 and 86). Limited historical regional bathymetry data exist this far west relative to the MRD; however, the NOAA data suggest a relatively flat apron

that transitions to a steeper slope offshore Southwest Pass (approximately  $0.03^\circ$  vs.  $0.2^\circ$ ) and then to a milder slope up to the shelf edge (approximately  $0.4^\circ$ ). No seafloor failures occurred along this cross section; the closest one occurred at WD 109, located approximately 8 km east of WD 107 on Section G-G'.

Shear strength data in shallow water (WD 48) indicate highly competent material; this section also correlates with sandy surficial and near-surface lithologies that extend at least as far as the bottom of the borehole at 14 m (47 feet). The remaining boreholes exhibit either normally consolidated behavior or a mix of normally consolidated and underconsolidated sediment. A marked transition occurs at WD 140, where a crustal layer appears to truncate at a depth of approximately 21 m (68 feet); below that point the sediment appears to be underconsolidated. Surficial and near-surface lithology is mostly clayey except for the sandy interval at WD 48.

Two strike-oriented cross sections were constructed across the MRDF, one closer to the delta and another farther out in deeper water (Figure 72). Cross Section H-H' is located along the periphery of the MRD and illustrates the bathymetric, geotechnical and lithological relationship of various locations with the MRD (Figures 87 and 88). Wide bathymetric variability can be seen in this profile in relation to the major passes of the MRD (i.e., Southwest Pass, South Pass and Pass a'Loutre). Wide variability in sediment shear strength is also evident and reflects a mix of normally and underconsolidated sediment. Cross Section I-I' is located 10-18 km distal relative to Cross Section H-H' and also reflects the wide variability that exists in seafloor bathymetry and shear strength (Figures 89-90). Surficial and near-surface lithology is predominantly clay, reflecting the more distal nature of the profile.

### **6.3 Geotechnical Characterization, MRDF Seafloor and Shallow Sediments**

#### **6.3.1 Shear Strength Characterization**

As discussed in the previous section, shear strength profiles in the GOM vary widely depending on location both in a macro sense as well as locally at specific sites (Hooper, 1980; Quiros et al., 1983). Most MRDF sediments contain shear strengths that are typically lower than

those elsewhere in the GOM. They are usually reflected by normally consolidated profiles with undrained shear strengths that increase at or above a profile that increases at a rate of approximately 8 psf foot<sup>-1</sup> (1.26 kPa m<sup>-1</sup>). In contrast, undrained shear strength profiles for remolded clay increase at or above a profile that increases at a rate of approximately 2 psf foot<sup>-1</sup> (3.14 x 10<sup>-1</sup> kPa m<sup>-1</sup>; Quiros et al., 1983). A description of undrained shear strength sample collection methods used in the GOM is provided in Appendix N.

A common artifact in MRDF shear strength profiles is the occurrence of a “crustal” zone that reflects unusually high shear strengths within the upper 15 m of sediment (Bohlke and Bennett, 1980). Prior work has indicated that increasing shear strengths within these crustal zones were the result of increases in silt-sized sediment and resulting decreases in the void ratio (Bea et al., 1975, Roberts et al., 1976). As the void ratio decreases, sediment water content likewise decreases, suggesting that remolding and dewatering of initially porous silty clay sediment has occurred (Bohlke and Bennett, 1980). Additional work indicates that these crusts are associated with zones of shearing during submarine sediment movement on the prodelta (Bea and Arnold, 1973; Bea and Audibert, 1980; Hooper, 1980). Shear strength profiles through these zones varies considerably with depth (Figure 91) as reflected in the existence of four main layers – an overlying crustal zone, a failure zone that indicates seafloor movement, a transition zone that begins reverting back to *in situ* conditions, and a “basement” zone comprised of undisturbed conditions (Figure 91).

The existence of crustal zones is evident on several boreholes depicted on the MRDF cross-section grid discussed in Section 6.1. In particular, shear strength profiles at SP 60 and SP 70 indicate the existence of crustal zones and therefore confirm the likelihood of past seafloor failures (Figure 78). Both of these blocks experienced past failure, with SP 60 failing during both Hurricanes Ivan and Katrina, and with SP 70 failing during Hurricane Camille. Additional failures occurred at SP 55 during Hurricane Ivan and at SP 38 during Hurricane Katrina. The profile at SP55 indicates the possible existence of a crustal zone but the shear strength data are

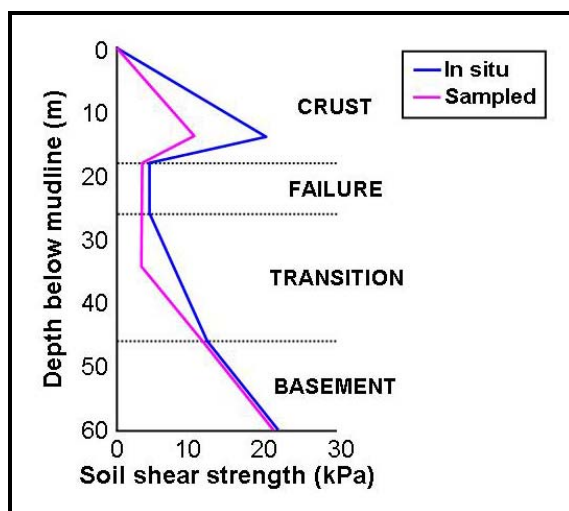


Figure 91: Typical shear strength profile through a crustal zone (modified from Bea and Arnold, 1973)

are relatively shallow and do not provide a complete record of shear strength integrity (Figure 84). The borehole acquisition date is also unknown and therefore cannot be used to reflect when prior failures may have occurred. The same holds true for the borehole from SP 38; although the profile does not reflect a typical crustal zone it cannot be used to conclusively demonstrate whether a prior failure occurred.

GOM shear strength distribution, as mapped in previous studies, indicates wide variations in shear strengths (Dunlap et al., 2004; Figure 92). A platform of relatively high shear strengths exists offshore Mississippi and Alabama, which coincides with areas containing coarser surficial sediments. Shear strengths decrease sharply further west in the Main Pass and upper Viosca Knoll Areas, reflecting finer-grained material adjacent to either side of the MRD. Isolated pockets of slightly higher shear strengths exist approximately 20 km and 40 km northeast and east, respectively, of the MRD. These higher shear strengths are evident in the boreholes comprising Cross Section A-A' (Figure 74) and the eastern end of Cross Section B-B' (Figure 76). Higher shear strengths were also mapped in the South Timbalier Area approximately 100 km west of the MRD, which also coincides with areas of coarser surficial sediments (Figure 92).



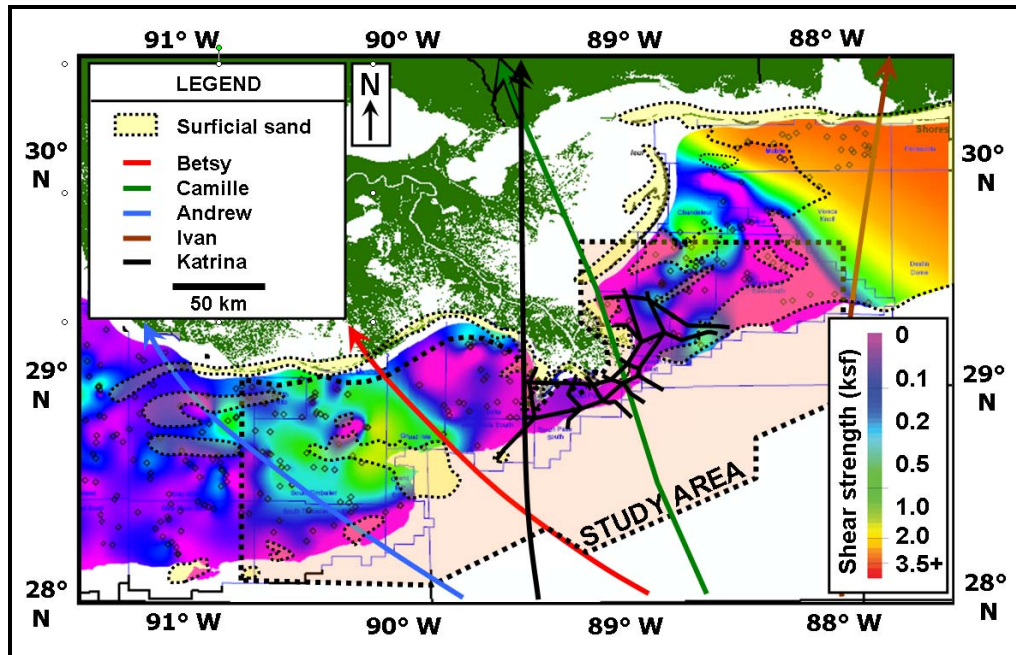


Figure 92: GOM shear strength distribution (modified from Dunlap et al., 2004)

Shear stresses along the seafloor were mapped for each hurricane as part of the MIKE 21 numerical wave model. Metocean impact is evident on shear stresses at maximum impact for each storm. Higher shear stresses during Hurricanes Ivan and Katrina, for example, increased in a trend that conforms to seafloor bathymetry (Figures 93 and 94). The outer limit of increased shear stress coincides roughly with the 100-meter isobath for each storm; the highest stresses coincide roughly with a 25-meter isobath.

### 6.3.2 Safety Factor Characterization

A criterion often used in geomechanics to assess relative seafloor stability is the safety factor (Henkel, 1970; Wright and Dunham, 1972; Nodine et al., 2006; Nodine, 2007). The factor of safety is broadly defined as the ratio of shear stresses to undrained soil shear strength:

$$F = \frac{c}{\tau} \quad (4)$$

Where:  $F$  = factor of safety  
 $c$  = undrained shear strength  
 $\tau$  = shear stresses developed along the length of a circular slip surface (Figure 9, Section 3.1.3; Henkel, 1970)

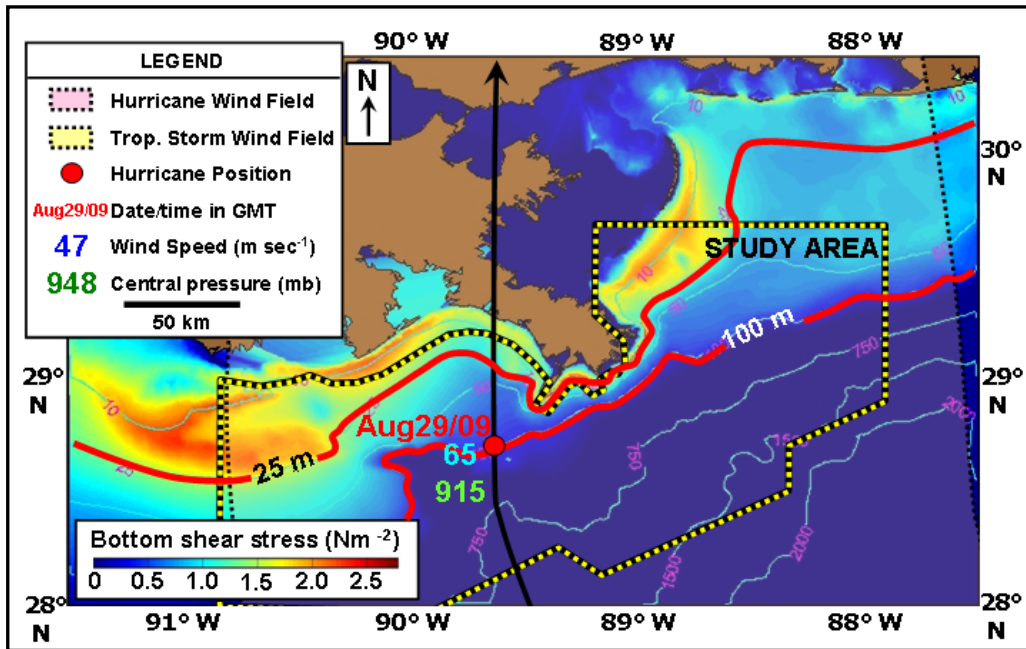


Figure 93: Bottom shear stress, Hurricane Katrina, 0900 UTC, August 29, 2005

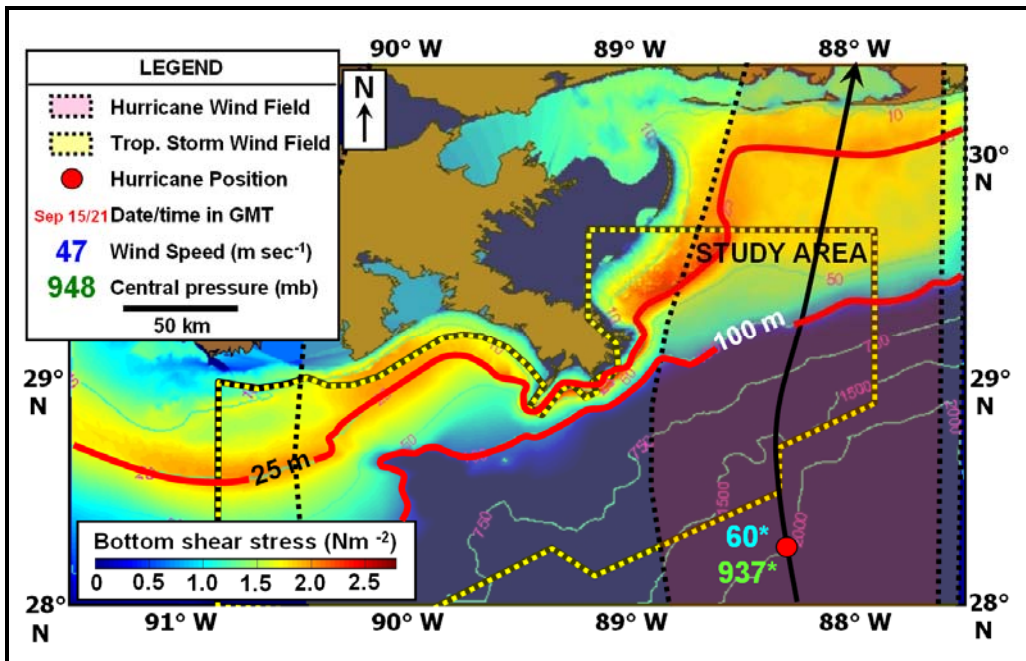


Figure 94: Bottom shear stress, Hurricane Ivan, 2100 UTC, September 15, 2004

Safety factor calculations are based on the circular slip surface theory described in Section 3.1.3 (Figure 11; Henkel, 1970). Factors of safety of less than 1.0 are generally assumed to indicate areas of potential instability containing a high risk of potential submarine failure. Areas containing safety factors greater than 1.0 are assumed to not be at risk of failing.

The metocean conditions present at a particular site must be known in order to calculate a safety factor that is reasonably accurate. Building on the metocean results presented for the five main hurricanes studied in this dissertation, characteristics such as maximum significant wave height and wave period can be used to determine the safety factors prevalent at specific sites at specific times during the approach of each storm. In order to calculate these site- and time-specific safety factors, a computer program compiled in Microsoft Excel by Nodine (2007) was used in which wave conditions and resulting seafloor pressure are integrated.

The steps used in the program to calculate safety factors are described in Appendix N. These steps are based on the assumption that shear strengths increase linearly with depth and that the following parameters were known: the slope angle ( $\beta$ ), water depth ( $d$ ), wavelength ( $L$ ), wave height ( $h$ ), wave period ( $T$ ), acceleration of gravity ( $g$ ; assumed as  $9.81 \text{ m sec}^{-2}$ ), submerged unit weight of soil ( $\gamma'_s$ ), unit weight of water ( $\gamma_w$ ), the shear strength of the soil at the mudline ( $c_0$ ) and the increase in shear strength with depth ( $c_z$ ).

An example of the inputs used in the safety factor model is shown in Figure 95. Each input (highlighted in blue) was entered into the model and the outputs (maximum wave pressure on the seafloor ( $P_{\max}$ ) and safety factor ( $F$ ); highlighted in yellow) were displayed interactively. Factors of safety are calculated for various slip circle trial heights, and the minimum factor of safety calculated is identified as the minimum factor of safety for that particular site given the assumed conditions. Once the trial height associated with the minimum factor of safety was identified, that value was entered as the “critical height” in the program and the radius was then calculated for a slip circle that corresponded to each depth in the input shear strength profile (Appendix Q).

Input factors were available from either observed seafloor conditions or from modeling results described in Chapter 5 except for wavelength and maximum pressure on the seafloor; these were calculated assuming linear wave theory described by Wiegel (1964):

Slope Angle (rad)	Water Depth (ft)	Wavelength (ft)	Wave Height (ft)	Submerged Soil Unit Wt. (pcf)	Water Unit Wt. (pcf)	Maximum Wave Pressure (psf)	Minimum Factor of Safety
$\beta$	d	L	h	$\gamma'_s$	$\gamma_w$	$P_{max}$	2.72
0.0032	300	1004	50	30.0	64	478.34	

Shear Strength Profile				
Trial Heights, h (ft)	Corresponding Factors of Safety	Critical Height, h (ft)	Depth (ft)	Shear Strength (psf)
50	3.384	325	0.0	50
75	3.109		9.0	154
100	2.959		13.0	66
125	2.870		17.0	88
150	2.813		23.0	308
175	2.775		25.0	132
200	2.750		31.0	242
225	2.734		35.0	154
250	2.725		49.0	484
275	2.720		59.5	418
300	2.718		69.5	418
325	2.720		79.5	484
350	2.724		89.5	528
375	2.729		110.0	924
400	2.737		139.5	946
425	2.745		149.5	902
450	2.755		159.0	1760
475	2.766		169.5	990
500	2.777		180.0	1276
525	2.790		189.0	1936
550	2.803		220.0	2200
575	2.816			
600	2.830			
625	2.845			
650	2.860			

Figure 95: Example of safety factor calculation, Main Pass 290 (format from Nodine, 2007); assumes a wave period of 14.0 sec and a corresponding wave length of 305 m (1004 feet)

1. Calculation the wavelength as a function of wave period:

$$L = \frac{gT^2}{2\pi} \tanh \frac{2\pi d}{L} \quad (5)$$

2. Calculation the maximum pressure on the seafloor using linear wave theory:

$$P_{max} = \frac{\gamma_w}{2} \left( \frac{h}{\cosh\left(\frac{2\pi}{L}d\right)} \right) \quad (6)$$

Using this methodology, safety factors were calculated along each of the cross-section profiles discussed in Section 6.2 (Figure 96-102). Given the time-series MIKE 21 numerical wave model results for the five hurricanes modeled in this dissertation, the factors of safety can be calculated along each profile at incremental steps during each storm as they approached the MRDF. The wave periods, corresponding wavelengths and resulting safety factors for boreholes on each cross-section are depicted in Appendix N (Tables N-1 through N-7).

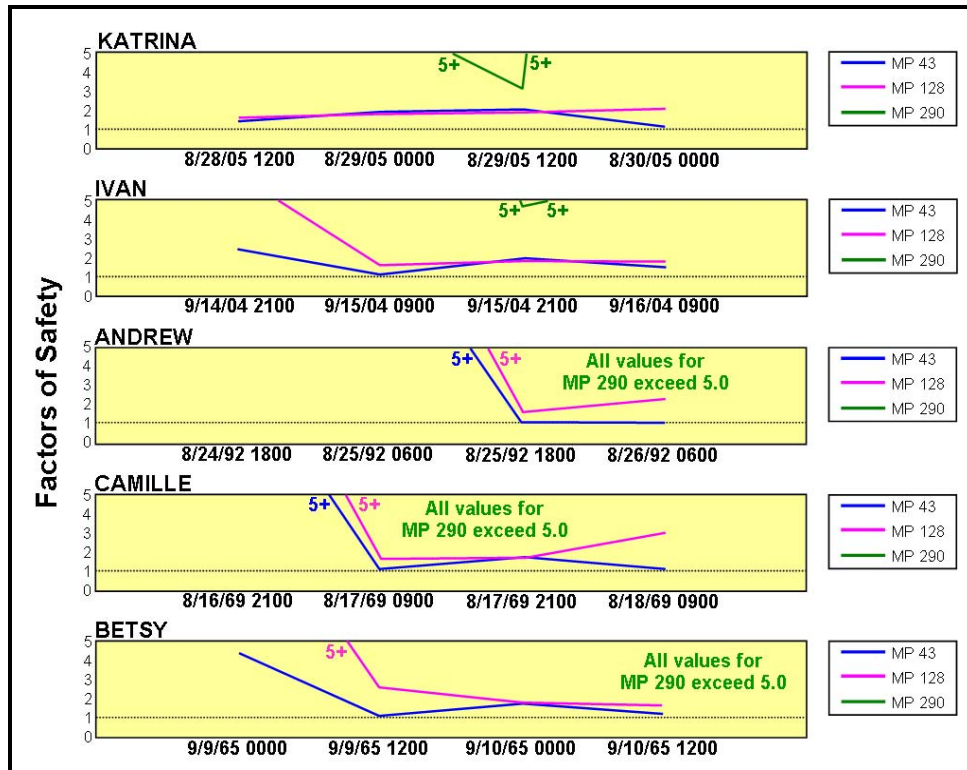


Figure 96: Factors of safety calculated along Cross Section A-A', Hurricanes Betsy through Katrina

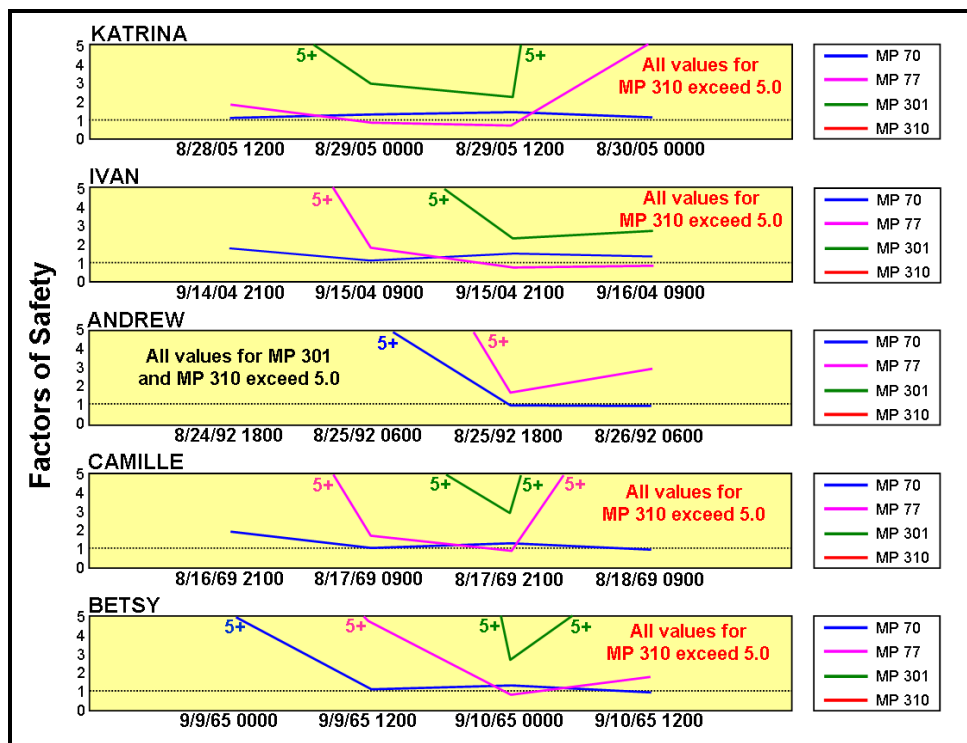


Figure 97: Factors of safety calculated along Cross Section B-B', Hurricanes Betsy through Katrina



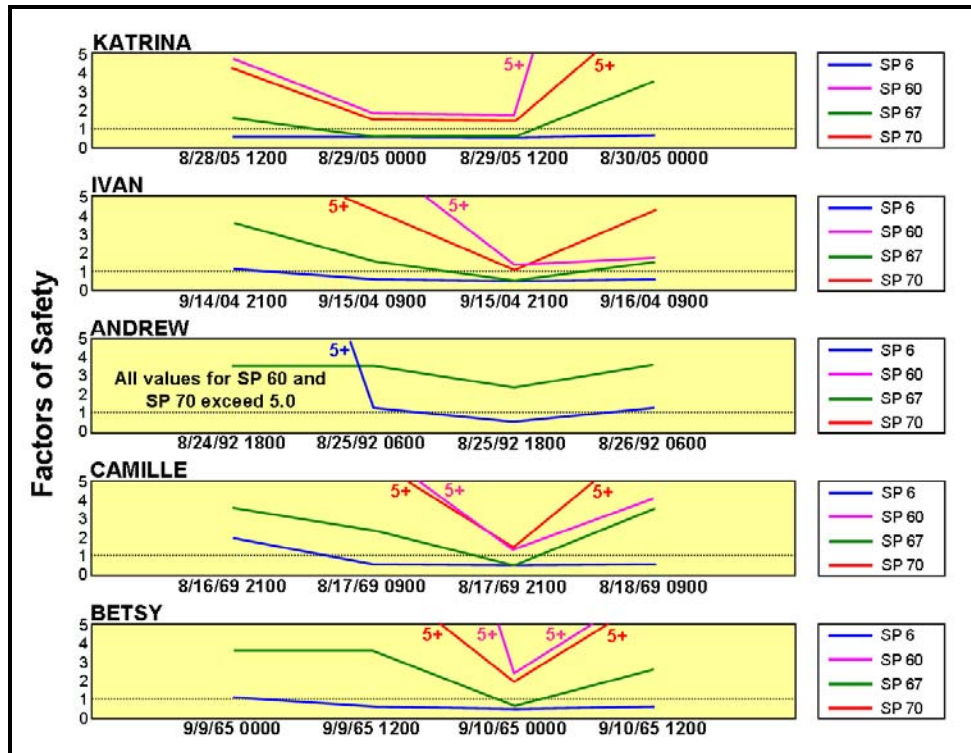


Figure 98: Factors of safety calculated along Cross Section C-C',  
Hurricanes Betsy through Katrina

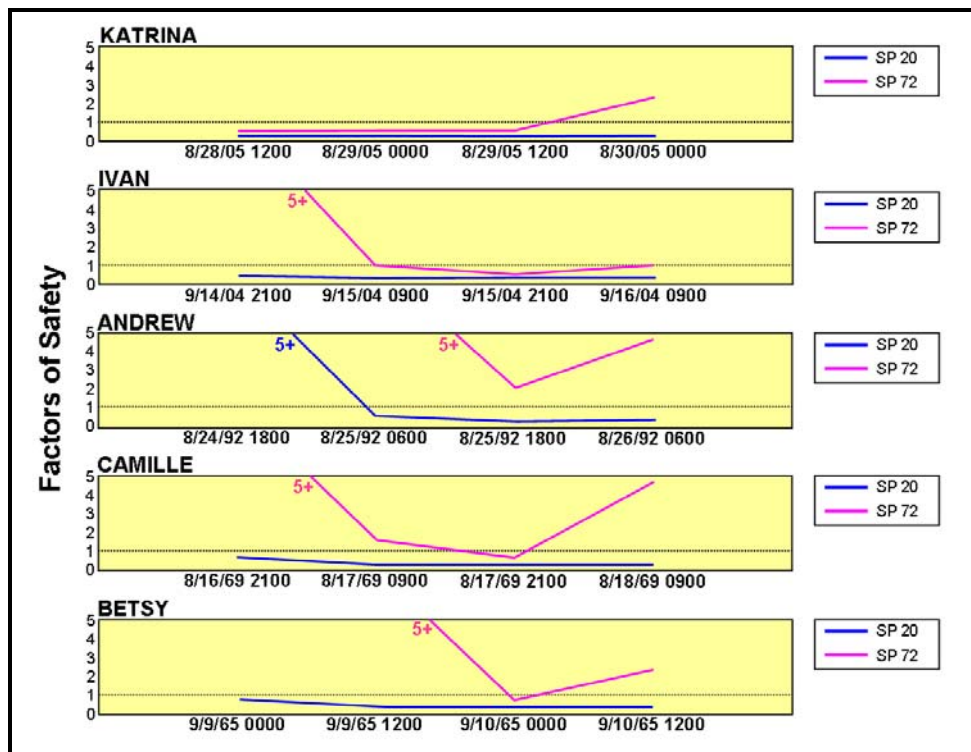


Figure 99: Factors of safety calculated along Cross Section D-D',  
Hurricanes Betsy through Katrina

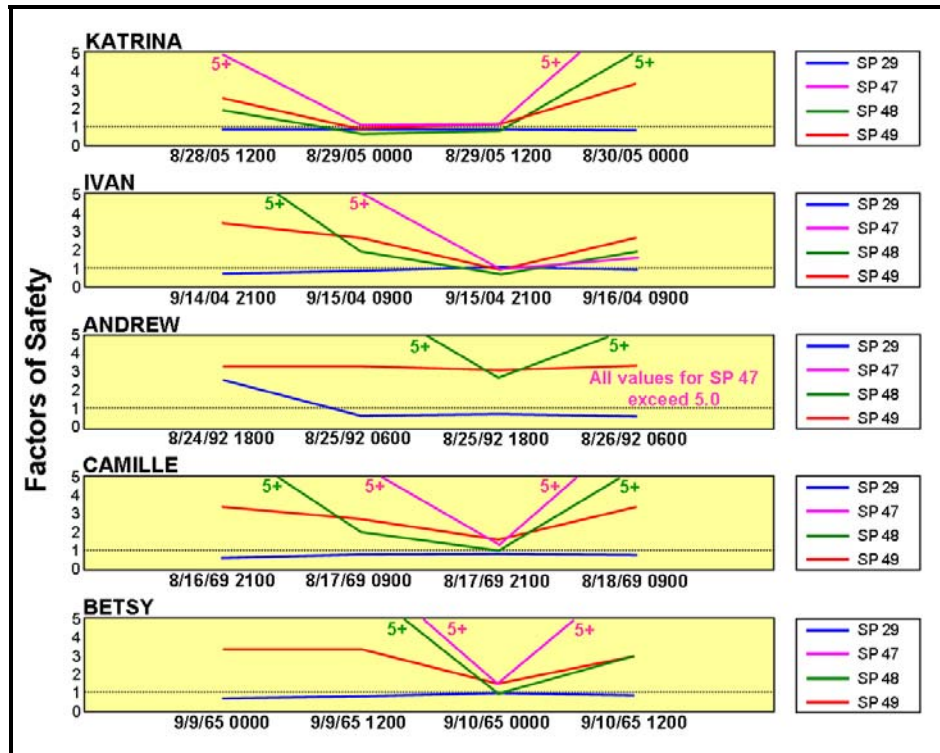


Figure 100: Factors of safety calculated along Cross Section E-E', Hurricanes Betsy through Katrina

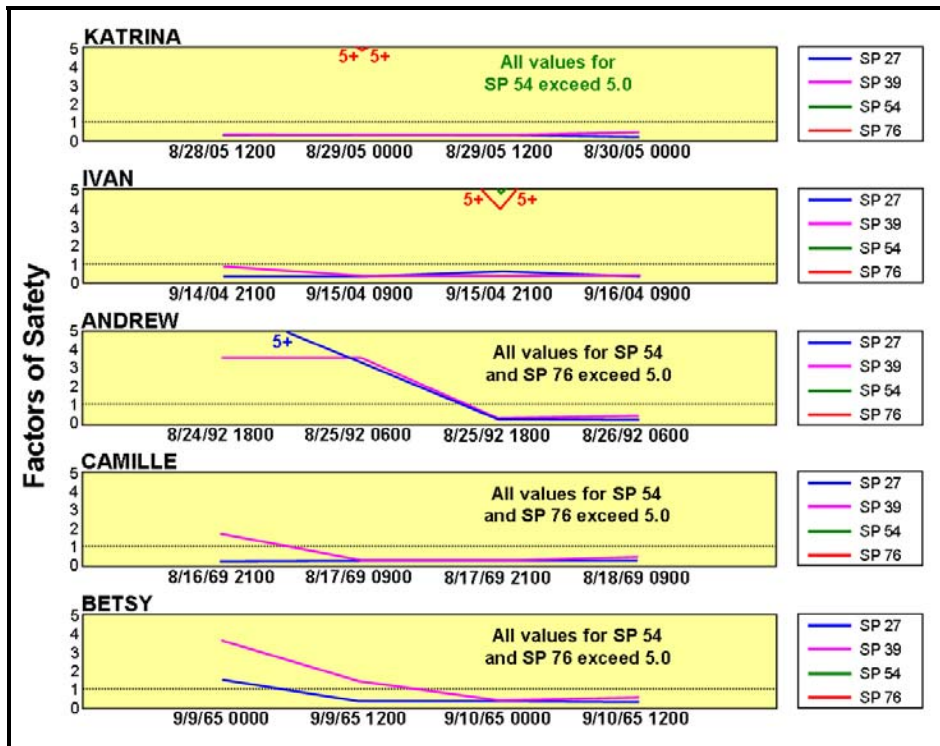


Figure 101: Factors of safety calculated along Cross Section F-F', Hurricanes Betsy through Katrina



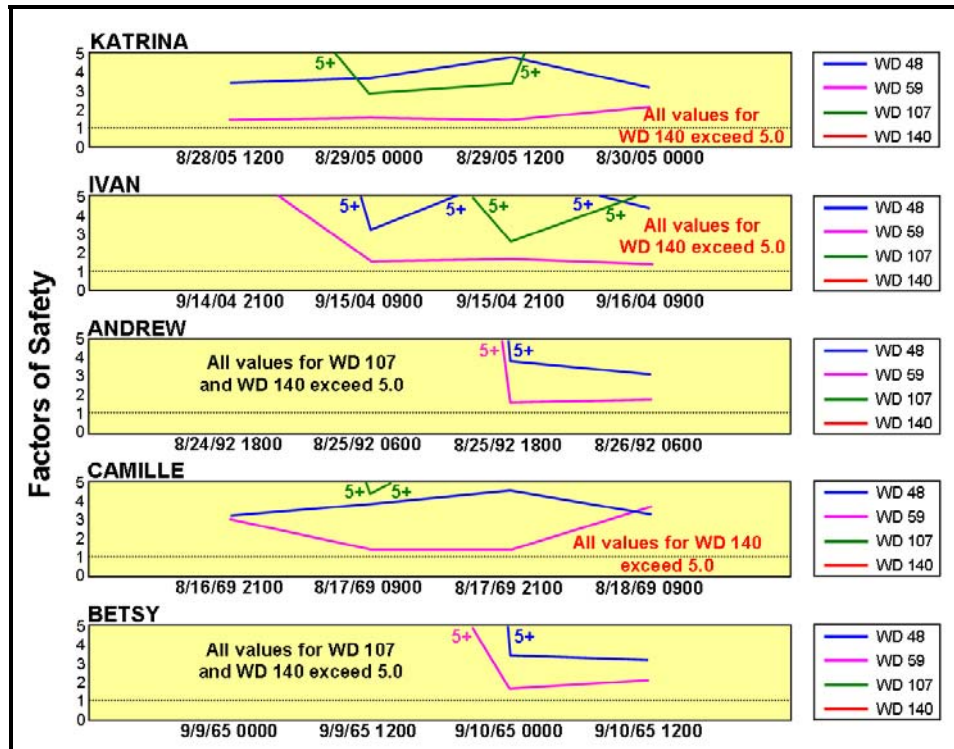


Figure 102: Factors of safety calculated along Cross Section G-G', Hurricanes Betsy through Katrina

Safety factors along Cross Section A-A' are relatively high and thus infer limited seafloor instability (Figure 96). No recorded instances of failure were noted during any of the five hurricanes studied. Although shear strength data were available for only three of the boreholes along this profile, safety factors all ranged above 1.0 over a 36-hour time span evaluated for each profile in the study area. Values for Hurricane Katrina were lower along a more extended time range, especially for Main Pass Blocks 43 and 128 (both boreholes were acquired prior to Katrina). Hurricane Andrew had the least effect on this area as lower safety factors were constrained with a narrower time window and the storm passed significantly farther to the west. The area near Main Pass Block 290 was the least affected, as it consistently yielded the highest safety factors of any borehole on this profile and leads to the hypothesis that this area is inherently more stable than areas closer to the MRD. Shear strength distribution as mapped by Dunlap et al. (2004) further quantifies higher shear strengths mapped on the eastern end of the profile near MP 290 (Figure 92).

Safety factors along Cross Section B-B' reflect similar overall trends, with lower safety factors nearer the MRD and higher safety factors farther east (Figure 97). The borehole most impacted by storm activity, both in terms of low safety factors and the time over which they prevailed, was at Main Pass Block 70 (acquired between Hurricanes Andrew and Ivan). Although these borehole data were relatively shallow, safety factors ranged at or slightly below 1.0 over a broad time span of each storm. These safety factors imply inherently unstable seafloor which is supported by seafloor failures that occurred on this block during both Hurricanes Ivan and Katrina. As with Cross Section A-A', the most stable areas are those farthest to the east at Main Pass Blocks 301 and 310 (acquired in 1988 and 1982, respectively). Hurricane Andrew impacted this area the least, passing farther to the west relative to the other four hurricanes. Safety factors for Main Pass Block 70 were consistently lowest, as wave periods were depicted by the MIKE 21 wave models as being longer closer to shore in relatively shallower water.

The area along Cross Section C-C' was at risk for seafloor failure for each hurricane except Andrew (Figure 98). Minimum safety factors for the South Pass (SP) Block 6 borehole (acquisition date unknown) fell consistently below the 1.0 failure threshold for all five hurricanes. Additionally, the area around SP 67 contained low safety factors for each hurricane except Andrew. Seafloor failure was reported at SP 60 during both Ivan and Katrina as well as at SP 70 during Camille (discussed in Section 3.3.2). Safety factors at both of those boreholes were at or near 1.0 during Katrina, Ivan and Camille; Hurricanes Andrew and Betsy passed farther to the west and had lesser impact. Soil conditions can vary greatly within a relatively small area on the seafloor and can yield highly variable safety factors and geotechnical properties depending on the exact location of a specific borehole (Quiros et al., 1983; Wright, 1976; Nodine et al., 2006; Nodine, 2007). Even though seafloor safety factors at SP 60 and SP 70 ranged at or above 1.0, the hypothesis exists that locally variable conditions would likely yield lower safety factors. Evidence for seafloor failure is illustrated by the variable nature of the seafloor bathymetry along Cross Section C-C' (Figure 78), which suggests that multiple seafloor failures occurred through

time. In addition, the sub-1.0 safety factors from the SP 6 borehole at least 24 hours prior to Katrina's maximum impact suggest that the seafloor is at risk of failure not only as a hurricane moves over a given area but also far in advance, and especially closer to shore where wavelengths and wave periods are higher in shallower water (Figure 98). At-risk safety factors at SP 6 actually precede Katrina's maximum impact by 48 hours (Appendix N, Table N-3). Likewise, low safety factors continued at the SP 6 location at least 12 hours after Katrina had passed through, suggesting that the seafloor continues to be at risk of failure even during post-storm sea-state recovery periods (Figure 95). A full return to non-risk safety factors occurred 36 hours after Katrina's maximum impact (Appendix N, Table N-3).

Only two boreholes from Cross Section D-D' contain shear strength information; however they yielded safety factors below 1.0 in most cases (the exception being SP 72 during Andrew; Figure 99). Safety factors for the area near SP 20 were consistently below 1.0 during a broad time range for each storm. Values for SP 72 indicate potential for failure during maximum impact except for Hurricane Katrina, which passed close by, and for Hurricane Betsy, which was a relatively fast-moving hurricane. As seen in SP 6 on Cross-Section C-C', safety factors during Hurricanes Betsy and Katrina ranged below 1.0 approximately 48 hours prior to maximum impact, demonstrating potential seafloor failure risk far in advance of maximum storm impact (Appendix N, Table N-4). Evidence for seafloor failure is illustrated by the highly variable seafloor bathymetry along this profile (Figure 80). No reports of seafloor failure exist at either SP 20 or SP 72; however the significant failure at Mississippi Canyon Block 20 lends further support to highly variable seafloor conditions and the potential for future seafloor failure.

Safety factors along Cross Section E-E' reflect seafloor risk for each hurricane except Andrew (Figure 100). Each borehole yielded a safety factor either near or below 1.0 during Ivan and Katrina. Hurricanes Camille and Betsy yielded shorter-duration response for SP 47 and, to some extent, SP 48, which is located only 5 km to the east. The response at SP 29, located in only 5 m of water, was much lengthier at or below the 1.0 safety factor threshold, thereby

implying seafloor failure risk throughout both the approach of and sea state recovery from a storm displaying similar metocean conditions. Although no seafloor failures were reported during any hurricane along this profile, the overall lower safety factors are consistent with implied historical seafloor failures elucidated from bathymetry change through time (Figure 82).

Safety factors along Cross Section F-F' vary considerably and appear grouped by water depth (Figure 101). Values for SP 27 and 39, which are located in 8 and 19 m of water, respectively, consistently fall below a 1.0 safety factor threshold for each storm evaluated. Safety factors for SP 54 and 76, located farther south and in deeper water, are higher and approach or exceed a value of 5.0, particularly during Hurricanes Camille and Betsy. MIKE 21-derived wave periods and wavelengths were much longer closer to shore (12 to 14 sec in shallower water vs. 8 to 10 sec in deeper water), thus increasing the maximum water pressure on the seafloor and thereby driving safety factors lower. Seafloor failure was reported at SP 38 during Hurricane Katrina, which is located 5 km east of SP 39 on Cross Section F-F' and consistent with expected safety factors (Figure 84). A seafloor failure was reported at SP 55 during Hurricane Ivan, approximately 5 km east of SP 54 on Cross Section F-F'; however, safety factors from the SP 54 borehole do not indicate a tendency for failure. The apparent discrepancy may result from widely variable soil conditions prevalent at SP 54 as well as the fact that the acquisition date for the SP 54 borehole is unknown and may not reflect conditions prevalent during Hurricane Ivan.

Lastly, safety factors along Cross Section G-G' consistently range above a 1.0 threshold for each of the five hurricanes studied (Figure 102). The lowest safety factors occur at West Delta (WD) Block 59, but even these consistently remain above 1.0. WD 59 is located approximately 15 km downdip from Southwest Pass of the MRD and thus the area is more vulnerable to higher sedimentation rates, resulting in underconsolidated sediment that can lead to increased instability and lower safety factor values. No seafloor failures occurred along this profile; the nearest failure occurred at WD 109, approximately 10 km east of WD 107 and downdip from the mouth of Southwest Pass (Figure 86). As in Cross Section F-F', boreholes

located in shallower water yielded lower safety factors, mainly as a function of the effects due to longer nearshore wavelengths and wave periods.

## **6.4 Shelf Failure Modeling**

### **6.4.1 1D Sediment Failure Modeling Program (BING)**

The characteristics of specific subaqueous mudflows were modeled using a 1D numerical model named BING, which was developed by researchers at the St. Anthony Halls Laboratory at the University of Minnesota (Imran et al., 2001a; 2001b). This model simulates muddy subaqueous and subaerial debris flows based on assumptions of initial mudflow size, thickness, viscosity, density (both mudflow and ambient conditions in which the mudflow fails), and rheology, all set against an initial bathymetric profile (see Figure 103 for a sample input panel). The underlying premise behind BING was to model muddy debris flows with sufficiently low permeabilities that prevent (or greatly inhibit) the loss of pore pressure during a non-hydroplaning mudslide failure (Imran et al., 2001b). One of two distinct rheological models can be used:

- Herschel-Bulkley model: Defined as a three-parameter rheological model of a non-Newtonian fluid (i.e. a fluid whose flow properties are not described by a single, constant viscosity value) under which fluids exhibit a non-linear (i.e., curved) shear-stress relationship (Hemphill et al., 1993).
- Bilinear model: Defined as a two-parameter rheological model under which fluids exhibit a linear shear-stress relationship (fluids following this relationship are referred to as Bingham plastic fluids; Hemphill et al., 1993).

Experiments with each rheological model indicated that frontal velocities calculated with Herschel-Bulkley accelerated more quickly, attained higher peak velocities, and then stopped very quickly. Frontal velocities simulated with the Bilinear model display similar trends until fluid flow reaches low strain rates during the deceleration phase, at which time fluids act as Newtonian fluids and display a “creeping” forward motion that continues indefinitely and never stops (Imran et al., 2001b).

The screenshot shows the 'BING...Input' window with the following sections and values:

- Initial Conditions:**
  - Position of Tail of Mud Deposit (m): 15000
  - Initial Length of Mud Deposit (m): 1200
  - Maximum Thickness of Mud Deposit (m): 5
  - Bed Elevation Data File: C:\Data\LSU\Dissemination\Mode (with 'Choose/Create File' button)
- Material Parameters:**
  - Rheology Model: ☒ Herschel-Bulkley, ☐ Bilinear
  - Reference Strain Rate (1/s): 2.5
  - Ratio of Strain Rates, r: 1
  - Apparent Yield Strength (Pa): 200
  - Mud Density (kg/m<sup>3</sup>): 1800
  - Ambient Fluid Density (kg/m<sup>3</sup>): 1025
- Numerical Model Parameters:**
  - Artificial Viscosity: .001
  - Number of Nodes in Domain: 21
  - Calculate Time Step (S): .0011573
  - Total Simulation Time (min): 1000
- Output:**
  - Output Display: ☒ Graphical, ☐ Numeric
  - Output Path: C:\Data\LSU\Dissemination (with 'Change Path' button)
  - OutFile Name: outfile.csv
  - FrontFile Name: frntfile.csv
  - Output Writing Interval (min): 5

At the bottom are two buttons: 'Run BING' and 'Exit'.

Figure 103: Input panel for the BING 1D numerical simulation failure model

A series of sediment failure models using the BING software program was run across the MRDF to quantify the extent to which seafloor failure occurred in the past. The outputs from these models, including mudflow final thickness, downslope extent traveled and the time required for the mudflow to reach its final downslope position, were used to help estimate the size and corresponding sediment volume of transported material. As BING is a 1D model, it does not provide estimates of width; however, an approximation of size and volume can be made based on historical evidence of past slides based on seafloor bathymetry data. Modeling these existing failures helped calibrate the BING model such that estimates of future failures could be predicted for a given set of input parameters.

The BING model does not account for hydroplaning of submarine failures. Abnormally long runout distances have been recorded with many failures, which are attributed to frontal pressure and lift forces that allow a layer of water to intrude underneath the slide, which in turn reduces friction and induces tensile stress behind the front of the failure (Mulder & Cochonat

1996; Ilstad et al., 2004; Bryn et al., 2002). In extreme cases, the front of the mudflow can become detached from the main body of the mudflow, resulting in an “outrunner block” that is far removed downdip from the rest of the failure. These phenomena have been noted in the GOM but were not modeled in the existing BING program.

#### **6.4.2 1D Sediment Failure Modeling, Prior MRDF Mudslides**

BING modeling runs were made along each of the dip profiles where time-series bathymetry data were available that could be used as a test for mudslide runout distance and where known cases of failure had taken place previously. A true dip profile along each cross section was created and then digitized using DigitizeIt software as the basis for existing bathymetry and in such a way as to eliminate the zigzag nature of certain cross sections due to borehole location. In addition to regional bathymetry data, locally available high-resolution bathymetry data were used as a basis for runout modeling in BING.

Historical regional bathymetry data as well as local high-resolution data are limited along Cross Section A-A', and therefore this section was not used for runout modeling purposes. Along Cross Section B-B', a failure occurred at Main Pass 70. However, historical regional bathymetry surveys are limited near MP 70 and only the 1940 and NOAA surveys cover the area (Figure 76).

Working with these available data, attempts were made to model bathymetry differences from 1940 and later surveys (the NOAA and regional 1997 Vastar surveys) along the western half of Cross Section B-B' (Figure 76). Models were run using the bilinear rheology option and were terminated when the final velocity of the failure reached  $0.25 \text{ m sec}^{-1}$ . Model sensitivities were run assuming failures of various failure lengths and thicknesses (Table 9). Results indicated that the eastern-most terminus of the bathymetry delta was reached by a failing mudslide only when initial mudslide thickness was at least 15 m given a 5000-meter mudslide length. In no case did the final thickness of the mud deposit reach the thickness of the bathymetry delta between any of the surveys. The maximum calculated thickness was approximately 7.5 m, yet thicknesses along Cross Section B-B' yielded values of approximately 10-11 m (Figure 76). These results support a



Table 9: Regional BING model sensitivities, Cross Section B-B'

Inputs			Outputs			
Initial position (m)	Mudslide length (m)	Mudslide thickness (m)	Runout length (m)	Time elapsed (min)	Maximum velocity (m sec <sup>-1</sup> )	Final velocity (m sec <sup>-1</sup> )
7000	2500	5	6,044	44.3	4.4	0.25
7000	2500	10	7,704	60.6	7.6	0.25
7000	2500	15	9,626	57.5	10.7	0.25
7000	5000	5	8,252	35.8	3.4	0.25
7000	5000	10	21,264	198.8	6.2	0.25
7000	5000	15	27,124	217.3	8.8	0.25
7000	7500	5	13,444	134.5	3.1	0.25
7000	7500	10	26,635	215.8	6.4	0.25
7000	7500	15	37,778	421.5	8.3	0.25

hypothesis that no single seafloor failure can account for the differences between the surveys and that the difference in bathymetry thickness must be the result of either multiple failures through time, progradation of the MRD, or a combination of both.

Results also indicate that mudslide thickness at shorter lengths has less effect on eventual runout distance than at longer lengths (Table 9). Runout distance for the maximum thickness case at 2500 m was 27% longer than the minimum case, yet runout distance for the maximum thickness case at 7500 m was 119% longer than the corresponding minimum. Total elapsed times at shorter mudslide lengths were grouped much closer together than those of longer mudslides; times for the thickest slides surpassed thinner slides by over a 3:1 ratio (Table 9). Maximum mudflow velocities attained were higher with increased mudslide thickness but were widely variable depending on initial mudslide length (i.e., the maximum velocity attained was not length-dependent; Table 9).

Along Cross Section C-C', the SP 70 failure during Hurricane Camille was modeled to generate a match with post-storm bathymetry and runout distance as delineated in post-storm seafloor surveys (Bea, 1971; Sterling and Strohbeck, 1975; Figures 15 and 16, Section 3.3.2). Models were run using the bilinear rheology option and were terminated when the final velocity of the failure reached 0.1 m sec<sup>-1</sup> (Table 10). A lower final velocity threshold was used in this

Table 10: BING model match, South Pass 70 failure

Inputs			Outputs			
Initial position (m)	Mudslide length (m)	Mudslide thickness (m)	Runout length (m)	Time elapsed (min)	Maximum velocity (m sec <sup>-1</sup> )	Final velocity (m sec <sup>-1</sup> )
12,300	730	1.8	490	52.7	0.39	0.10

case since the scale of the mudslide was smaller than those modeled in Cross Section B-B'. Results indicated that a relatively quick failure occurred at SP 70 that was comparable to failures with shorter initial mudslide lengths seen in Cross Section B-B'.

As discussed in Section 6.2, post-Camille shear strength data from boreholes at SP 70 suggest the presence of a crustal block at SP 70 that extends to a depth of approximately 24 m (80 feet; Bea et al., 1980). In addition, the net bathymetry difference between the 1874 and 1940 data is approximately 18 m (Figure 78). Sensitivity modeling in BING suggests that these are likely not the result of a singular event but instead are the result of cumulative, multiple failures that occurred through time and/or represent continued progradation of the MRD. Sediment thicknesses attained in the model ranged only from 2-8 m depending on variables used as input criteria (e.g., changing the slurry density, initial mudslide thickness or apparent yield strength).

Elsewhere along Cross Section C-C', seafloor failure occurred during both Hurricanes Ivan and Katrina at South Pass 60 (MMS, 2005a; 2005b). No high-resolution data were available over SP 60 to enable comparisons of seafloor bathymetry before and after each storm although differences between each regional bathymetry data set support a hypothesis that prior failures occurred through time (Figure 78).

Significant variation in seafloor bathymetry exists along Cross Section D'-D' (Figure 80). This profile's proximity to the MRD and sediment accumulation through time is can be seen in the profile, with each successive regional bathymetry dataset being, on average, shallower than the one that preceded it. In addition to normal delta progradation, the profile also suggests significant seafloor failures, one in particular that occurred at Mississippi Canyon Block 20 (MC 20) during Hurricane Ivan (MMS, 2005a). High-resolution multi-beam bathymetry data

over the southeastern quadrant of this block were obtained for use in this dissertation and are discussed in more detail in Section 7.2.3. These data indicate that the mudflow noses are approximately 20 m thick relative to the pre-2004 seafloor. Updip of the mudflow noses, high-resolution data exists and could help indicate potential failure thickness, but these data were unavailable for use. Instead, modeling in BING was carried out to estimate a range of estimated thicknesses and sediment properties required to yield the mudflow noses seen along this profile (Table 11). The models assumed failure approximately 12 km updip from MC 20 and extending either 6,500 m in length or 3,500 m in length. These lengths were chosen based on what appear to be previously existing mudflows and potentially unstable seafloor (Figure 80).

Table 11: BING model results, Cross section D-D'

Inputs			Outputs			
Initial position (m)	Mudslide length (m)	Mudslide thickness (m)	Runout length (m)	Time elapsed (min)	Maximum velocity (m sec <sup>-1</sup> )	Final velocity (m sec <sup>-1</sup> )
12,000	6,500	25	6,555	153.0	1.46	0.50
12,000	6,500	30	7,794	148.5	1.29	0.50
12,000	6,500	35	11,798	216.0	2.86	0.50
12,000	3,500	25	1,570	32.5	2.02	0.50
12,000	3,500	30	2,305	42.5	3.08	0.50
12,000	3,500	35	3,027	51.5	4.26	0.50

The best fit horizontally to existing, post-Ivan morphology was a sensitivity containing a failure thickness of 30 m and a length of 6,500 m. The resulting mudflow conforms to morphology seen in post-Ivan multi-beam bathymetry and terminates approximately 2 km past MC 20. However, the resulting mudflow thickness yielded from the model never exceeded 10 m, leading to a hypothesis that more than one mudflow occurred at MC 20 during Hurricane Ivan (Figure 104). As a further check, additional sensitivities were run and in no case did final mudflow thickness approach the 20 m mudflow thickness revealed by post-storm data. Cases run at thicknesses of 3,500 m (i.e., assumes that only the uppermost instability failed) never yielded a mudflow terminus that extended to the MC 20 failure. As a result, the failure that generated the MC 20 mudflow likely consisted of updip seafloor instability of considerable length.

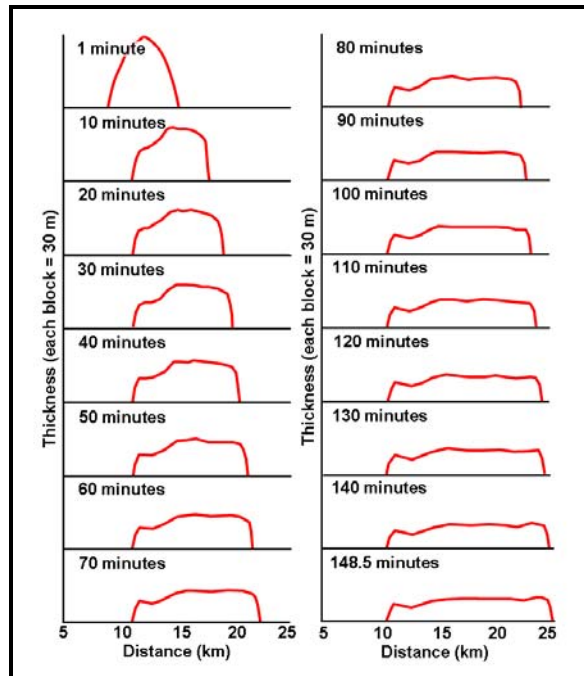


Figure 104: Shape of potential MC 20 seafloor failure and resulting mudflow nose during Hurricane Ivan as modeled in BING

Regional bathymetry along Cross Section E-E' depicts considerable variation through time (Figure 82). This profile is located proximal to South Pass of the MRD; the rapid deposition of sediment through time is implied by (1) the differences in regional bathymetry, and (2) shear strength profiles of the three southeastern-most boreholes that indicate the presence of underconsolidated sediment (profiles follow a trend of  $2 \text{ psf foot}^{-1}$  ( $3.14 \times 10^{-1} \text{ kPa m}^{-1}$ )). Prior seafloor failure along this cross section is evidenced by more recent bathymetry profiles occurring in places deeper than older bathymetry profiles. However, no seafloor failures were reported during either Hurricanes Ivan or Katrina in the vicinity of this cross section (MMS, 2005a; 2005b).

Seafloor failure occurred at South Pass Blocks 38 and 55 during Hurricanes Katrina and Ivan, respectively (MMS, 2005a; 2005b). These two locations are each one block (i.e., approximately 5 km) removed from boreholes located on Cross Section F-F' (Figure 84). High-resolution bathymetry over SP 38 acquired in 1995 indicate a relatively even seafloor except for two prior failures along the southern edge of the block that appear to have taken place between

1874 and 1940 (i.e., the failures do not appear on the 1874 data but appear on data from 1940 onward). Modeling these particular failures indicated considerably long runout distances, primarily because of a change in seafloor gradient and a relatively steeper slope proximal from the failures (Table 12). Resulting mudflow thicknesses were approximately 1 m, reflecting the broad agreement of regional bathymetry data from 1940 onward adjacent to and downdip of SP 38.

Table 12: BING model results, South Pass 38, Cross section F-F'

Inputs			Outputs			
Initial position (m)	Mudslide length (m)	Mudslide thickness (m)	Runout distance (m)	Time elapsed (min)	Maximum velocity (m sec <sup>-1</sup> )	Final velocity (m sec <sup>-1</sup> )
15,000	1200	5	4098	190.0	3.01	0.10

Historical regional bathymetry data as well as local high-resolution data are limited along Cross Section G-G', and therefore this section was not used for runout modeling purposes. No seafloor failures were reported in the vicinity of this cross section during Hurricanes Ivan or Katrina (MMS, 2005a; 2005b).

#### 6.4.3 1D Sediment Failure Modeling, Potential MRDF Mudslides

BING modeling runs were conducted along cases discussed in Section 6.4.2 to test the potential for future shelf failure in the vicinity of areas known to have experienced prior failure. The elevation basis used for these models was the most recent bathymetry data available (varied from regional to local bathymetry depending on location and data coverage).

A BING model using best-fit parameters identified in Section 6.4.2 was constructed along Cross Section C-C' and includes an area downdip from the prior SP 70 failure (Table 13). Runout lengths were 167% longer, likely because the location of any future mudslide would transcend the shelf edge directly adjacent to SP 70. If these predictive results are accurate, a future mudslide could pose a risk to a north-south pipeline extending southward from SP 70 and Viosca Knoll Block 983 (elements at risk are discussed further in Chapter 9). No platforms are immediately downdip from this potential mudslide area; however, a platform located in MC 21

Table 13: BING model results, South Pass 70 failure (future case)

Inputs			Outputs			
Initial position (m)	Mudslide length (m)	Mudslide thickness (m)	Runout length (m)	Time elapsed (min)	Maximum velocity (m sec <sup>-1</sup> )	Final velocity (m sec <sup>-1</sup> )
13,000	750	2.0	1309	108.5	1.22	0.10

could be at risk of future successive slides. Installed in 2005, it is located directly downdip of a major mudflow lobe identified from recent, post-Katrina bathymetry data (Enterprise Products Partners, LLC, 2005; discussed further in Section 7.2.3) and approximately 6 km east of the MC 20 platform destroyed during Hurricane Ivan. A small but dense network of pipelines also exists in MC Blocks 20 and 21 that is used to gather gas from nearby fields either along strike or farther offshore in deeper water and transport it onshore for processing.

An additional BING model was constructed along Cross Section D-D' in the vicinity of MC 20 using best-fit parameters identified in Section 6.4.2 (Table 14). Runout lengths were much higher than the original failure models (53% to 218% higher), likely because of steeper downdip slopes on which the models were based (i.e., downdip from previous failures and located on the upper continental slope). If these model results hold true, a future mudslide could pose a risk to an east-west pipeline extending from MC 65 to MC 68 (elements at risk are discussed further in Chapter 9). No platforms are located immediately downdip from this potential mudslide area.

A final model was run along Cross Section F-F' to test future seafloor impact using best-fit parameters identified in Section 6.4.2 (Table 15). A slightly longer runout distance was calculated for a subsequent mudslide than what was observed in the original model. If model results hold true, a future mudslide in this area could imperil two northwest-southeast oriented pipelines extending southward into SP 54 and 55 (elements at risk are discussed further in Chapter 9). However, because of the orientation of the pipelines (parallel to flow direction) the potential for pipeline rupture is minimized and the most prominent danger to the pipeline would occur from tensile stresses documented elsewhere in South Pass (Arnold, 1967). The closest

platform to this potential failure is located in SP 55. Installed in 1970 (MMS, 2009), it is likely too far downdip to be affected by an immediate, singular failure. However, if additional failures occur in succession this platform could face future mudflow hazards with time.

Table 14: BING model results, Cross Section D-D' (future case)

Inputs			Outputs			
Initial position (m)	Mudslide length (m)	Mudslide thickness (m)	Runout length (m)	Time elapsed (min)	Maximum velocity (m sec <sup>-1</sup> )	Final velocity (m sec <sup>-1</sup> )
18,000	6,500	25	10,030	175.8	3.73	0.50
19,000	6,500	30	13,548	218.5	6.03	0.50
24,000	6,500	35	16,739	257.0	8.24	0.50
18,000	3,500	25	4985	89.5	3.11	0.50
19,000	3,500	30	6657	109.5	4.47	0.50
24,000	3,500	35	8192	118.0	5.78	0.50

Table 15: BING model results, South Pass 38, Cross section F-F' (future case)

Inputs			Outputs			
Initial position (m)	Mudslide length (m)	Mudslide thickness (m)	Runout distance (m)	Time elapsed (min)	Maximum velocity (m sec <sup>-1</sup> )	Final velocity (m sec <sup>-1</sup> )
19,000	1200	5	4983	201.7	2.97	0.10



## **CHAPTER 7. MORPHOLOGIC CONTROLS**

Multiple bathymetric and geohazard studies have been conducted across the Mississippi River Delta Front (MRDF) and serve as the basis for an investigation into morphological change through time. The three regional grids (1874, 1940 and 1977) discussed in Section 4.1.1 were used to compute gross changes in seafloor bathymetry through time. While no direct hurricane implications can be drawn because of the time increment between these surveys, they are useful to help delineate the seaward advance of the MRDF. In addition to the regional surveys, this study incorporates results from 46 local MRDF bathymetric and geohazard surveys collected from 1964 through 2005 in the Main Pass, South Pass, Viosca Knoll, West Delta and Mississippi Canyon Protraction Areas (Figure 22, Section 4.1.1). These surveys, which contain bathymetry data and occasionally high-resolution seismic data, were used to help document incremental changes in seafloor morphology and near-surface stratigraphy through time.

### **7.1 Regional Bathymetric Changes in Study Area, 1874-1977**

The 1874 regional survey was collected across a relatively narrow area of the MRDF (Figure 23, Section 4.1.1). The reliability of such an early survey cannot be verified but the data were considered reliable for regional-scale studies. The 1940 survey was collected across a somewhat wider area and, unlike the 1874 survey, clearly delineates features associated with shelf failure including numerous mudflow gullies and mudflow noses downdip of the MRDF apron (Figure 24, Section 4.1.1). The 1977 survey covers a much wider swath of the MRDF than either the 1874 or 1940 surveys (Figure 25, Section 4.1.1).

A comparison between the 1874 and 1940 datasets, representing a time increment of 66 years, reveals several areas of net sediment deposition adjacent to Southwest Pass, South Pass and Pass a'Loutre (Figures 105 and 106). Other smaller, isolated pockets of net sediment gain line the periphery of the MRDF and likely represent new mudflow noses that formed downdip from shelf failures in shallower water. In addition, an area of net sediment loss exists in the southern part of the South Pass Area and the northwestern part of the Mississippi Canyon Area that most

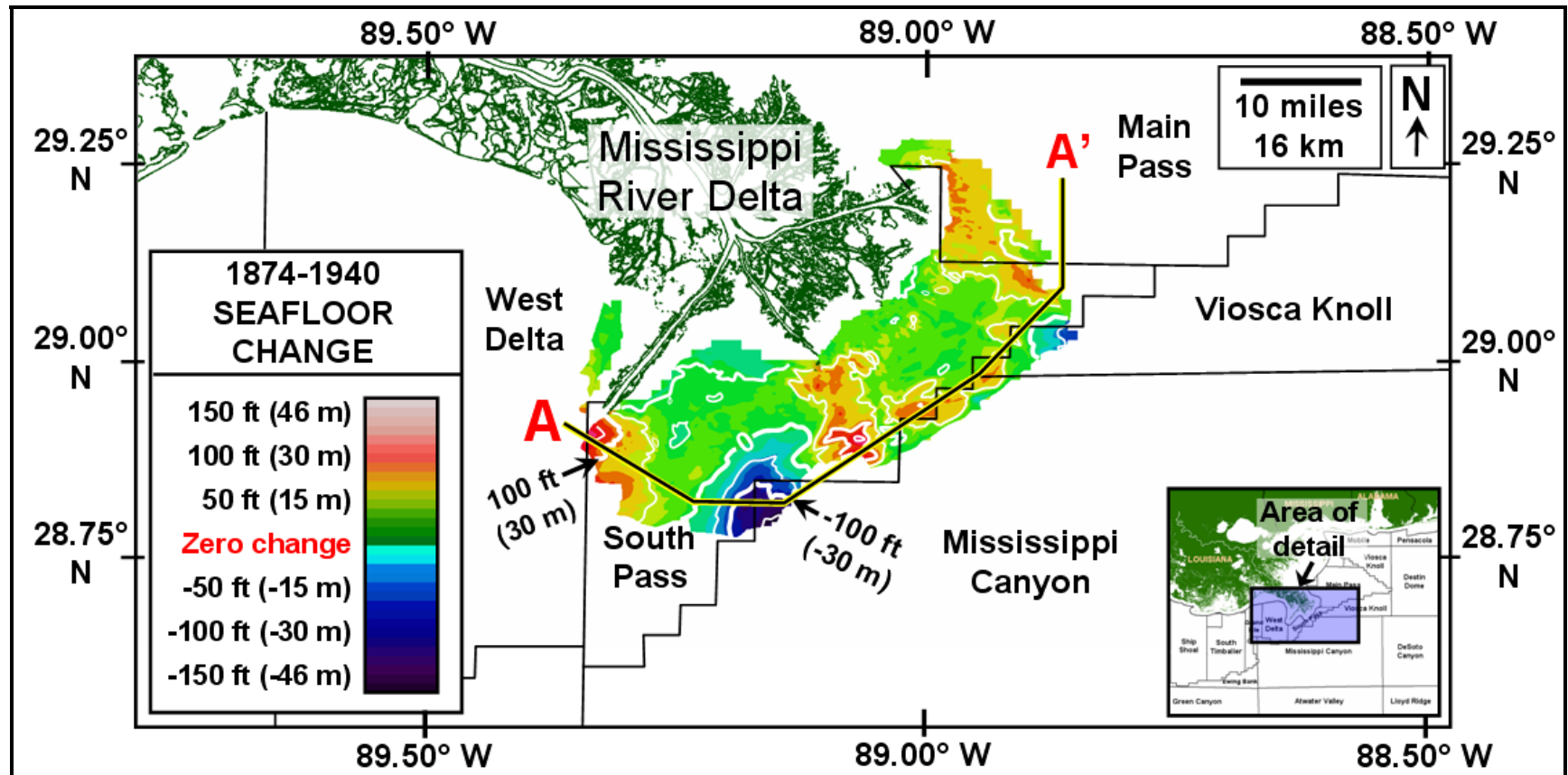


Figure 105: Net change in MRDF seafloor bathymetry, 1874-1940 (current Mississippi River Delta land profile used for illustration purposes)

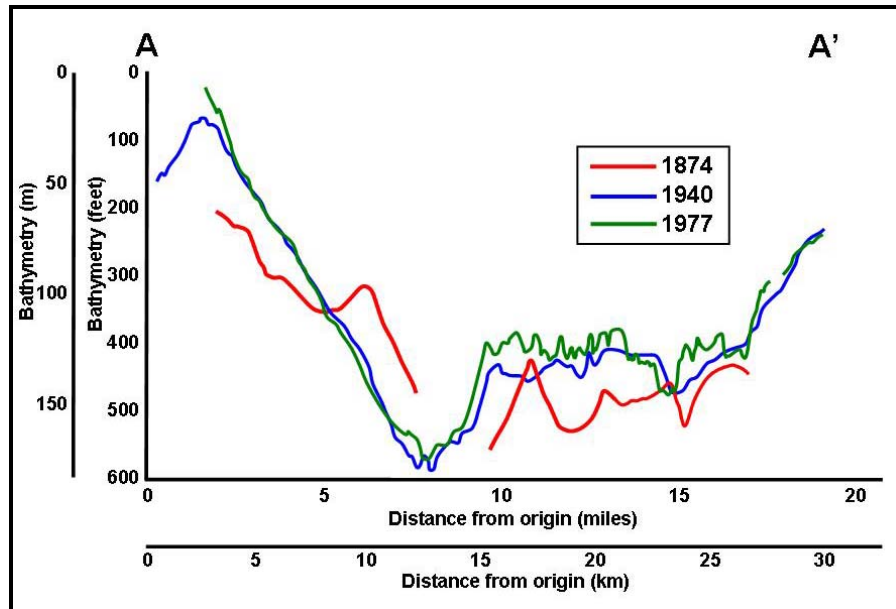


Figure 106: Regional MRDF bathymetry profiles, 1874-1977

likely represents the failure of a mudflow lobe depicted on the 1874 bathymetry data (Figures 25, 105 and 106).

During the period from 1874-1940, a total of ten hurricanes (Category 3 or greater) passed within 300 km of the MRDF (Table 1). Two of these, the Chenier Caminada Hurricane of 1893 and the New Orleans Hurricane of 1915, would have produced  $H_{s_{max}}$  exceeding 13 m by Hsu's (2006) wave height estimation method, which is slightly less than but still within range of conditions during Hurricane Ivan (Table 1; Figures 40, 41 and 43, Section 5.2.1). These hurricanes were also relatively slow-moving hurricanes and spent approximately seven hours traversing the MRDF study area, exactly in line with Hurricanes Andrew and Ivan and only slightly less than Hurricane Katrina (Figures 30, 33-35 and 38, Section 5.2.1). Therefore, the hypothesis that these hurricanes could have caused these seafloor failures is plausible, although it cannot be proved because of the lack of survey data during this time period.

A comparison between the 1940 and 1977 datasets, representing a time increment of 37 years, also reveals areas of net sediment deposition adjacent to Southwest Pass and, to a lesser extent, South Pass and Pass a'Loutre (Figure 107). The serrated contours of the 1940-1977 net

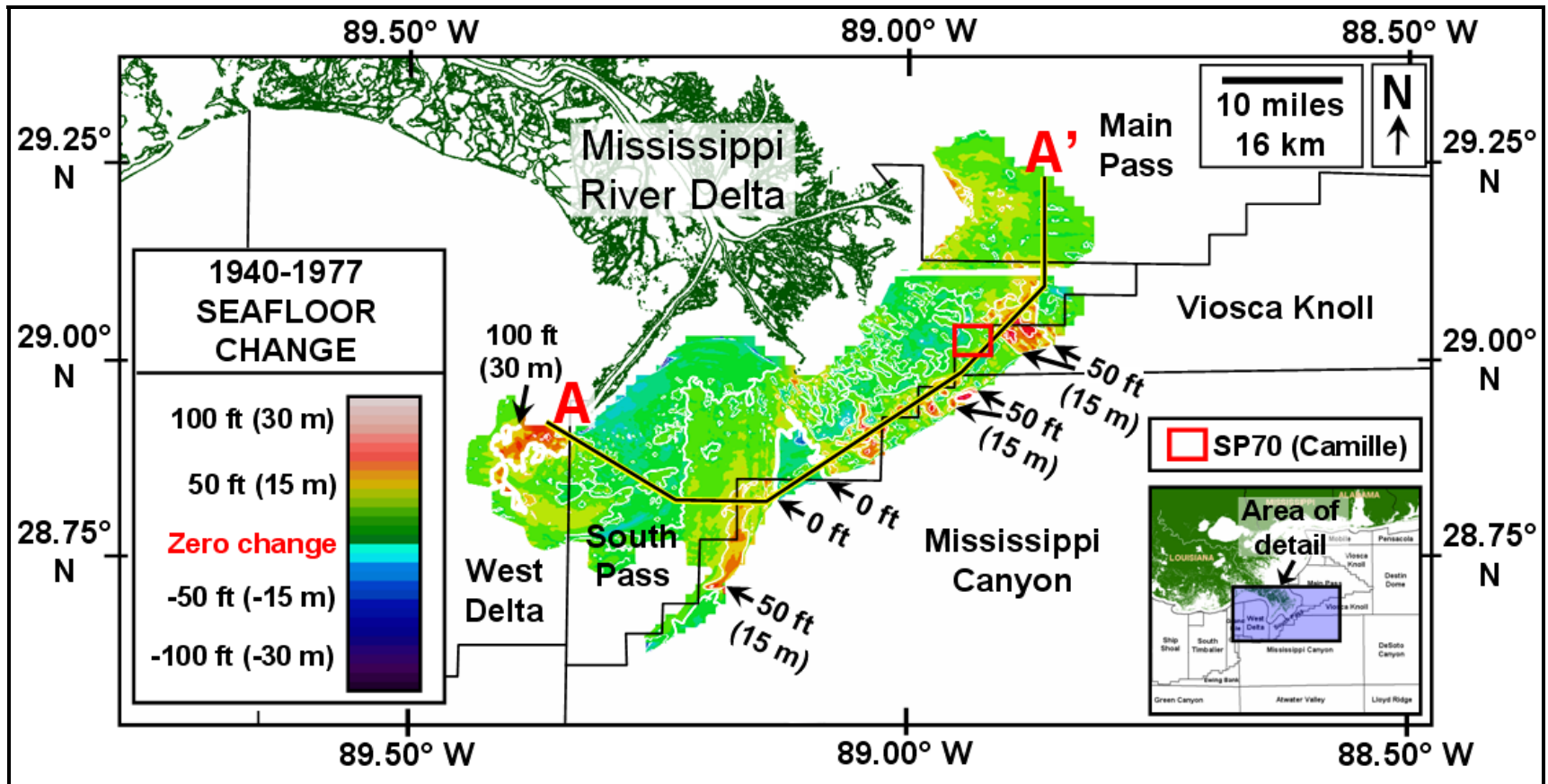


Figure 107: Net change in MRDF seafloor bathymetry, 1940-1977 (current Mississippi River Delta land profile used for illustration purposes)

bathymetry change indicate a complex, ephemeral system of mudflow gullies and sediment transport mechanisms (Figure 107).

During the period from 1940-1977, a total of five hurricanes (Category 3 or greater) passed within 300 km of the MRDF (Table 1; Figures 29 and 30, Section 5.1.2). Two of these, Hurricanes Betsy and Hilda, would have produced  $H_{s_{max}}$  exceeding 14 m by Hsu's (2006) wave height estimation method, which is within range of conditions during Hurricane Ivan (Table 1). Credence to these results is provided by bulk wave parameters simulated in the MIKE 21 wave model during Hurricane Betsy, which approached values of approximately 14 m as well (Figures 49 and 50, Section 5.2.2). Hurricane Camille, which was a small but intense storm, would have produced  $H_{s_{max}}$  near 21 m by Hsu's (2006) method. However, these values are higher than  $H_{s_{max}}$  simulated in the MIKE 21 wave model, which yielded values of approximately 15 m that more likely represent actual bulk wave parameters encountered (Table 1; Figures 45 and 46, Section 5.2.2).

## **7.2 Case Studies of Localized Bathymetric Changes in Study Area, 1964-2008**

The site-specific array of MRDF geohazard surveys was used to help quantify seafloor change in each Validation Test Area (VTA; Figure 22, Section 4.1; also Appendix K). Data quality varies from survey to survey but was considered sufficient for bathymetric comparison. Each VTA contains at minimum several surveys, some of which offer temporal repeatability of coverage across similar swaths of the shelf and upper slope. Variations in seafloor topography and steepness can then be utilized when assessing ultimate vulnerability for a given area.

### **7.2.1 Case Studies in Seafloor Failure – Validation Test Area One**

VTA 1 is located just east of the present-day Mississippi River Delta (Figure 22). A wide array of geohazard surveys spanning multiple time periods exists within the area, the most prominent of which include the regional MRDF surveys acquired in 1874, 1940 and 1977 as well as a semi-regional survey dating from 1997 (Vastar Resources, Inc., 1997a; Appendix K).

Additionally, the area is situated in a relatively mature oil producing area and therefore contains nine local, site-specific surveys acquired between 1975 and 2005 (Figure 22; also Appendix K).

The highest-quality (and therefore the most detailed) comparison datasets are two surveys that cover BP's Main Pass Oil Gathering System (MPOG). High-resolution multi-beam bathymetry data were collected after Hurricanes Ivan (Fugro GeoServices, Inc., 2004). Areas of slope failure can be seen along the 37 m (120 feet) isobath and where failure has retrograded back to the approximate level of the 34 m (110 feet) isobath (Figure 108; each color contour change represents 1.5 m (five feet) in bathymetric relief). Relatively large crustal blocks are detected immediately downslope from failed areas. These blocks also appear intact, commonly with topographic relief of approximately 3 m (10 feet), suggesting that movement occurred as a discrete block into deeper water. Additionally, these failures result in steep slopes along the updip end of the retrogressive failures, along the sides of each failure parallel to movement, and along the periphery of each failed crustal block (Figure 109).

These data were supplemented by an additional high-resolution survey acquired one year later immediately after Hurricane Katrina (Figure 110; Fugro GeoServices, Inc., 2005c). As with the post-Ivan data, areas of slope failure and downdip crustal movement were also detected and were confined primarily to areas immediately downdip of the steepest retrogressive slopes detected after Hurricane Ivan one year earlier, particularly along and just downdip from the 37 m (120 feet) isobath (Figures 111 and 112).

The impact of Hurricanes Ivan and Katrina on seafloor morphology is best revealed in comparisons to historical MRDF regional bathymetry. The 1940 dataset is the only one that covers the area, and its profile reflects a relatively smooth seafloor that also coincides with higher-relief, non-failed seafloor identified in the 2004-05 data (Figure 112). The resolution of the 1940 data was likely lower than the two MPOG surveys; however on a gross scale it reflects a relatively smooth seafloor that had not yet been impacted by recent hurricanes. A 14-year gap exists between 1940 and the Great Miami Hurricane of 1926, which had been the most recent

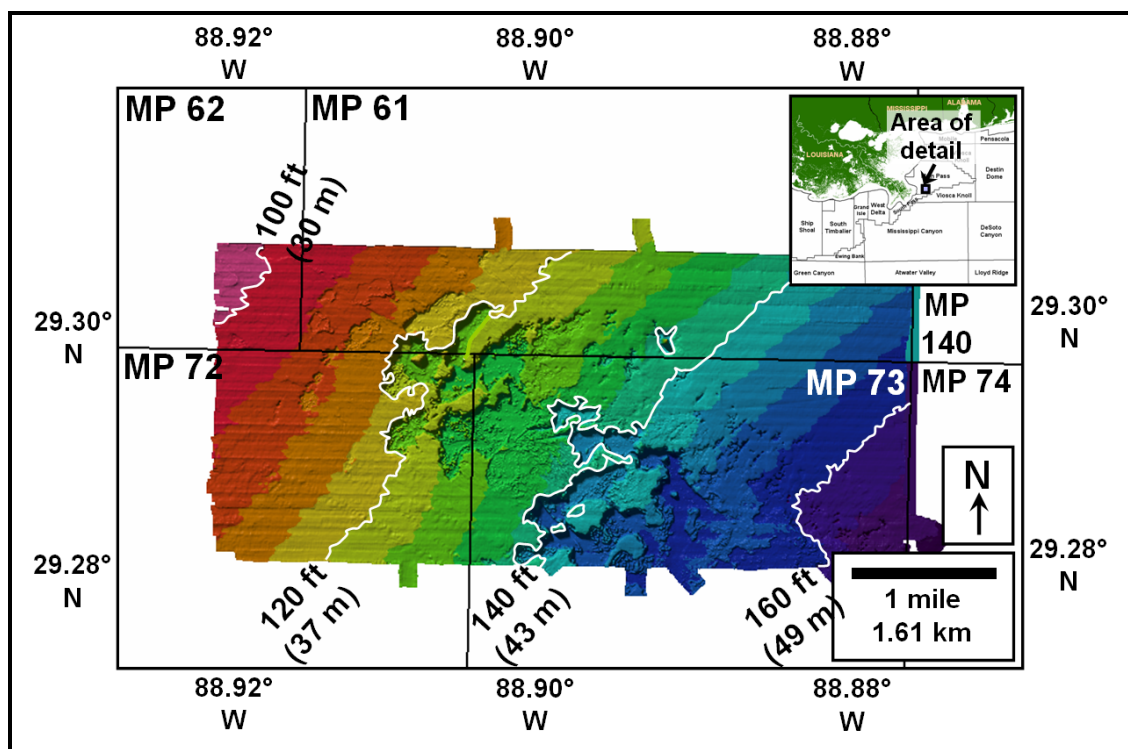


Figure 108: Post-Ivan (2004) bathymetry, Main Pass Oil Gathering System (MPOG; raw data from Fugro GeoServices, Inc., 2004)

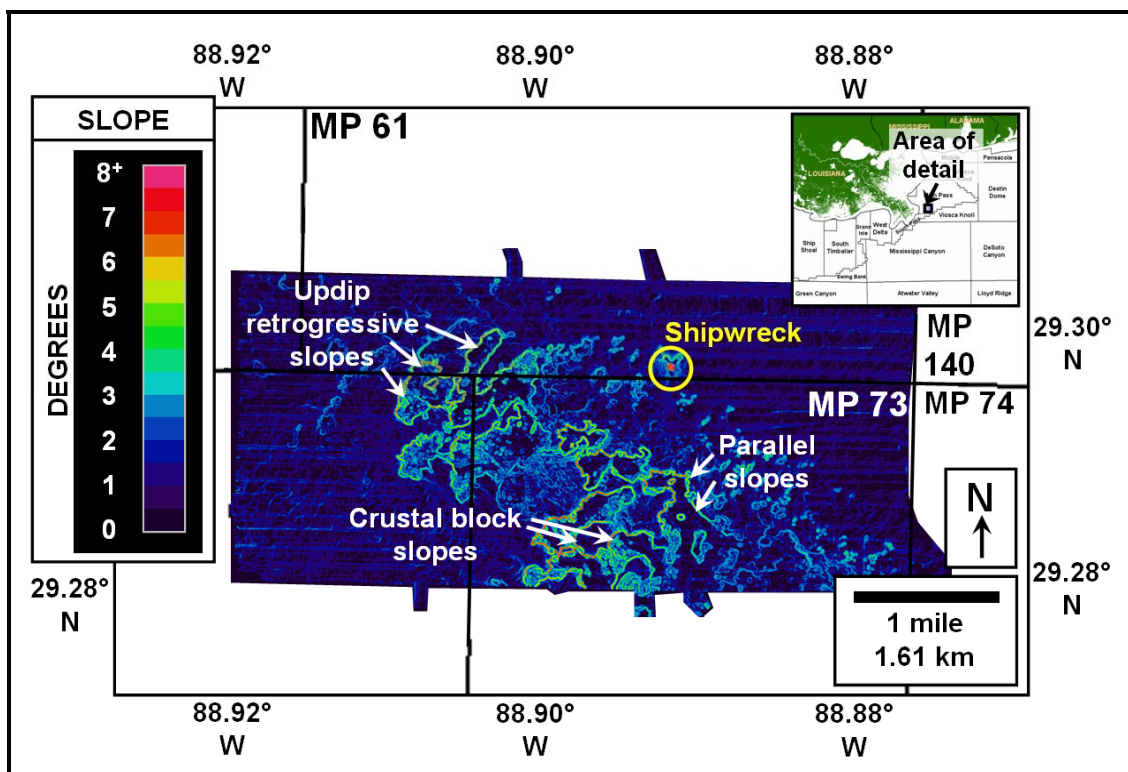


Figure 109: Slope steepness generated from post-Ivan (2004) bathymetry, Main Pass Oil Gathering System (MPOG; raw data from Fugro GeoServices, Inc., 2004)



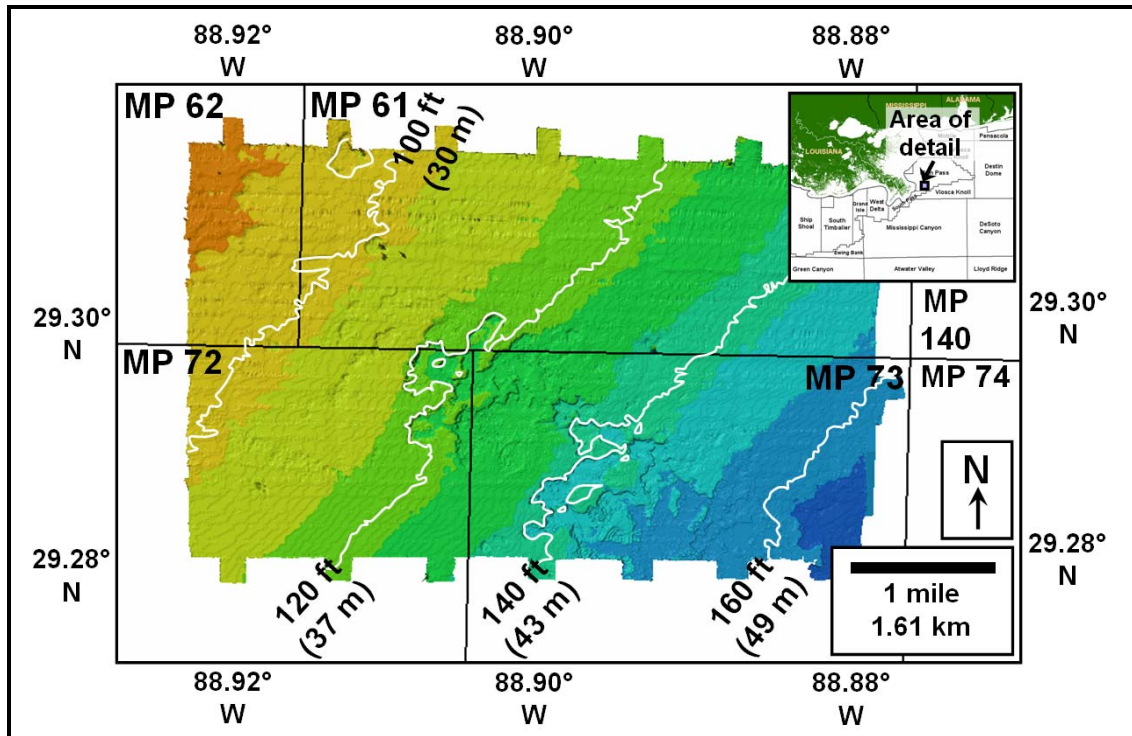


Figure 110: Post-Katrina (2005) bathymetry, Main Pass Oil Gathering System (MPOG; raw data from Fugro GeoServices, Inc., 2005c)

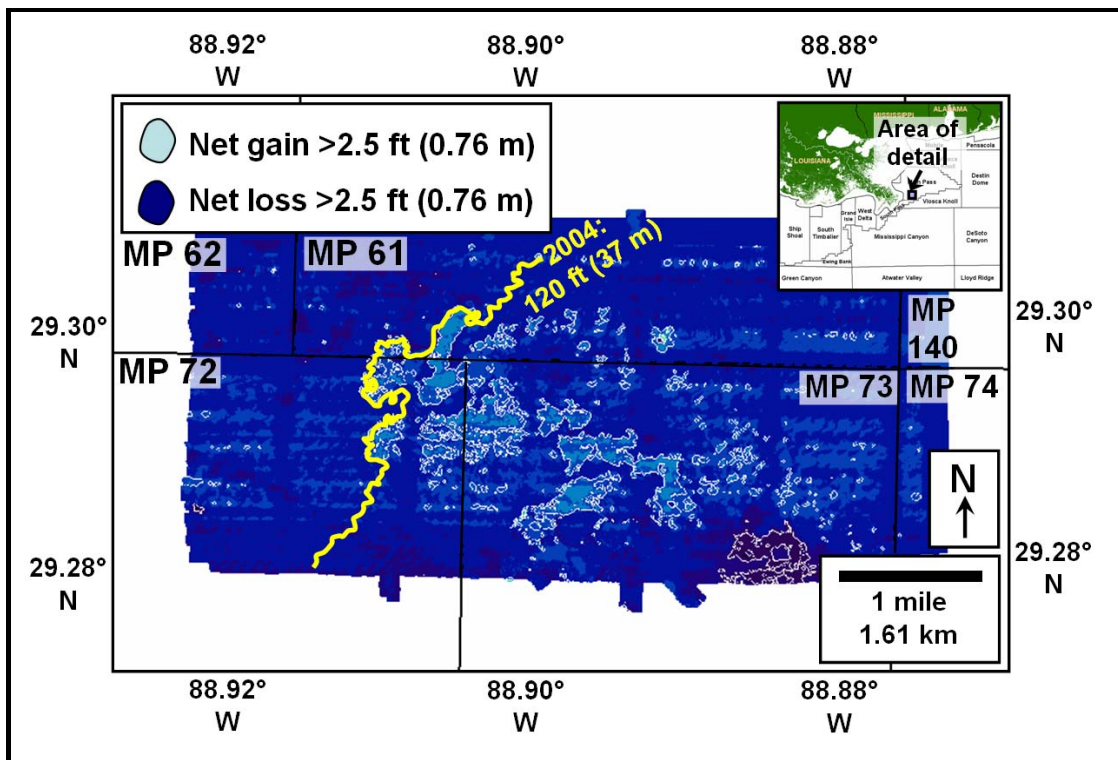


Figure 111: Net seafloor change, 2004-05, Main Pass Oil Gathering System (MPOG; raw data from Fugro GeoServices, Inc., 2004 and 2005c)

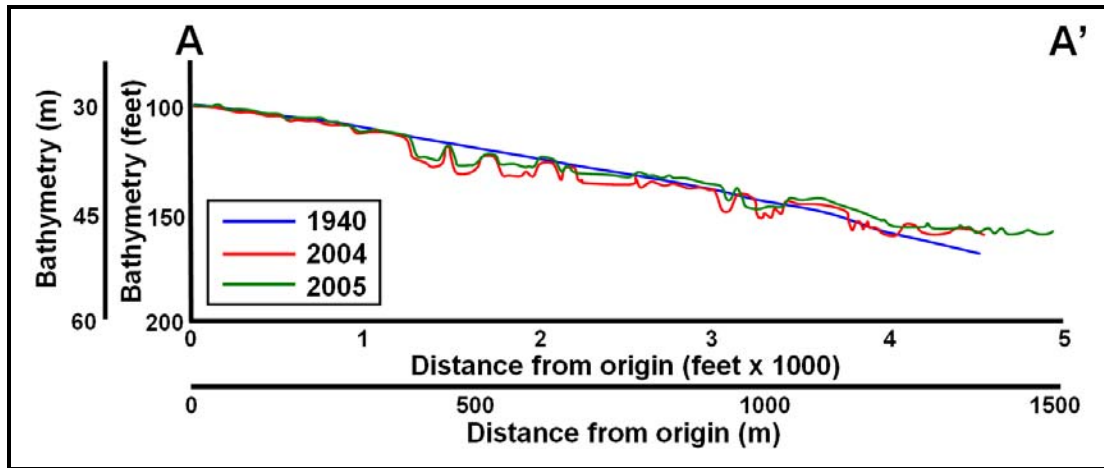


Figure 112: Bathymetric profile through time, Main Pass Oil Gathering System (MPOG; raw data from Fugro GeoServices, Inc., 2004 and 2005c)

hurricane to impact the area (landfall in Hancock County, Mississippi as a Category 3 hurricane). Post-1940, a gap of 29 years exists before the area was impacted by another severe hurricane (Camille). The hypothesis that Hurricane Camille could have caused the MPOG failures and that Hurricanes Ivan and Katrina merely exacerbated seafloor instability as they passed through the area cannot be definitively proven. No surveys were acquired in the MPOG area immediately after 1969 to compare against the 1940 data. However, the MPOG area is located approximately 24 km (15 miles) north of the South Pass Block 70 (SP 70) seafloor failure that occurred during Camille (discussed in Section 3.3.2). These two areas are situated parallel to the track of Hurricane Camille and therefore were exposed to similar metocean conditions as the hurricane approached the Mississippi coast. Spectral wave modeling performed using MIKE 21 indicates that these two areas experienced  $H_{s_{max}}$  exceeding 15 m and  $T_{02}$  wave periods exceeding 10 sec (Figures 45-48, Section 5.2.2). Conditions during Hurricane Ivan were modeled at similar levels although selected NDBC and ONR data suggest more extreme conditions (Figures 4 and 5; Section 2.2).

## 7.2.2 Case Studies in Seafloor Failure – Validation Test Area Two

VTA 2 is located east of VTA 1 and is therefore not covered by the regional MRDF surveys acquired in 1874, 1940 and 1977. However, a cluster of four local hazard surveys was

acquired in the area between 1988 and 1993 which provides a useful comparison relative to areas containing higher sedimentation rates farther west towards the MRDF (Figure 22; also Appendix K). In addition, the regional NOAA bathymetric dataset fully extends over the area.

This area is aligned along the current-day shelf edge, which itself is aligned east-northeast to west-southwest through the area. Although located beyond the delta front, the area was located directly in the path of Hurricane Ivan and was used as a base-line comparison in Chapter 9 to help determine future mudflow vulnerability. No failures were reported in the area during recent hurricanes. However, the absence of year-on-year data does not preclude a past event from having occurred, and in fact seafloor morphology reflected in local bathymetric data suggests that failures did occur in the past.

Several relict, small-scale mudflows are reflected in seafloor bathymetry data from Main Pass Blocks 294 and 295 through the appearance of topographical “aprons” depicted along the MRDF (Figure 113) and described in previous work (Hooper and Suhayda, 2005a and 2005b; William Lettis & Associates, Inc., 2005). These aprons represent the downdip extent of downslope mass sediment transfer associated with past failure events. Even though these aprons are clearly visible on colored bathymetry data, the vertical difference in topography is less than 1.5 m (five feet).

The shallow subsurface record reflects the relatively smooth present-day seafloor (Figure 114). However, beneath the shallowest 2 m (five feet) of strata a complex series of relict failures and subsequent depositional lobes can be seen, extending approximately 8 m (25 feet) below the present-day seafloor. These features occur in tandem with multiple series of prograding strata that could represent the distal advance of an older deltaic complex (Figure 114).

As none of the regional surveys extend this far to the east, the only bathymetry comparison that can be made is with the NOAA bathymetry (precise acquisition dates unknown but suspected to be approximately 1989). A comparison of these data with bathymetry data collected in 1994 indicates a difference of one to two meters (two to five feet) that reflects both

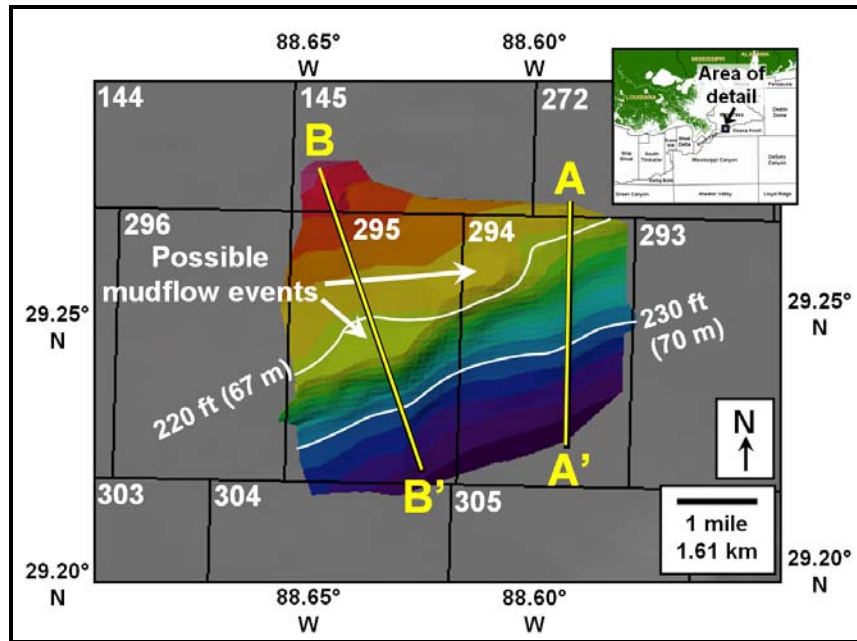


Figure 113: Seafloor bathymetry and prior mudflow morphology, Main Pass Blocks 294 and 295 (raw data from John E. Chance & Associates, 1994)

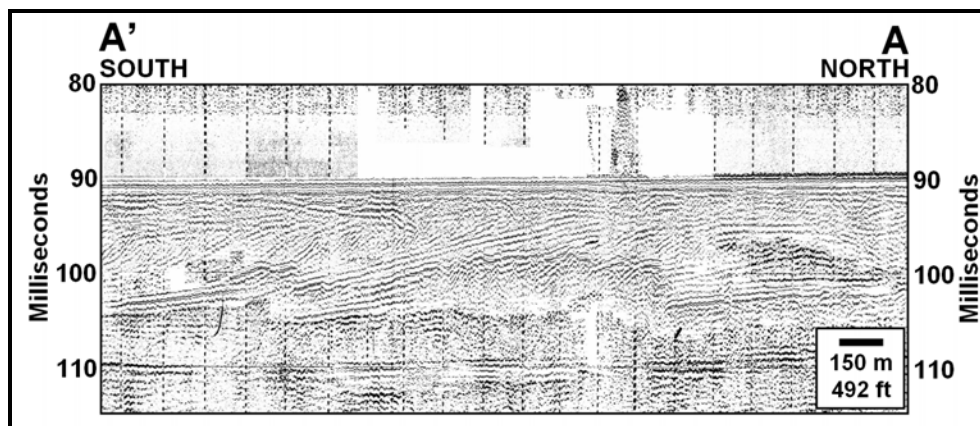
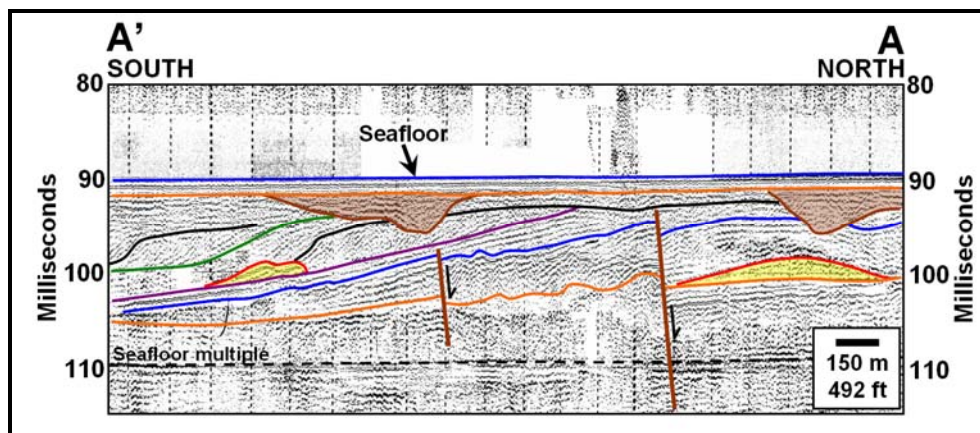


Figure 114: Line 6 (10 inch<sup>3</sup> sleeve gun; interpreted and non-interpreted), Main Pass Blocks 294 and 295 (data from John E. Chance & Associates, 1994)

failed seafloor and possible mudflow morphologies (Figure 115). No major hurricanes directly impacted the area between 1989 and 1994. The only significant hurricane to traverse the GOM during that time was Hurricane Andrew, which passed significantly farther west (Figure 1; also Appendix B, Figure B-3). However, the area could have been subjected to long-period waves in advance of Andrew's passage and the hypothesis that these small-scale mudflows could have been caused by Hurricane Andrew is valid.

Elsewhere in VTA 2, relatively smooth seafloor topography is revealed by the remaining site-specific surveys together with the relic deltaic facies indicated at Main Pass 294 and 295. No evidence or large-scale mudflows can be detected on visual scans of the seafloor through the use of side-scan sonar (Figure 116). The most striking feature detected in the area is the formation of authigenic hard grounds, which are precipitated through the bacterial oxidation of methane by chemosynthetic marine fauna (Sassen et al., 1998; Mannaerts et al., 2007). Support for this hypothesis can be seen in the numerous pock marks and apparent hydrocarbon seeps located throughout the area (Figure 116).

### **7.2.3 Case Studies in Seafloor Failure – Validation Test Area Three**

A wide array of data spanning multiple time periods exists within VTA 3. The most prominent surveys acquired in the area are the regional MRDF surveys in 1874, 1940 and 1977 as well as a semi-regional survey dating from 1997 (Vastar Resources, Inc., 1997a; Appendix K). Additionally, five local hazard surveys were acquired in the area between 1983 and 2006 post-Katrina (Figure 22; also Appendix K).

The upper delta front in this area is aligned northeast-southwest and contains numerous mudflow gullies that incise a progressively steeper slope with distance away from the delta (Figure 10, Section 3.2; Figures 23-26, Section 4.1.1). Mudflow noses become common with progressively deeper water and represent the distal extent of shelf failure events.

Regional changes in temporal seafloor morphology are evident in the surveys acquired in 1874, 1940 and 1977 (Figures 105 and 107, Section 7.1). Detailed temporal morphological



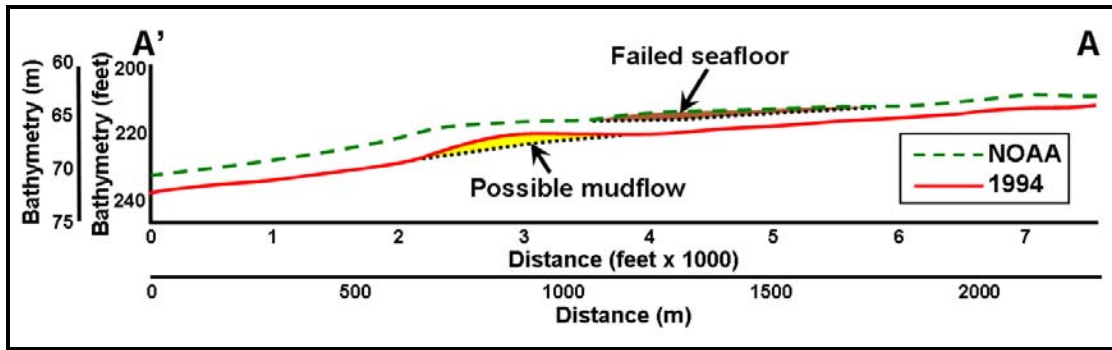


Figure 115: Seafloor bathymetry profile A-A', Main Pass Blocks 294 and 295

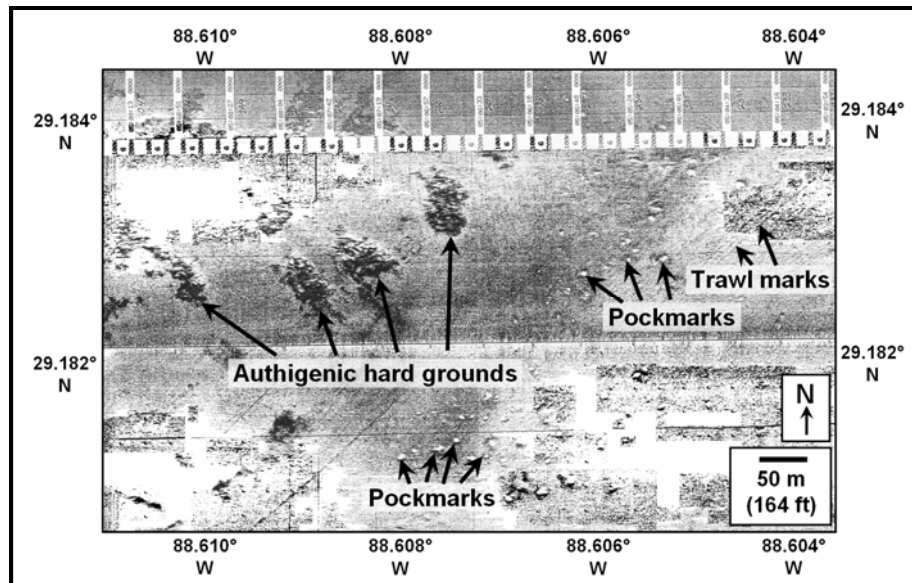


Figure 116: Side-scan sonar Line 111, Main Pass 308 and Viosca Knoll 914/915 survey (modified from raw data by Arco Oil and Gas Company, 1991a)

change is depicted on comparisons with local hazard surveys as well as regional surveys (pending available coverage). Comparing the 1977 regional MRDF survey to the 1997 Vastar survey, elongate areas of net seafloor gain can be seen nearer the delta in shallower water, which is indicative of mass wasting that occurred over the 20-year time interval between the two surveys (Figures 117-119). A large area of net seafloor loss, oriented northwest-southeast over westernmost Viosca Knoll and up to 12 m (40 feet) thick in places, can also be detected. The volume of this failed material, at least within the area overlapped by the two surveys, yields a calculation of  $0.43 \text{ km}^3$ .

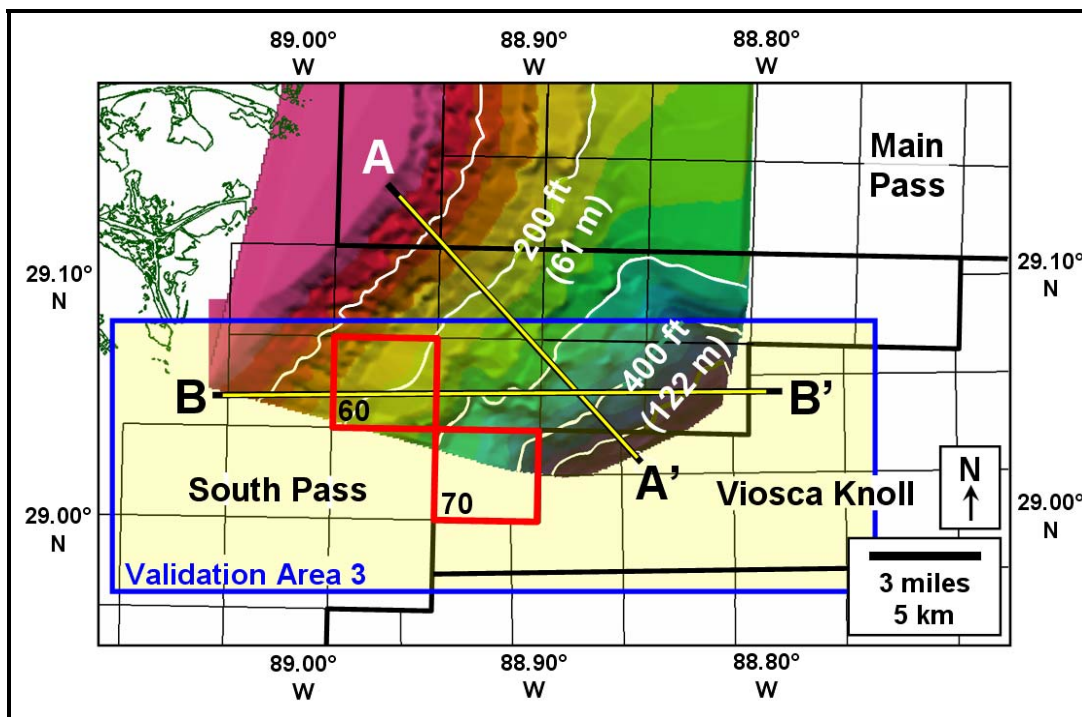


Figure 117: Semi-regional bathymetry data, South Pass Area (Vastar Resources, Inc., 1997a)

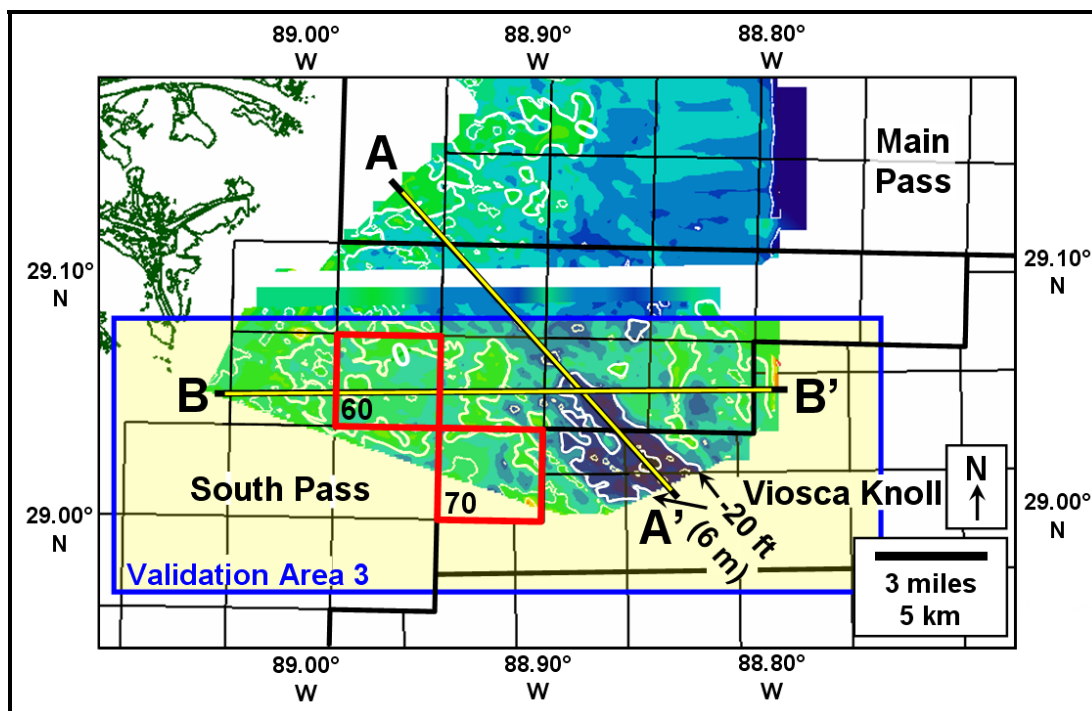


Figure 118: Net seafloor bathymetry change, 1977-1997, South Pass Protraction Area



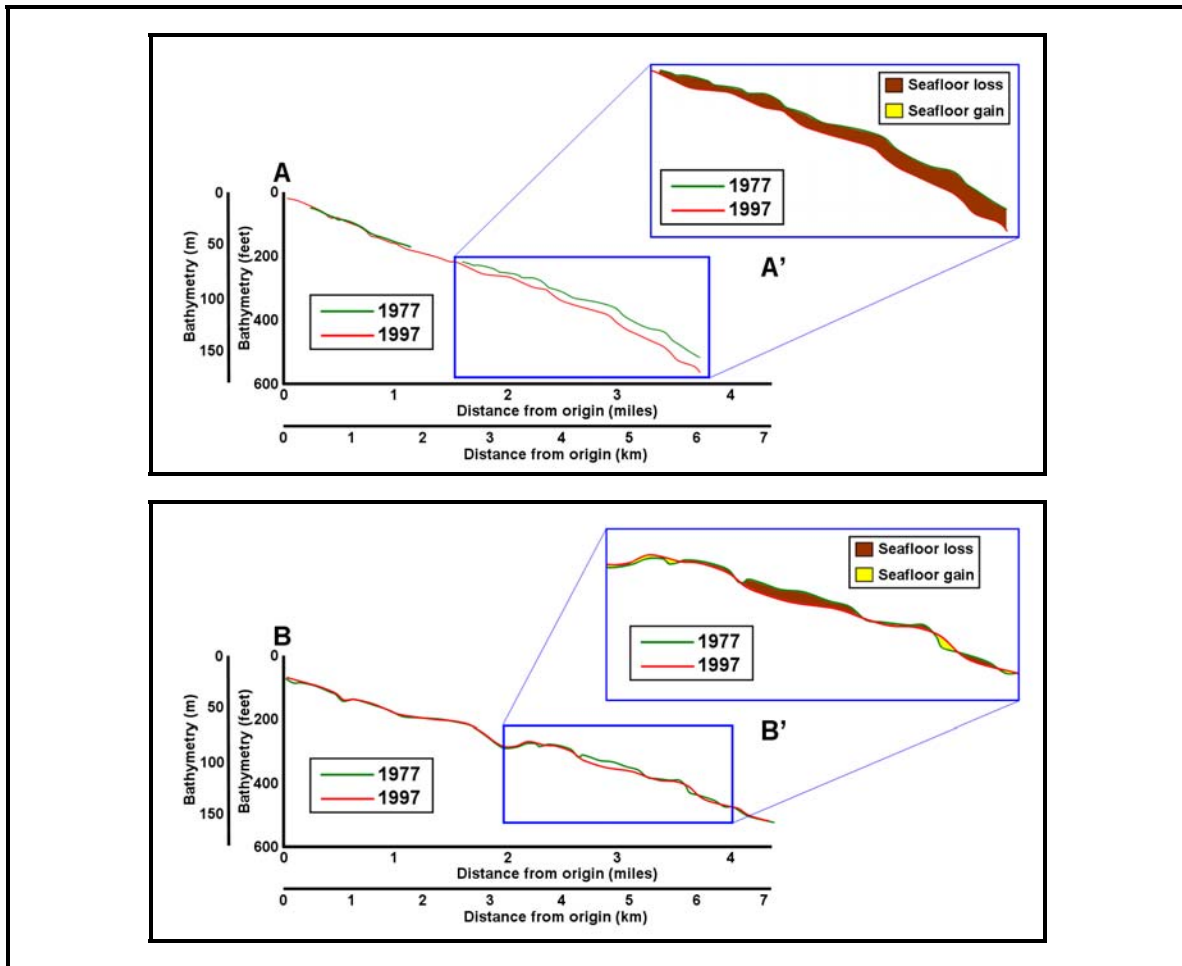


Figure 119: Cross-sectional grid and net seafloor bathymetry change, Validation Area 3

Although coverage of the 1997 survey ends towards the southeast at a water depth of approximately 168 m (550 feet), two high-resolution surveys are located directly downdip, one from 1983 and another from 2005 (Figures 120 and 121; John E. Chance & Associates, 1983; Enterprise Products Partners, LLC, 2005). The two most recent surveys overlap around Viosca Knoll (VK) Block 985 where classic mudflow nose morphology is displayed (Figure 122). Although the data quality of the older survey is lower, significant sediment accumulation occurred in this area between 1983 and 2005 based on a comparison of these surveys (Figures 123 and 124). Mudflow lobes seen on the 2005 data appear as areas of net sediment addition relative to 1983, thus implying significant seafloor change and mudflow deposition that occurred between 1983 and 2005 (Figure 124). The “fresh” nature of the mudflow noses on the 2005 data

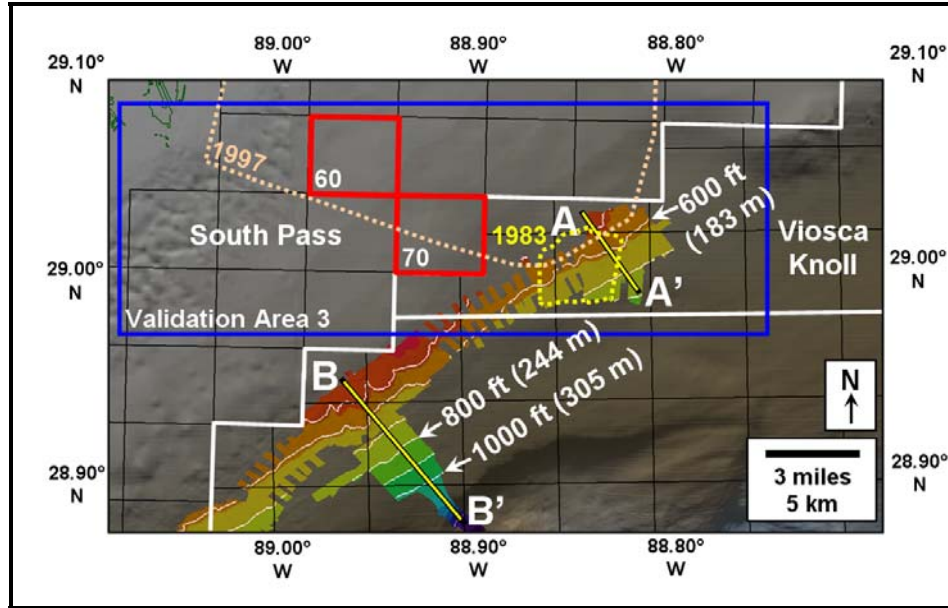


Figure 120: High-resolution bathymetry, Viosca Knoll and Mississippi Canyon Protraction Areas (Enterprise Products Partners, LLC, 2005 and overlies base regional bathymetry; NOAA, 2009)

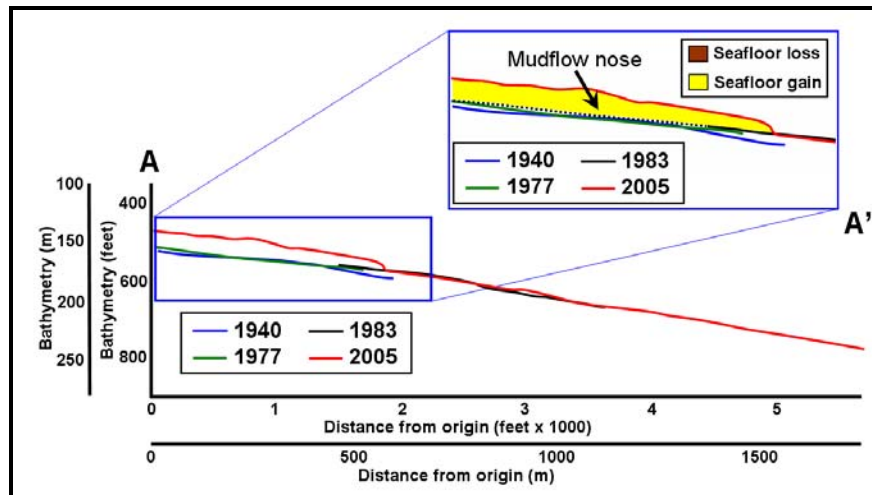


Figure 121: Net seafloor bathymetry change, Viosca Knoll Block 985 (Validation Area 3)

(i.e., distinct, visible pressure ridges across the mudflow noses and sharp edges; Figure 122) suggest that these mudflows occurred not long before the data were acquired, and certainly within the time frame to have been caused by Hurricane Ivan.

The volume of net sediment gain, constrained within the area overlapped by the 1983 and 2005 surveys, yields a minimum calculation of approximately  $2.04 \times 10^5 \text{ m}^3$  (the maximum cannot be calculated given the 2005 survey boundaries). Given the similar 1940, 1977 and 1983

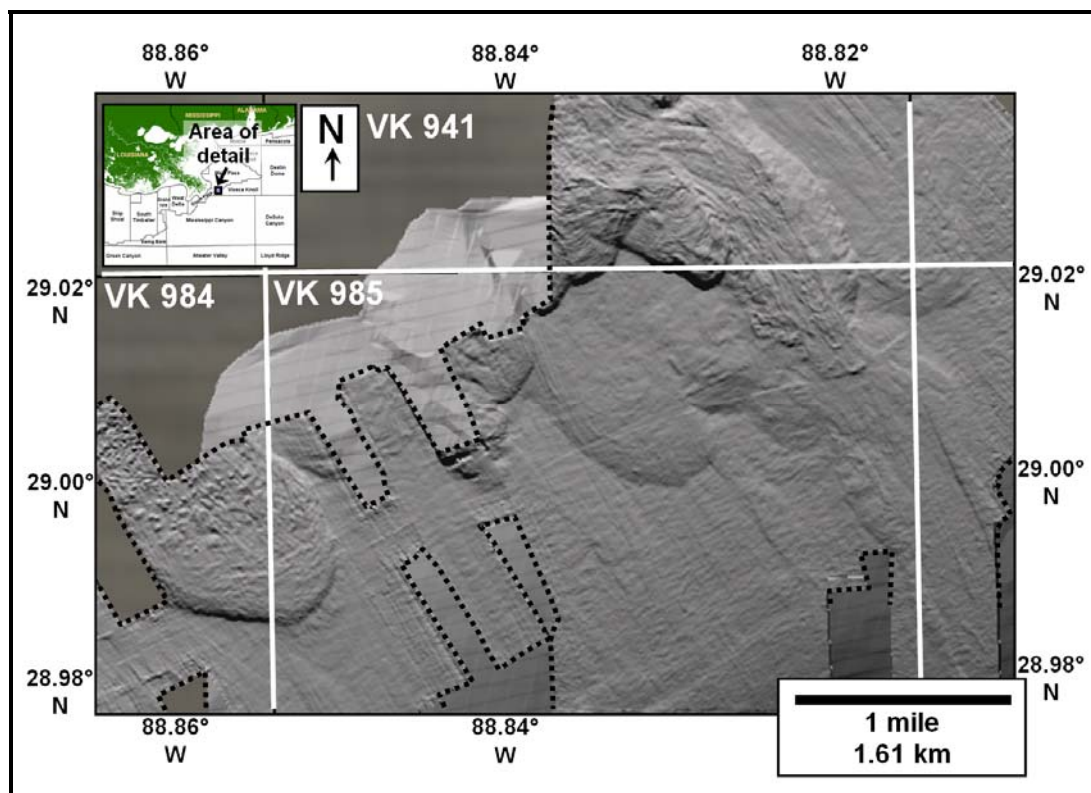
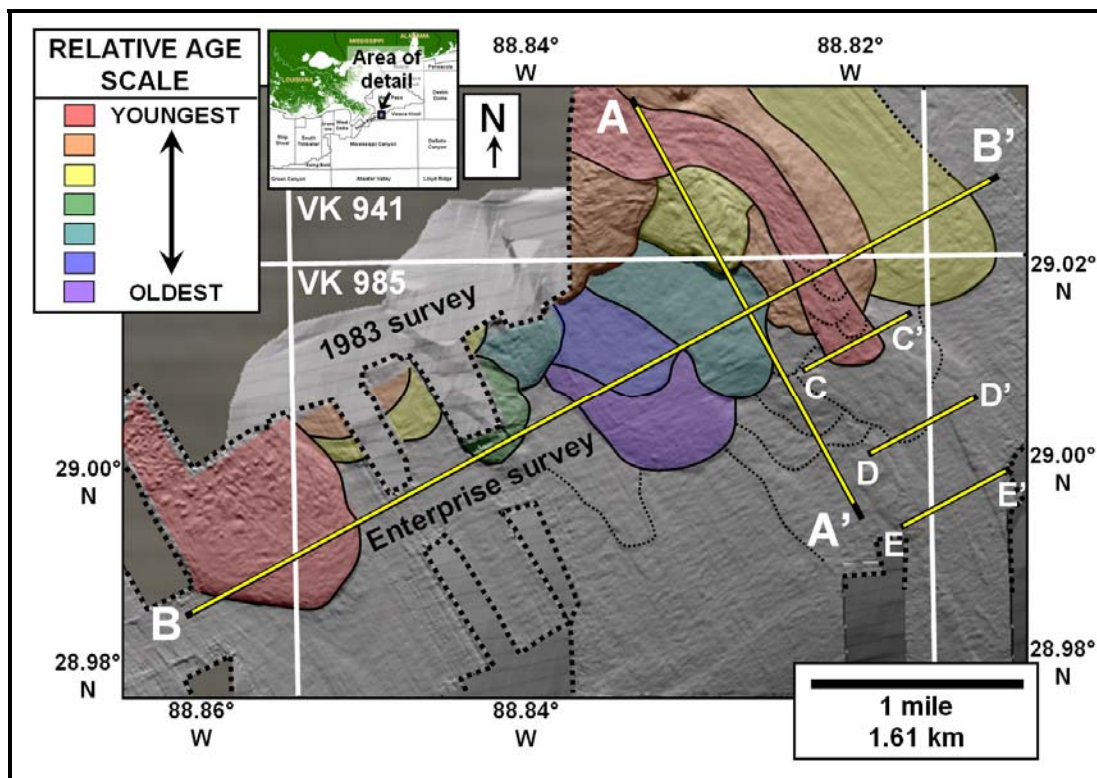


Figure 122: Generational mudflow history, Viosca Knoll Block 985 (raw data from Enterprise Products Partners, LLC, 2005)

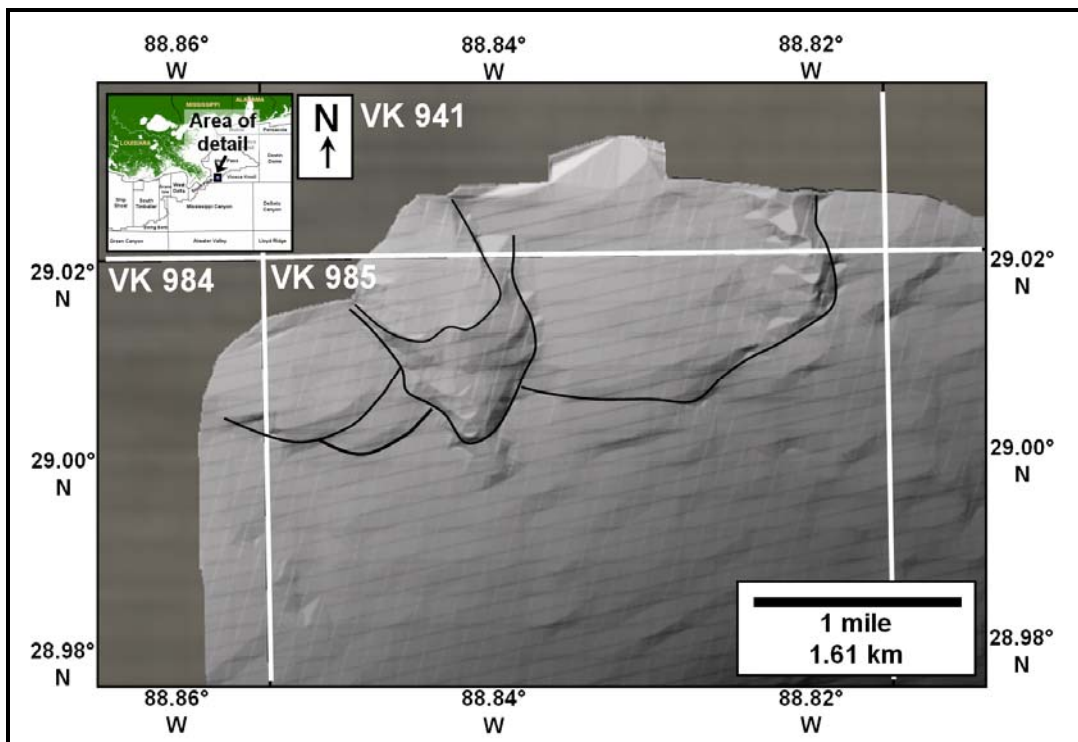
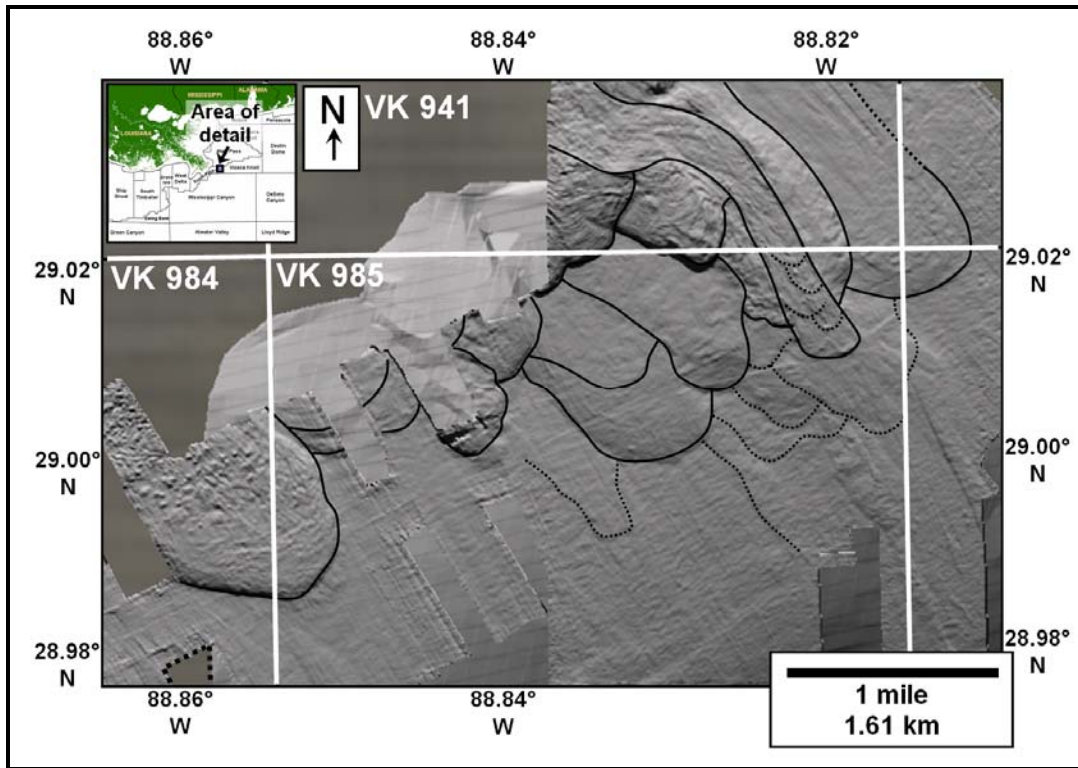


Figure 123: Comparison of high-resolution bathymetry survey acquired in 2005 (left side; raw data from Enterprise Products Partners, LLC, 2005) vs. survey acquired over same area in 1983 (right side; (raw bathymetry data from John E. Chance & Associates, 1983)



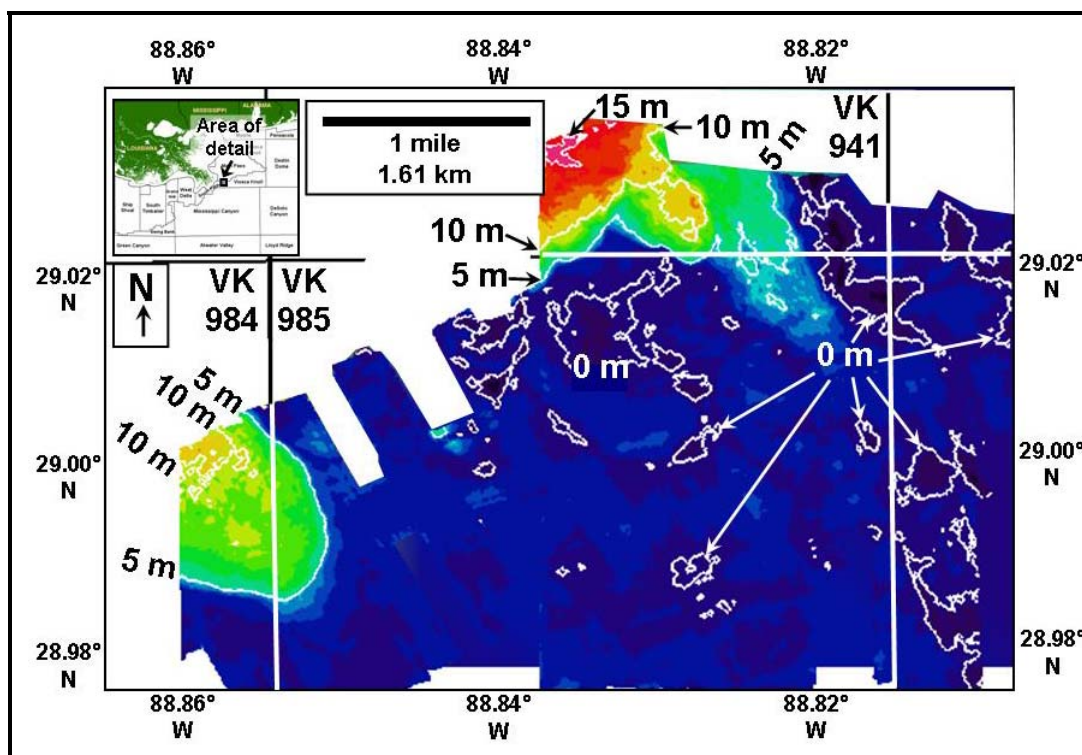


Figure 124: Surface difference, VK 985 vicinity, 1983-2005

seafloor profiles vs. the 2005 profile, it is unlikely that the sole source of the sediment gain in VK 985 occurred prior to 1997. Hurricanes Ivan and Katrina occurred between 1997 and 2005, and given their magnitude it is likely that failure occurred either in 2004 or in 2005. Two hurricanes passed near VK 985 between 1977 and 1997 (Frederic in 1979 and Elena in 1985) while two others (Andrew in 1992 and Opal in 1995) passed farther away (Table 1, Section 2.2; Figures 28 and 29, Section 5.1.1; NHC, 2009). Unlike Hurricane Ivan, Frederic approached the study area from the south-southeast (approximately 160°) and farther away than Ivan. Elena was a weaker and faster-moving storm; its lowest central pressure reached 953 mb (relative to 928 mb for Ivan) and it traveled through the study area in only 2.5 hours relative to the eight hours Ivan spent in the study area (Figure 30, Section 5.1.2; NHC, 2009). In addition, seafloor failure was reported during both Hurricanes Ivan and Katrina at South Pass Block 60 (outlined in red in Figures 117, 118 and 120), located 6.4 km updip of the sediment gain detected by 2005.

The morphology revealed on the 2005 survey indicates the ephemeral nature of the seafloor along the MRDF (Figures 122-123). Multiple mudflow noses overlap and coalesce, indicating a complex history of shelf failure and resulting deposition. Older mudflow noses appear more muted and ill-defined than fresh mudflows, presumably because of bottom currents that rework ocean floor sediment and/or because of hemipelagic drape that has infilled locally present topography along the seafloor (Figure 122; refer to the color code for relative age of each lobe). The net sediment difference revealed that a lobe to the southwest along the VK 984/985 boundary, as well as several lobes in south-central MK 941, were newer lobes not detected in 1983. The imagery of these lobes appears sharper than those around them and lends further credence to their being newly formed (Figure 124). Older mudflows are often eroded, cut by newer flows, or become reinitiated and move even further downdip than when initial failure occurred as described by Mohrig et al. (1999; Figure 122). Furthermore, the length of several mudflow lobes extends in a relatively narrow pattern several kilometers downslope and sometimes with disproportionate runout distances, which may provide evidence of hydroplaning (demonstrated elsewhere by Mohrig et al., 1998 and Masson et al., 2006).

This morphology is demonstrated by updip seafloor scour and subsequent, multiple pulses of sediment deposition downdip (colored in red in Figure 125 and 126) that post-dates an underlying debris flow (colored in orange). The downdip sediment pulses are located disproportionately farther downslope relative to any of the previous mudflow lobes; each downdip sediment terminus represents approximately 0.5 to 2.0 m of seafloor relief. These elongated features are themselves confined on both sides by relief of approximately 2 to 3 m, suggesting that flow was channeled downdip while sediment accumulated in occasional pulses internally within the scoured seafloor (Figure 126).

The 2005 Enterprise survey also details the downdip extent of classic mudflow noses that formed from updip shelf failure in the northwestern Mississippi Canyon Protraction Area (Figure 127). As with the mudflows in VK 985, a complex series of cross-cutting relationships

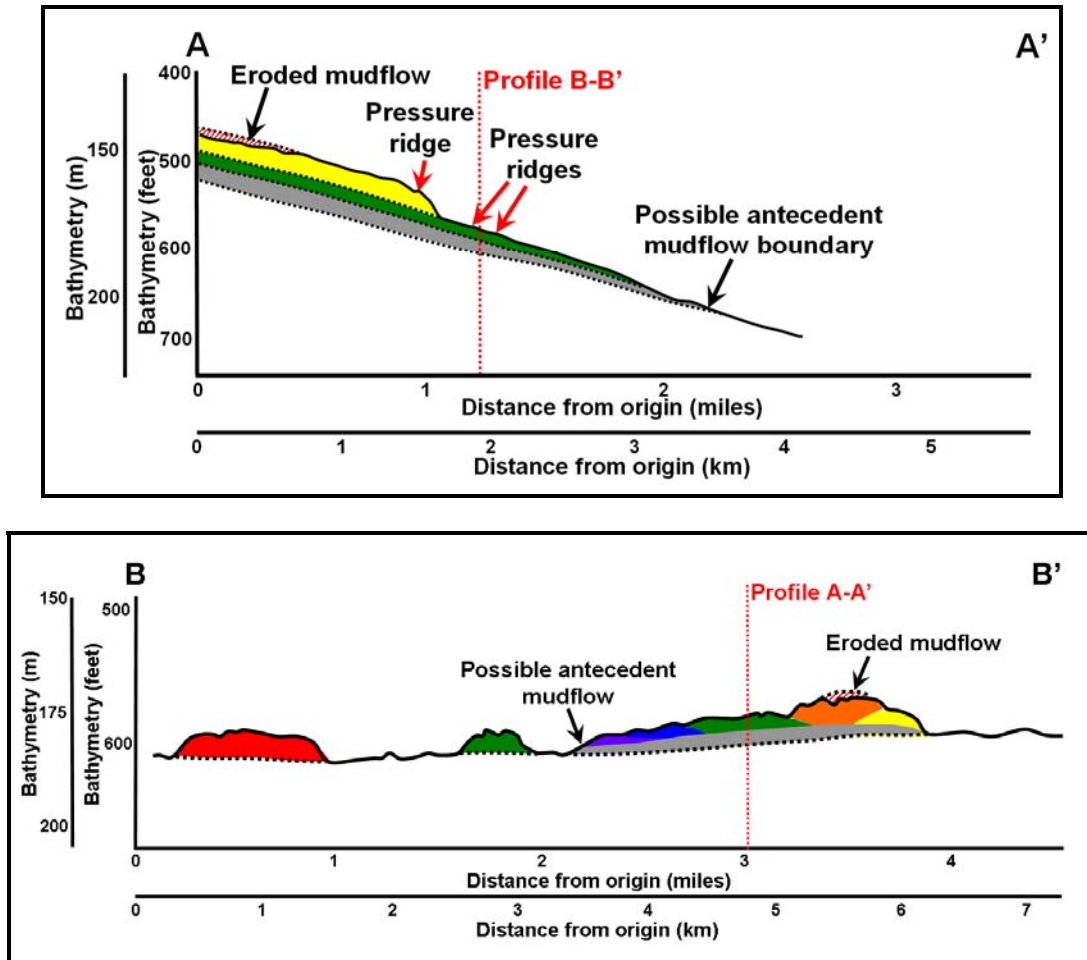


Figure 125: Mudflow nose topography, Viosca Knoll 985 and vicinity (raw data from Enterprise Products Partners, LLC, 2005)

exists in which older mudflows are truncated by newer flows (Figure 128). Shelf failure timing at MC 20 has been well documented as a result of infrastructure failure during Hurricane Ivan (MMS, 2005). A recent, elongate outrunner lobe traveled farther downslope than the rest of the underlying lobes, similar to that seen at VK 985 (Figure 127; mudflow oriented northwest-southeast and colored in red). This lobe appears to have been a failure of an earlier lobe (colored in green; Figures 127 and 128), further demonstrating the dynamic nature of the MRDF seafloor.

Mudflow noses can be further delineated by examining slope steepness on the periphery of each lobe as well as along internal pressure ridges on each lobe (Figure 129). Peripheral slopes on the largest noses average approximately four to seven degrees, with some slopes as steep as



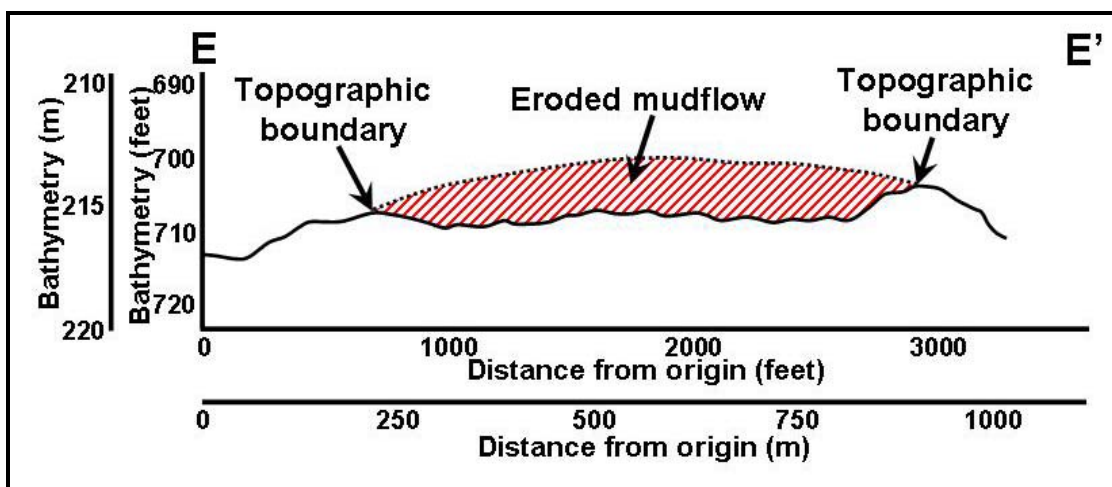
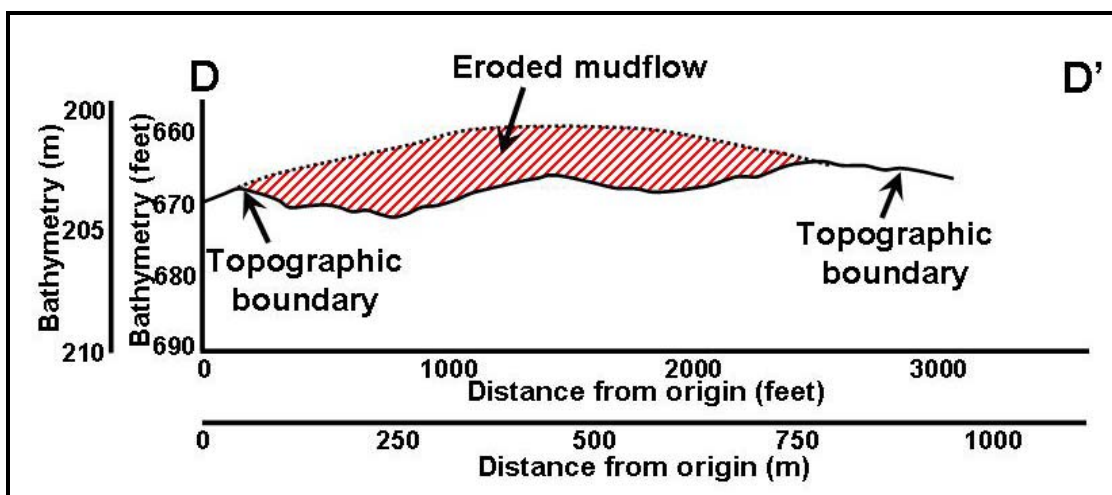
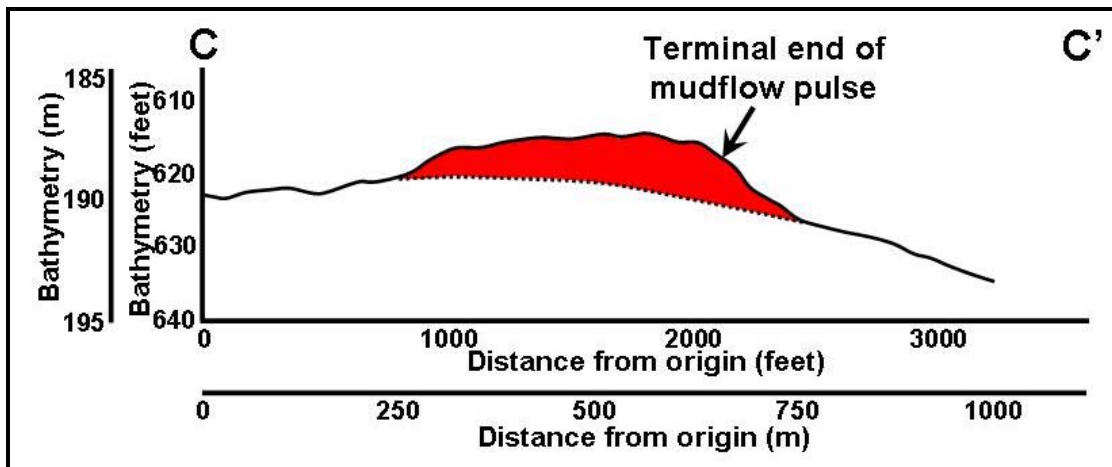


Figure 126: Terminus of elongated sediment flow (C-C') and downdip extent and confining boundary of elongated sediment flow (D-D' and E-E'), VK 985

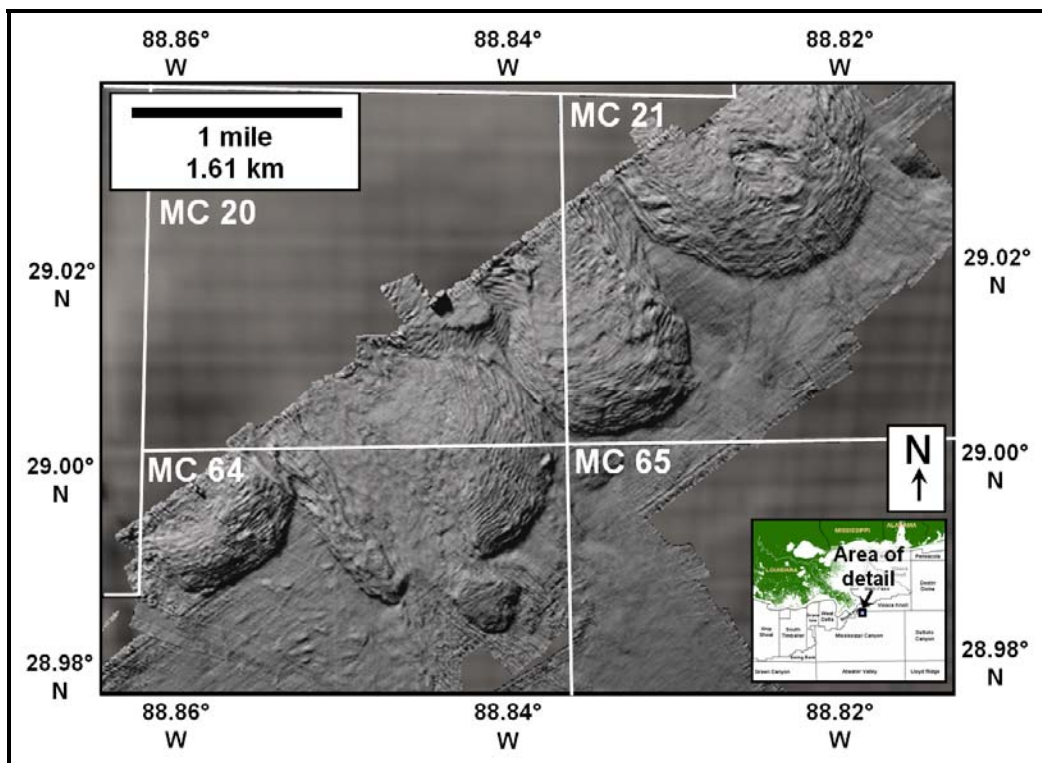
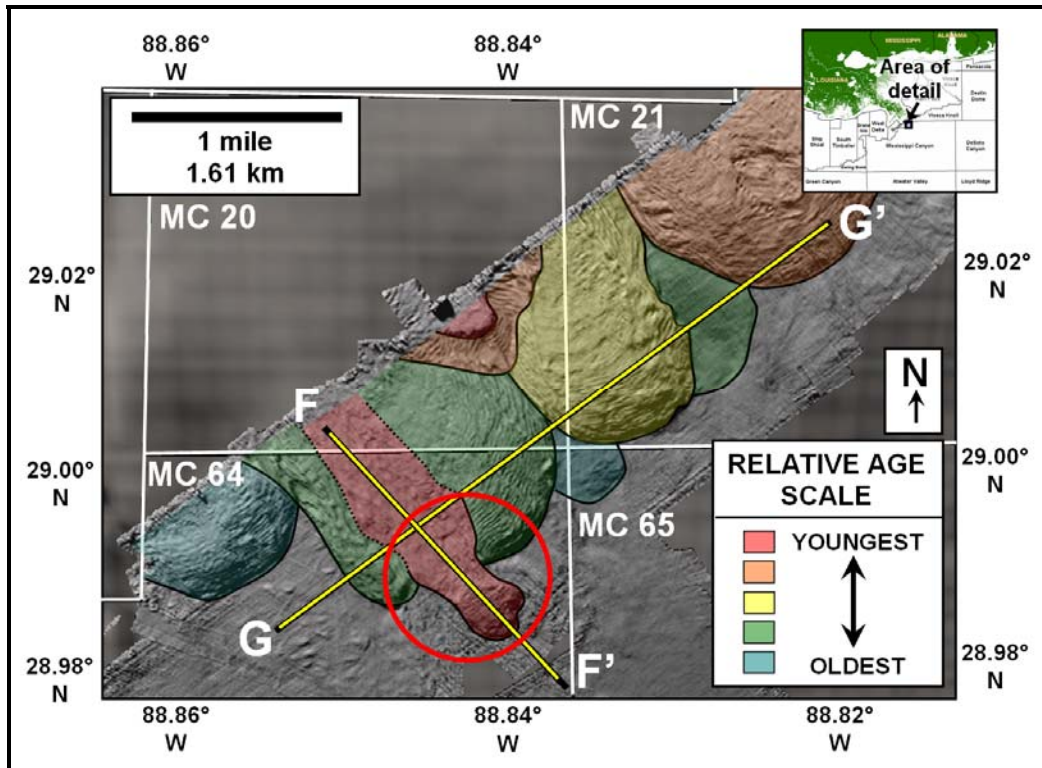


Figure 127: Generational mudflow history, northwest Mississippi Canyon (raw data from Enterprise Products Partners, LLC., 2005)

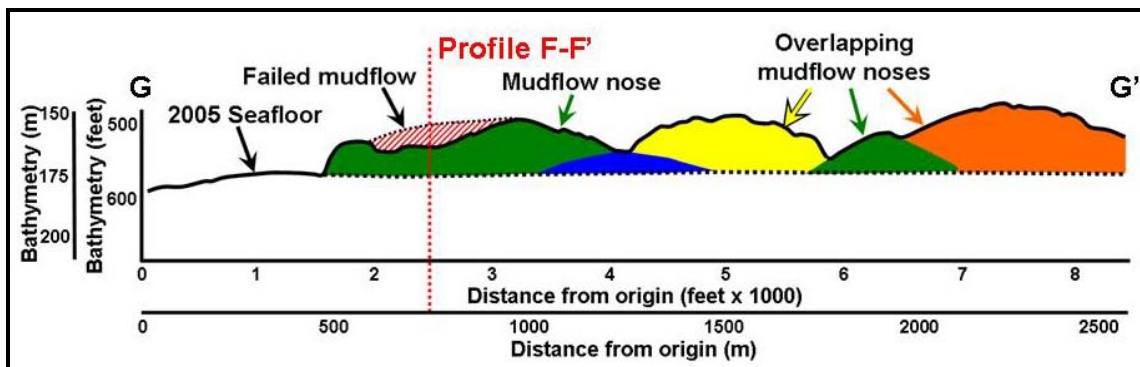
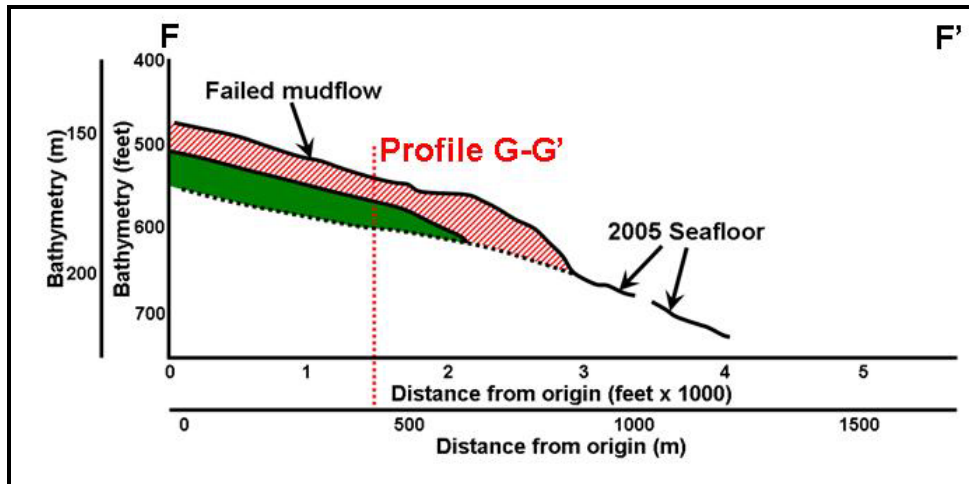


Figure 128: Mudflow nose topography, northwest Mississippi Canyon Protraction Area (colors correspond to colored mudflows in Figure 125; vertical exaggeration 20:1; based on raw data from Enterprise Products Partners, LLC, 2005)

twelve degrees. Internal pressure ridges found at the distal ends of these mudflow noses contain slopes of approximately two to four degrees.

As discussed in Sections 3.1.3 and 3.3.2, the seafloor failure that occurred at SP 70 during Hurricane Camille was located in VTA 3 (Bea, 1971; Sterling and Strohbeck, 1973). No recent survey data are available over the block; however the 1997 sub-regional survey across Main Pass and South Pass covers the area. Wide variations in water depth occur through time and reflect the ephemeral nature of an active mudslide area. From 1874 to 1940, a continuous layer of net sediment accumulation occurred along a dip profile from SP 60 to SP 70 (Figure 130). This layer ranges in thickness from approximately 6 m (20 feet) over SP 60 to approximately 15 m (50 feet) over SP 70. The next survey, acquired in 1977 eight years after

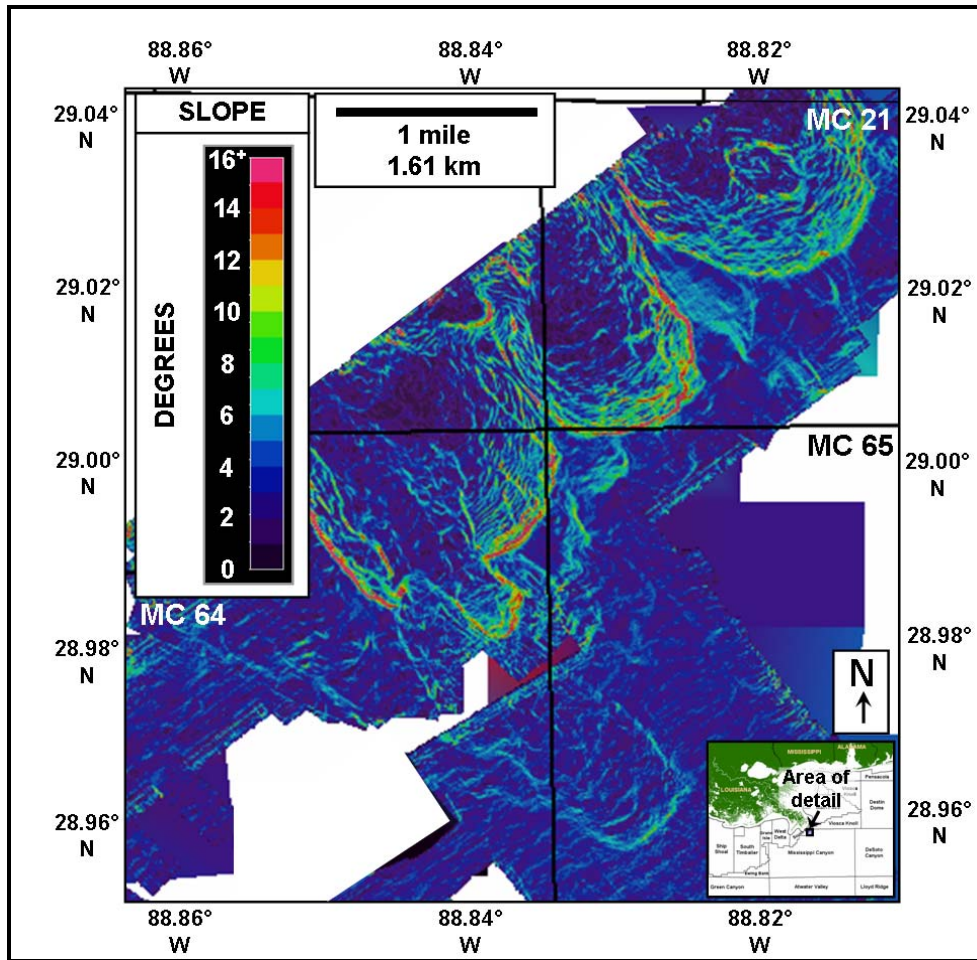


Figure 129: Mudflow lobes and internal pressure ridges as inferred from slope steepness, northwest Mississippi Canyon Protraction Area (based on raw data from Enterprise Products Partners, LLC, 2005)

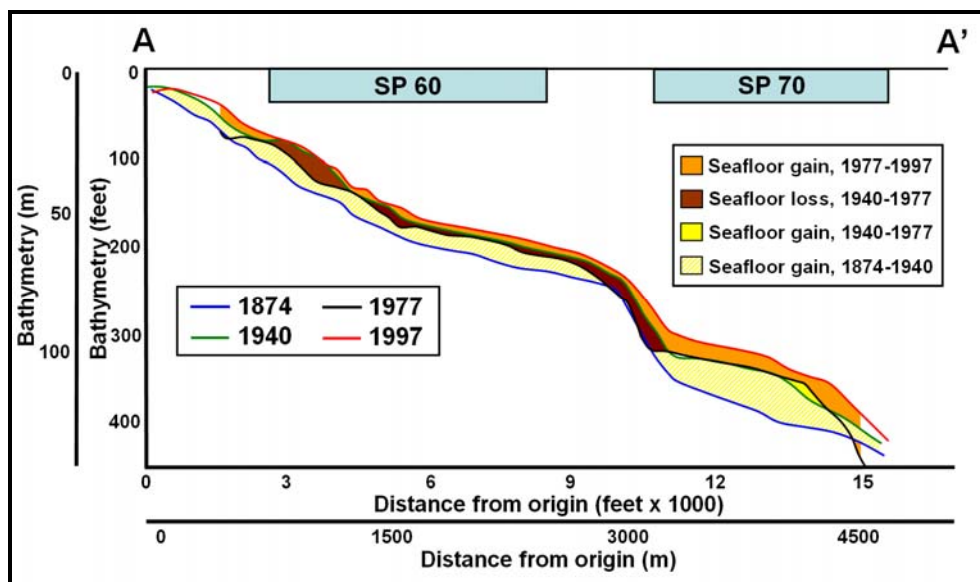


Figure 130: Bathymetric profiles through time, 1874-1997, South Pass Blocks 60 and 70



Hurricane Camille, reveals two areas of net seafloor loss – one in South Pass 60 and another immediately updip from South Pass 70 where a major mudslide toppled a platform during Hurricane Camille (Bea, 1971; Sterling and Strohbeck, 1973; Wright, 1976). This second area contains relatively steep seafloor dips of approximately seven degrees, providing a possible catalyst for seafloor failure. A small area of net seafloor gain occurred downdip in SP 70 during this same time period; however, insufficient sediment exists to fully account for the amount of failed material. Net sediment accumulation did occur, however, in the 20 years from 1977-1997, as a consistent addition of 3-5 m (10-15 feet) occurred throughout the area. The only major hurricane to impact the area during that period was Hurricane Frederic (1979), which made landfall along the Alabama coastline as a Category 4 storm albeit from an approach angle of 145° (south-southeast). Hurricane Elena (1985), a Category 3 hurricane, also passed nearby but from an approach angle of 105°, thereby impacting the MRDF with hurricane conditions for only 2.5 hours relative to six hours for Hurricane Frederic and eight hours for Hurricane Ivan (NHC, 2009).

#### **7.2.4 Case Studies in Seafloor Failure – Validation Test Area Four**

The most prominent regional surveys acquired within VTA 4 are the regional MRDF surveys acquired in 1874, 1940 and 1977 as well as a semi-regional survey acquired in the South Pass and northwestern Mississippi Canyon Areas in 1978 (McClelland Engineers, Inc., 1978; Figure 22; also Appendix M). Additionally, 15 local hazard surveys were acquired in the area between 1964 and 2006 post-Katrina (Figure 25; also Appendix K).

The upper delta front in this area is aligned east-northeast to west-southwest and contains numerous mudflow gullies that incise a progressively steeper slope with distance away from the delta (Figure 10; Figures 23-26, Section 4.1.1). As in VTA 3, mudflow noses are more pronounced downdip of failures funneled downslope by updip mudflow gullies, thereby representing the distal extent of shelf failure events.

Regional changes in temporal seafloor morphology are evident in this area from the surveys acquired in 1874, 1940 and 1977 (Figures 105-107, Section 7.1). Detailed morphological change through time can be seen on comparisons between the three regional surveys and the 15 local hazard surveys (pending available coverage and resolution quality, which vary greatly).

As an example of year-on-year bathymetric change before and after the passage of tropical systems, a series of geohazard surveys was previously acquired over South Pass Block 28 (Figures 131-136). An initial baseline survey was acquired in 1962 (Figure 131), a second survey was acquired in 1964 after the passage of Hurricane Hilda (Figure 132), and a third survey was acquired in 1965 after the passage of Hurricane Betsy (Figure 133; Arnold, 1967).

The post-Hilda survey revealed areas that underwent both net sediment gain as well as net sediment loss (Figure 132). Changes in seafloor bathymetry are also reflected in two profiles, one dip-oriented and one strike-oriented, across the block (Figures 137 and 138). A hypothesis to explain net addition in the northwest part of the survey is that a crustal block moved downslope relatively intact in response to repeated changes in differential pressure along the seafloor due to hurricane-driven waves (Figure 131). A hypothesis to explain sediment loss in the gully-like feature in the south-central part of the survey is that an existing, updip mudflow failed during Hurricane Hilda (Figure 131) and the resulting flow scoured up to 3 m (10 feet) of sediment immediately downslope (Figures 132 and 134).

The 1964 profile resulted in steep dips (up to 15°), which set the stage for additional failure one year later during Hurricane Betsy (Figures 132 and 135). Net sediment addition occurred along the headwall of the failure noted in 1964 and represents retrogressive erosion of the headwall of this prior failure (circled in red on Figure 136), thus inferring that failure vulnerability can occur not only downslope of the most distal ends of mudflow noses but also immediately downdip of mudflow gully headwalls through retrogressive erosion of steep slopes.

Another cluster of site-specific geohazard surveys was acquired approximately 16 km (10 miles) south-southwest of South Pass (Figure 22). Surveys were acquired over SP 50 and 51

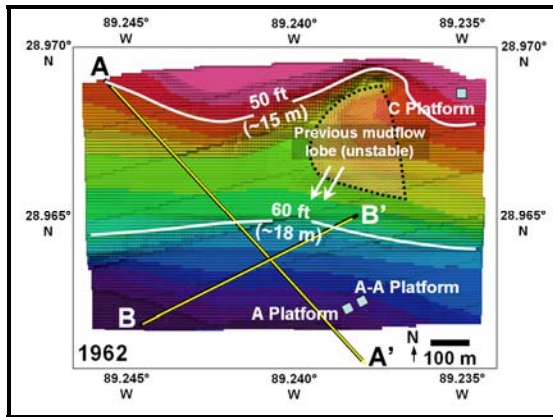


Figure 131: Seafloor bathymetry, South Pass Block 28, 1962 (pre-Hurricane Hilda; data from Arnold, 1967)

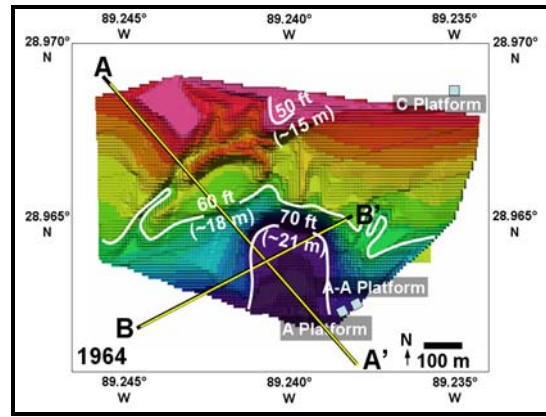


Figure 132: Seafloor bathymetry, South Pass Block 28, 1964 (post-Hilda/pre-Hurricane Betsy; data from Arnold, 1967)

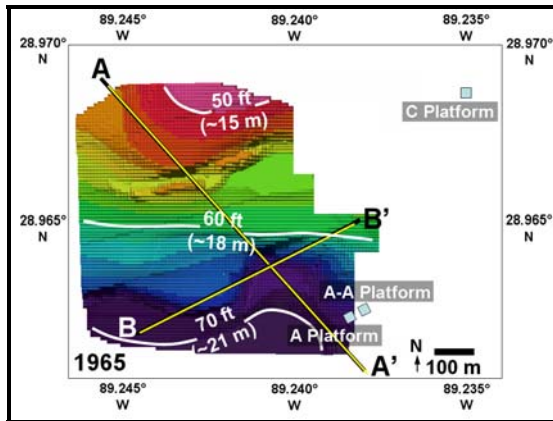


Figure 133: Seafloor bathymetry, South Pass Block 28, 1965 (post-Hurricane Betsy; data from Arnold, 1967)

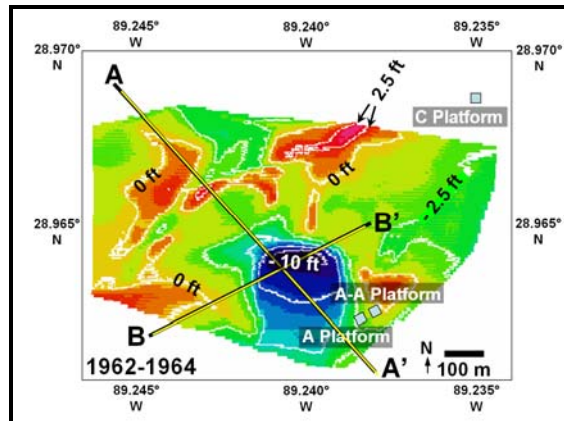


Figure 134: Net seafloor bathymetry change, 1962-1964, South Pass Block 28 (pre- and post-Hilda; data from Arnold, 1967)

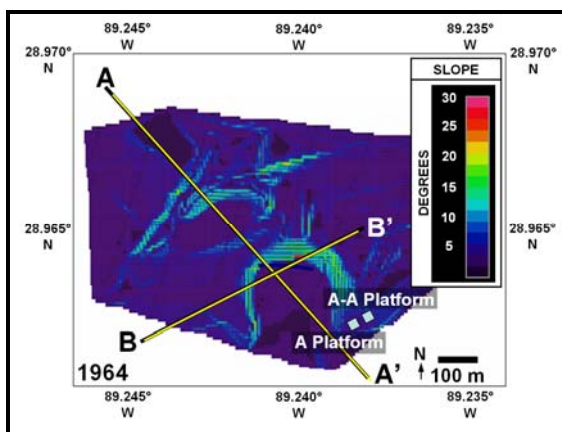


Figure 135: Slope map, South Pass Block 28, 1964 (post-Hilda/pre-Betsy; raw data from Arnold, 1967)

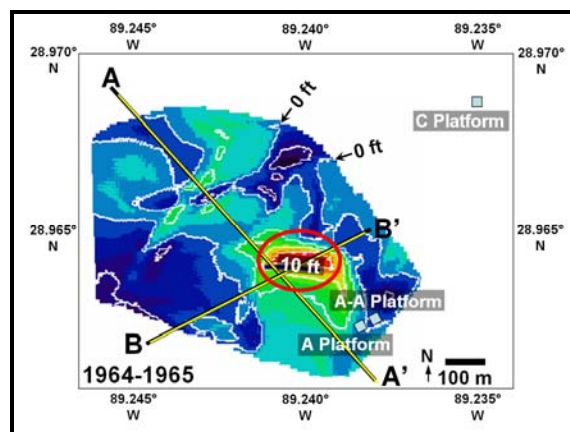


Figure 136: Net seafloor bathymetry change, 1964-1965, South Pass Block 28 (post-Hilda/post-Betsy; data from Arnold, 1967)



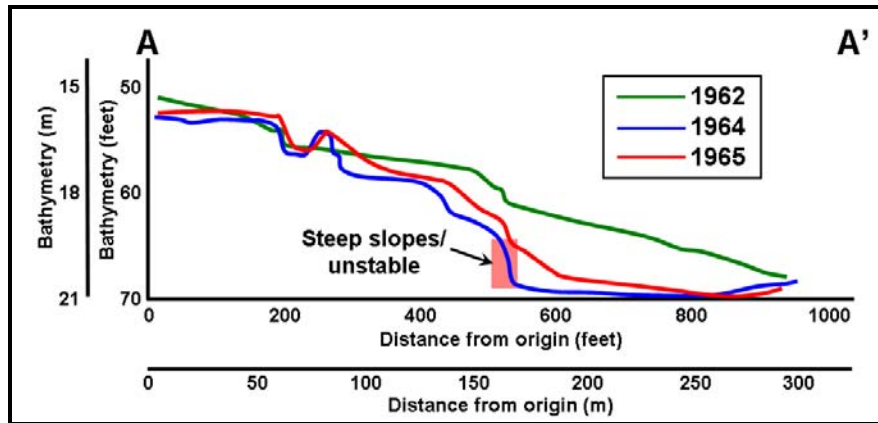


Figure 137: Time-series cross-sectional profile A-A', 1962-1965, South Pass Block 28 (pre-Hilda through post-Betsy)

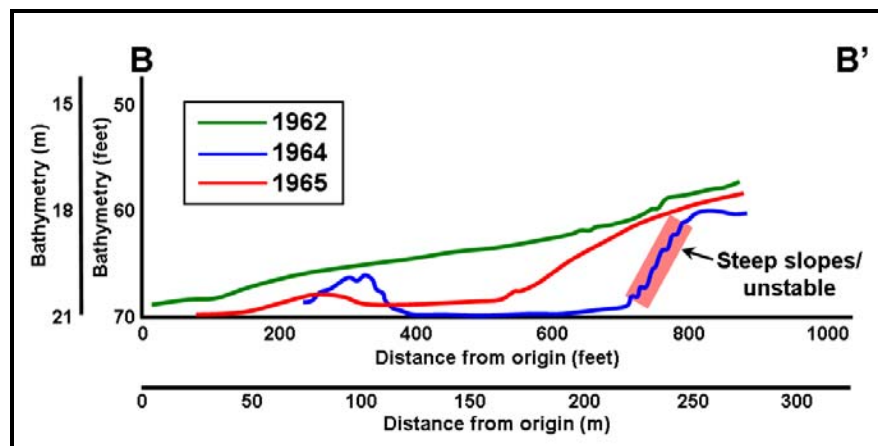


Figure 138: Time-series cross-sectional profile B-B', 1962-1965, South Pass Block 28 (pre-Hilda through post-Betsy)

in 1981, 1988 and 1990 (Racal-Decca, 1981; 1988; Arco Oil and Gas Company, 1990). Seafloor bathymetry data over these blocks indicates that no large-scale failures occurred in the nine-year time span covered by these surveys (Figures 139-142). This finding is substantiated by subbottom profiler data at SP 52 (5 km (3 miles) west; Figure 143) in which relatively little seafloor change occurred (1977-1985). No major tropical systems passed through the area during this time; only Hurricane Elena (1985) moved through the north-central GOM during this time as a Category 3 hurricane but it passed well north of these blocks. The lack of major failures in this area during this time interval lends initial support to the hypothesis that major subaqueous shelf failure is hurricane-driven. During Hurricane Ivan, a major shelf failure occurred at SP 55,

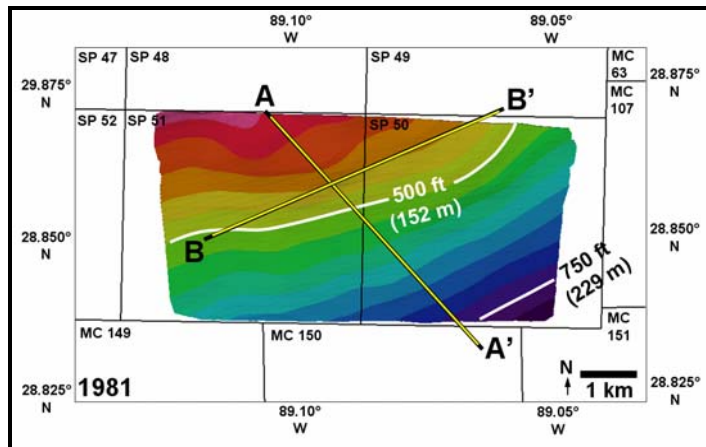


Figure 139: Seafloor bathymetry, South Pass Blocks 50 and 51, 1981. Image created in Fledermaus modeling software; artificial shading is applied from 330°; data from Racal-Decca, 1981.

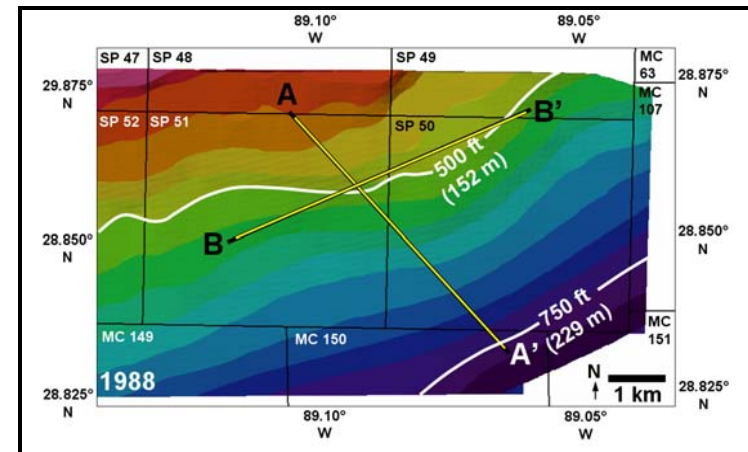


Figure 140: Seafloor bathymetry, South Pass Blocks 50 and 51, 1988. Image created in Fledermaus modeling software; artificial shading is applied from 330°; data from Racal-Decca, 1988.

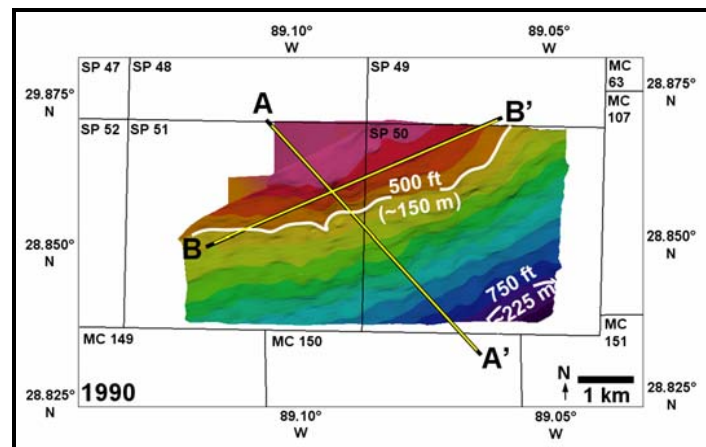


Figure 141: Seafloor bathymetry, South Pass Blocks 50 and 51, 1990. Image created in Fledermaus modeling software; artificial shading is applied from 330°; data from Arco Oil and Gas Company, 1990.

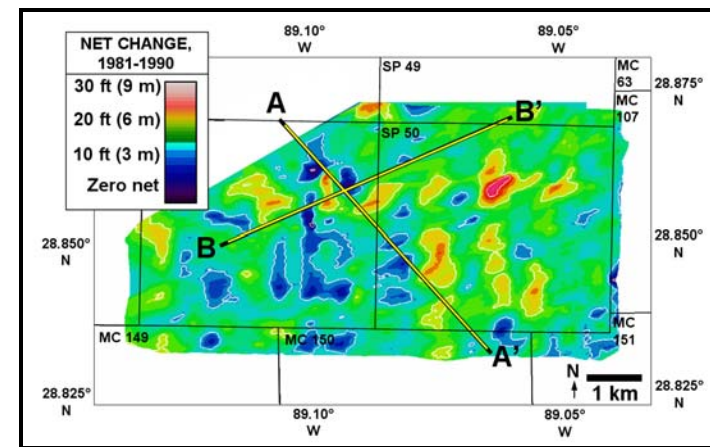


Figure 142: Net seafloor bathymetry change, 1981-1990, South Pass Blocks 50 and 51. Image created in Fledermaus modeling software; artificial shading is applied from 330°.

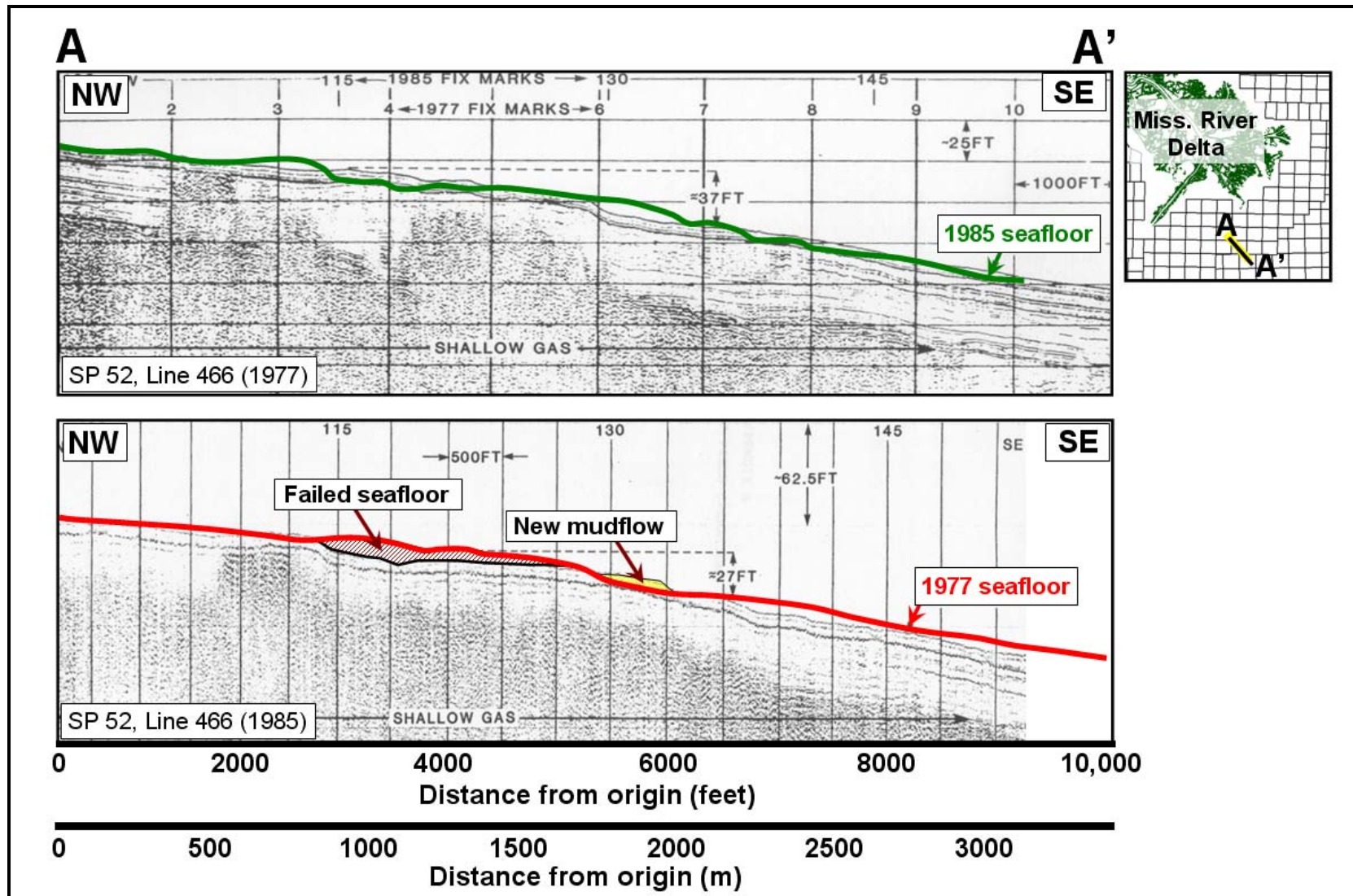


Figure 143: Seafloor and near-surface sediment change, 1977-1985, South Pass Block 52 (modified from McClelland Engineers, Inc., 1987)

approximately 19 km (12 miles) to the west. No site-specific data over this block was available for this study; however the lithologic and shear stress components of surficial and near-surface soils do not differ significantly from those in South Pass 50 and 51 (Figure 72, Section 6.1.2; Figure 74, Section 6.2; Figures 86 and 87, Section 6.3). In addition, a major seafloor failure occurred during Hurricane Katrina at South Pass Block 38, approximately 10 km (six miles) north of SP 55 and approximately 21 km (13 miles) west-northwest of SP 50 and 51. Again, no substantial difference exists in either surficial or near-surface sediments to suggest the area is unusually vulnerable to inter-hurricane shelf failures.

These findings corroborate evidence for limited inter-storm sediment movement previously substantiated 5 km (approximately three miles) to the northwest at South Pass Block 47 (SP 47; Hooper, 1996). A comparison of seafloor bathymetry between 1988 and 1993 was used to validate possible effects from Hurricane Andrew, which passed 80 km (approximately 50 miles) south of SP 47 in 1992. Even with the passage of a nearby hurricane, no changes in mudflow geometry, near-surface stratigraphy or surficial seafloor features were noted between the two surveys. Soil stability analyses predicted seafloor failure at wave periods up to 16 sec; however, since the seafloor remained relatively stable one must assume that wave periods were less than 16 sec and/or that the strength profile of near-surface sediments was greater than that assumed (Hooper, 1996).

The hypothesis that the SP 47 site experienced wave periods less than 16 sec was confirmed through numerical wave modeling carried out in this dissertation. Wave periods in this part of South Pass during Hurricane Andrew reached a maximum of approximately 11 sec on August 25, 1992 at 1800 Z and remained at that level through 2100 Z (Appendix O, Figure O-1). Wave conditions began to subside by August 26 at 0000Z (decreased to 8 sec) and continued a steady decline through August 27 at 0000Z, the last time sequence modeled in MIKE 21 for this study during Andrew. In no case did wave periods approach levels near 16 sec.

The effects of wave dampening at SP 47 as a result of soft or cohesive sediments along the seafloor were also addressed by Hooper (1996). These sediments, located *in situ* along the seafloor or comprising a prior mudflow, were shown through modeling to significantly reduce wave heights during severe storms (i.e., storms with wave periods of at least 15 sec). The wave fields simulated using MIKE 21 for Hurricane Andrew depicts  $H_{s_{max}}$  maxima of 8 m (27 feet) on August 25, 1992 at 1800 Z, coincident with the highest wave periods (Section 5.2.2; Appendix O, Figure O-2). Sea state conditions then began a steady decline through August 27 at 0000Z, the last time sequence in the Hurricane Andrew model.

Hooper (1996) also noted the effect of waves inducing shear stress levels equal to or exceeding that of the seafloor sediment, which leads to shelf failure conditions and implicit energy loss. Shear stress conditions at the seafloor at SP 47 during Hurricane Andrew, averaged approximately  $1.0 \text{ N m}^{-2}$  ( $2.09 \times 10^{-2}$  pounds feet<sup>2</sup>) on August 25, 1992 at 1800 Z, with localized areas approaching values of  $1.6 \text{ N m}^{-2}$  ( $3.34 \times 10^{-2}$  pounds feet<sup>2</sup>); Appendix O, Figure O-3). Although the scale of the data are insufficient to correlate directly with site-specific seafloor failures, the effect of seafloor bathymetry on seafloor shear stress was evident during Hurricane Andrew farther to the west, in particular along Ship Shoal (Appendix O, Figure O-3). Shear stresses there were markedly higher than background and range up to approximately  $1.6 \text{ N m}^{-2}$  ( $3.34 \times 10^{-2}$  pounds feet<sup>2</sup>) in an area roughly bounded by the 25-meter isobath.

### **7.3 Mississippi Canyon Morphologic Effects**

A modeling trial was performed to examine possible bathymetric controls on hydrodynamic conditions during severe hurricanes due to the existence of Mississippi Canyon and its proximity to the MRDF. During Hurricane Katrina a disproportionate number of platforms and pipelines suffered damage along the shelf in shallower water updip from the head of the canyon (discussed in more detail in Chapter 8). An attempt was made to determine the role that seafloor morphology plays and whether the canyon acts as a conduit for wave energy convergence and transfer upslope into shallower water. Prior work in the area has focused on the

effects of wave attenuation and the potential for the higher energy portion of an attenuated wave spectrum to shift closer to shore during severe hurricanes (Stone et al., 1995). In addition to the previous models discussed in Chapter 5, an additional model was constructed to examine modification in wave- and bottom-boundary layer parameters based on a “filled-in” canyon (i.e., assuming the canyon were non-existent). Any difference in values between existing and modeled conditions during Hurricane Katrina could then be inferred as resulting directly from the canyon’s existence and orientation.

Mississippi Canyon itself resulted from a massive submarine seafloor failure on an unstable continental margin approximately 25,000 to 27,000 years B.P. (Coleman et al., 1983). The canyon formed as a series of repeated failures, with each failure setting up steep headwall slopes that led to instability and additional failures. This process was repeated over and over, with the newly formed canyon acting as a downslope transport conduit for fresh sediment failure (Figure 144; Coleman et al., 1983).

### **7.3.1 MIKE 21 Modeling Trial**

For purposes of this trial, seafloor bathymetry was smoothed across the outer shelf to conform to bathymetric contours on either side of the existing canyon (Figure 144). A transect of ten data points oriented in a straight northwest-southeast profile was then outlined for use as model output locations (Table 16).

A distinct pattern of increasing  $H_{s_{max}}$  was noted in the existing canyon with increasing water depth and distance away from the coast as well as from the protective screen of the MRD, which would have restricted the fetch area at the height of the storm given Katrina’s counter-clockwise flow (Figures 144 and 145). The MIKE 21 “filled canyon” model revealed a decrease in  $H_{s_{max}}$  values of approximately 0.3 m in the shallowest water depths at the peak of Hurricane Katrina at Stations J and K (water depths 20 m or less; Figure 146). Moving downslope into deeper water, the maximum difference between actual and modeled bathymetry began to diverge in water depths of approximately 50 m beginning with Station F (Figures 144 and 146). As water



Table 16: Modeling stations, Mississippi Canyon Infilling Exercise

Station	Latitude (degrees)	Longitude (degrees)	Water Depth, Open Canyon (m)	Water Depth, “Filled” Canyon (m)
A	28.282090	-89.520500	958	670
B	28.393932	-89.646378	763	350
C	28.482472	-89.765985	587	170
D	28.558586	-89.852972	460	94
E	28.651786	-89.960152	216	68
F	28.675086	-89.997432	125	58
G	28.723239	-90.059565	46	46
H	28.824206	-90.169852	29	29
J	28.929833	-90.283245	18	18
K	29.019926	-90.385765	7	7

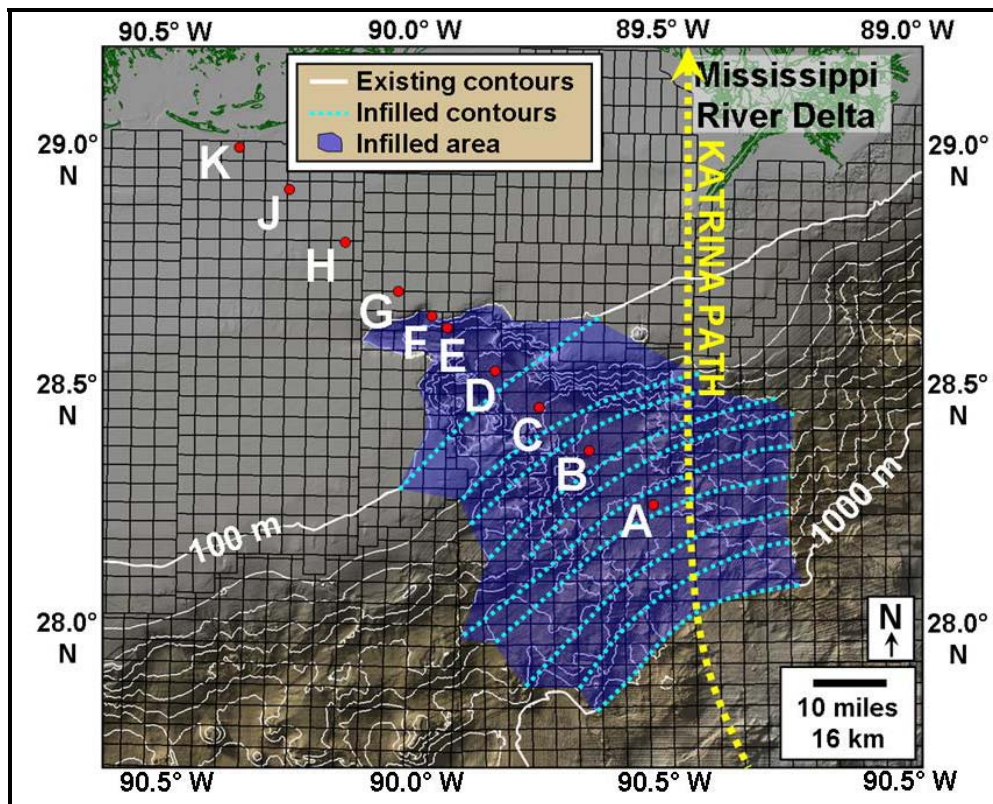


Figure 144: Seafloor rendering, MRDF and adjacent GOM continental shelf including Mississippi Canyon (image created in Fledermaus software with artificial shading applied from 340°; vertical exaggeration 25X; bathymetry data extracted from NOAA, 2009)



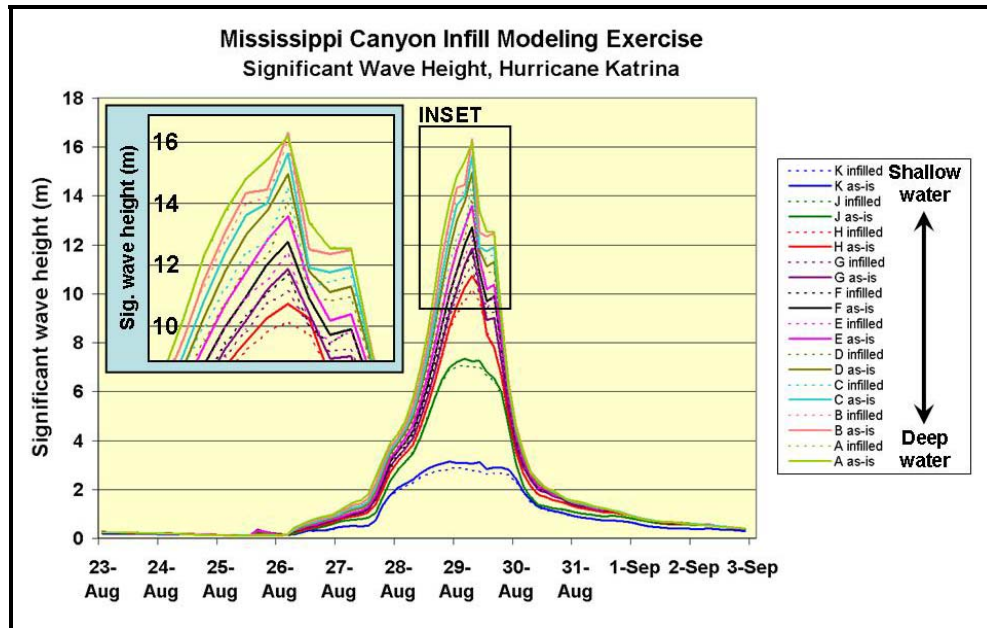


Figure 145: Significant wave height comparison between existing and modeled infilled Mississippi Canyon

depth increased, the wave attenuation effect of a filled canyon also began to increase, with the difference in  $H_{s_{max}}$  values for Stations G and H ranging from 0.58 to 0.75 m. Stations beyond Point F (inclusive) are located past the current-day shelf edge and thus the effects of become more pronounced. The greatest difference in  $H_{s_{max}}$  values (1.51 m) is seen at Station D in 460 m of water (existing; 94 m infilled).  $H_{s_{max}}$  values for both the infilled and existing canyon models continued to increase with distance offshore (Figure 147); however the differential between infilled and existing conditions began to decrease below Station C given increasingly negligible wave effects and the diminished effect of surface storm waves in ultra-deep water (Figure 146).

Wave periods for stations along the transect were clustered relatively close together, mostly in a range of 11-12 sec at the time of maximum impact (Figure 148). However, periods in the shallowest water, particularly at Stations J and K, fell in a range of approximately 13.5 sec at the time of maximum impact and were the highest periods recorded along the transect for both infilled and existing morphology along with Stations A and B in deeper water. This phenomenon can also be seen in the MIKE 21 runs for each storm modeled in Chapter 5, with longer periods

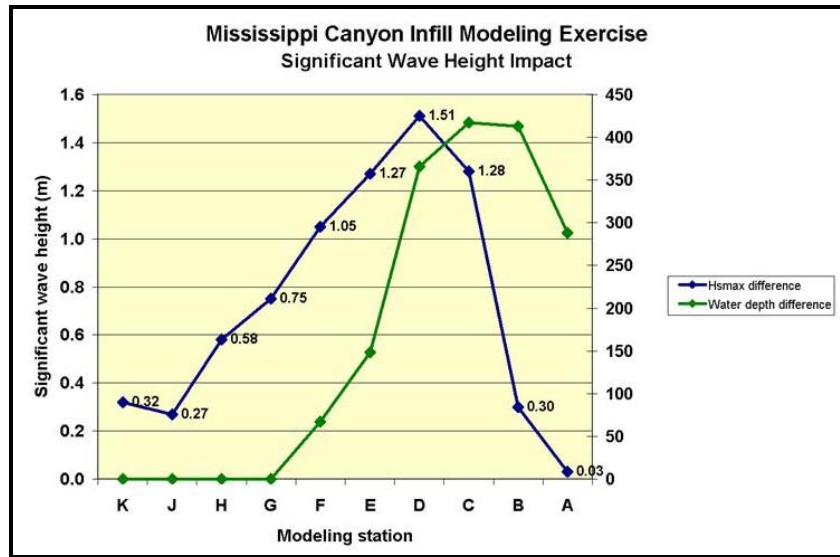


Figure 146: Maximum significant wave height difference between existing and modeled infilled canyon

adjacent to the immediate shoreline (Figures 39 and 44, Section 5.1.1 and Figures 47, 48, 51 and 52, Section 5.2.2). Modeled wave periods for Stations J and K became longer than those in deeper water beginning on August 27 and continued until August 31, consistent with wave effects in shallow water as waves slow down upon interaction with the seafloor closer to shore. Overall, little significant difference was detected in wave period values between infilled and existing conditions, with the maximum separation between the two being approximately 1.25 sec at Stations D and E; value differences elsewhere were less than 1 sec (Figures 147 and 149).

The most pronounced difference between infilled and existing conditions in Mississippi Canyon was exhibited among horizontal bottom particle velocities. A comparison of values from Stations A through D (along the shelf-slope break) revealed negligible velocity effects in the existing canyon while “filled” conditions revealed velocities up to  $0.7 \text{ m sec}^{-1}$  at Station D (Figure 147). However, beginning with Station E, the transect transitions from deep water into shallower continental shelf waters with abrupt variability in seafloor bathymetry (Figure 144). At this point the seafloor became impacted by storm wave base as reflected in bottom velocities (Stations A through C). As the transect continued into even shallower water, the effect of storm waves with the seafloor increased, and by Station G (with no difference between infilled and

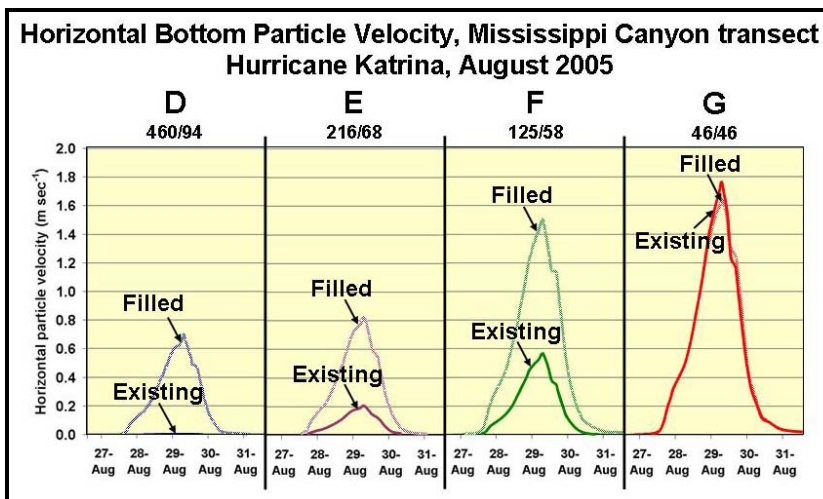
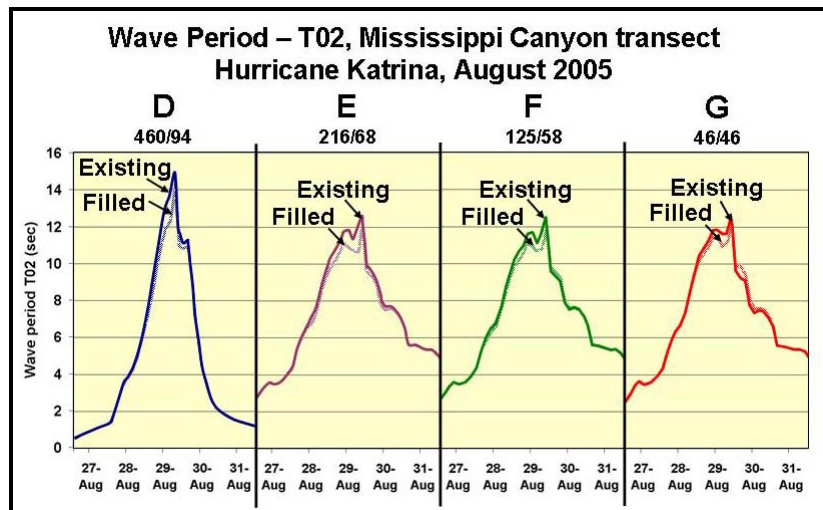
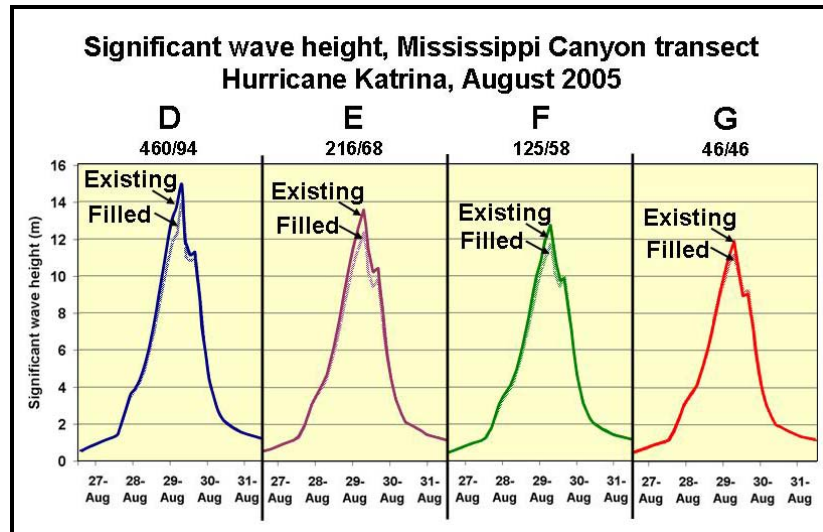


Figure 147: Comparison of significant wave height, wave period and horizontal particle velocity (seafloor) for canyon infill modeling exercise, Stations D, E, F and G, Mississippi Canyon transect (water depth for each station (m) denoted as actual/filled)

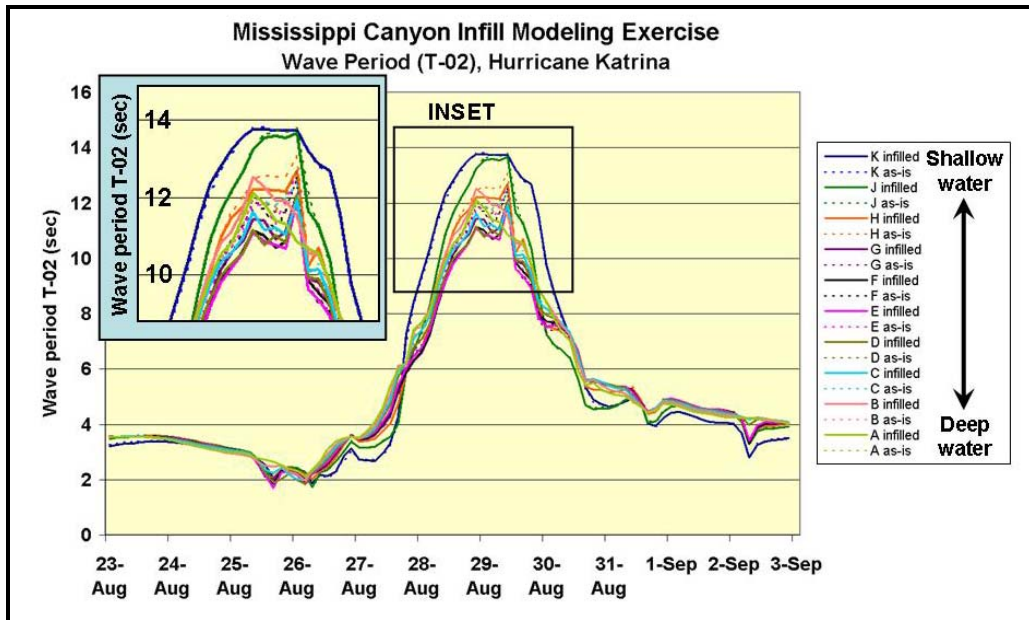


Figure 148: Wave period comparison between existing and modeled infilled Mississippi Canyon

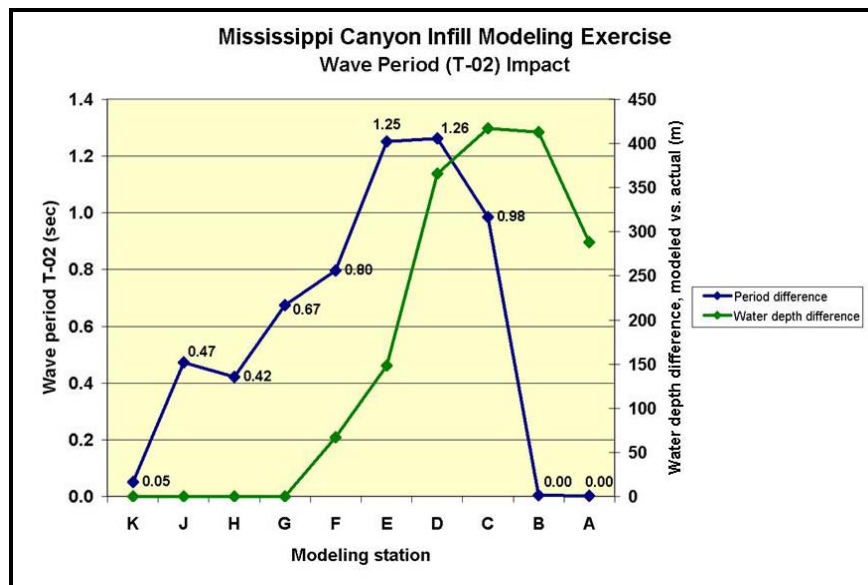


Figure 149: Maximum wave period difference between existing and modeled infilled canyon

existing bathymetry) there was broad agreement between the two sets of conditions (Figure 147). Of particular note are velocity differences at Stations C, D, E and F; in some cases the difference between infilled and existing conditions is approximately twice as high (infilled being higher; Figure 150). Horizontal velocities were generally highest at shallow water stations, with velocity maxima of approximately  $2.3 \text{ m sec}^{-1}$  at Stations H and J which are roughly consistent with but

slightly higher than observations described by Stone et al. (1995) during Hurricane Andrew (Figure 151). In this study, maximum near-bottom orbital velocities approached  $2.0 \text{ m sec}^{-1}$  in approximately 30 m of water (equivalent to Station H in this study, which registered a maximum velocity of  $2.3 \text{ m sec}^{-1}$  during Katrina).

### **7.3.2 Trial Ramifications**

The focus of this trial was to determine the extent to which energy and momentum transfer within Mississippi Canyon might be controlled by its bathymetry and/or orientation. No significant difference was observed in significant wave heights or in wave periods between filled and existing conditions; however horizontal orbital velocities exhibited significant differences.

Given the horizontal bottom velocities results, shear stress can be directly inferred as being directly proportional to the square of the bottom orbital velocity. Since the depth variability among stations located on the shelf edge (i.e., Stations D, E and F) is so abrupt, the same variability can be denoted for shear stress, and the variability becomes squared. Therefore, the amount of energy expended within a relatively short spatial period can be considerable. Also, the abrupt increase in velocity could impart higher momentum (defined as mass \* velocity). A disproportionate number of pipelines and platforms failed during Hurricane Katrina just north of the head of Mississippi Canyon (Figures 3 and 6, Chapter 2), and the hurricane-induced wave energy and the momentum involved could be responsible for these failures (albeit not from submarine mudslides). Inter-canyon turbulence has been shown to be orders of magnitude stronger than that along the shelf due to elevated internal wave fields (Petruncio et al., 1998; Kunze et al., 2002).

In addition, breaking near-inertial waves as a result of reflection off the seafloor can enhance inter-canyon turbulence, leading to elevated levels of energy dissipation along canyon boundaries (Jordi and Wang, 2008). Studies of Mississippi Canyon wave effects during Hurricane Ivan indicate that the highest rates of wave energy decay occurred northwest of Mississippi Canyon in depths of approximately 25-30 m (Stone et al., 1995).

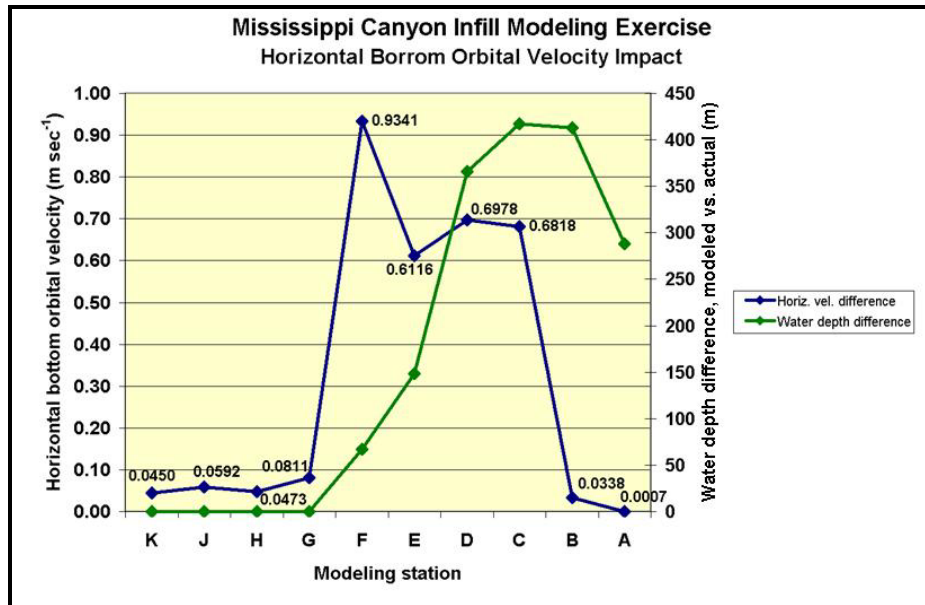


Figure 150: Horizontal bottom orbital velocity comparison between existing and modeled infilled Mississippi Canyon

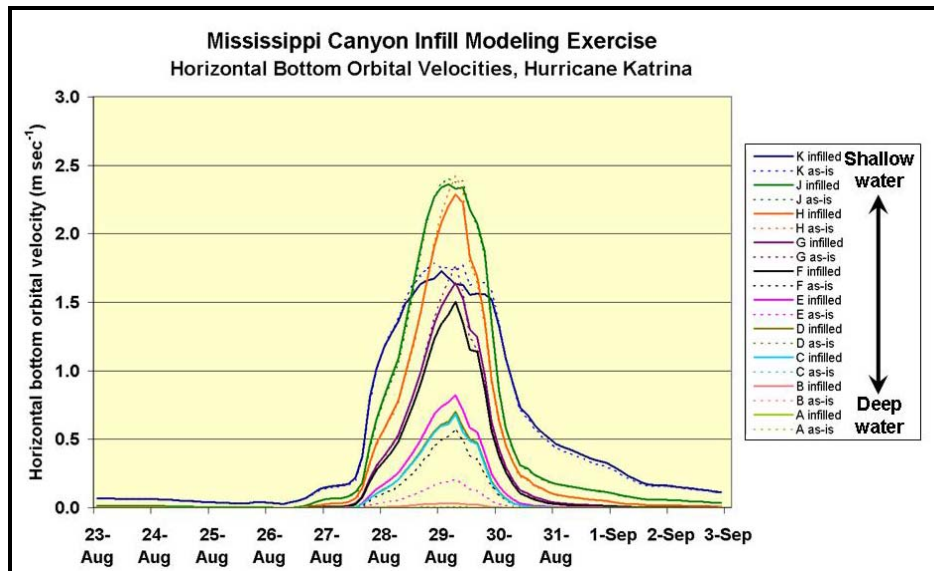


Figure 151: Horizontal bottom orbital velocity difference between existing and modeled infilled canyon

A vertical component (i.e., upwelling and downwelling) of energy propagation from inertial currents also likely exists during severe hurricanes. Within DeSoto Canyon in the northeastern GOM during Hurricane Ivan, a significant amount of vertical momentum transfer occurred as evidenced by an increase in bottom temperatures from 18° C to 26° C due to warmer surface waters being mixed downward (Stone et al., 2005). After Ivan passed through the area,

current speeds decreased, current direction changed, and bottom temperatures cooled rapidly from 26° C to 15.2° C, likely as a result of post-hurricane upwelling from deeper waters in DeSoto Canyon.

Strong bottom currents have been shown to prevail during extreme hurricanes. Hurricane Claudette generated currents of approximately 0.6 m sec<sup>-1</sup> from along the bottom at the height of the storm (Sheremet et al., 2005). These currents, which were in the direction of primary wind, abated to almost a complete standstill one day after landfall before transitioning to a strong return flow near the bottom afterwards. Similarly, bottom currents during Hurricane Ivan at the NRL moorings described in Section 2.2 ranged from 0.4 to 1.2 m sec<sup>-1</sup> and were sufficient to transport resuspended sediment and generate scour (Teague et al., 2006; 2007). Bottom scour at the NRL moorings as a result of Ivan was measured at 8, 32 and 36 cm at water depths of approximately 60 m. Scour of approximately 8-9 cm was detected at depths of approximately 90 m (Teague, 2006, 2007).

Pipelines in the GOM at these water depths are typically non-buried and are laid directly on the seafloor because the level of scour had been thought to be relatively insignificant. However, significant bottom scour can occur during hurricanes when orbital wave velocities generate sediment resuspension and background mean flow conditions are sufficient to transport the suspended sediment regardless of the actual depth of the bottom (Teague, 2007). Significant scour that occurs beneath pipelines could be a potential cause of failure. However, it appears unlikely that the dynamics required to initiate substantial submarine shelf failure and mudslides could have resulted from strong bottom currents and subsequent seafloor surface scour. These results also confirmed that the high momentum generated at the seafloor due to abrupt changes in morphology could also trigger these failures. Additional *in situ* observations of wave fields along Mississippi Canyon are recommended to further explore the role of canyons in effectively trapping hurricane-generated waves.



## **7.4 Climate Change and Anthropogenic Effects**

A comparison of the net sediment change maps between 1874-1940 and 1940-1977 illuminates the changed nature of Mississippi River sedimentation patterns. The 1874-1940 data reflect sediment buildup adjacent to Pass a'Loutre; the 1940-1977 data show practically no sediment buildup adjacent to the distributary. In addition, the area of sediment buildup from 1940-1977 is less than that for the period from 1874-1940. These findings were consistent with documented sediment load reduction during a time span that approximates the period between the 1940 and 1977 surveys (Rossi et al., 2009). Strong climatic influences, in addition to annual fluctuations, were postulated as related to well-known patterns such as ENSO (El Nino Southern Oscillation) sea level and ocean temperature anomalies. Results also indicated a decrease in sediment loading that was attributed to anthropogenic changes, such as the construction of large dams on the Missouri River in the 1950s. A reduction in average annual sediment load leads to the hypothesis of lower sediment rates and fewer slopes that are oversteepened, potentially resulting in the removal of several key triggers that can cause submarine shelf failure.

Kesel (2003) further described the many human modifications made within the Mississippi River flood plain beginning in the 1920s (e.g., extensive levee systems, dams and reservoirs, and channel cutoffs) and how they affected the overall channel and sediment budget. These modifications also served to reduce the overall sediment load and thus potentially reduce the influence of several triggering mechanisms for submarine shelf failure (discussed in more detail in Section 9.2.1).

After the 2005 hurricane season, which spawned Hurricanes Katrina, Rita and Wilma (all Category 5 hurricanes during their history), research focused on possible links between global climate change and the seeming increased frequency and severity of Atlantic Basin hurricanes (Arpe and Leroy, 2008). However, many other variables can influence tropical storm severity, chief among them being wind shear during El Nino events that can override warmer ocean temperatures and reduce hurricane severity. The implications of these findings on this

dissertation are that if GOM hurricanes occur more frequently or are more severe, then the potential for increased submarine shelf failure also increases (further discussed in Chapter 9). If other factors diminish the potential for severe storms, then one of the main triggering mechanisms responsible for submarine shelf failure is eliminated. As with all other risk factors described in Chapter 9, a thorough evaluation of all hazards and risks must be completed; the risk is not solely dependent on one variable.

## **CHAPTER 8. INFRASTRUCTURE CONTROLS AND STATISTICAL ANALYSIS**

Severe storm events such as the five hurricanes examined in this dissertation extract a huge toll on offshore oil and gas industry infrastructure. Damage and loss have been extensively noted among drilling rigs, producing platforms and pipelines, all of which can be affected by large waves propagated from hurricanes, tropical storms or even strong wintertime cold fronts (Arnold, 1967; Bea, 1971; Bea and Bernard, 1973; Sterling and Strohbeck, 1973; Bea and Audibert, 1980; MMS, 2005a; Hooper and Suhayda, 2005a, 2005b; MMS, 2005b; Thomson et al., 2005; MMS, 2005c, 2006a). This chapter examines damage and loss from a statistical standpoint within the dissertation study area (Figures 1 and 2, Chapter 2).

Photographic descriptions of the most common types of drilling rigs and production platforms active in the GOM are contained in Appendix A.

### **8.1 Historical Offshore Infrastructure Development, 1937-2008**

The first attempt at drilling offshore in the GOM occurred from a wooden structure located just offshore Cameron Parish, Louisiana in 1937 (Austin et al., 2004). This platform, which developed oil and gas reserves from Creole Field, was located approximately 2 km offshore in a water depth of approximately 4 m. The platform deck was constructed 4.5 m above sea level and was designed to be replaced should hurricane waves wash it away (Austin et al., 2004). An un-named Category 1 hurricane struck Cameron Parish from the southeast in August 1940 (NHC, 2009) during which waves tore the deck away. Additional wooden piles were driven for support and the deck was replaced, thus this platform became the first structure to “survive” a GOM hurricane (Austin et al., 2004).

Offshore drilling activity in the GOM began in earnest just after World War II. The first successful well drilled out of the sight of land was drilled in 1947 by Kerr-McGee in what is now Ship Shoal Block 28. As drilling technology continually improved, exploration activity moved into progressively deeper water, first on the continental shelf but eventually onto the continental

slope and, in recent years, beyond the Sigsbee Escarpment into ultra-deep water (3000 m; Figure 1). A dense production platform and pipeline network was constructed in order to produce hydrocarbons and transport them to onshore facilities. As of 2009, the GOM contained approximately 1500 platforms and 54,000 km of pipelines (Alvarado, 2006).

This dissertation evaluates infrastructure development and trends using snapshots taken at each of the five hurricanes evaluated. Statistics of offshore development through time were then compared to damage and loss patterns realized during each storm. Infrastructure information from the MMS was digitally imported into an ArcGIS database to create maps of platforms and pipeline segments in place during each storm (MMS, 2009). Platform installation dates prior to 1992 were reported only by year and therefore, for statistical purposes, platforms for Hurricanes Betsy and Camille were assumed to be in place in the year in which each hurricane occurred. Likewise, pipeline information was extracted from an MMS database into ArcGIS, manipulated to fit an approximate timeline, and displayed along with the appropriate platform information to provide an approximate infrastructure display (Figures 152-156).

## **8.2 Time-Sequenced Offshore Infrastructure Distribution**

Hurricane Betsy (1965) struck the southeast Louisiana coast approximately 90 km west of the Mississippi River Delta although its hurricane-force wind field extended broadly across most of offshore Louisiana's production grid (Figure 152). Hurricane Betsy was a relatively large hurricane but also a relatively fast one, as it traveled through the MRDF within approximately four hours (Figure 30, Section 5.1.1, and Figure 152; NHC, 2009). Industry development by 1965 was confined to the continental shelf in water depths of less than 150 m as drilling and production technology had not yet advanced sufficiently beyond the shelf edge (Figure 157).

A total of 380 platforms had been emplaced in the study area by 1965 (Figure 152; MMS, 2009). Most of these platforms were small, single-well installations set in water depths ranging

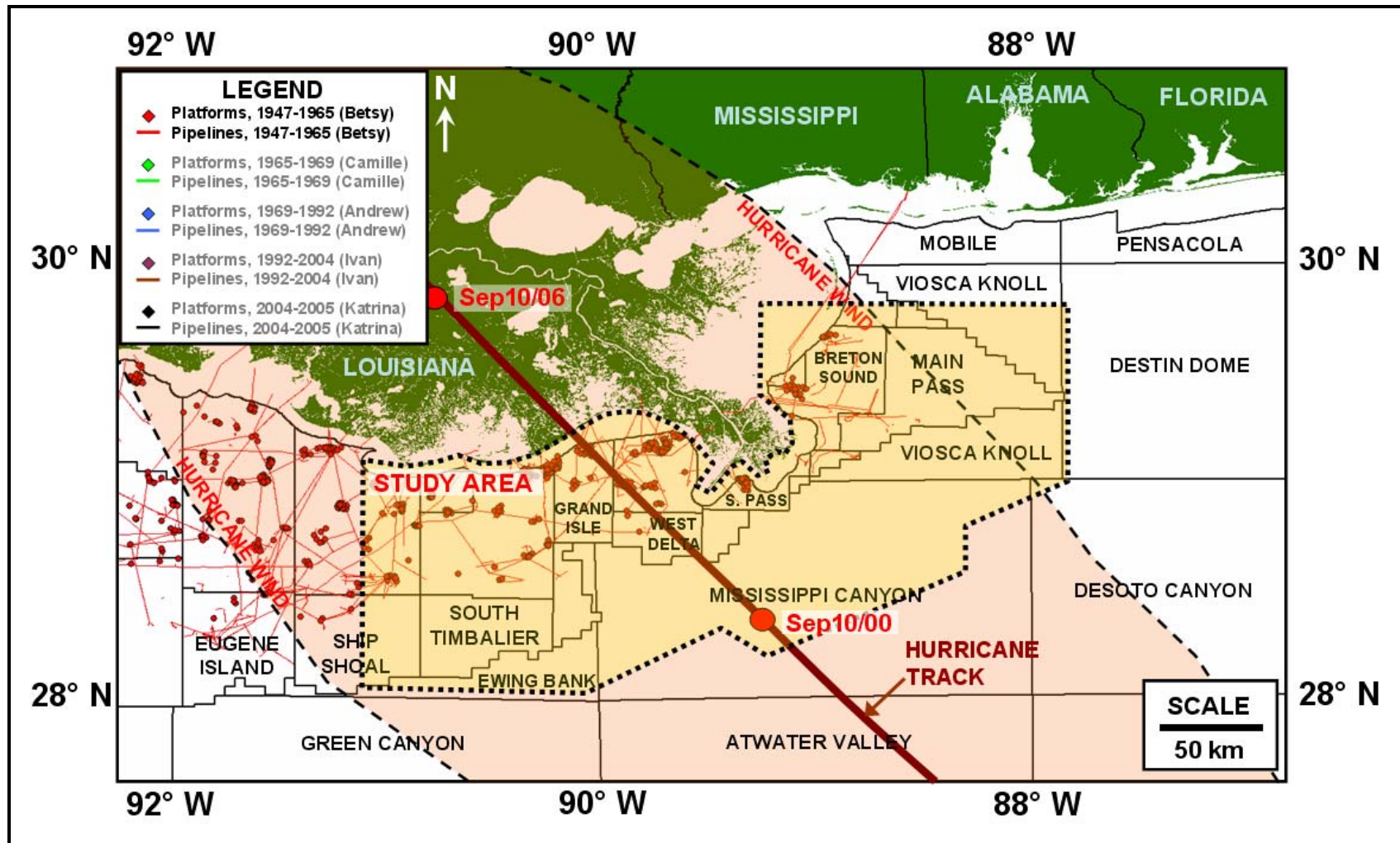


Figure 152: North-central GOM platform and pipeline infrastructure in place through end of 1965 (proxy for Hurricane Betsy landfall; platform data extracted from MMS, 2009 and imported into an ArcGIS database)

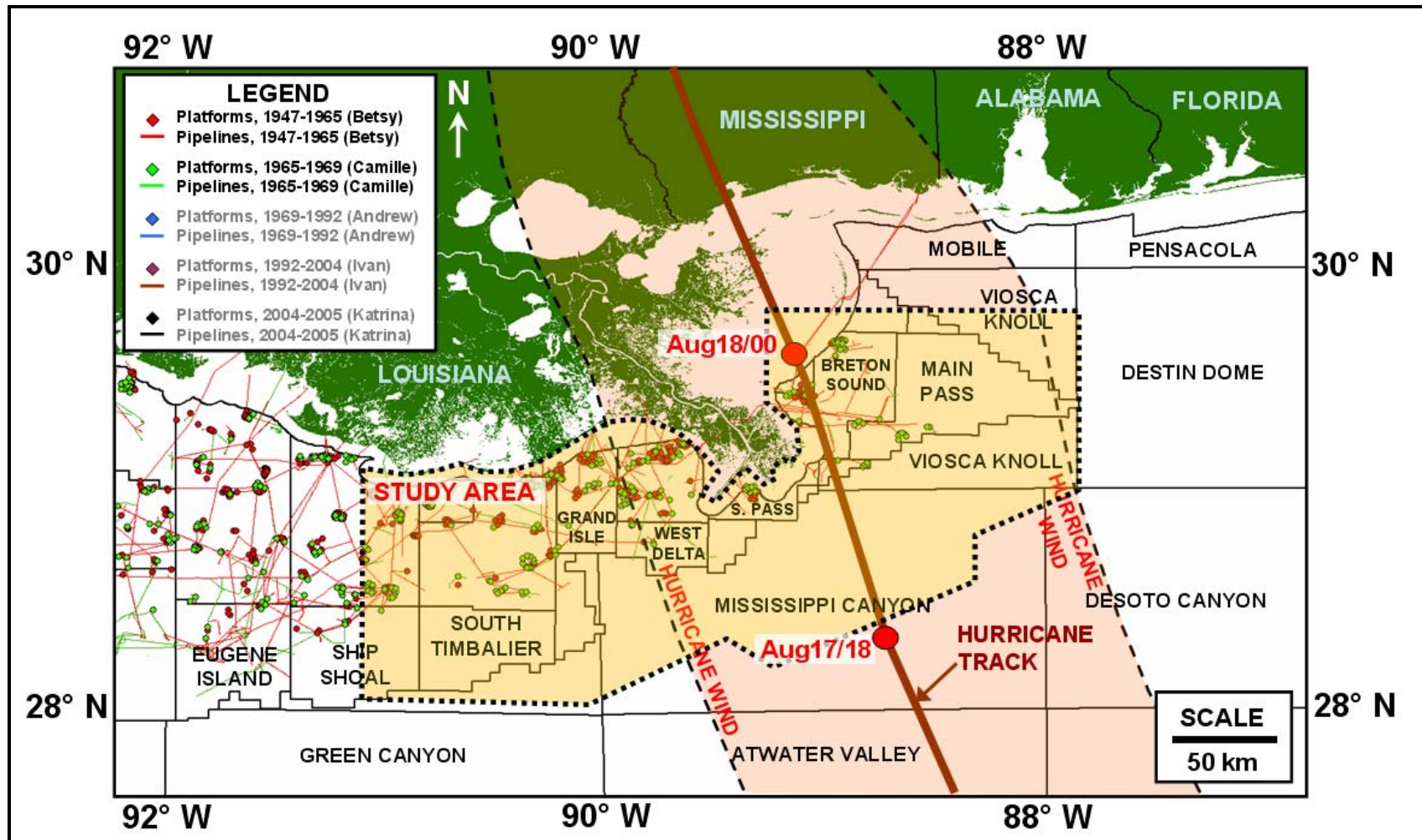


Figure 153: North-central GOM platform and pipeline infrastructure in place through end of 1969 (proxy for Hurricane Camille landfall; platform data extracted from MMS, 2009 and imported into an ArcGIS database)



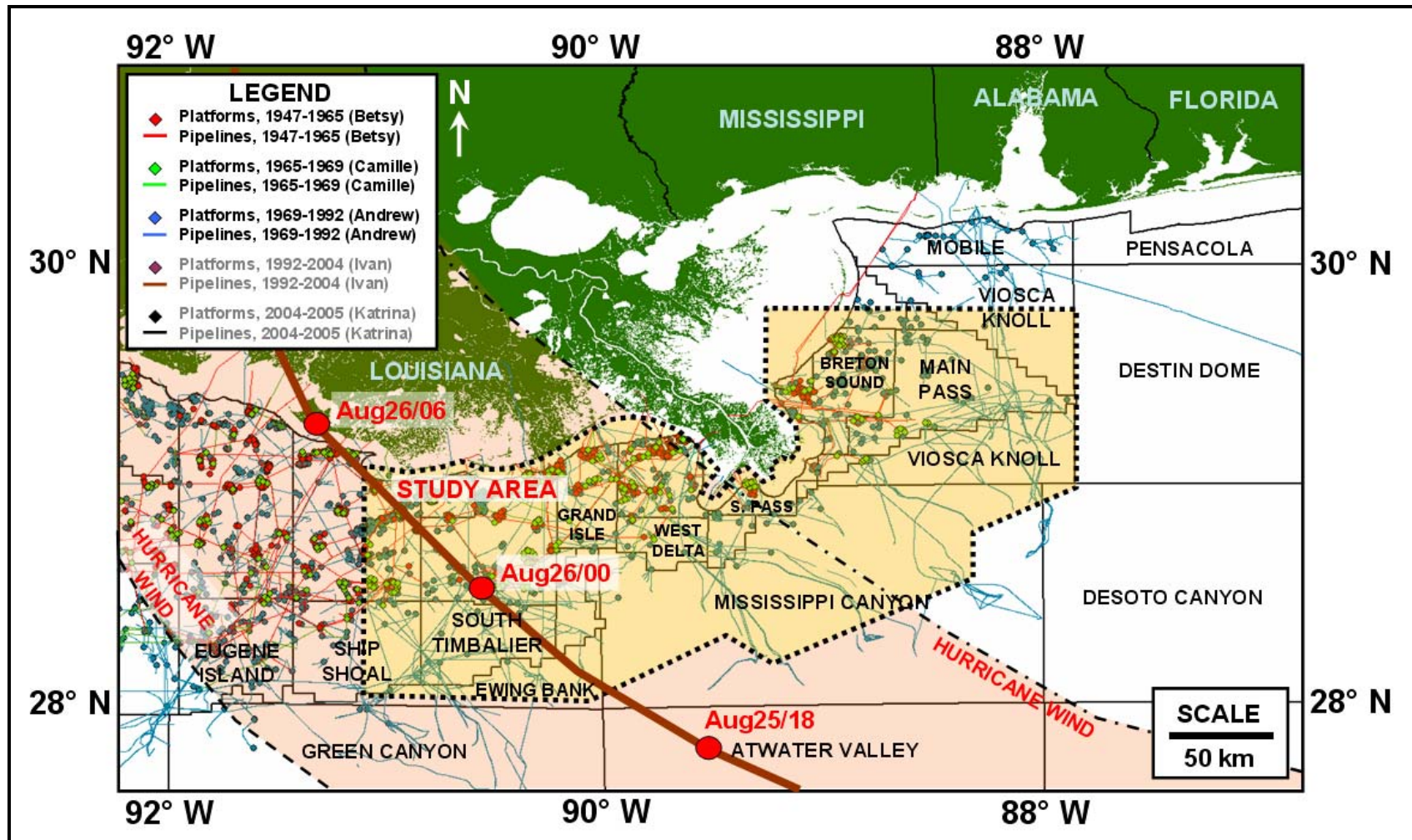


Figure 154: North-central GOM platform and pipeline infrastructure in place through Hurricane Andrew (August 1992; platform data extracted from MMS, 2009 and imported into an ArcGIS database)



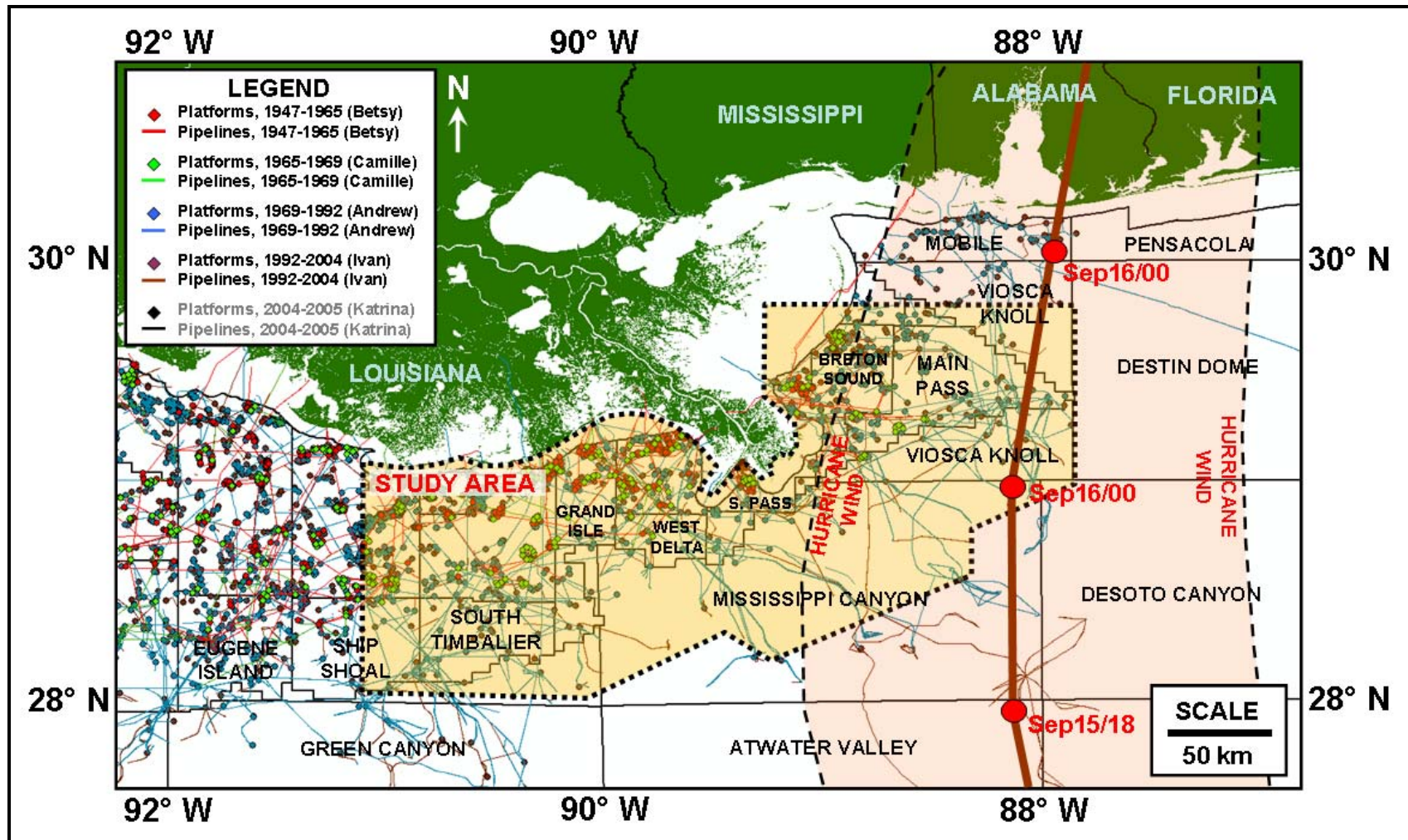


Figure 155: North-central GOM platform infrastructure in place through Hurricane Ivan (September 2004; platform data extracted from MMS, 2009 and imported into an ArcGIS database)

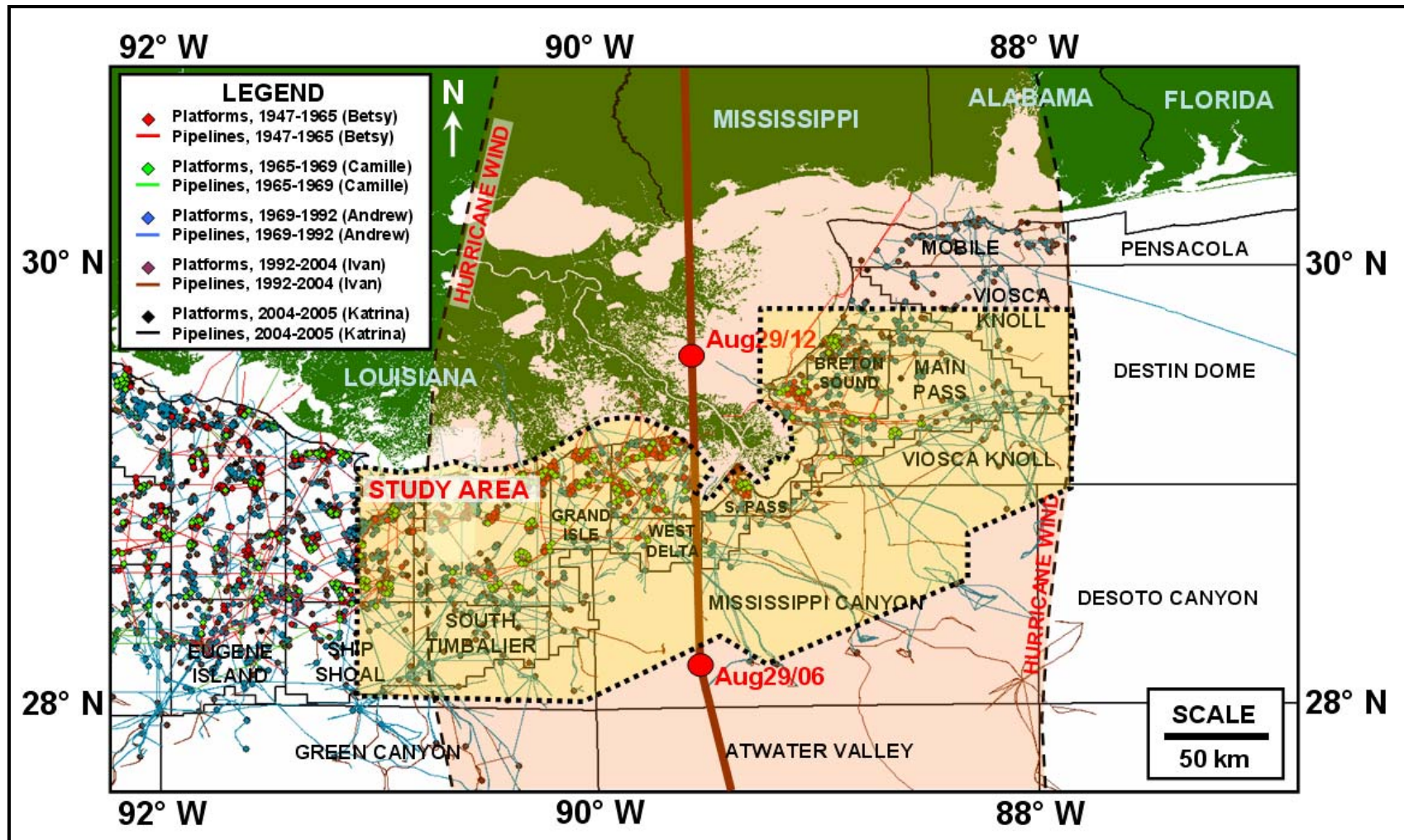


Figure 156: North-central GOM platform and pipeline infrastructure in place through Hurricane Katrina (August 2005; platform data extracted from MMS, 2009 and imported into an ArcGIS database)



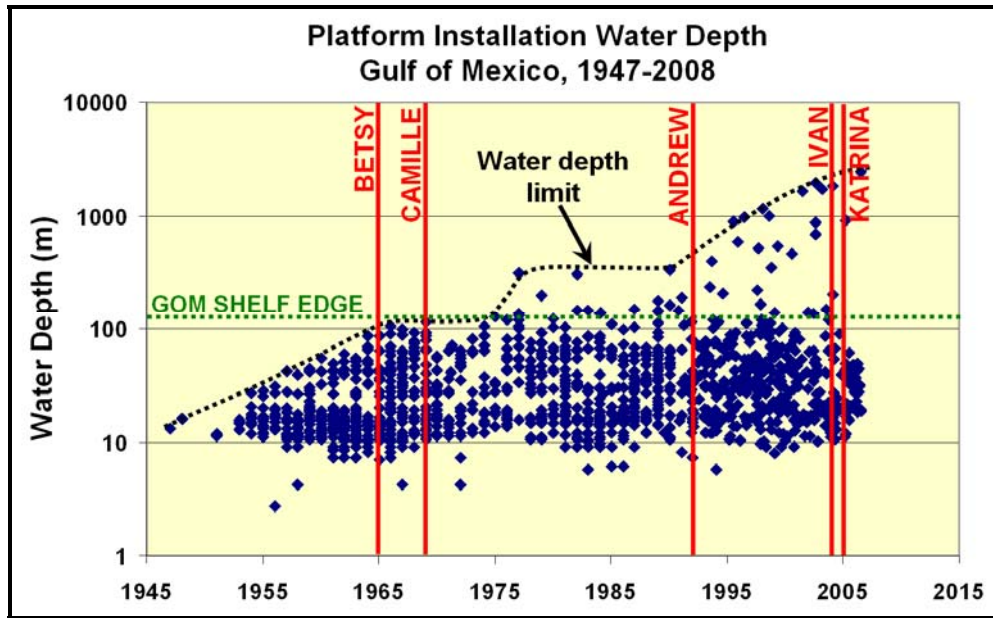


Figure 157: Historical water depth limits for installed Gulf of Mexico platforms, 1947-2008

between 10 and 85 m (Figure 157; also Appendix P). No platforms installed prior to Hurricane Betsy had been decommissioned (i.e., taken out of service) prior to the storm.

Hurricane Camille (1969) passed 35 km east of the Mississippi River Delta from a south-southeasterly angle (Figure 29, Section 5.1.1 and Figure 153). Its hurricane-force wind field extended in a relatively narrow band across the easternmost production area offshore Louisiana. Hurricane Camille was a relatively tight hurricane but also a relatively slow one, as it traveled through the MRDF within approximately eight hours (Figure 30, Section 5.1.1, and Figure 153; NHC, 2009). Industry development by 1969 was still confined to the continental shelf in water depths of less than 150 m although by 1969 development had moved further outward up to the shelf edge (Figures 153 and 157).

A total of 571 platforms had been emplaced in the study area by 1969 (MMS, 2009). Although many of these platforms were small, single-well installations, others were larger, more technologically advanced multi-well platforms set in water depths ranging between 10 and 103 m (Figure 153; also Appendix P). No platforms installed prior to 1969 had been decommissioned (i.e., taken out of service) by the time Camille struck the area. The pipeline network in the study

area (highlighted in green on Figure 153) grew steadily since Hurricane Betsy, extending nearly to the shelf edge in the Main Pass and Viosca Knoll Protraction Areas.

Hurricane Andrew (1992) passed 230 km west of the Mississippi River Delta from a southeasterly angle (Figure 29, Section 5.1.1 and Figure 154). Even though the eye of Andrew passed significantly west of the MRDF, its hurricane-force wind field extended over the study area. Hurricane Andrew traveled through the MRDF within approximately seven hours (Figure 30, Section 5.1.1, and Figure 154; NHC, 2009). Although facilities were still being installed on the shelf, GOM industry development by 1992 had moved into deep water, with a step-change having been achieved in 1978 with Shell's Cognac platform in 311 m of water in Mississippi Canyon Block 194 (Figure 157; Appendix P).

A total of 1122 platforms had been emplaced in the study area by 1992 (MMS, 2009). These platforms consisted of a mix of different types; most were fixed, multi-well platforms set in water depths ranging between 10 and 334 m (Figure 154; Appendix P). Of these, 120 had been decommissioned prior to Hurricane Andrew. The pipeline network in the study area (highlighted in blue on Figure 154) grew extensively in the 13-year interval between Hurricanes Camille and Andrew, extending far beyond the edge of the continental shelf and in particular throughout the Mississippi Canyon Protraction Area.

Hurricane Ivan (2004) passed 120 km east of the Mississippi River Delta from an angle slightly west of due south (Figure 29, Section 5.1.1 and Figure 155). The angle taken by the eye of Ivan skirted the eastern periphery of the study area; however its hurricane-force wind field covered the entire Main Pass and Viosca Knoll Protraction Areas as well as the eastern half of the Mississippi Canyon Protraction Area (Figure 155). Hurricane Ivan was a relatively slow-moving storm – it took over eight hours for the eye to move through the study area. The metocean effects from Ivan persisted even longer, with elevated wave heights and wave periods extending over 48 hours (see Section 5.2.1). As seen in earlier GOM development history, facilities were still being installed on the shelf but by 2004 several ultra-deep water developments had been installed,

the deepest being BP's NaKika facility in Mississippi Canyon Block 474 in 1939 m of water (Figure 157; also Appendix P).

A total of 1445 platforms had been emplaced in the study area by 2004 (MMS, 2009). These platforms consisted of a mix of different types; most were fixed, multi-well platforms although several of these consisted of floating production facilities (Figure 157; also Appendix P). Of the total, 449 had been decommissioned prior to Hurricane Ivan. The pipeline network in the study area (highlighted in brown on Figure 155) grew extensively in the 12-year interval between Hurricanes Andrew and Ivan, extending even further into deep water than the network had prior to Hurricane Andrew.

Hurricane Katrina (2005) passed approximately 50 km west of the Mississippi River Delta from an angle near due south (Figure 29, Section 5.1.1 and Figure 156). The relatively large hurricane-force wind field from Katrina blanketed the entire study area. The hurricane traveled through the MRDF within approximately seven hours although its metocean effects impacted the study area in excess of 48 hours (see Section 5.2.1). Only one year passed between Hurricanes Ivan and Katrina, therefore the infrastructure in place was not appreciably different between the two storms (Figures 155 and 156).

A total of 1473 platforms had been emplaced in the study area by 2005 (MMS, 2009). As with Hurricane Ivan, they consisted of a mix of different types (Figure 157; also Appendix P). Of this total, 467 had been decommissioned prior to Hurricane Katrina. The pipeline network in the study area (highlighted in black on Figure 156) was mostly unchanged from 2004-2005.

### **8.3 Infrastructure Damage and Loss, Major GOM Hurricanes**

Ever since the destruction of the Creole structure in 1940, offshore facilities have been vulnerable to extreme metocean conditions during severe storms. When the first fixed platforms were installed in shallow shelf waters, they contained an air gap of between 6-12 m based on then-conventional ideas of expected hurricane wave height and intensity (Austin et al., 2004; Benfield Group Limited, 2005). Hurricane Flossie (1956) was the first storm to cause a

significant impact to facilities and production (Lambert, 1956), which led to the initial efforts in setting standard recommended practices concerning platform design and construction (American Petroleum Institute (API), 1993, 2000). However, the design criteria that were adopted by industry varied by more than 200% for the same wave height considerations (Lee, 1963) and, as a result, significant damage occurred in the succession of Hurricanes Hilda, Betsy and Camille from 1964-1969 (Lambert, 1964, 1965; Sheffer, 1964, 1965; The Oil and Gas Journal, 1969a, 1969b; MMS, 2009). Subsequent efforts at platform design focused on ensuring that facilities could withstand a “100-year storm” (API, 1993; 2000). However, metocean and seafloor impact from Hurricanes Ivan, Katrina and Rita forced a re-evaluation of platform design criteria, which is still being debated (Benfield Group Limited, 2005).

#### **8.3.1 Hurricane Betsy (1965)**

Hurricane Betsy inflicted more damage to the offshore oil and gas industry than any previous hurricane, partly because of its intensity and partly because of the significant growth of offshore infrastructure in the years immediately preceding Betsy’s landfall (Lambert, 1965). Industry investment in the area affected by Hurricane Betsy (South and Main Pass, West Delta and Grand Isle Protraction Areas) was estimated at \$2 billion in 1965 (\$13.7 billion equivalent in 2009) and infrastructure damage (not counting lost oil and gas production from an estimated 8,000 producing wells in Betsy’s hurricane force wind field) amounted to \$100 million in 1965 (approximately \$685 million equivalent in 2009; Lambert, 1965; Sheffer, 1965). However, not all of this damage was due to seafloor movement and most of the losses were attributed to wave action that affected the topsides of numerous platforms in the hurricane’s path.

Several areas did, however, experience seafloor failure that precipitated damage and loss. Among them were Shell’s South Pass Block 27 Field located in East Bay, an interdistributary bay located between Southwest Pass and Main Pass offshore the Mississippi River delta (discussed further in Chapter 7). Water depths in the field range from 5-21 m. Seafloor movement during

Hurricane Betsy was inferred when numerous pipeline breaks occurred and when several risers were twisted loose from an overlying platform and pulled to the southwest (Arnold, 1967).

Subsequent post-hurricane divers' reports indicated 32 pipeline breaks in the area of which eight (25%) were ascribed to seafloor failure (Arnold, 1967; Table 17). However, previous studies conducted after previous storms (e.g. Carla in 1961 and Hilda in 1964) indicated an additional 59 pipeline breaks, of which 34 (58%) were ascribed to seafloor failure. The ephemeral nature of seafloor topography was indicated in bathymetric surveys conducted in the area after Hurricanes Carla, Hilda and Betsy moved through the GOM. In each successive survey, topographic changes were detected on the seafloor, many of which were located near numerous pipeline breaks.

Table 17: Summary of flow line and transfer line breaks, South Pass Block 27 Field Area (from Arnold, 1967)

	1958-1965 (excluding hurricanes)	Carla (1961)	Hilda (1964)	Betsy (1965)	Total
Corrosion	79	N/A	N/A	N/A	79
Anchor or spud	23	N/A	N/A	N/A	23
Leak in clamp	19	N/A	1	1	21*
Rubbing	21	1	2	1	25*
Line into mud	10	5	5	5	25*
Line in tension	2	5	5	0	12*
Riser pulled	3	4	6	1	15*
Breaks above	0	4	4	14	22
Unknown mechanical breaks	22	11	6	10	49
TOTAL	180	30	29	32	271

\* Due to soil movements or currents

Pipeline diameter played a significant role in determining which pipelines failed. Larger-diameter pipelines (i.e. greater than 4 inches (10.2 cm) in diameter) failed in shear whereas smaller pipelines were flexible enough to move in tandem with changing seafloor conditions. Smaller pipelines, when they did fail, did so as a result of tensile forces in the part of the line that anchored it to a more stable region (Arnold, 1967).



Storm-related impact was also detected in the Bay Marchand Protraction Area east of the delta where 90 flow lines were destroyed. Six additional lines were reported destroyed in the Main Pass Protraction Area although the precise locations of these lines are unknown (Lambert, 1965). Despite the proximity to wind and waves from Hurricane Betsy, certain regions in the northern, shallower parts of the West Delta and Grand Isle Protraction Areas were disproportionately unaffected. Several hypotheses proposed to explain this fact include (1) that the Mississippi River delta acted as a barrier to higher waves, and (2) that Hurricane Betsy's fast forward speed of 35 km hour<sup>-1</sup> (22 miles hour<sup>-1</sup>) curtailed time-dependent wave generation and therefore prevented prolonged exposure to severe metocean conditions (Blumberg, 1965; discussed previously in Chapter 5).

### **8.3.2 Hurricane Camille (1969)**

Infrastructure damage offshore Louisiana caused by Hurricane Camille consisted of damage to numerous platforms and pipelines adjacent to the Mississippi River delta. However, total losses were less than those incurred in Hurricane Betsy because of Camille's more easterly track relative to Betsy. Total damage and loss costs were estimated between \$50 million to \$100 million in 1969 (\$294 million to \$587 million equivalent in 2009; The Oil and Gas Journal, 1969a; 1969b). Although much of this loss can be linked to extreme wave action that directly impacted platforms, several cases of seafloor movement leading to platform loss were described.

One of the most significant losses during Hurricane Camille was the South Pass Block 70 "B" Platform, which was discussed previously in Section 3.3.2. Additional losses were detected in the South Pass Protraction Area, notably at South Pass Block 61, 5 km west of South Pass Block 70, and also at South Pass Block 60 which is 5 km northwest and adjacent to mudslide events that took place during Hurricanes Ivan and Katrina over 30 years later. Platform failure reports for the earliest hurricanes (i.e. Camille and earlier) are provided in Table 18 (PMB Engineering, Inc, 2006). However, it should be noted that these failure reports include all causes,

Table 18: Platform failures from all causes in hurricanes prior to Hurricane Andrew (from PMB Engineering, Inc., 1993)

<u>Hurricane</u>		<u>Operator</u> <u>Name</u>	<u>Area*/</u> <u>Block</u>	<u>Platform Characteristics</u>			
<u>Name</u>	<u>Date</u>			<u>Name</u>	<u>Year</u> <u>Installed</u>	<u>Water</u> <u>Depth (m)</u>	<u>Number</u> <u>of Piles</u>
Grand Island	1948	Humble	N/A	2	N/A	15	N/A
	1948	Humble	N/A	1	N/A	15	N/A
Carla	1961	Placid	EI 198	N/A	N/A	31	2
		Shell	EC (N/A)	N/A	N/A	N/A	4
		Zapata	VM 104	N/A	1959	18	4
Hilda	1964	CATC	EI 208	A	N/A	30	8
		CATC	EI 208	C	1959	29	8
		CATC	EI 208	D	N/A	29	8
		Gulf	SS 154	B	N/A	18	6
		Gulf	SS 154	H	N/A	18	6
		Gulf	SS 169	A	1961	18	4
		Placid	EI 198	B	1961	31	2
		Pure	SS 253	N/A	1964	52	8
		Signal	SS 149	B	N/A	15	8
		Sinclair	EI 175	A	1955	27	16
		Shell	EI 188	N/A	1958	21	4
		Tenneco	SS 198	C	1959	26	8
		Tenneco	SS 199	A	1959	31	8
		Union	EI 276	N/A	1964	52	8
Betsy	1965	CATC	WD 69	1	N/A	38	3
		CATC	WD 70	3	N/A	38	3
		Forest	WD 97	N/A	N/A	51	4
		Gulf	WD 117	A	1962	63	8
		Gulf	WD 117	B	N/A	66	8
		Phillips	MP 129	N/A	N/A	28	4
		Pure	WD 118	N/A	N/A	59	4
		Shell	SP 24	N/A	N/A	18	4
Camille	1969	Gulf	SP 61	A	1968	85	8
		Shell	SP 70	A	1969	98	16
		Shell	SP 70	B	1969	100	16
Carmen	1974	Odeco	SS 119	A	N/A	16	36
		Odeco	SS 119	F	N/A	16	36
Frederic	1979	Odeco	SP 19	4	N/A	9	3
		Odeco	SP 19	11	N/A	9	3
		Odeco	SP 19	13	N/A	9	3
Juan	1985	Odeco	SP 19	OBM	1961	9	4
		Odeco	SP 19	SWP	N/A	9	3
		Odeco	ST 86	A	1955	29	16

\* Protraction Area Legend:

EC: East Cameron

EI: Eugene Island

MP: Main Pass

SP: South Pass

SS: Ship Shoal

ST: South Timbalier

VM: Vermilion

WD: West Delta

not just those from submarine mudslides. Failures in Table 18 due to known mudslides are denoted in yellow.

### **8.3.3 Hurricane Andrew (1992)**

By 1992, offshore Louisiana infrastructure had significantly grown since Hurricane Camille passed through the study area in 1969 – 1,002 structures were located in the study area by 1992 compared to only 571 in 1969 (data retrieved from archives at MMS, 2009). However, the impact to oil and gas facilities from Hurricane Andrew was less than Hurricanes Betsy and Camille due to Andrew's more westerly track through the GOM and away from the higher-density concentration of oil and gas infrastructure offshore southeastern Louisiana (Figure 1). Total damage to offshore facilities amounted to approximately \$500 million in 1992 (approximately \$768 million equivalent in 2009).

A total of 485 GOM-wide pipeline damage incidents were reported as a result of the storm (Den Norske Veritas, 2007; Table 19). Of the damaged segments, 10 of them (approximately 2%) were attributed to known mudslide events, mostly in the South Timbalier Protraction Area and well west of the MRDF. No known, large-scale seafloor failure events occurred within the MRDF proper as a result of Andrew. A total of 22 production platforms were destroyed during Hurricane Andrew, of which five were located in the study area and none of which appear to be the result of storm-induced seafloor failure (Den Norske Veritas, 2007; Table 20). An additional 65 platforms were significantly damaged, of which 19 were located in the study area.

Despite the lack of relative damage to offshore infrastructure within the MRDF proper, Andrew is still considered a major reference storm in this research because of its intensity as it traversed the GOM and because it provides a useful comparison between storms that caused major damage in the MRDF and those that did not.

Table 19: Reported pipeline damage due to natural hazards (from Den Norske Veritas, 2007)

<u>Hurricane</u>	<u>Total damage reports</u>	<u>Due to adjacent platform</u>	<u>Due to Mudflow</u>	<u>Due to riser</u>	<u>Due to pipe displacement</u>	<u>Due to outside force</u>	<u>Other/ Unknown</u>
Andrew	485	253	10	103	44	18	57
Lili	120	120	16	N/A	78	N/A	6
Ivan	168	20	16	67	38	9	18
Katrina	299	139	1	66	61	9	14
Rita	243	94	0	89	31	8	21
Total	1315	626	43	325*	252	44*	116
Average	263	125	9	65*	50	9*	23

\* record incomplete; could be higher

Table 20: Reported platform damage due to natural hazards (from Den Norske Veritas, 2007)

<u>Hurricane</u>	<u>Platforms Exposed to Hurricane Force</u>	<u>Platforms Destroyed</u>	<u>Platforms Damaged</u>	<u>Percentage of Exposed Platforms Destroyed</u>	<u>Percentage of Exposed Platforms Damaged</u>
Andrew	~700	22	65	3.1	9.3
Lili	~800	2	17	0.3	2.1
Ivan	~150	7	31	4.7	20.1
Katrina	~1000	47	20	4.7	2.0
Rita	~2050	66	32	3.3	1.6
Total	~4700	144	165	3.1	3.5
Average	~900	29	33	3.1	3.5

#### 8.3.4 Hurricane Ivan (2004)

Seven production platforms were destroyed during Hurricane Ivan and significant damage occurred to 31 others (Figure 4; also Appendix C, Table C-1; MMS, 2005a). Of the seven platforms that were destroyed, one was destroyed by a seafloor failure (a platform at Mississippi Canyon Block 20); the others were likely destroyed as a result of wave loading (Puskar et al., 2006). Most of the platforms that failed during Ivan were designed to withstand lower metocean conditions and therefore contained lower strength characteristics than platforms designed for more rigid metocean conditions as required by updated industry specifications (API, 1993; 2000; Puskar et al., 2006).

Hurricane Ivan initiated 168 pipeline damage incidents in the GOM, with 16 of them being attributed to mudslides (approximately 9.5%, a much higher percentage than during

Andrew). One example of this damage was the BP-operated Main Pass Oil and Gas Gathering system (MPOG) previously discussed in Section 7.2.1. This pipeline underwent horizontal translation in three separate areas but remained intact as demonstrated by side-scan sonar surveys taken after Hurricane Ivan (Thomson et al., 2005).

The eye of Ivan passed over a part of the GOM that contains relatively fewer platforms and pipelines compared to areas further to the west (Figure 155; Tables 19 and 20). The percentage of platforms destroyed and damaged was 4.7% and 20.1%, respectively, which is far above the statistical average of the most recent hurricanes that moved through the area. The number of pipeline damage reports attributed to submarine mudslides was relatively high (16 compared to the statistical average of nine), especially when compared to those from Hurricane Katrina where the network of pipelines is much denser (Figure 156). Pipeline age did not appear to be a factor, as approximately 30% of the pipelines damaged in the most recent hurricanes were less than ten years old and the distribution of damaged pipelines is approximately equal across an installation year spectrum (Den Norske Veritas, 2007). Also, most of the pipeline damage incidents reported (67%) were from pipelines less than 6 inches ( $1.52 \times 10^{-1}$  m) in diameter and therefore more susceptible to failure. Pipeline damage tends to be a better indicator of submarine mudslide activity, and the hypothesis that submarine mudflows may have caused much of the damage during Hurricane Ivan appears valid.

#### **8.3.5 Hurricane Katrina (2005)**

Like its predecessor Ivan, Katrina severely impacted oil and gas infrastructure. Forty-seven platforms (including many small ones) were destroyed during Katrina and 20 others were significantly damaged (MMS, 2006b; Figure 4; also Appendix C, Table C-2). Katrina followed a more westerly path as it passed through the study area and was a more intense storm than Ivan in terms of barometric pressure (938 mb for Ivan vs. 915 mb for Katrina; Table 1). In addition to the impact on platforms, 299 pipeline segments across 61 different pipelines were damaged during Katrina (Alvarado, 2006; MMS, 2006b; Table 19; also Appendix C, Table C-3). The

number of pipeline failures attributed to mudslide events varies from one (Den Norske Veritas, 2007) to six (Alvarado, 2006), or up to 2% of the total.

Only one platform failure during Katrina was attributed to mudslides or foundation failure (Den Norske Veritas, 2007; Energo Engineering, Inc., 2007). Most of the platform damage that occurred during Katrina was located west of the eye path and likely caused by wave loading on platform jackets. Platforms located east of the eye were subjected to extreme metocean conditions during Hurricane Ivan only the year before, and any weak structures were likely eliminated from the available platform pool at that time. In any case, observed platform performance during Katrina was much better than anticipated (Energo Engineering, Inc., 2006). Several hypotheses used to explain this include the fact that (1) platform pile capacity increases with time (thereby accounting for an increase in design capacity, approximately 2-3 times beyond that which was anticipated), and (2) many platforms in this area were designed more conservatively given inherent variability in local soil conditions, which resulted in a more robust platform design (Energo Engineering, Inc., 2007).

Caution must be taken, however, in evaluating damage pipeline damage patterns as the incidence of damage largely depends on operator diligence when reporting damage to the MMS. In addition, many reports depend on how well pipeline damage can be observed through visual inspection or inferred from hydrocarbon leaks and/or reduced pipeline pressure. Most of the pipeline damage during Hurricanes Ivan and Katrina was attributed to adjacent platform failure, riser damage or anchor dragging; in fewer cases the damage resulted from a loss of cover and subsequent pipeline movement nearshore and in shallower water (Den Norske Veritas, 2007). Since data on what triggered each pipeline failure are incomplete, attributing the ultimate cause of any pipeline failure remains difficult.

## **CHAPTER 9. RESULTS AND VULNERABILITY MATRIX**

Various controls on shelf failure and subaqueous mudslides (discussed in Chapters 5, 6 and 7) each exert unique influence upon the probability of mudslide occurrence. These controls, when integrated as part of an overall hazard model, can help quantify and predict seafloor vulnerability to future mudslides given specific metocean, lithologic, geotechnical and morphological characteristics. The net result of the evaluation is a composite Mississippi River Delta Front (MRDF) vulnerability profile that can be used to highlight the potential for future seafloor failure for a specific area given a range of conditions.

### **9.1 Common Hazard Framework**

Hazard estimation studies the past several decades have focused on defining and integrating various risk parameters into a common framework that allows for interpretation consistency on a global basis (Vaunat and Leroueil, 2002). This framework, while constructed initially for subaerial landslides, can be adapted to subaqueous environments in general and, by extension, to those in the MRDF (Leroueil et al., 2003). Although certain characteristics of submarine mudslides may differ from subaerial slope movements (in particular the post-failure stage, in which movement may occur as a relatively intact or undisturbed body extending unusually long distances), the underlying framework has been quantified in prior landslide research and is assumed valid (Leroueil et al., 1996; Locat and Lee, 2002; Leroueil et al., 2003). This dissertation aims to apply the framework specifically to the MRDF environment.

#### **9.1.1 Hazard and Vulnerability Assessment History**

Initial studies in subaerial landslides in the 1970s concentrated on distinguishing differences between what were termed “basic” maps and “synthesis” maps (Vaunat and Leroueil, 2002). Basic maps corresponded to specific factors that underpinned failure (e.g., topographic, geological, morphological and geotechnical) whereas synthesis maps focused on better defining the actual hazard through sets of hazard and risk management maps (e.g., land-use, planning and development constraints; Froelich et al., 1978; Ives and Krebs, 1978).



Work in the 1980s evolved towards developing a common methodology for hazard and risk analysis (Vaunat and Leroueil, 2002). Risk factors were defined on the basis of probabilistic concepts consistent with other natural hazards. These factors were ultimately consolidated by the International Geotechnical Society (IGS) of the United Nations Educational, Scientific and Cultural Organization (UNESCO), thus ensuring their use on a global basis.

The probabilistic concepts formalized by IGS include several basic definitions commonly associated with landslide occurrence (Hansen, 1984; Varnes, 1984; Hartlen and Viberg, 1988; Einstein, 1988; Edris, 1988; Alexander, 2002; Crozier and Glade, 2005). These definitions, which are referred to in subsequent sections for consistency, include the following:

- **Danger:** Defined as the event that could actually take place (in the initial case, a landslide). In this dissertation, danger is defined as the process of slope change before, during and after a potential subaqueous mudslide or shelf failure event.
- **Magnitude:** Defined as the energy released during the failure event with which it is associated. Magnitude can be quantified by the area, volume, travel distance and velocity of a given failure (discussed in Chapters 6 and 7).
- **Hazard:** Defined as the probability that a given event (i.e., a landslide), triggered by events and conditions quantified in Chapter 5, will occur in the future.
- **Risk:** the expected consequences that occur as a result of a specific event (landslide).

In order for a risk evaluation to be effective it should incorporate the following:

- **Inventory:** Defined as a quantification of the elements at risk. In this dissertation, elements at risk include various offshore infrastructure types (e.g., production platforms and pipelines; discussed in Chapter 8).
- **Vulnerability:** For each element, a number is assigned on a predetermined scale to reflect the degree of damage (i.e., that which is sustained by offshore infrastructure during severe hurricanes and subsequent mudslide events).

- Total risk: is equal to the product of the hazard, the value of all the risk elements, and their vulnerability (Varnes, 1984).

These concepts underpin the terminology used when characterizing MRDF risk and vulnerability in this chapter. Despite the framework adopted by IGS it should be noted that considerable uncertainty exists, whether in the data available over a certain area, the lack of accurate slope behavior models, or in time effects due to pore pressure changes and creep, and the strict use of a probabilistic framework remains difficult in many cases (IUGS, 1997; Vaunat and Leroueil, 2002).

### **9.1.2 MRDF Hazard Application and Vulnerability Framework**

A common landslide risk estimation framework accepted for geotechnical use worldwide is one advanced by Vaunat et al. (1992) and Vaunat and Leroueil, 2002). This framework relies on a series of factors that, when activated, characterize a particular danger that could be faced. The danger, in turn, can then be characterized by conducting a hazard assessment that estimates the occurrence probability of seafloor failure and the evolution of the slope before, during and after failure. These dangers are quantified by a magnitude that can itself be characterized by the area, volume, travel distance and velocity of a particular seafloor failure. The hazard assessment, in turn, defines the occurrence probability of dangers within a given time interval, within a given area, and for a given magnitude. Following from the hazard assessment, the risk assessment evaluates damage suffered by a particular element during a given hazard (Figure 158). The conceptual relationship between hazard, vulnerability and elements at risk has been summarized by Alexander (2002; Figure 159). An asset (i.e., an element at risk) is not at risk unless it is threatened by something (i.e., a submarine mudslide), and a hazard is not hazardous unless it threatens something (i.e., an element at risk). The intersection of hazard and vulnerability therefore combine to define the anticipated risk (Figure 159).

This framework is adapted to the MRDF environment to evaluate and characterize the vulnerability and risk associated with subaqueous shelf failure. The factors defined in Figure 158

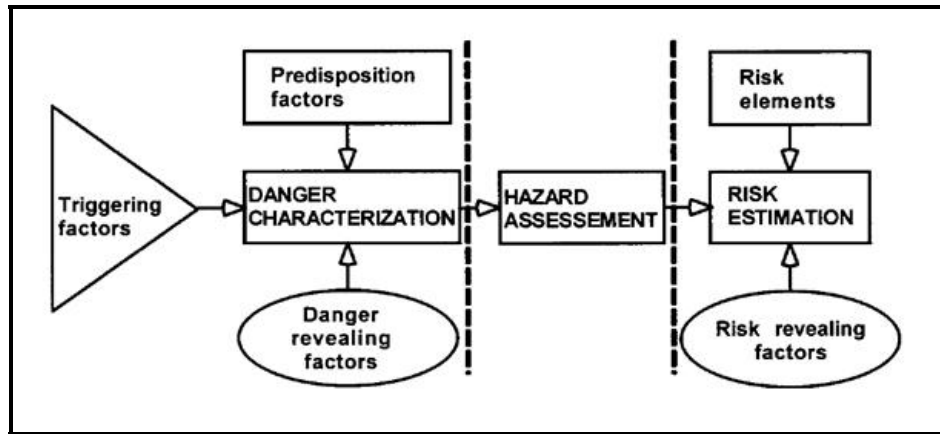


Figure 158: Landslide hazard and risk analysis (from Vaunat and Leroueil, 2002)

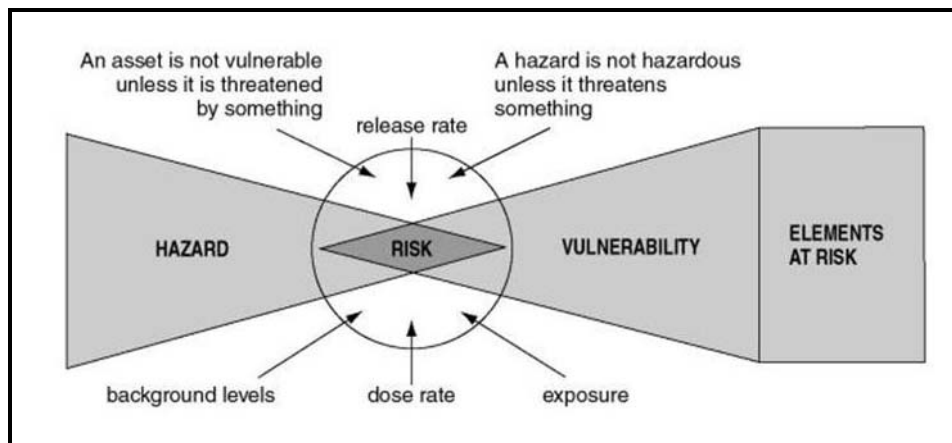


Figure 159: Conceptual relationship between hazard, elements at risk, vulnerability and risk (from Alexander, 2002)

can be broken down into three main types – triggering, predisposition, and revealing factors. Triggering factors, as related to subaqueous mudslides, include the effects of extreme metocean conditions experienced during severe hurricanes (e.g., extreme significant wave heights, wave periods, bottom currents and the amount of time that a given point on the seafloor endures extreme metocean conditions). Revealing factors related to subaqueous mudslides include evidence of prior events (e.g., antecedent mudflow lobes), element vulnerability (e.g., damaged or destroyed infrastructure), or any other factor that reveals the occurrence potential for a future event.

Predisposition factors can be defined as permanent factors that help determine seafloor slope response (Vaunat and Leroueil, 2002). These factors, as related to subaqueous mudslides,

include the effects of lithological and geotechnical parameters comprising the ocean floor and immediate subsurface (e.g., grain size, soil type, shear strengths, slope steepness of the existing seafloor and time elapsed since previous mudslides).

The hazard assessment follows on the characterization of the dangers involved. Previous risk assessments discussed in the literature have been adapted for submarine failure and build on earlier landslide hazard and risk analysis results (Leroueil et al., 2003; Figure 160). However, none have been specifically adapted for use along the MRDF and its unique metocean, lithologic, geotechnical and infrastructure characteristics. The evaluation procedure that follows is an adaptation of that model to the MRDF, which is a major contribution of this dissertation. Individual components of the risk model (e.g., various factors, the danger characterization, the elements at risk and the total risk estimation) are integrated into a new MRDF model discussed in Section 9.3.

## **9.2 MRDF Risk Synthesis**

### **9.2.1 Danger Characterization**

The principal danger evaluated in this work is that of submarine shelf failure occurring along and adjacent to the MRDF. This danger can be characterized by three primary factors as they relate to MRDF shelf failure as identified in Section 9.1.2 – triggering factors, revealing factors, and predisposition factors (Figure 158).

#### **9.2.1.1 Triggering Factors**

Primary triggering factors include temporal exposure to extreme metocean conditions during severe hurricanes as discussed in Chapter 5. These factors include effects from extreme significant wave heights, wave periods, bottom currents and the amount of time that a given point on the seafloor endures extreme bulk wave and bottom boundary layer conditions. Prolonged exposure to such conditions can exacerbate triggers for submarine mudslides and therefore can increase the likelihood of an occurrence. In addition, the *intensity* of bulk wave and bottom

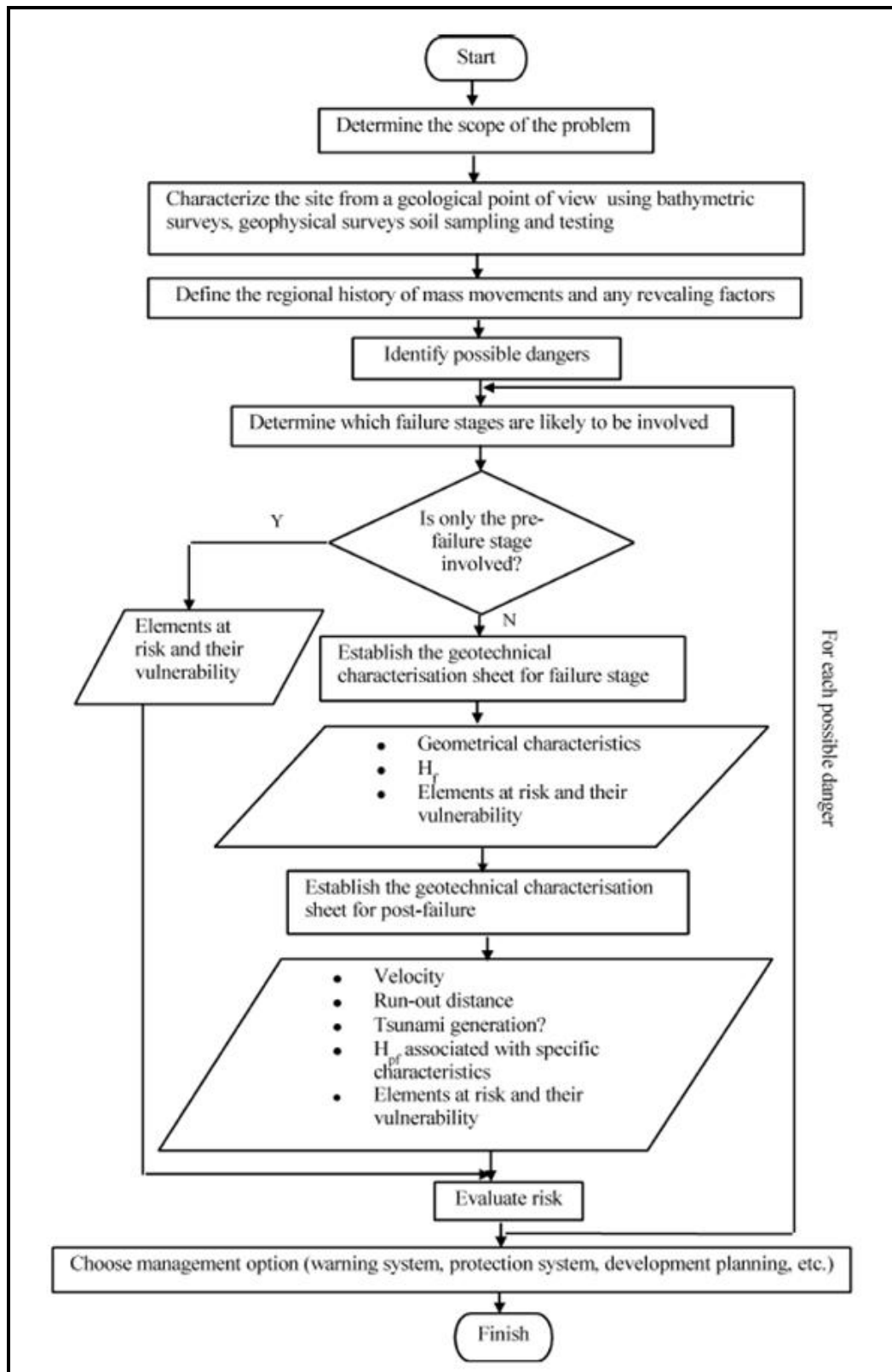



Figure 160: Risk management procedure for submarine landslides (from Leroueil et al., 2003)

boundary layer conditions within a given area on the seafloor is assumed to influence the probability and severity of a potential event.

Scaling matrices are proposed to capture the influence of triggering factors relative to MRDF submarine mudslides (Tables 21-26). The descriptors selected for each category (i.e., “Catastrophic”, “Extreme”, etc.) were chosen to most accurately reflect the danger relative to hurricane conditions and thus help define the hazard (i.e., the probability) of a future event.

Table 21: Significant wave height matrix, MRDF study area

<u>Category</u>	<u>H<sub>smax</sub> (m)</u>	<u>Score</u>	<u>Relative scale</u>
Catastrophic	20+	5	High impact
Extreme	15-20	4	
Severe	10-15	3	
Strong	5-10	2	
Elevated	< 5	1	Low impact


Observed bulk wave conditions, together with MIKE 21 numerical wave model results described in Chapter 5, yielded peak significant wave height ( $H_{smax}$ ) values between 15-17 m for Hurricanes Ivan and Katrina (Figures 33, 38, 40 and 43, Section 5.2.1). These values score as “Extreme” on the matrix in Table 21.

The  $H_{smax}$  matrix for prior hurricanes (Camille, Andrew and Betsy) score between “Severe” and “Catastrophic” (Figures 45-46, 49-50, Section 5.2.2; also Figure O-2, Appendix O). Hurricane Camille was one of only three Category 5 hurricanes to strike the United States, with peak winds of approximately  $85 \text{ m sec}^{-1}$  (Simpson et al., 1970).  $H_{smax}$  values derived from Hsu’s (2006) wave height estimation method, based on a conversion from barometric pressure, yielded results of approximately 20.8-21.6 m, thereby placing Camille well into the “Catastrophic” category. In addition,  $H_{smax}$  values recorded by the Baylor Company program yielded results of at least 21.6 m (the maximum that could be measured by the equipment; Hamilton and Ward, 1974; Ward, 1974). Peak  $H_{smax}$  as simulated in the MIKE 21 wave model yielded results of at least 15 m (Figures 45 and 46, Section 5.2.2). Peak  $H_{smax}$  values for Hurricanes Andrew and

Betsy within the MRDF study area were approximately 15 and 12 m, respectively. The lower values for Hurricane Andrew reflect the fact that the storm passed significantly farther west than the other hurricanes evaluated (Figure 1, Chapter 2).

Observed wave periods (T-02), together with MIKE 21 numerical wave model results described in Chapter 5, yielded peak wave period values between 12-16 sec for Hurricanes Katrina and Ivan, respectively (Figures 33, 39, 40 and 44, Section 5.2.1). These values score as “Severe” to “Extreme” on the matrix in Table 22. Wave periods in Katrina were lower relative to those during Ivan; as discussed in Section 5.2.1, an explanatory hypothesis is that Katrina’s initial motion pushed waves from the south and southeast as it crossed southern Florida, but once it moved into the GOM its counter-clockwise wind field impacted the bulk wave parameters as evidenced by a distinct “step” in the data at 1800 Z on August 25, 2005 and a change in mean wave direction from 155° to 105° (Figure 33).

Table 22: Wave period (T-02) matrix, MRDF study area

<u>Category</u>	<u>Period T-02 (sec)</u>	<u>Score</u>	<u>Relative scale</u>
Catastrophic	20+	5	High impact
Extreme	15-20	4	
Severe	10-15	3	
Strong	5-10	2	
Elevated	< 5	1	Low impact

Simulated peak wave periods for earlier storms ranged from 12 sec during Hurricanes Camille and Betsy to 8 sec during Hurricane Andrew (Figures 47-48, 51-52; also Figure O-1, Appendix O). These values correspond to categories ranging from “Strong” (Andrew) to “Severe” (Camille and Betsy, although Betsy just crosses over the threshold between the two). Even though Camille was a more intense system, its relatively small size leads to the hypothesis that the generation of larger wave periods was precluded as opposed to Betsy, which was a relatively large storm with a resulting larger wave field fetch area given its angle of approach towards the MRDF (Figure 1, Chapter 2). Additionally, the scale in Table 22 is appropriate for




use not only during peak MRDF hurricane conditions but also far in advance of a tropical system, as long-period waves begin advancing into the GOM days prior to a system's arrival in the MRDF. The MIKE 21 wave model demonstrated that spectral energy in advance of Hurricane Katrina, manifested as high-frequency waves, first arrived at NDBC buoys adjacent to the MRDF four days prior to peak sea-state conditions and the hurricane's eventual landfall in Louisiana (discussed in Section 5.3).

A final triggering factor is the amount of time that a given area of the MRDF is exposed to severe metocean conditions (Figure 30, Section 5.1.1). Hurricane forward speed is quite variable in the GOM, resulting in elevated bulk wave conditions that range from less than three hours for Hurricanes Elena (1985) and Eloise (1975) to approximately ten hours for the 1906 and Last Island (1856) Hurricanes (NHC, 2009; Figure 30, Section 5.1.1). A hypothesis is proposed that extended exposure to severe conditions, and the corresponding repeated changes in differential pressure along the seafloor, can be used as a proxy to estimate the degree of potential danger (Table 23). If a storm moves quickly through the area (e.g., Hurricane Betsy) the amount of exposure time is reduced; slower storms (e.g., Hurricanes Camille and Ivan) can potentially cause more damage. This hypothesis appears to be borne out in operator-reported seafloor movements in the South Pass and Mississippi Canyon Protraction Areas, respectively, during Camille and Ivan (Sections 3.3.2 and 6.2). Based on the scale in Table 23, both hurricanes would be scored as "Slow" whereas a faster-moving storm such as Betsy would be scored as "Fast". Katrina would be scored as an upper-level "Moderate". The Last Island Hurricane comes closest to the "Lingering" category, spending approximately ten hours in MRDF waters (NHC, 2009; assumes historical hurricane data are reliable).

#### **9.2.1.2 Revealing Factors**


Primary revealing factors include evidence of prior shelf failure events such as antecedent mudflows as seen in seafloor bathymetric data (described in Chapters 6 and 7) or through element vulnerability (e.g., damaged or destroyed infrastructure) from an earlier event (described in

Table 23: Temporal exposure matrix, MRDF study area

<u>Category</u>	<u>Exposure (hours)</u>	<u>Score</u>	<u>Relative scale</u>
Lingering	10.0+	5	High impact
Slow	7.5-10.0	4	
Moderate	5.0-7.5	3	
Fast	2.5-5.0	2	
Rapid	< 2.5	1	Low impact

Chapter 8). Prior mudflow evidence can occur either on a regional scale, such as the descriptors used in prior MRDF seafloor morphology work (Figure 21, Section 4.1; Coleman et al., 1980b), or on a local scale such as case studies within the four Validation Test Areas (VTAs) described in Sections 7.2.1 through 7.2.4. Morphologic seafloor type can be scaled to reflect the potential for future events, as they help “reveal” the existence of prior events (Table 24; William Lettis & Associates, Inc., 2005).

Table 24: Morphology type matrix, MRDF study area

<u>Morphology type</u>	<u>Score</u>	<u>Relative scale</u>
Mudflow gully	4	High
Mudflow lobe	3	
Slightly disturbed seafloor	2	
Undisturbed seafloor	1	Low

Mudflow gullies, which act as conduits for failed sediment as it is transported down dip, are scaled as least stable given their relatively steeper head scarps and sides. Sediments within mudflow gullies are typically composed of blocks of undisturbed seafloor transported within a matrix of remolded, slurry-like clay (Prior and Suhayda, 1979; Hooper, 1996). Even though undisturbed sediments are scaled as least likely to fail, their existence within a mudflow gully overrides any local morphological consideration given their overall, regional setting. Prior mudflow lobes (or noses) are scaled as next unstable given the possibility of sediment movement re-initiation under certain circumstances. The scale continues downward to the most stable morphology, which is undisturbed seafloor. The net result from evaluating morphologic type is a

“danger map” that highlights the potential danger of future failures based on morphology and their inherent stability scored in Table 24 (Figure 161).

#### **9.2.1.3 Predisposition Factors**

Primary predisposition factors include criteria that potentially influence seafloor slope response and the degree to which seafloor movement can be “predisposed” to occur. These factors include existing lithological and geotechnical parameters of the ocean floor and immediate subsurface, such as seafloor grain size characteristics and soil type, slope steepness of an existing seafloor, the shear strength profile of the immediate subsurface at a given point, and the amount of time that has elapsed since any prior seafloor movement.

Slope steepness is considered a primary predisposition factor because of the potential for increased seafloor instability linked to steeper slopes (Lewis, 1971; Prior and Coleman, 1978a; 1978b; McGregor, 1981). The rapid sedimentation rate associated with Mississippi River deposits has resulted in oversteepening; the seafloor failure process along the MRDF serves to make these slopes less steep (McAdoo et al., 2000; discussed in Section 3.1.1).

Slope steepness was computed from seafloor bathymetry datasets in each of the four VTAs using Fledermaus imaging software (Figure 22, Section 4.1; Figures 162-169). These test areas are located in varying morphological settings ranging from stable shelf platforms to the relatively steeper shelf edge. The steepest seafloor slopes were found along the walls of mudflow gullies and along the periphery of crustal blocks that slid downslope intact (slopes typically of 3-5° but occasionally up to 8°; best exemplified by Figure 109, Section 7.2.1 and Figures 166-167). Steep slopes were also found along internal pressure ridges on top of mudflow lobes (slopes typically of 4-6°) as well as at their terminal ends (slopes up to 14°; all best exemplified by Figure 129, Section 7.2.3).

A scaling system to account for predisposition danger associated with seafloor slopes and the inherent instability they lead to is included in Table 25. The scale has been adjusted to account for “clusters” of slope ranges that are dependent on various morphological types. This

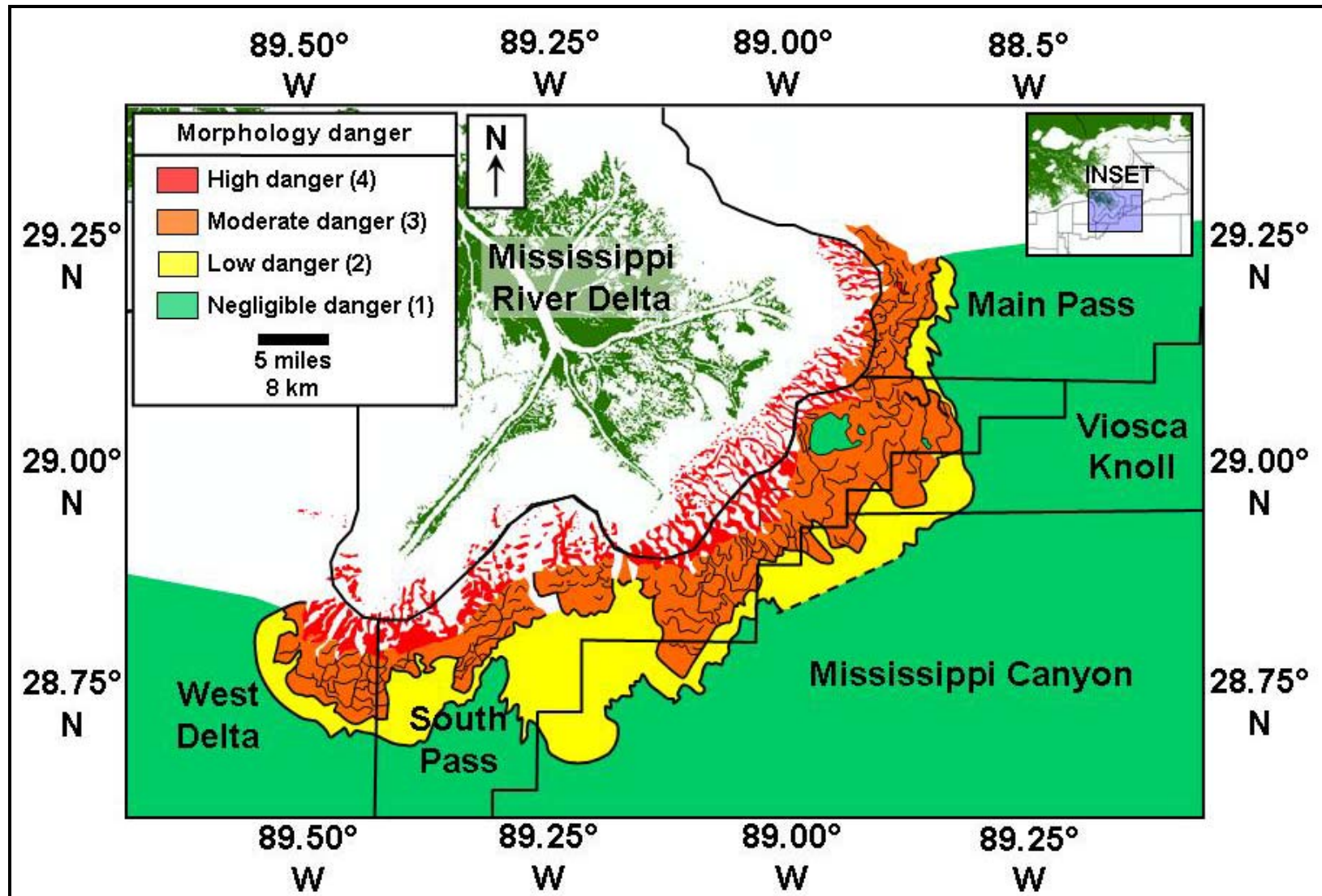


Figure 161: Morphology scaling map, MRDF (adapted and modified from morphology identified by Coleman et al., 1980b)

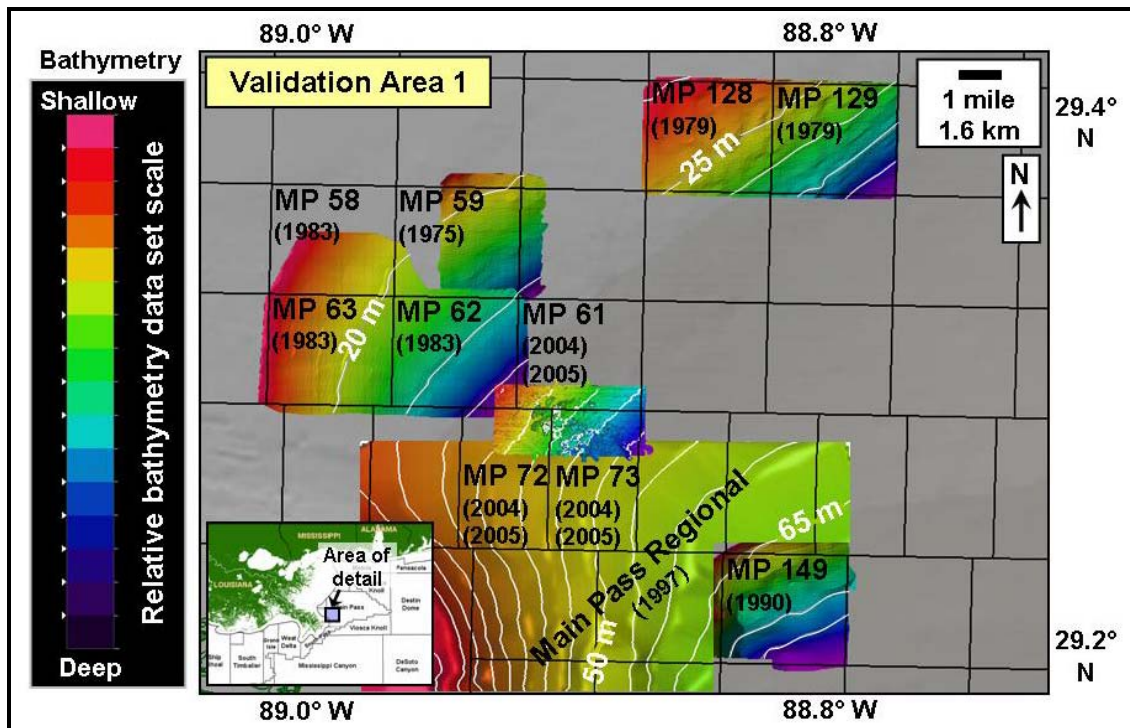


Figure 162: High-resolution bathymetry superimposed on regional NOAA bathymetry grid, Validation Area 1 (contour interval = 5 m)

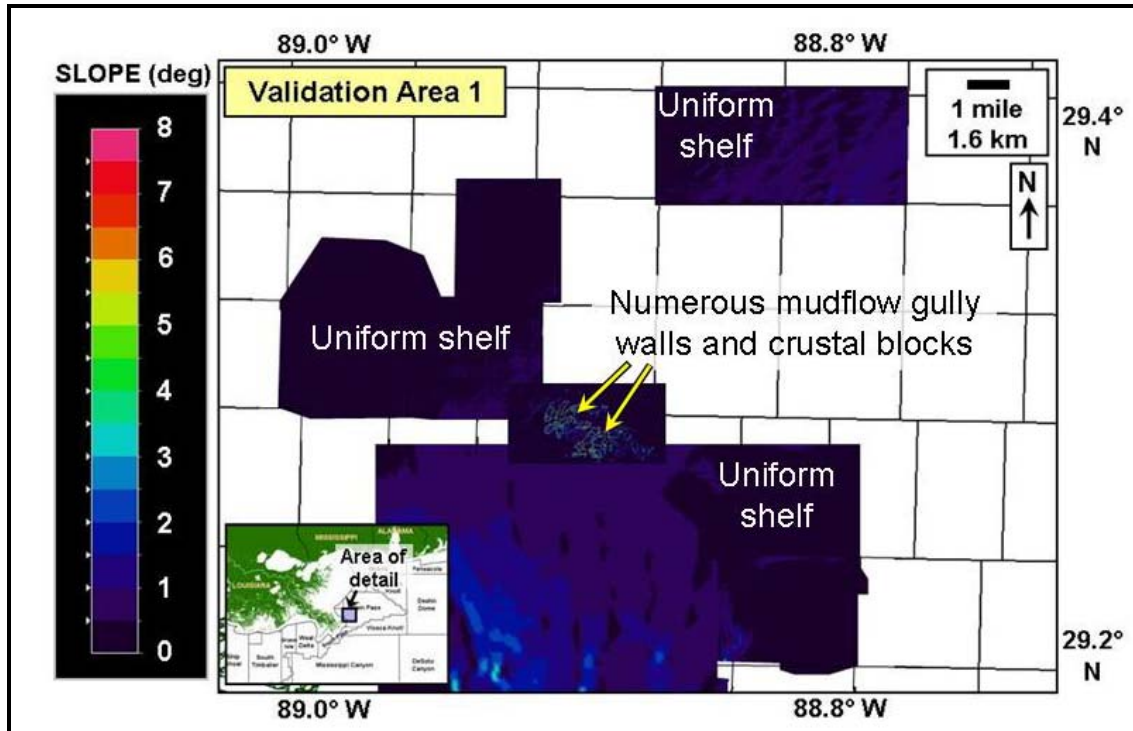


Figure 163: Slope steepness computed from high-resolution bathymetry, Validation Area 1



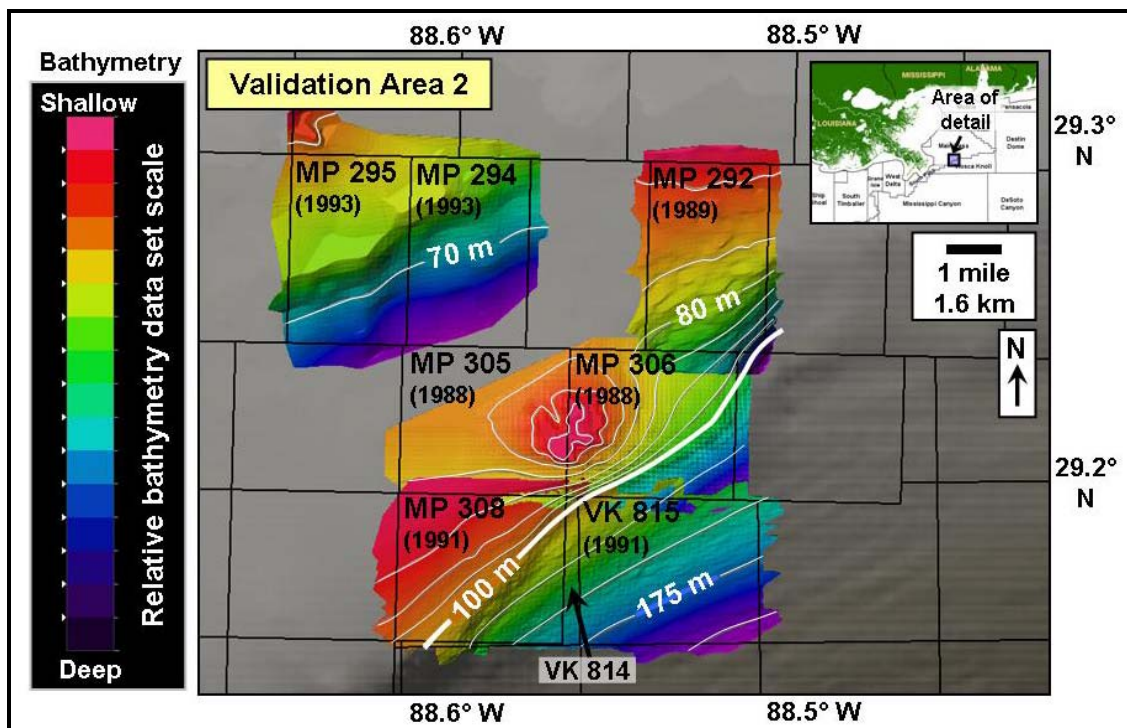


Figure 164: High-resolution bathymetry superimposed on regional NOAA bathymetry grid, Validation Area 2 (contour interval = 5 m when < 100 m depth; 25 m when > 100 m depth)

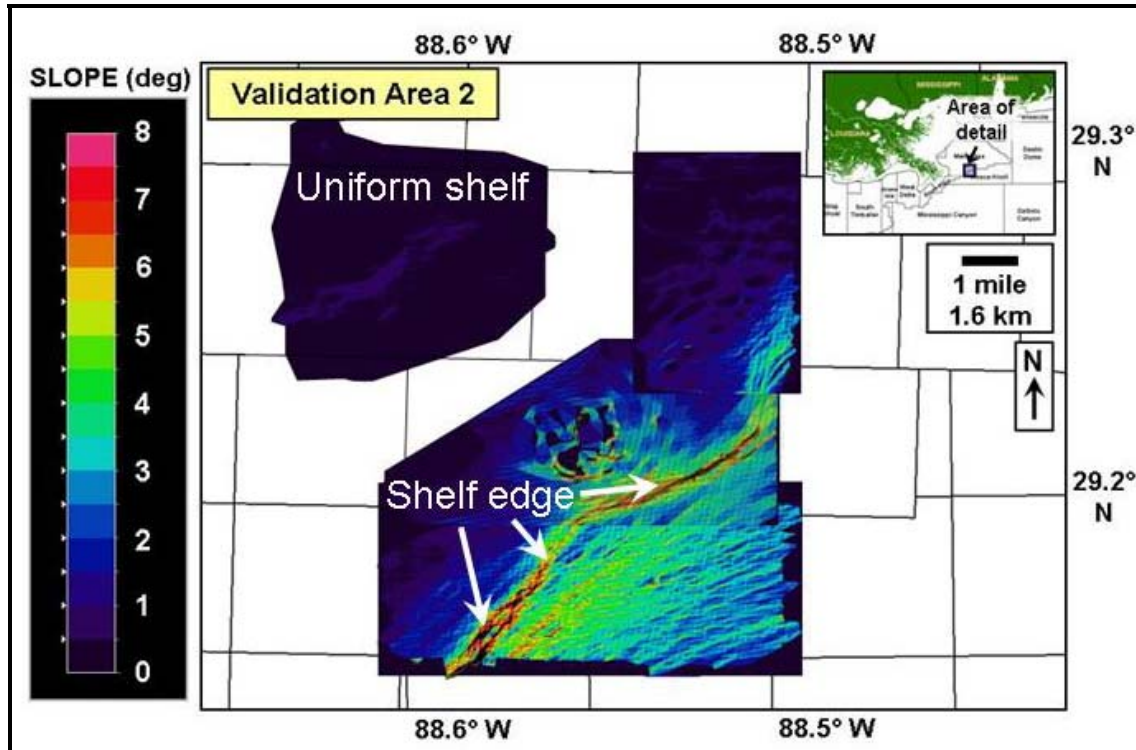


Figure 165: Slope steepness computed from high-resolution bathymetry, Validation Area 2

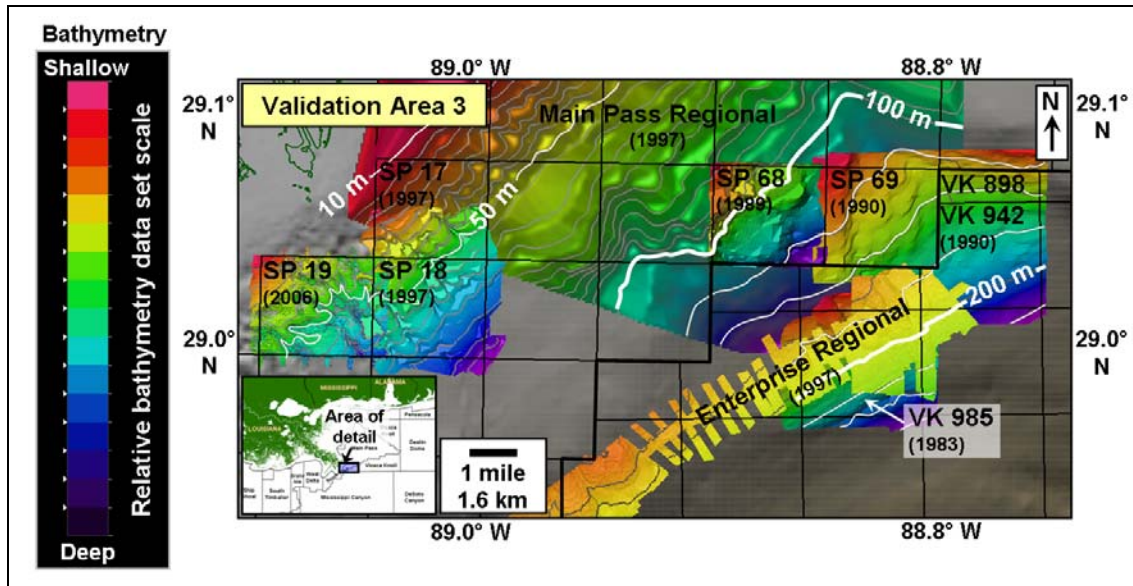


Figure 166: High-resolution bathymetry superimposed on regional NOAA bathymetry grid, Validation Area 3 (contour interval = 5 m when < 100 m depth; 25 m when > 100 m depth)

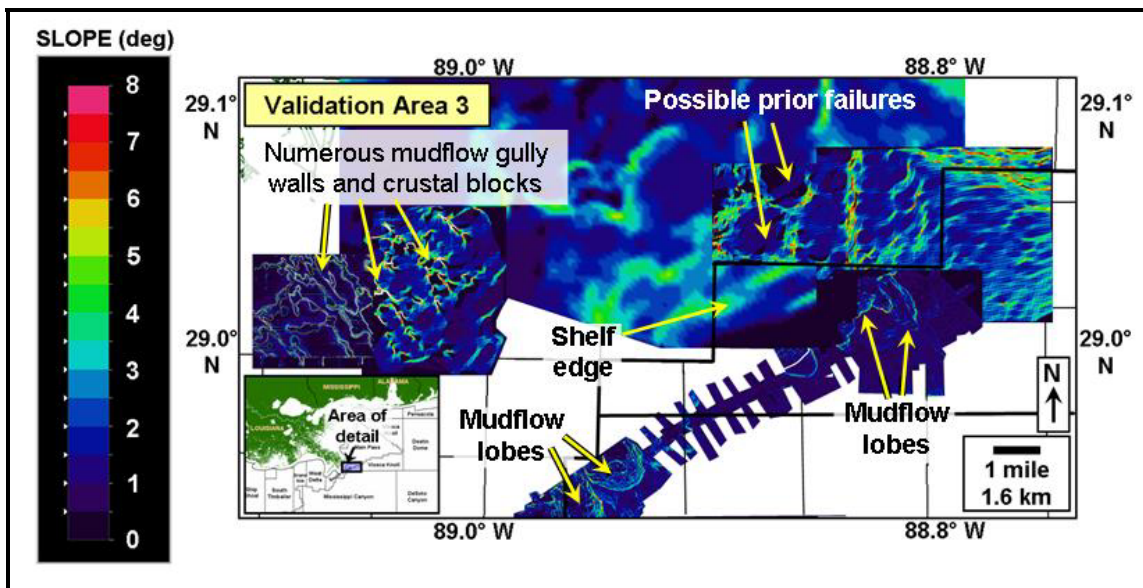


Figure 167: Slope steepness computed from high-resolution bathymetry, Validation Area 3



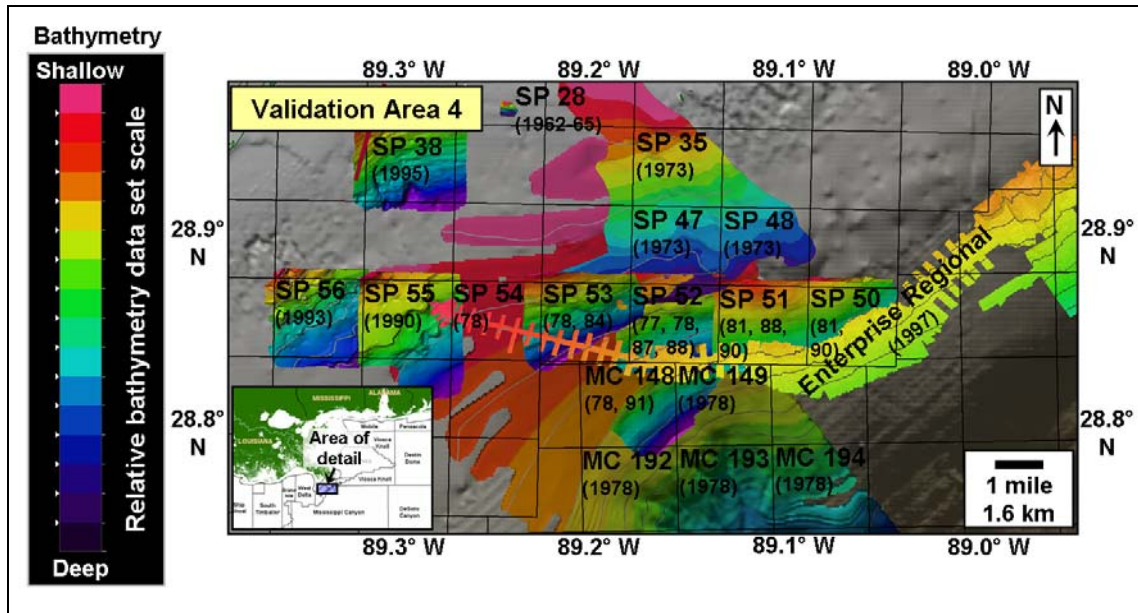


Figure 168: High-resolution bathymetry superimposed on regional NOAA bathymetry grid, Validation Area 4 (contour interval = 5 m when < 100 m depth; 25 m when > 100 m depth)

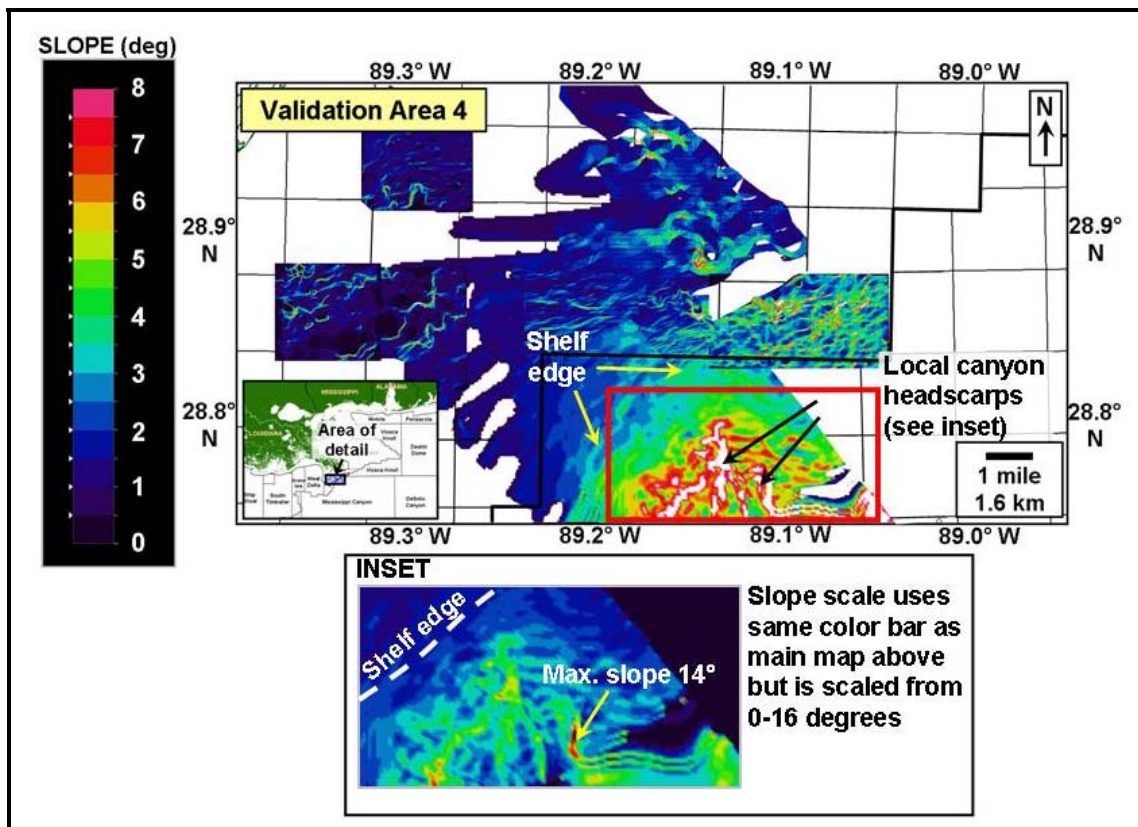



Figure 169: Slope steepness computed from high-resolution bathymetry, Validation Area 4 (maximum canyon headscarp slopes calculated at 14°; off-scale on main map)

scaling differentiates between gradients typically found in a shelf environment (low-angled slopes of 1-2°; Figures 162-163 in VTA 1; updip shelf portions of Figures 164-165 in VTA 2) vs. those associated with either the shelf edge and/or prior shelf failure events that resulted in locally steeper slopes (southeastern portions of Figures 162-163 and 166-167 as they transition from continental shelf to continental slope environments).

Table 25: MRDF vulnerability matrix – slope steepness

<u>Category</u>	<u>Slope (degrees)</u>	<u>Score</u>	<u>Relative scale</u>
Hazardous slope	> 8.0	7	High impact
Extreme slope	6.0 – 8.0	6	
Steep slope	4.0 – 6.0	5	
Moderate slope	3.0 – 4.0	4	
Gentle slope	2.0 – 3.0	3	
Low slope	1.0 – 2.0	2	
Negligible	< 1.0	1	Low impact

Slope gradients mapped in Figures 163, 165, 167 and 169 can be transformed accordingly based on the scale in Table 25 and then incorporated into the total MRDF risk characterization described in Section 9.2.5. Areas with higher slope scores will be considered as being potentially more hazardous.

An additional predisposition factor is the rate of seafloor change through time. The occurrence of prior mudflows over a given area results in altered seafloor slopes and shear strength conditions that lead an area to be predisposed to future events. Temporal differences in sediment deposition and scour on a regional scale were calculated using the 1874, 1940 and 1977 bathymetric surveys (Figures 105 and 107, Section 7.1). Local changes in seafloor profiles were obtained from available geohazard and bathymetric surveys, some of which overlapped areally through time and over multiple hurricane approaches (Appendix K).

The most recent rate of regional seafloor change, either positive or negative, can be scored based on differences in bathymetry measured between 1940 and 1977 (Table 26). The regional NOAA bathymetry data were not used in computing seafloor change rates because of its

varying spatial resolution relative to the most recent (i.e., 1977) regional MRDF bathymetry data. The areas of maximum seafloor change (positive) were located immediately downdip of the shelf edge along the South Pass/Mississippi Canyon Protraction Area boundary, in the westernmost Viosca Knoll Protraction Area, and in the east-central West Delta Protraction Area adjacent to Southwest Pass of the Mississippi River (Figure 107, Section 7.1). These areas rank as extreme on the scale in Table 26. The MRDF as a whole exhibited a low to moderate increase from 1940-1977, reflecting overall advancement of the MRDF. The area of maximum seafloor change (negative) was located downslope of an interdistributary area known as East Bay located between Southwest and South Passes of the Mississippi River (Figure 107; Section 7.1). This area ranks as low to moderate on the scale in Table 26.

Table 26: MRDF vulnerability matrix – rate of seafloor change  
(based on a model from William Lettis & Associates, Inc., 2005)

<u>Relative change</u>	<u>Rate of seafloor change (m)</u>	<u>Score</u>	<u>Relative scale</u>
Increase – extreme	> 25	4	High impact
Increase – high	15 – 25	3	↕
Increase – moderate	5 – 15	2	
Increase – low	0 – 5	1	
Decrease – low	0 – -5	1	↕
Decrease – moderate	-5 – -15	2	
Decrease – high	-15 – -25	3	
Decrease – extreme	> -25	4	High impact

Long-term patterns of sediment transport and deposition can be elucidated from these results. Areas of maximum temporal change are used to infer relative sediment stability and the potential for areas at risk of future seafloor failure. Areas with higher rates of increase support the hypothesis of oversteepening potential, leading to future failures and a higher hazard for areas located immediately downdip. Areas with higher rates of decrease support the hypothesis of long-term seafloor instability and higher susceptibility to future sediment failure.

Final predisposition factors involve the soil characteristics of areas susceptible to failure. Seafloor sediment grain size (i.e., soft cohesive soils vs. harder and coarser soils) and shear strengths (both at the seafloor as well as the immediate subsurface) can influence seafloor failure occurrence – softer seafloors potentially dampen wave heights and alter wave periods, thereby changing the metocean dynamics that drive changes in differential pressure along the seafloor and contribute to sediment failure (Suhayda, 1977; Dalrymple and Liu, 1978; Rosenthal, 1978; Forristall et al., 1985, Hsiao and Shemdin, 1980; Kraft et al., 1990; Sheremet et al., 2005).

Sediment grain size, identified from GOM borehole arrays, varies across the study area in patterns of relatively finer- and coarser-grained material (Figures 70-71, Section 6.1.2). Seafloor shear strengths also vary across the study area, with relatively stronger material located toward the northeast offshore Mississippi, Alabama and Florida coincident with coarser seafloor sediment (Figure 92, Section 6.2.1). Weaker material exists farther west in the Main Pass and upper Viosca Knoll Protraction Areas separated by isolated pockets of slightly higher shear strengths approximately 20 km and 40 km northeast and east, respectively, of the MRD.

In addition, shear stresses modeled in the MIKE 21 model for each hurricane indicate higher stresses coincident with shallower areas, particularly at Ship Shoal and at a shoal in Main Pass, with the 25-meter isobath (examples for Hurricanes Katrina and Ivan in Figures 93-94, respectively; Section 6.2.1). In the event that shear stresses equal or exceed sediment strength, seafloor failure conditions can be assumed (Hooper, 1996). To quantify predisposition factors associated with existing soil conditions, areas of lower shear strengths were superimposed on top of maximum shear stresses encountered during Katrina and Ivan (Figures 170-171, respectively). Shoals stand out as areas of higher shear strengths and coarser-grained material; areas away from shoals correspond to lower shear strengths (i.e., where shear stresses from hurricanes equal or exceed sediment strength) and relatively finer-grained material (Figures 172-173; highlighted by red circles).

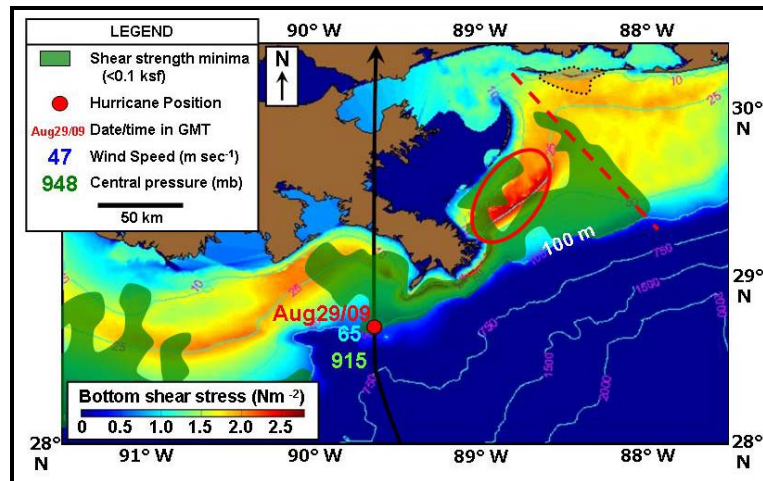


Figure 170: Shear strength vs. bottom shear stresses, Hurricane Katrina 29 August 2005, 0900 Z

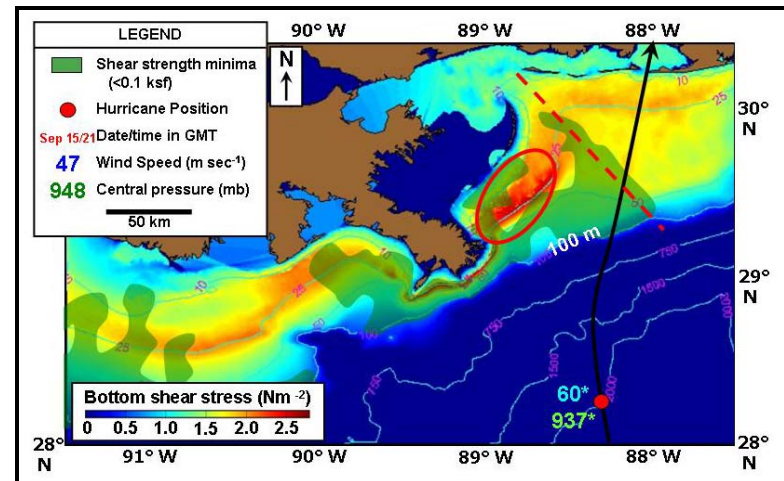


Figure 171: Shear strength vs. bottom shear stresses, Hurricane Ivan 15 September 2004, 2100 Z

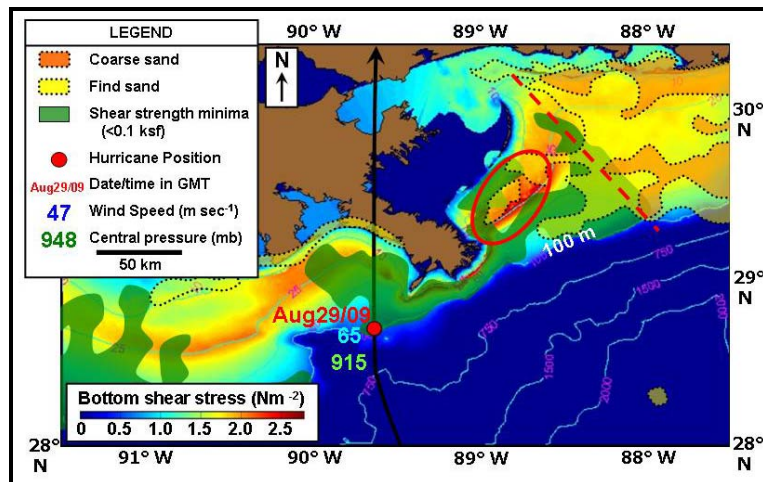


Figure 172: Shear strength, bottom shear stresses and sediment grain size, Hurricane Katrina, 29 August 2005, 0900 Z

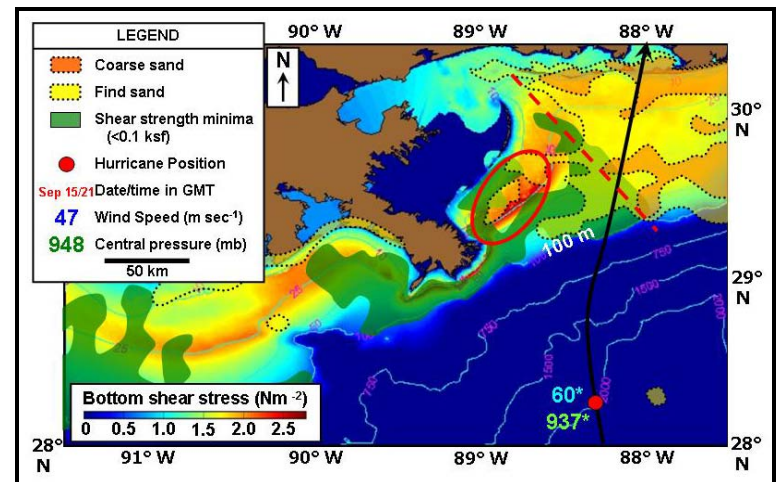



Figure 173: Shear strength, bottom shear stresses and sediment grain size, Hurricane Ivan, 15 September 2004, 2100 Z

Submarine mudflow occurrence during Hurricanes Ivan and Katrina, as manifested through platform and pipeline damage, was confined to areas of lower shear strengths and softer seafloors (Figure 3, Section 2.1). Most damage east of the MRD occurred along the shelf edge in areas of relatively finer-grained, cohesive soils and away from higher-relief areas containing coarser material. A submarine mudslide susceptibility matrix can then be defined based on a quantitative combination of seafloor grain size and sediment shear strength (Table 27).

Table 27: Submarine mudslide susceptibility, seafloor sediment characteristics

<u>Relative sediment grain size</u>	<u>Shear strength (kips feet<sup>2</sup>)</u>	<u>Score</u>	<u>Relative scale</u>
Clay	< 0.1	5	High impact
Silt	0.1-0.5	4	
Very fine sand	0.5-1.0	3	
Fine sand	1.0-3.5	2	
Coarse sand	< 3.5	1	Low impact

### 9.2.2 Magnitude Characterization

Magnitude is defined as the energy released during a failure event and can be quantified by the area, volume, travel distance and velocity of a given failure (Hansen, 1984; Varnes, 1984; Hartlen and Viberg, 1988; Einstein, 1988; Edris, 1988). Typical magnitude parameters that quantify submarine sediment failure were discussed in significant detail in Section 6.3.2. These parameters represent outputs generated by the 1D sediment failure modeling performed using the BING software program (Imran et al., 2001a; 2001b).

Magnitude can best be quantified through the modeling of mudslide movement along several MRDF cross sections covered in Section 6.2 to match observed mudslide evidence inferred from prior hurricanes. Shelf failure was modeled along Cross Section B-B' (Figures 75-76, Section 6.2) to match evidence assumed from a failure at Main Pass Block 70 (MP 70) during Hurricane Camille (Table 9, Section 6.3.2). Model sensitivities, which were performed using a bilinear rheology option of varying failure lengths and thicknesses, indicated maximum runout lengths of approximately 37 km and maximum velocities that ranged from 4.4 to 10.7 m sec<sup>-1</sup>



depending on varying mudslide length and mudslide thickness. However, based on the fact that in no case did modeling match the observed mudslide thickness, the hypothesis that multiple mudslides account for local bathymetry change at MP 70 seems valid.

Shelf failure was also modeled along Cross Section C-C' (Figures 77-78, Section 6.2) to match evidence from a failure at South Pass Block 70 (SP 70), also during Hurricane Camille (Table 10, Section 6.3.2). Model sensitivities indicated a relatively quick failure given the smaller scale of the mudslide; runout lengths were calculated at 490 m and a maximum velocity of  $0.39 \text{ m sec}^{-1}$  over a time span of less than one hour (Table 10, Section 6.3.2). Failure was also modeled along Cross Section D-D' (Figures 79-80, Section 6.2) as a significant failure occurred at Mississippi Canyon Block 20 (MC 20) during Hurricane Ivan (MMS, 2005a). Model sensitivities, based on varying mudslide lengths and mudslide thicknesses, yielded a most-likely runout length of approximately 7.8 km and a maximum velocity of approximately  $1.3 \text{ m sec}^{-1}$  (Table 11, Section 6.3.2). Other cases support faster maximum velocities but final results did not match observed conditions so this case was assumed the best fit. However, even the most likely case fails to yield a mudflow terminus that perfectly matches observed conditions from the post-Ivan bathymetry data (Enterprise Products Partners, LLC (EPP), 2005), which supports a hypothesis that the failure that generated the mudflow at MC 20 and the surrounding area likely consisted of updip seafloor instability of considerable length.

A final shelf failure was modeled along Cross Section F-F' (Figures 83-84, Section 6.2) to match evidence from failures at South Pass Blocks 38 and 55 during Hurricanes Katrina and Ivan, respectively (MMS, 2005a; 2005b). Model sensitivities yielded relatively long runout distances relative to the size of the initial mudslide primarily because of local changes in seafloor gradients and relatively steeper slopes downdip of and proximal from the two failures (Table 12, Section 6.3.2). Runout distances were calculated at approximately 4 km and maximum velocities were approximately  $3 \text{ m sec}^{-1}$ .



Sediment failure area and volume vary considerably across the MRDF based on morphology type (i.e., mudflow lobe vs. internal crustal block within a mudflow gully, etc.). Mudflow lobes were best exemplified by the Enterprise high-resolution bathymetry dataset (EPP, 2005). Mudflow lobes on these datasets were considered typical in size given a visual comparison with other, albeit lower resolution, bathymetry data (mostly the regional 1874, 1940 and 1977 datasets where mudflow lobe presence was inferred from locally flat slopes that did not conform to local slope gradient and typically bulged slightly downslope in map view). The average areal extent of these lobes ranged from approximately 1.46 km<sup>2</sup> to 10.2 km<sup>2</sup> and, when assuming a range of thicknesses from 5 to 20 m, the average volume calculations range from approximately 7.28 x 10<sup>3</sup> m<sup>3</sup> to 4.66 x 10<sup>4</sup> m<sup>3</sup>.

### **9.2.3 Hazard Characterization**

Hazard characterization quantifies the occurrence probability of an event as defined by the probability of dangers within a given time interval within a given area and for a given magnitude. Alternately, since calculating precise mudslide event probability is difficult, a hazard can be defined as the process of recognizing and accounting for all possible dangers that might occur within the place and time period of interest (Crozier and Glade, 2005). For purposes of this dissertation, hazard will be considered equal to the product of dangers outlined in Section 9.2.1.1 above a pre-defined threshold associated with a corresponding magnitude (first proposed by Vaunat and Leroueil (2002) but now modified for use across the MRDF). Initial attempts at determining probabilistic estimates of *subaerial* landslides were difficult due to the uncertain timing of primary triggers (e.g., earthquakes; Masson et al., 2006); however, the subaqueous MRDF environment comprises triggers that can be quantified with more certainty given evidence of past sediment failures and the ability to predict hurricane paths and sea-state conditions in advance.

Hurricane Recurrence Interval (RI) serves as the base triggering factor. Based on meteorological records dating to 1851 (Table 1, Section 2.2; Table 5, Section 5.1.1), MRDF

tropical storm and hurricane RI was quantified based on distance from South Pass of the Mississippi River (a proxy to measure distance from the MRDF; Table 4 and Figure 28, Section 5.1.1). These results indicated RI of 5.4, 6.0 and 13.6 years for Category 3 hurricanes striking 300, 200 and 100 km, respectively, of the MRDF. From these numbers, the probability of a Category 3 hurricane striking within 100 km of the MRDF (and thus potentially impacting the seafloor) in any given year equals approximately 7%. This number excludes any effects from decadal cyclic occurrence patterns observed in the Atlantic Basin, and even within cyclical periods of activity the number of severe hurricanes (i.e., Category 3+) appears unrelated to hurricane occurrence (Figure 28, Section 5.1.1). Increasing the distance from the MRDF to 300 km yields a higher probability of approximately 18%.

Successive triggering factors include oceanographic response to severe hurricanes as manifested in  $H_{s_{max}}$  and wave period, and the amount of time that a given area experiences extreme metocean conditions.  $H_{s_{max}}$  categories introduced in Table 21 can be applied to past hurricanes using Hsu's (2006) method for estimating wave height from central pressure. Based on shelf failure observations during Hurricanes Katrina, Ivan and Camille, seemingly limited failures during Hurricanes Andrew and Betsy, and what is known regarding significant wave heights and the time exposure for all these storms, a hypothesis is drawn that  $H_{s_{max}}$  required to initiate shelf failure meets a threshold of 15 m with a time exposure of seven hours.

Evaluating the historical hurricane record from 1851 reveals that only three hurricanes met this threshold across the MRDF in that same time interval (Katrina, Ivan and Camille (depicted by the upper-right box in Figure 30, Section 5.1.1). Hurricane Opal, while containing sufficient intensity to generate extreme  $H_{s_{max}}$ , passed farther to the east and therefore its effects were not as great. The MRDF was exposed to extreme oceanographic conditions for over seven hours but it too passed farther away from the MRDF (in this case, to the west) and its effects were also minimal at the MRDF. No submarine failures were reported to the MMS during either hurricane. Several hurricanes in the historical record (the New Orleans Hurricane of 1915 and the

Last Island Hurricane of 1856) approach the criteria required for generating extensive submarine mudslides. Although no offshore infrastructure was in place in 1915, bathymetry comparisons between the 1874 and 1940 regional surveys suggest considerable seafloor bathymetry change during the intervening years (Figures 105-106; Section 7.1). Since no other severe hurricanes traversed near the MRDF during that time, the hypothesis exists that most of these changes were due to the 1915 hurricane.

These triggering factors can be combined with various revealing factors (mudflow morphology) and predisposition factors (e.g., slope steepness, surficial sediment parameters and the rate of seafloor change through time) to characterize the overall submarine mudslide hazard facing the MRDF (Tables 21-27, Section 9.2.1). Individual hazard maps of these parameters for each VTA were constructed in a traffic-light approach such that the highest dangers are shown in red and the least dangers are shown in green (Figures 174-189).

The product of these categories was then integrated with metocean parameters (significant wave height, wave period and temporal exposure to hurricane conditions) to compute a total hazard score for the five hurricanes modeled in MIKE 21 assuming constant morphologic, slope and sediment characteristics (i.e., a mudflow lobe, a slope between 2°-3° and surficial clay were assumed; Table 28). The product of all these parameters indicated that Hurricanes Ivan and Camille each scored over 5000. In addition, scores were also calculated for hurricanes in the historical record where barometric pressure readings were available (Table 28), thus leading to estimates of  $H_{s_{max}}$  (from Hsu, 2006); wave periods were assumed to be equal in severity relative to  $H_{s_{max}}$ . Although the precision of these historical records is unknown, they still contain value for comparing hurricane conditions on a relative scale. Given that the Last Island Hurricane also scored above 5000 and that failures occurred during Ivan and Camille, it seems reasonable that the Last Island Hurricane also spawned similar shelf failure in 1856.

Hurricane Katrina scored above 4000, as did Hurricanes Opal, Carmen and the New Orleans Hurricane of 1915. However, shelf failure was minimal during Opal and Carmen, mainly

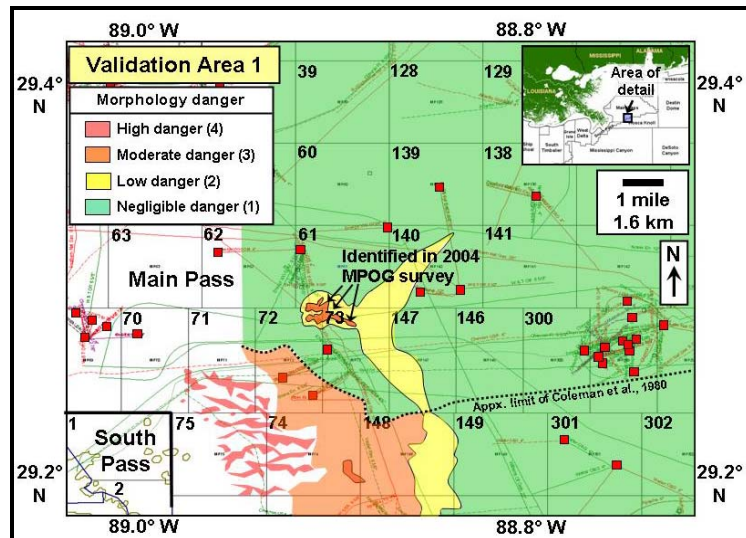


Figure 174: Morphology type hazard map, Validation Test Area 1

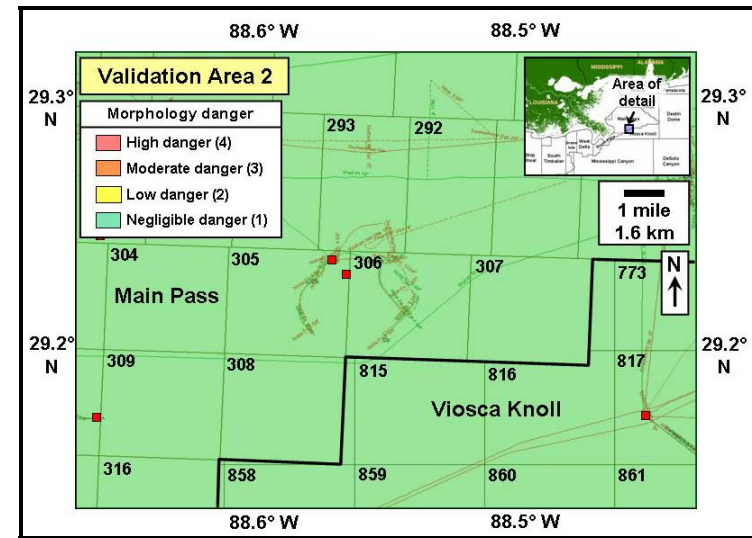


Figure 175: Morphology type hazard map, Validation Test Area 2

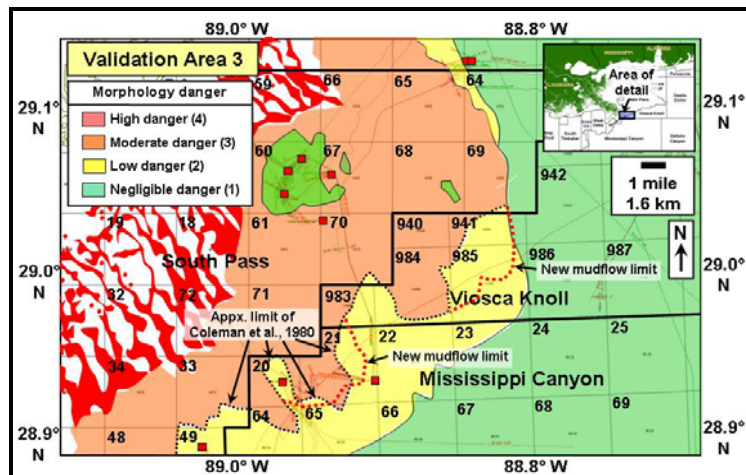


Figure 176: Morphology type hazard map, Validation Test Area 3

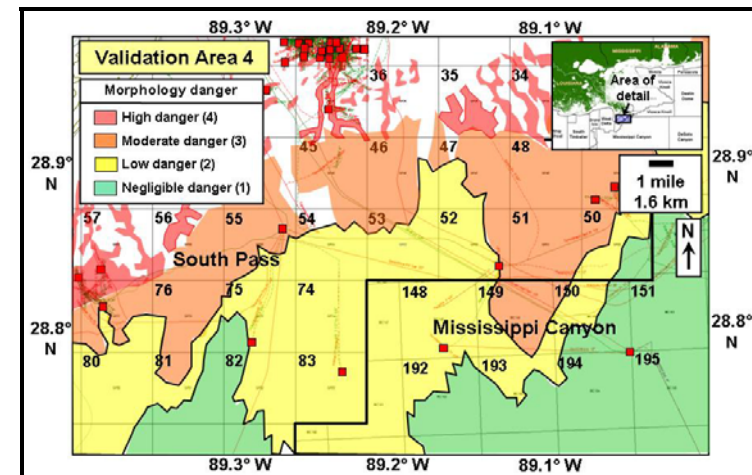


Figure 177: Morphology type hazard map, Validation Test Area 4

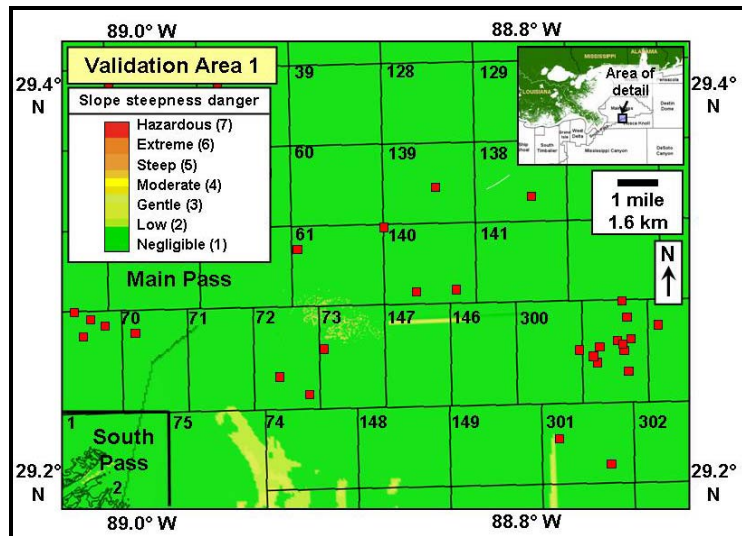


Figure 178: Slope steepness hazard map, Validation Test Area 1

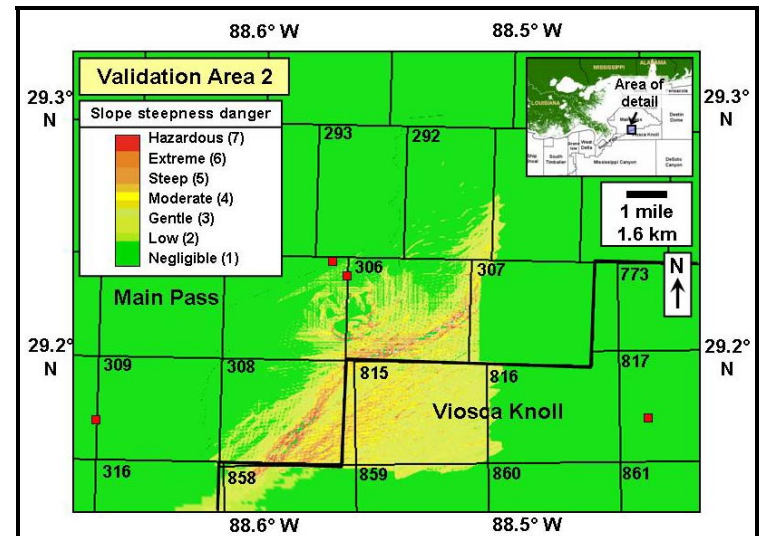


Figure 179: Slope steepness hazard map, Validation Test Area 2

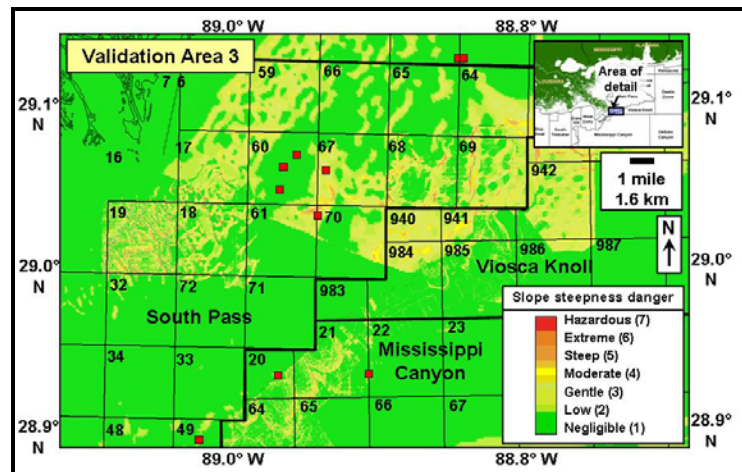


Figure 180: Slope steepness hazard map, Validation Test Area 3

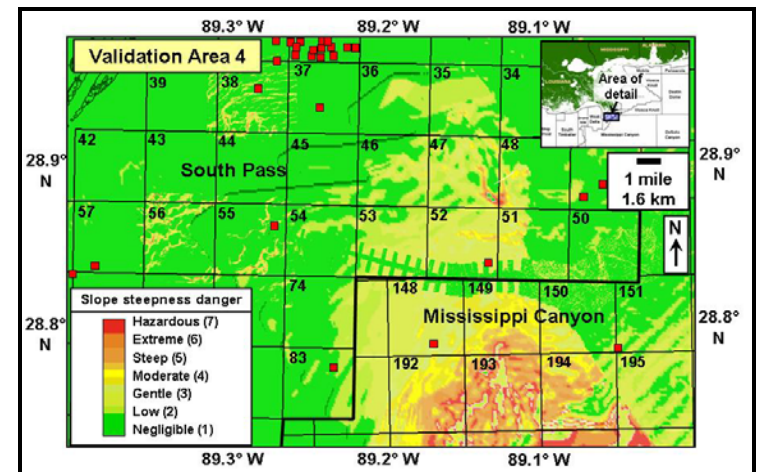


Figure 181: Slope steepness hazard map, Validation Test Area 4



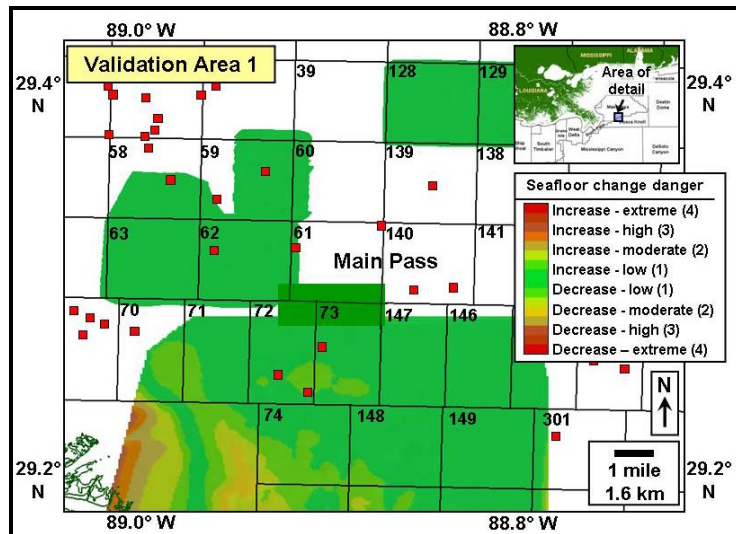


Figure 182: Seafloor change, NOAA to local, Validation Test Area 1

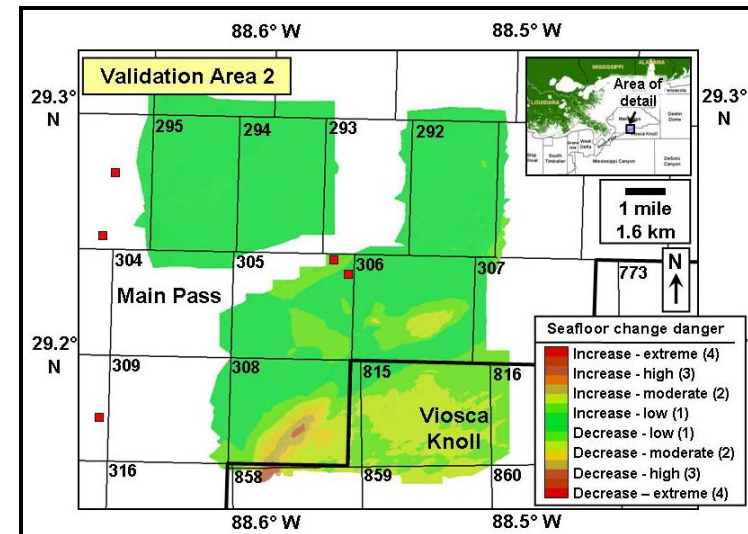


Figure 183: Seafloor change, NOAA to local, Validation Test Area 2

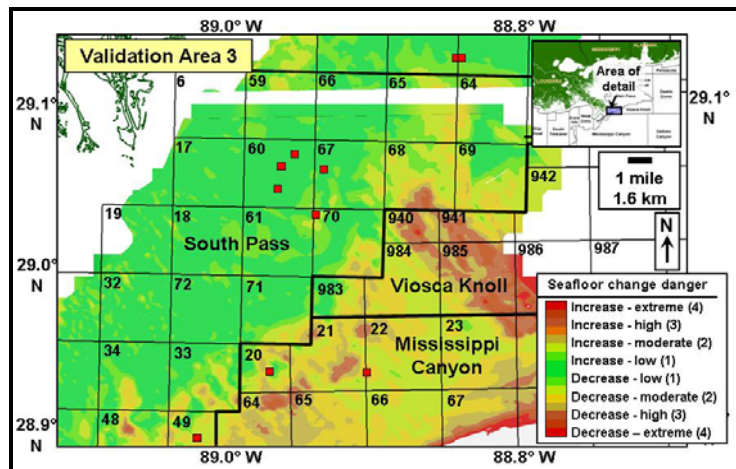


Figure 184: Seafloor change, NOAA to 1977, Validation Test Area 3

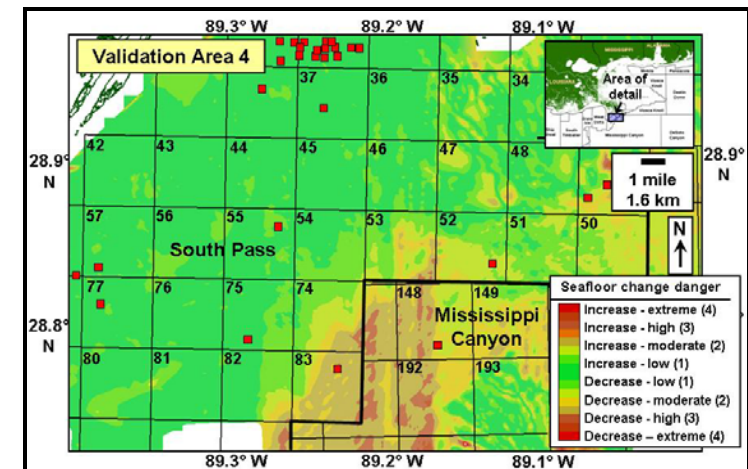


Figure 185: Seafloor change, NOAA to 1977, Validation Test Area 4

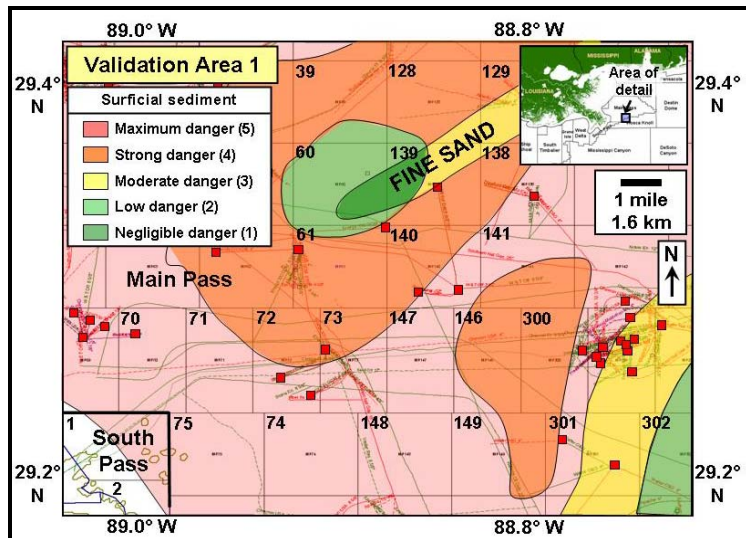


Figure 186: Seafloor sediment susceptibility, Validation Test Area 1

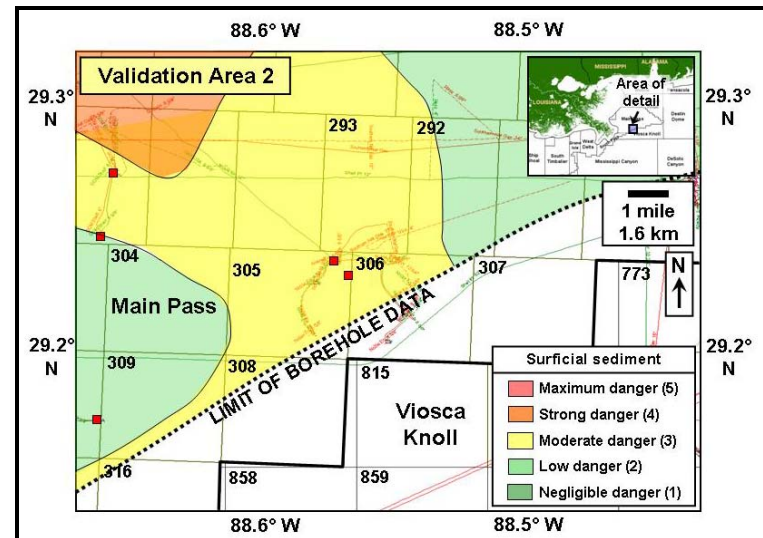


Figure 187: Seafloor sediment susceptibility, Validation Test Area 2

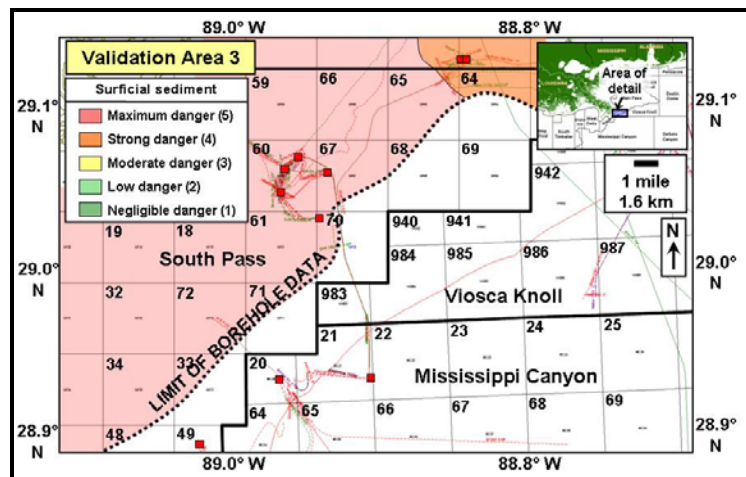


Figure 188: Seafloor sediment susceptibility, Validation Test Area 3

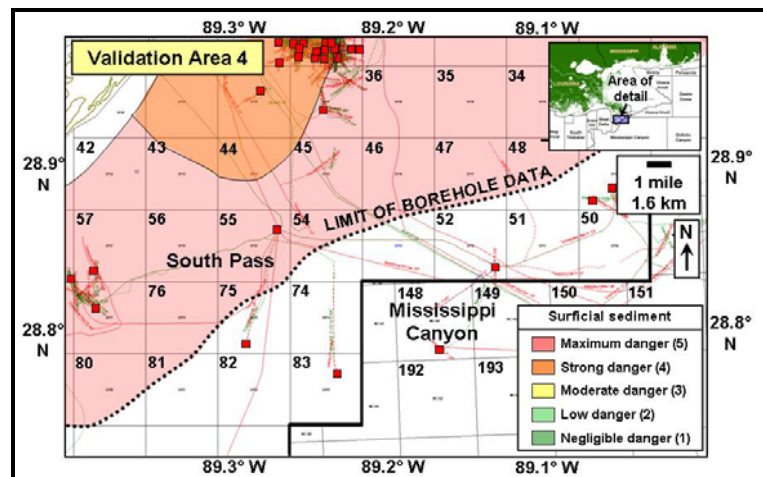


Figure 189: Seafloor sediment susceptibility, Validation Test Area 4



Table 28: Hazard scoring matrix, prior MRDF Hurricanes

<u>MIKE 21 modeled hurricanes</u>								
<u>Hurricane</u>	<u>Hsmax</u>	<u>Wave period</u>	<u>Time</u>	<u>Morphology</u> * <sup>1</sup>	<u>Slope</u> * <sup>2</sup>	<u>Sed. Rate</u> * <sup>3</sup>	<u>Surficial</u> * <sup>4</sup>	<u>Total score</u>
Katrina	4	4	3	3	3	2	5	4320
Ivan	4	4	4	3	3	2	5	5760
Andrew	3	2	3	3	3	2	5	1620
Camille	5	3	4	3	3	2	5	5400
Betsy	3	3	2	3	3	2	5	1620
<u>Hurricanes from the historical record (not modeled)</u>								
<u>Hurricane</u>	<u>Hsmax</u> *	<u>Wave period</u>	<u>Time</u>	<u>Morphology</u> * <sup>1</sup>	<u>Slope</u> * <sup>2</sup>	<u>Sed. Rate</u> * <sup>3</sup>	<u>Surficial</u> * <sup>4</sup>	<u>Total score</u>
Gustav	3	3	2	3	3	2	5	1620
Lili	3	3	3	3	3	2	5	2430
Opal	4	4	3	3	3	2	5	4320
Elena	3	3	1	3	3	2	5	810
Frederic	3	3	3	3	3	2	5	2430
Eloise	3	3	2	3	3	2	5	1620
Carmen	4	4	3	3	3	2	5	4320
Hilda	3	3	4	3	3	2	5	3240
New Orleans	4	4	3	3	3	2	5	4320
Grand Isle	3	3	3	3	3	2	5	2430
1906	3	3	4	3	3	2	5	3240
Chenier Caminada	3	3	3	3	3	2	5	2430
1882	3	3	2	3	3	2	5	1620
Last Island	4	4	4	3	3	2	5	5760

\*<sup>1</sup> Morphology assumed constant as a mudflow lobe (scaled “3” from Table 24)

\*<sup>2</sup> Slope steepness assumed constant as 2°-3° (scaled “3” from Table 25)

\*<sup>3</sup> Rate of seafloor change through time assumed constant as a moderate increase or decrease (scaled “2” from Table 26)

\*<sup>4</sup> Surficial sediment characteristics (i.e., sediment size and shear strength characteristics) assumed constant as clay/low shear strength (scaled “5” from Table 27)

\*<sup>5</sup> Hs<sub>max</sub> based on Hsu (2006)

because they tracked away from the MRDF as they approached landfall. Notably, Hurricane Frederic made a nearly identical landfall to Ivan but Frederic approached the MRDF from a more southeasterly angle than Ivan ( $165^{\circ}$  vs.  $185^{\circ}$  for Ivan) and from farther east (145 km vs. 120 km for Ivan; Figure 29, Section 5.1.1).

As a forward-looking exercise, the product of each category was then integrated with metocean parameters to compute a total hazard score for a series of projected future tropical systems with varying intensities (Table 29). These storms, named Alpha (most intense), Beta, Gamma, Delta and Epsilon (least intense), reflect the spectrum of hurricane conditions that could be reasonably expected across the MRDF. Using the same scoring criteria and assumptions from prior storms, shelf failure conditions could be expected for each scenario except one in Hurricane Alpha and for half the conditions in Hurricane Beta (the exceptions being a fast hurricane over a mudflow lobe). These conditions (i.e., scores over 5000) equate to those at least as severe as Hurricanes Ivan and Camille. Successively weaker storms produced lower scores, culminating in the least damaging scenario of Hurricane/Tropical Storm Epsilon with a score of 180 (Table 29).

The probability that the MRDF will experience a hurricane of the magnitude of any of these storms is difficult to predict given the decadal cycles of increased and decreased activity experienced since 1851 (and even since 1718; Figures 28 and 31, Table 4, Section 5.1.1). However, given the RI discussed earlier in this section, a Hurricane Gamma-like hurricane (roughly equivalent to a Category 3 storm) would impact the MRDF every 5.4, 6.0 and 13.6 years when striking 300, 200 and 100 km away, respectively.

#### **9.2.4 Risk Characterization**

Risk is quantified as the expected consequences that occur as a result of a specific event which, in the case of the MRDF, is assumed to be a submarine mudslide. Risk is characterized by evaluating two parameters – the inventory, which quantifies the value of the elements at risk (i.e., MRDF production platforms and pipelines), and the vulnerability for each element, which is

Table 29: Sample scoring matrix, projected MRDF Hurricanes

	<u>Hsmax</u>	<u>Period</u>	<u>Time exposure</u>	<u>Morphology</u>	<u>Slope</u>	<u>Sediment rate</u>	<u>Surficial sediment</u>	<u>Total score</u>
<b>Hurricane Alpha</b>								
Slow hurricane, gentle slopes, mudflow gully	5	5	5	4	3	2	5	15,000
Slow hurricane, gentle slopes, mudflow lobe	5	5	5	3	3	2	5	11,250
Slow hurricane, low slopes, mudflow gully	5	5	5	4	2	2	5	10,000
Slow hurricane, low slopes, mudflow lobe	5	5	5	3	2	2	5	7,500
Fast hurricane, gentle slopes, mudflow gully	5	5	3	4	3	2	5	9,000
Fast hurricane, gentle slopes, mudflow lobe	5	5	3	3	3	2	5	6,750
Fast hurricane, low slopes, mudflow gully	5	5	3	4	2	2	5	6,000
Fast hurricane, low slopes, mudflow lobe	5	5	3	3	2	2	5	4,500
<b>Hurricane Beta</b>								
Slow hurricane, gentle slopes, mudflow gully	4	4	5	4	3	2	5	9,600
Slow hurricane, gentle slopes, mudflow lobe	4	4	5	3	3	2	5	7,200
Slow hurricane, low slopes, mudflow gully	4	4	5	4	2	2	5	6,400
Slow hurricane, low slopes, mudflow lobe	4	4	5	3	2	2	5	4,800
Fast hurricane, gentle slopes, mudflow gully	4	4	3	4	3	2	5	5,760
Fast hurricane, gentle slopes, mudflow lobe	4	4	3	3	3	2	5	4,320
Fast hurricane, low slopes, mudflow gully	4	4	3	4	2	2	5	3,840
Fast hurricane, low slopes, mudflow lobe	4	4	3	3	2	2	5	2,880
<b>Hurricane Gamma</b>								
Slow hurricane, gentle slopes, mudflow gully	3	3	5	4	3	2	5	5,400
Slow hurricane, gentle slopes, mudflow lobe	3	3	5	3	3	2	5	4,050
Slow hurricane, low slopes, mudflow gully	3	3	5	4	2	2	5	3,600
Slow hurricane, low slopes, mudflow lobe	3	3	5	3	2	2	5	2,700
Fast hurricane, gentle slopes, mudflow gully	3	3	3	4	3	2	5	3,240
Fast hurricane, gentle slopes, mudflow lobe	3	3	3	3	3	2	5	2,430
Fast hurricane, low slopes, mudflow gully	3	3	3	4	2	2	5	2,160
Fast hurricane, low slopes, mudflow lobe	3	3	3	3	2	2	5	1,620
<b>Hurricane Delta</b>								
Slow hurricane, gentle slopes, mudflow gully	2	2	5	4	3	2	5	2,400
Slow hurricane, gentle slopes, mudflow lobe	2	2	5	3	3	2	5	1,800
Slow hurricane, low slopes, mudflow gully	2	2	5	4	2	2	5	1,600
Slow hurricane, low slopes, mudflow lobe	2	2	5	3	2	2	5	1,200
Fast hurricane, gentle slopes, mudflow gully	2	2	3	4	3	2	5	1,440
Fast hurricane, gentle slopes, mudflow lobe	2	2	3	3	3	2	5	1,080
Fast hurricane, low slopes, mudflow gully	2	2	3	4	2	2	5	960
Fast hurricane, low slopes, mudflow lobe	2	2	3	3	2	2	5	720
<b>Hurricane/Tropical Storm Epsilon</b>								
Slow hurricane, gentle slopes, mudflow gully	1	1	5	4	3	2	5	600
Slow hurricane, gentle slopes, mudflow lobe	1	1	5	3	3	2	5	450
Slow hurricane, low slopes, mudflow gully	1	1	5	4	2	2	5	400
Slow hurricane, low slopes, mudflow lobe	1	1	5	3	2	2	5	300
Fast hurricane, gentle slopes, mudflow gully	1	1	3	4	3	2	5	360
Fast hurricane, gentle slopes, mudflow lobe	1	1	3	3	3	2	5	270
Fast hurricane, low slopes, mudflow gully	1	1	3	4	2	2	5	240
Fast hurricane, low slopes, mudflow lobe	1	1	3	3	2	2	5	180

quantified by a number representing the degree of damage ranging from zero (no loss) to one (total loss)

An inventory of elements at risk during each storm modeled in this dissertation is displayed in Figures 152-156, Section 8.2. A detailed view of elements at risk (platforms and pipelines) in each of the VTAs is displayed in Figures 190-193.

VTA 1 contains 20 platforms of various sizes that all consist of fixed structures installed directly on the ocean floor (Figure 190; also Appendix P, Table P-3). Numerous pipelines cross the area, most notably a series of oil pipelines that carry production from the Main Pass (MP) 299 Field as well as a series of regional, east-west transport pipelines located in MP 71-73 and MP 146-147 (e.g., the MPOG pipeline discussed in Section 7.2.1). Many of these pipelines were initially routed to minimize disruption from potential submarine failures (i.e., routed perpendicular to seafloor dip). Assuming an approximate replacement cost of \$30-50 million per platform (although platform cost varies greatly depending on water depth and the number of producing wells) and \$1 million per mile of pipeline (these costs also vary widely depending on pipeline diameter, maximum pressure and the overall length of pipeline – longer pipelines are cheaper per mile due to economies of scale), the total elements at risk value in VTA 1 is approximately \$600 million to \$900 million. These costs exclude platforms and pipelines located at MP 299 Field; the additional structures and pipelines located there boost costs to approximately \$480 million to \$820 million. Overall pipeline costs may be lower as only local pipeline segments, and not an entire pipeline, would most likely be affected by local slides. In those cases the replacement cost would involve repairing individual pipeline segments at the point of rupture. Given the size of past and expected future submarine mudslides, these costs would likely approximate only \$1-2 million in each instance of failure.

VTA 2 contains three platforms installed directly on the ocean floor (Figure 191; also Appendix P, Tables P-3 and P-6). Relatively few pipelines cross the area, most notably local transport pipelines within the MP 305/306 Field as well as regional transport pipelines that carry

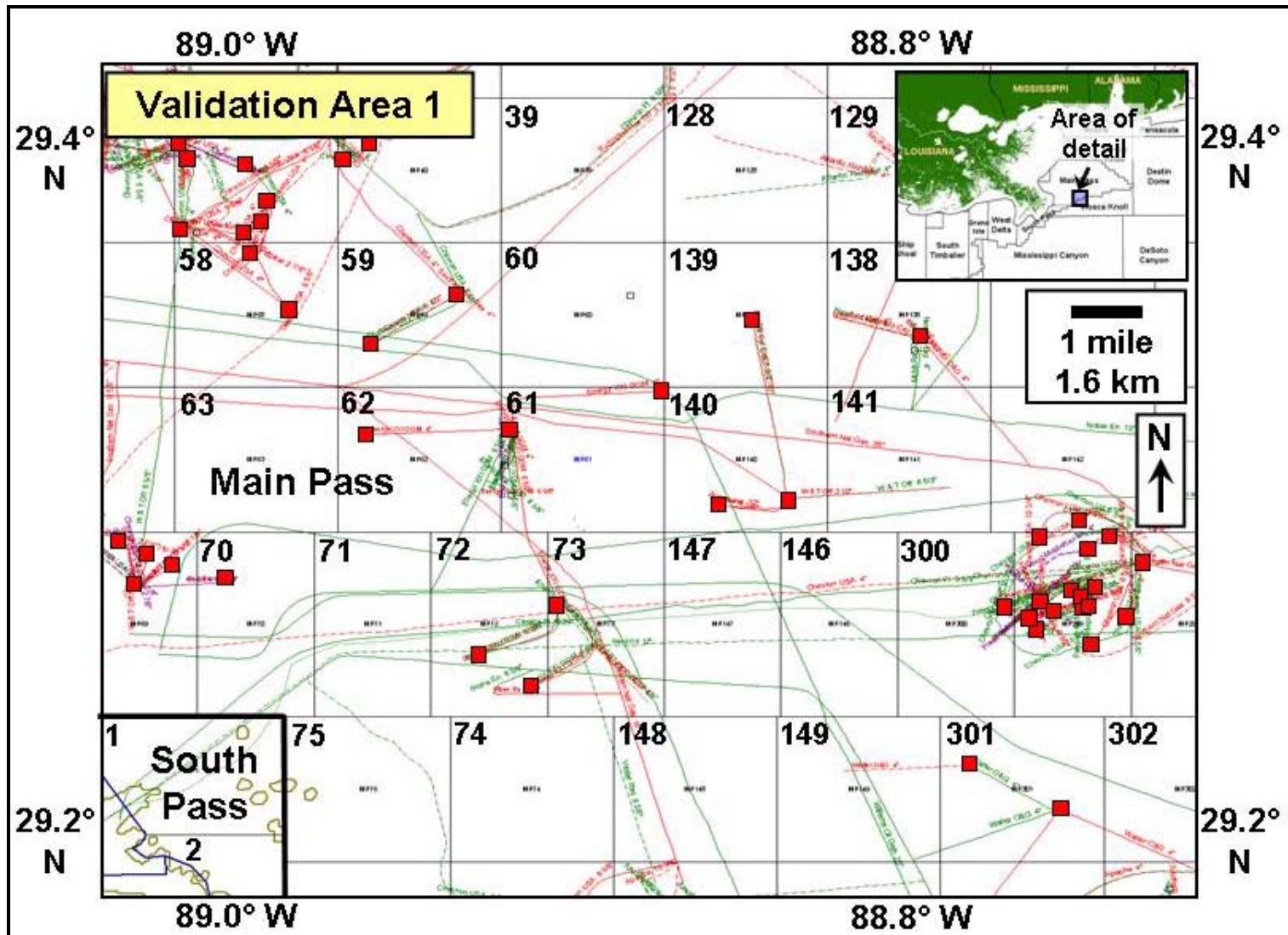


Figure 190: Infrastructure and elements at risk, Validation Test Area 1

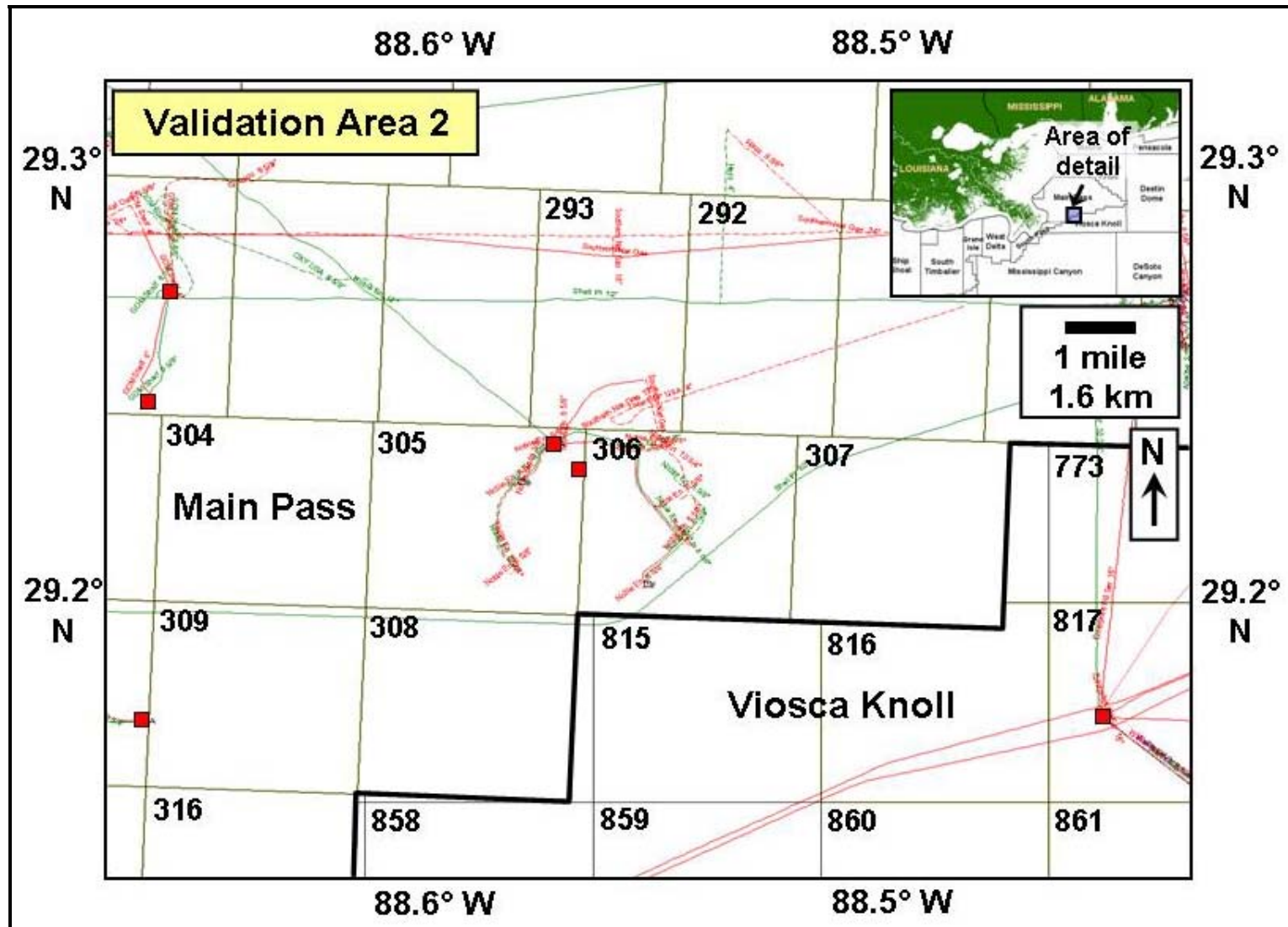


Figure 191: Infrastructure and elements at risk, Validation Test Area 2



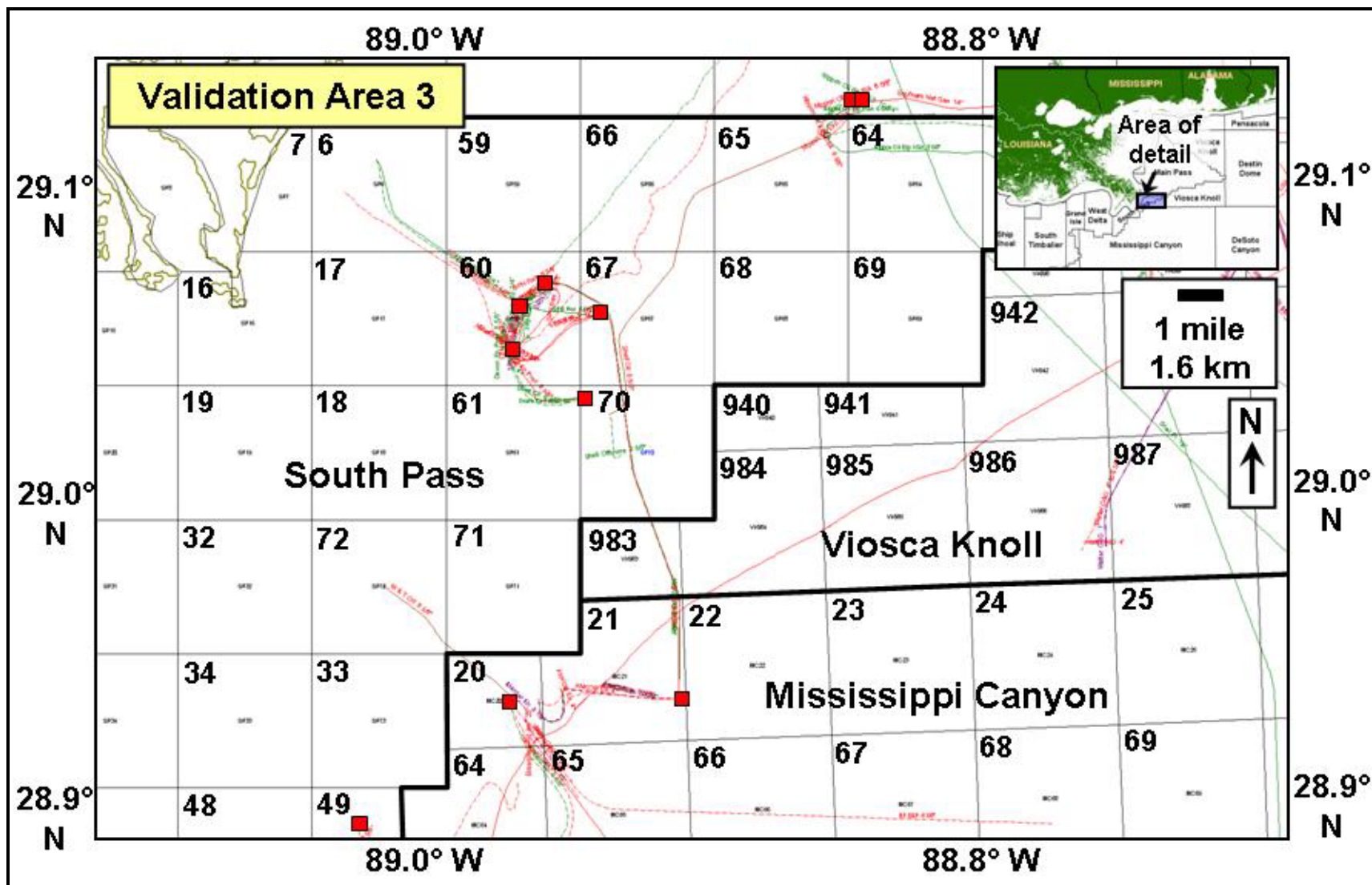


Figure 192: Infrastructure and elements at risk, Validation Test Area 3



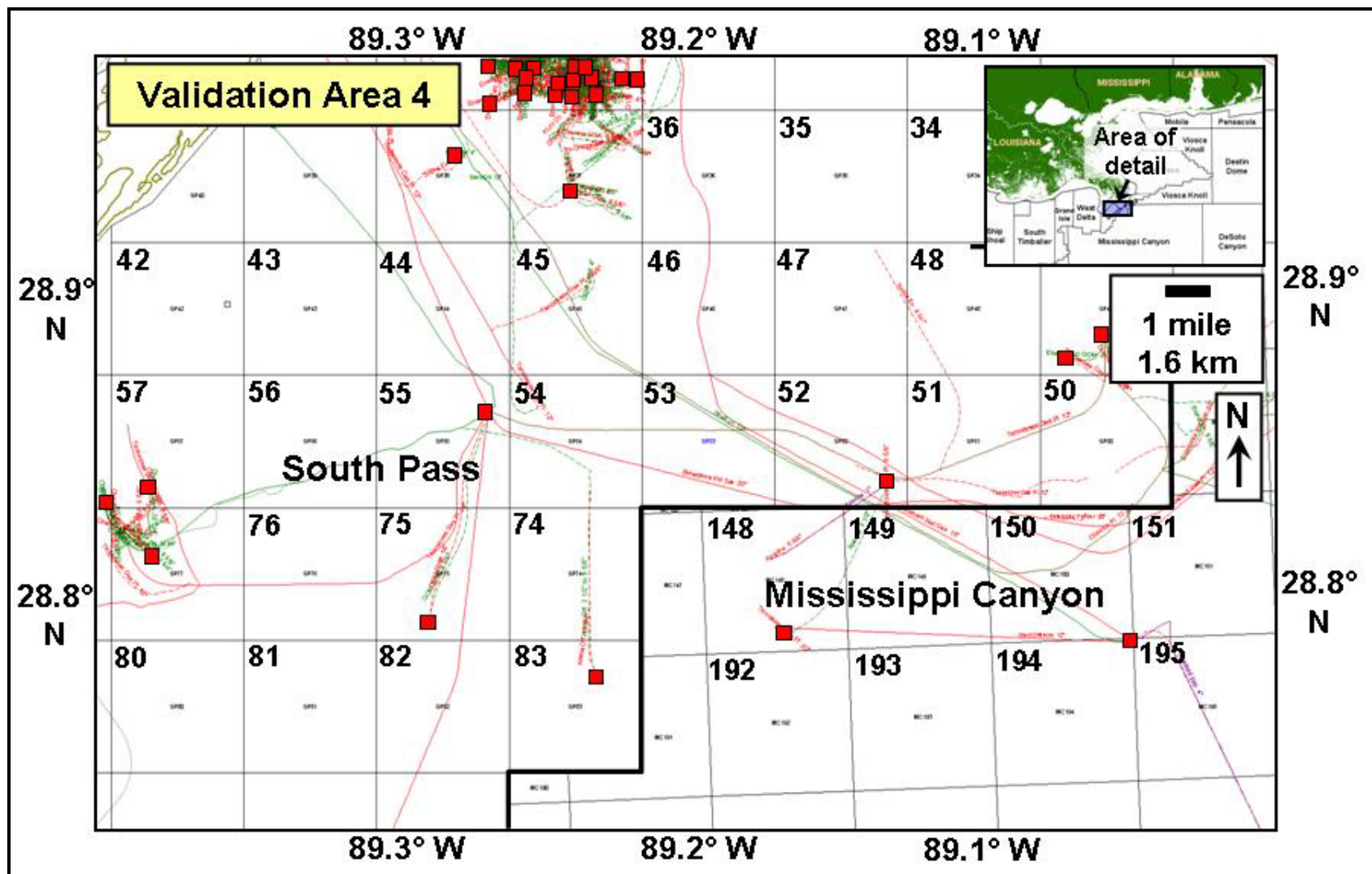


Figure 193: Infrastructure and elements at risk, Validation Test Area 4

production from MP 305/306 as well as from Viosca Knoll 817 (and points east) to shore. Several east-west regional pipelines also cross through the northern part of the test area. Assuming an approximate cost of \$50-70 million per platform (water depths are slightly deeper compared to VTA 1) and \$1 million per mile of pipeline, the total elements at risk value in VTA 2 is approximately \$230 million to \$290 million (although local pipeline replacement cost may be lower).

VTA 3 contains seven platforms installed directly on the ocean floor (Figure 192; also Appendix P, Tables P-4, P-5 and P-6). Pipeline density is high in places, notably around the South Pass Block 60 Field. Several regional transport pipelines exist farther to the south, mainly in the northwestern portion of the Mississippi Canyon (MC) Protraction Area. Assuming an approximate cost of \$30-50 million per platform on the shelf (South Pass Area), \$100-250 million per platform beyond the shelf edge (the MC Area), and \$1 million per mile of pipeline, the total elements at risk value in VTA 3 is approximately \$200 million to \$550 million.

VTA 4 contains a dense platform network along its northern periphery within the SP 28 Field (82 structures) as well as eight platforms elsewhere throughout the VTA (Figure 193; also Appendix P, Tables P-4 and P-5). Platform types vary considerably, ranging from older single-well platforms on the shelf to larger, multi-well platforms in deep water. Pipeline density is high throughout the VTA, especially within SP 28 Field but also extending in a northwest-southeast pattern from the SP 52 and MC 148 and 195 Fields. Assuming an approximate cost of \$30-50 million per platform on the shelf (excluding SP 28), \$100-250 million per platform in deep water, and \$1 million per mile of pipeline, the total elements at risk value in VTA 4 is approximately \$360-680 million.

The combined inventory replacement cost for the four VTAs falls within a range of \$1.27 billion to \$2.34 billion (with lower downside pipeline costs depending on localized damage to individual pipeline segments), which is only a small window on overall offshore infrastructure costs and the total number of elements at risk in future hurricanes. However, given that the

boundaries of the VTAs were chosen based on evidence from past mudslides, these totals may represent a reasonable estimate of losses due to hurricane-initiated mudslides.

A final element at risk is the value of the lost production as a result of a platform or pipeline that could be lost to a potential submarine mudslide. Kaiser (2007) estimated GOM production trends due to extreme weather by using empirical models to analyze historic production trends and weather events from 1950-2003. These results, together with production losses after the most recent GOM hurricanes (MMS, 2005a; 2005b), indicate significant potential for value destruction in the event of infrastructure damage or loss. Daily production from fields in each VTA varies significantly but all together totals approximately  $3.3 \times 10^4$  barrels of oil and  $1.08 \times 10^8$  feet<sup>3</sup> of gas (PI/Dwights Energy Database, 2009; Appendix Q, Table Q-1). Assuming an oil price of \$60 per barrel and a gas price of \$4.50 per 10<sup>3</sup> feet<sup>3</sup>, these daily production rates yield a value of \$2.47 million.

Vulnerability, for purposes of this dissertation and as applied to infrastructure loss due to submarine landslides, is considered an all-or-nothing event. If a platform fails as a result of sediment movement, it is usually non-salvageable and therefore considered a total loss. A pipeline may bend or otherwise be removed from its original position but as long as flow continues (assuming there are no leaks) it is considered useable; if the pipeline breaks then the failed segment is considered a loss and must be replaced. Therefore, for purposes of calculating risk in Section 9.2.5, vulnerability is assumed equal to one (i.e., failure).

#### **9.2.5 Total MRDF Risk**

Total risk is defined as the product of hazard, value of elements and vulnerability. Varnes (1984) defined total risk ( $R_T$ ) as the set of damages resulting from the occurrence of an event through the following equation:

$$R_T = \sum H R_i V_i \quad (7)$$

Where:  $H$  = hazard occurrence probability within a given area and a given time period (from Tables 28 and 29)

- $R_i$  = (for  $i = 1$  to  $n$ ) are the elements at risk potentially damaged by the phenomenon (from Appendix Q, Table Q-1)
- $V_i$  = vulnerability of each element represented by a damage degree ranging from zero (no loss) to one (total loss)

The point system displayed in Table 29, Section 9.2.3 for five theoretical topical systems that could approach the MRDF represent a quantifiable measure of the hazard occurrence. Elements at risk, and their values, were described in Section 9.2.4 as was their vulnerability. Given the scoring combinations possible and the elements at risk value for each VTA, the total risk was calculated for each potential hurricane/tropical storm category (i.e., Alpha through Epsilon; Tables 30-32). The total risk score was displayed using a divisor of  $10^4$  to keep the numbers to a manageable level. Elements at risk used in the calculations represent the range of threats (i.e., the value) faced by singular platforms within a VTA, not the entire infrastructure value. Similarly, pipeline elements at risk assumed singular failures along a given pipeline route, not failure of the entire pipeline.

In VTA 1, total risk results indicate highest risk above values of 25 in Hurricane Alpha and a slow Hurricane Beta, similar to conditions during Hurricanes Ivan and Camille (Table 30). Total risk scores between 15 and 25 represent borderline risk range equivalent to conditions seen in a fast Hurricane Beta and a slow Hurricane Gamma. Scores below approximately 15 represent successively weaker storms, culminating in the least damaging scenario of Hurricane/Tropical Storm Epsilon (Table 30). These values are, of course, entirely dependent on the value of the elements at risk; higher infrastructure values will result in higher values of total risk. However, for shelf environments in water depths less than 30 m, these numbers remain valid.

VTA 2 results indicate slightly higher risk thresholds given slightly deeper water closer to the shelf edge (deeper water requires slightly more expensive platforms, thereby increasing the elements at risk). Total risk scores above approximately 35 (Hurricanes Alpha and a slow Hurricane Beta) indicate the highest risk (Table 31). Total risk scores between 20 and 35

Table 30: Total risk calculations, VTA 1, 3 and 4 (shelf environment)

Validation Test Area 1, 3(shelf) and 4						
	Total score	Elements at risk (min)	Elements at risk (max)	Vulnerability	Min total risk (x 10 <sup>4</sup> )	Max total risk (x 10 <sup>4</sup> )
	(H)	(R <sub>i</sub> )	(R <sub>j</sub> )	(V <sub>i</sub> )	(R <sub>i</sub> )	(R <sub>j</sub> )
<b>Hurricane Alpha</b>						
Slow hurricane, gentle slopes, mudflow gully	15,000	35	55	1.0	52.50	82.50
Slow hurricane, gentle slopes, mudflow lobe	11,250	35	55	1.0	39.38	61.88
Slow hurricane, low slopes, mudflow gully	10,000	35	55	1.0	35.00	55.00
Slow hurricane, low slopes, mudflow lobe	7,500	35	55	1.0	26.25	41.25
Fast hurricane, gentle slopes, mudflow gully	9,000	35	55	1.0	31.50	49.50
Fast hurricane, gentle slopes, mudflow lobe	6,750	35	55	1.0	23.63	37.13
Fast hurricane, low slopes, mudflow gully	6,000	35	55	1.0	21.00	33.00
Fast hurricane, low slopes, mudflow lobe	4,500	35	55	1.0	15.75	24.75
<b>Hurricane Beta</b>						
Slow hurricane, gentle slopes, mudflow gully	9,600	35	55	1.0	33.60	52.80
Slow hurricane, gentle slopes, mudflow lobe	7,200	35	55	1.0	25.20	39.60
Slow hurricane, low slopes, mudflow gully	6,400	35	55	1.0	22.40	35.20
Slow hurricane, low slopes, mudflow lobe	4,800	35	55	1.0	16.80	26.40
Fast hurricane, gentle slopes, mudflow gully	5,760	35	55	1.0	20.16	31.68
Fast hurricane, gentle slopes, mudflow lobe	4,320	35	55	1.0	15.12	23.76
Fast hurricane, low slopes, mudflow gully	3,840	35	55	1.0	13.44	21.12
Fast hurricane, low slopes, mudflow lobe	2,880	35	55	1.0	10.08	15.84
<b>Hurricane Gamma</b>						
Slow hurricane, gentle slopes, mudflow gully	5,400	35	55	1.0	18.90	29.70
Slow hurricane, gentle slopes, mudflow lobe	4,050	35	55	1.0	14.18	22.28
Slow hurricane, low slopes, mudflow gully	3,600	35	55	1.0	12.60	19.80
Slow hurricane, low slopes, mudflow lobe	2,700	35	55	1.0	9.45	14.85
Fast hurricane, gentle slopes, mudflow gully	3,240	35	55	1.0	11.34	17.82
Fast hurricane, gentle slopes, mudflow lobe	2,430	35	55	1.0	8.51	13.37
Fast hurricane, low slopes, mudflow gully	2,160	35	55	1.0	7.56	11.88
Fast hurricane, low slopes, mudflow lobe	1,620	35	55	1.0	5.67	8.91
<b>Hurricane Delta</b>						
Slow hurricane, gentle slopes, mudflow gully	2,400	35	55	1.0	8.40	13.20
Slow hurricane, gentle slopes, mudflow lobe	1,800	35	55	1.0	6.30	9.90
Slow hurricane, low slopes, mudflow gully	1,600	35	55	1.0	5.60	8.80
Slow hurricane, low slopes, mudflow lobe	1,200	35	55	1.0	4.20	6.60
Fast hurricane, gentle slopes, mudflow gully	1,440	35	55	1.0	5.04	7.92
Fast hurricane, gentle slopes, mudflow lobe	1,080	35	55	1.0	3.78	5.94
Fast hurricane, low slopes, mudflow gully	960	35	55	1.0	3.36	5.28
Fast hurricane, low slopes, mudflow lobe	720	35	55	1.0	2.52	3.96
<b>Hurricane/Tropical Storm Epsilon</b>						
Slow hurricane, gentle slopes, mudflow gully	600	35	55	1.0	2.10	3.30
Slow hurricane, gentle slopes, mudflow lobe	450	35	55	1.0	1.58	2.48
Slow hurricane, low slopes, mudflow gully	400	35	55	1.0	1.40	2.20
Slow hurricane, low slopes, mudflow lobe	300	35	55	1.0	1.05	1.65
Fast hurricane, gentle slopes, mudflow gully	360	35	55	1.0	1.26	1.98
Fast hurricane, gentle slopes, mudflow lobe	270	35	55	1.0	0.95	1.49
Fast hurricane, low slopes, mudflow gully	240	35	55	1.0	0.84	1.32
Fast hurricane, low slopes, mudflow lobe	180	35	55	1.0	0.63	0.99

Table 31: Total risk calculations, VTA 2 (outer shelf environment)

Validation Test Area 2 (outer shelf)							
	<u>Total score</u>	<u>Elements at risk (min)</u> <u>(millions of dollars)</u>	<u>Elements at risk (max)</u> <u>(millions of dollars)</u>	<u>Vulnerability</u>	<u>Min total risk (x 10<sup>4</sup>)</u>	<u>Max total risk (x 10<sup>4</sup>)</u>	
<b>Hurricane Alpha</b>	<b>(H)</b>	<b>(R<sub>i</sub>)</b>	<b>(R<sub>i</sub>)</b>	<b>(V<sub>i</sub>)</b>	<b>(R<sub>i</sub>)</b>	<b>(R<sub>i</sub>)</b>	
Slow hurricane, gentle slopes, mudflow gully	15,000	35	55	1.0	52.50	82.50	
Slow hurricane, gentle slopes, mudflow lobe	11,250	35	55	1.0	39.38	61.88	
Slow hurricane, low slopes, mudflow gully	10,000	35	55	1.0	35.00	55.00	
Slow hurricane, low slopes, mudflow lobe	7,500	35	55	1.0	26.25	41.25	
Fast hurricane, gentle slopes, mudflow gully	9,000	35	55	1.0	31.50	49.50	
Fast hurricane, gentle slopes, mudflow lobe	6,750	35	55	1.0	23.63	37.13	
Fast hurricane, low slopes, mudflow gully	6,000	35	55	1.0	21.00	33.00	
Fast hurricane, low slopes, mudflow lobe	4,500	35	55	1.0	15.75	24.75	
<b>Hurricane Beta</b>							
Slow hurricane, gentle slopes, mudflow gully	9,600	35	55	1.0	33.60	52.80	
Slow hurricane, gentle slopes, mudflow lobe	7,200	35	55	1.0	25.20	39.60	
Slow hurricane, low slopes, mudflow gully	6,400	35	55	1.0	22.40	35.20	
Slow hurricane, low slopes, mudflow lobe	4,800	35	55	1.0	16.80	26.40	
Fast hurricane, gentle slopes, mudflow gully	5,760	35	55	1.0	20.16	31.68	
Fast hurricane, gentle slopes, mudflow lobe	4,320	35	55	1.0	15.12	23.76	
Fast hurricane, low slopes, mudflow gully	3,840	35	55	1.0	13.44	21.12	
Fast hurricane, low slopes, mudflow lobe	2,880	35	55	1.0	10.08	15.84	
<b>Hurricane Gamma</b>							
Slow hurricane, gentle slopes, mudflow gully	5,400	35	55	1.0	18.90	29.70	
Slow hurricane, gentle slopes, mudflow lobe	4,050	35	55	1.0	14.18	22.28	
Slow hurricane, low slopes, mudflow gully	3,600	35	55	1.0	12.60	19.80	
Slow hurricane, low slopes, mudflow lobe	2,700	35	55	1.0	9.45	14.85	
Fast hurricane, gentle slopes, mudflow gully	3,240	35	55	1.0	11.34	17.82	
Fast hurricane, gentle slopes, mudflow lobe	2,430	35	55	1.0	8.51	13.37	
Fast hurricane, low slopes, mudflow gully	2,160	35	55	1.0	7.56	11.88	
Fast hurricane, low slopes, mudflow lobe	1,620	35	55	1.0	5.67	8.91	
<b>Hurricane Delta</b>							
Slow hurricane, gentle slopes, mudflow gully	2,400	35	55	1.0	8.40	13.20	
Slow hurricane, gentle slopes, mudflow lobe	1,800	35	55	1.0	6.30	9.90	
Slow hurricane, low slopes, mudflow gully	1,600	35	55	1.0	5.60	8.80	
Slow hurricane, low slopes, mudflow lobe	1,200	35	55	1.0	4.20	6.60	
Fast hurricane, gentle slopes, mudflow gully	1,440	35	55	1.0	5.04	7.92	
Fast hurricane, gentle slopes, mudflow lobe	1,080	35	55	1.0	3.78	5.94	
Fast hurricane, low slopes, mudflow gully	960	35	55	1.0	3.36	5.28	
Fast hurricane, low slopes, mudflow lobe	720	35	55	1.0	2.52	3.96	
<b>Hurricane/Tropical Storm Epsilon</b>							
Slow hurricane, gentle slopes, mudflow gully	600	35	55	1.0	2.10	3.30	
Slow hurricane, gentle slopes, mudflow lobe	450	35	55	1.0	1.58	2.48	
Slow hurricane, low slopes, mudflow gully	400	35	55	1.0	1.40	2.20	
Slow hurricane, low slopes, mudflow lobe	300	35	55	1.0	1.05	1.65	
Fast hurricane, gentle slopes, mudflow gully	360	35	55	1.0	1.26	1.98	
Fast hurricane, gentle slopes, mudflow lobe	270	35	55	1.0	0.95	1.49	
Fast hurricane, low slopes, mudflow gully	240	35	55	1.0	0.84	1.32	
Fast hurricane, low slopes, mudflow lobe	180	35	55	1.0	0.63	0.99	

Table 32: Total risk calculations, VTA 3 (deep water environment)

Validation Test Area 3 (deep water; upper slope)							
	Total score	Elements at risk (min) (millions of dollars)	Elements at risk (max) (millions of dollars)	Vulnerability	Min total risk (x 10 <sup>4</sup> )	Max total risk (x 10 <sup>4</sup> )	
	(H)	(R <sub>i</sub> )	(R <sub>j</sub> )	(V <sub>i</sub> )	(R <sub>i</sub> )	(R <sub>j</sub> )	
<b>Hurricane Alpha</b>							
Slow hurricane, gentle slopes, mudflow gully	15,000	105	255	1.0	157.50	382.50	
Slow hurricane, gentle slopes, mudflow lobe	11,250	105	255	1.0	118.13	286.88	
Slow hurricane, low slopes, mudflow gully	10,000	105	255	1.0	105.00	255.00	
Slow hurricane, low slopes, mudflow lobe	7,500	105	255	1.0	78.75	191.25	
Fast hurricane, gentle slopes, mudflow gully	9,000	105	255	1.0	94.50	229.50	
Fast hurricane, gentle slopes, mudflow lobe	6,750	105	255	1.0	70.88	172.13	
Fast hurricane, low slopes, mudflow gully	6,000	105	255	1.0	63.00	153.00	
Fast hurricane, low slopes, mudflow lobe	4,500	105	255	1.0	47.25	114.75	
<b>Hurricane Beta</b>							
Slow hurricane, gentle slopes, mudflow gully	9,600	105	255	1.0	100.80	244.80	
Slow hurricane, gentle slopes, mudflow lobe	7,200	105	255	1.0	75.60	183.60	
Slow hurricane, low slopes, mudflow gully	6,400	105	255	1.0	67.20	163.20	
Slow hurricane, low slopes, mudflow lobe	4,800	105	255	1.0	50.40	122.40	
Fast hurricane, gentle slopes, mudflow gully	5,760	105	255	1.0	60.48	146.88	
Fast hurricane, gentle slopes, mudflow lobe	4,320	105	255	1.0	45.36	110.16	
Fast hurricane, low slopes, mudflow gully	3,840	105	255	1.0	40.32	97.92	
Fast hurricane, low slopes, mudflow lobe	2,880	105	255	1.0	30.24	73.44	
<b>Hurricane Gamma</b>							
Slow hurricane, gentle slopes, mudflow gully	5,400	105	255	1.0	56.70	137.70	
Slow hurricane, gentle slopes, mudflow lobe	4,050	105	255	1.0	42.53	103.28	
Slow hurricane, low slopes, mudflow gully	3,600	105	255	1.0	37.80	91.80	
Slow hurricane, low slopes, mudflow lobe	2,700	105	255	1.0	28.35	68.85	
Fast hurricane, gentle slopes, mudflow gully	3,240	105	255	1.0	34.02	82.62	
Fast hurricane, gentle slopes, mudflow lobe	2,430	105	255	1.0	25.52	61.97	
Fast hurricane, low slopes, mudflow gully	2,160	105	255	1.0	22.68	55.08	
Fast hurricane, low slopes, mudflow lobe	1,620	105	255	1.0	17.01	41.31	
<b>Hurricane Delta</b>							
Slow hurricane, gentle slopes, mudflow gully	2,400	105	255	1.0	25.20	61.20	
Slow hurricane, gentle slopes, mudflow lobe	1,800	105	255	1.0	18.90	45.90	
Slow hurricane, low slopes, mudflow gully	1,600	105	255	1.0	16.80	40.80	
Slow hurricane, low slopes, mudflow lobe	1,200	105	255	1.0	12.60	30.60	
Fast hurricane, gentle slopes, mudflow gully	1,440	105	255	1.0	15.12	36.72	
Fast hurricane, gentle slopes, mudflow lobe	1,080	105	255	1.0	11.34	27.54	
Fast hurricane, low slopes, mudflow gully	960	105	255	1.0	10.08	24.48	
Fast hurricane, low slopes, mudflow lobe	720	105	255	1.0	7.56	18.36	
<b>Hurricane/Tropical Storm Epsilon</b>							
Slow hurricane, gentle slopes, mudflow gully	600	105	255	1.0	6.30	15.30	
Slow hurricane, gentle slopes, mudflow lobe	450	105	255	1.0	4.73	11.48	
Slow hurricane, low slopes, mudflow gully	400	105	255	1.0	4.20	10.20	
Slow hurricane, low slopes, mudflow lobe	300	105	255	1.0	3.15	7.65	
Fast hurricane, gentle slopes, mudflow gully	360	105	255	1.0	3.78	9.18	
Fast hurricane, gentle slopes, mudflow lobe	270	105	255	1.0	2.84	6.89	
Fast hurricane, low slopes, mudflow gully	240	105	255	1.0	2.52	6.12	
Fast hurricane, low slopes, mudflow lobe	180	105	255	1.0	1.89	4.59	



represent borderline risk ranges equivalent to a fast Hurricane Beta and a slow Hurricane Gamma. Scores below approximately 20 represent weaker storms. These scores represent a typical profile for an area located along an outer shelf environment in the GOM.

VTA 3 risk results can be broken into two separate profiles. Shelf areas contain a risk profile similar to that in VTA 1 given their location on the shelf in shallower water (Table 30). However, part of VTA 3 overlaps the shelf edge and the upper continental slope, thereby requiring more expensive platforms. The higher values for these elements at risk are reflected in the total risk values calculated for VTA3 in deep water (Table 32). In these scenarios, total risk scores above 60 in the minimum case and 125 in the maximum case equate to the most destructive storms; scores between 40 and 60 (minimum case) and 100 and 125 (maximum case) equate to moderate storms, and values below 40 and 60 equate to weaker storms in minimum and maximum cases, respectively.

VTA 4 results are similar in scope to those in VTA 1 (i.e., shelf environment; Table 30).

### **9.3 Risk Results Testing**

A quick-look series of tests were conducted to assess the validity of the risk model outlined in Section 9.2 by comparing various triggering, revealing and predisposition factors to potential MRDF hurricane hazard scores. As an example, seafloor morphology types outlined in Table 24 were compared to hazard scores for the range of possible hurricanes (Figure 194). The impact from these storms is constrained upward by the maximum hazard score assigned to hurricanes from the historical record (5760 in Hurricane Ivan, although Camille would have scored 7200 had wave periods been comparable to those in Ivan; Table 28). Impact is constrained downward by comparing hazard scores in Table 29 to actual observations quantified in Table 28 (i.e., red or yellow highlights in Table 29). Results indicate that Hurricane Alpha would impact mudflow gullies and mudflow lobes, and possibly slightly undisturbed seafloor. Undisturbed seafloor would not be considered at risk since empirical evidence suggests that failures have not occurred in similar conditions. Likewise, Hurricane Beta would impact a mudflow gully and possibly a mudflow lobe; no other morphology types would be impacted. Hurricane Gamma would impact mudflow gullies only (Figure 194).

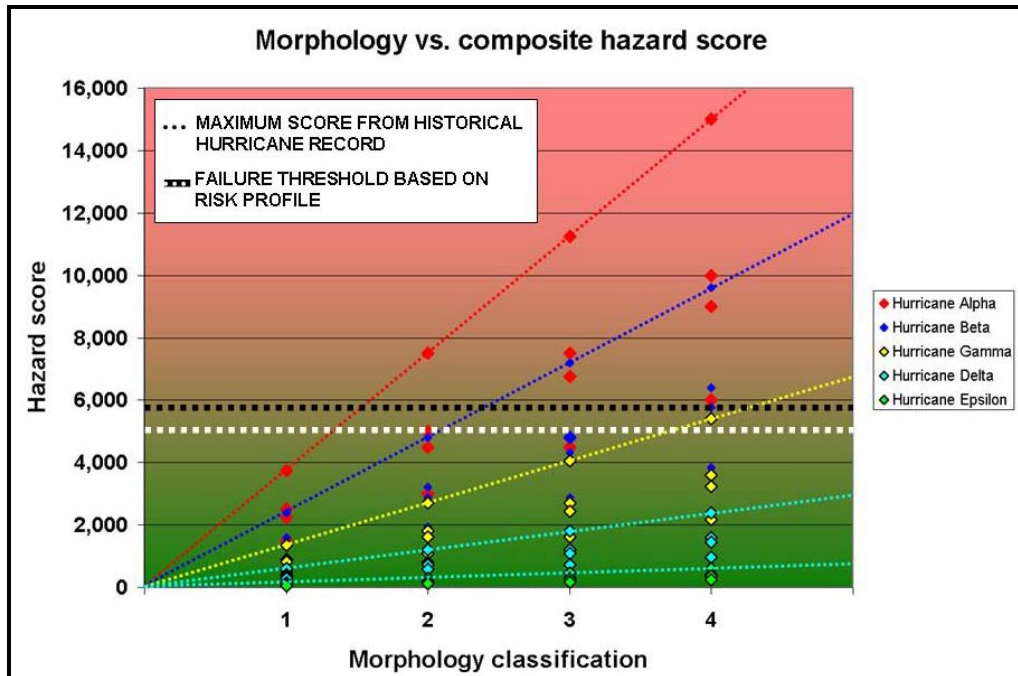


Figure 194: MRDF morphology type vs. composite hazard score

Rates of seafloor change (either positive or negative) were similarly ranked on a scale of 1-4 and produced a profile similar to that portrayed in Figure 194, thereby implying similar effects from potential hurricanes. Other external factors such as temporal hurricane exposure and surficial sediment characteristics were valued on a scale of 1-5 and are portrayed in an example plot in Figure 195. This plot reveals that for any of these factors, Hurricane Alpha and marginally Hurricane Beta would initiate conditions susceptible to seafloor failure.

Slope steepness was the only factor ranked on a scale of 1-7. Test results indicate that Hurricane Alpha would initiate failure conditions across all slopes and morphology types, Hurricane Beta would initiate failure conditions for slopes exceeding  $1.0^{\circ}$  in a mudflow gully and for all dips steeper than that regardless of morphology type, and that Hurricane Gamma would initiate failure in a mudflow gully with slopes exceeding  $2^{\circ}$  (Figure 196). Hurricanes Delta and Epsilon would not initiate failure regardless of slope angle except in the case of dips exceeding  $8^{\circ}$  within mudflow gullies.

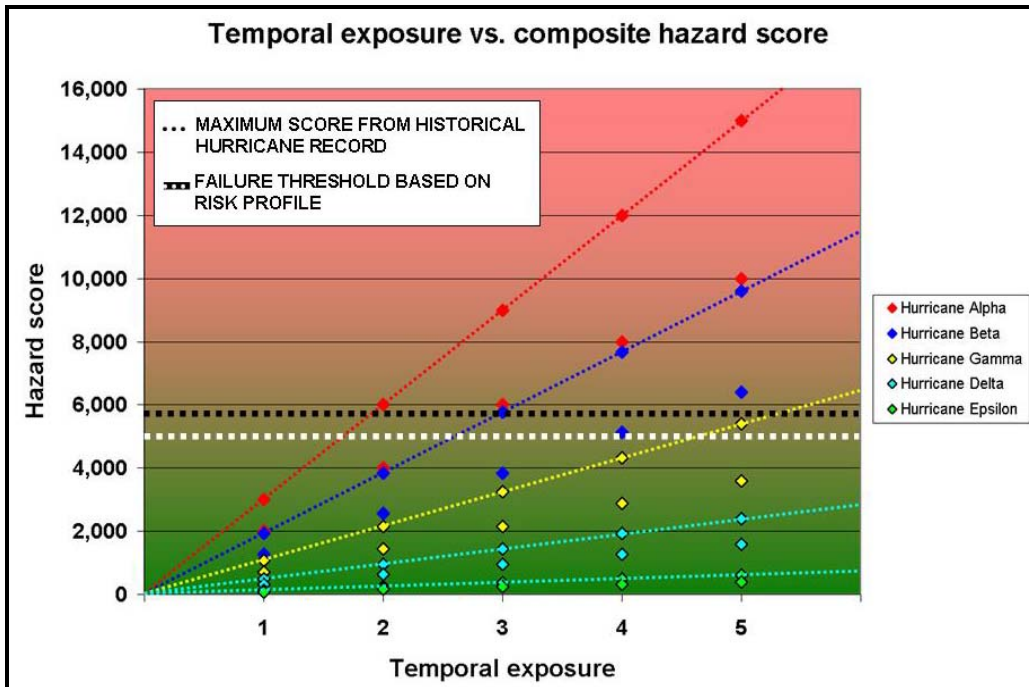


Figure 195: MRDF hurricane temporal exposure vs. composite hazard score

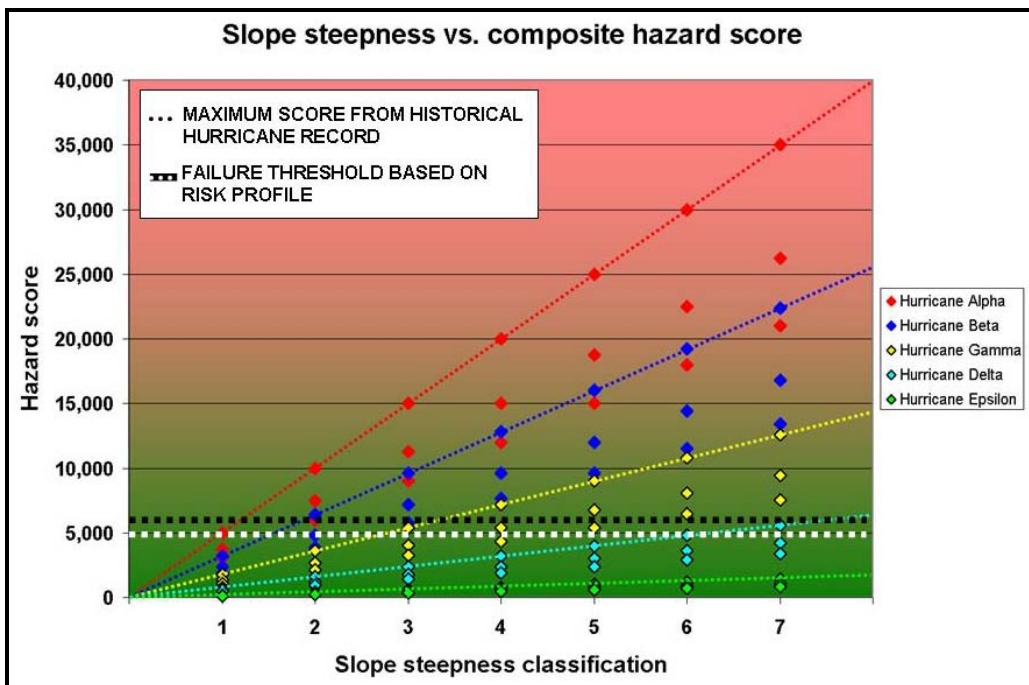


Figure 196: MRDF slope steepness vs. composite hazard score

Given these risk parameters, however, it should be pointed out that this total risk model represents a scoping, first pass attempt to place various hazard and risk factors across the MRDF into a total risk model appropriate for the MRDF environment. A more robust scaling matrix is required that can more effectively isolate variables linked to submarine shelf failure hazards. Additional statistical analyses, such as regression comparisons, should be performed to provide additional texture to hazard and risk results and to identify the parameters that are truly statistically significant

#### **9.4 Risk Results Application Guidelines**

The risk results contained in this chapter can be used by a variety of decision-makers when considering potential platform and pipeline routing locations.

With respect to pipelines, and as evidenced in Section 9.2.4, they can be considered at risk when located downdip of antecedent and relatively fresh mudflow lobes and therefore be exposed to perpendicular stresses. Pipelines can also be considered at risk if they cross or lie within mudflow gullies and therefore be exposed to tensile stresses. The risks increase proportionately given the factors that comprise the hazard and total risk scores for hurricanes of varying intensity. Operators should use these results in order to minimize potential risk with respect to where pipeline routes are eventually located. Given the mudslide runout calculations performed in Sections 6.4.1 and 6.4.2, pipelines can be routed to ensure adequate distance away and downdip from potential slides given assumptions on previous mudslide length, underlying topography, viscosity and mudflow slurry density.

With respect to platforms, these results can be used to determine the safest locations (i.e., areas least prone to failure) in the event of severe hurricanes. The safety factor calculations described in Section 6.3.2 offer specific guidance in potential seafloor behavior given hurricanes of varying intensity. However, the work in this dissertation also illuminates the widely varying soil conditions prevalent within the MRDF, and a sufficiently rigorous geotechnical program should be undertaken as part of any platform location exercise.

Lastly, offshore operators are often faced with decisions regarding evacuations and the safety of offshore personnel when tropical storms and hurricanes approach their facilities. Despite the results outlined in this chapter and the fact that they illuminate the risks of potential submarine seafloor movement, they are not intended to be, nor should they be used as, a proxy for making decisions with respect to the personal safety of offshore personnel.

## CHAPTER 10. CONCLUSIONS

### 10.1 Key Project Conclusions

Several hypotheses regarding submarine shelf failure and the conditions under which it is initiated were outlined in Chapters 1 and 2. The evaluation of these hypotheses helped guide this research and culminated in several original contributions to knowledge involving subaqueous mudslides along the Mississippi River Delta Front (MRDF). They include:

- Observed bulk wave and bottom boundary layer conditions during Hurricanes Ivan and Katrina were used to calibrate a series of MIKE 21 numerical wave models that were subsequently used to estimate conditions for earlier MRDF hurricanes with no direct or reliable observations (Betsy, Camille and Andrew). Model calibration was carried out by adjusting model inputs to derive results similar to those obtained from offshore National Data Buoy Center (NDBC) buoys and from wind field calculations based on prior hindcast models. Significant wave height ( $H_{s_{max}}$ ) and wave period exceeded 15 m and 12 sec, respectively, during recent hurricanes. Prior-hurricane MIKE 21 models revealed varying levels of metocean impact depending on storm intensity and proximity of individual hurricane tracks to the MRDF. In addition to storm intensity, a major factor in MRDF failures includes forward speed, thereby influencing temporal exposure to severe hurricane conditions for a given area.
- Spectral frequency data help quantify pre-storm effects long before hurricane arrival at the MRDF. These findings represent one of the major results of this research. During Hurricane Katrina, a transition from higher-frequency to lower-frequency spectra was observed at several NDBC buoys approximately 48 hours prior proximal passage of the hurricane, indicating a range of slightly less than 0.20 Hz to approximately 0.14 Hz from the east and southeast. Pre-storm spectra were not recorded at lower frequencies for these buoys during Katrina; however, they likely portray the available wave spectra accurately. At peak hurricane proximity to each

buoy, frequencies decreased to approximately 0.06 Hz. These frequencies correspond roughly to wave periods of 16-17 sec and compare favorably to wave periods measured during Hurricane Katrina. In addition, pre-storm spectra for Hurricane Ivan at several NDBC buoys appear bimodal. Two foci of energy appear, one from approximately 0.12 Hz to 0.20 Hz, and another around 0.07 Hz, possibly representing a combination of remotely generated swells and local wind-generated sea waves.

- Temporal seafloor change can be quantified by comparing a mix of regional bathymetry and local bathymetry acquired during site-specific geohazard surveys, some of which were repeated in time. Significant differences in bathymetry exist both on a regional scale, exacerbated by prior seafloor failures as well as overall sedimentation rates associated with Mississippi River progradation, as well as on a local scale revealed by comparisons of local bathymetry through time. This dissertation drew extensively upon bathymetry and shallow subsurface seismic data that are not publicly available but for which approval was granted for use. This interrelated network of regional and local data helped quantify the morphological response associated with submarine shelf failure.
- Bathymetry effects at Mississippi Canyon during Hurricane Katrina were evaluated to determine the influence of the canyon on possible wave energy. A distinct pattern of increasing  $H_{s_{max}}$  was noted in the canyon with increasing water depth and distance away from the coast as well as from the protective screen of the Mississippi River Delta, which would have restricted the fetch area at the height of the storm given Katrina's counter-clockwise flow. The amount of energy expended within a relatively short spatial period can be considerable and may be responsible for disproportionate infrastructure damage in the West Delta and Grand Isle Protraction Areas during Hurricane Katrina.



- Lithological and geotechnical parameters comprise a significant part of the triggering mechanism required to initiate hurricane-induced MRDF shelf failure. Variation in differential pressure along the seafloor due to bulk wave impact contributes to a full set of physical process conditions that govern hurricane-initiated subaqueous shelf failure. These conditions include bottom shear stress, which was modeled as part of the MIKE 21 numerical wave model run for each hurricane studied. The models revealed that higher bottom stresses coincided with shallower along offshore shoals. The outer limit of increased shear stress coincides roughly with the 100-meter isobath for each storm; the highest stresses coincide roughly with the 25-meter isobath.
- Considerable variation exists in shear strength properties from block to block, and even locally. However, the correlation of weaker shear strengths to areas of known failure is not clear, likely due to when the data were collected and due to wide variations in near-surface sediment properties across the MRDF.
- Safety factors computed along an MRDF cross-sectional profile and compared to results of known hurricane-initiated seafloor failure revealed that soil conditions can yield highly variable safety factors and geotechnical properties depending on borehole location and hurricane intensity. Seafloor safety factors at SP 60 and SP 70 ranged at or above 1.0 yet seafloor failure occurred within both blocks, leading to the hypothesis that locally variable conditions likely account for lower safety factors. In addition, sub-1.0 safety factors at SP 6 at least 24 hours prior to Katrina's maximum impact suggest that seafloor failure risk exists not only during maximum hurricane impact but also far in advance, and especially closer to shore where wavelengths and wave periods are higher in shallower water. Likewise, low safety factors continued at the SP 6 location at least 12 hours after Katrina had passed, suggesting that seafloor failure risk remains even during post-storm sea-state recovery.

- Past failures were evaluated via one-dimensional sediment failure models (BING) to match observed thickness and lateral extent downdip. The calibrated models were then used to predict potential future changes in seafloor morphology in the vicinity of past failures and identify elements at risk in the paths of future mudslides. Results indicate that mudslide thickness at shorter lengths had less effect on eventual runout distance than at longer lengths. Total elapsed times at shorter mudslide lengths were grouped much closer together than those of longer mudslides; times for the thickest slides surpassed thinner slides by over a 3:1 ratio. Maximum mudflow velocities attained were higher with increased mudslide thickness but were widely variable depending on initial mudslide length (i.e., the maximum velocity attained was not length-dependent). This dissertation represents the first attempt at modeling failures to determine past history and potential future extent.
- MRDF failure potential was placed into an overall risk framework that clearly outlines the hazard, consisting of triggering, revealing and predisposition factors, the elements at risk involved (offshore infrastructure at risk and its value) and vulnerability. Hazard factors were mapped and integrated into a multiplicative matrix to derive a total risk score calibrated to prior MRDF hurricanes. Risk scores indicated that Hurricanes Ivan and Camille contained the highest risk along with the Last Island Hurricane of 1856. A second tier of risked hurricanes includes Hurricanes Katrina, Opal, Carmen, and the New Orleans Hurricane of 1915. Interestingly, this second tier does not include Hurricanes Hilda or Betsy, which were responsible for moderate infrastructure damage levels in the GOM (albeit due to wave activity, not submarine shelf failure, and to platform standards that were insufficient to safeguard against high sea-state energy levels). This risk model was subsequently used to characterize the effects from five hypothetical hurricanes of varying intensity to impact the MRDF in the future. These tests revealed that that

Hurricane Alpha (most intense) and marginally Hurricane Beta would initiate conditions susceptible to seafloor failure. This dissertation represents the first attempt at scoring MRDF seafloor impact within a risk framework that clearly outlines potential future potential hurricane impact.

## **10.2 Recommendations for Future Study**

Through the research carried out in this dissertation, several key opportunities for further work have been identified. They include research both in terms of additional data that could be collected as well as additional studies that could help better quantify subaqueous shelf failure. These recommendations include:

- This dissertation relies on numerous local bathymetry datasets collected over a wide area of the MRDF over an approximately 40-year period. This study also relies on three regional MRDF bathymetry datasets that are widely separated in time. A coordinated effort should be undertaken by industry and/or academia to update regional MRDF bathymetry so that the effects of recent hurricanes can be better understood on a regional scale. Data acquired should also be of a sufficient resolution to permit detailed evaluation of seafloor bathymetry. Such an acquisition will be expensive but may be money well spent.
- The 1D numerical model (BING) used in quantifying shelf failure does not take hydroplaning into account. An updated version of BING now takes hydroplaning into account and should be used in evaluating the potential for submarine mudflows to extend much farther than expected. The actual runout distances of individual mudflows often exceeded modeled results, and efforts should be made to better quantify abnormally high runout potential.
- A more robust evaluation of the probabilities associated with hazard definition should be attempted, either through a Monte Carlo simulation or another package that can

adequately evaluate all the different outcome combinations associated with submarine sediment failure and their effects.

- The total risk model presented in Chapter 9 represents a scoping, first pass attempt to place various hazard and risk factors into a total MRDF risk model. A more robust scaling matrix is required that can more effectively isolate variables comprising submarine shelf failure hazards. Additional statistical analyses, such as regression comparisons, should be performed to provide additional texture to hazard and risk results and to identify the parameters that are truly statistically significant.
- Additional *in situ* observations of wave fields along Mississippi Canyon should be undertaken to further explore the role that canyon bathymetry plays in effectively trapping hurricane-generated waves. In addition, a better understanding of the dynamics associated with intercanyon turbulence in Mississippi Canyon could help further refine models that link wave energy during severe storms to updip oceanographic effects observed on the shelf.

## REFERENCES

- Adams, C.E. and Roberts, H.H., 1993. A model of the effects of sedimentation rate on the stability of Mississippi Delta sediments. *Geo-Marine Letters*, 13: 17-23.
- Alexander, D.E., 2002. *Principles of Emergency Planning and Management*. Oxford University Press, New York, 340 pp.
- Allison, M.A., Sheremet, A., Goni, M.A. and Stone, G.W., 2005. Storm layer deposition on the Mississippi-Atchafalaya subaqueous delta generated by Hurricane Lili in 2002. *Continental Shelf Research*, 25: 2213-2232.
- Alvarado, A., 2006. *Update on MMS Regulatory Issues for Offshore Operators*. Available at: <http://www.southerngas.org/EVENTS/documents/SGAOGO06Alvarado.pdf>.
- American Petroleum Institute (API), 1993. *Recommended Practice for Planning, Designing and Constructing Fixed Offshore Platforms*. API Recommended Practice 2A (RP 2A)-LRFD, 224 pp.
- \_\_\_\_\_, 2000. *Recommended Practice for Planning, Designing and Constructing Fixed Offshore Platforms*. API Recommended Practice 2A (RP 2A)-WSD, 226 pp.
- Aquatronics, Inc./Decca Survey Systems, Inc., 1973. "Multi-Pak" Marine Engineering/Exploration Survey, Blocks 29, 30, 35, 36, 46, 47, 48, 52 and 53, South Pass Area, Louisiana. Houston, 5 pp.
- Arco Oil and Gas Company, 1987. *A High Resolution Geophysical Survey Report of South Pass Area Block 52, OCS-G-7796*. Houston, 15 pp.
- \_\_\_\_\_, 1988. *A High Resolution Geophysical Survey Report of South Pass Area Block 50 and 51*. Bathymetry map only; no other data available.
- \_\_\_\_\_, 1990. *A High Resolution Geophysical Report of South Pass Blocks 50 and 51 (OCS-G-9699 and 9700)*. ARCO Oil and Gas Company, Houston, 21 pp.
- \_\_\_\_\_, 1991a. *A High Resolution Geophysical Report of Main Pass (South & East Addition) Block 308 (OCS-G-13038) & Viosca Knoll Blocks 814 and 815 (OCS-G-13061 and G-13062)*. Houston, 11 pp.
- \_\_\_\_\_, 1991b. *A High Resolution Geophysical Report of a Proposed Pipeline Route, South Pass 52 to Mississippi Canyon 148*. Houston, 7 pp.
- \_\_\_\_\_, 1991c. *A High Resolution Geophysical Report of West Delta Block 129 (OCS-G-12070)*. Houston, 13 pp.
- \_\_\_\_\_, 1992. *A High Resolution Geophysical Report and Cultural Resource Assessment of West Delta Area Blocks 26 & 49 (OCS-G-10874 & 10877)*. Houston, 28 pp.
- \_\_\_\_\_, 1993a. *A High Resolution Geophysical Report of South Pass Block 56 (OCS-G-13646)*. Houston, 13 pp.

- \_\_\_\_\_, 1993b. *A High Resolution Geophysical Report of West Delta (South Addition) Block 149 (OCS-G-12075)*. Houston, 9 pp.
- \_\_\_\_\_, 1994. *A High Resolution Geophysical Report of West Delta Block 102 (OCS-G-13947)*. Houston, 12 pp.
- Arnold, K.E., 1967. *Soil movements and their effects on pipelines in the Mississippi Delta Region*. M.S. Thesis, Tulane University, New Orleans, 75 pp.
- Arpe, K. and Leroy, S.A.G., 2008. Atlantic hurricanes – testing impacts of local SSTs, ENSO, stratospheric QBO – implications for global warming. *Quaternary International*, 195: 4-14.
- Austin, D., Carriker B., McGuire T., Pratt J., Priest T., and Pulsipher, A. G., 2004. *History of the Offshore Oil and Gas Industry in Southern Louisiana: Interim report; Volume I: Papers on the Evolving Offshore Industry (OCS Study MMS 2004-049)*. U.S. Dept. of the Interior, Minerals Management Service, Gulf of Mexico OCS Region, New Orleans, 102 pp.
- Bea, R.G., 1971. How sea floor slides affect offshore structures. *Oil and Gas Journal*, 69 (November 29, 1971): 88-92.
- \_\_\_\_\_, 1974. Gulf of Mexico hurricane wave heights. *Proceedings of the Offshore Technology Conference*, 6: 791-810.
- \_\_\_\_\_, 1998. Reliability characteristics of a platform in the Mississippi River Delta. *Journal of Geotechnical and Geoenvironmental Engineering*, 124: 729-738.
- \_\_\_\_\_, 2002. Human and organizational factors in reliability assessment and management of offshore structures. *Risk Analysis* 22(1): 29-45.
- \_\_\_\_\_, 2006. Reliability and human factors in geotechnical engineering. *Journal of Geotechnical and Geoenvironmental Engineering*, 132(5): 631-643.
- Bea, R.G. and Arnold, P., 1973. Movements and forces developed by wave-induced slides in soft clays. *Proceedings of the Offshore Technology Conference*, 5: 731-742.
- Bea, R.G. and Audibert, J.M.E., 1980. Performance of offshore platforms and pipelines in the Mississippi River Delta. *Journal of Geotechnical Engineering*, American Society of Civil Engineering, New York, New York.
- Bea, R.G., Audibert, J.M.E., Lai, N.W. and Schafer, D., 1980. An assessment of facilities siting – South Pass Blocks 42/43. In: D.W. Folger and J.C. Hathaway (Editors), *Conference on Continental Margin Mass Wasting and Pleistocene Sea-Level Changes, August 13-15, 1980*. U.S. Geological Survey Circular 961, 9 pp.
- Bea, R.G. and Aurora, R.P., 1983. Design of pipelines in mudslide areas. *Proceedings of the Offshore Technology Conference*, 15: 1985-1995.
- Bea, R.G. and Bernard, H.A., 1973. Movements of bottom soils in the Mississippi Delta offshore. *Lafayette Geological Society Special Publication*, 13-28.

- Bea, R.G., Bernard, H.A., Arnold, P. and Doyle, E.H., 1975. Soil movements and forces developed by wave-induced slides in the Mississippi delta. *Journal of Petroleum Technology*, 27: 500-514.
- Bea, R.G., Wright, S.G., Sircar, P. and Niedoroda, A.W., 1980. Wave-induced slides in South Pass Block 70, Mississippi Delta. *Journal of Geotechnical Engineering*, 109: 619-644.
- Benfield Group Limited, 2005. A 65-Year History of Hurricanes and Some of their Resultant Impacts on the Offshore Industry. Benfield Corporate Risk, London, UK, 5 pp.
- Best, A.I., Clayton, C.R.I., Longva, O. and Szuman, M., 2003. The role of free gas in the activation of submarine slides in Finneidfjord. In: J. Locat and J. Mienert (Editors), *Submarine Mass Movements and Their Consequences*. Kluwer Academic Publishers, Dordrecht, The Netherlands, pp. 491-498.
- Bohlke, B.M. and Bennett, R.H., 1980. Mississippi prodelta crusts: a clay fabric and geotechnical analysis. *Marine Geotechnology*, 4(1): 55-82.
- Blumberg, R., 1965. An oceanographer looks at Hurricane Betsy. *World Oil*, 159(6): 11-25.
- \_\_\_\_\_, 1974. Hurricane winds, waves and currents test marine pipeline design. *Pipeline Industry* (Reprint), June-November, 1974.
- Booth, J.S., 1979. Recent history of mass-wasting on the upper continental slope, northern Gulf of Mexico, as interpreted from the consolidation states of the sediment. In: L.J. Doyle and O.H. Pilkey (Editors), *Geology of continental slopes*. Society of Economic Paleontologists and Mineralogists Special Publication 27, Tulsa, Oklahoma, pp. 153-164.
- Brooks, J.M. and Sackett, W.M., 1973. Sources, sinks and concentrations of light hydrocarbons in the Gulf of Mexico. *Journal of Geophysical Research*, 78: 5248-5258.
- Bryn, P., Solheim, A., Berg, K., Lien, R., Forsberg, C.F., Haflidason, H., Ottosen, D. and Rise, L., 2002. The Storegga slide complex: repeated large scale sliding in response to climatic cyclicity. In: J. Locat and J. Mienert (Editors), *Submarine Mass Movement and Their Consequences*. Advances in Natural and Technological Hazard Research, pp. 215-222.
- Buczkowski, B.J., Reid, J.A., Jenkins, Chris J., Reid, J.M., Williams, S.J. and Flocks, J.G., 2006. usSEABED: Gulf of Mexico and Caribbean (Puerto Rico and U.S. Virgin Islands) Offshore Surficial Sediment Data Release. United States Geological Survey Data Series 146, Version 1.0. Washington, D.C., 50 pp.
- \_\_\_\_\_, 2005. *High-Resolution Survey of the Main Pass Oil Gathering System, Offshore Louisiana*. Lafayette LA, 10 pp.
- Cardone, V.J., Cox, A.T. and Forristall, G.Z., 2007. Hindcast of winds, waves and currents in northern Gulf of Mexico in Hurricanes Katrina (2005) and Rita (2005). *Proceedings of the Offshore Technology Conference*, Paper No. 18652.
- Cardone, V.J., Cox, A.T., Lisaeter, K.A. and Szabo, D., 2004. Hindcast of winds, waves and current in the northern Gulf of Mexico in Hurricane Lili (2002). *Proceedings of the Offshore Technology Conference*, Paper No. 16821.



- Cardone, V.J., Jensen, R.E., Resio, D.T., Swail, V.R. and Cox, A.T., 1996. Evaluation of contemporary ocean wave models in rare extreme events: Halloween storm of October 1991; Storm of the century of March 1993. *Journal of Atmospheric and Oceanographic Technology*, 13: 198-230.
- Chaney, R.C. and Demars, K.R., 1984. Strength Testing of Marine Sediments: Laboratory and In-situ Measurements: A Symposium Sponsored by ASTM Committee D-18 on Soil Rock, San Diego, CA, 26-27 January 1984, 588 pp.
- Chouinard, L.E. and Liu, C., 1997. Model for recurrence rate of hurricanes in the Gulf of Mexico. *Journal of Waterway, Port Coastal and Ocean Engineering*, 123(3): 113-119.
- Chouinard, L.E., Liu, C. and Cooper, C.K., 1997. Model for severity of hurricanes in the Gulf of Mexico. *Journal of Waterway, Port Coastal and Ocean Engineering*, 123(3): 120-129.
- Coleman, J.M. and Garrison, L.E., 1977. Geological aspects of marine slope instability, northwestern Gulf of Mexico. *Marine Geotechnology*, 2: 9-44.
- Coleman, J.M. and Prior, D.B., 1978. Submarine landslides in the Mississippi River delta. *Proceedings of the Offshore Technology Conference*, 10: 1067-1072.
- \_\_\_\_\_, 1980a. Marine sediment instabilities in the Mississippi River delta. In: *Forefronts of Ocean Technology*, Marine Technical Society, Washington, D.C., pp. 12-114.
- \_\_\_\_\_, 1980b. *Subaqueous sediment instabilities in the offshore Mississippi River delta*. BLM Open File Report 80-01, The United States Department of the Interior Bureau of Land Management, New Orleans, 60 pp.
- \_\_\_\_\_, 1988. Mass wasting on continental margins. *Annual Review of Earth and Planetary Sciences*, 16: 101-119.
- Coleman, J.M., Prior, D.B. and Garrison, L.E., 1980. Subaqueous sediment instabilities in the offshore Mississippi River delta. In: L.R. Handley (Editor), *Environmental Information on Hurricanes, Deep Water Technology, and Mississippi Delta Mudslides in the Gulf of Mexico*. U.S. Department of Labor, Bureau of Land Management, Open File Report 80-02, 171 pp.
- \_\_\_\_\_, 1983. Deltaic influences on shelf edge instability processes. In: D.J. Stanley and G.T. Moore (Editors), *The Shelf Break: Critical Interface on Continental Margins*. Society of Economic Paleontologists and Mineralogists Special Publication 33, Tulsa, Oklahoma, pp. 121-137.
- Coleman, J.M. and Roberts, H.H., 1988a. Late Quaternary depositional framework of the Louisiana Continental Shelf and upper Continental Slope. *Transactions of the Gulf Coast Association of Geological Societies*, 38: 407-419.
- \_\_\_\_\_, 1988b. Sedimentary development of the Louisiana continental shelf related to sea level cycles: Part I – Sedimentary sequences. *Geo-Marine Letters*, 8: 63-108.
- Coleman, J.M., Roberts, H.H. and Stone, G.W., 1998. Mississippi River Delta: an overview. *Journal of Coastal Research*, 14(3), 699-716.

- Coleman, J.M., Suhayda, J.N., Whelan III, T. and Wright, L.D., 1974. Mass movement of Mississippi River delta sediments. *Transactions of the Gulf Coast Association of Geological Societies*, 24: 49-68.
- Comap Geosurveys, Inc., 1984. Geological Hazards Survey, West Delta Blocks 129 and 144 for Exxon Company USA. Project No. A4891/2. Houston, 22 pp.
- Cooper, A.K. and Hart, P.E., 2003. High-resolution seismic reflection investigation of the northern Gulf of Mexico gas-hydrate stability zone. *Marine and Petroleum Geology*, 19 (2003): 1275-1293.
- Cox, A.T., Cardone, V.J., Counillon, F. and Szabo, C., 2005. Hindcast study of winds, waves and currents in the northern Gulf of Mexico in Hurricane Ivan. *Proceedings of the Offshore Technology Conference*, Paper No. 17736.
- Coyne, M.J. and Dollar, J.J., 2005. Shell Pipeline's response and repairs after Hurricane Ivan. *Proceedings of the Offshore Technology Conference*, Paper No. 17734, 10 pp.
- Crozier, M.J. and Glade, T., 2005. Landslide hazard and risk: issues, concepts and approach. In: T. Glade, M. Anderson and M.J. Crozier (Editors), *Landslide Hazard and Risk*. J. Wiley, Hoboken, New Jersey, 802 pp.
- Daemrich, K.-F., Mai, S., Ohle, N. and Tautenhain, E., 2004. Influence of spectral density distribution on wave parameters and simulation in time domain. 2nd Chinese-German Joint Symposium on Coastal and Ocean Engineering, October 11-20, 2004, Nanjing, China.
- Dalrymple, R.A. and Liu, P., 1978. Waves over soft muds: a two-layer fluid model. *Journal of Physical Oceanography*, 8: 1121-1131.
- Daniels, G.R., 1994. *Hurricane Andrew's Impact on Natural Gas and Oil Facilities on the Outer Continental Shelf: Interim Report, as of November 1993*. OCS Report MMS 94-0031, The United States Department of the Interior, Minerals Management Service, Engineering and Technology Division, Herndon, Virginia, 49 pp.
- De Blasio, F.V., Elverhoi, A., Issler, D., Harbitz, C.B., Bryn, P. and Lien, R., 2005. On the dynamics of subaqueous clay-rich gravity mass flows – the giant Storegga slide, Norway. *Marine and Petroleum Geology*, 22 (1/2): 179-86.
- De Blasio, F.V., Harbitz, C.B. and Lien, R., 2004. Flow models of small- to medium-scale debris flows originating from compacted clay materials. *Marine Geology*, 213: 439-455.
- Decca Survey Systems, Inc., 1975. *A Multi-Sensor Engineering Survey of a Portion of Main Pass Area Block 59 for Amoco Production Company*. Houston, 16 pp.
- Den Norske Veritas, 2007. *Pipeline Damage Assessment from Hurricanes Katrina and Rita in the Gulf of Mexico*. MMS Project No. 581, Houston, 104 pp.
- Dengler, A.T., Wilde, P., Noda, E.K. and Normark, W.R., 1984. Turbidity currents generated by Hurricane Iwa. *Geo-Marine Letters*, 4: 5-11.
- DHI Software, 2005. MIKE 21 SW Spectral Waves FM Module User Guide.

- DiMarco, S.F., Kelly, F.J., Zhang, J. and Guinasso, N., 1995. Directional wave spectra on the Louisiana-Texas Shelf during Hurricane Andrew. *Journal of Coastal Research*, Special Issue 21, 295-305.
- Dingle, R.V., 1977. The anatomy of a large submarine slump on a sheared continental margin (SE Africa). *Journal of the Geological Society of London*, 134 (3), 293-310.
- Dott, R.H., 1963. Dynamics of subaqueous gravity depositional processes. *American Association of Petroleum Geologists Bulletin*, 47: 104-128.
- Dunlap, W., Holcombe, L. and Holcombe, T., 2004. *Shear Strength Maps of Shallow Sediments in the Gulf of Mexico*. MMS/OTRC Cooperative Research Agreement 1435-01-99-CA-31003, Task Order 17007, Project 367, 14 pp.
- Dunn, G.E., Moore, P.L., Clark, G.B., Frank, N.L., Hill, E.C., Kraft, R.H. and Sugg, A.L., 1965. The hurricane season of 1964. *Monthly Weather Review*, 93(3): 175-187.
- Earle, M.D., 1975. Extreme wave conditions during Hurricane Camille. *Journal of Geophysical Research*, 80 (3): 377-379.
- Edris, H.H., 1988. Special lecture: evaluation of risks associated with slope instability. In: C. Bonnard (Editor), *Proceedings of the 5<sup>th</sup> Symposium on Landslides*. Balkema, Rotterdam, pp. 1491-1496.
- Einstein, H.H., 1988. Special lecture: landslide risk assessment procedure. In: C. Bonnard (Editor), *Proceedings of the 5<sup>th</sup> Symposium on Landslides*. Balkema, Rotterdam, pp. 1037-1058.
- Emrich, W.J., 1971. Performance study of soil sampler for deep-penetration marine borings. In: *Sampling of Soil and Rock*, ASTM Special Technical Publication 483, American Society for Testing and Materials, Philadelphia, PA, pp. 30-50.
- Energco Engineering, Inc., 2006. *Assessment of Fixed Offshore Platform Performance in Hurricanes Andrew, Lili and Ivan*. MMS Project No. 549, Houston, 90 pp.
- \_\_\_\_\_, 2007. *Assessment of Fixed Offshore Platform Performance in Hurricanes Katrina and Rita*. MMS Project No. 578, Houston, 59 pp.
- Enterprise Products Partners, LLC, 2005. *Multi-beam bathymetry data, South Pass 53 to Viosca Knoll 985 Pipeline Route*. Digital data only.
- Environmental Geosciences, 1987. *Shallow Geohazards Study Based on a High-Resolution Geophysical Survey of West Delta Block 72, OCS-G-1082, Gulf of Mexico*. Report prepared for Exxon Company, USA Offshore/Alaska Division. The Woodlands, TX, 10 pp.
- Esrig, M.I., Ladd, R.S. and Bea, R.G., 1975. Material properties of submarine Mississippi Delta sediments under simulated wave loadings. *Proceedings of the Offshore Technology Conference*, Paper No. 2188.
- Fernandez-Partagas, J. and Diaz, H.F., 1996. Atlantic hurricanes in the second half of the 19<sup>th</sup> century. *American Meteorological Society Bulletin*, 77(12): 2899-2906.

- Fine, I.V., Rabinovich, A.B., Bornhold, B.D., Thomson, R.E. and Kulikov, E.A., 2005. The Grand Banks landslide-generated tsunami of November 18, 1929: preliminary analysis and numerical modeling. *Marine Geology*, 215: 45-57.
- Fisk, H.N. and McClelland, B., 1959. Geology of continental shelf off Louisiana: its influence on offshore foundation design. *Geological Society of America Bulletin*, 10: 1369-1394.
- Forristall, G.Z., 2007a. Wave crest heights and deck damage in Hurricanes Ivan, Katrina and Rita. *Proceedings of the Offshore Technology Conference*, Paper No. 18620.
- Forristall, G.Z., 2007b. Comparing hindcasts with wave measurements from Hurricanes Lili, Ivan, Katrina and Rita. *10<sup>th</sup> International Workshop on Wave Hindcasting and Forecasting and Coastal Hazard Symposium*, Oahu HI, November 11-16, 2007.
- Forristall, G.Z., Reece, A.M., Thro, M.E., Ward, E.G., Doyle, E.H. and Hamilton, R.C., 1985. Measurements of sea wave attenuation due to deformable bodies: The SWAMP Experiment. *Journal of Geophysical Research*, 90: 3367-3380.
- Frazier, D.E., 1974. *Depositional Episodes – Their Relationship to the Quaternary Stratigraphy Framework in the Northwestern Portion of the Gulf Basin*. Texas Bureau of Economic Geology Circular 74-1, 28 pp.
- Froehlich, A.J., Garnas, A.D. and Van Dreil, J.N., 1978. Franconia area: Fairfax County, Virginia: planning a new community in an urban setting. In: G.D. Robinson and A.M. Spieker (Editors), *Nature to be Commanded – Earth Science Maps Applied to Land and Water Management*. Geological Survey Professional Paper 950, U.S. Government Printing Office, Washington DC, pp. 69-89.
- Fugro GeoServices, Inc., 2004. *High-Resolution Survey of the Main Pass Oil Gathering System, Offshore Louisiana*. Houston, 12 pp.
- \_\_\_\_\_, 2005a. *Anchor Clearance Survey, Block 70 (OCS-G-00182) and Block 94 (OCS-G-00839), West Delta Area*. Report prepared for BP America Inc., Report No. 2405-1293, Houston, 1 pp.
- \_\_\_\_\_, 2005b. *Structure Investigation Survey, OCS-G-00839 “G” Structure, Block 94, West Delta Area*. Report prepared for BP America Inc., Report No. 2405-1278-WD94G, Houston, 1 pp.
- \_\_\_\_\_, 2005c. *High-Resolution Survey of the Main Pass Oil Gathering System, Offshore Louisiana*. Houston, 12 pp.
- Gauer, P., Elverhoi, A., Issler, D and De Blasio, F., 2006. On numerical simulations of subaqueous slides: back-calculations of laboratory experiments of clay-rich slides. *Norwegian Journal of Geology*, 86: 295-300.
- Gauer, P., Kvalstad, T.J., Forsberg, C.F., Bryn, P and Berg, K., 2005. The last phase of the Storegga Slide: simulation of retrogressive slide dynamics and comparison with slide-scar morphology. *Marine and Petroleum Geology*, 22: 171-178.

- Geoscience Earth & Marine Services, Inc. (GEMS), 2006. *Regional Northern Gulf of Mexico Bathymetry Map*. Houston; 1 plate.
- Gilbert, R.B., 2003. Risk assessment for slope failures – what is this reference?
- Gilbert, R.B., Nodine, M.C., Wright, S.G., Cheon, J.Y., Wrzyszczyński, M., Coyne, M. and Ward, E.G., 2007. Impact of hurricane-induced mudslides on pipelines. *Proceedings of the Offshore Technology Conference*, Paper No. 18983.
- Gray, W.M., Landsea, C.W., Mielke, P.W. and Berry, K.J., 1993. Predicting Atlantic Basin seasonal tropical cyclone activity by 1 August. *Weather Forecasting*, 8: 73-86.
- Grozic, J.L., 2003. Liquefaction potential of gassy marine sands. In: J. Locat and J. Mienert (Editors), *Submarine mass movements and their consequences*. Kluwer Academic Publishers, Dordrecht, pp. 37-46.
- Grymes III, J.M. and Stone, G.W., 1995. A review of key meteorological and hydrological aspects of Hurricane Andrew. *Journal of Coastal Research* (SI), 21: 6-23.
- Haflidason, H., Nygaard, H., Torgersen, B. and Sulebakk, J.R., 2002. *Morphological analyses of the seafloor in the Storegga Slide Area*. Final Report to NorskHydro AS 100-03/02, Department of Geology, University of Bergen, Bergen, Norway.
- Hamilton, R.C. and Ward, E.G., 1974. Ocean Data Gathering Program – quality and reduction of data. *Proceedings of the Offshore Technology Conference*, 6: 749-770.
- Hance, J.J., 2003. *Development of a database and assessment of seafloor slope stability based on published literature*. M.S. Thesis, The University of Texas at Austin, 245 pp.
- Hansen, A., 1984. Landslide hazard analysis. In: D. Brunsden and D.B. Prior (Editors), *Slope Instability*. John Wiley & Sons Ltd., Chichester, UK, pp. 523-602.
- Hart Publications, 1997. *50 Years of Offshore Oil and Gas Development*. Hart Publications, Houston, 176 pp.
- Hartlen, J. and Viberg, L., 1988. General report: evaluation of landslide hazard. In: C. Bonnard (Editor), *Proceedings of the 5<sup>th</sup> Symposium on Landslides*. Balkema, Rotterdam, pp. 1037-1058.
- Hasselmann, K., 1974. On the spectral dissipation of ocean waves due to white-capping. *Boundary Layer Meteorology*, 6: 107-127.
- Hasselmann, S., Hasselmann, K., Allender, J.H. and Barnett, T.P., 1985. Computations and parameterizations of the non-linear energy transfer in gravity wave spectrum, Part II: Parameterizations of non-linear energy transfer for applications in wave models. *Journal of Physical Oceanography*, 15: 1369-1377.
- Helwick, S.J. and Bryant, W.R., 1978. Geotechnical characteristics of Mississippi Delta sediments, southeast Louisiana. *Marine Geotechnology*, 3(2): 183-198.

- Hemphill, T., Campos, W. and Pilehvari, A., 1993. Yield-power law model more accurately predicts mud rheology. *The Oil and Gas Journal*, 91(34): 45-50.
- Henkel, D.J., 1970. The role of waves in causing submarine landslides. *Geotechnique*, 20: 75-80.
- Hitchcock, C., Angell, M. Givler, R. and Hooper, J., 2008. Transport and depositional features associated with submarine mudflows, Mississippi Delta, Gulf of Mexico. *Transactions of the Gulf Coast Association of Geological Societies*, 58: Paper 801-9.
- Ho, F. P., Su, J. C., Hanevich, K. L., Smith, R. J. and Richards, F. P., 1987. *Hurricane climatology for the Atlantic and Gulf Coasts of the United States*. National Oceanic and Atmospheric Administration Technical Report NWS 38. National Oceanic and Atmospheric Administration, Washington DC.
- Hooper, J.R., 1980. Crustal layers in Mississippi Delta region of the Gulf of Mexico mudflows. *Proceedings of the Offshore Technology Conference*, Paper No. 3770.
- \_\_\_\_\_, 1996. Foundation soil motion in South Pass 47. *Proceedings of the Offshore Technology Conference*, Paper No. 7953.
- Hooper, J.R. and Suhayda, J.N., 2005a. Hurricane Ivan as a geologic force: Mississippi Delta Front seafloor failures. *Proceedings of the Offshore Technology Conference*, Paper No. 17737.
- \_\_\_\_\_, 2005b. Hurricane-induced seafloor failures in the Mississippi Delta. *Proceedings of the 2005 Offshore Hurricane Readiness Conference*, American Petroleum Institute, Houston TX, July 26-28, 2005.
- Hsiao, S.V. and Shemdin, O.H., 1980. Interaction of ocean waves with a soft bottom. *Journal of Physical Oceanography*, 10: 605-610.
- Hsu, S.A., 2006. Nowcasting the significant wave height during a hurricane. *Mariners Weather Log*, 50 (3): 1-3.
- Ilstad, T., De Blasio, F.V., Elverhoi, A., Harbitz, C.B., Engvik, L. Longva, O. and Marr, J.G., 2004. On the frontal dynamics and morphology of submarine debris flows. *Marine Geology*, 213: 481-497.
- Imran, J., Harff, P. and Parker, G., 2001a. A numerical model of submarine debris flows with graphical user interface. *Computers & Geosciences*, 27: 717-729.
- Imran, J., Parker, G., Locat, J. and Lee, H., 2001b. 1D numerical model of muddy subaqueous and subaerial debris flows. *Journal of Hydraulic Engineering*, 127: 959-968.
- IUGS – Working Group on Landslides, Committee on Risk Assessment, 1997. Quantitative risk assessment for slopes and landslides – the state of the art. In: D.M. Cruden and R. Fell (Editors), *Landslide Risk Assessment*, Balkema, Rotterdam, pp. 3-12.

- Ives, J.D. and Krebs, P.V., 1978. Natural hazards research and land-use planning responses in mountainous terrain: the town of Vail, Colorado, Rocky Mountains, USA. *Arctic and Alpine Research*. 10: 213-222.
- Janssen, P.A.E.M., 1989. Wave-induced stress and the drag of airflow over sea waves. *Journal of Physical Oceanography*, 19: 745-754.
- \_\_\_\_\_, 1991. Quasi-linear theory of wind-wave generation applied to wave forecasting. *Journal of Physical Oceanography*, 21: 1631-1642.
- John E. Chance & Associates, Inc., 1983. *Shallow Hazards Survey Report of Viosca Knoll Block 985 for Arco Exploration Company*. Houston, 44 pp.
- \_\_\_\_\_, 1984a. *Hazard Study of Block 53 (OCS-G-6793), South Pass Area, Offshore Louisiana for Arco Exploration Company*. Houston, 13 pp.
- \_\_\_\_\_, 1984b. *Hazard Study of Block 989 and Block 990, Viosca Knoll Area for Sohio Petroleum Company*. Houston, 12 pp.
- \_\_\_\_\_, 1988a. *Hazard Study of Blocks 305 and 306 (OCS-G-9373) for Freeport-McMoRan Resource Partners, Ltd.* Lafayette LA, 13 pp.
- \_\_\_\_\_, 1988b. *Hazard Study of Block 101 (OCS-G-9688), West Delta Area, Offshore Louisiana for Anadarko Petroleum Company*. Houston, 15 pp.
- \_\_\_\_\_, 1989. *A High Resolution Geophysical Survey Report of Main Pass Area, East and South Addition Block 292, OCS-G-10912, for Arco Oil and Gas Company*. Houston, 15 pp.
- \_\_\_\_\_, 1990a. *Hazard Study of Block 55 (OCS-G-10891) for FMP Operating Company*. Houston, 17 pp.
- \_\_\_\_\_, 1990b. *Hazard Study of Block 69, South Pass Area and Blocks 898 and 942, Viosca Knoll Area, for Amerada Hess Corporation*. Houston, 11 pp.
- \_\_\_\_\_, 1990c. *Hazard Study of Blocks 90 and 92 (OCS-G-12081 and 12082), South Pass Area for BP Exploration Inc.* Houston, 20 pp.
- \_\_\_\_\_, 1990d. *A High Resolution Geophysical Survey Report and Cultural Resource Assessment of Main Pass Area Block 149, OCS-G-12000, for Arco Oil and Gas Company*. Houston, 26 pp.
- \_\_\_\_\_, 1994. *A High Resolution Geophysical Report, Main Pass (South & East Addition), Blocks 294 and 295 (OCS # G-13036 and 13037) for Arco Oil and Gas Company*. Houston, 21 pp.
- \_\_\_\_\_, 1995. *A High Resolution Geophysical report & Cultural Resource Evaluation of South Pass Block 38 (OCS-G\_14572) for Vastar Resources, Inc.* Houston, 19 pp.
- Jordi, A. and Wang, D.P., 2008. Near-inertial motions in and around the Palamos submarine canyon (NW Mediterranean) generated by a severe storm. *Continental Shelf Research*, 28: 2523-2534.



- Jose, F., Kobashi, D. and Stone, G.W., 2007. Spectral Wave Transformation over an Elongated Sand Shoal off South-Central Louisiana, U.S.A. *Journal of Coastal Research, SI 50 (Proceedings of the 9th International Coastal Symposium)*, 757-761. Gold Coast, Australia.
- Jose, F. and Stone, G.W., 2006. Forecast of nearshore wave parameters using MIKE 21 spectral wave model. *Transactions of the Gulf Coast Association of Geological Societies*, 56: 323-327.
- Jose, F., Stone, G.W., Kobashi, D., Siadatmousavi, S.M. and Liu, B., 2009. Hydrodynamic response of a transgressive shoal to the proposed mining for restoring adjacent beaches and barriers: Sabine Bank off Louisiana-Texas coast, United States. *Coastal Dynamics '09*, (in press), Tokyo, Japan.
- Kaiser, M.J. 2007. The impact of extreme weather on offshore production in the Gulf of Mexico. *Applied Mathematical Modeling*, 32: 1996-2018.
- Keen, T.R. and Glenn, S.M., 1999. Shallow water currents during Hurricane Andrew. *Journal of Geophysical Research*, 104: 23,443-23,458.
- Keim, B.D., Muller, R.A. and Stone, G.W., 2004. Spatial and temporal variability of coastal storms in the North Atlantic Basin. *Marine Geology*, 210: 7-15.
- \_\_\_\_\_, 2007. Spatiotemporal patterns and return periods of tropical storm and hurricane strikes from Texas to Maine. *Journal of Climate*, 20: 3498-3509.
- Kesel, R.H., 2003. Human modifications to the sediment regime of the Lower Mississippi River flood plain. *Geomorphology*, 56(3-4): 325-334.
- Kindinger, J.L., 1988. Seismic stratigraphy of the Mississippi-Alabama shelf and upper continental slope. *Marine Geology*, 83: 79-94.
- \_\_\_\_\_, 1989. Depositional history of the Lagniappe Delta, northern Gulf of Mexico. *Geo-Marine Letters*, 9:59-66.
- Kindinger, J.L., Penland, S., Williams, S.J. and Suter, J.R., 1989. Inner shelf deposits of the Louisiana-Mississippi region, Gulf of Mexico. *Transactions of the Gulf Coast Association of Geological Societies*, 39: 413-420.
- Kinsella, Cook & Associates, Inc., 1989. *Geophysical Survey Report, Block 68, South Pass Area, East Addition, Offshore Louisiana (OCS-G-10892)*. Report prepared for Louisiana Land and Exploration Company. Baton Rouge, 11 pp.
- Knabb, R.D., Rhome, J.R. and Brown, D.P., 2005. *Tropical Cyclone Report: Hurricane Katrina, 23-30 August 2005* (online at [http://www.nhc.noaa.gov/pdf/TCR-AL122005\\_Katrina.pdf](http://www.nhc.noaa.gov/pdf/TCR-AL122005_Katrina.pdf)), National Hurricane Center, Miami, Florida, 43 pp.
- Kobashi, D., Stone, G.W., Khalil, S.M., Kerper, D., 2009. Impacts of sand removal from a shore-parallel Holocene transgressive shoal on hydrodynamics over the shoal and shoreface of barrier islands, south-central Louisiana, U.S.A. In: G.W. Stone (Editor), *Environmental Investigation of the Long-term Use of Ship Shoal Sand Resources for Large Scale Beach and Coastal Restoration in Louisiana*. OCS Study MMS 2009-024, 99-126.

- Komen, G.J., Cavaleri, L., Donelan, M., Hasselmann, K., Hasselmann, S. And Janssen, P.A.E.M., 1994. *Dynamics and Modeling of Ocean Waves*. Cambridge University Press, New York, 532 pp.
- Kraft, L.M., Suhayda, J.N., Helfrich, S.C. and Marin, J.E., 1990. Ocean wave attenuation due to soft seafloor sediments. *Marine Geotechnology*, 9: 227-242.
- Kunze, E., Rosenfeld, L.K., Carter, G.S. and Gregg, M.C., 2002. Inter waves in Monterey Submarine Canyon. *Journal of Physical Oceanography*, 32: 1890–1913.
- Lambert, D.E., 1956. Offshore operators look at Flossie's damage. *World Oil*, 151(6): 73-75.
- \_\_\_\_\_, 1964. Operators look at Hilda's damage. *World Oil*, 159(6): 11-25.
- \_\_\_\_\_, 1965. Hurricane Betsy – petroleum's most expensive storm. *World Oil*, 161(5), 11-20.
- Landsea, C.W., Pielke Jr., R.A., Mestas-Nunez, A.M. and Knaff, J.A., 1999. Atlantic basin hurricanes: indices of climate changes. *Climatic Change*, 42: 89-129.
- Layas, F.M., 1982. *Response and Stability of Ocean Floor Soils under Random Waves*. Ph.D. Dissertation, North Carolina State University, Raleigh, 158 pp.
- Lee, G.C., 1963. Offshore platform construction extended to 400-foot water depths. *Journal of Petroleum Technology*, April 1963: 385.
- Lee, H.J., Schwab, W.C., Edwards, B.D. and Kayen, R.E., 1991. Quantitative controls on submarine slope failure morphology. *Marine Geotechnology*, 10: 143-157.
- Leroueil, S., Locat, J., Levesque, C. and Lee, H.J., 2003. Towards an approach for the assessment of risk associated with submarine mass movements. *First International Symposium on Submarine Mass Movements and their Consequences*, April 2003, Nice, France, pp. 59-67.
- Leroueil, S., Vaunat, J., Picarelli, L., Locat, J., Faure, R. and Lee, H., 1996. A geotechnical characterisation of slope movements. *Proceedings of the 7<sup>th</sup> International Symposium on Landslides*. Balkema, Rotterdam, pp. 53-74.
- Lewis, K.B., 1971. Slumping on a continental slope inclined at 1°-4°. *Sedimentology*, 16: 97-110.
- Lindsay, J.F., Prior, D.B. and Coleman, J.M., 1984. Distributary-mouth bar development and role of submarine landslides in delta growth, South Pass, Mississippi delta. *American Association of Petroleum Geologists Bulletin*, 68: 1732-1743.
- Locat, J. and Lee, H.J., 2002. Submarine landslides: advances and challenges. *Canadian Geotechnical Journal*, 39: 193-212.
- Lowe, D.R., 1979. Sediment gravity flows: their classification and some problems of application to natural flows and deposits. In: L.J. Doyle and O.H. Pilkey (Editors), *Geology of*

*Continental Slopes*. Society of Economic Paleontologists and Mineralogists Special Publication 27, Tulsa, Oklahoma, pp. 75-82.

Ludwick, J.C., 1964. Sediments in northwestern Gulf of Mexico. In: R.L. Miller (Editor), *Papers in Marine Geology, Shepard Commemorative Volume*. Macmillan Company, New York, pp. 204-238.

Mannaerts, H.M., Guidroz, W.S., Scherschel, C.A., Weiland, R.J., Taylor, M. and Care, B., 2007. The role of ROV technology in offshore shallow geohazard observation and monitoring: environment stewardship in the Gulf of Mexico. *Proceedings of the 6<sup>th</sup> International Offshore Site Investigation and Geotechnics Conference: Confronting New Challenges and Sharing Knowledge*, 11-13 September 2007, London, UK.

Marine Technical Services, Inc., 1987. *Shallow Geohazards Study Based on a High-Resolution Geophysical Survey of West Delta Block 87, Gulf of Mexico*. Houston, 7 pp.

Masson, D.G., Harbitz, C.B., Wynn, R.B., Pedersen, G. and Lovholt, F., 2006. Submarine landslides: processes, triggers and hazard prediction. *Philosophical Transactions of the Royal Society: Mathematical, Physical and Engineering Sciences*, 364: 2009-2039.

Mayfield, M., Avila, L. and Rappaport, E.N., 1994. Atlantic hurricane season of 1992. *Monthly Weather Review*, 122(3): 517-538.

Mazzullo, J. and Bates, C., 1985. Sources of Pleistocene sand for the northeast Gulf of Mexico Shelf and Mississippi Fan. *Transactions of the Gulf Coast Association of Geological Societies*, 35: 457-466.

McAdoo, B.G., Pratson, L.F. and Orange, D.L., 2000. Submarine landslide geomorphology, US continental slope. *Marine Geology*, 169: 103-136.

McBride, R.A. and Byrnes, M.R., 1995. Surficial sediments and morphology of the southwestern Alabama/western Florida panhandle coast and shelf. *Transactions of the Gulf Coast Association of Geological Societies*, 45: 393-404.

McClelland Engineers, Inc., 1978. *Geotechnical Engineering Study, Block 148, Mississippi Canyon Area, Volume 1: Geologic Evaluations and Geotechnical Engineering Analyses*. Report prepared for Atlantic Richfield Company. Houston, 51 pp.

\_\_\_\_\_, 1982. *Soil and Foundation Investigation, Geology and Engineering Analyses, Block 77, Main Pass Area, Boring 3*. Report to Gulf Oil Exploration and Production Company, New Orleans, 16 pp.

\_\_\_\_\_, 1987. *Soil and Foundation Investigation, Block 52, South Pass Area, Gulf of Mexico, Volume 1: Investigation of Shallow Geologic Conditions*. Report No. 0585-5044, Ventura CA, 23 pp.

McGregor, B.A., 1981. Smooth seaward-dipping horizons – an important factor in seafloor stability. *Marine Geology*, 39: M89-M98.

Meade, R.H., 1996. River-sediment inputs to major deltas. In: Milliman, J., Haq, B. (Editors), *Sea-Level Rise and Coastal Subsidence*. Kluwer, London, pp. 63–85.

- Milliman, J.D. and Meade, R.H., 1983. World-wide delivery of river sediment to the ocean. *Journal of Geology*, 91: 1-21.
- Minerals Management Service, 2005a. *Oil and gas production in the Gulf of Mexico continues to stabilize; MMS issues damage assessment and review of Hurricane Ivan*. Minerals Management Service Office of Public Affairs New Release No. 3223. U.S. Department of the Interior, Washington, D.C., 2 pp.
- \_\_\_\_\_, 2005b. *Damage Caused by Hurricanes Katrina and Rita*. Minerals Management Service Notice to Lessees No. 2005-G20. U.S. Department of the Interior, Washington, D.C., pp. 1-2.
- \_\_\_\_\_, 2005c. *Hurricane Katrina/Hurricane Rita Evacuation and Production Shut-in Statistics Report as of Thursday, December 29, 2005*. Minerals Management Service Office of Public Affairs New Release No. 3447. U.S. Department of the Interior, Washington, D.C., pp. 1-2.
- \_\_\_\_\_, 2006a. *Impact Assessment of Offshore Facilities from Hurricanes Katrina and Rita*. Minerals Management Service Office of Public Affairs New Release No. 3418. U.S. Department of the Interior, Washington, D.C., pp. 1-11.
- \_\_\_\_\_, 2006b. *MMS Updates Hurricanes Katrina and Rita Damage*. Minerals Management Service Office of Public Affairs New Release No. 3486. U.S. Department of the Interior, Washington, D.C., pp. 1-11.
- \_\_\_\_\_, 2008. *Minerals Management Website, Gulf of Mexico Region*. U.S. Department of the Interior, Washington (available online at <http://www.gomr.mms.gov>).
- Mohrig, D., Elverhoi, A. and Parker, G., 1999. Experiments on the relative mobility of muddy subaqueous and subaerial debris flows, and their capacity to remobilize antecedent deposits. *Marine Geology*, 154: 117-129.
- Mohrig, D., Whipple, K.X., Hondzo, M., Ellis, C. and Parker, G., 1998. Hydroplaning of subaqueous debris flows. *Geological Society of America Bulletin*, 110 (3): 387-394.
- Moon, I.-J., Ginis, I., Hara, T., Tolman, H.L., Wright, C.W. and Walsh, E.J., 2003. Numerical simulation of sea surface directional wave spectra under hurricane wind forcing. *Journal of Physical Oceanography*, 33: 1680-1706.
- Moragne, J. and Woodward, J., 1982. *Development and Infilling of the South Pass Shelf-Edge Failure Bowl, Offshore Mississippi Delta*. M.S. Thesis, Stanford University, Palo Alto CA, 79 pp.
- Mulder, T. and Cochonat, P., 1996. Classification of offshore mass movements. *Journal of Sedimentary Research*, 66: 43-57.
- Muller, R.A. and Stone, G.W., 2001. A climatology of tropical storm and hurricane strikes to enhance vulnerability prediction for the southeast U.S. coast. *Journal of Coastal Research*, 16(4): 949-956.

- Murray, S. P., 1970. Bottom currents near the coast during Hurricane Camille. *Journal of Geophysical Research*, 75: 4579-4582.
- National Data Buoy Center, 2004. Archive available at website of National Data Buoy Center ([http://www.ndbc.noaa.gov/view\\_text\\_file.php?filename=42040h2004.txt.gz&dir=data/historical/stdmet/](http://www.ndbc.noaa.gov/view_text_file.php?filename=42040h2004.txt.gz&dir=data/historical/stdmet/)).
- \_\_\_\_\_, 2005. National Data Buoy Center online archive ([http://www.ndbc.noaa.gov/view\\_text\\_file.php?filename=42040h2005.txt.gz&dir=data/historical/stdmet/](http://www.ndbc.noaa.gov/view_text_file.php?filename=42040h2005.txt.gz&dir=data/historical/stdmet/)).
- National Hurricane Center, 2009. Archive available at website of National Hurricane Center (<http://www.nhc.noaa.gov/>).
- National Oceanographic and Atmospheric Administration (NOAA), Atlantic Oceanographic and Meteorological Laboratory, Hurricane Research Division, 2007. *Gridded Surface Wind Analysis* ([http://www.aoml.noaa.gov/hrd/data\\_sub/wind.html](http://www.aoml.noaa.gov/hrd/data_sub/wind.html)).
- \_\_\_\_\_, 2009. Regional GOM bathymetry data available at: <http://www.ngdc.noaa.gov/mgg/bathymetry/relief.html>.
- Neumann, C. J., Jarvinen, B. R. and Elms, J., 1987. *Tropical Cyclones of the North Atlantic Ocean, 1871-1986*. National Climatic Data Center, National Oceanic and Atmospheric Administration, U.S. Department of Commerce, 186 pp.
- Neumann, C. J., Jarvinen, B. R., McAdie, C.J. and Elms, J., 1993. *Tropical Cyclones of the North Atlantic Ocean, 1871-1992*. National Climatic Data Center, National Oceanic and Atmospheric Administration, U.S. Department of Commerce, 193 pp.
- Neurauter, T.W. and Bryant, W.R., 1989. Gas hydrates and their association with mud diapir/mud volcanoes on the Louisiana continental slope. *Proceedings of the Offshore Technology Conference*, 21: 599-607.
- New York Mercantile Exchange, 2006. *Monthly reports of West Texas Intermediate Oil and Henry Hub Natural Gas Pricing* (<http://quotes.ino.com/exchanges>).
- Noble Drilling Services, Inc., 2007. Rig fleet descriptions available at website of Noble Drilling Services, Inc. (<http://www.noblecorp.com/rig/foverviewfrX.html>)
- Nodine, M.C., Wright, S.G., Gilbert, R.B. and Ward, E.G., 2006. Mudflows and mudslides during Hurricane Ivan. *Proceedings of the Offshore Technology Conference*, Paper No. 18328.
- \_\_\_\_\_, 2007. *Mudslides during Hurricane Ivan and an Assessment of the Potential for Future Mudslides in the Gulf of Mexico*. Phase I Project Report, MMS/OTRC Cooperative Research Agreement 1435-01-04-CA-35515, Task Order 39239, MMS Project Number 552 (<http://www.mms.gov/tarprojects/552/IvanMudslidesFinalPhaseIReport.pdf>), 44 pp.
- Normark, W.R., Wilde, P., Campbell, J.F., Chase, T.E. and Tsutsui, B., 1993. Submarine slope failures initiated by Hurricane Iwa, Kahe Point, Oahu, Hawaii. In: H.J. Lee and D.C. Twichell (Editors), *Submarine Landslides: Selected Studies in the US Exclusive Economic Zone*. United States Geological Survey Bulletin, 1993, pp. 197-204.

- Oceanweather, Inc., 1992. *Hindcast Study of Hurricane Andrew (1992)*. Prepared for Minerals Management Service, Study and Hindcast of Wind and Wave Fields for Hurricane Andrew, Project No. 193 (available online at <http://www.mms.gov/tarprojects/193/193.pdf>, 158 pp.
- \_\_\_\_\_, 2003. *Final Report, MMS Hindcast Study of Hurricane Lili (2002), Offshore Northern Gulf of Mexico*. Prepared for Minerals Management Service, Hindcast Study of Winds, Waves, and Currents in N. GOM in Hurricane Lili (2002), Project No. 467 (available online at <http://www.mms.gov/tarprojects/467/MMS%20Lili%202002%20Hindcast.pdf>), 67 pp.
- \_\_\_\_\_, 2006. Hindcast data on winds, waves and currents in northern Gulf of Mexico in Hurricanes Katrina and Rita. Prepared for Minerals Management Service, Project No. 580 (available online at <http://www.mms.gov/tarprojects/580.htm>, 174 pp.
- \_\_\_\_\_, 2007a. Website of Oceanweather, Inc. (<http://www.oceanweather.com>).
- \_\_\_\_\_, 2007b. Wind hindcast results, Hurricanes Camille (1969) and Andrew (1992). Data purchased from Oceanweather, Inc.
- Odom Offshore Surveys, 1979. *A Drilling and Construction Hazard Survey of Block 129, Main Pass Area, Offshore Louisiana*. Report No. 79-102-00501, Baton Rouge LA, 16 pp.
- \_\_\_\_\_, 1983a. *A High Resolution Geophysical Survey of Block 58, Main Pass Area, Offshore Louisiana*. Report No. 83-169-12001, Baton Rouge LA, 16 pp.
- \_\_\_\_\_, 1983b. *A High Resolution Geophysical Survey of Block 62, Main Pass Area, Offshore Louisiana*. Report No. 83-158-12002, Baton Rouge LA, 16 pp.
- \_\_\_\_\_, 1983c. *A High Resolution Geophysical Survey of Block 63, Main Pass Area, Offshore Louisiana*. Report No. 83-159-12001, Baton Rouge LA, 16 pp.
- Panchang, V.G. and Gupta, R.C., 1989. On the determination of three-parameter Weibull MLEs. *Communications in Statistics, Simulation and Computation*, 18: 1037-1057.
- Panchang, V.G. and Li, D., 2006. Large waves in the Gulf of Mexico caused by Hurricane Ivan. *American Meteorological Society Bulletin*, 84(4): 481-489.
- Patterson, M.M., 1974. Oceanographic data from Hurricane Camille. *Proceedings of the Offshore Technology Conference*, 6: 781-790.
- Pepper, D.A., 2000. *Hydrodynamics, Bottom Boundary Layer Processes and Sediment Transport on the South-Central Louisiana Inner Shelf: The Influence of Extratropical Storms and Bathymetric Modification*. Ph.D. Dissertation, Louisiana State University, 159 pp.
- Petruncio, E.T., Rosenfeld, L.K. and Paduan, J.D., 1998. Observations of the internal tide in Monterey Canyon. *Journal of Physical Oceanography*, 28: 1873-1903.
- PI/Dwights Energy Database, 2009. Offshore production database accessed through license agreement at BP.

- Pielke, R.A. and Landsea, C.W., 1999. La Nina, El Nino, and Atlantic hurricane damages in the United States. *American Meteorological Society Bulletin*, 80: 2027-2033.
- Plains Resources, 2006. *Multi-beam bathymetry data, South Pass Block 19*. Digital data only.
- PMB Engineering, Inc., 1993. *Hurricane Andrew – Effects on Offshore Platforms*. Prepared for Minerals Management Service, API/Hurricane Foundation Study, Joint Industry Project Final Report, 330 pp.
- \_\_\_\_\_, 1995. *Further Evaluation of Offshore Structures Performance in Hurricane Andrew: Development of Bias Factors for Pile Foundation Capacity*. Prepared for Minerals Management Service, API/Hurricane Foundation Study, Project No. 207, 150 pp.
- Postma, G., 1986. Classification for sediment gravity-flow deposits based on flow conditions during sedimentation. *Geology*, 14: 291-294.
- Powell, M.D., Houston, S.H., Amat, L.R. and Morisseau-Leroy, N., 1998. The HRD real-time hurricane wind analysis system. *Journal of Wind Engineering and Industrial Aerodynamics*, 77: 53-64.
- Prior, D.B., Bornhold, B.D. and Johns, M.W., 1984. Depositional characteristics of a submarine debris flow. *Journal of Geology*, 92: 707-727.
- Prior, D.B. and Coleman, J.M., 1978a. Disintegrating retrogressive landslides on very low angle subaqueous slopes, Mississippi Delta. *Marine Geotechnology*, 3: 37-60.
- \_\_\_\_\_, 1978b. Submarine landslides on the Mississippi River delta-front slope. *Geoscience and Man*, 19: 41-53.
- \_\_\_\_\_, 1979. Submarine landslides – geometry and nomenclature. *Zeitschrift für Geomorphologie*, 23: 415-426.
- \_\_\_\_\_, 1982. Active slides and flows in underconsolidated marine sediments on the slope of the Mississippi Delta. In: S. Saxov and J.K. Nieuwenhuis (Editors), *Marine slides and other mass movements: Proceedings of a North Atlantic Treaty Organization (NATO) workshop on marine slides and other mass movements*, pp. 21-49.
- \_\_\_\_\_, 1984. Submarine slope instability. In: D. Brunsden and D.B. Prior (Editors), *Slope Instability*. John Wiley & Sons Ltd., Chichester, UK, pp. 419-455.
- Prior, D.B. and Suhayda, J.N., 1979. Submarine mudslide morphology and development mechanisms, Mississippi Delta. *Proceedings of the Offshore Technology Conference*, 11: 1055-1061.
- Prior, D.B., Suhayda, J.N., Lu, N.Z., Bornhold, B.D., Keller, G.H., Wiseman, W.J., Wright, L.D. and Yang, Z.-S., 1989. Storm wave reactivation of a submarine landslide. *Nature*, 341: 47-50.
- Prior, D.B., Yang, Z.S., Bornhold, B.D., Keller, G.H., Lu, N.Z., Wiseman, Jr., W.J., Wright, L.D. and Zhang, J., 1986. Active slope failure, sediment collapse, and silt flows on the modern subaqueous Huanghe (Yellow River) delta. *Geo-Marine Letters*, 6: 85-95.



- Puskar, F.J., Spong, R.E., Ku, A., Gilbert, R.B. and Choi, Y.J., 2006. Assessment of fixed offshore platform performance in Hurricane Ivan. *Proceedings of the Offshore Technology Conference*, Paper No. 18325.
- Quiros, G.W., Young, A.G., Pelletier, J.H. and Chan, J.H., 1983. Shear strength interpretation for Gulf of Mexico clays. In: S. Wright (Editor), *Proceedings of the Conference on Geotechnical Practice in Offshore Engineering, April 27-29, 1983*, Austin, Texas, pp. 144-165.
- Racal-Decca Surveys, Inc., 1981. *Archaeological and Engineering Survey for The Superior Oil Company*. Bathymetry map only; no other data available.
- \_\_\_\_\_, 1988. *Archaeological and Engineering Survey, South Pass Block 51*. Bathymetry map only; no other data available.
- Roberts, H.H., Cratsley, D. and Whelan, T., III, 1976. Stability of Mississippi delta sediments as evaluated by analysis of structural features in sediment borings. *Proceedings of the Offshore Technology Conference*, 8: 9-28.
- Roberts, N.C., 1969. *The Story of Extreme Hurricane Camille*. Privately published, New Orleans, 160 pp.
- Rosenthal, W., 1978. Energy exchange between surface waves and motion of sediments. *Journal of Geophysical Research*, 83: 1980-1982.
- Rossi, A., Massei, N., Laignel, B., Sebag, D. and Copard, Y., 2009. The response of the Mississippi River to climate fluctuations and reservoir construction as indicated by wavelet analysis of streamflow and suspended-sediment load, 1950-1975. *Journal of Hydrology*, article in press.
- Sager, W.W., Schroeder, W.W., Davis, K.S. and Rezak, R., 1999. A tale of two deltas: seismic mapping of near surface sediments on the Mississippi-Alabama outer shelf and implications for recent sea level fluctuations. *Marine Geology*, 160(1999): 119-136.
- Sassen, R., MacDonald, I.R., Guinasso, N.L., Joye, S., Requejo, A.G., Sweet, S.T., Alcalá-Herrera, J., DeFreitas, D.A. and Schink, D.R., 1998. Bacterial methane oxidation in sea-floor gas hydrate: Significance to life in extreme environments. *Geology*, 26(9): 851-854.
- Schapery, R.A. and Dunlap, W.A., 1978. Prediction of storm-induced sea bottom movement and platform forces. *Proceedings of the Offshore Technology Conference*, 10: 1789-1796.
- Schlumberger Corp., 2007. *Online Oilfield Glossary* (available at <http://www.glossary.oilfield.slb.com/Default.cfm>).
- Shapiro, L.J., 1987. Month-to-month variability of the Atlantic tropical circulation and its relationship to tropical storm formation. *Monthly Weather Review*, 115: 1598-1614.
- Sheffer, L., 1964. Hilda's damage may hit \$100 million. *Offshore*, 22(4), 15-22.
- \_\_\_\_\_, 1965. Hurricane Betsy takes savage toll from Gulf oil industry. *Offshore*, 24(4): 24-29.

- Shelton, M.K., 1977. *Wave Analysis of Hurricane Camille*. M.S. Thesis, University of Houston, Houston, 91 pp.
- Shemdin, O.H., 1977. *Hurricane waves, storm surge and currents: As assessment of the state of the art*. U.S. – Southeast Asia Symposium on Engineering for Natural Hazards Protection. Manila, The Philippines.
- Sheremet, A., Mehta, A.J., Liu, B. and Stone, G.W., 2005. Wave-sediment interaction on a muddy inner shelf during Hurricane Claudette. *Estuarine, Coastal and Shelf Science*, 63: 225-233.
- Sheremet, A. and Stone, G.W., 2003. Observations of nearshore wave dissipation over muddy sea beds. *Journal of Geophysical Research*, 108 (C11), 3357, doi: 10.1029/2003JC001885, 2003, pp. 21(1)-21(11).
- Simpson, R.H., Sugg, A.L., Clark, G.B., Frank, N.L., Hope, J.R., Hebert, P.J., Kraft, R.H. and Pelissier, J.M., 1970. The Atlantic hurricane season of 1969. *Monthly Weather Review*, 98(4): 293-306.
- Sorensen, O.R., Kofoed-Hansen, H., Rugbjerg, M. And Sorensen, L.S., 2004. A third-order generation spectral wave model using an unstructured finite volume technique. *Proceedings of the 5<sup>th</sup> International Conference on Coastal Engineering*, 29: 894-906.
- Spaziani, A.L., Jose, F. and Stone, G.W., 2009. Sediment dynamics on an inner shelf shoal during storm events in the northeastern Gulf of Mexico, USA. *Proceedings of the 10<sup>th</sup> International Coastal Symposium 2009*, April 13-16, 2009. Lisbon, Portugal.
- Sterling, G. H. and Strohbeck, E. E., 1973. The Failure of South Pass 70 "B" Platform in Hurricane Camille. *Proceedings of the Offshore Technology Conference*, 5: 720-724.
- Stewart, S.R., 2005. *Tropical Cyclone Report: Hurricane Ivan, 2-26 September 2004*. National Hurricane Center Tropical Prediction Center, Coral Gables, Florida.
- Stone, G.W., Grymes III, J.M., Dingler, J.R. and Pepper, D.A., 1997. Overview and significance of hurricanes on the Louisiana coast, U.S.A. *Journal of Coastal Research*, 13: 656-669.
- Stone, G.W. and Stapor, F.W., 1996. A nearshore sediment transport model for the northeast Gulf of Mexico coast, USA. *Journal of Coastal Research*, 12: 786-792.
- Stone, G.W., Walker, N.D., Hsu, S.A., Babin, A., Liu, B., Keim, B.D., Teague, W., Mitchell, D. and Leben, R., 2005. Hurricane Ivan's impact along the northern Gulf of Mexico. *Eos, Transactions, American Geophysical Union*, 86(48): 497-508.
- Stone, G.W., Wang, P., Pepper, D.A., Grymes III, J.M., Roberts, H.H., Zhang, X., Hsu, S.A. and Huh, O.K., 1999. Studying the importance of hurricanes to the northern Gulf of Mexico coast. *Eos, Transactions, American Geophysical Union*, 80: 301-305.
- Stone, G.W., Xu, J.P. and Zhang, X., 1995. Estimation of the wave field during Hurricane Andrew and morphological change along the Louisiana coast. *Journal of Coastal Research*, 21: 234-253.

- Sugg, A.L., 1966. The hurricane season of 1965. *Monthly Weather Review*, 94(3): 183-191.
- Suhayda, J.N., 1977. Surface waves and bottom sediment response. *Marine Geotechnology* 2: 135-146.
- Suhayda, J.N. and Prior, D.B., 1978. Explanation of submarine landslide morphology by stability analysis and rheological models. *Proceedings of the Offshore Technology Conference*, 10: 1073-1080.
- Sultan, N., Cochonat, P., Canals, M., Cattaneo, A., Dennielou, B., Haflidason, H., Laberg, J.S., Long, D., Mienert, J., Trincardi, F., Urgeles, R., Vorren, T. and Wilson, C., 2004. Triggering mechanisms of slope instability processes and sediment failures on continental margins: A geotechnical approach. *Marine Geology*, 213: 291-321.
- Suter, J.R. and Berryhill, H.L., 1985. Late Quaternary shelf-margin deltas, northwest Gulf of Mexico. *American Association of Petroleum Geologists Bulletin*, 69: 77-91.
- Sydow, J. and Roberts, H.H., 1994. Stratigraphic framework of a late Pleistocene shelf-edge delta, northeast Gulf of Mexico. *American Association of Petroleum Geologists Bulletin*, 78: 1276-1312.
- Tannehill, I.R., 1956. *Hurricanes, Their Nature and History, Particularly Those of the West Indies and the Southern Coasts of the United States*. Princeton University Press, Princeton, 308 pp.
- Teague, W. J., Jarosz, E., Carnes, M. R., Mitchell, D. A. and Hogan, P. J., 2006. Low-frequency current variability observed at the shelf break in the northeastern Gulf of Mexico. *Continental Shelf Research*, 26: 2559-2582.
- Teague, W.J., Jarosz, E., Wang, D.W. and Mitchell, D.A., 2007. Observed oceanic response over the upper continental slope and outer shelf during Hurricane Ivan. *Journal of Physical Oceanography*, 37:2181-2206.
- Terzaghi, K., Peck, R.B. and Mesri, G., 1996. *Soil Mechanics in Engineering Practice*. Wiley-IEEE, New York, NY, 549 pp.
- The Oil and Gas Journal, 1969a. Oil installations hit hard by Camille. *The Oil and Gas Journal*, August 25, 1969.
- \_\_\_\_\_, 1969b. Operators assess ruin left by Camille. *The Oil and Gas Journal*, September 1, 1969, pp. 74-75.
- \_\_\_\_\_, 1974. Carmen goes easy on oil operations. *The Oil and Gas Journal*, September 16, 1974, p. 40.
- Thom, H.C.S. and Marshall, R.D., 1971. Wind and surge damage due to Hurricane Camille. *Waterways, Harbors and Coastal Engineering Division of the American Society of Civil Engineers*, 97 (WW2): 335-363.
- Thomson, J., Garrett, M., Taylor, M., George, T., Melancon, M. and Behrens, K., 2005. Sonar surveys for pipeline inspection show extent of pipeline displacement and seafloor instability

- following Hurricane Ivan. *Proceedings of the Offshore Technology Conference*, Paper No. 17738.
- Trabant, P.K., Bryant, W.R. and Coleman, J.M., 1979. Submarine geomorphology and geology of the Mississippi River Delta Front. *Proceedings of the Offshore Technology Conference*, 11: 1887-1898.
- Transocean Corp., 2007. Rig fleet descriptions available at Transocean Corporation website ([http://www.deepwater.com/fw/main/Our\\_Rigs-14.html](http://www.deepwater.com/fw/main/Our_Rigs-14.html)).
- Tripsanas, E.K., Bryant, W.R. and Phaneuf, B.A., 2004. Slope instability processes caused by salt movements in a complex deep-water environment, Bryant Canyon area, northwest Gulf of Mexico. *American Association of Petroleum Geologists Bulletin*, 88: 801-823.
- Tripsanas, E.K., Bryant, W.R., Prior, D.B. and Phaneuf, B.A., 2003. Interplay between salt activities and slope instabilities, Bryant Canyon area, northwest Gulf of Mexico. In: J. Locat and J. Mienert (Editors), *Submarine Mass Movements and Their Consequences*. Kluwer Academic Publishers, Dordrecht, pp. 307-316.
- United States Coast and Geodetic Survey, 1957. *Gulf Coast Hydrographic Survey Index, New Orleans, Louisiana to Sabine Pass, Texas*. Washington, 12 pp.
- United States Weather Bureau, 1969. *Preliminary Report on Hurricane Camille, August 14-22, 1969*. U.S. Department of Commerce, Environmental Science Services Administration. Washington, 21 pp.
- Varnes, D.J., 1984. Landslide hazard zonation: a review of the principles and practice. *The IAGE Commission on Landslides and other Mass Movements on Slopes*. UNESCO, Paris, France.
- Vastar Resources, Inc., 1995. *A High Resolution Geophysical Report of South Pass Area, East Addition, Block 69 (OCS-G-14574)*. Houston, 11 pp.
- \_\_\_\_\_, 1997a. *A High-Resolution Geophysical Report of Mississippi Delta Regional Study, South Pass and Main Pass Areas, Gulf of Mexico*. Houston, 7 pp.
- \_\_\_\_\_, 1997b. *A High Resolution Geophysical Report and Cultural Resource Assessment of South Pass Area Blocks 17 and 18, OCS-G-14568 and 14569, Offshore Louisiana, Gulf of Mexico, for Vastar Resources, Inc.* Houston, 22 pp.
- Vaunat, J and Leroueil, S., 2002. Analysis of post-failure slope movements within the framework of hazard and risk analysis. *Natural Hazards*, 26: 83-109.
- Walker, J.R. and Messingill, J.V., 1970. Slump features on the Mississippi Fan, Northeastern Gulf of Mexico. *Geological Society of America Bulletin*, 81 (10), 3101-3108.
- Wang, D.W., Mitchell, D.A., Teague, W.J., Jarosz, E. and Hulbert, M.S., 2005. Extreme waves under Hurricane Ivan. *Science*, 309: 896.
- Ward, E.G., 1974. Ocean Data Gathering Program – an overview. *Proceedings of the Offshore Technology Conference*, 6: 771-780.

- Watkins, D.J. and Kraft, L.M., 1976. Stability of continental shelf and slope off Louisiana and Texas – geotechnical aspects. In: A.H. Bouma, G.T. Moore and J.M. Coleman (Editors), *Beyond the Shelf Break*. American Association of Petroleum Geologists Short Course, New Orleans, II: B1-B34.
- WAVCIS (Wave-Current Information System), 2009. Online oceanographic data gathering and reporting system, Coastal Studies Institute, Louisiana State University (<http://www.wavcis.lsu.edu>).
- Wentworth, C.K., 1922. A scale of grade and class terms for clastic sediments. *Journal of Geology*, 30: 377–392.
- Whalen, J.E. and Ochi, M.K., 1978. Variability of wave spectral shapes associated with hurricanes. *Proceedings of the Offshore Technology Conference*, 10: 1515-1522
- Whelan, III, T., Coleman, J.M., Suhayda, J.N. and Garrison, L.E., 1975. The geochemistry of recent Mississippi River delta sediments: gas concentration and sediment stability. *Proceedings of the Offshore Technology Conference*, 7: 71-84.
- Wiegel, R.L., 1964. *Oceanographic Engineering*. Prentice Hall, Englewood Cliffs, 532 pp.
- William Lettis & Associates, Inc., 2005. *A Pilot Study for Regionally Consistent Hazard Susceptibility Mapping of Submarine Mudslides, Offshore Gulf of Mexico*. Walnut Creek, California, 29 pp.
- Wright, C.W., Walsh, E.J., Vandemark, D., Krabill, W.B., Garcia, A.W., Houston, S.H., Powell, M.D., Black, P.G. and Marks, F.D., 2001. Hurricane directional wave spectrum spatial variation in the open ocean. *Journal of Physical Oceanography*, 31: 2472-2488.
- Wright, L.D., Swaye, F.J. and Coleman, J.M., 1970. Effects of Hurricane Camille on the landscape of the Breton-Chandeleur Island Chain and the eastern portion of the Lower Mississippi Delta. *Coastal Studies Institute Technical Report 76*, 34 pp.
- Wright, S.G., 1976. Analyses for wave induced sea-floor movements. *Proceedings of the Offshore Technology Conference*, 8: 41-50.
- Wright, S.G., 2002. *Forum on Risk Assessment for Submarine Slope Stability: Report of a Forum Held in Houston, Texas on May 10 and 11, 2002*. MMS/Offshore Technology Research Center Cooperative Research Agreement No. 1435-01-99-CA-31003, 40 pp.
- Wright, S.G. and Dunham, R.S., 1972. Bottom stability under wave-induced loads. *Proceedings of the Offshore Technology Conference*, Paper No. 1603.
- Young, I.R., 1998. Observations of the spectra of hurricane-generated waves. *Ocean Engineering*, 25(4-5): 261-276.
- \_\_\_\_\_, 2003. A review of the sea state generated by hurricanes. *Marine Structures*, 16: 201-218.

## APPENDIX A: COMMON TYPES OF OFFSHORE INDUSTRY INFRASTRUCTURE



Figure A-1: Jack-up drilling rig - fixed on seafloor; legs penetrate seafloor and rig is “jacked-up” along legs (rig: Noble Ronald Hope; from Noble Drilling Services Inc., 2007)



Figure A-2: Jack-up drilling rig adjacent to small production platform – legs fixed on seafloor and derrick overlays platform (rig: Noble Eddie Paul; from Noble Drilling Services Inc., 2007)



Figure A-3: Semi-submersible drilling rig – floats on ocean surface and rig is dynamically positioned (rig: Deepwater Horizon; from Transocean Corp., 2007)



Figure A-4: Drill ship – floats on ocean surface and rig is dynamically positioned (rig: Discoverer 534; from Transocean Corp., 2007)

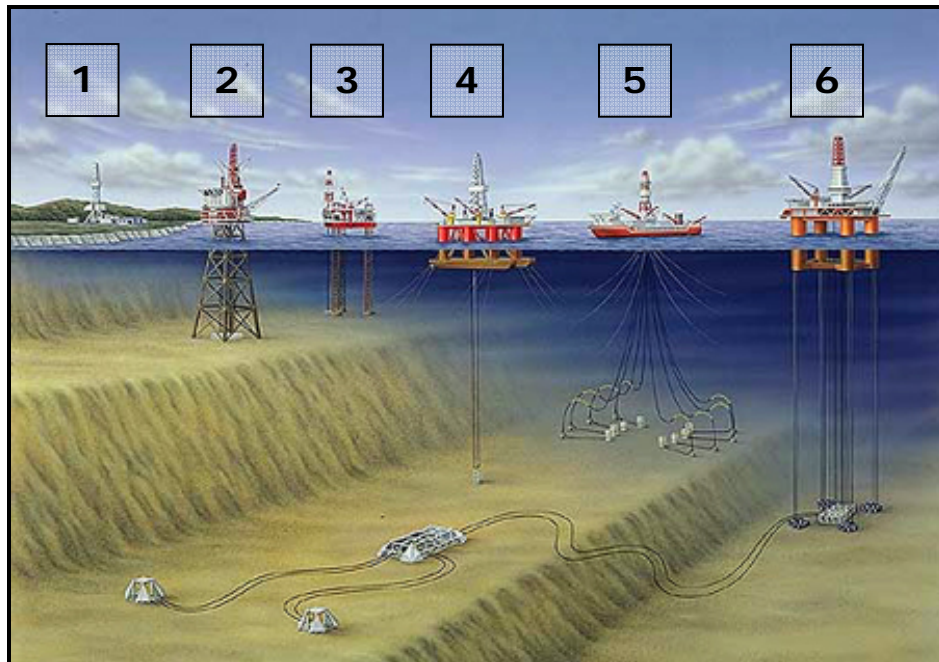


Figure A-5: Common types of offshore drilling and producing facilities in the Gulf of Mexico relative to water depth (from MMS, 2009; available at: <http://www.gomr.mms.gov/homepg/offshore/deepwatr/options.html>)

- |                              |                                   |
|------------------------------|-----------------------------------|
| 1. Onshore drilling platform | 4. Semi-submersible drilling rig  |
| 2. Fixed producing platform  | 5. Drilling ship                  |
| 3. Jack-up drilling rig      | 6. Tension-leg producing platform |



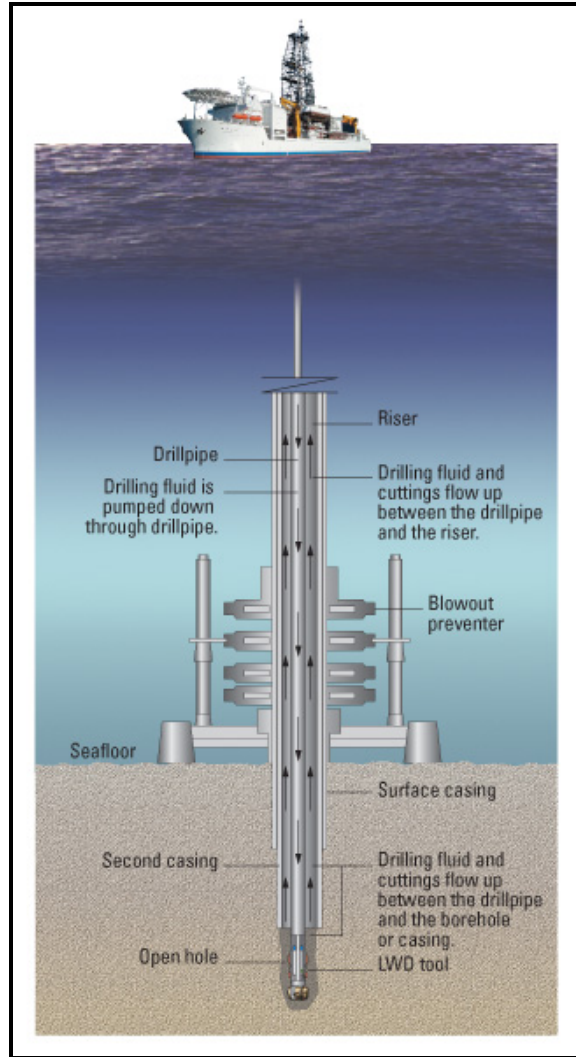


Figure A-6: Depiction of a typical seafloor drilling assembly used in the GOM  
(from Schlumberger, 2007)

The riser is a buoyant “pipe” that extends from a drilling rig or platform at the water surface down to the seafloor (Figure A-6). Drilling mud and cuttings from the borehole are returned to the surface through the riser. The top of the riser is attached to the rig or platform while its bottom is secured at the seafloor. The riser pipe diameter is large enough to allow drill pipe, logging tools and multiple casing strings to pass through (Schlumberger, 2007).

## APPENDIX B: KEY HURRICANE ROUTES AND STORM INTENSITY HISTORY

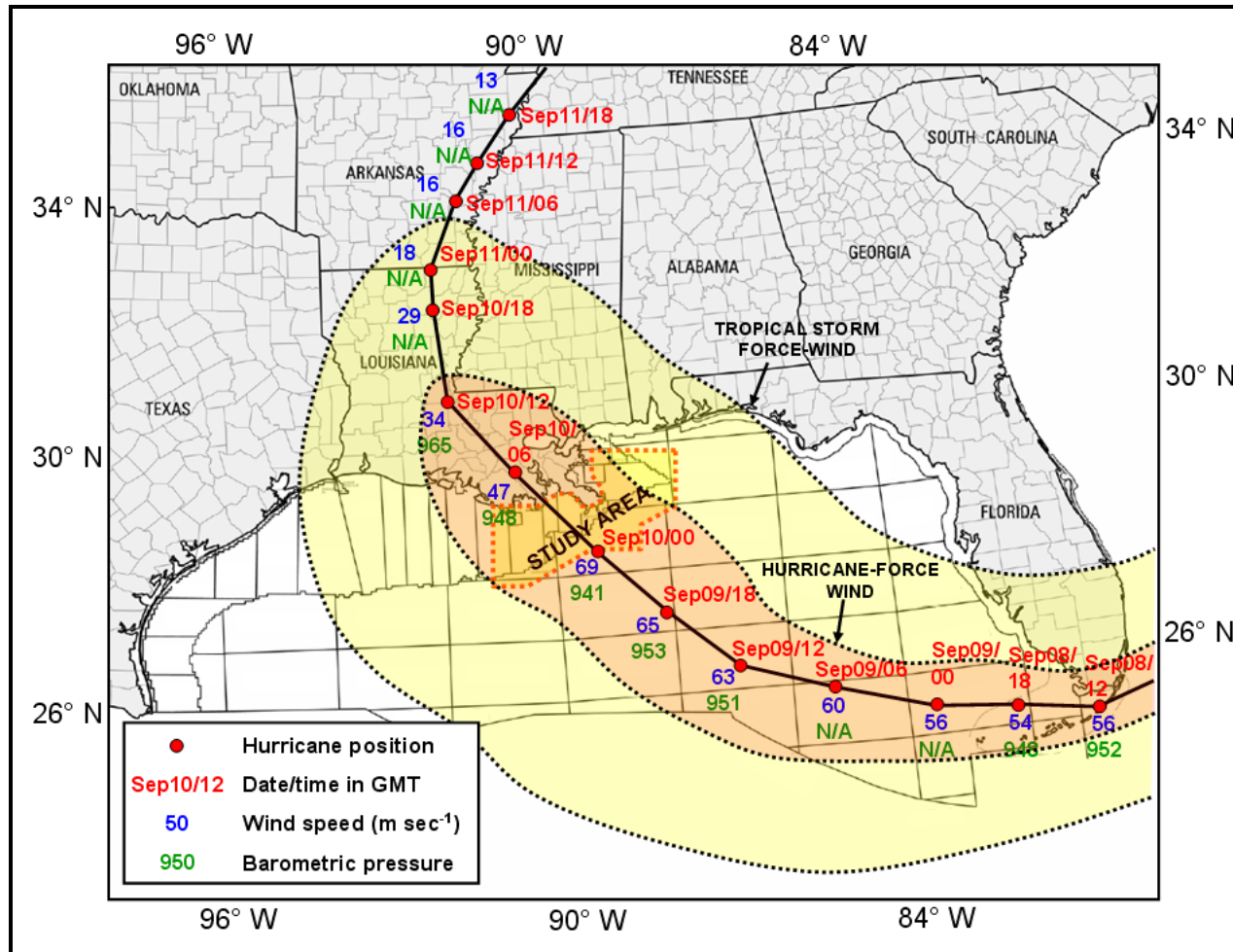


Figure B-1: Hurricane track and intensity history, Hurricane Betsy (1965)  
(data extracted from archives at NHC, 2009 and NOAA, 2007)

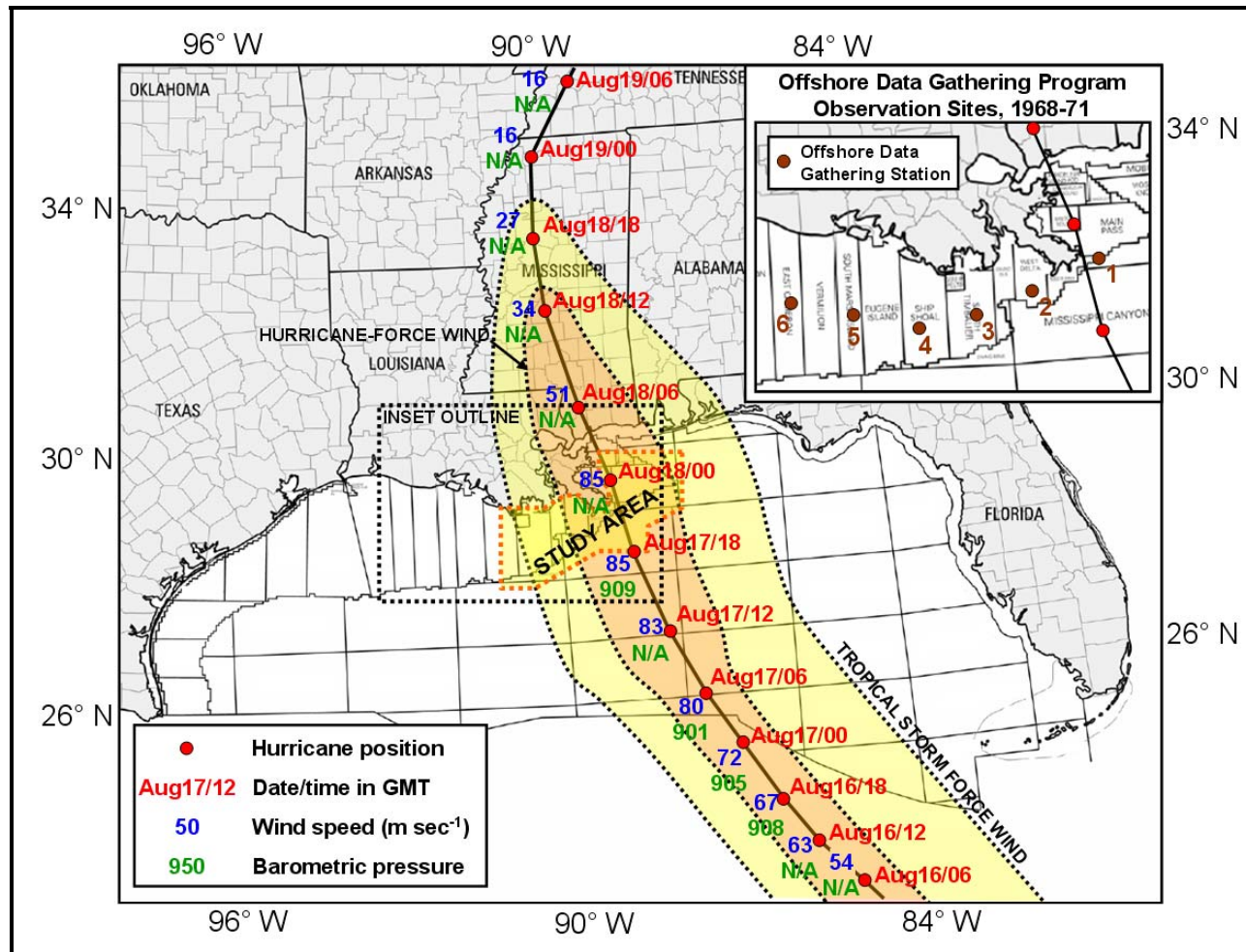


Figure B-2: Hurricane track and intensity history, Hurricane Camille (1969) plus locations of Offshore Data Gathering Sites (ODGS), 1968-1971 (data extracted from archives at NHC, 2009 and Oceanweather, 2007b; ODGS locations modified from Ward, 1974)

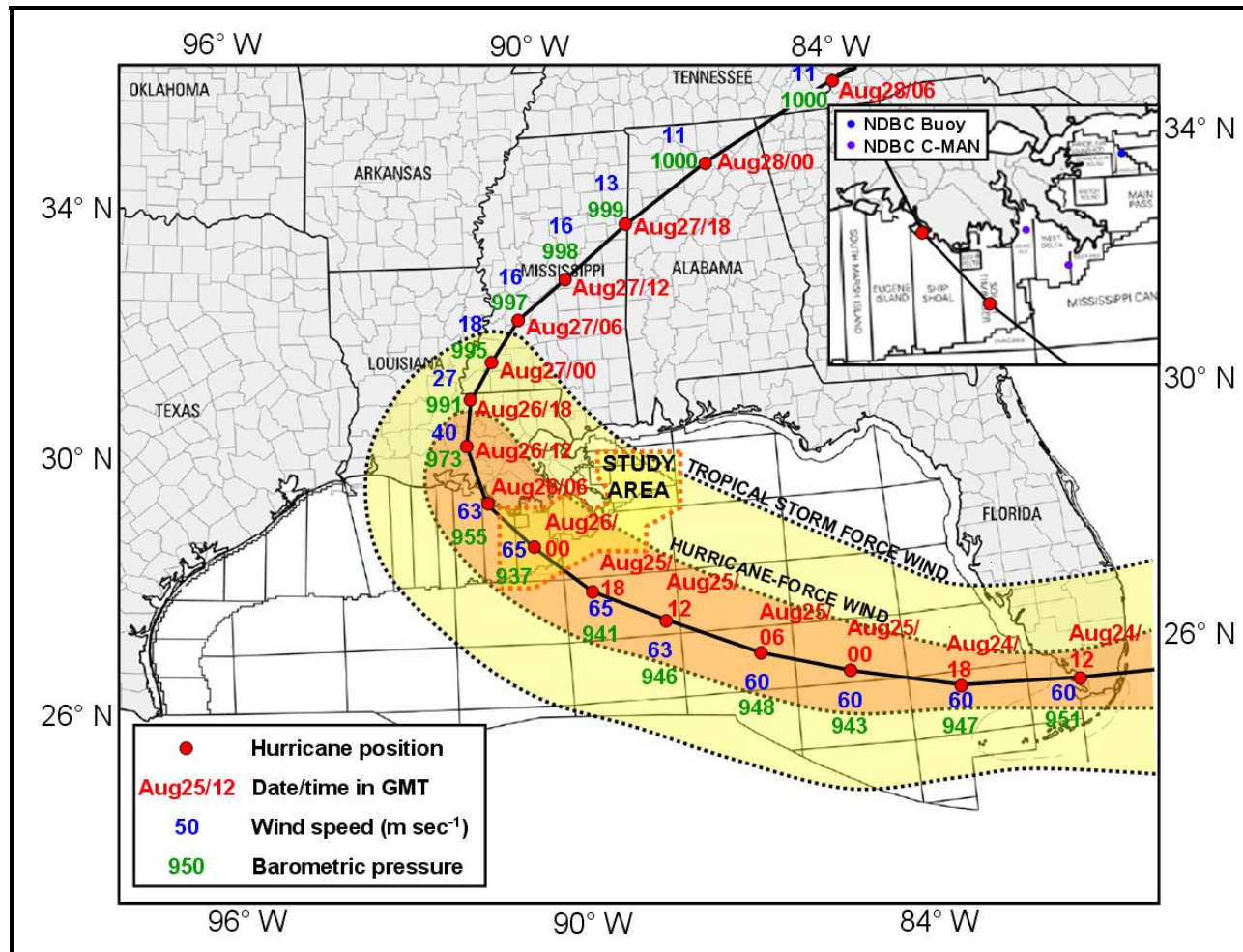


Figure B-3: Hurricane track and intensity history, Hurricane Andrew (1992) plus locations of NDBC measuring stations as of 1992 (data extracted from NHC, 2009 and Oceanweather, 2007b; NDBC locations modified from NDBC, 2009)



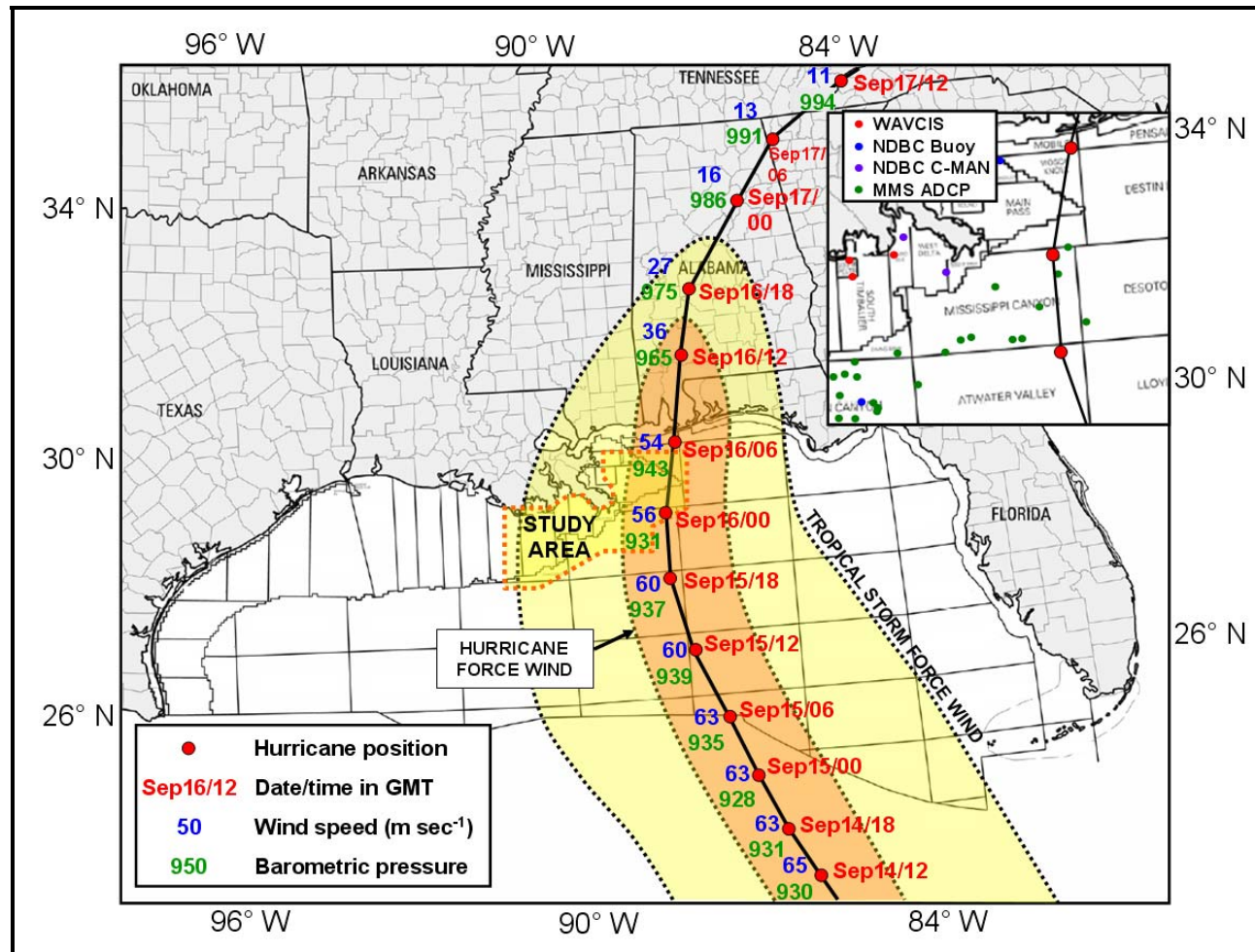


Figure B-4: Hurricane track and intensity history, Hurricane Ivan (2004) plus locations of NDBC measuring stations as of 2004 (data extracted from NHC, 2009 and NOAA, 2007; NDBC locations modified from NDBC, 2009)



# **APPENDIX C: INFRASTRUCTURE DAMAGE AND LOSS, HURRICANE IVAN (2004)**

Table C-1: Platforms destroyed by Hurricane Ivan (from MMS, 2005a)

<b>Operator</b>	<b>Map area</b>	<b>Block number</b>	<b>Facility</b>	<b>Facility Type</b>	<b>Water Depth (ft)</b>
Taylor Energy	MC	20	A	8-pile	479
Forest Energy	MP	98	A	Braced caisson	79
Noble Energy, Inc.	MP	293	“Sonat”	4-pile	232
Noble Energy, Inc.	MP	293	A	8-pile	247
Noble Energy, Inc.	MP	305	C	8-pile	244
Noble Energy, Inc.	MP	306	E	8-pile	255
Noble Energy, Inc.	VK	294	A	Braced caisson	119

Area Key: MC: Mississippi Canyon  
MP: Main Pass  
VK: Viosca Knoll



Table C-2: Platforms destroyed during Hurricane Katrina (sorted by protraction area/block; MMS, 2006b)

Operator	Map Area	Block Number	Facility	Water Depth (ft)
BP America Production Company	GI	40	B	83
BP America Production Company	GI	40	F	86
BP America Production Company	GI	47	C	88
BP America Production Company	GI	48	D	86
BP America Production Company	GI	41	A	91
BP America Production Company	GI	32	J	106
Newfield Exploration Company	MP	138	A	158
Southern Natural Gas Company	MP	298	B-Valve	222
Noble Energy, Inc.	MP	306	D	255
Apache Corporation	MP	312	JA	248
Dominion Exploration & Production, Inc.	MP	270	A	205
Energy Resource Technology, Inc.	PL	20	39	30
Apache Corporation	SP	62	A	340
Apache Corporation	SP	62	B	322
Marlin Energy Offshore, L.L.C.	ST	21	1	37
Marlin Energy Offshore, L.L.C.	ST	21	22	36
Marlin Energy Offshore, L.L.C.	ST	21	25	40
Marlin Energy Offshore, L.L.C.	ST	21	27	40
Marlin Energy Offshore, L.L.C.	ST	21	31	36
Marlin Energy Offshore, L.L.C.	ST	21	66	45
Marlin Energy Offshore, L.L.C.	ST	21	67	46
Marlin Energy Offshore, L.L.C.	ST	21	71	48
Marlin Energy Offshore, L.L.C.	ST	21	75	47
Marlin Energy Offshore, L.L.C.	ST	21	E	40
Chevron U.S.A. Inc.	ST	135	M	116
Chevron U.S.A. Inc.	ST	151	I	128
Chevron U.S.A. Inc.	ST	151	O	137
Apache Corporation	ST	161	A	117
Chevron U.S.A. Inc.	ST	176	A	140
Chevron U.S.A. Inc.	ST	151	G	137
Apache Corporation	ST	161	B	120
BP America Production Company	WD	69	C	121
BP America Production Company	WD	69	K	134
BP America Production Company	WD	95	#5 Well	150
Apache Corporation	WD	103	A	223
Apache Corporation	WD	103	B	228
Apache Corporation	WD	104	C	228
Anglo-Suisse Offshore Partners	WD	117	C	214
Anglo-Suisse Offshore Partners	WD	117	D	195
Anglo-Suisse Offshore Partners	WD	117	E	208
Anglo-Suisse Offshore Partners	WD	117	F	200

--- continued on following page ---

**Area Key:** GI: Grand Isle MP: Main Pass PL: South Pelto  
SP: South Pass ST: South Timbalier WD: West Delta

<b>Operator</b>	<b>Map Area</b>	<b>Block Number</b>	<b>Facility</b>	<b>Water Depth (ft)</b>
Anglo-Suisse Offshore Partners	WD	117	QRT	214
Apache Corporation	WD	133	B	285
El Paso Production GOM Inc.	WD	137	A	310
BP America Production Company	WD	94	G	153
BP America Production Company	WD	70	H	141

**Area Key:**      GI: Grand Isle      MP: Main Pass      PL: South Pelto  
                      SP: South Pass      ST: South Timbalier      WD: West Delta

Table C-3: Large-diameter pipelines (10 inches or greater) damaged during Hurricane Katrina (sorted by protraction area/block; MMS, 2006b)

Operator	Map Area	Block Number (starting point)	Diameter	Product
Tennessee Gas Pipeline Company	GI	47	12	Gas
Trunkline Gas Company LLC	GI	94	24	Gas
Total E&P USA Inc	MC	243	10	Gas
Chevron USA Inc.	MC	292	12	Bulk Gas
Chevron USA Inc.	MC	292	12	Bulk Gas
Noble Energy Inc	MC	365	12	Gas/Cond.
Equilon Pipeline Company, LLC	MC	807	18	Oil
Equilon Pipeline Company, LLC	MC	807	14	Gas
Equilon Pipeline Company, LLC	MC	809	18	Oil
Equilon Pipeline Company, LLC	MC	809	18	Gas
Chandeleur Pipeline Company	MO	908	12	Gas
Chandeleur Pipeline Company	MP	41	12	Gas
Chandeleur Pipeline Company	MP	42	16	Gas
Destin Pipeline Company, LLC	MP	260	36	Gas
Shell Offshore, Inc.	MP	290	12	Oil
Southern Natural Gas Company	MP	291	24-Dec	Gas
Southern Natural Gas Company	MP	298	26	Gas
Southern Natural Gas Company	MP	298	12	Gas
Chevron Pipeline Company	MP	299	10	Oil
Noble Energy Inc	MP	305	12	Oil
Noble Energy Inc	MP	305	10	Gas
Southern Natural Gas Company	MP	306	18	Gas
SPN Resources LLC	SP	60	12	Gas
SPN Resources LLC	SP	60	10	Gas
Apache Corporation	SP	62	10	Lift
Apache Corporation	SP	62	10	Gas
Shell Oil Company	SP	62	12	Oil
Southern Natural Gas Company	SP	62	20	Gas
Southern Natural Gas Company	SP	62	14	Gas
Chevron USA Inc.	SP	77	10	Bulk Oil
Chevron USA Inc.	SP	77	10	Bulk Oil
Exxon Mobil Corporation	SP	93	10	Gas
Tennessee Gas Pipeline Company	SS	145	26	Gas
Tennessee Gas Pipeline Company	SS	168	20	Gas
Transcontinental Gas Pipeline	SS	169	10	Gas
Transcontinental Gas Pipeline	SS	169	10	Gas
Tennessee Gas Pipeline Company	SS	198	26	Gas
Marlin Energy Offshore LLC	ST	20	14	Gas

--- continued on following page ---

<b>Area Key:</b>	EI: Eugene Island	GC: Green Canyon	GI: Grand Isle
	MC: Mississippi Canyon	MO: Mobile	MP: Main Pass
	SM: South Marsh Island	SP: South Pass	SS: Ship Shoal
	ST: South Timbalier	VK: Viosca Knoll	VR: Vermilion
	WC: West Cameron	WD: West Delta	

Operator	Map Area	Block Number (starting point)	Diameter	Product
Gulf South Pipeline Company LP	ST	26	12	Gas
Tennessee Gas Pipeline Company	ST	37	20	Gas
Tennessee Gas Pipeline Company	ST	55	12	Gas
Chevron USA Inc.	ST	134	10	Bulk Oil
Chevron USA Inc.	ST	151	10	Bulk Gas
Gulf South Pipeline Company LP	ST	26	12	Gas
Tennessee Gas Pipeline Company	ST	37	20	Gas
Tennessee Gas Pipeline Company	ST	55	12	Gas
Chevron USA Inc.	ST	134	10	Bulk Oil
Chevron USA Inc.	ST	151	10	Bulk Gas
Venice Energy Services Company	ST	151	26	Gas/Cond.
Apache Corporation	ST	160	10	Gas
Chevron USA Inc.	ST	176	10	Bulk Gas
Enterprise Field Services LLC	VK	817	20	Gas
Venice Gathering System LLC	WD	41	26	Gas
BP America Production Company	WD	69	16	Gas
BP America Production Company	WD	69	10	Gas/Oil
BP America Production Company	WD	70	12	Gas
BP America Production Company	WD	70	10	Gas
Venice Gathering System LLC	WD	79	20-22	Gas
BP America Production Company	WD	94	12	Gas
BP America Production Company	WD	94	10	Bulk Oil
Equilon Pipeline Company, LLC	WD	104	12	Oil
Apache Corporation	WD	105	10	Gas
Apache Corporation	WD	122	12	Bulk Oil
Southern Natural Gas Company	WD	133	12	Gas

**Area Key:**

EI: Eugene Island	GC: Green Canyon	GI: Grand Isle
MC: Mississippi Canyon	MO: Mobile	MP: Main Pass
SM: South Marsh Island	SP: South Pass	SS: Ship Shoal
ST: South Timbalier	VK: Viosca Knoll	VR: Vermilion
WC: West Cameron	WD: West Delta	

# APPENDIX D: MRDF HURRICANE PATHS, 1947-2005

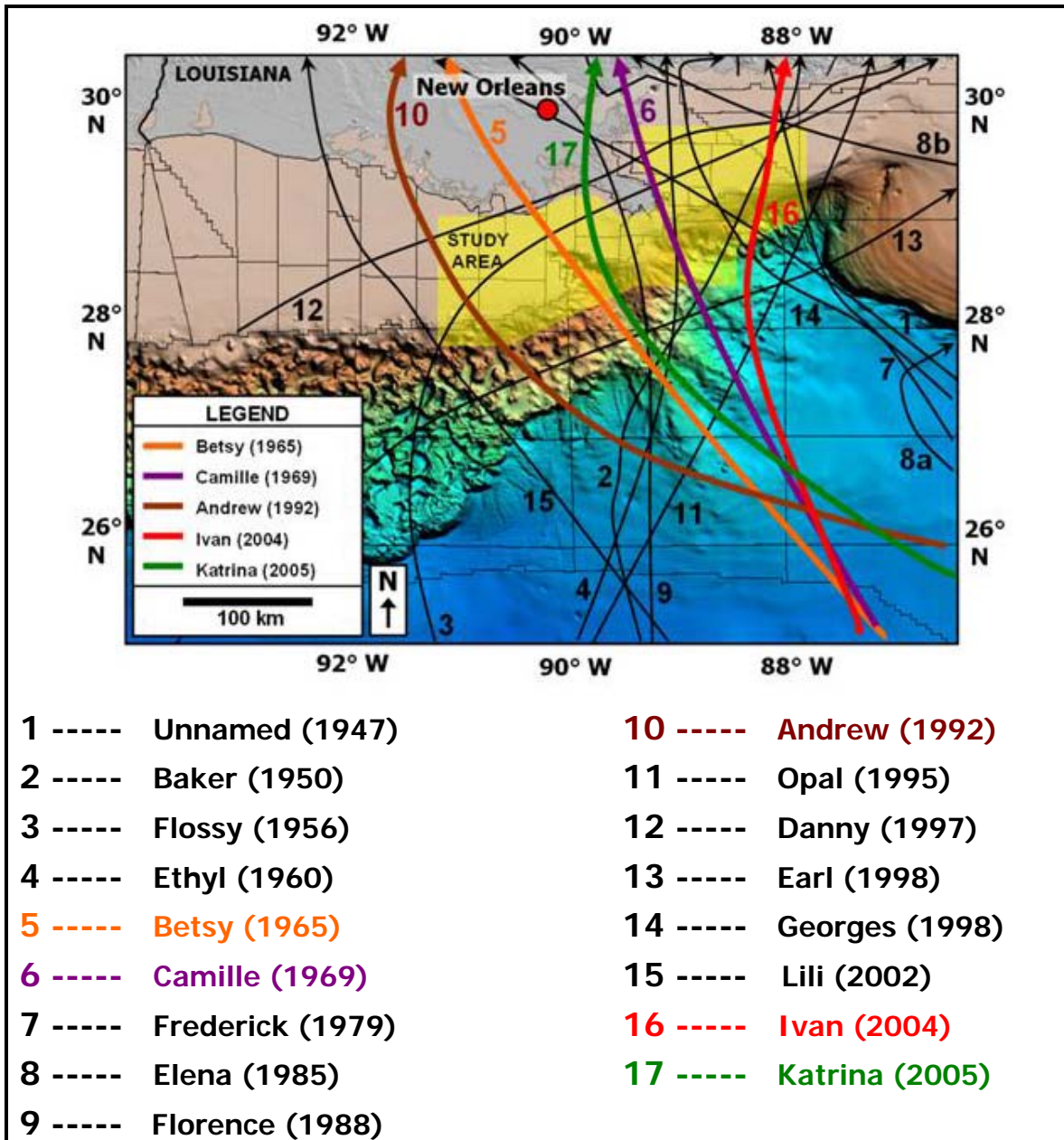


Figure D1: Hurricane tracks through study area, 1947-2005  
(Betsy, Camille, Andrew, Ivan and Katrina highlighted in bold tracks; NHC, 2009)

## APPENDIX E: RISK ASSESSMENT FOR SUBMARINE SLOPE FAILURES, HOUSTON FORUM 2002

Contributing Elements	Importance to Design Decisions	Current State of Knowledge	Knowledge Needs
<p>Magnitude and frequency (spatial and temporal) of slope failure mechanisms</p> <ul style="list-style-type: none"> <li>• How big?</li> <li>• How many?</li> <li>• How old?</li> <li>• Where?</li> <li>• What type?</li> </ul>	High	Variable by geographic area	Quantify the recurrence intervals by regional studies. Definition of active vs. relict.
State-of-the-art geologic/geophysical data supported by appropriate geotechnical data for integrated analysis		An imbalance exists between geophysical and geotechnical data; volume and quality. Limitation due to cost of acquiring geological and geotechnical data.	Innovative and inexpensive ways to develop geotechnical parameters and integration with seismic data.
<p>Characterization of triggers:</p> <p>Identification of key factors responsible for cause of failures.</p>	High	Varies from location to location depending on mechanism. We don't know how to define regional and local, and there is an imbalance between the understanding of the two	Quantify factors on local and regional scales. Apply the earthquake risk methodology as a "go by".
Consistent standards for slope instability risk assessment criteria and procedures	High	Non-existent	Guidelines: some kind of recommended practice the industry can generally approve.

# APPENDIX F: OFFSHORE LOUISIANA BATHYMETRIC DATASETS, 1868-2007

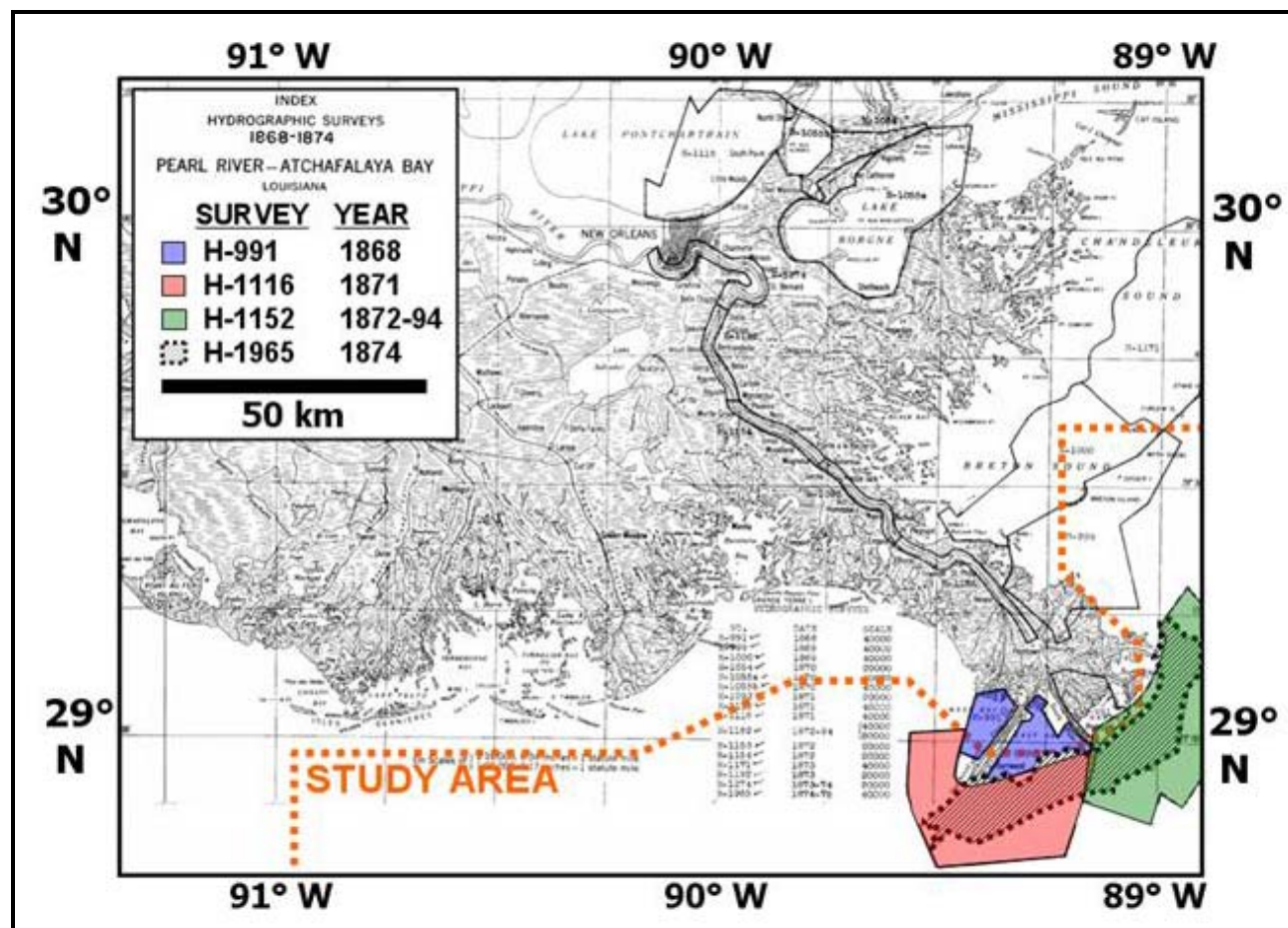
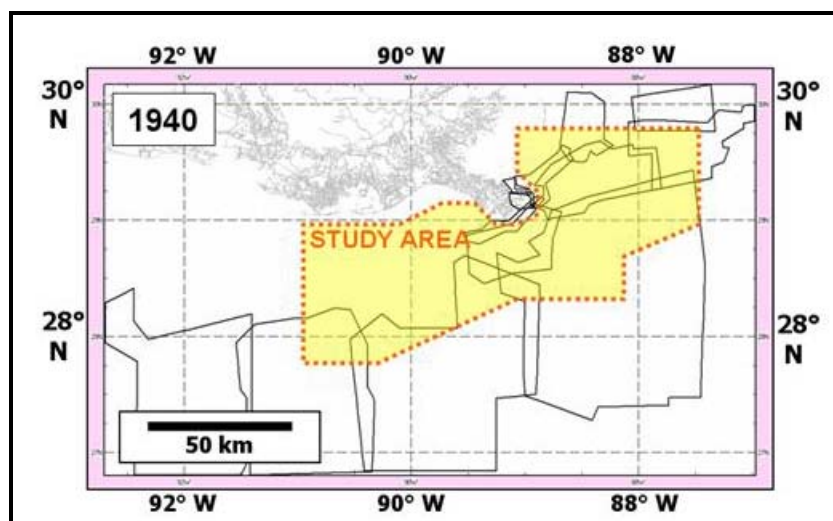


Figure F-1: Hydrographic survey areal coverage, 1868-1894 (modified from U.S. Coast and Geodetic Survey, 1957)

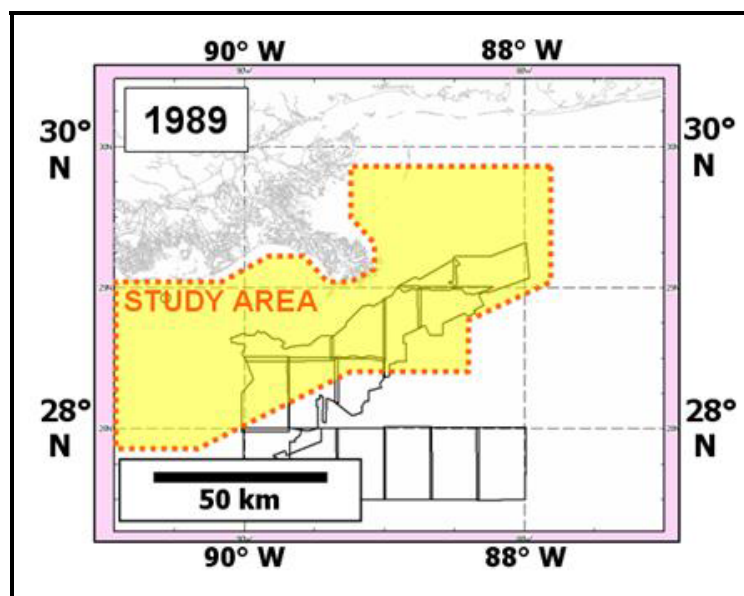




HYD93 Header (page 1 of 2)

survey	NGDC Num	SF	cr-date	source institution	
4 H06502	HYD93 03071030	S	19791231	National Ocean Survey, N.O.A.A.	01
country	platform	name	c	type	chief scientist(s)
U.S.A.	HYDROGRAPHER	1	SHIP	G.C. MATTISON	02
Project	type of survey	styr	endyr	scale	
		1940	1940	120,000	03
area-general	area-specific				
GULF OF MEXICO	OFF LOUISIANA COAST				04
quality of survey description	processing status description				
					05
position determination					
					06
hdrCode	horizontal datum (in records)	hdcCode	horizontal datum (original)		
NOS06	North American Datum 1927	NOS06	North American Datum 1927		07
vdCode	vertical datum	aveTide	original units		
02	Mean Low Water		fathoms		08
sounding method					
Digital Echo Sounder w/ Graphical Record assumed					09
HYD93 Header (page 1 of 2)					
HYD93 Header (page 2 of 2)					
svCode	sound velocity correction				
1	Corrected for actual sound velocity				10
data processing methodology					
Smooth sheets digitized for N.O.S. under Ashville Contract					11
HYD93 Ascii format	TopLat	BotLat	LeftLon	RightLon	
SURV,LAT,LOH,VAL,TYP,CCODE(A8,F9.6,F10.6,F6.1,I1,I3)	+28.38	+26.83	-92.68	-91.39	12

Figure F-2: Areal coverage and hydrographic survey details, 1940



HYD93 Header (page 1 of 2)									
survey	NGDC Num	SF	cr-date	source institution					
4	B00191	HYD93	03082014	S	1993012	National Ocean Survey, N.O.A.A.			
country	platform	name	c	type	chief scientist(s)				
U.S.A.	WHITING		1	SHIP	D.R. SEIDEL				
Project		type of survey		styr	endyr	scale			
K535-WH-89		EEZ Bathymetric Survey		1989	1989	50,000			
area-general		area-specific							
LOUISIANNA		27 NM SOUTHEAST OF SOUTH PASS, LA							
quality of survey description					processing status description				
position determination									
ARGO									
hdrCode	horizontal datum (in records)			hdcCode	horizontal datum (original)				
NOS31	North American Datum 1983			NOS31	North American Datum 1983				
vdCode	vertical datum			aveTide	original units				
04	Mean Lower Low Water				meters				
sounding method									
HYDROCHART II GENERAL INSTRUMENTS UNKNOWN 17 Beams 36 KHZ									
HYD93 Header (page 1 of 2)									
HYD93 Header (page 2 of 2)									
svCode	sound velocity correction								
1	Corrected, Vertical-cast Sound Velocity Table 89202-2031.VEL;9								
data processing methodology									
NOS Pacific Hydro Section - standard SEABEAM processing									
HYD93 Ascii format				TopLat	BotLat	LeftLon	RightLon		
SURV,LAT,LON,VAL,TYP,CODE(A6,F9.6,F10.6,F6.1,I1,I3)				+29.02	+28.37	-89.02	-88.73		
additional documentation									
This data is a subset of SEABEAM file. 5 Beams of actual data were extracted									
from each return. Sampling rate varies from 10 to 30 seconds along track.									

Figure F-3: Areal coverage and survey details, 1989 regional Gulf of Mexico bathymetry acquired by NOAA

## APPENDIX G: METOCEAN CONDITIONS, HURRICANE CAMILLE (1969)

Table G-1: Wave parameters during Hurricane Camille, August 17, 1969 (from Earle, 1975)

Time	H (m)	H <sub>RMS</sub> (m)	H <sub>S</sub> (m)	H <sub>MAX</sub> (m)	T (sec)	T <sub>S</sub> (sec)	T <sub>HMAX</sub>	Number of waves
0615-0645	2.82	3.16	4.44	7.02	7.2	8.7	9.8	249
0645-0715	2.90	3.30	4.73	8.39	7.2	9.1	10.6	249
0715-0745	3.05	3.41	4.79	7.67	7.4	9.6	7.7	242
0745-0815	3.10	3.49	4.92	8.50	7.5	9.4	11.0	238
0815-0845	3.50	3.90	5.49	8.54	8.3	10.3	8.6	216
0845-0915	3.85	4.26	5.92	9.49	8.4	10.5	10.4	214
0915-0945	3.87	4.36	6.20	9.58	8.2	10.7	10.9	218
0945-1015	4.60	5.12	7.16	12.12	8.6	10.7	11.4	209
1015-1045	4.65	5.15	7.05	12.02	9.0	11.1	9.7	199
1045-1115	5.37	6.10	8.72	12.15	9.2	11.8	9.3	193
1115-1145	5.84	6.52	9.17	15.12	9.4	11.5	10.5	190
1145-1215	6.23	7.07	9.90	23.60	9.8	12.4	12.5	183
1215-1245	6.38	7.21	10.26	15.18	9.9	12.3	9.1	182
1245-1315	6.32	7.22	10.19	21.37	9.8	12.3	12.1	182
1315-1345	7.58	8.47	11.82	19.26	11.0	12.6	11.4	162
1345-1415	6.97	7.76	10.69	18.99	9.6	11.8	12.9	187
1415-1445	7.00	7.85	11.11	16.02	9.4	12.0	10.1	191
1445-1515	7.75	8.58	12.00	18.82	9.8	11.5	12.4	183
1515-1545	8.35	9.40	13.45	22.99	10.0	11.8	11.9	179
1545-1615	8.12	9.34	13.36	22.22	9.3	11.5	13.7	192

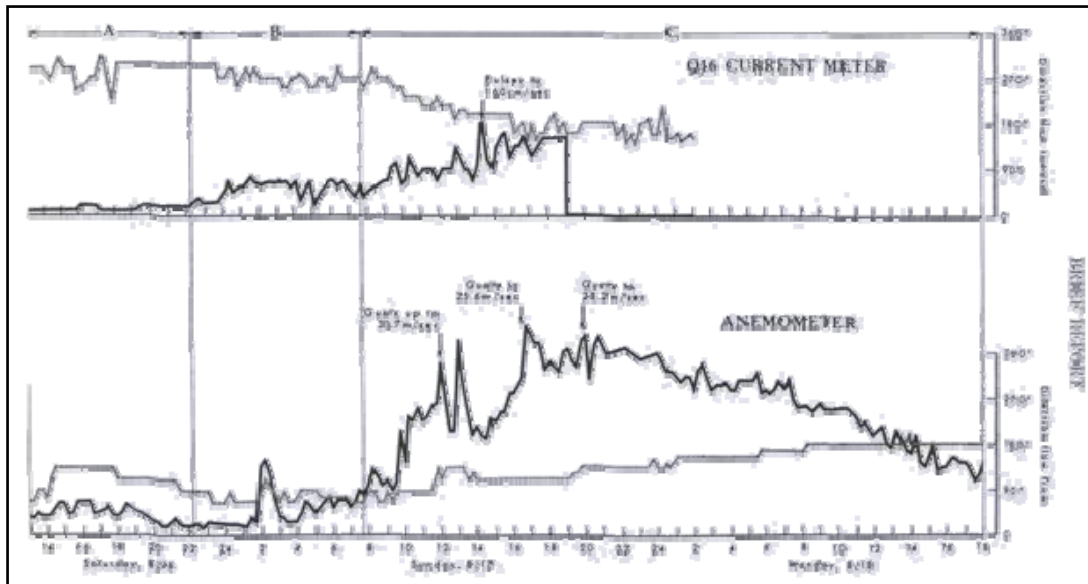


Figure G-1: Current speed and direction records, Hurricane Camille (from Earle, 1975)

## APPENDIX H: NATIONAL DATA BUOY CENTER GULF OF MEXICO BUOYS

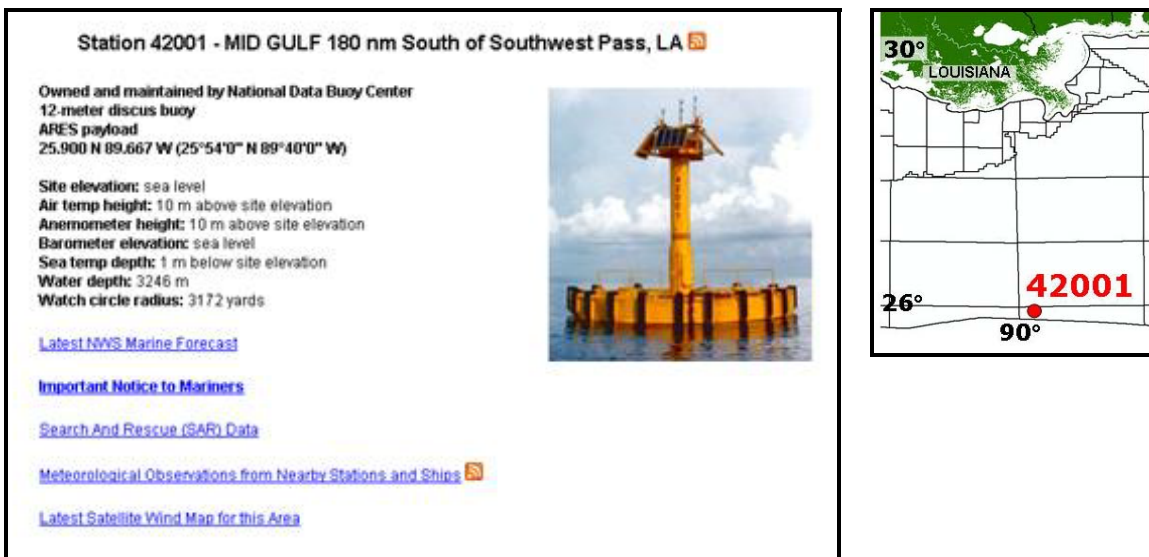


Figure H-1: Descriptor information, NDBC Data Buoy Number 42001 and proximity of buoy to MRDF (NDBC, 2009)



Figure H-2: Descriptor information, NDBC Data Buoy Number 42002 and proximity of buoy to MRDF (NDBC, 2009)

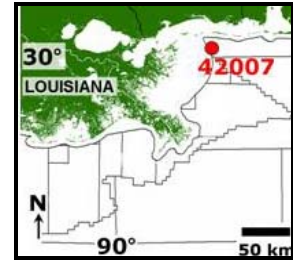
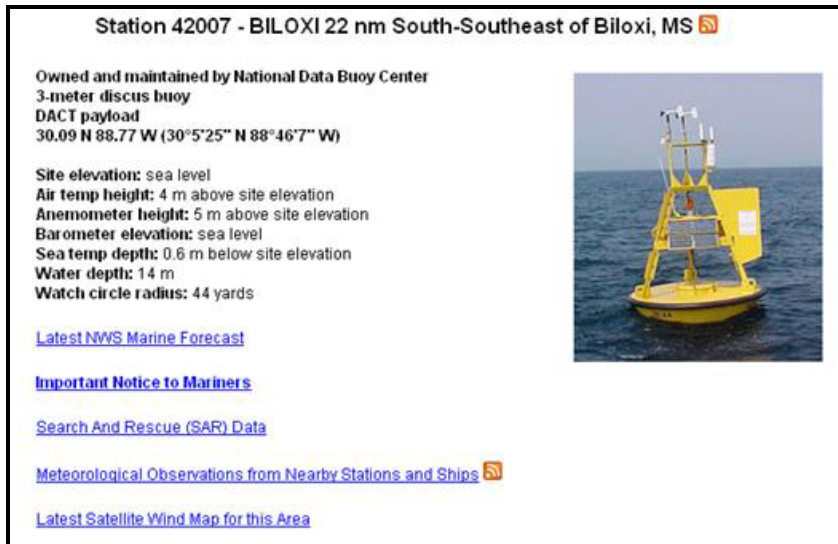


Figure H-3: Descriptor information, NDBC Data Buoy Number 42007 and proximity of buoy to MRDF (NDBC, 2009)

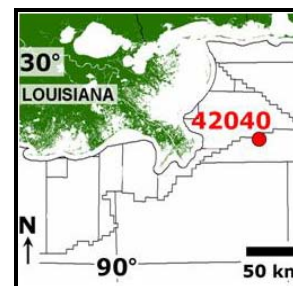
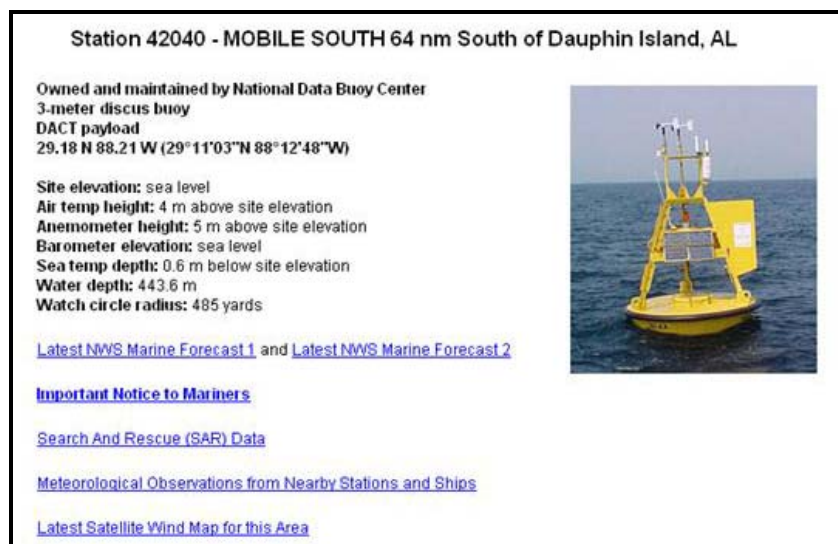


Figure H-4: Descriptor information, NDBC Data Buoy Number 42040 and proximity of buoy to MRDF (NDBC, 2009)

# **APPENDIX I: SUMMARY OF OFFSHORE INFRASTRUCTURE DAMAGE, HURRICANE ANDREW (1992)**

Table I-1: Areas of platform exposure and damage, Hurricane Andrew (from Daniels, 1994)

<b>Protraction Area</b>	<b>Undamaged</b>	<b>Damaged</b>	<b>Total</b>
Ship Shoal	159	12	171
Mississippi Canyon	6	-	6
West Delta	99	-	99
Eugene Island	128	-	128
South Timbalier	118	22	140
South Pelto	16	2	18
Ewing Bank	2	-	2
Grand Isle	60	-	60
South Pass	10	-	10
Green Canyon	1	-	1
<b>Total</b>	<b>599</b>	<b>36</b>	<b>635</b>

Table I-2: Full platforms exposed to hurricane force wind during Hurricane Andrew (from Daniels, 1994)

<b>Year Installed</b>	<b>Undamaged *</b>	<b>Damaged **</b>	<b>Total</b>
1950-1960	57	4	61
1961-1965	87	16	103
1966-1970	113	5	118
1971-1975	76	1	77
1976-1980	91	1	92
1981-1985	87	3	90
1986-1990	72	2	74
1990-1992	16	2	18
Undetermined	-	2	2
<b>Total</b>	<b>599</b>	<b>36</b>	<b>635</b>

\* Undamaged – no apparent damage

\*\* Damaged – platform was either bent significantly, completely toppled, or had significant topside damage



## APPENDIX J: SEA-STATE CONDITIONS DURING HURRICANE IVAN (2004) AS RECORDED BY U.S. NAVAL RESEARCH LABORATORY MOORINGS



U.S. Naval Research Laboratory moorings being retrieved after Hurricane Ivan and proximity of moorings to track of Hurricane Ivan, 2004 (NDBC, 2009)

A complete range of sea-state conditions was captured by a series of shelf and slope moorings maintained by the United States Naval Research Laboratory near the vicinity of Buoy 42040. Ivan moved directly over these moorings as it approached the Alabama coastline (Wang et al., 2005; Teague et al., 2007).

Table J1: Hourly reported conditions during Hurricane Ivan, September 15-16, 2004

<u>Year</u>	<u>Day</u>	<u>Hour</u>	<u>Maximum wave height (m)</u>	<u>Significant wave height (m)</u>
2004	15-Sep	3	4.0	6.6
2004		5	5.2	8.2
2004		7	6.1	8.7
2004		9	8.1	12.8
2004		12	8.1	9.6
2004		15	11.7	23.0
2004		18	17.6	21.8
2004		20	17.9	27.7
2004	16-Sep	22	7.7	12.9
2004		0	5.6	9.7
2004		3	9.6	18.1
2004		6	6.2	7.9
2004		8	4.0	5.0
2004		10	3.4	4.9



## **APPENDIX K: LOCAL BATHYMETRY DATASETS AND ACQUISITION PARAMETERS (ARRANGED IN TIME-CHRONOLOGICAL ORDER)**

**Survey 1: South Pass 28 (1964-1966):** No survey acquisition details are available for this study. The only data available are bathymetry maps acquired over a portion of SP 28 through time to illustrate changes in seafloor bathymetry as a result of Hurricanes Hilda and Betsy (Arnold, 1967).

**Survey 2: South Pass 35, 47 and 48 (1973):** Survey coverage consisted of 12 northwest-southeast track lines spaced 500 feet (~150 m) apart and six southwest-northeast tie lines spaced (850 m) apart. Shot points were recorded at 500 foot (~150 m) intervals. Data collection was performed in June 1973. Horizontal positioning of the survey vessel was accomplished with the Decca Hi-Fix navigation system. Data collected included side scan sonar, 3.5 kHz subbottom profiler, Atlas Echosounder, and a 4.2 kilojoule sparker system (Aquatronics, Inc./Decca Survey Systems, Inc., 1973).

**Survey 3: Main Pass 59 (1975):** Survey coverage consisted of 22 north-south track lines spaced 500 feet (~150 m) apart and six east-west tie lines spaced 850 m apart. Shot points were recorded at 500 foot (~150 m) intervals. Data collection was performed on August 24-25, 1975 aboard the M/V Mr. Jake. Horizontal positioning of the survey vessel was accomplished with the Decca Hi-Fix navigation system. Data collected included magnetometer, side scan sonar, 7.0 kHz subbottom profiler, Precision Echosounder, and a 4.2 kilojoule sparker system (Decca Survey Systems, Inc., 1975).

**Survey 4: West Delta 44 (1976):** No survey acquisition details are available for this study. The only data available are bathymetry maps over WD 44 and the western half of WD 45.

**Survey 5: South Pass 52 (1977):** No survey acquisition details are available for this study. The only data available are bathymetry maps over SP 52.

**Survey 6: Semi-Regional MRDF Survey, South Pass and Main Pass (1978):** Survey coverage consisted of northwest-southeast track lines parallel to regional dip spaced 1000 feet

(305 m) apart, and northeast-southwest tie lines perpendicular to regional dip spaced 3000 feet (914 m) apart. Shot points were recorded at 1000-foot (305 m) intervals. Data collection was performed from July 18 to August 6, 1977 aboard the M/V Java Seal. Horizontal positioning of the initial survey vessel was accomplished with a RAC/type N Radist radio positioning system. Data collected included side scan sonar, 3.5 kHz subbottom profiler, and an Acoustipulse single-channel, high resolution marine reflection seismic survey (McClelland Engineers, Inc., 1978).

**Survey 7: Main Pass 128 and 129 (1979):** Data collection was performed on June 10-19, 1979 aboard the M/V Benjamin. Horizontal positioning of the survey vessel was accomplished with a Hydrotrac/Navtrace navigation system. Data collected included magnetometer, side scan sonar, 3.5 kHz subbottom profiler, and a 24-fold medium-penetration seismic profiler. Sea conditions were good (0.0 to 1.0 m) and had no adverse impact on data quality (Odom Offshore Surveys, Inc., 1979).

**Survey 8: South Pass 50 and 51 (1981):** No survey acquisition details are available for this study. The only data available are bathymetry maps over SP 51 (Racal-Decca Surveys, Inc., 1981).

**Survey 9: Main Pass 58 (southern half; 1983):** Survey coverage consisted of 16 parallel lines spaced 500 feet (152 m) apart and six tie lines spaced 3,000 feet (914 m) apart. Shot points were recorded at 12.5-meter intervals. Data collection was performed on June 11-20, 1983 aboard the M/V Chad Michael. Horizontal positioning of the survey vessel was accomplished with a Trisponder/Navtrace navigation system. Data collected included 24 kHz echo sounder, side scan sonar, 3.5 kHz subbottom profiler, and a 24-fold medium-penetration seismic profiler. Sea conditions were good (0.3 to 1.3 m) and had no adverse impact on data quality (Odom Offshore Surveys, Inc., 1983a).

**Survey 10: Main Pass 62 (1983):** Survey coverage consisted of 16 parallel lines spaced 500 feet (152 m) apart and six tie lines spaced 3,000 feet (914 m) apart. Shot points were recorded at 12.5-meter intervals. Data collection was performed on June 11-20, 1983 aboard the

M/V Chad Michael. Horizontal positioning of the survey vessel was accomplished with a Trisponder/Navtrace navigation system. Data collected included 24 kHz echo sounder, side scan sonar, 3.5 kHz subbottom profiler, and a 24-fold medium-penetration seismic profiler. Sea conditions were good (0.3 to 1.3 m) and had no adverse impact on data quality (Odom Offshore Surveys, Inc., 1983b).

**Survey 11: Main Pass 63 (1983):** Survey coverage consisted of 16 parallel lines spaced 500 feet (152 m) apart and six tie lines spaced 3,000 feet (914 m) apart. Shot points were recorded at 12.5-meter intervals. Data collection was performed on June 11-20, 1983 aboard the M/V Chad Michael. Horizontal positioning of the survey vessel was accomplished with a Trisponder/Navtrace navigation system. Data collected included 24 kHz echo sounder, side scan sonar, 3.5 kHz subbottom profiler, and a 24-fold medium-penetration seismic profiler. Sea conditions were good (0.3 to 1.3 m) and had no adverse impact on data quality (Odom Offshore Surveys, Inc., 1983c).

**Survey 12: Viosca Knoll 985 (1983):** Survey coverage consisted of 24 parallel lines spaced 800 feet (244 m) apart and six tie lines spaced 2,950 feet (900 m) apart. Shot points were recorded at 12.5-meter intervals. Data collection was performed on October 20-22, 1983 aboard the M/V Geodetic Surveyor. Horizontal positioning of the survey vessel was accomplished with an Autotape navigation system. Data collected included side scan sonar, 3.5 kHz subbottom profiler, and a medium-penetration seismic profiler. Sea conditions were moderate (1.0 to 1.6 m) but had no adverse impact on data quality (John E. Chance & Associates, 1983).

**Survey 13: South Pass 53 (1984):** Survey coverage consisted of 17 north-south track lines spaced 300 m apart and 16 east-west tie lines spaced 300 m apart. Shot points were recorded at 50-meter intervals. Data collection was performed on July 25-28, 1984 aboard the M/V Chad Michael. Horizontal positioning of the survey vessel was accomplished with a Trisponder/Navtrace navigation system. Data collected included magnetometer, side scan sonar, 24 kHz echo sounder, 3.5 kHz subbottom profiler, and a high resolution seismic survey (12-fold,

24 trace) with a 160 in<sup>3</sup> (2,622 cm<sup>3</sup>) water gun. Sea conditions were moderate (0.5 to 1.0 m) but were considered acceptable for record quality (John E. Chance & Associates, 1984a).

**Survey 14: Viosca Knoll 989 and 990 (1984):** No survey acquisition details are available for this study. The only available data are bathymetry maps over VK 989 and 990 (John E. Chance & Associates, 1984b).

**Survey 15: West Delta 129 and 144 (1984):** Survey coverage consisted of 17 north-south track lines spaced 300 m apart and two east-west tie lines spaced 900 m apart. Shot points were recorded at 50-meter intervals. Data collection was performed on May 26-June 4, 1984 aboard the M/V Pine River. Horizontal positioning of the survey vessel was accomplished with a GULFSYL Syledis navigation system. Data collected included side scan sonar, fathometer, 3.5 kHz subbottom profiler, and a 24-channel seismic data acquisition system (Comap Geosurveys, Inc., 1984).

**Survey 16: South Pass 52 (1987):** Survey coverage consisted of a partial re-shoot of larger, regionally focused grid acquired in 1977 (McClelland Engineers, Inc., 1978). Survey coverage consisted of northwest-southeast track lines parallel to regional dip spaced 1000 feet (305 m) apart, and northeast-southwest tie lines perpendicular to regional dip spaced 3000 feet (914 m) apart. Shot points were recorded at 1000-foot (305 m) intervals. Initial data collection was performed from July 18 to August 6, 1977 aboard the M/V Java Seal; the portion of the survey re-acquired in 1986 was performed by Pelagos. Horizontal positioning of the initial survey vessel was accomplished with a RAC/type N Radist radio positioning system. Data collected included side scan sonar, 3.5 kHz subbottom profiler, and an Acoustipulse single-channel, high resolution marine reflection seismic survey. Sea conditions were not reported for the new survey (Arco Oil and Gas Company, 1987).

**Survey 17: West Delta 72 (1987):** Survey coverage consisted of 16 north-south track lines spaced 150 m apart and three east-west tie lines spaced 900 m apart. Shot points were recorded at 24.6-foot (7.5 m) intervals. Data collection was performed on October 7-9, 1987

aboard the M/V Stephanie. Horizontal positioning of the survey vessel was accomplished with a Microphase/Syledis navigation system. Data collected included magnetometer, side scan sonar, Innerspace Model 440 Echosounder bathymetry, 3.5 kHz subbottom profiler, and a high-resolution seismic survey acquired via a 48-channel hydrophone streamer. Sea conditions were considered acceptable for record quality (Environmental Geosciences, 1987).

**Survey 18: West Delta 87 (1987):** Survey coverage consisted of 30 north-south track lines spaced 150 m apart and eight east-west tie lines spaced 900 m apart. Data collection was performed on September 19-27, 1987. Horizontal positioning of the survey vessel was accomplished with a Microphase navigation system. Data collected included magnetometer, side scan sonar, 3.5 kHz subbottom profiler, water gun (near-channel) and depth sounder. In addition, all 48 channels of the water gun data were digitally recorded to a two-way travel time of 2.0 sec (Marine Technical Services, Inc., 1987).

**Survey 19: Main Pass 305 and 306 (1988):** Survey coverage consisted of 16 east-west track lines spaced 300 m apart and 11 north-south tie lines spaced 900 m apart. Shot points were recorded at 500-foot (152 m) intervals. Data collection was performed on July 4-5, 1988 aboard the M/V L'Arpenteur. Horizontal positioning of the survey vessel was accomplished with a Starfix navigation system. Data collected included magnetometer, side scan sonar, EDO Narrow Beam Bathymetric System, 3.5 kHz subbottom profiler, and a 4 kilojoule sparker seismic survey. Sea conditions were moderate (0.7 to 1.0 m) and were considered acceptable for record quality (John E. Chance & Associates, 1988a).

**Survey 20: South Pass 50, 51 and 52 (1988):** No survey acquisition details are available for this study. The only data available are bathymetry maps over SP 50, 51 and 52 (Arco Oil and Gas Company, 1988).

**Survey 21: West Delta 101 (1988):** Survey coverage consisted of 12 north-south track lines spaced 300 m apart and eight east-west tie lines spaced 900 m apart. Shot points were recorded at 150 m intervals. Data collection was performed on August 30-31, 1988 aboard the

M/V Geodetic Surveyor. Horizontal positioning of the survey vessel was accomplished with a Starfix navigation system. Data collected included magnetometer, side scan sonar, 3.5 kHz subbottom profiler, and a 160 in<sup>3</sup> (2,624 cm<sup>3</sup>) water gun profiler. Sea conditions were calm (0.3 to 1.3 m) and were considered acceptable for record quality (John E. Chance & Associates, 1988b).

**Survey 22: Main Pass 292 (1989):** Survey coverage consisted of 12 north-south track lines spaced 300 m apart and six east-west tie lines spaced 900 m apart. Shot points were recorded at 50-meter intervals. Data collection was performed on October 2-4, 1989 aboard the M/V Geodetic Surveyor. Horizontal positioning of the survey vessel was accomplished with a Starfix navigation system. Data collected included magnetometer, side scan sonar, 24 kHz echo sounder, 3.5 kHz subbottom profiler, 48-channel multi-fold seismic survey. Sea conditions were moderate (0.3 to 1.3 m) but were considered acceptable for record quality (John E. Chance & Associates, 1989).

**Survey 23: South Pass 68 (1989):** Survey coverage consisted of 15 north-south track lines spaced 300 m apart and four east-west tie lines spaced 900 m apart. Shot points were recorded at 50-meter intervals. Data collection was performed on November 19-20, 1989 aboard the R/V Albuquerque. Horizontal positioning of the survey vessel was accomplished with a Trisponder positioning system and a Sentinel computer system. Data collected included magnetometer, side scan sonar, 41 kHz echo sounder, and 3.5 kHz subbottom profiler (Kinsella, Cook & Associates, Inc., 1989).

**Survey 24: Main Pass 149 (1990):** Survey coverage consisted of 13 north-south track lines spaced 300 m apart and six east-west tie lines spaced 900 m apart. A shipping fairway is positioned diagonally in a northwest-southeast direction across the western one-third of the block. As a result, only the east-west tie lines were acquired over the fairway; north-south track lines end at the fairway boundary. Shot points were recorded at 50-meter intervals. Data collection was performed on July 14-15, 1990 aboard the M/V Geodetic Surveyor. Horizontal positioning

of the survey vessel was accomplished with a Starfix navigation system. Data collected included magnetometer, side scan sonar, 24 kHz echo sounder, 3.5 kHz subbottom profiler, and a high-resolution seismic survey acquired via a 48-channel hydrophone streamer. Sea conditions were good (0.3 to 1.0 m) and were considered acceptable for record quality (John E. Chance & Associates, 1990d).

**Survey 25: South Pass 50 and 51 (1990):** Survey coverage consisted of 31 north-south track lines spaced 300 m apart and five east-west tie lines spaced approximately 900 m apart. Shot points were recorded at 150-meter intervals. A shipping fairway is oriented northeast-southwest through SP 51; therefore the survey does not cover the extreme northwestern quadrant of the block. Data collection was performed on December 2-6, 1989 aboard the M/V Geodetic Surveyor. Horizontal positioning of the survey vessel was accomplished with a Starfix navigation system. Data collected included magnetometer, side scan sonar, Echosounder bathymetry, 3.5 kHz subbottom profiler, and a 48-channel multifold seismic survey. Sea conditions were variable (0.3 to 3.0 m) and were discontinued for one day (December 4) to wait for better weather. Conditions during the remainder of the survey were considered acceptable for record quality (Arco Oil and Gas Company, 1990).

**Survey 26: South Pass 55 (1990):** Survey coverage consisted of 16 north-south track lines spaced 300 m apart and eight east-west tie lines spaced 900 m apart. Shot points were recorded at 150-meter intervals. Data collection was performed on August 27-29, 1989 aboard the M/V L'Arpenteur. However, complete side-scan sonar coverage was not obtained during the original survey and most lines were re-acquired on January 27-29 aboard the M/V Geodetic Surveyor. Horizontal positioning of the survey vessel was accomplished with a Starfix navigation system. Data collected included magnetometer, side scan sonar, Echotrac bathymetry, and a 3.5 kHz subbottom profiler. Sea conditions were moderate but were considered acceptable for record quality (John E. Chance & Associates, 1990a).



**Survey 27: South Pass 69 and Viosca Knoll 898 and 942 (1990):** Survey coverage consisted of 29 north-south track lines spaced 300 m apart and nine east-west tie lines spaced approximately 800 m apart. Shot points were recorded at 150-meter intervals. Data collection was performed on April 28-29, May 7-8, and May 14-16, 1990 aboard the M/V El Topografo. Horizontal positioning of the survey vessel was accomplished with a Starfix navigation system. Data collected included magnetometer, side scan sonar, Echotrac bathymetry, 3.5 kHz subbottom profiler, and a 24-channel multifold seismic survey. Sea conditions were moderate but were considered acceptable for record quality (John E. Chance & Associates, 1990b).

**Survey 28: South Pass 90, 91 and 92 (1990):** Survey coverage consisted of 16 north-south track lines spaced 300 m apart and 11 east-west tie lines spaced approximately 900 m apart, all of which were designed to avoid a shipping fairway that covers most of SP 90. Shot points were recorded at 150-meter intervals. Data collection was performed on May 14-16, 1990 aboard the M/V L'Arpenteur. Horizontal positioning of the survey vessel was accomplished with a Starfix navigation system. Data collected included magnetometer, side scan sonar, Echotrac bathymetry, 3.5 kHz subbottom profiler, and a 48-channel multifold seismic survey. Sea conditions were good and considered acceptable for record quality (John E. Chance & Associates, 1990c).

**Survey 29: Main Pass 308 and Viosca Knoll 814 and 815 (1991):** Survey coverage consisted of 17 east-west track lines spaced 300 m apart and 11 north-south tie lines spaced 900 m apart. Shot points were recorded at 50-meter intervals. Data collection was performed on June 20-July 5, 1991 aboard the R/V Albuquerque by Kinsella, Cook & Associates, Inc. under contract to Arco Oil and Gas Company. Horizontal positioning of the survey vessel was accomplished via three portable Del Norte transponders located on platforms in the vicinity of the survey area. Data collected included magnetometer, side scan sonar, 41 kHz echo sounder, 3.5 kHz subbottom profiler, a medium-penetration profiler survey using a 10 in<sup>3</sup> (164 cm<sup>3</sup>) sleeve gun, and a multi-fold seismic survey acquired by a 100 in<sup>3</sup> (1,640 cm<sup>3</sup>) sleeve air gun as a source and a 48-channel

streamer as a receiver. Sea conditions were good (less than 0.7 m) and were considered acceptable for record quality (Arco Oil and Gas Company, 1991a).

**Survey 30: Pipeline Route, South Pass 52 to Mississippi Canyon 148 (1991):** Survey coverage consisted of 18 northeast-southwest track lines spaced 300 m apart (oriented parallel to the proposed pipeline route) and seven northwest-southeast tie lines spaced 900 m apart (oriented perpendicular to the proposed pipeline route). Shot points were recorded at 50-meter intervals. Data collection was performed on May 6-9, 1991 aboard the M/V Global Surveyor. Horizontal positioning of the survey vessel was accomplished with a Starfix navigation system. Data collected included magnetometer, side scan sonar, 200 kHz echo sounder, and a 3.5 kHz subbottom profiler. Sea conditions were moderate (1.0 to 2.0 m) but were considered acceptable for record quality (Arco Oil and Gas Company, 1991b).

**Survey 31: West Delta 129 (1991):** Survey coverage consisted of 20 north-south track lines spaced 300 m apart and five east-west tie lines spaced 900 m apart. Shot points were recorded at 50-meter intervals. Data collection was performed from August 22 through September 2, 1990 aboard the M/V Global Surveyor (August 22-24) and the M/V Geodetic Surveyor (September 1-2). Horizontal positioning of the survey vessel was accomplished with a Starfix navigation system. Data collected included magnetometer, side scan sonar, 200 kHz echo sounder, 3.5 kHz subbottom profiler, a medium-penetration seismic survey with a 10 in<sup>3</sup> sleeve air gun, and a 48-channel multi-fold seismic survey. Sea conditions were moderate (0.5 to 1.0 m) but were considered acceptable for record quality (Arco Oil and Gas Company, 1991c).

**Survey 32: West Delta 26 and 49 (1992):** Survey coverage consisted of 22 north-south track lines spaced 150 m apart and 14 east-west tie lines spaced 900 m apart. Shot points were recorded at 50-meter intervals. Data collection was performed from June 15-20, 1990 aboard the M/V Geodetic Surveyor. Horizontal positioning of the survey vessel was accomplished with a Starfix navigation system. Data collected included magnetometer, side scan sonar, 200 kHz echo sounder, 3.5 kHz subbottom profiler, a medium-penetration seismic survey with a 10 in<sup>3</sup> sleeve

air gun, and a 48-channel multi-fold seismic survey. Sea conditions were moderate (0.5 to 1.0 m) but were considered acceptable for record quality (Arco Oil and Gas Company, 1992).

**Survey 33: Main Pass 294 and 295 (1993):** Survey coverage consisted of 23 north-south track lines spaced 300 m apart and seven east-west tie lines spaced 900 m apart. Shot points were recorded at 50-meter intervals. Data collection was performed on May 28-June 1, 1993 and from June 28-July 5, 1993 aboard the M/V L'Arpenteur. Horizontal positioning of the survey vessel was accomplished with a Starfix navigation system. Data collected included magnetometer, side scan sonar, 200 kHz echo sounder, 3.5 kHz subbottom profiler, a medium-penetration seismic survey with a 10 in<sup>3</sup> sleeve air gun, and a 48-channel multi-fold seismic survey. Sea conditions were moderate (0.5 to 1.0 m) but were considered acceptable for record quality (John E. Chance & Associates, 1994).

**Survey 34: South Pass 56 (1993):** Survey coverage consisted of 16 north-south track lines spaced 300 m apart and five east-west tie lines spaced 900 m apart. Shot points were recorded at 50-meter intervals. Data collection was performed on May 21-23, 1993 aboard the M/V L'Arpenteur. Horizontal positioning of the survey vessel was accomplished with a Starfix differential GPS navigation system. Data collected included magnetometer, side scan sonar, 200 kHz echo sounder, 3.5 kHz subbottom profiler, and a 48-channel multi-fold seismic survey. Sea conditions were considered acceptable for record quality (Arco Oil and Gas Company, 1993a).

**Survey 35: West Delta 149 (1993):** Survey coverage consisted of 11 southwest-northeast track lines spaced 300 m apart and four northwest-southeast tie lines spaced 900 m apart. Shot points were recorded at 50-meter intervals. Data collection was performed on May 26-27, 1993 aboard the M/V L'Arpenteur. Horizontal positioning of the survey vessel was accomplished with a Starfix differential GPS navigation system. Data collected included magnetometer, side scan sonar, 200 kHz echo sounder, 3.5 kHz subbottom profiler, a medium-penetration seismic survey with a 10 in<sup>3</sup> sleeve air gun, and a 48-channel multi-fold seismic

survey. Sea conditions were moderate (0.5 to 1.0 m) but were considered acceptable for record quality (Arco Oil and Gas Company, 1993b).

**Survey 36: West Delta 102 (1994):** Survey coverage consisted of 12 north-south track lines spaced 300 m apart and seven east-west tie lines spaced 900 m apart. Data collection was performed on October 12-13, 1993 aboard the M/V Albuquerque. Horizontal positioning of the survey vessel was accomplished with a differential GPS navigation system. Data collected included magnetometer, side scan sonar, 208 kHz echo sounder, 3.5 kHz subbottom profiler, and a 48-channel multi-fold seismic survey (Arco Oil and Gas Company, 1994).

**Survey 37: South Pass 38 (1995):** Survey coverage consisted of 16 east-west track lines spaced 300 m apart and six north-south tie lines spaced 900 m apart. Shot points were recorded at 50-meter intervals. Data collection was performed on February 21-26, 1995 aboard the M/V Seis Surveyor. Horizontal positioning of the survey vessel was accomplished with a Starfix navigation system. Data collected included magnetometer, side scan sonar, 200 kHz echo sounder, 3.5 kHz subbottom profiler, and a medium-penetration, multi-fold seismic survey acquired by a 100 in<sup>3</sup> (1640 cm<sup>3</sup>) sleeve air gun as a source and a 48-channel streamer as a receiver. Sea conditions were good (no precise conditions were reported) and were considered acceptable for record quality (John E. Chance & Associates, 1995).

**Survey 38: South Pass 69 (1995):** Survey coverage consisted of 11 east-west track lines spaced 300 m apart and four north-south tie lines spaced 900 m apart. Shot points were recorded at 50-meter intervals. A shipping fairway is oriented northeast-southwest through SP 69; therefore the survey covers only the northwest quadrant and the extreme southeast quadrant of the block. Data collection was performed on May 30, 1995 aboard the R/V Albuquerque. Horizontal positioning of the survey vessel was accomplished with a differential GPS navigation system. Data collected included magnetometer, side scan sonar, 24 kHz echo sounder, 3.5 kHz subbottom profiler, and a medium-penetration, multi-fold seismic survey acquired by a 100 in<sup>3</sup> (1640 cm<sup>3</sup>) sleeve air gun as a source and a 48-channel streamer as a receiver. Sea conditions were good (no

precise conditions were reported) and were considered acceptable for record quality (Vastar Resources, Inc., 1995).

**Survey 39: Mississippi Delta Regional Study (1997):** This regional survey was acquired as advance support for a subsequent, regional-scale, bottom-cable exploration seismic survey conducted by Western Geophysical in the summer of 1997. Survey coverage consisted of 186 lines spaced at varying intervals of 100 m and 150 m over approximately 900 km<sup>2</sup>. Shot points were recorded at 50-meter intervals. Data collection was performed on May 12-June 1, 1997 by John Chance & Associates aboard the M/V Polo Pony. Horizontal positioning of the survey vessel was accomplished with a Starfix differential GPS navigation system. Data collected included side scan sonar, 200 kHz echo sounder, and a 3.5 kHz subbottom profiler (Vastar Resources, Inc., 1997a).

**Survey 40: South Pass 17 and 18 (1997):** Survey coverage consisted of 16 north-south track lines spaced 300 m apart and six east-west tie lines spaced 900 m apart. Shot points were recorded at 50-meter intervals. Data collection was performed on September 16-18, 1997 aboard the R/V Albuquerque. Horizontal positioning of the survey vessel was accomplished with a differential GPS navigation system and Sentinel navigation software. Data collected included magnetometer, side scan sonar, 200 kHz echo sounder, 3.5 kHz subbottom profiler, and a medium-penetration, multi-fold seismic survey acquired by a 100 in<sup>3</sup> (1640 cm<sup>3</sup>) sleeve air gun as a source and a 48-channel streamer as a receiver. Sea conditions were good (0.5 to 1.0 m) and were considered acceptable for record quality (Vastar Resources, Inc., 1997b).

**Survey 41: MPOG Pipeline Route, Main Pass 61, 73, 140 and 147 (2005):** Coverage of this post-Ivan survey consisted of 36 east-west track lines spaced 75 m apart and three northwest-southeast tie lines spaced at variable distances of approximately 900 m. Data collected included magnetometer, side scan sonar, echo sounder, and a 3.5 kHz subbottom profiler (Fugro GeoServices, Inc., 2004).

**Survey 42: West Delta 70 and 94 (2005):** Survey coverage consisted of 23 north-south track lines and 42 east-west tie lines, all spaced approximately 100 m apart. Data collection was performed on September 6-8, 2005 aboard the R/V Geodetic Surveyor. Horizontal positioning of the survey vessel was accomplished with Fugro Starfix differential global positioning system. Data collected included magnetometer, side scan sonar, 3.5 kHz subbottom profiler, and Echotrac bathymetry (Fugro GeoServices, Inc., 2005a).

**Survey 4543 West Delta 94 (2005):** Survey coverage consisted of four northeast-southwest track lines and four northwest-southeast tie lines, all spaced 150 m apart. Data collection was performed on September 4, 2005 aboard the R/V Geodetic Surveyor. Horizontal positioning of the survey vessel was accomplished with Fugro Starfix differential global positioning system. Data collected included side scan sonar and Echotrac bathymetry (Fugro GeoServices, Inc., 2005b).

**Survey 44: Enterprise Pipeline Route, South Pass 53 to Viosca Knoll 985 (2005):** No survey acquisition details are available for this study. Data provided include side scan sonar and multi-beam bathymetry obtained after Hurricane Katrina along a 20-inch (0.5-meter) pipeline route (Enterprise Products Partners, LLC; 2005).

**Survey 45: MPOG Pipeline Route, Main Pass 61, 73, 140 and 147 (2005):** Coverage of this post-Katrina survey consisted of 36 east-west track lines spaced 75 m apart and three northwest-southeast tie lines spaced at variable distances of approximately 900 m. Data collected included magnetometer, side scan sonar, echo sounder, and a 3.5 kHz subbottom profiler (Fugro GeoServices, Inc., 2005c).

**Survey 46: South Pass 19 (2006):** Data collection was performed on December 16-21, 2006. No additional survey acquisition details are available for this study. Data provided include side scan sonar and multi-beam bathymetry obtained approximately one year after Hurricane Katrina moved through the area (Plains Resources, 2006).

## APPENDIX L: MRDF GEOTECHNICAL BOREHOLE DATABASE

Table L-1: Texas A&M/MMS Geotechnical Borehole Database (arranged in time-sequential order; from Dunlap et al., 2004)

Number	Protraction Area	Block	Latitude	Longitude	Lith (mm) *	Depth (m)	Depth (ft)	Date	Operator
1	Main Pass	127	29.442904	-88.851724	0.005	-17.98	-59.00	1970-01-15	Chevron
2	Main Pass	127	29.446689	-88.841024	0.005	-17.98	-59.00	1970-06-15	Chevron
<b>CARMEN</b>									
3	South Timbalier	140	28.662715	-90.504265	0.005	-20.12	-66.00	1974-12-21	HughesDenny
<b>ELOISE</b>									
4	South Timbalier	86	28.783994	-90.234244	0.005	-27.43	-90.00	1977-03-06	Odeco
5	Main Pass	114	29.455259	-88.848842	0.005	-17.07	-56.00	1978-01-21	DiamondShamrock
6	Main Pass	114	29.508999	-88.808654	0.005	-14.63	-48.00	1978-01-23	DiamondShamrock
7	South Pelto	19	28.899152	-90.699405	0.100	-9.14	-30.00	1978-10-16	Odeco
8	West Delta	63	29.052263	-89.691632	0.005	-32.00	-105.00	1979-03-26	Arco
9	South Timbalier	53	28.854895	-90.458482	0.005	-19.20	-63.00	1979-08-24	Unocal
<b>FREDERIC</b>									
10	South Timbalier	53	28.844109	-90.439448	0.005	-19.81	-65.00	1981-05-13	Unocal
11	Main Pass	77	29.182196	-88.903839	0.005	-45.42	-149.00	1981-09-15	Gulf
12	South Timbalier	34	28.918355	-90.476697	0.005	-16.15	-53.00	1981-09-19	KerrMcGee
13	South Timbalier	34	28.914261	-90.486855	0.005	-16.15	-53.00	1981-09-20	KerrMcGee
14	Main Pass	114	29.455045	-88.848976	0.005	-17.68	-58.00	1981-12-02	DiamondShamrock
15	Main Pass	310	29.187399	-88.683473	0.005	-74.98	-246.00	1982-02-10	Shell
16	South Timbalier	54	28.833397	-90.416734	0.005	-20.12	-66.00	1982-02-18	Exxon
17	South Pelto	25	28.830110	-90.526643	0.050	-19.51	-64.00	1982-11-17	Shell
18	South Timbalier	221	28.395185	-90.493362	0.005	-47.24	-155.00	1983-10-19	Amoco
19	Main Pass	165	29.621748	-88.450381	0.005	-41.76	-137.00	1983-11-18	HallHouston
20	Mobile Bay	952	30.042397	-88.296877	0.100	-21.34	-70.00	1983-12-20	Odeco
21	Mobile Bay	953	30.032632	-88.275234	0.100	-22.25	-73.00	1983-12-20	Odeco
22	Main Pass	128	29.381160	-88.869235	0.005	-22.86	-75.00	1984-01-27	Arco
23	South Timbalier	147	28.596526	-90.471930	0.005	-30.18	-99.00	1984-08-25	Tenneco
24	Main Pass	93	29.619733	-88.790621	0.100	-14.02	-46.00	1984-09-04	KerrMcGee
25	South Timbalier	245	28.292344	-90.659306	0.005	-58.52	-192.00	1984-11-26	Amoco
26	Main Pass	243	29.364577	-88.282417	0.100	-59.74	-196.00	1985-03-06	HallHouston
27	South Timbalier	143	28.595952	-90.622281	0.005	-22.10	-72.50	1985-03-26	HallHouston
28	Mobile Bay	861	30.109849	-88.443817	0.005	-16.46	-54.00	1985-04-28	Chevron
29	Mobile Bay	861	30.118101	-88.446774	0.100	-15.24	-50.00	1985-05-09	Chevron
30	Main Pass	64	29.324652	-89.049397	0.050	-12.19	-40.00	1985-05-15	Howell
31	Main Pass	64	29.324652	-89.049397	0.020	-12.19	-40.00	1985-05-15	Linder
32	South Timbalier	53	28.845466	-90.461494	0.005	-20.12	-66.00	1985-06-09	Unocal
<b>ELENA</b>									
33	South Timbalier	76	28.761603	-90.674979	0.005	-18.59	-61.00	1985-12-10	CNG
34	Mobile Bay	827	30.177533	-87.939341	0.100	-14.33	-47.00	1986-01-26	Exxon
35	Mobile Bay	823	30.188845	-88.163075	0.020	-12.50	-41.00	1986-01-27	Mobil
36	Mobile Bay	991	30.000873	-88.555107	0.100	-25.60	-84.00	1986-04-11	Gulfstar
37	Chandeleur Sound	30	29.691968	-88.763618	0.005	-15.24	-50.00	1986-09-13	HallHouston
38	Main Pass	124	29.413911	-88.720545	0.005	-42.06	-138.00	1986-11-15	DiamondShamrock
39	Main Pass	125	29.419765	-88.735510	0.005	-39.32	-129.00	1986-11-16	DiamondShamrock
40	Main Pass	56	29.352664	-89.102600	0.100	-9.14	-30.00	1986-12-03	Walter
41	Chandeleur Sound	40	29.703514	-88.518763	0.005	-32.92	-108.00	1986-12-29	Phillips
42	Main Pass	95	29.622444	-88.709832	0.005	-17.98	-59.00	1987-01-01	South Pelto
43	Mobile Bay	870	30.137972	-88.002639	0.100	-17.68	-58.00	1987-02-24	SantaFe
44	Main Pass	101	29.569683	-88.735724	0.100	-15.24	-50.00	1987-03-10	Samedan
45	Main Pass	244	29.370240	-88.240078	0.100	-60.35	-198.00	1987-04-17	HallHouston
46	South Timbalier	51	28.897868	-90.476356	0.005	-18.59	-61.00	1987-05-27	Chevron
47	West Delta	18	29.180034	-89.723437	0.005	-14.33	-47.00	1987-05-29	Samedan
48	Main Pass	209	29.471207	-88.464269	0.005	-54.25	-178.00	1987-07-03	HallHouston
49	Main Pass	202	29.498721	-88.451108	0.005	-52.43	-172.00	1987-07-07	HallHouston
50	Main Pass	227	29.398339	-88.156872	0.100	-60.66	-199.00	1987-07-10	HallHouston
51	Mobile Bay	872	30.153658	-87.900060	0.100	-11.89	-39.00	1987-08-28	Texaco
52	South Timbalier	151	28.616266	-90.249653	0.005	-43.59	-143.00	1987-10-16	Chevron
53	Mobile Bay	916	30.081812	-87.886439	0.100	-16.15	-53.00	1987-11-06	Union
54	Mobile Bay	914	30.077709	-88.012679	0.100	-20.73	-68.00	1987-11-29	SantaFe
55	Main Pass	252	29.360902	-87.885817	0.100	-84.43	-277.00	1987-12-05	Shell
56	Mobile Bay	961	30.054560	-87.870675	0.100	-19.20	-63.00	1987-12-06	Union
57	Grand Isle	41	28.981122	-89.977425	0.005	-27.74	-91.00	1987-12-16	Conoco
58	Mobile Bay	915	30.077761	-87.963757	0.100	-17.83	-58.50	1987-12-26	Union
59	Mobile Bay	904	30.084645	-88.496458	0.100	-18.59	-61.00	1988-01-11	Union
60	Chandeleur Sound	38	29.723262	-88.482103	0.005	-33.83	-111.00	1988-01-15	Samedan
61	Chandeleur Sound	34	29.725371	-88.543500	0.005	-30.48	-100.00	1988-02-18	HallHouston
62	South Timbalier	160	28.584125	-90.374247	0.005	-36.73	-120.50	1988-02-25	Amoco
63	South Timbalier	75	28.767511	-90.743135	0.005	-18.59	-61.00	1988-03-13	CNG
64	South Timbalier	107	28.703632	-90.355081	0.005	-23.47	-77.00	1988-03-29	Century
65	Main Pass	208	29.471467	-88.440229	0.005	-54.56	-179.00	1988-04-27	South Pelto
66	Grand Isle	82	28.685641	-89.959122	0.005	-61.87	-203.00	1988-05-16	HallHouston
67	West Delta	89	28.901862	-89.612664	0.005	-64.01	-210.00	1988-05-23	McMoRan
68	South Timbalier	198	28.449277	-90.685233	0.005	-39.62	-130.00	1988-05-29	UnionPacific
69	Main Pass	108	29.551950	-88.666057	0.005	-19.81	-65.00	1988-06-18	KerrMcGee
70	West Delta	33	29.161016	-89.740673	0.005	-16.92	-55.50	1988-07-24	Samedan

--- continued on following page ---

\* Grain sizes in "Lithology" column assigned as an average of the lithologic descriptor from each borehole based on grain size standards from Wentworth (1922); VTA boreholes in yellow.



Number	Protraction Area	Block	Latitude	Longitude	Lith (mm) *	Depth (m)	Depth (ft)	Date	Operator
71	Main Pass	301	29.206919	-88.767317	0.005	-68.88	-226.00	1988-08-18	Walter
72	Mobile Bay	1002	29.994775	-88.027417	0.125	-24.99	-82.00	1988-08-26	Union
73	Mobile Bay	1003	30.007236	-87.974489	0.150	-22.25	-73.00	1988-08-26	Unocal
74	South Timbalier	206	28.429870	-90.308174	0.005	-52.88	-173.50	1988-09-21	Amerada
75	South Timbalier	205	28.433975	-90.346830	0.005	-50.44	-165.50	1988-09-23	Amerada
76	West Delta	100	28.859329	-89.746261	0.005	-60.05	-197.00	1988-10-15	Exxon
77	Mobile Bay	869	30.139132	-88.078609	0.100	-14.33	-47.00	1988-10-28	Texaco
78	Chandeleur Sound	24	29.738450	-88.649669	0.005	-19.81	-65.00	1988-11-12	Century
79	Chandeleur Sound	41	29.708418	-88.473235	0.005	-35.97	-118.00	1988-12-19	Odeco
80	South Timbalier	225	28.385787	-90.300826	0.005	-57.30	-188.00	1988-12-24	TXP
81	West Delta	140	28.697819	-89.707012	0.005	-91.74	-301.00	1989-01-15	Amoco
82	West Delta	63	29.004194	-89.678954	0.005	-42.37	-139.00	1989-02-26	Walter
83	West Delta	97	28.859511	-89.844576	0.005	-49.38	-162.00	1989-03-19	Zilkha
84	South Timbalier	197	28.474118	-90.720593	0.005	-36.58	-120.00	1989-04-01	KerrMcGee
85	Main Pass	108	29.552887	-88.659923	0.005	-21.03	-69.00	1989-05-13	KerrMcGee
86	Main Pass	107	29.530497	-88.690648	0.100	-18.75	-61.50	1989-05-14	KerrMcGee
87	West Delta	62	29.022133	-89.663760	0.005	-37.80	-124.00	1989-06-22	Walter
88	Main Pass	112	29.505649	-88.719811	0.100	-17.98	-59.00	1989-08-07	DiamondShamrock
89	Main Pass	112	29.511442	-88.699050	0.100	-18.29	-60.00	1989-08-07	DiamondShamrock
90	Grand Isle	79	28.750975	-89.865792	0.005	-61.87	-203.00	1989-08-14	South Pelto
91	Main Pass	93	29.648825	-88.780290	0.005	-14.02	-46.00	1989-08-23	KerrMcGee
92	West Delta	86	28.904461	-89.531549	0.005	-58.52	-192.00	1989-08-26	Marathon
93	Grand Isle	102	28.414004	-90.065963	0.005	-78.33	-257.00	1989-09-06	Agip
94	Main Pass	186	29.546996	-88.329963	0.100	-45.72	-150.00	1989-09-15	HallHouston
95	Main Pass	187	29.525870	-88.280397	0.100	-47.24	-155.00	1989-09-20	Cockrell
96	Main Pass	94	29.633110	-88.755139	0.005	-13.41	-44.00	1989-11-09	KerrMcGee
97	South Timbalier	226	28.410372	-90.279793	0.005	-55.17	-181.00	1990-03-23	Elf
98	Mobile Bay	864	30.108464	-88.326155	0.100	-19.20	-63.00	1990-04-01	Arco
99	Viosca Knoll	69	29.926012	-88.478353	0.005	-31.09	-102.00	1990-05-06	HallHouston
100	West Delta	22	29.175985	-89.609253	0.005	-10.67	-35.00	1990-06-12	Samedan
101	South Timbalier	38	28.936474	-90.313988	0.005	-18.29	-60.00	1990-06-20	Elf
102	Grand Isle	55	28.886123	-89.863644	0.005	-44.81	-147.00	1990-06-23	Elf
103	Viosca Knoll	22	29.972976	-88.604176	0.005	-23.77	-78.00	1990-07-01	SantaFe
104	West Delta	28	29.131168	-89.579034	0.005	-12.19	-40.00	1990-07-26	Chevron
105	West Delta	20	29.176689	-89.669862	0.005	-13.11	-43.00	1990-08-27	Samedan
106	South Timbalier	30	28.958593	-90.361267	0.005	-15.24	-50.00	1990-11-10	ATP
107	West Delta	97	28.839494	-89.838611	0.005	-52.12	-171.00	1990-12-09	Zilkha
108	Main Pass	181	29.542857	-88.562200	0.005	-41.76	-137.00	1991-01-05	DiamondShamrock
109	Viosca Knoll	203	29.781278	-88.333452	0.100	-37.49	-123.00	1991-01-25	Murphy
110	Viosca Knoll	203	29.794521	-88.359465	0.005	-36.58	-120.00	1991-01-26	Murphy
111	Viosca Knoll	204	29.785661	-88.299646	0.005	-37.49	-123.00	1991-01-27	Murphy
112	Mobile Bay	865	30.137295	-88.257210	0.100	-19.05	-62.50	1991-03-20	Scana
113	Mobile Bay	916	30.094382	-87.883185	0.100	-15.54	-51.00	1991-03-20	Unocal
114	South Timbalier	143	28.625292	-90.628925	0.005	-20.73	-68.00	1991-07-01	Apache
115	South Timbalier	144	28.593912	-90.595697	0.005	-25.30	-83.00	1991-07-02	HallHouston
116	South Timbalier	136	28.649698	-90.292965	0.100	-28.35	-93.00	1991-08-25	GreatWestern
117	Main Pass	310	29.163938	-88.665371	0.100	-80.47	-264.00	1991-10-03	Shell
118	South Timbalier	194	28.507408	-90.629630	0.005	-34.44	-113.00	1991-12-06	Newfield
119	Main Pass	175	29.578009	-88.354872	0.100	-42.67	-140.00	1992-01-16	GenAtlantic
120	West Delta	103	28.880423	-89.663031	0.005	-64.62	-212.00	1992-05-03	Amoco
121	South Pelto	19	28.893857	-90.698431	0.100	-11.58	-38.00	1992-05-06	Odeco
122	Grand Isle	102	28.414289	-90.066441	0.005	-78.33	-257.00	1992-08-10	Agip
ANDREW									
123	Main Pass	154	29.656416	-88.235499	0.100	-40.08	-131.50	1992-10-06	Gulfstar
124	Chandeleur Sound	37	29.743153	-88.445972	0.005	-35.36	-116.00	1992-10-25	Gulfstar
125	Main Pass	90	29.653423	-88.797089	0.100	-13.41	-44.00	1992-12-08	KerrMcGee
126	South Timbalier	227	28.251126	-90.505566	0.005	-70.10	-230.00	1993-01-02	GenAtlantic
127	Main Pass	301	29.219668	-88.793170	0.005	-69.19	-227.00	1993-01-08	Walter
128	South Timbalier	86	28.782124	-90.221882	0.005	-29.57	-97.00	1993-06-11	Murphy
129	South Timbalier	86	28.782301	-90.222385	0.005	-29.57	-97.00	1993-06-11	Murphy
130	Chandeleur Sound	37	29.737411	-88.429496	0.005	-36.88	-121.00	1993-06-23	Gulfstar
131	Main Pass	141	29.297353	-88.796301	0.005	-57.30	-188.00	1993-08-31	Pennzoil
132	Viosca Knoll	31	29.949018	-88.160375	0.100	-31.09	-102.00	1993-09-01	SantaFe
133	Viosca Knoll	76	29.906018	-88.115136	0.100	-35.05	-115.00	1993-09-02	SantaFe
134	Main Pass	111	29.515731	-88.653382	0.005	-28.35	-93.00	1993-09-09	DiamondShamrock
135	Main Pass	181	29.564115	-88.590816	0.005	-28.04	-92.00	1993-11-01	Diamond Sha
136	Mobile Bay	916	30.098988	-87.902326	0.100	-15.85	-52.00	1993-11-12	Unocal
137	Mobile Bay	822	30.156220	-88.221441	0.100	-16.76	-55.00	1993-11-24	OEDC
138	Main Pass	123	29.419217	-88.648402	0.005	-49.99	-164.00	1993-12-15	Pogo
139	South Timbalier	111	28.656786	-90.671973	0.005	-16.15	-53.00	1993-12-18	Newfield
140	South Pelto	13	28.927530	-90.651196	0.100	-9.45	-31.00	1994-01-05	Zilkha
141	West Delta	106	28.831417	-89.557862	0.005	-76.81	-252.00	1994-01-17	Walter
142	West Delta	107	28.829378	-89.526551	0.005	-69.80	-229.00	1994-01-24	Walter
143	South Timbalier	99	28.675956	-90.745322	0.005	-18.90	-62.00	1994-02-22	OPS
144	West Delta	48	29.054808	-89.521989	0.100	-11.89	-39.00	1994-03-09	PG&E
145	Mobile Bay	864	30.150081	-88.287357	0.100	-17.37	-57.00	1994-03-11	Chevron
146	South Timbalier	112	28.668578	-90.710610	0.005	-17.68	-58.00	1994-03-16	OPS
147	West Delta	94	28.900619	-89.793667	0.005	-50.29	-165.00	1994-06-13	HallHouston
148	West Delta	94	28.895312	-89.772453	0.005	-52.43	-172.00	1994-06-14	HallHouston

--- continued on following page ---

\* Grain sizes in "Lithology" column assigned as an average of the lithologic descriptor from each borehole based on grain size standards from Wentworth (1922); VTA boreholes in yellow.

Number	Protraction Area	Block	Latitude	Longitude	Lith (mm) *	Depth (m)	Depth (ft)	Date	Operator
149	South Timbalier	206	28.456233	-90.301252	0.005	-51.21	-168.00	1994-06-17	Amerada
150	Main Pass	70	29.275982	-89.001634	0.005	-17.68	-58.00	1994-07-14	Chevron
151	Mobile Bay	959	30.066438	-87.954489	0.100	-14.94	-49.00	1994-07-15	OEDC
152	Mobile Bay	960	30.055707	-87.902840	0.100	-18.29	-60.00	1994-07-16	OEDC
153	South Timbalier	112	28.661524	-90.681275	0.005	-17.53	-57.50	1994-07-24	OPS
154	Main Pass	89	29.653757	-88.730595	0.005	-16.15	-53.00	1994-08-11	EnergyDev
155	South Pelto	23	28.845745	-90.652070	0.050	-18.59	-61.00	1994-09-28	Stone
156	South Pelto	23	28.843560	-90.611957	0.050	-19.51	-64.00	1994-10-02	Stone
157	South Pelto	5	29.007370	-90.529638	0.050	-9.14	-30.00	1994-10-11	Zikha
158	Main Pass	18	29.584513	-88.877555	0.100	-11.58	-38.00	1994-10-13	Mobil
159	West Delta	17	29.171488	-89.751706	0.005	-16.46	-54.00	1994-10-15	Seneca
160	Mobile Bay	961	30.044011	-87.864054	0.100	-19.81	-65.00	1994-11-09	Unocal
161	South Timbalier	229	28.385972	-90.135788	0.005	-69.49	-228.00	1994-12-05	LL&E
162	Main Pass	107	29.549498	-88.688945	0.100	-16.76	-55.00	1995-01-25	KerrMcGee
163	South Timbalier	193	28.514740	-90.572884	0.005	-35.05	-115.00	1995-02-20	Newfield
164	Main Pass	223	29.391779	-87.956488	0.100	-81.99	-269.00	1995-02-22	Coastal
165	South Pelto	9	28.955469	-90.666383	0.050	-11.28	-37.00	1995-03-16	Mobil
166	West Delta	59	28.998422	-89.557553	0.005	-20.42	-67.00	1995-03-19	Oryx
167	Viosca Knoll	155	29.837066	-88.561872	0.005	-27.43	-90.00	1995-03-28	SantaFe
168	South Timbalier	252	28.324954	-90.377712	0.005	-59.59	-195.50	1995-04-13	Dalen Res.
169	South Timbalier	148	28.589457	-90.420767	0.005	-33.22	-109.00	1995-05-05	Newfield
170	South Timbalier	265	28.298468	-90.474605	0.005	-60.35	-198.00	1995-05-28	KerrMcGee
171	South Timbalier	172	28.516622	-90.572664	0.005	-35.36	-116.00	1995-07-23	Samedan
172	Main Pass	225	29.399397	-88.042723	0.100	-78.03	-256.00	1995-07-24	CNG
173	South Timbalier	241	28.347432	-90.631222	0.005	-49.99	-164.00	1995-09-06	Meridian
OPAL									
174	South Timbalier	35	28.927851	-90.467233	0.005	-15.24	-50.00	UNKNOWN	Chevron
175	South Timbalier	35	28.944489	-90.464902	0.005	-15.24	-50.00	UNKNOWN	Chevron
176	West Delta	33	29.156599	-89.740705	0.005	-18.29	-60.00	UNKNOWN	Samedan

\* Grain sizes in "Lithology" column assigned as an average of the lithologic descriptor from each borehole based on grain size standards from Wentworth (1922). Boreholes in test validation areas are highlighted in yellow.

Table L-2: Coastal Studies Institute/Louisiana State University Geotechnical Borehole Database  
(arranged in time-sequential order where available)

Number	Protraction Area	Block	Latitude	Longitude	Lith (mm) *	Lith description	Date
1	Main Pass	69	29.254590	-89.040724	0.010	Clayey Silt	1948
2	Main Pass	68	29.241074	-89.045893	0.005	Clay	1949
3	Main Pass	80	29.204694	89.036448	0.010	Silty Clay	1949
4	Main Pass	34	29.420994	89.438605	0.100	Clay	1951
5	Main Pass	32	29.460171	89.416681	0.010	Clayey Silt	1952
6	Main Pass	68	29.247463	89.058189	0.005	Clay	1954
7	Main Pass	68	29.242050	89.060252	0.005	Clay	1954
8	Main Pass	69	29.277018	89.027281	0.005	Soft Gray Clay	1954
9	Empire Jetty-X-1	N/A	29.267539	89.597567	0.005	Soft Gray Clay	1955
10	Main Pass	31	29.459001	89.382021	0.020	Soft Gray Sandy Clay with Shells and Organics	1955
11	Main Pass	67	29.264626	89.082128	0.005	Clay	1955
12	South Pass	10	29.090530	89.266898	0.010	Layered Clay and Silt	1955
13	South Pass	Unknown	29.081533	89.271952	0.005	Silty Clay	1955
14	West Delta	53	29.025702	89.341400	0.020	Soft Gray Clay with Silt and Sand And Organics	1955
15	Main Pass	40	29.399924	88.960821	0.050	Gray Fine Sand with Clay	1956
16	Main Pass	41	29.373011	88.968067	0.050	Fine Sand	1956
17	Main Pass	59	29.356003	88.950566	0.100	Fine Sand	1956
18	Main Pass	45	29.395365	89.191444	0.010	Soft Gray Clay	1957
19	Main Pass	58	29.351156	88.982138	0.010	Layered Soft Gray Clay and Silty Sand	1957
20	Main Pass	59	29.367376	88.955640	0.010	Layered Gray Silty Sand and Clay	1957
21	South Pass	Unknown	29.065136	89.312065	0.005	Soft Gray Clay with Organics	1957
<b>AUDREY ETHYL</b>							
22	Breton Sound	49	29.435137	89.300049	0.005	Soft Gray Clay with Sand	1961
23	Main Pass	40	29.383497	88.949913	0.100	Layered Soft Gray Clay and Sand	1961
24	Main Pass	69	29.255517	89.032724	0.005	Soft Gray Clay	1961
<b>CARLA</b>							
25	Bay Marchand	165	28.578614	90.576447	0.005	Clay	1962
26	Main Pass	67	29.284406	89.098344	0.005	Soft Gray Clay with Silt & Shells	1962
27	Main Pass	107	29.563389	88.725971	0.100	Gray Fine Sand	1962
28	Main Pass	112	29.501847	88.711766	0.010	Gray Fine Sand	1962
29	Main Pass	42	29.409793	89.026356	0.010	Soft Gray Clay with Silt	1964
30	Main Pass	42	29.400782	89.034905	0.050	Layered Gray Silty Sand and Clay	1964
31	Main Pass	42	29.409793	89.026356	0.005	Clay	1964
<b>HILDA</b>							
32	Breton Sound	41	29.484942	89.002615	0.050	Gray Silty Sand with Clay and Shells	1965
33	Breton Sound	55	29.413580	89.038498	0.005	Soft Gray Clay with Sand and Shells	1965
34	Breton Sound	55	29.416515	89.014634	0.005	Soft Gray Clayey Sand	1965
35	Main Pass	Unknown	29.645945	88.889147	0.100	Fine Sand	1965
36	Main Pass	41	29.409552	88.982356	0.050	Soft Gray Sandy Clay	1965
37	Main Pass	42	29.405959	89.051001	0.050	Gray Silty Sand with Shells	1965
38	Main Pass	42	29.390526	89.025756	0.050	Gray Sandy Silt	1965
39	Main Pass	42	29.405959	89.051001	0.050	Silty Sand	1965
40	Main Pass	42	29.390526	89.025756	0.050	Sandy Silt	1965
41	Main Pass	42	29.391889	89.051268	0.050	Sandy Silt	1965
42	Main Pass	42	29.391889	89.051268	0.050	Gray Sandy Silt	1965
<b>BETSY</b>							
43	Main Pass	43	29.403332	89.077917	0.005	Gray Silty Sand With Clay	1966
44	Bay Marchand	189	28.500347	90.394349	0.005	Clay	1967
45	Main Pass	142	29.287193	88.759754	0.020	Layered Soft Gray Clay and Silty Sand with Shells	1967
46	Main Pass	208	29.451240	88.493594	0.005	Soft Gray Clay	1967
47	Main Pass	236	29.436545	88.587866	0.005	Soft Gray Clay	1967
48	Main Pass	290	29.254497	88.451944	0.050	Gray Silty Sand	1967
49	South Pass	61	29.018016	88.954031	0.005	Clay	1967
50	Grand Isle	75	28.729456	90.067170	0.005	Clay	1968
51	Main Pass	289	29.258251	88.442783	0.050	Gray Silty Sand with Shells	1968
52	Main Pass	289	29.258480	88.441227	0.005	Greenish Gray Clayey Sand with Shells	1968
53	South Pass	70	29.024124	88.934464	0.005	Soft Gray Clay	1968
54	South Pass	70	29.011798	88.930515	0.005	Soft Gray Clay	1968
55	Main Pass	43	29.390859	89.100096	0.050	Dark Gray Fine Silty Sand	1969
56	Main Pass	95	29.628960	88.701039	0.020	Layered Soft Gray Clay and Sand	1969
57	Main Pass	209	29.452704	88.439642	0.020	Soft Gray Clay with Sand	1969
58	Main Pass	209	29.475261	88.432518	0.020	Soft Gray Clay with Shells	1969
<b>CAMILLE</b>							
59	Main Pass	127	29.440419	88.870167	0.010	Soft Gray Clay with Silt	1970
60	South Pass	60	29.055431	88.964604	0.005	Soft Gray Clay	1970
61	South Pass	60	29.057230	88.965798	0.005	Soft Gray Clay	1970
62	South Pass	60	29.057344	88.962383	0.005	Soft Gray Clay	1970
63	South Pass	70	29.024261	88.934010	0.005	Soft Gray Clay	1970
64	South Pass	70	29.011060	88.930648	0.005	Soft Gray Clay	1970
65	South Pass	60	29.068844	88.948053	0.005	Soft Gray Clay	1971
66	South Pass	60	29.066823	88.949763	0.005	Soft Dark Gray Clay	1971
67	South Pass	60	29.065129	88.950091	0.005	Soft Gray Clay	1971
68	South Pass	60	29.065652	88.951012	0.005	Soft Gray Clay	1971
69	South Pass	60	29.065015	88.958155	0.005	Soft Gray Clay with Organics	1972
70	South Pass	60	29.065049	88.954717	0.005	Soft Gray Clay with Organics	1972

--- continued on following page ---

\* Grain sizes in "Lithology" column assigned as an average of the lithologic descriptor from each borehole based on grain size standards from Wentworth (1922). Boreholes in test validation areas are highlighted in yellow.

Number	Protraction Area	Block	Latitude	Longitude	Lith (mm) *	Lith description	Date
71	South Pass	60	29.062880	88.958424	0.005	Soft Gray Clay	1972
72	South Pass	60	29.064375	88.955625	0.005	Soft Gray Clay with Organics	1972
73	South Pass	60	29.062323	88.959111	0.005	Soft Gray Clay	1972
74	South Pass	60	29.063800	88.956058	0.005	Soft Gray Clay	1972
75	South Pass	60	29.069063	88.984820	0.005	Soft Gray Clay	1972
76	South Pass	60	29.066716	88.982051	0.005	Soft Gray Clay	1972
77	South Pass	60	29.070958	88.981745	0.005	Soft Gray Clay With Gas	1972
78	South Pass	60	29.064089	88.989046	0.005	Soft Gray Clay	1973
CARMEN							
FREDERIC							
79	Main Pass	76	29.176016	88.954793	0.005	Clay	1980
80	Main Pass	79	29.140598	88.955794	0.005	Clay	1980
81	Grand Isle	32	29.018573	89.878197	0.005	Clay	1982
82	Grand Isle	47	28.942714	90.011383	0.005	Clay	1984
END OF TIME-SEQUENTIAL DATA							
83	Bay Marchand	47	28.885323	90.306487	0.005	Clay	Unknown
84	Bay Marchand	54	28.679025	90.393614	0.005	Clay	Unknown
85	Bay Marchand	63	28.809060	90.213327	0.050	Silty Fine Sand	Unknown
86	Grand Isle	32	29.035247	89.891812	0.005	Clay	Unknown
87	Grand Isle	40	28.968866	90.021359	0.005	Clay	Unknown
88	Grand Isle	90	28.564695	90.066118	0.005	Clay	Unknown
89	Grand Isle	90	28.573147	90.087065	0.005	Clay	Unknown
90	Grand Isle	91	28.588464	90.034356	0.005	Clay	Unknown
91	Main Pass	24	29.521976	89.460132	0.005	Clay	Unknown
92	Main Pass	41	29.375654	89.012250	0.010	Gray Fine Silty Sand with Shells	Unknown
93	Main Pass	41	29.373805	89.012352	0.050	Gray Silty Sand	Unknown
94	Main Pass	68	29.253176	89.056425	0.005	Soft Dark Gray Clay with Organics	Unknown
95	Main Pass	68	29.258411	89.048290	0.005	Soft Dark Gray Clay with Organics	Unknown
96	Main Pass	68	29.267650	89.058196	0.005	Soft Gray Clay	Unknown
97	Main Pass	69	29.273776	89.027183	0.005	Soft Gray Clay with Organics	Unknown
98	Main Pass	92	29.618667	88.836909	0.050	Gray Fine Silty Sand	Unknown
99	Main Pass	144	29.292781	88.669221	0.005	Soft Gray Clay	Unknown
100	Main Pass	289	29.252014	88.439519	0.005	Soft Gray Clay with Shells	Unknown
101	Main Pass	290	29.252411	88.470673	0.005	Gray Clay	Unknown
102	Main Pass	290	29.256513	88.450023	0.050	Gray Silty Sand with Shells	Unknown
103	Main Pass	290	29.256460	88.451750	0.020	Layered Gray Clayey Sand and Shell	Unknown
104	Main Pass	295	29.248821	88.639590	0.005	Soft Gray Clay with Shells	Unknown
105	Main Pass	198	29.275263	88.741927	0.005	Clay	Unknown
106	Main Pass	299	29.270171	88.771627	0.005	Soft Gray Clay	Unknown
107	Main Pass	299	29.252537	88.757104	0.005	Soft Gray Clay	Unknown
108	Main Pass	300	29.263722	88.781667	0.005	Soft Gray Clay	Unknown
109	Main Pass	312	29.174376	88.765302	0.005	Soft Gray Clay with Sand and Shells	Unknown
110	Main Pass		29.272438	89.242758	0.005	Clay	Unknown
111	Main Pass		29.276028	89.241952	0.005	Clay	Unknown
112	Main Pass		29.272438	89.242758	0.005	Clay	Unknown
113	Ship Shoal	198	28.591436	91.251096	0.005	Clay	Unknown
114	South Pass	5	29.150974	89.015141	0.005	Soft Gray Clay	Unknown
115	South Pass	5	29.117511	89.027846	0.050	Gray Sandy Silt	Unknown
116	South Pass	6	29.086754	89.001516	0.005	Soft Dark Gray Clay with Organics	Unknown
117	South Pass	6	29.080379	88.998467	0.005	Soft Dark Gray Clay with Organics and Gas	Unknown
118	South Pass	20	28.830434	89.107815	0.005	Soft Dark Gray Clay	Unknown
119	South Pass	23	29.034755	89.263605	0.010	Layered Soft Gray Silty Clay and Silt	Unknown
120	South Pass	23	29.033760	89.240938	0.005	Soft Dark Gray Clay	Unknown
121	South Pass	24	29.012648	89.279328	0.010	Gray Clayey Silt	Unknown
122	South Pass	24	29.001270	89.306176	0.005	Soft Gray Clay	Unknown
123	South Pass	26	28.986222	89.338055	0.010	Layered Soft Gray Clay and Silt	Unknown
124	South Pass	27	28.997165	89.306956	0.005	Soft Gray Clay	Unknown
125	South Pass	27	28.984342	89.268551	0.005	Soft Gray Clay	Unknown
126	South Pass	28	28.979777	89.225613	0.020	Dark Gray Silt	Unknown
127	South Pass	28	28.963982	89.264277	0.005	Soft Gray Clay	Unknown
128	South Pass	28	28.975113	89.262544	0.005	Soft Gray Clay	Unknown
129	South Pass	28	28.968964	89.265557	0.005	Layered Soft Gray Clay and Soft Dark Gray Clay	Unknown
130	South Pass	29	28.994093	89.199482	0.010	Layered Clay and Silt	Unknown
131	South Pass	29	28.984784	89.185290	0.100	Gray Fine Silty Sand	Unknown
132	South Pass	29	28.984784	89.185290	0.010	Layered Soft Gray Clay and Silt	Unknown
133	South Pass	29	28.994093	89.199482	0.020	Layered Clay and Sand	Unknown
134	South Pass	33	28.927867	89.071407	0.005	Clay	Unknown
135	South Pass	39	28.938465	89.334432	0.005	Soft Dark Gray Clay	Unknown
136	South Pass	39	28.944531	89.354159	0.005	Soft Gray Clay	Unknown
137	South Pass	39	28.938648	89.356151	0.010	Soft Dark Gray Clay with Silt	Unknown
138	South Pass	40	28.937099	89.366407	0.050	Layered Soft Gray Clay and Silty Sand	Unknown
139	South Pass	40	28.946657	89.364451	0.005	Soft Gray Clay	Unknown
140	South Pass	40	28.940414	89.363795	0.050	Gray Fine Silty Sand	Unknown
141	South Pass	40	28.927532	89.362696	0.010	Soft Dark Gray Clay with Silt	Unknown
142	South Pass	40	28.936923	89.363863	0.005	Soft Gray Sandy Clay	Unknown
143	South Pass	40	28.924742	89.402294	0.020	Layered Gray Silty Sand and Clay	Unknown
144	South Pass	41	28.918223	89.438899	0.005	Soft Gray Clay	Unknown
145	South Pass	42	28.909158	89.364358	0.005	Soft Dark Gray Clay	Unknown
146	South Pass	42	28.908324	89.367453	0.005	Soft Dark Gray Clay	Unknown

--- continued on following page ---

\* Grain sizes in "Lithology" column assigned as an average of the lithologic descriptor from each borehole based on grain size standards from Wentworth (1922). Boreholes in test validation areas are highlighted in yellow.

Number	Protraction Area	Block	Latitude	Longitude	Lith (mm) *	Lith description	Date
147	South Pass	47	28.892836	89.134723	0.005	Soft Dark Gray Clay with Organics	Unknown
148	South Pass	47	28.877235	89.163003	0.005	Soft Gray Clay	Unknown
149	South Pass	47	28.905248	89.160765	0.005	Soft Gray Clay	Unknown
150	South Pass	48	28.856742	89.127700	0.005	Soft Gray Clay	Unknown
151	South Pass	54	28.865716	89.264987	0.005	Clay	Unknown
152	South Pass	56	28.852815	89.332765	0.005	Clay	Unknown
153	South Pass	57	28.863046	89.406936	0.005	Clay	Unknown
154	South Pass	57	28.867648	89.401974	0.005	Clay	Unknown
155	South Pass	57	28.843684	89.399497	0.005	Clay	Unknown
156	South Pass	59	29.075955	88.951594	0.005	Clay	Unknown
157	South Pass	66	29.086430	88.940926	0.005	Soft Dark Gray Clay with Gas	Unknown
158	South Pass	67	29.057047	88.924852	0.005	Clay	Unknown
159	South Pass	70	29.021370	88.910651	0.005	Soft Gray Clay	Unknown
160	South Pass	70	29.001801	88.933606	0.005	Soft Gray Clay	Unknown
161	South Pass	70	29.021370	88.910651	0.005	Soft Gray Clay	Unknown
162	South Pass	70	29.021869	88.938054	0.005	Soft Gray Clay	Unknown
163	South Pass	70	29.020229	88.934585	0.005	Soft Gray Clay With Gas	Unknown
164	South Pass	70	29.024165	88.937311	0.005	Soft Gray Clay	Unknown
165	South Pass	70	29.010705	88.930613	0.005	Soft Gray Clay	Unknown
166	South Pass	70	29.021262	88.910725	0.005	Soft Gray Clay	Unknown
167	South Pass	70	29.030069	88.943507	0.005	Soft Gray Clay	Unknown
168	South Pass	70	29.028708	88.943217	0.005	Soft Gray Clay With Gas	Unknown
169	South Pass	70	29.030682	88.941984	0.005	Soft Gray Clay with Organics	Unknown
170	South Pass	70	29.032074	88.944258	0.005	Soft Dark Gray Clay	Unknown
171	South Pass	72	28.990766	89.020298	0.005	Clay	Unknown
172	South Pass	76	28.815798	89.332116	0.005	Clay	Unknown
173	South Pass	76	28.824063	89.411677	0.005	Clay	Unknown
174	South Pass	28	28.827150	89.412150	0.005	Clay	Unknown
175	South Pass	28	28.830367	89.410215	0.005	Clay	Unknown
176	South Pass	88	28.710881	89.424502	0.005	Soft Gray Clay	Unknown
177	South Timbalier	276	28.231138	90.533654	0.005	Clay	Unknown
178	South Timbalier	320	28.069424	90.524631	0.005	Clay	Unknown

\* Grain sizes in “Lithology” column assigned as an average of the lithologic descriptor from each borehole based on grain size standards from Wentworth (1922). Boreholes in test validation areas are highlighted in yellow.

## **APPENDIX M: MIKE 21 NUMERICAL MODELING**

In order to quantify bulk wave parameters and bottom-boundary layer variables associated with the passage of GOM hurricanes used in this research, a series of wave simulations were performed. These simulations were run using the MIKE 21 software package, a two-dimensional numerical modeling suite developed by DHI Water & Environment, Inc.

The MIKE 21 SW module is a spectral wind-wave model based on an unstructured mesh that simulates the growth, decay and transformation of wind-generated waves and swell in offshore and coastal areas (DHI, 2005). Two formulations are included in the model, a fully spectral formulation and a directional de-coupled parametric formulation. The fully spectral method was used in this dissertation given complex wave-wave interaction and energy transfer between frequencies, especially during the approach phase of a hurricane. The fully spectral formulation is based on the wave action conversation equation (Komen et al., 1994). For this formulation, directional-frequency wave action spectrum is the dependent variable.

The MIKE 21 SW model is capable of parameterizing the following physical phenomena:

- Wave growth by wind action
- Non-linear wave-wave interaction
- Dissipation due to white capping
- Dissipation due to bottom friction
- Dissipation due to depth-limited wave breaking
- Refraction and shoaling due to depth variations
- Wave-current interaction

The unstructured mesh approach provides the model with a high degree of flexibility. Integration over time is based on a fractional step approach in which propagation steps are solved using an explicit method (Sorenson et al., 2004). Wind input, the main source function in the equation, is based on Janssen's quasi-linear theory of wind-wave generation (Janssen, 1989;

1991) and implemented as in WAV Cycle 4. Non-linear energy transfer through four-wave interaction is represented by a discrete interaction approximation proposed by Hasselmann et al. (1985). Dissipation due to white capping is implemented based on Hasselmann (1974) and is further tuned based on Janssen (1989). Detailed descriptions of all source functions and numerical methods used in the model are discussed in Sorensen et al. (2004).

The discretization in geographical and spectral space is performed using a cell-centered finite volume method. In the geographical domain, an unstructured mesh is used. The spatial domain is discretized by subdivision of the continuum into non-overlapping elements. The elements can take the form of arbitrarily shaped polygons. However, in this dissertation only triangles are considered as elements. Wave action density is represented as a piecewise constant over the elements and stored at the geometric centers. In frequency space, a logarithmic discretization is used:

$$\sigma_1 = \sigma_{\min} \quad \sigma_l = f_\sigma \sigma_{l-1} \quad \Delta\sigma_l = \sigma_{l+1} - \sigma_l \quad l = 2, N_\sigma \quad (\text{M1})$$

Where  $f_\sigma$  is a given factor,  $\sigma_{\min}$  is the minimum discrete angular frequency, and  $N_\sigma$  is the number of discrete frequencies.

In the directional space, an equidistant discretization is used (where  $N_\theta$  equals the number of discrete directions):

$$\Theta_m = (m-1)\Delta\theta \quad \Delta\Theta_m = \frac{2\pi}{N_\theta} \quad m = 1, N_\theta \quad (\text{M2})$$

The action density is represented as piecewise constant over the discrete intervals,  $\Delta\sigma$  and  $\Delta\sigma_m$ , in the frequency and directional space.

A fully spectral in-stationary approach was used for computation of bulk wave parameters. A logarithmic frequency discretization with 25 frequencies was used. The lowest discrete frequency was  $\sigma_{\min} = 0.055$  Hz and the ratio between successive frequencies was chosen as 1.1. The number of discrete directions was chosen as 16. The time step interval chosen for the simulation was 60s. The white capping parameters were included in the model ( $C_{\text{dis}} = 2$  and



$\Delta_{\text{dis}} = 0.8$ ). For the wave breaking parameters, a constant value of  $\gamma = 0.8$  and  $\alpha = 1$  were used. Given the orientation of the Mississippi River Delta, diffraction effects were also included in hurricane simulations. As discussed earlier, quadruplet-wave interactions were chosen for the energy transfer parameterization. For bottom friction computation, median grain size data were compiled from various sources (e.g., usSEABED, the Texas A&M and Coastal Studies Institute databases). Initial conditions for the model were set using the Joint North Sea Wave Observation Project (JONSWAP) spectra with a maximum fetch length of 100 km, maximum peak frequency of 0.4 Hz and maximum Philips constant of 0.0081.

The Mississippi River Delta Front (MRDF) domain (Figures M-1 and M-2) was developed with three distinct spatial resolutions – an outer boundary resolution of 5 km, a study area-wide scale of 2 km, and a high resolution scale in each of the four Validation Test Areas of 0.5 km (Figure M-1). The model grid (flexible mesh) was developed using the mesh generation module provided with the MIKE ZERO<sup>®</sup> package. Bathymetric data underlying the grid generation were compiled from various data sources, with the National Geophysical Data Center (NGDC) Coastal Elevation Model serving as the base data while being supplemented by additional bathymetry data from regional and local sources described in Section 4.1.1.

The MRDF domain (Figure M1) was nested with a regional wave model developed for the Gulf of Mexico (GOM; Jose et al., 2006). A series of simulations were run for Hurricanes Ivan and Katrina after which the simulated bulk wave parameters were calibrated and skill-assessed using time series data from National Data Buoy Center (NDBC) buoy network. The model was calibrated throughout the process to ensure the best agreement with observed conditions.

Archived metocean data from a number of NDBC buoys deployed in the GOM were used for skill assessment of the wave model. Mooring location coordinates of buoys used in this dissertation are provided in Table M-1; additional background information on each buoy is contained in Appendix H.

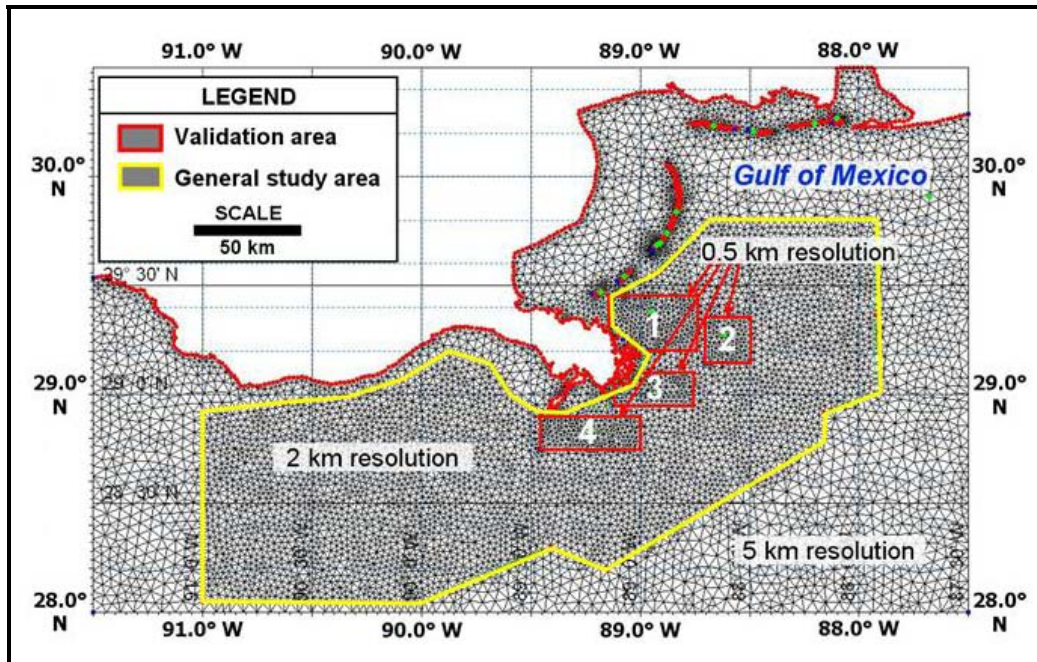


Figure M-1: Mesh resolution, MIKE 21 numerical wave model

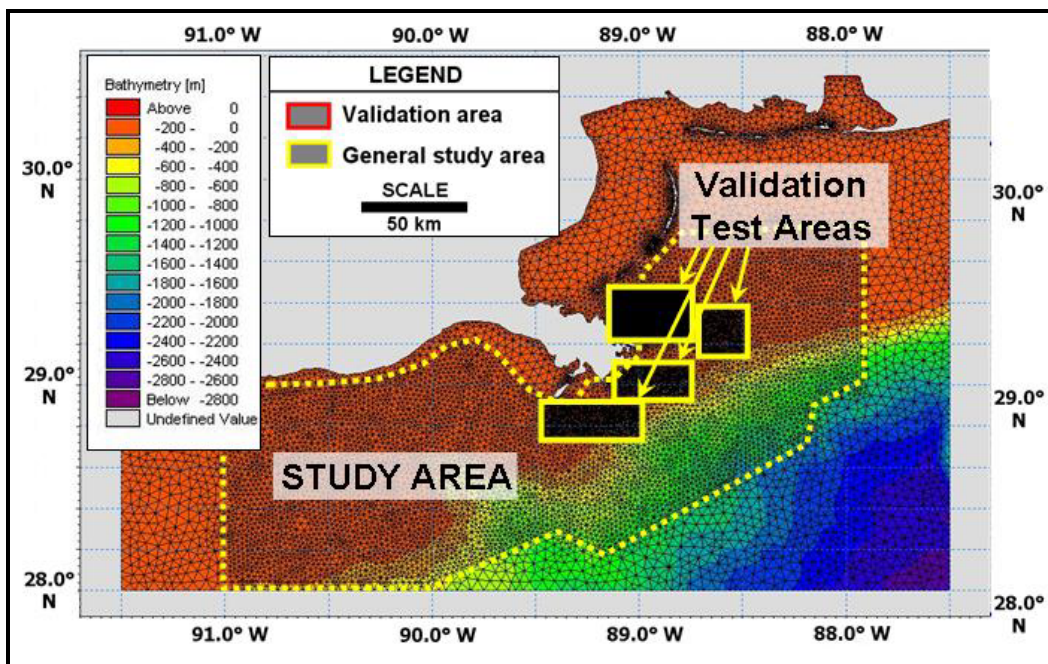


Figure M-2: Mesh density and bathymetry of the MIKE 21 computational domain (coastal grid nested with a regional wave model)

Table M-1: Location of NDBC buoys used in MIKE 21 wave model skill assessment

<u>NDBC Buoy</u>	<u>Latitude (degrees)</u>	<u>Longitude (degrees)</u>	<u>Latitude (decimal)</u>	<u>Longitude (decimal)</u>
42001	25° 54' 00" N	89° 40' 00" W	25.900° N	89.670° W
42002	25° 10' 00" N	94° 25' 00" W	25.167° N	94.417° W
42007	30° 05' 25" N	88° 46' 07" W	30.090° N	88.769° W
42040	29° 11' 03" N	88° 12' 48" W	29.184° N	88.213° W

Calibration parameters were fine-tuned to ensure the best fit of modeled to observed conditions during Hurricanes Ivan and Katrina (the recent hurricanes studies). Once both Katrina and Ivan were calibrated to a satisfactory level compared with the observed conditions (mainly from bulk wave and bottom boundary layer parameters obtained from the NDBC buoys described in Table M-1), simulations were then performed for the remaining three hurricanes evaluated (Andrew, Camille and Betsy). Wave boundary conditions for the MRDF coastal model were obtained by forcing the Gulf-wide model using high resolution 2D wind data (Section 5.2.1). Then, using the same 2D wind data and employing boundary conditions from the regional model, hurricane-generated wave fields were simulated for the entire study area.

## **APPENDIX N: SHEAR STRENGTH SAMPLE COLLECTION METHODS**

A variety of collection methods are used to obtain shear strength data. They include:

- Unconfined compression test: This test is used to determine the consistency of saturated clays and other cohesive soils. A vertical cylindrical specimen with a 2:1 height-to-diameter ratio and at least 39 mm in diameter is set up between two end plates. Vertical loads are applied incrementally at rates to produce a vertical strain of approximately 1% to 2% per minute. The unconfined compressive strength is considered to be equal to the load at which failure occurs, or at which the axial strain reaches 20% if no sudden failure occurs (Terzaghi et al., 1996).
- Unconsolidated, undrained triaxial compression test (UU): This test is similar to the unconfined compression test but this test reduces the likelihood of premature failure along possible fracture planes. The UU test consists of enclosing a sample in a membrane, placing it in a triaxial apparatus, and subjecting it to a confining pressure. No drainage is permitted from the sample under the influence of either the confining pressure or the axial stress (Figure N-1; Terzaghi et al., 1996).
- Miniature vane test: This test consists of inserting a small, four-bladed vane (usually 1.27 to 1.90 cm in diameter and 1.27 to 3.30 cm in height) into a sediment sample so that its top is at least as far below the sediment surface as the vane height. The vane is rotated until a peak torque is reached. The undrained shear strength is then calculated assuming full-strength mobilization along a right circular cylinder inscribed about the vane (Figure N-2; Chaney et al., 1984).

A distinction can be made between drained and undrained shear strengths. In drained tests, changes in stress are applied slowly to allow pore pressures to dissipate, and the resulting shear stresses are expressed in terms of effective stress. Undrained tests are adopted in cases where the rate of loading is much greater than the rate at which pore water pressures generated due to the action of shearing the soil may dissipate.

The preferred undrained strength test for offshore collection is the unconfined compression test, followed closely by the unconsolidated, undrained triaxial compression test, followed by the miniature vane (Nodine et al., 2006). Prior research on the results of shear strength in the GOM indicates that pushed samples yield higher strengths than percussion samples (Emrich, 1971). Also, vane tests in which samples fail along predetermined planes yield higher strengths than those where failure occurred along natural planes, such as in unconfined compression tests.

Shear strength data used in the mapping exercise described in Dunlap et al. (2004) were derived from various testing and sampling methods, all of which can affect values of reported undrained shear strength. The data were corrected to remove the effects of various testing and sampling methods using a modification process developed in the Dunlap study (Table N-1). This process adjusts shear strengths to the reference strength of an unconfined compression test performed on a sample obtained using a 3-inch, thin-walled sampler pushed into the soil (Nodine et al., 2006; 2007).

Table N-1: Shear strength modification factors (from Dunlap et al., 2004)

<u>Sampler type</u>	<u>Insertion method</u>	<u>Strength test</u>	<u>*Modification factor, <math>S_u/S_u'</math></u>	
			<u>Based on Emrich, 1971</u>	<u>Based on Nodine et al., 2006</u>
2 ¼" thin-walled	Percussion	Unconfined compression	1.56	1.50
2 ¼" thin-walled	Percussion	Miniature vane	1.06	1.10
3" thin-walled	Push	Unconfined compression	1.05	1.00
3" thin-walled	Push	Miniature vane	0.76	0.80
In-site measurement		Remote vane	0.69	0.70

- \*  $S_u$  = undrained shear strength determined by unconfined compression tests on 3-inch fixed-piston samples  
 $S_u'$  = undrained shear strength determined by other strength tests or with other sample types, as indicated

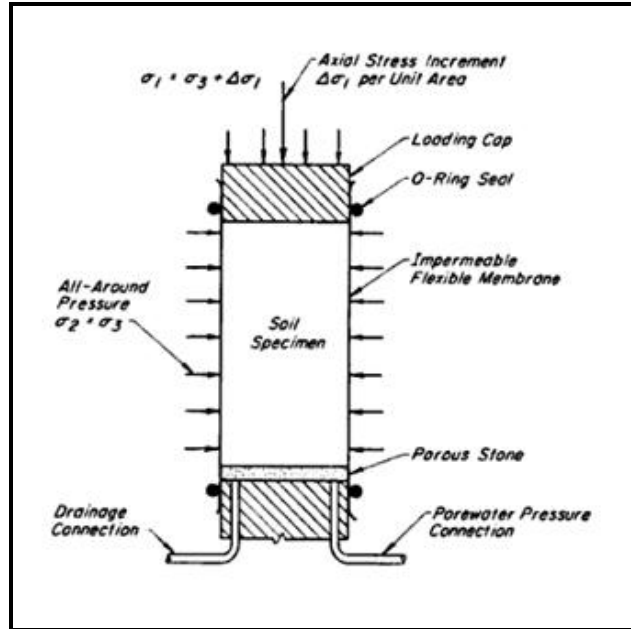


Figure N-1: Sampling apparatus, UU shear strength test (from Terzaghi et al., 1996)

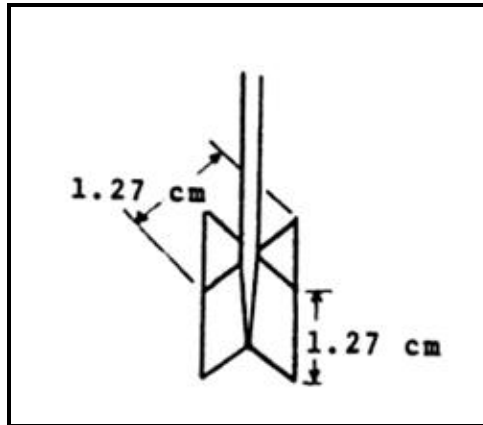


Figure N-2: Sampling apparatus, miniature vane shear strength test (from Chaney et al., 1984)

The following steps were programmed into the safety factor program developed by Nodine (2007):

1. Calculate the wavelength as a function of wave period assuming linear wave theory described by Wiegel (1964):

$$L = \frac{gT^2}{2\pi} \tanh \frac{2\pi d}{L} \quad (4)$$

2. Calculate the maximum pressure on the seafloor using linear wave theory described by Wiegel (1964):

$$P_{\max} = \frac{\gamma_w}{2} \left( \frac{h}{\cosh\left(\frac{2\pi}{L}d\right)} \right) \quad (5)$$

3. Calculate the dimensionless constant:  $\frac{\gamma L \tan \beta}{P_{\max}}$  (6)

4. Calculate the dimensionless constant:  $\frac{c_z L}{c_o}$  (7)

5. Using the calculated answers from Steps 3 and 4, determine the value of  $N_z$ : from the chart in Figure 92:

$$N_z = \frac{c_z L}{P_{\max} F} \quad (8)$$

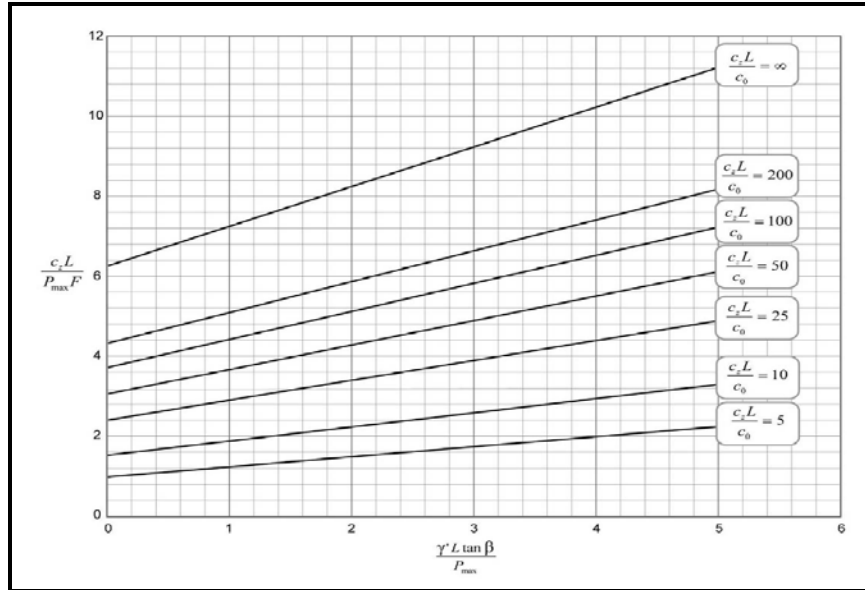


Figure N-3: Stability chart for limit equilibrium slope stability model (from Nodine, 2007)

6. Calculate the factor of safety (F) using  $N_z$  and known values of  $c_z$ ,  $L$  and  $P_{\max}$ :

$$F = \frac{1}{N_z} \left( \frac{c_z L}{P_{\max}} \right) \quad (9)$$



Table N-2: Parameters used in safety factor calculations, Cross Section A-A'

	<u>Betsy</u>			<u>Camille</u>			<u>Andrew</u>			<u>Ivan</u>			<u>Katrina</u>		
	<u>Sep 9 0000 Z</u>			<u>Aug 16 2100 Z</u>			<u>Aug 24 1800 Z</u>			<u>Sep 14 2100 Z</u>			<u>Aug 28 1200 Z</u>		
<u>Borehole</u>	<u>P</u>	<u>L</u>	<u>F</u>	<u>P</u>	<u>L</u>	<u>F</u>	<u>P</u>	<u>L</u>	<u>F</u>	<u>P</u>	<u>L</u>	<u>F</u>	<u>P</u>	<u>L</u>	<u>F</u>
MP 43	4.2	90	4.35	3.5	63	11.9	2.5	32	190	4.5	104	2.36	10.8	597	1.46
MP 128	4.6	108	13.0	4.5	104	15.2	3.5	63	156	5.1	138	6.35	10.0	512	1.57
MP 290	5.0	128	75.6	4.8	118	75.7	3.5	63	75.6	5.7	166	75.7	8.4	361	25.6
	<u>Sep 9 1200 Z</u>			<u>Aug 17 0900 Z</u>			<u>Aug 25 0600 Z</u>			<u>Sep 15 0900 Z</u>			<u>Aug 29 0000 Z</u>		
<u>Borehole</u>	<u>P</u>	<u>L</u>	<u>F</u>	<u>P</u>	<u>L</u>	<u>F</u>	<u>P</u>	<u>L</u>	<u>F</u>	<u>P</u>	<u>L</u>	<u>F</u>	<u>P</u>	<u>L</u>	<u>F</u>
MP 43	5.7	166	1.15	7.0	251	1.07	3.5	63	11.9	7.6	296	1.10	13.5	933	1.92
MP 128	6.3	203	2.54	8.0	328	1.62	4.5	104	15.2	8.4	361	1.57	12.5	800	1.77
MP 290	6.3	203	75.5	8.0	328	35.0	4.5	104	75.6	8.4	361	25.6	10.5	564	7.03
	<u>Sep 10 0000 Z</u>			<u>Aug 17 2100 Z</u>			<u>Aug 25 1800 Z</u>			<u>Sep 15 2100 Z</u>			<u>Aug 29 1200 Z</u>		
<u>Borehole</u>	<u>P</u>	<u>L</u>	<u>F</u>	<u>P</u>	<u>L</u>	<u>F</u>	<u>P</u>	<u>L</u>	<u>F</u>	<u>P</u>	<u>L</u>	<u>F</u>	<u>P</u>	<u>L</u>	<u>F</u>
MP 43	12.4	787	1.71	12.5	800	1.73	8.0	328	1.13	13.5	933	1.92	14.0	1004	1.99
MP 128	11.6	689	1.73	11.0	620	1.68	8.0	328	1.62	12.5	800	1.77	14.0	1004	1.89
MP 290	10.8	597	6.15	11.0	620	5.66	8.0	328	35.0	11.5	677	4.73	13.2	892	3.09
	<u>Sep 10 1200 Z</u>			<u>Aug 18 0900 Z</u>			<u>Aug 26 0600 Z</u>			<u>Sep 16 0900 Z</u>			<u>Aug 30 0000 Z</u>		
<u>Borehole</u>	<u>P</u>	<u>L</u>	<u>F</u>	<u>P</u>	<u>L</u>	<u>F</u>	<u>P</u>	<u>L</u>	<u>F</u>	<u>P</u>	<u>L</u>	<u>F</u>	<u>P</u>	<u>L</u>	<u>F</u>
MP 43	8.4	361	1.17	6.5	216	1.04	6.5	216	1.09	10.8	597	1.46	7.6	296	1.10
MP 128	7.6	296	1.72	6.0	184	2.98	6.5	216	2.33	11.6	689	1.73	6.8	237	2.07
MP 290	8.4	361	25.6	6.5	216	75.3	6.5	216	75.3	10.8	597	6.15	6.8	237	74.9

P = wave period

L = wavelength

F = safety factor

MP = Main Pass Protraction Area

Table N-3: Parameters used in safety factor calculations, Cross Section B-B'

	<u>Betsy</u>			<u>Camille</u>			<u>Andrew</u>			<u>Ivan</u>			<u>Katrina</u>		
	<u>Sep 9 0000 Z</u>			<u>Aug 16 2100 Z</u>			<u>Aug 24 1800 Z</u>			<u>Sep 14 2100 Z</u>			<u>Aug 28 1200 Z</u>		
<u>Borehole</u>	<u>P</u>	<u>L</u>	<u>F</u>	<u>P</u>	<u>L</u>	<u>F</u>	<u>P</u>	<u>L</u>	<u>F</u>	<u>P</u>	<u>L</u>	<u>F</u>	<u>P</u>	<u>L</u>	<u>F</u>
MP 70	4.6	108	5.13	5.5	155	1.93	3.5	63	49.2	5.7	166	1.69	10.8	597	1.08
MP 77	5.0	128	14.0	4.5	104	14.1	3.5	63	14.0	5.1	133	14.0	8.4	361	1.77
MP 301	5.0	128	2262	4.5	104	3638	3.5	63	3615	5.1	133	1846	8.4	361	7.98
MP 310	5.0	128	929	4.5	104	930	3.5	63	930	5.1	133	928	8.4	361	41.6
	<u>Sep 9 1200 Z</u>			<u>Aug 17 0900 Z</u>			<u>Aug 25 0600 Z</u>			<u>Sep 15 0900 Z</u>			<u>Aug 29 0000 Z</u>		
<u>Borehole</u>	<u>P</u>	<u>L</u>	<u>F</u>	<u>P</u>	<u>L</u>	<u>F</u>	<u>P</u>	<u>L</u>	<u>F</u>	<u>P</u>	<u>L</u>	<u>F</u>	<u>P</u>	<u>L</u>	<u>F</u>
MP 70	6.9	244	1.08	10.5	564	1.05	4.5	104	5.75	10.8	597	1.08	12.5	800	1.28
MP 77	6.9	244	4.70	8.5	370	1.69	4.5	104	14.1	8.4	361	1.77	10.5	564	0.84
MP 301	6.9	244	38.0	8.5	370	7.41	4.5	104	3638	8.4	361	7.98	10.5	564	2.89
MP 310	7.5	288	102	8.5	370	38.2	4.5	104	930	8.4	361	41.6	10.5	564	12.5
	<u>Sep 10 0000 Z</u>			<u>Aug 17 2100 Z</u>			<u>Aug 25 1800 Z</u>			<u>Sep 15 2100 Z</u>			<u>Aug 29 1200 Z</u>		
<u>Borehole</u>	<u>P</u>	<u>L</u>	<u>F</u>	<u>P</u>	<u>L</u>	<u>F</u>	<u>P</u>	<u>L</u>	<u>F</u>	<u>P</u>	<u>L</u>	<u>F</u>	<u>P</u>	<u>L</u>	<u>F</u>
MP 70	12.4	787	1.27	12.5	800	1.28	10.0	512	1.01	13.5	933	1.43	13.2	892	1.38
MP 77	10.8	597	0.79	10.5	564	0.84	8.5	370	1.69	11.5	677	0.70	11.6	689	0.69
MP 301	10.8	597	2.65	10.5	564	2.89	8.5	370	7.41	11.5	677	2.26	11.6	689	2.21
MP 310	10.8	597	11.3	10.5	564	12.5	8.5	370	38.2	12.5	800	7.45	12.4	787	7.58
	<u>Sep 10 1200 Z</u>			<u>Aug 18 0900 Z</u>			<u>Aug 26 0600 Z</u>			<u>Sep 16 0900 Z</u>			<u>Aug 30 0000 Z</u>		
<u>Borehole</u>	<u>P</u>	<u>L</u>	<u>F</u>	<u>P</u>	<u>L</u>	<u>F</u>	<u>P</u>	<u>L</u>	<u>F</u>	<u>P</u>	<u>L</u>	<u>F</u>	<u>P</u>	<u>L</u>	<u>F</u>
MP 70	8.4	361	0.95	9.0	415	0.95	7.5	288	0.99	12.5	800	1.28	6.8	237	1.11
MP 77	8.4	361	1.77	6.0	184	11.7	6.5	216	2.94	10.8	597	0.79	6.8	237	5.13
MP 301	8.4	361	7.98	7.0	251	33.1	7.5	288	17.9	10.0	597	2.65	6.8	237	44.1
MP 310	8.4	361	41.6	7.0	251	194	7.5	288	102	10.0	597	11.3	7.6	296	90.1

P = wave period

MP = Main Pass Protraction Area

L = wavelength

F = safety factor

Table N-4: Parameters used in safety factor calculations, Cross Section C-C'

	<u>Betsy</u>			<u>Camille</u>			<u>Andrew</u>			<u>Ivan</u>			<u>Katrina*</u>		
	<u>Sep 9 0000 Z</u>			<u>Aug 16 2100 Z</u>			<u>Aug 24 1800 Z</u>			<u>Sep 14 2100 Z</u>			<u>Aug 28 1200 Z</u>		
<u>Borehole</u>	<u>P</u>	<u>L</u>	<u>F</u>	<u>P</u>	<u>L</u>	<u>F</u>	<u>P</u>	<u>L</u>	<u>F</u>	<u>P</u>	<u>L</u>	<u>F</u>	<u>P</u>	<u>L</u>	<u>F</u>
SP 6	6.3	203	1.08	5.5	155	1.97	3.5	63	23.2	6.3	203	1.08	12.4	787	0.50*
SP 60	5.4	149	25.4	4.5	104	25.5	3.5	63	25.5	5.7	166	25.6	9.2	433	4.66
SP 67	5.4	149	3.57	5.5	104	3.57	3.5	63	3.57	5.7	166	3.58	9.2	433	1.51
SP 70	5.0	128	7.67	5.5	104	7.67	3.5	63	7.67	5.7	166	7.67	9.2	433	4.26
	<u>Sep 9 1200 Z</u>			<u>Aug 17 0900 Z</u>			<u>Aug 25 0600 Z</u>			<u>Sep 15 0900 Z</u>			<u>Aug 29 0000 Z</u>		
<u>Borehole</u>	<u>P</u>	<u>L</u>	<u>F</u>	<u>P</u>	<u>L</u>	<u>F</u>	<u>P</u>	<u>L</u>	<u>F</u>	<u>P</u>	<u>L</u>	<u>F</u>	<u>P</u>	<u>L</u>	<u>F</u>
SP 6	8.1	336	0.61	10.5	564	0.56	6.0	184	1.30	11.6	689	0.53	13.5	933	0.49
SP 60	6.9	244	24.3	8.5	370	6.64	5.0	128	25.5	8.4	361	7.06	11.5	677	1.74
SP 67	6.9	244	3.52	8.5	370	2.39	5.0	128	3.57	9.2	433	1.51	11.5	677	0.51
SP 70	6.3	203	7.67	8.5	370	6.19	5.0	128	7.67	9.2	433	4.26	11.5	677	1.42
	<u>Sep 10 0000 Z</u>			<u>Aug 17 2100 Z</u>			<u>Aug 25 1800 Z</u>			<u>Sep 15 2100 Z</u>			<u>Aug 29 1200 Z</u>		
<u>Borehole</u>	<u>P</u>	<u>L</u>	<u>F</u>	<u>P</u>	<u>L</u>	<u>F</u>	<u>P</u>	<u>L</u>	<u>F</u>	<u>P</u>	<u>L</u>	<u>F</u>	<u>P</u>	<u>L</u>	<u>F</u>
SP 6	11.6	689	0.53	12.5	800	0.50	10.5	564	0.56	14.5	1076	0.49	14.0	1004	0.49
SP 60	10.8	597	2.26	12.5	800	1.30	8.5	370	6.64	12.5	800	1.30	11.6	689	1.68
SP 67	10.8	597	0.66	11.5	677	0.51	8.5	370	2.39	11.5	677	0.51	11.6	689	0.50
SP 70	10.8	597	1.88	11.5	677	1.42	8.5	370	6.19	12.5	800	1.04	12.4	787	1.37
	<u>Sep 10 1200 Z</u>			<u>Aug 18 0900 Z</u>			<u>Aug 26 0600 Z</u>			<u>Sep 16 0900 Z</u>			<u>Aug 30 0000 Z</u>		
<u>Borehole</u>	<u>P</u>	<u>L</u>	<u>F</u>	<u>P</u>	<u>L</u>	<u>F</u>	<u>P</u>	<u>L</u>	<u>F</u>	<u>P</u>	<u>L</u>	<u>F</u>	<u>P</u>	<u>L</u>	<u>F</u>
SP 6	8.4	361	0.58	9.5	461	0.55	6.0	184	1.30	12.4	787	0.50	10.6	575	0.57*
SP 60	8.4	361	7.06	9.5	461	4.13	7.5	288	13.7	11.6	689	1.68	6.0	184	25.5
SP 67	8.4	361	2.56	7.0	251	3.52	7.5	288	3.63	9.2	433	1.51	6.8	237	3.53
SP 70	8.4	361	6.51	7.0	251	7.68	7.5	288	7.72	9.2	433	4.26	6.8	237	7.66

P = wave period  
L = wavelength  
F = safety factor

SP = South Pass Area

*SP 6 Katrina pre- and post-storm safety factor limit: (pre-storm at Aug 27 0000 Z; post-storm at Aug 30 1200 Z)	6.4	212	1.00
---	-----	-----	------

Table N-5: Parameters used in safety factor calculations, Cross Section D-D'

	<u>Betsy</u>			<u>Camille</u>			<u>Andrew</u>			<u>Ivan</u>			<u>Katrina*</u>		
	<u>Sep 9 0000 Z</u>			<u>Aug 16 2100 Z</u>			<u>Aug 24 1800 Z</u>			<u>Sep 14 2100 Z</u>			<u>Aug 28 1200 Z</u>		
<u>Borehole</u>	<u>P</u>	<u>L</u>	<u>F</u>	<u>P</u>	<u>L</u>	<u>F</u>	<u>P</u>	<u>L</u>	<u>F</u>	<u>P</u>	<u>L</u>	<u>F</u>	<u>P</u>	<u>L</u>	<u>F</u>
SP 20	5.4	149	0.72	5.5	155	0.65	3.5	63	7.97	6.3	203	0.42	12.4	787	0.30
SP 72	5.4	149	8.78	5.5	155	8.78	3.5	63	8.78	5.7	166	8.77	11.6	689	0.58
	<u>Sep 9 1200 Z</u>			<u>Aug 17 0900 Z</u>			<u>Aug 25 0600 Z</u>			<u>Sep 15 0900 Z</u>			<u>Aug 29 0000 Z</u>		
<u>Borehole</u>	<u>P</u>	<u>L</u>	<u>F</u>	<u>P</u>	<u>L</u>	<u>F</u>	<u>P</u>	<u>L</u>	<u>F</u>	<u>P</u>	<u>L</u>	<u>F</u>	<u>P</u>	<u>L</u>	<u>F</u>
SP 20	6.9	244	0.35	10.5	564	0.29	5.5	155	0.65	11.6	689	0.30	13.5	933	0.28
SP 72	6.9	244	7.70	9.0	415	1.56	5.5	155	8.78	10.0	512	0.95	11.5	677	0.59
	<u>Sep 10 0000 Z</u>			<u>Aug 17 2100 Z</u>			<u>Aug 25 1800 Z</u>			<u>Sep 15 2100 Z</u>			<u>Aug 29 1200 Z</u>		
<u>Borehole</u>	<u>P</u>	<u>L</u>	<u>F</u>	<u>P</u>	<u>L</u>	<u>F</u>	<u>P</u>	<u>L</u>	<u>F</u>	<u>P</u>	<u>L</u>	<u>F</u>	<u>P</u>	<u>L</u>	<u>F</u>
SP 20	11.6	689	0.30	12.5	800	0.30	8.5	370	0.30	14.5	1076	0.28	13.2	892	0.29
SP 72	10.8	597	0.72	11.0	620	0.67	8.5	370	2.15	12.5	800	0.49	11.6	689	0.58
	<u>Sep 10 1200 Z</u>			<u>Aug 18 0900 Z</u>			<u>Aug 26 0600 Z</u>			<u>Sep 16 0900 Z</u>			<u>Aug 30 0000 Z</u>		
<u>Borehole</u>	<u>P</u>	<u>L</u>	<u>F</u>	<u>P</u>	<u>L</u>	<u>F</u>	<u>P</u>	<u>L</u>	<u>F</u>	<u>P</u>	<u>L</u>	<u>F</u>	<u>P</u>	<u>L</u>	<u>F</u>
SP 20	9.2	433	0.29	10.0	512	0.29	6.5	216	0.39	12.4	787	0.30	9.8	491	0.29
SP 72	8.4	361	2.31	7.5	288	4.67	7.5	288	4.67	10.0	512	0.95	8.4	361	2.31

P = wave period

L = wavelength

F = safety factor

SP = South Pass Protraction Area

\*SP 20 Katrina pre- and post-storm safety factor limit:  
(Katrina pre-storm at Aug 27 0000 Z; post-storm at Aug 30 1200 Z)

\*SP 72 Katrina pre- and post-storm safety factor limit:  
(Katrina pre-storm at Aug 27 0000 Z)

5.1 133 1.00

9.9 500 1.00

Table N-6: Parameters used in safety factor calculations, Cross Section E-E'

	<u>Betsy</u>			<u>Camille</u>			<u>Andrew</u>			<u>Ivan</u>			<u>Katrina</u>		
	<u>Sep 9 0000 Z</u>			<u>Aug 16 2100 Z</u>			<u>Aug 24 1800 Z</u>			<u>Sep 14 2100 Z</u>			<u>Aug 28 1200 Z</u>		
<u>Borehole</u>	<u>P</u>	<u>L</u>	<u>F</u>	<u>P</u>	<u>L</u>	<u>F</u>	<u>P</u>	<u>L</u>	<u>F</u>	<u>P</u>	<u>L</u>	<u>F</u>	<u>P</u>	<u>L</u>	<u>F</u>
SP 29	6.3	203	0.63	6.5	216	0.64	3.5	63	2.60	7.5	288	0.69	12.4	787	0.86
SP 47	5.0	128	7.92	5.5	155	7.92	3.5	63	7.92	5.7	166	7.92	9.2	433	4.97
SP 48	5.0	128	6.96	5.5	155	6.97	3.5	63	6.96	5.7	166	6.97	9.2	433	1.85
SP 49	5.4	149	3.35	6.5	216	3.35	3.5	63	3.35	5.7	166	3.35	9.2	433	2.58
	<u>Sep 9 1200 Z</u>			<u>Aug 17 0900 Z</u>			<u>Aug 25 0600 Z</u>			<u>Sep 15 0900 Z</u>			<u>Aug 29 0000 Z</u>		
<u>Borehole</u>	<u>P</u>	<u>L</u>	<u>F</u>	<u>P</u>	<u>L</u>	<u>F</u>	<u>P</u>	<u>L</u>	<u>F</u>	<u>P</u>	<u>L</u>	<u>F</u>	<u>P</u>	<u>L</u>	<u>F</u>
SP 29	8.1	336	0.73	10.5	564	0.79	5.0	128	0.71	11.6	689	0.83	13.5	933	0.93
SP 47	6.3	203	7.93	9.0	415	5.64	5.0	128	7.92	9.2	433	4.97	12.5	800	1.13
SP 48	6.3	203	6.91	9.0	415	2.05	5.0	128	6.96	9.2	433	1.85	11.5	800	0.63
SP 49	6.9	244	3.36	9.0	415	2.75	5.0	128	3.35	9.2	433	2.58	11.5	800	0.63
	<u>Sep 10 0000 Z</u>			<u>Aug 17 2100 Z</u>			<u>Aug 25 1800 Z</u>			<u>Sep 15 2100 Z</u>			<u>Aug 29 1200 Z</u>		
<u>Borehole</u>	<u>P</u>	<u>L</u>	<u>F</u>	<u>P</u>	<u>L</u>	<u>F</u>	<u>P</u>	<u>L</u>	<u>F</u>	<u>P</u>	<u>L</u>	<u>F</u>	<u>P</u>	<u>L</u>	<u>F</u>
SP 29	13.2	892	0.91	12.0	737	0.85	9.5	461	0.79	14.5	1076	1.00	13.2	892	0.91
SP 47	11.6	689	1.52	12.0	737	1.32	8.5	370	7.92	13.5	933	0.89	12.4	787	1.17
SP 48	10.8	597	0.94	10.5	564	1.03	8.5	370	2.79	12.5	800	0.63	11.6	689	0.75
SP 49	10.8	597	1.44	10.5	564	1.60	8.5	370	3.13	12.5	800	0.86	11.6	689	1.11
	<u>Sep 10 1200 Z</u>			<u>Aug 18 0900 Z</u>			<u>Aug 26 0600 Z</u>			<u>Sep 16 0900 Z</u>			<u>Aug 30 0000 Z</u>		
<u>Borehole</u>	<u>P</u>	<u>L</u>	<u>F</u>	<u>P</u>	<u>L</u>	<u>F</u>	<u>P</u>	<u>L</u>	<u>F</u>	<u>P</u>	<u>L</u>	<u>F</u>	<u>P</u>	<u>L</u>	<u>F</u>
SP 29	10.0	512	0.79	9.0	415	0.80	8.0	328	0.72	12.4	787	0.86	10.8	597	0.80
SP 47	8.4	361	7.84	7.5	288	7.69	7.5	288	7.69	11.6	689	1.52	7.6	296	7.64
SP 48	8.4	361	2.98	7.5	288	5.48	7.5	288	5.48	9.2	433	1.85	7.6	296	5.12
SP 49	9.2	433	2.58	7.5	288	3.37	7.5	288	3.37	9.2	433	2.58	7.6	296	3.37

P = wave period

SP = South Pass Protraction Area

L = wavelength

F = safety factor

Table N-7: Parameters used in safety factor calculations, Cross Section F-F'

	<u>Betsy</u>			<u>Camille</u>			<u>Andrew</u>			<u>Ivan</u>			<u>Katrina</u>		
	<u>Sep 9 0000 Z</u>			<u>Aug 16 2100 Z</u>			<u>Aug 24 1800 Z</u>			<u>Sep 14 2100 Z</u>			<u>Aug 28 1200 Z</u>		
<u>Borehole</u>	<u>P</u>	<u>L</u>	<u>F</u>	<u>P</u>	<u>L</u>	<u>F</u>	<u>P</u>	<u>L</u>	<u>F</u>	<u>P</u>	<u>L</u>	<u>F</u>	<u>P</u>	<u>L</u>	<u>F</u>
SP 27	3.8	74	1.51	6.5	216	0.24	2.5	32	6.43	8.2	344	0.26	13.2	892	0.31
SP 39	4.2	90	3.60	5.5	155	1.71	3.5	63	3.63	6.3	203	0.82	12.4	787	0.32
SP 54	4.6	108	29.1	6.5	216	29.1	3.5	63	29.1	5.7	166	29.1	10.8	597	8.92
SP 76	5.0	128	23.3	6.5	216	23.3	3.5	63	23.3	5.7	166	23.3	10.0	597	8.40
	<u>Sep 9 1200 Z</u>			<u>Aug 17 0900 Z</u>			<u>Aug 25 0600 Z</u>			<u>Sep 15 0900 Z</u>			<u>Aug 29 0000 Z</u>		
<u>Borehole</u>	<u>P</u>	<u>L</u>	<u>F</u>	<u>P</u>	<u>L</u>	<u>F</u>	<u>P</u>	<u>L</u>	<u>F</u>	<u>P</u>	<u>L</u>	<u>F</u>	<u>P</u>	<u>L</u>	<u>F</u>
SP 27	6.3	203	0.24	12.0	737	0.28	3.5	63	3.43	13.5	933	0.24	14.5	1076	0.33
SP 39	5.7	166	1.36	10.5	564	0.35	3.5	63	3.63	11.6	689	0.32	13.5	933	0.32
SP 54	6.3	203	29.1	9.0	415	17.1	4.5	104	29.1	9.2	433	15.8	12.5	800	5.94
SP 76	6.3	203	23.3	9.0	415	13.2	4.5	104	23.3	9.2	433	12.0	11.5	677	4.95
	<u>Sep 10 0000 Z</u>			<u>Aug 17 2100 Z</u>			<u>Aug 25 1800 Z</u>			<u>Sep 15 2100 Z</u>			<u>Aug 29 1200 Z</u>		
<u>Borehole</u>	<u>P</u>	<u>L</u>	<u>F</u>	<u>P</u>	<u>L</u>	<u>F</u>	<u>P</u>	<u>L</u>	<u>F</u>	<u>P</u>	<u>L</u>	<u>F</u>	<u>P</u>	<u>L</u>	<u>F</u>
SP 27	14.0	1004	0.32	12.0	737	0.28	12.5	800	0.29	15.0	1152	0.34	13.2	892	0.31
SP 39	12.4	787	0.32	12.0	737	0.32	10.0	512	0.37	15.0	1152	0.33	11.6	689	0.32
SP 54	11.6	689	7.13	12.0	737	6.53	8.5	370	21.1	12.5	800	4.84	10.8	597	8.82
SP 76	10.8	597	6.18	11.0	620	5.76	8.5	370	16.5	12.5	800	3.87	10.8	597	6.18
	<u>Sep 10 1200 Z</u>			<u>Aug 18 0900 Z</u>			<u>Aug 26 0600 Z</u>			<u>Sep 16 0900 Z</u>			<u>Aug 30 0000 Z</u>		
<u>Borehole</u>	<u>P</u>	<u>L</u>	<u>F</u>	<u>P</u>	<u>L</u>	<u>F</u>	<u>P</u>	<u>L</u>	<u>F</u>	<u>P</u>	<u>L</u>	<u>F</u>	<u>P</u>	<u>L</u>	<u>F</u>
SP 27	10.0	512	0.26	8.5	370	0.26	8.5	370	0.26	12.4	787	0.29	10.8	597	0.26
SP 39	8.4	361	0.42	7.5	288	0.49	7.5	288	0.49	11.6	689	0.32	10.2	533	0.36
SP 54	8.4	361	22.0	7.5	288	29.8	7.5	288	29.8	10.0	512	11.5	8.4	361	22.0
SP 76	8.4	361	17.3	7.5	288	23.0	7.5	288	23.0	9.2	433	12.0	7.6	296	22.5

P = wave period

SP = South Pass Protraction Area

L = wavelength

F = safety factor

Table N-8: Parameters used in safety factor calculations, Cross Section G-G'

	<u>Betsy</u>			<u>Camille</u>			<u>Andrew</u>			<u>Ivan</u>			<u>Katrina</u>		
	<u>Sep 9 0000 Z</u>			<u>Aug 16 2100 Z</u>			<u>Aug 24 1800 Z</u>			<u>Sep 14 2100 Z</u>			<u>Aug 28 1200 Z</u>		
<u>Borehole</u>	<u>P</u>	<u>L</u>	<u>F</u>	<u>P</u>	<u>L</u>	<u>F</u>	<u>P</u>	<u>L</u>	<u>F</u>	<u>P</u>	<u>L</u>	<u>F</u>	<u>P</u>	<u>L</u>	<u>F</u>
WD 48	3.0	46	424	8.5	370	3.18	3.5	63	119	3.9	78	32.1	9.2	433	3.28
WD 59	3.4	59	66.0	6.5	216	3.02	3.5	63	66.0	5.1	133	6.82	11.6	689	1.41
WD 107	4.2	90	28.2	6.5	216	28.8	2.5	32	28.2	5.1	133	28.2	8.4	361	11.4
WD 140	4.6	108	57.8	6.5	216	57.8	3.5	63	57.8	6.3	203	57.8	8.4	361	40.8
	<u>Sep 9 1200 Z</u>			<u>Aug 17 0900 Z</u>			<u>Aug 25 0600 Z</u>			<u>Sep 15 0900 Z</u>			<u>Aug 29 0000 Z</u>		
<u>Borehole</u>	<u>P</u>	<u>L</u>	<u>F</u>	<u>P</u>	<u>L</u>	<u>F</u>	<u>P</u>	<u>L</u>	<u>F</u>	<u>P</u>	<u>L</u>	<u>F</u>	<u>P</u>	<u>L</u>	<u>F</u>
WD 48	3.3	56	177	10.5	564	3.84	2.5	32	3234	8.4	361	3.16	13.5	933	5.43
WD 59	4.5	104	14.1	10.5	564	1.40	2.5	32	65.6	9.2	433	1.50	14.0	1004	1.57
WD 107	5.7	166	28.2	10.5	564	4.44	3.5	63	28.2	8.4	361	11.4	12.5	800	2.86
WD 140	6.3	203	57.8	9.0	415	28.8	4.5	104	57.8	8.4	361	40.8	11.5	677	10.0
	<u>Sep 10 0000 Z</u>			<u>Aug 17 2100 Z</u>			<u>Aug 25 1800 Z</u>			<u>Sep 15 2100 Z</u>			<u>Aug 29 1200 Z</u>		
<u>Borehole</u>	<u>P</u>	<u>L</u>	<u>F</u>	<u>P</u>	<u>L</u>	<u>F</u>	<u>P</u>	<u>L</u>	<u>F</u>	<u>P</u>	<u>L</u>	<u>F</u>	<u>P</u>	<u>L</u>	<u>F</u>
WD 48	9.2	433	3.38	12.0	737	4.56	10.5	564	3.84	14.5	1076	6.08	12.4	787	4.78
WD 59	8.4	361	1.70	10.5	564	1.40	8.5	370	1.67	14.5	1076	1.62	12.4	787	1.44
WD 107	9.2	433	7.41	9.0	415	8.16	8.5	370	10.7	13.5	933	2.56	10.0	512	5.26
WD 140	10.0	512	17.3	11.0	620	11.7	8.5	370	38.4	13.5	933	6.23	9.2	433	25.9
	<u>Sep 10 1200 Z</u>			<u>Aug 18 0900 Z</u>			<u>Aug 26 0600 Z</u>			<u>Sep 16 0900 Z</u>			<u>Aug 30 0000 Z</u>		
<u>Borehole</u>	<u>P</u>	<u>L</u>	<u>F</u>	<u>P</u>	<u>L</u>	<u>F</u>	<u>P</u>	<u>L</u>	<u>F</u>	<u>P</u>	<u>L</u>	<u>F</u>	<u>P</u>	<u>L</u>	<u>F</u>
WD 48	8.4	361	3.16	6.0	184	3.29	8.5	370	3.18	11.6	689	4.35	8.4	361	3.16
WD 59	7.6	296	2.11	6.0	184	3.67	8.0	328	1.85	10.8	597	1.40	7.6	296	2.11
WD 107	8.4	361	11.4	7.5	288	19.6	7.5	288	19.6	10.0	512	5.26	7.6	296	18.5
WD 140	8.4	361	40.8	7.5	288	58.2	7.5	288	58.2	10.0	512	17.3	8.4	361	40.8

P = wave period

SP = South Pass Protraction Area

L = wavelength

F = safety factor



**APPENDIX O: MIKE 21 WAVE MODELING RESULTS,  
HURRICANE ANDREW (1992)**

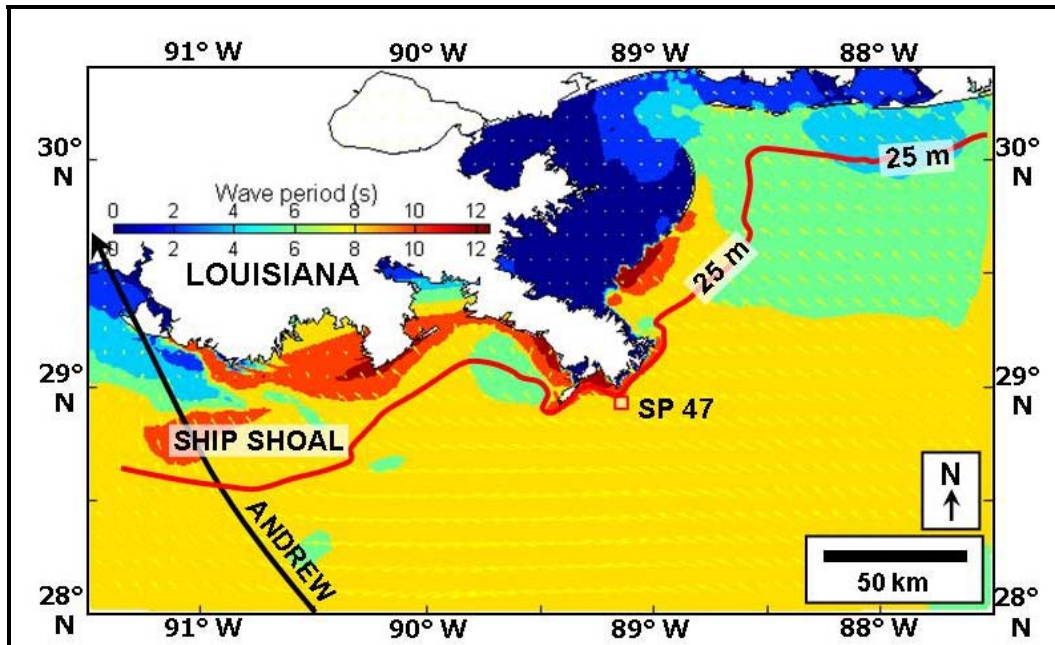


Figure O-1: Zero-crossing wave period (T-02) computed during Hurricane Andrew, August 25, 1992 at 1800 Z

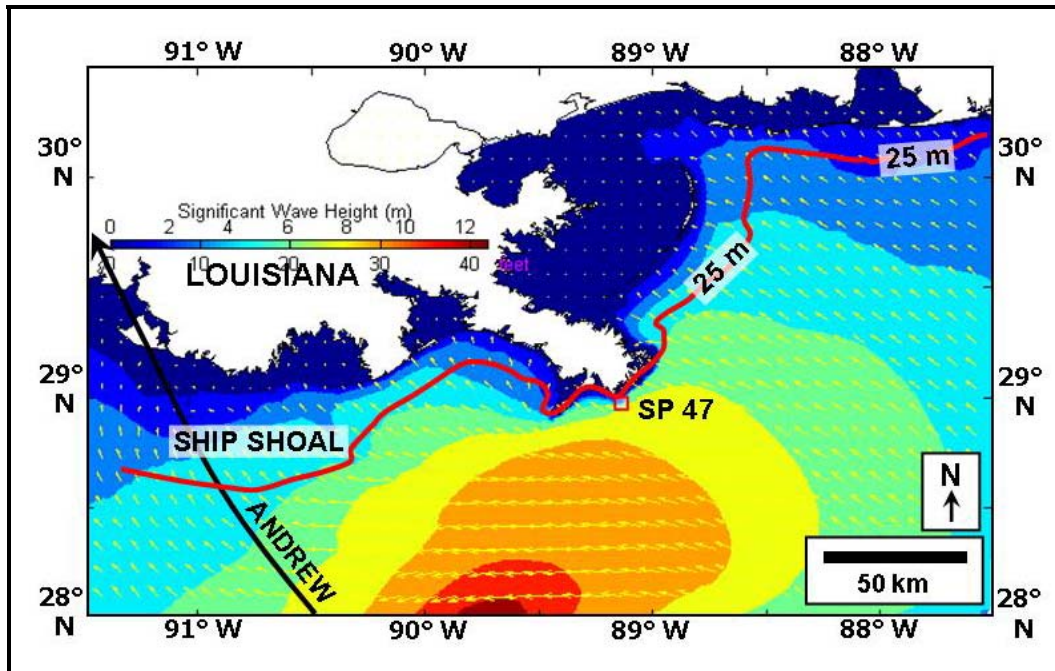


Figure O-2: Significant wave height computed during Hurricane Andrew, August 25, 1992 at 1800 Z

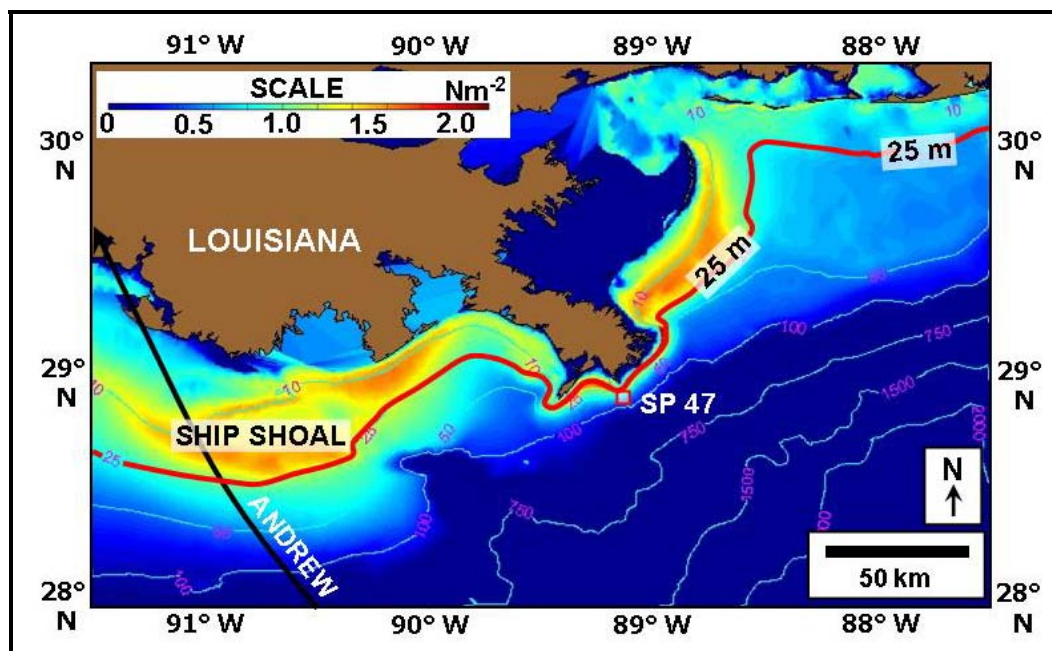


Figure O-3: Bottom shear stress computed during Hurricane Andrew, August 25, 1992 at 1800 Z

## APPENDIX P: STUDY AREA PLATFORM HISTORY (SORTED BY PROTRACTION AREA)

Table P-1: Ewing Banks Protraction Area: Platform History and Statistical Analysis (data from MMS, 2009)

EWING BANKS Platform Data - INSTALLED												
Searched by Area and Structure Installed Date Sorted by Installation Date												
Area Code	Block Number	Field	Structure Name	Struc Type	Operator	Install Date	Removal Date	Water Depth	Latitude	Longitude	Ptfm X Location	Ptfm Y Location
EW	305	EW305	A	FIXED	Stone Energy Corporation	1/1/1985		271	28.6658	-89.9695	2,612,202	10,415,141
ELENA												
EW	826	EW826	A	FIXED	Apache Corporation	1/1/1988		483	28.1633	-90.3586	2,491,380	10,229,440
EW	947	EW947	A	FIXED	Newfield Exploration Company	1/1/1990		477	28.0360	-90.8911	2,320,575	10,179,797
ANDREW												
EW	482	MC441	A	FIXED	W & T Offshore, Inc.	11/29/1992		371	28.4692	-89.9703	2,613,725	10,343,645
EW	873	EW873	A (LOBSTER)	FIXED	Marathon Oil Company	7/2/1994		775	28.1010	-90.2021	2,542,338	10,207,929
OPAL												
EW	921	EW921	A-Morpeth East	MTLP	Eni US Operating Co. Inc.	8/10/1998		1,700	28.0348	-90.0228	2,600,750	10,185,223
GEORGES												
EW	910	EW910	A	FIXED	Offshore Shelf LLC	10/16/1998		549	28.0535	-90.5476	2,431,255	10,188,253
EW	1003	EW958	A-Prince TLP	TLP	El Paso E&P Company, L.P.	7/18/2001		1,500	27.9927	-90.3258	2,503,306	10,167,636
LILI												
IVAN												
KATRINA												
RITA												

Index to "Structural Type" field:			
CAIS	Caisson	SPAR	SPAR Platform - floating production system
CT	Compliant tower	SSANC	Fixed anchors or mooring piles used to secure a structure to the seafloor
FIXED	Fixed Leg Platform	SSMNF	Subsea Manifold
FPSO	Floating production, storage, and offloading	SSTMP	Subsea templates
MOPU	Mobile Production Unit	TLP	Tension leg platform
MTLP	Mini Tension Leg Platform	UCOMP	Underwater completion or subsea caisson
SEMI	Semi Submersible (Column Stabilized Unit) Floating Production System	WP	Well Protector

Table P-2: Grand Isle Protraction Area: Platform History and Statistical Analysis (data from MMS, 2009)

GRAND ISLE Platform Data - INSTALLED													
Searched by Area and Structure Installed Date Sorted by Installation Date													
Area Code	Block Number	Field	Structure Name	Struc Type Code	Operator	Install Date	Removal Date	Water Depth	Latitude	Longitude	Ptfm X Location	Ptfm Y Location	
GI	16	GI016	A	WP	Freeport-McMoRan Energy LLC	1/1/1948	12/31/1976	43	29.1314	-90.0126	2,421,682	171,447	
GI	22	GI016	C	WP	Exxon Mobil Corporation	1/1/1949	12/31/1976	53	29.1272	-89.9594	2,438,682	170,117	
GI	23	GI016	G	FIXED	Exxon Mobil Corporation	1/1/1954	12/31/1975	42	29.1227	-90.0215	2,418,876	168,224	
GI	23	GI016	J	FIXED	Exxon Mobil Corporation	1/1/1955		53	29.1008	-89.9944	2,427,622	160,364	
GI	47	GI047	A	FIXED	GOM Shelf LLC	1/1/1955		89	28.9455	-90.0311	2,416,556	103,782	
GI	22	GI016	L-CMP-VALVE	FIXED	Exxon Mobil Corporation	1/1/1956		55	29.1014	-89.9786	2,432,694	160,669	
GI	22	GI016	L-PRD	FIXED	Exxon Mobil Corporation	1/1/1956		55	29.1014	-89.9779	2,432,894	160,669	
GI	22	GI016	L-QTR	FIXED	Exxon Mobil Corporation	1/1/1956		55	29.1014	-89.9782	2,432,794	160,669	
GI	23	GI016	K	FIXED	Exxon Mobil Corporation	1/1/1956	9/19/2001	50	29.0986	-90.0102	2,422,611	159,501	
GI	26	BM002	P	WP	Chevron U.S.A. Inc.	1/1/1956		40	29.0873	-90.1161	2,388,831	155,016	
GI	40	GI047	B	FIXED	GOM Shelf LLC	1/1/1956		83	28.9713	-90.0357	2,414,986	113,145	
GI	22	GI016	P	FIXED	Exxon Mobil Corporation	1/1/1957		55	29.1086	-89.9700	2,435,402	163,319	
GI	26	BM002	1	CAIS	Chevron U.S.A. Inc.	1/1/1957	7/16/2004	42	29.0718	-90.1117	2,390,278	149,419	
GI	29	GI016	N	FIXED	Exxon Mobil Corporation	1/1/1957	12/31/1984	62	29.0865	-89.9593	2,438,902	155,319	
GI	47	GI047	C	FIXED	GOM Shelf LLC	1/1/1957		88	28.9604	-90.0235	2,418,926	109,215	
AUDREY													
GI	37	BM002	FLR	FIXED	Chevron U.S.A. Inc.	1/1/1958	12/21/1994	49	29.0434	-90.1213	2,387,328	139,061	
GI	37	BM002	R	FIXED	Chevron U.S.A. Inc.	1/1/1958		49	29.0430	-90.1209	2,387,458	138,923	
GI	48	GI047	E	FIXED	GOM Shelf LLC	1/1/1958		91	28.9342	-90.0435	2,412,630	99,611	
GI	26	BM002	X	FIXED	Chevron U.S.A. Inc.	1/1/1959		43	29.0563	-90.1162	2,388,920	143,742	
GI	26	BM002	CH	WP	Chevron U.S.A. Inc.	1/1/1959	8/2/2004	44	29.0656	-90.1170	2,388,609	147,138	
GI	48	GI047	D	FIXED	GOM Shelf LLC	1/1/1959		86	28.9604	-90.0436	2,412,486	109,145	
GI	37	BM002	Y	FIXED	Chevron U.S.A. Inc.	1/1/1960		47	29.0378	-90.1100	2,390,947	137,044	
GI	40	GI047	F	FIXED	GOM Shelf LLC	1/1/1960		86	28.9692	-90.0210	2,419,686	112,405	
ETHYL													
GI	22	GI016	Q	FIXED	Exxon Mobil Corporation	1/1/1961		55	29.0946	-89.9898	2,429,144	158,119	
GI	22	GI016	R	FIXED	Exxon Mobil Corporation	1/1/1961		55	29.1227	-89.9662	2,436,551	168,440	
GI	26	BM002	BB	FIXED	Chevron U.S.A. Inc.	1/1/1961	4/9/2005	47	29.0535	-90.1079	2,391,578	142,771	
GI	37	BM002	CO	FIXED	Chevron U.S.A. Inc.	1/1/1961		50	29.0341	-90.1220	2,387,128	135,661	
CARLA													
GI	23	GI016	T	FIXED	Exxon Mobil Corporation	1/1/1962		48	29.1109	-90.0239	2,418,158	163,946	
GI	26	BM002	CB	WP	Chevron U.S.A. Inc.	1/1/1962	8/10/2004	45	29.0671	-90.1145	2,389,404	147,687	
GI	37	BM002	FLR	FIXED	Chevron U.S.A. Inc.	1/1/1962	11/14/1995	50	29.0274	-90.1190	2,388,121	133,251	
GI	37	BM002	CZ	WP	Chevron U.S.A. Inc.	1/1/1962	12/31/1984	50	29.0274	-90.1199	2,387,821	133,251	
GI	37	BM002	CS	FIXED	Chevron U.S.A. Inc.	1/1/1962		48	29.0407	-90.1256	2,385,978	138,061	
GI	37	BM002	CR	WP	Chevron U.S.A. Inc.	1/1/1962	12/31/1984	52	29.0298	-90.1099	2,391,028	134,161	
GI	22	GI016	U	FIXED	Exxon Mobil Corporation	1/1/1963		60	29.0969	-89.9645	2,437,193	159,060	
GI	41	GI041	A	FIXED	GOM Shelf LLC	1/1/1964		91	28.9845	-89.9623	2,438,402	118,203	
HILDA													
GI	32	GI043	J	FIXED	GOM Shelf LLC	1/1/1965		106	29.0104	-89.8576	2,471,756	128,027	
BETSY													
GI	21	GI016	W	FIXED	Exxon Mobil Corporation	1/1/1966		65	29.0948	-89.9421	2,444,360	158,383	
GI	21	GI016	X	FIXED	Exxon Mobil Corporation	1/1/1966	12/31/1984	65	29.0953	-89.9250	2,449,809	158,636	
GI	37	BM002	GG	FIXED	Chevron U.S.A. Inc.	1/1/1966		54	29.0202	-90.1091	2,391,309	130,640	
GI	41	GI041	B	FIXED	GOM Shelf LLC	1/1/1966		91	28.9985	-89.9590	2,439,402	123,303	
GI	21	GI016	Z	FIXED	Exxon Mobil Corporation	1/1/1967	2/11/1994	62	29.1090	-89.9326	2,447,325	163,578	
GI	29	GI016	Y	WP	Exxon Mobil Corporation	1/1/1967	12/31/1980	62	29.0830	-89.9704	2,435,363	153,979	
GI	42	GI041	C	FIXED	BP America Production Company	1/1/1967		100	28.9988	-89.9378	2,446,176	123,485	
GI	43	GI043	Q	FIXED	GOM Shelf LLC	1/1/1967		140	28.9982	-89.8829	2,463,709	123,511	
GI	63	GI072	A	FIXED	Conoco Inc.	1/1/1967	3/3/1989	60	28.8090	-90.0763	2,402,628	53,963	
GI	85	ST131	I	FIXED	Chevron U.S.A. Inc.	1/1/1967	8/26/1998	192	28.7088	-90.1225	2,388,232	17,380	
GI	37	BM002	21	CAIS	Chevron U.S.A. Inc.	1/1/1968	7/21/1999	54	29.0198	-90.1088	2,391,408	130,503	
GI	40	GI047	G	FIXED	GOM Shelf LLC	1/1/1968		85	28.9696	-90.0003	2,426,309	112,662	
GI	41	GI041	D	FIXED	GOM Shelf LLC	1/1/1968		90	28.9936	-89.9671	2,436,809	121,494	
GI	41	GI041	E	FIXED	GOM Shelf LLC	1/1/1968		85	28.9929	-89.9854	2,430,973	121,182	
GI	43	GI043	AA-SEP	FIXED	GOM Shelf LLC	1/1/1968		110	29.0007	-89.8583	2,471,568	124,503	
GI	43	GI043	AA-RSR	FIXED	GOM Shelf LLC	1/1/1968		110	29.0012	-89.8583	2,471,568	124,703	
GI	43	GI043	AA-PRD	FIXED	GOM Shelf LLC	1/1/1968		110	29.0012	-89.8589	2,471,368	124,703	
GI	43	GI043	AA-QRT	FIXED	GOM Shelf LLC	1/1/1968		110	29.0010	-89.8589	2,471,368	124,603	
GI	43	GI043	AA-CMP	FIXED	GOM Shelf LLC	1/1/1968		110	29.0012	-89.8592	2,471,268	124,703	
GI	17	GI016	1-PRD	FIXED	Freeport-McMoRan Energy LLC	1/1/1969	8/25/2002	55	29.1300	-89.9896	2,429,043	171,001	
GI	17	GI016	2-TWR	FIXED	Freeport-McMoRan Energy LLC	1/1/1969	8/25/2002	55	29.1300	-89.9896	2,429,043	171,001	
GI	17	GI016	1-TWR	FIXED	Freeport-McMoRan Energy LLC	1/1/1969	8/25/2002	55	29.1300	-89.9896	2,429,043	171,001	
GI	17	GI016	QTRS	FIXED	Freeport-McMoRan Energy LLC	1/1/1969	8/25/2002	55	29.1300	-89.9896	2,429,043	171,001	
GI	17	GI016	PP	FIXED	Freeport-McMoRan Energy LLC	1/1/1969	8/25/2002	55	29.1300	-89.9896	2,429,043	171,001	
GI	17	GI016	4-TWR	FIXED	Freeport-McMoRan Energy LLC	1/1/1969	8/25/2002	55	29.1300	-89.9896	2,429,043	171,021	
GI	17	GI016	2-PRD	WP	Freeport-McMoRan Energy LLC	1/1/1969	8/25/2002	55	29.1300	-89.9896	2,429,043	171,001	
GI	17	GI016	3-TWR	FIXED	Freeport-McMoRan Energy LLC	1/1/1969	8/25/2002	55	29.1300	-89.9896	2,429,043	171,001	
GI	17	GI016	WRHOUSE	FIXED	Freeport-McMoRan Energy LLC	1/1/1969	8/25/2002	55	29.1300	-89.9896	2,429,043	171,001	
GI	17	GI016	BLEEDWATER	FIXED	Freeport-McMoRan Energy LLC	1/1/1969	8/25/2002	50	29.1336	-89.9887	2,429,308	172,307	
GI	37	BM002	#2	CAIS	Pogo Producing Company	1/1/1969	7/20/1999	90	29.0212	-90.1044	2,392,803	131,023	
GI	37	BM002	22	CAIS	Chevron U.S.A. Inc.	1/1/1969		50	29.0352	-90.1256	2,385,978	136,069	
CAMILLE													
GI	40	GI047	I	FIXED	GOM Shelf LLC	1/1/1970		86	28.9687	-90.0215	2,419,518	112,233	
GI	47	GI047	H	FIXED	GOM Shelf LLC	1/1/1970		90	28.9458	-90.0335	2,415,791	103,857	
GI	81	GI082	A	FIXED	MidCon Exploration Company - Gulf Coast	1/1/1971	12/31/1986	177	28.7200	-89.9490	2,443,809	22,081	
GI	26	BM002	15	CAIS	Chevron U.S.A. Inc.	1/1/1972	6/21/2000	47	29.0536	-90.1079	2,391,584	142,803	
GI	32	GI043	W	FIXED	Conoco Inc.	1/1/1972	12/31/1980	92	29.0353	-89.8919	2,460,660	136,961	
GI	47	GI047	AQ QTRS	FIXED	GOM Shelf LLC	1/1/1972		89	28.9455	-90.0308	2,416,656	103,782	
GI	26	BM002	14	CAIS	Chevron U.S.A. Inc.	1/1/1973	7/19/2004	24	29.0643	-90.1197	2,387,750	146,672	
GI	48	GI047	J	FIXED	GOM Shelf LLC	1/1/1973		24	28.9450	-90.0535	2,409,400	103,502	
GI	76	GI076	A	FIXED	Forest Oil Corporation	1/1/1973		150	28.7383	-90.0262	2,418,994	28,436	
GI	95	GI095	A	FIXED	BP Exploration & Production Inc.	1/1/1973		210	28.5159	-90.1231	2,388,778	-52,793	
GI	94	GI095	B	FIXED	Apache Corporation	1/1/1974		210	28.5258	-90.0979	2,396,828	-49,093	
CARMEN													
GI	37	BM002	YA	CAIS	Chevron U.S.A. Inc.	1/1/1975		47	29.0378	-90.1104	2,390,832	137,058	
GI	42	GI041	F	FIXED	BP America Production Company	1/1/1975		100	29.0036	-89.9444	2,444,017	125,210	
GI	93	GI095	C	FIXED	Apache Corporation	1/1/1975		210	28.5489	-90.0687	2,406,128	-40,593	
ELOISE													
GI	45	GI045	3	CAIS	Conoco Inc.	1/1/1976	2/24/1989	90	28.9617	-89.9260	2,450,102	110,045	
GI	48	GI047	K	FIXED	GOM Shelf LLC	1/1/1976		90	28.9371	-90.0653	2,405,636	100,577	
GI	37	BM002	17	WP	Chevron U.S.A. Inc.	1/1/1979	6/20/2000	54	29.0137	-90.1250	2,386,268	128,222	

GRAND ISLE Platform Data - INSTALLED													
Searched by Area and Structure Installed Date Sorted by Installation Date													
Area Code	Block Number	Field	Structure Name	Struc Type Code	Operator	Install Date	Removal Date	Water Depth	Latitude	Longitude	Ptfm X Location	Ptfm Y Location	
GI	75	GI076	JA	WP	Forest Oil Corporation	1/1/1979		150	28.7360	-90.0515	2,410,878	27,512	
FREDERIC													
GI	83	GI076	A	FIXED	Coldren Resources LP	1/1/1980		153	28.7200	-90.0234	2,419,950	21,793	
GI	19	GI018	3	FIXED	Exxon Mobil Corporation	1/1/1981		55	29.1499	-89.8974	2,458,382	178,587	
GI	20	GI020	A	FIXED	Apache Corporation	1/1/1982		60	29.1229	-89.8969	2,458,660	168,777	
GI	20	GI020	1	CAIS	Apache Corporation	1/1/1983		40	29.1182	-89.8991	2,457,989	167,057	
GI	47	GI047	L	FIXED	GOM Shelf LLC	1/1/1983		100	28.9329	-90.0262	2,418,178	99,197	
GI	37	BM002	Z	FIXED	Chevron U.S.A. Inc.	1/1/1984		50	29.0274	-90.1203	2,387,721	133,251	
GI	48	GI047	14	CAIS	GOM Shelf LLC	1/1/1984		19	28.9485	-90.0834	2,399,822	104,688	
GI	90	GI090	A	FIXED	Apache Corporation	1/1/1985		218	28.5751	-90.0724	2,404,818	-31,057	
GI	33	GI033	A	FIXED	Apache Corporation	3/22/1985		86	29.0314	-89.9241	2,450,406	135,421	
ELENA													
GI	47	GI047	6	CAIS	Conoco Inc.	1/1/1986	3/24/1991	100	28.9428	-90.0113	2,422,907	102,841	
GI	86	ST131	AA	FIXED	Chevron U.S.A. Inc.	1/1/1986		219	28.6700	-90.1292	2,386,225	3,253	
GI	17	GI016	STRG	FIXED	Freeport-McMoran Energy LLC	1/1/1987	8/25/2002	55	29.1300	-89.9896	2,429,043	171,001	
GI	41	GI041	H	FIXED	GOM Shelf LLC	1/1/1988		91	28.9811	-89.9774	2,433,586	116,919	
GI	59		LOOP (PUMP)	FIXED	LOOP,LLC.	12/31/1988		115	28.8850	-90.0250	2,418,758	81,790	
GI	82	EW305	A	FIXED	Apache Corporation	1/1/1989		203	28.6856	-89.9592	2,440,673	9,541	
GI	79	GI079	A	FIXED	Samedan Oil Corporation	1/1/1990	1/15/2001	203	28.7510	-89.8658	2,470,321	33,683	
GI	32	GI043	CC	WP	GOM Shelf LLC	1/1/1991		92	29.0367	-89.8950	2,459,668	137,467	
GI	55	GI043	A	FIXED	J. M. Huber Corporation	1/1/1991	5/29/2003	147	28.8863	-89.8634	2,470,467	82,896	
GI	47	GI047	AP	FIXED	GOM Shelf LLC	1/1/1992		89	28.9456	-90.0312	2,416,532	103,804	
GI	47	GI047	AX	FIXED	GOM Shelf LLC	1/1/1992		89	28.9455	-90.0308	2,416,656	105,782	
ANDREW													
GI	102	GI102	A	FIXED	Eni US Operating Co. Inc.	2/8/1994		255	28.4142	-90.0663	2,407,441	-89,549	
GI	39	GI047	4	CAIS	GOM Shelf LLC	1/1/1995		19	29.0058	-90.0733	2,402,828	125,553	
GI	40	GI041	M	WP	GOM Shelf LLC	5/16/1995		90	28.9914	-90.0126	2,422,284	120,537	
OPAL													
GI	102	GI102	B	FIXED	Eni Petroleum Co. Inc.	5/28/1996	1/23/2002	239	28.4272	-90.0899	2,399,777	-84,908	
GI	104		A	FIXED	Walter Oil & Gas Corporation	9/2/1996		303	28.4377	-89.9832	2,434,045	-80,710	
GI	78		A	FIXED	Arena Offshore, LLC	9/22/1996		185	28.7298	-89.9241	2,451,753	25,755	
GI	82		A	FIXED	Arena Offshore, LLC	5/21/1997		175	28.7216	-89.9655	2,438,503	22,577	
GI	45		CAIS.A(PLTF.A)	FIXED	Apache Corporation	6/3/1997		114	28.9626	-89.9147	2,453,725	110,435	
GI	115	GI115	SEAHORSE PRC	FIXED	Walter Oil & Gas Corporation	8/22/1997		366	28.3076	-90.0220	2,422,132	-128,169	
GI	65	GI065	A	FIXED	Walter Oil & Gas Corporation	8/1/1998	1/9/2003	137	28.8234	-89.9672	2,437,510	59,609	
GEORGES													
GI	63	WILD	A	FIXED	Walter Oil & Gas Corporation	9/4/1999	10/21/2003	116	28.8092	-90.0796	2,401,578	54,042	
GI	68	GI068	A	FIXED	Devon Energy Production Company, L.P.	10/28/1999		195	28.7630	-89.8660	2,470,218	38,039	
GI	30	WILD	A	FIXED	El Paso Production GOM Inc.	12/18/1999	10/20/2004	75	29.0720	-89.9130	2,453,759	150,230	
GI	116	GI116	A (HICKORY)	FIXED	Apache Corporation	8/26/2000		326	28.3093	-90.0705	2,406,489	-127,737	
GI	31	GI030	B	CAIS	El Paso Production GOM Inc.	9/26/2000	10/24/2004	75	29.0830	-89.8657	2,468,818	154,419	
GI	41	GI041	I	CAIS	GOM Shelf LLC	11/15/2000		100	28.9737	-89.9541	2,441,052	114,295	
GI	33	GI033	B	FIXED	Apache Corporation	1/17/2001		82	29.0449	-89.9348	2,446,902	140,261	
GI	103	GI102	A	FIXED	Newfield Exploration Company	9/3/2001		260	28.4053	-90.0415	2,415,454	-92,705	
GI	20	GI020	B	CAIS	Apache Corporation	9/4/2001		70	29.0956	-89.8583	2,471,113	159,010	
GI	26	BM002	CAIS.#40	CAIS	Chevron U.S.A. Inc.	11/1/2001		41	29.0529	-90.1097	2,390,987	142,548	
GI	28	WILD	A	FIXED	Hunt Petroleum (AEC), Inc.	7/6/2002		57	29.0841	-90.0059	2,424,017	154,273	
LILI													
IVAN													
GI	34	WILD	A	CAIS	Arena Offshore, LLC	5/31/2005		80	29.0282	-89.9616	2,438,411	134,094	
KATRINA													
RITA													
GI	72	WILD	B	FIXED	Contango Operators, Inc.	3/5/2006		127	28.7713	-90.0817	2,401,078	40,255	
GI	46	GI047	N	WP	GOM Shelf LLC	6/7/2006		111	28.9404	-89.9523	2,441,799	102,208	
GI	47		C-AUX	CAIS	BP America Production Company	12/6/2006		90	28.9608	-90.0234	2,418,940	109,353	
GI	32	GI043	GG	CAIS	GOM Shelf LLC	4/7/2007		102	29.0375	-89.8560	2,472,118	137,911	
GI	47	GI047	O	FIXED	GOM Shelf LLC	4/8/2007		91	28.9593	-90.0189	2,420,411	108,843	

Index to "Structural Type" field:			
CAIS	Caisson	SPAR	SPAR Platform - floating production system
CT	Compliant tower	SSANC	Fixed anchors or mooring piles used to secure a structure to the seafloor
FIXED	Fixed Leg Platform	SSMNF	Subsea Manifold
FPSO	Floating production, storage, and offloading	SSTMP	Subsea templates
MOPU	Mobile Production Unit	TLP	Tension leg platform
MTLP	Mini Tension Leg Platform	UCOMP	Underwater completion or subsea caisson
SEMI	Semi Submersible (Column Stabilized Unit) Floating Production System	WP	Well Protector



Table P-3: Main Pass Protraction Area: Platform History and Statistical Analysis (data from MMS, 2009)

MAIN PASS Platform Data - INSTALLED													
Searched by Area and Structure Installed Date Sorted by Installation Date													
Area Code	Block Number	Field	Structure Name	Struc Type	Operator	Install Date	Removal Date	Water Depth	Latitude	Longitude	Ptfm X Location	Ptfm Y Location	
MP	69	MP069	D	FIXED	W & T Offshore, Inc.	1/1/1954		52	29.2740	-89.0272	2,735,238	228,243	
MP	41	MP041	A	FIXED	Chevron U.S.A. Inc.	1/1/1956		43	29.3738	-89.0124	2,739,240	264,637	
MP	58	MP041	AB(N)	FIXED	Chevron U.S.A. Inc.	1/1/1957		62	29.3512	-88.9821	2,749,050	256,615	
AUDREY													
MP	41	MP041	AD	FIXED	Chevron U.S.A. Inc.	1/1/1958		53	29.3725	-88.9946	2,744,900	264,280	
MP	41	MP041	AC	CAIS	Chevron U.S.A. Inc.	1/1/1958		53	29.3758	-88.9890	2,746,650	265,530	
MP	41	MP041	CA	FIXED	Chevron U.S.A. Inc.	1/1/1959		39	29.3936	-89.0102	2,739,772	271,860	
MP	58	MP041	AA	FIXED	Chevron U.S.A. Inc.	1/1/1959		53	29.3671	-88.9930	2,745,460	262,330	
ETHYL													
MP	41	MP041	B	FIXED	Chevron U.S.A. Inc.	1/1/1961		51	29.3999	-88.9697	2,752,621	274,414	
MP	41	MP041	5	FIXED	Chevron U.S.A. Inc.	1/1/1961		47	29.4046	-88.9748	2,750,985	276,072	
CARLA													
MP	40	MP041	3	CAIS	Chevron U.S.A. Inc.	1/1/1963		55	29.3999	-88.9608	2,755,455	274,469	
MP	42	MP041	CB	FIXED	Chevron U.S.A. Inc.	1/1/1963		38	29.4063	-89.0200	2,736,579	276,410	
MP	42	MP041	DB	WP	Chevron U.S.A. Inc.	1/1/1963		34	29.4096	-89.0348	2,731,832	277,501	
MP	42	MP041	DA	WP	Chevron U.S.A. Inc.	1/1/1963	6/16/1999	35	29.4094	-89.0346	2,731,885	277,420	
MP	7	MP006	1	FIXED	MOBIL OIL EXPLORATION & PRODUCING	1/1/1964	7/25/2004	33	29.6417	-88.8817	2,778,750	362,880	
MP	41	MP041	C	FIXED	Chevron U.S.A. Inc.	1/1/1964		39	29.3984	-89.0123	2,739,084	273,583	
MP	42	MP041	D	FIXED	Chevron U.S.A. Inc.	1/1/1964		35	29.4008	-89.0349	2,731,862	274,300	
MP	42	MP041	EA	FIXED	Chevron U.S.A. Inc.	1/1/1964		37	29.4086	-89.0145	2,738,310	277,284	
MP	42	MP041	E	FIXED	Chevron U.S.A. Inc.	1/1/1964		36	29.4099	-89.0263	2,734,532	277,656	
MP	91	MP006	2	CAIS	OXY USA Inc.	1/1/1964	7/16/1993	34	29.6532	-88.8473	2,789,600	367,330	
MP	91	MP006	1	CAIS	OXY USA Inc.	1/1/1964	9/18/1992	35	29.6532	-88.8585	2,786,050	367,240	
MP	92	MP006	A-CF	FIXED	MOBIL OIL EXPLORATION & PRODUCING	1/1/1964	7/22/2004	24	29.6437	-88.8600	2,785,650	363,780	
HILDA													
MP	7	MP006	9	CAIS	MOBIL OIL EXPLORATION & PRODUCING	1/1/1965	1/22/2004	33	29.6384	-88.8764	361,730	2,780,475	
MP	7	MP006	8	WP	MOBIL OIL EXPLORATION & PRODUCING	1/1/1965	7/23/2004	35	29.6388	-88.8852	2,777,681	361,822	
MP	7	MP006	3	WP	MOBIL OIL EXPLORATION & PRODUCING	1/1/1965	6/26/2004	33	29.6384	-88.8764	2,780,475	361,730	
MP	41	MP041	JA	FIXED	Chevron U.S.A. Inc.	1/1/1965		42	29.4058	-88.9944	2,744,733	276,396	
MP	41	MP041	AE	CAIS	Chevron U.S.A. Inc.	1/1/1965		47	29.3728	-89.0078	2,740,708	264,309	
MP	42	MP041	6	CAIS	Chevron U.S.A. Inc.	1/1/1965	5/18/1992	27	29.4105	-89.0583	2,724,350	277,680	
MP	42	MP041	I(E)	FIXED	Chevron U.S.A. Inc.	1/1/1965		33	29.3919	-89.0513	2,726,717	270,963	
MP	42	MP041	GA	CAIS	Chevron U.S.A. Inc.	1/1/1965	6/16/2000	30	29.4058	-89.0508	2,726,750	276,030	
MP	42	MP041	H	FIXED	Chevron U.S.A. Inc.	1/1/1965	3/24/2005	37	29.3929	-89.0261	2,734,739	271,485	
MP	42	MP041	G	FIXED	Chevron U.S.A. Inc.	1/1/1965	6/16/2000	30	29.4061	-89.0513	2,726,614	276,147	
MP	92	MP006	7	CAIS	MOBIL OIL EXPLORATION & PRODUCING	1/1/1965	6/28/2004	35	29.6487	-88.8243	2,796,940	365,830	
BETSY													
MP	41	MP041	BA	WP	Chevron U.S.A. Inc.	1/1/1966		43	29.4095	-88.9824	2,748,522	277,822	
MP	41	MP041	J	FIXED	Chevron U.S.A. Inc.	1/1/1966		40	29.4039	-89.0045	2,741,519	275,614	
MP	43	MP041	KA	WP	Chevron U.S.A. Inc.	1/1/1966	12/31/1976	23	29.4088	-89.0738	2,719,427	276,969	
MP	92	MP006	12	CAIS	MOBIL OIL EXPLORATION & PRODUCING	1/1/1966	6/26/2004	34	29.6409	-88.8477	2,789,565	362,830	
MP	298	MP299	A	FIXED	Chevron U.S.A. Inc.	1/1/1966		210	29.2753	-88.7420	2,826,140	230,680	
MP	7	MP006	2	CAIS	MOBIL OIL EXPLORATION & PRODUCING	1/1/1967	7/27/2004	33	29.6499	-88.8730	2,781,450	365,920	
MP	43	MP041	K	FIXED	Chevron U.S.A. Inc.	1/1/1967		27	29.4005	-89.0738	2,719,472	273,953	
MP	43	MP041	KB	FIXED	Chevron U.S.A. Inc.	1/1/1967		24	29.3997	-89.0911	2,713,967	273,534	
MP	91	MP006	2	CAIS	MOBIL OIL EXPLORATION & PRODUCING	1/1/1967	10/11/1988	34	29.6565	-88.8384	2,792,400	368,580	
MP	92	MP006	2	CAIS	MOBIL OIL EXPLORATION & PRODUCING	1/1/1967	12/31/1979	38	29.6224	-88.8599	2,785,850	356,030	
MP	92	MP006	3	CAIS	MOBIL OIL EXPLORATION & PRODUCING	1/1/1967	12/31/1981	39	29.6413	-88.8341	2,793,900	363,080	
MP	300	MP299	B	FIXED	Chevron U.S.A. Inc.	1/1/1967		210	29.2637	-88.7817	2,813,598	226,183	
MP	91	MP006	1	CAIS	MOBIL OIL EXPLORATION & PRODUCING	1/1/1968	12/16/1997	36	29.6526	-88.8242	2,796,940	367,240	
MP	91	MP006	3	CAIS	MOBIL OIL EXPLORATION & PRODUCING	1/1/1968	12/16/1997	35	29.6513	-88.8413	2,791,525	366,680	
MP	92	MP006	13	CAIS	MOBIL OIL EXPLORATION & PRODUCING	1/1/1968	12/31/1983	34	29.6428	-88.8672	2,783,350	363,380	
MP	92	MP006	4	CAIS	MOBIL OIL EXPLORATION & PRODUCING	1/1/1968	1/24/2004	36	29.6473	-88.8360	2,793,225	365,230	
MP	92	MP006	14	CAIS	MOBIL OIL EXPLORATION & PRODUCING	1/1/1968	1/23/2004	34	29.6486	-88.8543	2,787,425	365,580	
MP	92	MP006	15	CAIS	MOBIL OIL EXPLORATION & PRODUCING	1/1/1968	8/7/2004	40	29.6425	-88.8540	2,787,565	363,380	
MP	92	MP006	16	CAIS	MOBIL OIL EXPLORATION & PRODUCING	1/1/1968	1/22/2004	36	29.6372	-88.8375	2,792,825	361,580	
MP	92	MP006	7	CAIS	MOBIL OIL EXPLORATION & PRODUCING	1/1/1968	10/14/1994	35	29.6189	-88.8474	2,789,850	354,830	
MP	92	MP006	5	CAIS	MOBIL OIL EXPLORATION & PRODUCING	1/1/1968	8/9/2004	37	29.6449	-88.8424	2,791,225	364,330	
MP	92	MP006	5	CAIS	MOBIL OIL EXPLORATION & PRODUCING	1/1/1968	1/21/2004	33	29.6488	-88.8649	2,784,050	365,580	
MP	144	MP144	A	FIXED	Chevron U.S.A. Inc.	1/1/1968		207	29.2924	-88.6691	2,849,241	237,421	
MP	289	MP290	B	FIXED	Apache Corporation	1/1/1968		320	29.2585	-88.4415	2,922,071	226,863	
MP	290	MP290	A	FIXED	Apache Corporation	1/1/1968		289	29.2564	-88.4515	2,918,904	225,998	
MP	69	MP069	1	CAIS	Chevron U.S.A. Inc.	1/1/1969	12/18/1997	30	29.2862	-89.0299	2,734,290	232,679	
MP	92	MP006	10	CAIS	MOBIL OIL EXPLORATION & PRODUCING	1/1/1969	7/3/2004	41	29.6158	-88.8309	2,795,100	353,830	
MP	92	MP006	9	CAIS	MOBIL OIL EXPLORATION & PRODUCING	1/1/1969	12/31/1979	39	29.6232	-88.8424	2,791,400	356,430	
MP	92	MP006	6	CAIS	MOBIL OIL EXPLORATION & PRODUCING	1/1/1969	6/30/2004	38	29.6120	-88.8252	2,796,940	352,490	
MP	92	MP006	B	FIXED	MOBIL OIL EXPLORATION & PRODUCING	1/1/1969	7/2/2004	38	29.6184	-88.8371	2,793,100	354,730	
MP	92	MP006	6	CAIS	MOBIL OIL EXPLORATION & PRODUCING	1/1/1969	7/2/2004	38	29.6187	-88.8373	2,793,050	354,830	
MP	92	MP006	8	CAIS	MOBIL OIL EXPLORATION & PRODUCING	1/1/1969	1/22/2004	40	29.6116	-88.8247	2,797,100	352,330	
MP	103	MP103	1	CAIS	MOBIL OIL EXPLORATION & PRODUCING	1/1/1969	7/28/2004	38	29.5814	-88.8689	2,783,300	341,080	
MP	103	MP103	CF	FIXED	MOBIL OIL EXPLORATION & PRODUCING	1/1/1969	7/30/2004	38	29.5801	-88.8685	2,783,450	340,580	
MP	103	MP106	2	CAIS	MOBIL OIL EXPLORATION & PRODUCING	1/1/1969	1/23/2004	38	29.6096	-88.8430	2,791,300	351,500	
MP	142	MP299	C	FIXED	Chevron U.S.A. Inc.	1/1/1969		201	29.2872	-88.7597	2,820,394	234,864	
MP	293	MP306	A	FIXED	Noble Energy, Inc.	1/1/1969		247	29.2307	-88.5643	2,883,165	215,772	
MP	305	MP306	C	FIXED	Noble Energy, Inc.	1/1/1969		244	29.1982	-88.5834	2,877,372	203,814	
MP	305	MP306	A	FIXED	Noble Energy, Inc.	1/1/1969		180	29.2254	-88.5761	2,879,472	213,772	
MP	305	MP306	B	FIXED	Noble Energy, Inc.	1/1/1969		241	29.2168	-88.5830	2,877,326	210,590	
MP	306	MP306	E	FIXED	Noble Energy, Inc.	1/1/1969		255	29.2149	-88.5466	2,888,972	210,172	
MP	306	MP306	D	FIXED	Noble Energy, Inc.	1/1/1969		255	29.2249	-88.5526	2,886,972	213,772	
CAMILLE													
MP	18	MP103	3	CAIS	Apache Corporation	1/1/1970	7/14/2004	37	29.5736	-88.8902	2,776,600	338,080	
MP	18	MP103	4	CAIS	Apache Corporation	1/1/1970	8/17/2004	37	29.5826	-88.8737	2,781,750	341,480	
MP	19	MP103	2	CAIS	Apache Corporation	1/1/1970	9/16/1991	38	29.5604	-88.8778	2,780,642	333,375	
MP	38	MP127	3	WP	Chevron U.S.A. Inc.	1/1/1970	6/24/1999	51	29.4369	-88.8842	2,779,550	288,430	
MP	42	MP041	M-QTR	FIXED	Chevron U.S.A. Inc.	1/1/1970		35	29.4008	-89.0352	2,731,762	274,300	
MP	42	MP041	L	FIXED	Chevron U.S.A. Inc.	1/1/1970		35	29.4008	-89.0386	2,730,688	274,300	
MP	103	MP103	4	CAIS	MOBIL OIL EXPLORATION & PRODUCING	1/1/1970	12/312						

# MAIN PASS Platform Data - INSTALLED

Searched by Area and Structure Installed Date													
Sorted by Installation Date													
Area Code	Block Number	Field	Structure Name	Struc Type	Operator	Install Date	Removal Date	Water Depth	Latitude	Longitude	Ptfm X Location	Ptfm Y Location	
MP	19	MP103	5	CAIS	Apache Corporation	1/1/1971	8/4/2004	39	29.5697	-88.8957	2,774,890	336,630	
MP	41	MP041	BB	FIXED	Chevron U.S.A. Inc.	1/1/1971		51	29.3999	-88.9700	2,752,521	274,414	
MP	41	MP041	N(N)	FIXED	Chevron U.S.A. Inc.	1/1/1971		39	29.3984	-89.0123	2,739,088	273,583	
MP	42	MP041	HA(N)	WP	Chevron U.S.A. Inc.	1/1/1971	8/26/2004	37	29.3934	-89.0258	2,734,822	271,661	
MP	103	MP103	5	CAIS	MOBIL OIL EXPLORATION & PRODUCING	1/1/1971	8/20/2004	38	29.5833	-88.8643	2,784,750	341,780	
MP	107	MP107	A	FIXED	Chevron U.S.A. Inc.	1/1/1971	6/27/1988	51	29.5519	-88.6904	2,840,270	331,590	
MP	107	MP107	6	CAIS	Chevron U.S.A. Inc.	1/1/1971	6/26/1988	51	29.5415	-88.6910	2,840,170	327,820	
MP	127	MP127	A	FIXED	Chevron U.S.A. Inc.	1/1/1971	6/12/2000	58	29.4406	-88.8698	2,784,102	289,865	
MP	133	MP133	A	FIXED	Petro Ventures, Inc.	1/1/1971		180	29.3982	-88.6280	2,861,427	276,195	
MP	41	MP041	CC	FIXED	Chevron U.S.A. Inc.	1/1/1972		44	29.3921	-88.9936	2,745,080	271,412	
MP	41	MP041	O	FIXED	Chevron U.S.A. Inc.	1/1/1972		51	29.3999	-88.9697	2,752,621	274,414	
MP	93	MP006	4	CAIS	ExxonMobil Oil Corporation	1/1/1972	12/31/1980	40	29.6143	-88.8106	2,801,560	353,430	
MP	293		SONAT	FIXED	Southern Natural Gas Company	3/20/1972	8/23/2005	232	29.2707	-88.5641	2,882,900	230,330	
MP	298		B-VALVE	FIXED	Southern Natural Gas Company	3/20/1972		222	29.2697	-88.7168	2,834,225	228,830	
MP	92	MP006	QRTS	FIXED	MOBIL OIL EXPLORATION & PRODUCING	1/1/1973	7/22/2004	24	29.6429	-88.8595	2,785,800	363,480	
MP	140	MP140	B	FIXED	Apache Corporation	1/1/1973		150	29.2955	-88.8423	2,794,017	237,321	
MP	140	MP140	A	FIXED	Apache Corporation	1/1/1973		165	29.2939	-88.8617	2,787,850	236,580	
CARMEN													
MP	254	MP253	A	FIXED	Hughes Eastern Petroleum, Inc.	1/1/1975	8/2/2000	280	29.3624	-87.8059	3,123,528	270,300	
ELOISE													
MP	44	MP041	KC	FIXED	Chevron U.S.A. Inc.	1/1/1976		60	29.3969	-89.1071	2,708,911	272,433	
MP	288	MP290	A	FIXED	Stone Energy Corporation	1/1/1976		420	29.2398	-88.4095	2,932,462	220,332	
MP	73	MP073	A	FIXED	Energy XXI GOM, LLC	1/1/1977		141	29.2664	-88.9080	2,773,312	226,289	
MP	236	MP133	B	FIXED	Petro Ventures, Inc.	1/1/1977		180	29.4054	-88.5844	2,875,250	279,130	
MP	133	MP133	C	FIXED	Petro Ventures, Inc.	1/1/1978		180	29.4001	-88.6093	2,867,350	277,030	
MP	306	MP306	F	FIXED	Noble Energy, Inc.	1/1/1978		271	29.1948	-88.5553	2,886,372	202,814	
MP	72	MP073	B	FIXED	Pogo Producing Company	1/1/1979		120	29.2533	-88.9306	2,766,180	221,372	
MP	72	MP073	C	FIXED	Pogo Producing Company	1/1/1979		137	29.2445	-88.9163	2,770,837	218,257	
MP	73	MP073	CF	FIXED	Energy XXI GOM, LLC	1/1/1979		141	29.2669	-88.9088	2,773,055	226,437	
MP	91	MP006	4	CAIS	OXY USA Inc.	1/1/1979	9/18/1992	35	29.6535	-88.8634	2,784,497	367,327	
MP	311	MP311	A	FIXED	GOM Shelf LLC	1/1/1979		250	29.1642	-88.7461	2,825,740	190,256	
FREDERIC													
MP	311	MP311	BB	FIXED	GOM Shelf LLC	1/1/1980		250	29.1834	-88.7369	2,828,530	197,299	
MP	114	MP115	1	WP	Diamond Shamrock Offshore Partners Limit	1/1/1981	11/18/1990	48	29.5090	-88.8086	2,803,047	315,170	
MP	115	MP115	1	WP	Diamond Shamrock Offshore Partners Limit	1/1/1981	12/31/1985	48	29.4994	-88.8505	2,789,800	311,380	
MP	120	MP120	CA	WP	Arena Offshore, LLC	1/1/1981		180	29.4620	-88.6494	2,854,087	299,227	
MP	133	MP133	CB	WP	Petro Ventures, Inc.	1/1/1981		180	29.3795	-88.6324	2,860,203	269,356	
MP	144	MP144	BA	FIXED	Chevron U.S.A. Inc.	1/1/1981		210	29.2904	-88.6651	2,850,517	236,732	
MP	296	MP144	C	FIXED	GOM Shelf LLC	1/1/1981		220	29.2574	-88.6608	2,852,195	224,772	
MP	40	MP041	BC	FIXED	Chevron U.S.A. Inc.	1/1/1982		55	29.4001	-88.9607	2,755,491	274,530	
MP	59	MP041	A	FIXED	Chevron U.S.A. Inc.	1/1/1982		69	29.3544	-88.9345	2,764,188	258,088	
MP	64	MP064	3	CAIS	Medco Energi US LLC	1/1/1982		30	29.3068	-89.0569	2,725,547	239,994	
MP	116	MP127	A	FIXED	Hunt Petroleum (AEC), Inc.	1/1/1982		58	29.4574	-88.8304	2,796,536	296,233	
MP	132	MP133	CC	WP	Chevron U.S.A. Inc.	1/1/1982	6/21/2000	178	29.3917	-88.6456	2,855,893	273,703	
MP	151	MP151	A	FIXED	Apache Corporation	1/1/1982		174	29.1886	-88.8866	2,780,741	198,153	
MP	296	MP144	B	FIXED	GOM Shelf LLC	1/1/1982		225	29.2336	-88.6649	2,851,060	216,072	
MP	313	MP311	A	FIXED	Chevron U.S.A. Inc.	1/1/1982		270	29.1265	-88.7793	2,815,473	176,296	
MP	40	MP041	P	FIXED	Chevron U.S.A. Inc.	1/25/1982		48	29.4087	-88.9586	2,756,097	277,676	
MP	41	MP041	CD	FIXED	Chevron U.S.A. Inc.	1/1/1983		53	29.3815	-88.9875	2,747,100	267,580	
MP	42	MP041	15	CAIS	Chevron U.S.A. Inc.	1/1/1983		36	29.4100	-89.0265	2,734,461	277,691	
MP	64	MP064	1	CAIS	Medco Energi US LLC	1/1/1983		30	29.3052	-89.0509	2,727,470	239,438	
MP	64	MP064	A	FIXED	Medco Energi US LLC	1/1/1983		35	29.3019	-89.0547	2,726,284	238,242	
MP	64	MP064	10	CAIS	Medco Energi US LLC	1/1/1983		30	29.3032	-89.0501	2,727,737	238,727	
MP	64	MP064	5	CAIS	Medco Energi US LLC	1/1/1983		30	29.3043	-89.0451	2,729,318	239,152	
MP	64	MP064	8	CAIS	Medco Energi US LLC	1/1/1983		30	29.3157	-89.0543	2,726,308	243,255	
MP	64	MP064	AQ	FIXED	Medco Energi US LLC	1/1/1983		35	29.3017	-89.0550	2,726,182	238,136	
MP	64	MP064	6	CAIS	Medco Energi US LLC	1/1/1983		30	29.3107	-89.0526	2,726,865	241,432	
MP	64	MP064	2	CAIS	Medco Energi US LLC	1/1/1983		35	29.3017	-89.0552	2,726,126	238,165	
MP	64	MP064	7	CAIS	Medco Energi US LLC	1/1/1983		30	29.2969	-89.0532	2,726,790	236,399	
MP	64	MP064	9	CAIS	Medco Energi US LLC	1/1/1983		30	29.3121	-89.0584	2,725,036	241,898	
MP	64	MP064	B	FIXED	Medco Energi US LLC	1/1/1983		40	29.3006	-89.0495	2,727,946	237,801	
MP	77	MP151	A	FIXED	Chevron U.S.A. Inc.	1/1/1983		130	29.1808	-88.9031	2,775,531	195,189	
MP	265	MP265	A	FIXED	El Paso Exploration & Production Managem	1/1/1983		208	29.3467	-88.2816	2,972,200	260,230	
MP	296	MP144	D	FIXED	GOM Shelf LLC	1/1/1983		214	29.2804	-88.6616	2,851,718	233,106	
MP	310	MP310	A	FIXED	Apache Corporation	1/1/1983		248	29.1875	-88.6834	2,845,556	199,164	
MP	55	MP064	PIG-TRAP	CAIS	Medco Energi US LLC	1/1/1984		40	29.3463	-89.1080	2,708,969	254,046	
MP	64	MP064	12	CAIS	Medco Energi US LLC	1/1/1984		30	29.2984	-89.0589	2,724,960	236,938	
MP	64	MP064	13	CAIS	Medco Energi US LLC	1/1/1984		30	29.3083	-89.0604	2,724,397	240,527	
MP	64	MP064	11	CAIS	Medco Energi US LLC	1/1/1984		30	29.3033	-89.0595	2,724,725	238,716	
MP	65	MP064	A	WP	Medco Energi US LLC	1/1/1984		33	29.3107	-89.0652	2,722,855	241,348	
MP	91	MP006	5	CAIS	OXY USA Inc.	1/1/1984	9/18/1992	34	29.6533	-88.8584	2,786,070	367,282	
MP	100	MP107	A	FIXED	Century Exploration New Orleans, Inc.	1/1/1984		60	29.5882	-88.7107	2,833,505	-344,654	
MP	126	MP126	1	CAIS	Burlington Resources Offshore Inc.	1/1/1984	6/24/1996	100	29.4293	-88.8199	2,800,093	286,107	
MP	153	SP065	C	FIXED	Nippon Oil Exploration U.S.A. Limited	1/1/1984		275	29.1174	-88.8489	2,793,324	172,498	
MP	299	MP299	DA	FIXED	Chevron U.S.A. Inc.	1/1/1984		217	29.2605	-88.7472	2,824,602	225,241	
MP	39	MP039	1	CAIS	Diamond Shamrock Offshore Partners Limit	1/1/1985	11/16/1990	50	29.3834	-88.9011	2,774,585	268,848	
MP	40	MP041	7	CAIS	Chevron U.S.A. Inc.	1/1/1985		53	29.3988	-88.9580	2,756,350	274,080	
MP	41	MP041	34	CAIS	Chevron U.S.A. Inc.	1/1/1985		40	29.4048	-88.9686	2,752,950	276,180	
MP	41	MP041	36	CAIS	Chevron U.S.A. Inc.	1/1/1985		53	29.4006	-88.9679	2,753,200	274,680	
MP	64	MP064	17	CAIS	Medco Energi US LLC	1/1/1985		35	29.3177	-89.0602	2,724,404	243,927	
MP	64	MP064	14	CAIS	Medco Energi US LLC	1/1/1985		36	29.3060	-89.0605	2,724,400	239,680	
MP	64	MP064	15	CAIS	Medco Energi US LLC	1/1/1985		32	29.3009	-89.0606	2,724,400	237,830	
MP	93	MP093	4	CAIS	Offshore Shelf LLC	1/1/1985		45	29.6330	-88.7950	2,806,359	360,345	
MP	93	MP093	A	FIXED	Offshore Shelf LLC	1/1/1985		45	29.6197	-88.7907	2,807,850	355,530	
MP	98	MP098	B	FIXED	Forest Oil Corporation	1/1/1985	7/10/1989	80	29.5790	-88.6188	2,862,800		



# MAIN PASS Platform Data - INSTALLED

Searched by Area and Structure Installed Date													
Sorted by Installation Date													
Area Code	Block Number	Field	Structure Name	Struc Type	Operator	Install Date	Removal Date	Water Depth	Latitude	Longitude	Ptfm X Location	Ptfm Y Location	
MP	127	MP127	5	CAIS	Chevron U.S.A. Inc.	1/1/1985	6/19/1999	55	29.4467	-88.8474	2,791,200	292,230	
MP	128	MP128	A	CAIS	Atlantic Richfield Company	1/1/1985	1/22/1994	72	29.3799	-88.8691	2,784,800	267,800	
MP	297	MP144	A	FIXED	Chevron U.S.A. Inc.	1/1/1985	9/17/1996	250	29.2394	-88.6929	2,842,110	217,972	
ELENA													
MP	59	MP041	AA	WP	Chevron U.S.A. Inc.	1/1/1986		67	29.3409	-88.9593	2,756,390	253,003	
MP	103	MP103	6	CAIS	MOBIL OIL EXPLORATION & PRODUCINC	1/1/1986	8/19/2004	40	29.5852	-88.8693	2,783,150	342,430	
MP	117	MP127	2	CAIS	Diamond Shamrock Offshore Partners Limit	1/1/1986	11/21/1990	48	29.4808	-88.8175	2,800,450	304,830	
MP	299	MP299	AA	FIXED	Chevron U.S.A. Inc.	1/1/1986		207	29.2830	-88.7517	2,822,993	233,413	
MP	40	MP041	BF	CAIS	Chevron U.S.A. Inc.	6/12/1986		53	29.3928	-88.9656	2,753,999	271,832	
MP	30	MP030	A	FIXED	Chevron U.S.A. Inc.	1/1/1987		40	29.4686	-88.9501	2,758,337	299,490	
MP	56	MP056	3	CAIS	General Atlantic Resources, Inc.	1/1/1987	6/1/1991	40	29.3527	-89.1025	2,710,673	256,391	
MP	89	MP089	1	WP	Hall-Houston Oil Company	1/1/1987	12/8/1992	35	29.6776	-88.7560	2,818,391	376,821	
MP	96	MP096	1	CAIS	Energy Development Corporation	1/1/1987	6/1/1991	59	29.6244	-88.6786	2,843,418	358,057	
MP	101	MP107	A	WP	Samedan Oil Corporation	1/1/1987	7/9/1992	49	29.5697	-88.7357	2,825,719	337,738	
MP	106	MP107	1	CAIS	Murphy Exploration & Production Company	1/1/1987	10/12/1993	53	29.5661	-88.7413	2,823,980	336,413	
MP	106	MP107	2	CAIS	Murphy Exploration & Production Company	1/1/1987	10/12/1993	58	29.5657	-88.7464	2,822,351	336,213	
MP	127	MP127	7	CAIS	Chevron U.S.A. Inc.	1/1/1987	7/3/1999	60	29.4467	-88.8410	2,793,225	292,280	
MP	127	MP127	6	CAIS	Chevron U.S.A. Inc.	1/1/1987	7/3/1999	60	29.4429	-88.8517	2,789,850	290,830	
MP	165	MP164	B	CAIS	Callon Petroleum Operating Company	1/1/1987	11/20/2001	129	29.6380	-88.4424	2,918,321	364,790	
MP	165	MP164	A	FIXED	Callon Petroleum Operating Company	1/1/1987	12/3/2001	156	29.6220	-88.4505	2,915,893	358,915	
MP	202	MP202	A	FIXED	W & T Offshore, Inc.	1/1/1987	11/20/1999	170	29.4987	-88.4510	2,916,871	314,089	
MP	39	MP039	3	CAIS	Diamond Shamrock Offshore Partners Limit	1/1/1988	12/31/1990	50	29.3834	-88.9012	2,774,577	268,848	
MP	68	MP068	1-A	CAIS	Noble Energy, Inc.	1/1/1988	9/20/2006	30	29.2872	-89.0585	2,725,166	232,850	
MP	95	MP096	A	FIXED	Samedan Oil Corporation	1/1/1988	6/26/2001	55	29.6225	-88.7099	2,833,500	357,111	
MP	106	MP107	A	FIXED	Murphy Exploration & Production Company	1/1/1988	10/12/1993	55	29.5415	-88.7776	2,812,650	327,185	
MP	106	MP107	4	CAIS	Murphy Exploration & Production Company	1/1/1988	10/12/1993	54	29.5582	-88.7414	2,824,012	333,534	
MP	106	MP107	B	FIXED	Murphy Exploration & Production Company	1/1/1988	12/31/1993	55	29.5406	-88.7333	2,826,733	327,185	
MP	107	MP107	#1(A)	CAIS	Kerr-McGee Corporation	1/1/1988	4/26/1995	60	29.5306	-88.6905	2,840,429	323,843	
MP	108	MP108	B	FIXED	Offshore Shelf LLC	1/1/1988		69	29.5451	-88.6499	2,853,202	329,438	
MP	116	MP127	B	FIXED	Hunt Petroleum (AEC), Inc.	1/1/1988		55	29.4552	-88.8490	2,790,628	295,308	
MP	124	MP124	A	FIXED	Vintage Petroleum, Inc.	1/1/1988	11/3/2000	78	29.4137	-88.7203	2,831,909	281,133	
MP	125	MP125	A	FIXED	Vintage Petroleum, Inc.	1/1/1988	1/10/2005	78	29.4199	-88.7372	2,826,478	283,288	
MP	128	MP128	B	CAIS	Atlantic Richfield Company	1/1/1988	1/15/1994	74	29.3978	-88.8621	2,786,910	274,363	
MP	129	MP129	A	FIXED	Apache Corporation	1/1/1988	10/13/2000	95	29.3920	-88.8144	2,802,129	272,533	
MP	202	MP202	B	WP	Devon SFS Operating, Inc.	1/1/1988	5/20/1997	170	29.4969	-88.4305	2,923,381	313,605	
MP	208	MP202	A	WP	Apache Corporation	1/1/1988	12/12/1995	170	29.4712	-88.4642	2,912,921	303,995	
MP	227	MP227	A	WP	El Paso Exploration & Production Managem	1/1/1988	5/28/2005	195	29.4163	-88.1659	3,008,350	286,530	
MP	243	MP265	A	WP	El Paso Exploration & Production Managem	1/1/1988	6/22/2000	192	29.3651	-88.3107	2,962,750	266,701	
MP	244	MP265	A	WP	El Paso Exploration & Production Managem	1/1/1988	4/20/2000	193	29.3746	-88.2623	2,978,091	270,542	
MP	289	MP290	C	FIXED	Apache Corporation	1/1/1988		338	29.2485	-88.4414	2,922,205	223,222	
MP	301	MP311	A	FIXED	Walter Oil & Gas Corporation	1/1/1988		223	29.2069	-88.7673	2,818,635	205,624	
MP	94	MP096	1	CAIS	Offshore Shelf LLC	1/1/1989		50	29.6364	-88.7575	2,818,263	361,825	
MP	113	MP107	5	CAIS	Odeco Oil & Gas Company	1/1/1989	10/12/1993	58	29.5075	-88.7414	2,824,429	315,107	
MP	113	MP107	2	CAIS	Odeco Oil & Gas Company	1/1/1989	10/12/1993	54	29.5058	-88.7562	2,819,727	314,371	
MP	159	MP159	1	CAIS	Callon Petroleum Operating Company	1/1/1989	8/8/2006	130	29.6491	-88.4647	2,911,121	368,676	
MP	160	MP163	5	CAIS	Callon Petroleum Operating Company	1/1/1989	8/10/2006	115	29.6616	-88.5256	2,891,683	372,738	
MP	161	CA040	1	CAIS	Callon Petroleum Operating Company	1/1/1989	8/2/2003	115	29.6785	-88.5518	2,883,221	378,651	
MP	163	MP163	B	FIXED	Callon Petroleum Operating Company	1/1/1989	8/17/2006	130	29.6271	-88.5216	2,893,257	360,215	
MP	163	MP163	1	CAIS	Callon Petroleum Operating Company	1/1/1989	8/12/2006	120	29.6436	-88.5410	2,886,943	366,072	
MP	163	MP163	A-1	CAIS	Callon Petroleum Operating Company	1/1/1989	8/17/2006	130	29.6271	-88.5219	2,893,156	360,215	
MP	163	MP163	2-A	CAIS	Callon Petroleum Operating Company	1/1/1989	8/15/2006	110	29.6247	-88.5380	2,888,069	359,228	
MP	209	MP202	A	FIXED	Energy Development Corporation	1/1/1989	6/9/1999	175	29.4715	-88.4403	2,920,500	304,300	
MP	94	MP096	B	FIXED	Offshore Shelf LLC	1/1/1990		47	29.6332	-88.7551	2,819,052	360,687	
MP	99	MP099	1	CAIS	BP Exploration Inc.	1/1/1990	2/25/1991	47	29.5879	-88.6829	2,842,346	344,748	
MP	99	MP099	2	CAIS	Torch Energy Services, Inc.	1/1/1990	5/28/2000	47	29.5880	-88.6829	2,842,346	-344,768	
MP	105	WILD	1	CAIS	Atlantic Richfield Company	1/1/1990	12/31/1990	56	29.5481	-88.7974	2,806,299	329,451	
MP	108	MP108	1	CAIS	Offshore Shelf LLC	1/1/1990		64	29.5521	-88.6723	2,846,011	331,800	
MP	108	MP108	A	FIXED	Offshore Shelf LLC	1/1/1990		70	29.5527	-88.6600	2,849,916	332,132	
MP	112	MP107	2	CAIS	Hunt Petroleum (AEC), Inc.	1/1/1990		65	29.5057	-88.7199	2,831,292	314,591	
MP	112	MP107	1	CAIS	Hunt Petroleum (AEC), Inc.	1/1/1990		65	29.5115	-88.6991	2,837,833	316,834	
MP	186	MP186	A	FIXED	Devon SFS Operating, Inc.	1/1/1990	5/31/1997	150	29.5471	-88.3299	2,954,917	332,670	
MP	244	MP265	B	FIXED	El Paso Exploration & Production Managem	1/1/1990	4/20/2000	46	29.3702	-88.2401	2,985,196	269,152	
MP	252	MP252	A	FIXED	Shell Offshore Inc.	1/1/1990		277	29.3609	-87.8858	3,098,092	268,975	
MP	273	MP273	A	FIXED	Hess Corporation	1/1/1990	9/27/1999	216	29.2941	-88.5395	2,890,526	239,037	
MP	64	MP064	18	CAIS	Medco Energi US LLC	8/6/1990		40	29.3148	-89.0583	2,725,050	242,880	
MP	64	MP064	19	CAIS	Medco Energi US LLC	1/1/1991		36	29.3072	-89.0514	2,727,288	240,157	
MP	138	MP138	A	FIXED	Newfield Exploration Company	1/1/1991		158	29.3392	-88.8028	2,806,246	253,454	
MP	181	MP181	A	FIXED	Magnum Hunter Production, Inc.	1/1/1991		130	29.5429	-88.5622	2,881,104	329,278	
MP	299	MP299	QRT	FIXED	Freeport-McMoRan Energy LLC	1/1/1991	7/20/2003	210	29.2615	-88.7693	2,817,564	225,458	
MP	299	MP299	PP	FIXED	Freeport-McMoRan Energy LLC	1/1/1991	7/20/2003	210	29.2609	-88.7703	2,817,233	225,216	
MP	299	MP299	PRD2RIG	FIXED	Freeport-McMoRan Energy LLC	1/1/1991		210	29.2675	-88.7632	2,819,450	227,700	
MP	299	MP299	PRD1RIG	FIXED	Freeport-McMoRan Energy LLC	1/1/1991		210	29.2657	-88.7581	2,821,080	227,050	
MP	299	MP299	A	FIXED	Freeport-McMoRan Energy LLC	1/1/1991		209	29.2632	-88.7592	2,820,753	226,150	
MP	299	MP299	BW	FIXED	Freeport-McMoRan Energy LLC	1/1/1991		209	29.2793	-88.7580	2,821,000	232,000	
MP	299	MP299	FP	FIXED	Freeport-McMoRan Energy LLC	1/1/1991		209	29.2647	-88.7721	2,816,640	226,608	
MP	299	MP299	STR	FIXED	Freeport-McMoRan Energy LLC	1/1/1991		210	29.2607	-88.7748	2,815,805	225,140	
MP	299	MP299	BS-Y	WP	Freeport-McMoRan Energy LLC	1/1/1991	7/20/2003	212	29.2633	-88.7662	2,818,520	226,121	
MP	299	MP299	BS	WP	Freeport-McMoRan Energy LLC	1/1/1991		212	29.2675	-88.7619	2,819,881	227,692	
MP	299												

# MAIN PASS Platform Data - INSTALLED

Searched by Area and Structure Installed Date Sorted by Installation Date													
Area Code	Block Number	Field	Structure Name	Struc Type	Operator	Install Date	Removal Date	Water Depth	Latitude	Longitude	Ptfm X Location	Ptfm Y Location	
MP	64	MP064	20	CAIS	Medco Energi US LLC	11/26/1992		40	29.2955	-89.0397	2,731,107	235,982	
MP	175	MP175	A	FIXED	Magnum Hunter Production, Inc.	12/12/1992		137	29.5780	-88.3549	2,946,676	343,720	
MP	92	MP006	17	CAIS	MOBIL OIL EXPLORATION & PRODUCING	1/1/1993	7/22/2004	24	29.6440	-88.8604	2,785,500	363,880	
MP	90	MP093	1	CAIS	Kerr-McGee Corporation	1/29/1993	8/16/1998	45	29.6534	-88.7971	2,805,542	367,744	
MP	299	MP299	BB	FIXED	Chevron U.S.A. Inc.	6/11/1993		231	29.2573	-88.7730	2,816,414	223,888	
MP	234	MP234	A	WP	W & T Offshore, Inc.	11/11/1993	11/15/1999	185	29.4089	-88.4676	2,912,400	281,330	
MP	154	MP154	A	WP	Chevron U.S.A. Inc.	1/1/1994		131	29.6564	-88.2355	2,983,845	373,206	
MP	301	MP301	B	FIXED	Walter Oil & Gas Corporation	1/1/1994		227	29.2197	-88.7932	2,810,287	210,088	
MP	93	MP093	6	CAIS	Offshore Shelf LLC	2/9/1994		40	29.6415	-88.7947	2,806,407	363,414	
MP	187	MP186	CAIS.#3	FIXED	Maritech Resources, Inc.	2/25/1994	7/12/2003	155	29.5358	-88.2961	2,965,759	328,871	
MP	187	MP186	A	FIXED	Maritech Resources, Inc.	2/25/1994	7/5/2003	155	29.5266	-88.3033	2,963,547	325,440	
MP	141	MP141	A	WP	W & T Offshore, Inc.	5/11/1994		188	29.2975	-88.7964	2,808,620	238,350	
MP	18	MP103	5	CAIS	Apache Corporation	7/23/1994	8/17/2004	40	29.5845	-88.8769	2,780,739	342,145	
MP	18	MP103	6	CAIS	Apache Corporation	8/21/1994	8/7/2004	40	29.5770	-88.8745	2,781,547	339,419	
MP	181	MP181	B	WP	Magnum Hunter Production, Inc.	9/9/1994		130	29.5573	-88.5870	2,873,097	334,348	
MP	111	MP107	A-1	CAIS	Hunt Petroleum (AEC), Inc.	9/13/1994		95	29.5157	-88.6534	2,852,350	318,726	
MP	259	MP259	A	FIXED	Devon Energy Production Company, L.P.	9/16/1994		392	29.3257	-88.0201	3,055,700	254,935	
MP	255	MP255	A	FIXED	Devon Energy Production Company, L.P.	9/26/1994		332	29.3204	-87.8125	3,121,884	254,949	
MP	89	MP089	6	CAIS	Samedan Oil Corporation	10/15/1994	10/7/2001	53	29.6538	-88.7306	2,826,661	368,346	
MP	123	MP133	A	FIXED	Pogo Producing Company	11/6/1994		158	29.4190	-88.6486	2,854,692	283,581	
MP	93	MP093	7	CAIS	Offshore Shelf LLC	1/1/1995		45	29.6271	-88.8105	2,801,479	358,080	
MP	93	MP093	8	CAIS	Offshore Shelf LLC	1/1/1995		45	29.6413	-88.7891	2,808,185	363,377	
MP	103	MP103	7	CAIS	MOBIL OIL EXPLORATION & PRODUCING	1/1/1995	8/21/2004	41	29.5812	-88.8552	2,787,642	341,081	
MP	245	MP811	A	FIXED	Walter Oil & Gas Corporation	5/5/1995	12/4/2001	226	29.3545	-88.1875	3,002,100	263,880	
MP	70	MP069	1	CAIS	W & T Offshore, Inc.	6/3/1995		50	29.2762	-89.0020	2,743,260	229,230	
MP	107	MP108	A-1	FIXED	Kerr-McGee Oil & Gas Corporation	7/21/1995	1/12/2004	55	29.5486	-88.6888	2,840,798	330,432	
OPAL													
MP	40	MP041	8	FIXED	Chevron U.S.A. Inc.	1/1/1996		55	29.4082	-88.9561	2,756,900	277,500	
MP	225	MP225	A	FIXED	Dauphin Island Gathering Partners	1/19/1996		255	29.3998	-88.0428	3,047,717	281,647	
MP	91	MP006	B	FIXED	Apache Corporation	2/17/1996		35	29.6532	-88.8648	2,784,043	367,201	
MP	262	MP262	A	FIXED	Nexen Petroleum Offshore U.S.A. Inc.	3/11/1996	4/21/2000	288	29.3231	-88.1662	3,009,202	252,652	
MP	91	MP006	A	WP	Apache Corporation	3/13/1996		37	29.6529	-88.8494	2,788,945	367,197	
MP	37	MP041	BE	FIXED	Chevron U.S.A. Inc.	4/30/1996		55	29.4268	-88.9208	2,767,981	284,494	
MP	252	MP252	B	FIXED	Shell Offshore Inc.	5/6/1996		277	29.3606	-87.8848	3,098,432	268,864	
MP	223		A	FIXED	Maritech Resources, Inc.	6/12/1996		269	29.3923	-87.9562	3,075,364	279,729	
MP	94	MP094	3	FIXED	Offshore Shelf LLC	6/28/1996		45	29.6340	-88.7543	3,060,980	2,819,300	
MP	92		12	CAIS	Apache Corporation	1/25/1997	9/8/2006	34	29.6165	-88.8657	2,784,037	353,830	
MP	139	MP139	A	WP	Eni US Operating Co. Inc.	4/23/1997		116	29.3455	-88.8513	2,790,742	255,422	
MP	120		CE	FIXED	Arena Offshore, LLC	6/4/1997		110	29.4644	-88.6859	2,842,446	299,829	
MP	313	MP311	B	WP	Chevron U.S.A. Inc.	8/15/1997		283	29.1155	-88.7683	2,819,060	172,405	
MP	104	WILD	A	FIXED	Apache Corporation	8/16/1997		46	29.5676	-88.8346	2,794,302	336,282	
MP	217		B	FIXED	El Paso Exploration & Production Management	10/23/1997	9/12/2003	174	29.4446	-88.0577	3,042,483	297,785	
MP	138	MP129	B	FIXED	Newfield Exploration Company	11/2/1997	9/28/2006	158	29.3459	-88.8280	2,798,165	255,745	
MP	312	WILD	JA	FIXED	Apache Corporation	11/20/1997		248	29.1800	-88.7650	2,819,605	195,857	
MP	261	MP261	A	FIXED	Transcontinental Gas Pipe Line Corporation	1/1/1998		282	29.3474	-88.1133	3,025,794	261,976	
MP	198	MP198	A	FIXED	El Paso Exploration & Production Management	2/10/1998	9/11/2002	161	29.4812	-88.2307	2,987,100	309,555	
MP	199	MP186	A	FIXED	Vastar Resources, Inc.	3/4/1998	2/23/2004	163	29.5122	-88.3042	2,963,429	320,226	
MP	226	MP226	A	FIXED	Nippon Oil Exploration U.S.A. Limited	8/14/1998		175	29.4304	-88.1169	3,023,798	292,096	
MP	260		P	FIXED	Destin Pipeline Company, L.L.C.	9/1/1998		300	29.3430	-88.0671	3,040,551	260,785	
GEORGES													
MP	91	WILD	CAIS.#1	CAIS	Apache Corporation	10/25/1998	9/13/2006	42	29.6525	-88.8267	2,796,148	367,208	
MP	279	MP283	B	FIXED	Dominion Exploration & Production, Inc.	11/9/1998	2/22/2006	290	29.2783	-88.2577	2,980,491	235,581	
MP	256	WILD	A	FIXED	Dauphin Island Gathering Partners	11/18/1998		348	29.3321	-87.8779	3,100,945	258,589	
MP	280		C	WP	Dominion Exploration & Production, Inc.	11/26/1998		302	29.2888	-88.2118	2,995,009	239,803	
MP	250		B	FIXED	Maritech Resources, Inc.	12/10/1998		319	29.3574	-87.9786	3,068,593	266,817	
MP	281		A	FIXED	Eni US Operating Co. Inc.	1/3/1999		307	29.2854	-88.1795	3,005,339	238,849	
MP	216	WILD	C	FIXED	Millennium Offshore Group, Inc.	4/12/1999	8/25/2005	169	29.4484	-88.0966	3,030,090	298,837	
MP	162	MP162	A	FIXED	Maritech Resources, Inc.	6/13/1999		95	29.6245	-88.5730	2,876,969	358,873	
MP	63	WILD	1	CAIS	Devon Louisiana Corporation	7/26/1999	11/2/2003	67	29.3092	-88.9765	2,751,145	241,400	
MP	283	MP283	A	FIXED	MOBIL OIL EXPLORATION & PRODUCING	8/15/1999		300	29.2694	-88.2375	2,987,003	232,522	
MP	90	WILD	1	FIXED	Apache Corporation	9/6/1999		49	29.6529	-88.7779	2,811,650	367,680	
MP	225	MP225	D	FIXED	Millennium Offshore Group, Inc.	9/9/1999		227	29.4017	-88.0711	3,038,683	282,097	
MP	93	WILD	1	CAIS	Apache Corporation	10/2/1999	9/10/2006	42	29.6419	-88.8208	2,798,100	363,380	
MP	264	MP264	A	FIXED	The Houston Exploration Company	3/2/2000		234	29.3272	-88.2401	2,985,614	253,525	
MP	242	WILD	A	FIXED	Maritech Resources, Inc.	4/15/2000		196	29.3639	-88.3524	2,949,489	265,914	
MP	7		A	FIXED	Apache Corporation	6/12/2000		40	29.6417	-88.8817	2,778,750	362,880	
MP	277	WILD	A	FIXED	El Paso E&P Company, L.P.	8/24/2000		223	29.3063	-88.3352	2,955,524	245,117	
MP	7	WILD	B	FIXED	Apache Corporation	9/24/2000		39	29.6139	-88.8714	2,782,252	352,875	
MP	86	WILD	1	FIXED	McMoran Oil & Gas LLC	11/29/2000		70	29.6544	-88.6201	2,861,739	369,397	
MP	20	WILD	1	CAIS	Devon Energy Production Company, L.P.	12/8/2000		34	29.5603	-88.9448	2,759,347	332,869	
MP	86	WILD	2	CAIS	McMoran Oil & Gas LLC	12/21/2000		75	29.6678	-88.6287	2,858,900	374,196	
MP	61	WILD	A	FIXED	Energy XXI GOM, LLC	5/13/2001		91	29.3162	-88.9204	2,768,951	244,310	
MP	275	WILD	A	FIXED	Apache Corporation	5/19/2001		231	29.2845	-88.4433	2,921,256	236,304	
MP	164	MP164	A	FIXED	Magnum Hunter Production, Inc.	7/18/2001		135	29.6367	-88.4877	2,903,952	363,967	
MP	178	MP178	A	FIXED	Magnum Hunter Production, Inc.	9/26/2001		150	29.5767	-88.4728	2,909,221	342,290	
MP	261		JP	FIXED	Williams Field Services - Gulf Coast Comp	10/20/2001		299	29.3308	-88.1019	3,029,600	256,030	
MP	94	MP096	4	FIXED	Offshore Shelf LLC	1/2/2002		47	29.6331	-88.7552	2,819,023	360,662	
MP	61	MP061	B	WP	Energy XXI GOM, LLC	1/14/2002		102	29.2976	-88.9204	2,769,092	237,523	
LILI													
MP	107	WILD	CAIS.#1	CAIS	Offshore Shelf LLC	11/1/2002		55	29.5552	-88.7185	2,831,317	332,584	
MP	61	MP061	C	FIXED	Energy XXI GOM, LLC	11/26/2002		97	29.3060	-88.9219	2,768,550	240,580	
MP	270	WILD	A	FIXED	Eni US Operating Co. Inc.	1/12/2003		205	29.3338	-88.5271	2,894,129	253,547	
MP	57	WILD	CAIS.#1	CAIS	Palace Operating Company	2/1/2003		37	29.3309	-89.0538	2,726,340	248,782	
MP	101	MP101	D	FIXED	Hunt Petroleum (AEC), Inc.	3/17/2003		56	29.5709	-88.7722	2,814,125	337,907	
MP	61	MP061	D	FIXED	Energy								

MAIN PASS Platform Data - INSTALLED													
Searched by Area and Structure Installed Date Sorted by Installation Date													
Area Code	Block Number	Field	Structure Name	Struc Type	Operator	Install Date	Removal Date	Water Depth	Latitude	Longitude	Ptfm X Location	Ptfm Y Location	
MP	104	MP103	B	CAIS	Apache Corporation	5/10/2004		46	29.5555	-88.8489	2,789,848	331,779	
MP	116	MP127	8	CAIS	Hunt Petroleum (AEC), Inc.	6/9/2004		58	29.4573	-88.8304	2,796,507	296,228	
MP	287	MP287	A	FIXED	Stone Energy Corporation	6/9/2004		285	29.2669	-88.3794	2,941,804	230,430	
MP	99	MP099	A	WP	Magnum Hunter Production, Inc.	7/18/2004		65	29.5669	-88.6592	2,850,076	337,287	
MP	108	MP108	#7	WP	Offshore Shelf LLC	8/23/2004		59	29.5598	-88.6634	2,848,783	334,673	
IVAN													
MP	19	WILD	G	FIXED	Petsec Energy Inc.	11/27/2004		40	29.5589	-88.8819	2,779,342	332,796	
MP	88	WILD	A	CAIS	Hunt Petroleum (AEC), Inc.	1/1/2005		52	29.6591	-88.7245	2,828,537	370,323	
MP	69	MP069	E	CAIS	W & T Offshore, Inc.	1/11/2005		48	29.2831	-89.0235	2,736,360	231,580	
MP	100	MP107	B	FIXED	Century Exploration New Orleans, Inc.	1/21/2005		54	29.5995	-88.7235	2,829,350	348,680	
MP	207		A	FIXED	Magnum Hunter Production, Inc.	2/9/2005		174	29.4640	-88.5379	2,889,515	300,782	
MP	161	WILD	C	CAIS	Walter Oil & Gas Corporation	2/20/2005		71	29.6515	-88.5897	2,871,431	368,575	
MP	7	MP006	2	CAIS	Apache Corporation	3/19/2005		35	29.6187	-88.9001	2,773,109	354,415	
MP	95	MP096	3	CAIS	Offshore Shelf LLC	4/9/2005		60	29.6295	-88.7018	2,836,001	359,740	
KATRINA													
RITA													
MP	166	WILD	A	FIXED	Forest Oil Corporation	9/30/2005		130	29.6109	-88.4018	2,931,469	355,300	
MP	118	WILD	A	FIXED	Hunt Petroleum (AEC), Inc.	12/18/2005		69	29.4594	-88.7661	2,816,962	297,432	
MP	20	MP020	B	FIXED	LLOG Exploration Offshore, Inc.	2/5/2006		36	29.5357	-88.9529	2,756,942	323,881	
MP	29	WILD	1	CAIS	Hunt Petroleum (AEC), Inc.	3/9/2006		55	29.4721	-88.8779	2,781,290	301,274	
MP	92	WILD	1	CAIS	Legacy Resources Co., L.P.	3/9/2006		39	29.6428	-88.8542	2,787,480	363,485	
MP	138	MP129	G	FIXED	Newfield Exploration Company	10/15/2006		157	29.3359	-88.8054	2,805,463	252,260	
MP	120	MP120	A	CAIS	Arena Offshore, LLC	5/23/2007		103	29.4763	-88.6768	2,845,243	304,203	

Index to "Structural Type" field:			
CAIS	Caisson	SPAR	SPAR Platform - floating production system
CT	Compliant tower	SSANC	Fixed anchors or mooring piles used to secure a structure to the seafloor
FIXED	Fixed Leg Platform	SSMNF	Subsea Manifold
FPSO	Floating production, storage, and offloading	SSTMP	Subsea templates
MOPU	Mobile Production Unit	TLP	Tension leg platform
MTLP	Mini Tension Leg Platform	UCOMP	Underwater completion or subsea caisson
SEMI	Semi Submersible (Column Stabilized Unit) Floating Production System	WP	Well Protector

Table P-4: Mississippi Canyon Protraction Area: Platform History and Statistical Analysis (data from MMS, 2009)

MISSISSIPPI CANYON Platform Data - INSTALLED													
Searched by Area and Structure Installed Date Sorted by Installation Date													
Area Code	Block Number	Field	Structure Name	Struc Type	Operator	Install Date	Removal Date	Water Depth	Latitude	Longitude	Ptfm X Location	Ptfm Y Location	
MC	194	MC194	A-Cognac	FIXED	Shell Offshore Inc.	1/1/1978		1,023	28.7910	-89.0564	981,880	10,454,000	
MC	268	MC311	A	FIXED	Exxon Mobil Corporation	1/1/1978		343	28.6521	-89.7865	746,822	10,408,280	
MC	311	MC311	A	FIXED	Apache Corporation	1/1/1978		428	28.6426	-89.7942	744,244	10,404,880	
FREDERIC													
MC	148	MC148	A	FIXED	Apache Corporation	1/1/1980		651	28.7951	-89.1768	943,327	10,456,200	
MC	63	SP049	B	FIXED	Pogo Producing Company	1/1/1983		480	28.9017	-89.0235	993,096	10,494,079	
MC	280	MC281	A-Lena CT	CT	Exxon Mobil Corporation	1/1/1983		1,000	28.6627	-89.1578	948,570	10,407,935	
MC	20	MC020	A	FIXED	Taylor Energy Company LLC	1/1/1984		475	28.9380	-88.9710	1,010,135	10,507,008	
ELENA													
MC	486	MC486	A	FIXED	Sojitz Energy Venture, Inc.	1/1/1990		582	28.4559	-89.8522	724,020	10,337,409	
MC	109	MC109	A-Amberjack	FIXED	Stone Energy Corporation	1/1/1991		1,100	28.8647	-88.9308	1,022,550	10,480,130	
MC	397	MC397	A-Alabaster	FIXED	Exxon Mobil Corporation	10/3/1991		476	28.5464	-89.9296	699,950	10,370,930	
MC	365	MC365	A (Crystal)	FIXED	Noble Energy, Inc.	1/1/1992		619	28.6010	-89.3113	898,888	10,386,416	
ANDREW													
MC	807	MC807	A-Mars TLP	TLP	Shell Offshore Inc.	7/18/1996		2,933	28.1695	-89.2229	924,373	10,229,010	
OPAL GEORGES													
MC	809	MC810	A-Ursa TLP	TLP	Shell Offshore Inc.	12/28/1998		3,800	28.1540	-89.1036	962,722	10,222,690	
MC	127	MC084	A-Horn Mountain	SPAR	BP Exploration & Production Inc.	6/29/2002		5,400	28.8660	-88.0563	1,302,433	10,477,093	
LILI													
MC	474	A-NaKika FPDS		SEMI	BP Exploration & Production Inc.	8/2/2003		6,378	28.5209	-88.2888	1,226,668	10,352,377	
MC	243	MC243	A-Matterhorn	MTLP	TOTAL E&P USA, INC.	8/3/2003		2,850	28.7423	-88.8256	1,055,524	10,435,094	
MC	582	MC582	A-Medusa Spar	SPAR	Murphy Exploration & Production Company	8/8/2003		2,223	28.3924	-89.4535	851,717	10,311,485	
MC	773	MC773	A/DEVILS TOWER SPAR	SPAR	Eni US Operating Co. Inc.	2/19/2004		5,610	28.2088	-88.7375	1,080,968	10,240,719	
IVAN													
MC	778	MC778	A/Thunder Horse	SEMI	BP Exploration & Production Inc.	1/16/2005		6,037	28.1906	-88.4956	1,158,783	10,233,084	
MC	21	MC020	B SIMBA	FIXED	Taylor Energy Company LLC	1/23/2005		667	28.9373	-88.9120	1,029,000	10,506,419	
KATRINA RITA													
MC	711	MC755	A (GOMEZ)	SEMI	ATP Oil & Gas Corporation	3/8/2006		2,975	28.2207	-89.6151	798,393	10,250,124	
MC	920	A/Independence		SEMI	Anadarko Petroleum Corporation	6/11/2007		8,000	28.0851	-87.9858	1,322,640	10,193,040	

Index to "Structural Type" field:			
CAIS	Caisson	SPAR	SPAR Platform - floating production system
CT	Compliant tower	SSANC	Fixed anchors or mooring piles used to secure a structure to the seafloor
FIXED	Fixed Leg Platform	SSMNF	Subsea Manifold
FPSO	Floating production, storage, and offloading	SSTMP	Subsea templates
MOPU	Mobile Production Unit	TLP	Tension leg platform
MTLP	Mini Tension Leg Platform	UCOMP	Underwater completion or subsea caisson
SEMI	Semi Submersible (Column Stabilized Unit) Floating Production System	WP	Well Protector

Table P-5: South Pass Protraction Area: Platform History and Statistical Analysis (data from MMS, 2009)

SOUTH PASS Platform Data - INSTALLED													
Searched by Area and Structure Installed Date Sorted by Installation Date													
Area Code	Block Number	Field	Structure Name	Struc Type	Operator	Install Date	Removal Date	Water Depth	Latitude	Longitude	Ptfm X Location	Ptfm Y Location	
SP	27	SP027	28	WP	Energy Partners, Ltd.	1/1/1958		35	28.9786	-89.2734	2,658,702	119,375	
SP	28	SP027	40	WP	Energy Partners, Ltd.	1/1/1958		36	28.9813	-89.2459	2,667,462	120,484	
SP	28	SP027	41	WP	Energy Partners, Ltd.	1/1/1958		36	28.9785	-89.2666	2,660,862	119,375	
SP	28	SP027	SAT #42	WP	Energy Partners, Ltd.	1/1/1958		36	28.9784	-89.2584	2,663,502	119,375	
SP	28	SP027	49	WP	Energy Partners, Ltd.	1/1/1958		36	28.9782	-89.2460	2,667,462	119,375	
SP	28	SP027	46	WP	Energy Partners, Ltd.	1/1/1958		38	28.9848	-89.2417	2,668,782	121,804	
SP	28	SP027	51	WP	Energy Partners, Ltd.	1/1/1958		36	28.9783	-89.2501	2,666,142	119,375	
SP	28	SP027	54	WP	Energy Partners, Ltd.	1/1/1958		38	28.9847	-89.2376	2,670,106	121,796	
SP	28	SP027	55	WP	Energy Partners, Ltd.	1/1/1958		36	28.9811	-89.2377	2,670,102	120,484	
SP	28	SP027	50	WP	Energy Partners, Ltd.	1/1/1958		36	28.9812	-89.2418	2,668,782	120,484	
SP	28	SP027	53	WP	Energy Partners, Ltd.	1/1/1958		36	28.9781	-89.2418	2,668,782	119,375	
SP	28	SP027	187	WP	Energy Partners, Ltd.	1/1/1958		35	28.9818	-89.2593	2,663,172	120,589	
SP	27	SP027	35(SL 1011)	FIXED	Energy Partners, Ltd.	1/1/1959		35	28.9816	-89.2733	2,658,702	120,445	
SP	27	SP027	37(SL1011)	WP	Energy Partners, Ltd.	1/1/1959		35	28.9787	-89.2775	2,657,382	119,375	
SP	28	SP027	1(V)	WP	Energy Partners, Ltd.	1/1/1959		36	28.9767	-89.2646	2,661,522	118,715	
SP	28	SP027	58	WP	Energy Partners, Ltd.	1/1/1959		36	28.9783	-89.2542	2,664,822	119,375	
SP	28	SP027	8	WP	Energy Partners, Ltd.	1/1/1959		35	28.9749	-89.2667	2,660,862	118,055	
SP	28	SP027	6(V)	WP	Energy Partners, Ltd.	1/1/1959		14	28.9748	-89.2626	2,662,182	118,055	
SP	28	SP027	5(Z)	WP	Energy Partners, Ltd.	1/1/1959		45	28.9764	-89.2481	2,666,802	118,717	
SP	28	SP027	9(Z)	WP	Energy Partners, Ltd.	1/1/1959		35	28.9746	-89.2460	2,667,462	118,055	
SP	28	SP027	59	WP	Energy Partners, Ltd.	1/1/1959		36	28.9781	-89.2377	2,670,102	119,375	
SP	28	SP027	60	WP	Energy Partners, Ltd.	1/1/1959		36	28.9813	-89.2500	2,666,142	120,484	
SP	28	SP027	2	WP	Energy Partners, Ltd.	1/1/1959		35	28.9766	-89.2604	2,662,846	118,707	
SP	28	SP027	30	WP	Energy Partners, Ltd.	1/1/1960		50	28.9616	-89.2463	2,667,458	113,332	
SP	28	SP027	24	WP	Energy Partners, Ltd.	1/1/1960		60	28.9673	-89.2462	2,667,462	115,415	
SP	28	SP027	17(VV)	WP	Energy Partners, Ltd.	1/1/1960		35	28.9712	-89.2598	2,663,082	116,735	
SP	28	SP027	AA WEST	FIXED	Energy Partners, Ltd.	1/1/1960		65	28.9623	-89.2387	2,669,902	113,645	
SP	28	SP027	33	WP	Energy Partners, Ltd.	1/1/1960		35	28.9648	-89.2377	2,670,202	114,545	
SP	28	SP027	V	FIXED	Energy Partners, Ltd.	1/1/1960		56	28.9707	-89.2641	2,661,702	116,541	
SP	28	SP027	23	WP	Energy Partners, Ltd.	1/1/1960		35	28.9709	-89.2420	2,668,782	116,735	
SP	28	SP027	Z	FIXED	Energy Partners, Ltd.	1/1/1960		75	28.9698	-89.2453	2,667,740	116,316	
SP	28	SP027	12	WP	Energy Partners, Ltd.	1/1/1960		35	28.9712	-89.2626	2,662,178	116,743	
SP	28	SP027	15	WP	Energy Partners, Ltd.	1/1/1960		40	28.9710	-89.2461	2,667,462	116,735	
SP	28	SP027	16	WP	Energy Partners, Ltd.	1/1/1960		35	28.9746	-89.2502	2,666,142	118,055	
SP	28	SP027	21(V)	WP	Energy Partners, Ltd.	1/1/1960		35	28.9685	-89.2668	2,660,862	115,715	
SP	28	SP028	AA-EAST	FIXED	Energy Partners, Ltd.	1/1/1960		65	28.9623	-89.2384	2,670,002	113,645	
SP	28	SP027	18	WP	Energy Partners, Ltd.	1/1/1960		35	28.9676	-89.2627	2,662,182	115,415	
SP	28	SP027		FIXED	Energy Partners, Ltd.	1/1/1960		65	28.9629	-89.2387	2,669,902	113,845	
SP	37	SP027	A	WP	Hunt Oil Company	1/1/1960	12/31/1975	100	28.9525	-89.2461	2,667,600	110,016	
ETHYL													
SP	28	SP027	37	WP	Energy Partners, Ltd.	1/1/1961		35	28.9607	-89.2381	2,670,102	113,055	
SP	28	SP027	45	WP	Energy Partners, Ltd.	1/1/1961		35	28.9690	-89.2351	2,671,000	116,081	
SP	28	SP027	38	WP	Energy Partners, Ltd.	1/1/1961		55	28.9656	-89.2524	2,665,482	114,755	
SP	28	SP027	A-49	WP	Energy Partners, Ltd.	1/1/1961		55	28.9765	-89.2620	2,662,352	118,675	
SP	28	SP027	69	WP	Energy Partners, Ltd.	1/1/1961		36	28.9780	-89.2336	2,671,418	119,383	
SP	28	SP027	58	WP	Energy Partners, Ltd.	1/1/1961		40	28.9744	-89.2362	2,670,602	118,055	
SP	28	SP027	10	WP	Energy Partners, Ltd.	1/1/1961		40	28.9745	-89.2419	2,668,786	118,047	
SP	37	SP027	C	FIXED	Hunt Oil Company	1/1/1961	11/18/2003	105	28.9488	-89.2504	2,666,255	108,648	
CARLA													
SP	28	SP027	60	WP	Energy Partners, Ltd.	1/1/1962		65	28.9648	-89.2365	2,670,572	114,545	
SP	28	SP027	110	WP	Energy Partners, Ltd.	1/1/1962		36	28.9798	-89.2397	2,669,467	120,000	
SP	28	SP027	122	WP	Energy Partners, Ltd.	1/1/1962		24	28.9759	-89.2423	2,668,660	118,545	
SP	28	SP027	29	WP	Energy Partners, Ltd.	1/1/1962		50	28.9747	-89.2543	2,664,826	118,047	
SP	28	SP027	66	WP	Energy Partners, Ltd.	1/1/1962		55	28.9628	-89.2631	2,662,102	113,685	
SP	28	SP027	A71	WP	Energy Partners, Ltd.	1/1/1962		45	28.9656	-89.2445	2,668,012	114,805	
SP	28	SP027	68	WP	Energy Partners, Ltd.	1/1/1962		40	28.9728	-89.2395	2,669,582	117,455	
SP	28	SP027	52(SL1012)T	CAIS	Energy Partners, Ltd.	1/1/1962		36	28.9849	-89.2499	2,666,146	121,796	
SP	37	SP027	B	FIXED	Hunt Oil Company	1/1/1962	12/31/1978	108	28.9466	-89.2308	2,672,521	107,976	
SP	37	SP037	B	FIXED	Hunt Oil Company	1/1/1963	6/24/2003	140	28.9310	-89.2375	2,670,492	102,257	
SP	37	SP037	A	FIXED	Hunt Oil Company	1/1/1963	11/18/2003	130	28.9309	-89.2485	2,666,976	102,168	
SP	28	SP027	79	WP	Energy Partners, Ltd.	1/1/1964		45	28.9686	-89.2625	2,662,242	115,768	
SP	28	SP027	130	WP	Energy Partners, Ltd.	1/1/1964		36	28.9797	-89.2647	2,661,472	119,795	
SP	37	SP037	C	FIXED	Hunt Oil Company	1/1/1964	11/18/2003	140	28.9259	-89.2312	2,672,520	100,429	
HILDA													
SP	28	SP027	45	WP	Energy Partners, Ltd.	1/1/1965		50	28.9785	-89.2625	2,662,182	119,375	
BETSY													
SP	28	SP027	T	FIXED	Energy Partners, Ltd.	1/1/1966		36	28.9839	-89.2482	2,666,702	121,424	
SP	28	SP027	89	WP	Energy Partners, Ltd.	1/1/1966		35	28.9657	-89.2242	2,674,510	114,966	
SP	28	SP027	13(V)	WP	Energy Partners, Ltd.	1/1/1966		65	28.9713	-89.2668	2,660,858	116,743	
SP	28	SP027	TT	FIXED	Energy Partners, Ltd.	1/1/1966		36	28.9840	-89.2487	2,666,552	121,474	
SP	28	SP027	47(SL 1012)	CAIS	Energy Partners, Ltd.	1/1/1966		38	28.9849	-89.2458	2,667,466	121,796	
SP	28	SP027	93	WP	Energy Partners, Ltd.	1/1/1967		50	28.9727	-89.2573	2,663,880	117,300	
SP	28	SP027	SP28M (SL 1012)	WP	Energy Partners, Ltd.	1/1/1967		35	28.9861	-89.2682	2,660,302	122,129	
SP	28	SP027	85W(SL 1012)	FIXED	Energy Partners, Ltd.	1/1/1967		35					
SP	28	SP027	48	WP	Energy Partners, Ltd.	1/1/1967		70	28.9622	-89.2525	2,665,482	113,525	
SP	62	SP062	A	FIXED	Apache Corporation	1/1/1967		340	29.0795	-88.7439	2,827,149	159,482	
SP	28	SP027	99	WP	Energy Partners, Ltd.	1/1/1968		35	28.9662	-89.2293	2,672,858	115,090	
SP	28	SP027	20	WP	Energy Partners, Ltd.	1/1/1968		14	28.9748	-89.2584	2,663,502	118,055	
SP	28	SP027	VV-AUX	FIXED	Energy Partners, Ltd.	1/1/1968		56	28.9707	-89.2652	2,661,377	116,541	
SP	28	SP027	160	CAIS	Energy Partners, Ltd.	1/1/1968		36	28.9870	-89.2358	2,670,660	122,624	
SP	28	SP027	5	WP	Energy Partners, Ltd.	1/1/1968		60	28.9720	-89.2754	2,658,096	116,942	
SP	28	SP027	102(T)	CAIS	Energy Partners, Ltd.	1/1/1968		36	28.9821	-89.2606	2,662,762	120,700	
SP	62	SP062	B	FIXED	Apache Corporation	1/1/1968		322	29.0924	-88.7214	2,834,228	164,319	
SP	62	SP062	C	FIXED	Apache Corporation	1/1/1968		325	29.0876	-88.7338	2,830,297	162,495	
SP	65	SP065	A	FIXED	Nippon Oil Exploration U.S.A. Limited	1/1/1969		300	29.1071	-88.8573	2,790,710	168,697	
CAMILLE													
SP	54	SP054	A	FIXED	Texaco Exploration and Production Inc.	1/1/1970	4/20/2002	280	28.8661	-89.2609	2,663,428	78,526	
SP	55	SP054	A-VALVE	FIXED	Tennessee Gas Pipeline Company	1/1/1970		260	28.8655	-89.2783	2,657,872	78,220	
SP	60	SP061	A	FIXED	SPN Resources, LLC	1/1/1971		185	29.0579	-88.9642	2,756,945	150,107	
SP	60	SP061	B	FIXED	SPN Resources, LLC	1/1/1972		206	29.0443	-88.9666	2,756,286	145,134	
SP	28	SP027	3	WP	Energy Partners, Ltd.	1/1/1973		14	28.9764	-89.2439	2,668,122	118,715	
SP	28	SP027	201 V	WP	Energy Partners, Ltd.	1/1/1973		14	28.9772	-89.2626	2,662,152	118,925	

--- continued on following page ---

SOUTH PASS Platform Data - INSTALLED													
Searched by Area and Structure Installed Date Sorted by Installation Date													
Area Code	Block Number	Field	Structure Name	Struc Type	Operator	Install Date	Removal Date	Water Depth	Latitude	Longitude	Ptfm X Location	Ptfm Y Location	
SP	60	SP061	C	FIXED	SPN Resources, LLC	1/1/1973		192	29.0637	-88.9560	2,759,532	152,272	
SP	28	SP027	149	WP	Energy Partners, Ltd.	1/1/1974		40	28.9754	-89.2468	2,667,224	118,350	
SP	28	SP027	85(SL 1012)(w)	WP	Energy Partners, Ltd.	1/1/1974		43	28.9844	-89.2628	2,662,049	121,529	
SP	70	SP061	C	FIXED	Devon Energy Production Company, L.P.	1/1/1974		264	29.0295	-88.9427	2,764,028	139,902	
CARMEN													
SP	28	SP027	220	WP	Energy Partners, Ltd.	1/1/1975		50	28.9827	-89.2556	2,664,348	120,951	
SP	28	SP027	229 T	WP	Energy Partners, Ltd.	1/1/1975		40	28.9793	-89.2501	2,666,139	119,755	
SP	28	SP027	225 (SL 1012)T	WP	Energy Partners, Ltd.	1/1/1975		48	28.9879	-89.2407	2,669,085	122,925	
SP	61	SP061	B	WP	Chevron U.S.A. Inc.	1/1/1975	12/31/1980	230	29.0312	-88.9537	2,760,492	140,471	
ELOISE													
SP	28	SP027	157	WP	Energy Partners, Ltd.	1/1/1976		45	28.9719	-89.2466	2,667,298	117,074	
SP	28	SP027	98(SL 1012)(M)	WP	Energy Partners, Ltd.	1/1/1977		47	28.9818	-89.2658	2,661,105	120,568	
SP	28	SP027	271(SL 1012)	WP	Energy Partners, Ltd.	1/1/1977		45	28.9832	-89.2709	2,659,457	121,041	
SP	60	SP061	D	FIXED	SPN Resources, LLC	1/1/1977		185	29.0569	-88.9636	2,757,139	149,755	
SP	70	SP061	D	FIXED	Devon Energy Production Company, L.P.	1/1/1977		264	29.0289	-88.9437	2,763,719	139,709	
SP	77	SP078	A	FIXED	Chevron U.S.A. Inc.	1/1/1977		216	28.8308	-89.4061	2,617,178	64,892	
SP	78	SP078	A	FIXED	Maritech Resources, Inc.	1/1/1978	9/22/2004	227	28.8239	-89.4117	2,615,403	62,342	
SP	89	SP089	A	FIXED	Marathon Oil Company	1/1/1978	6/6/2004	395	28.7031	-89.3910	2,622,786	18,518	
SP	93	SP089	A	FIXED	Exxon Mobil Corporation	1/1/1978		446	28.6629	-89.4082	2,617,530	3,823	
SP	28	SP027	193	WP	Energy Partners, Ltd.	1/1/1979		48	28.9748	-89.2578	2,663,700	118,052	
SP	28	SP027	189	WP	Energy Partners, Ltd.	1/1/1979		36	28.9669	-89.2397	2,669,553	115,304	
FREDERIC													
SP	28	SP027	235 T	WP	Energy Partners, Ltd.	1/1/1980		36	28.9825	-89.2388	2,669,711	120,980	
SP	28	SP027	267(V)	WP	Energy Partners, Ltd.	1/1/1980		36	28.9800	-89.2594	2,663,172	119,944	
SP	49	SP049	A	FIXED	Pogo Producing Company	1/1/1980		300	28.8854	-89.0638	2,726,384	86,750	
SP	57	SP078	B	FIXED	Chevron U.S.A. Inc.	1/1/1980		194	28.8439	-89.3966	2,620,128	69,692	
SP	60	SP061	E	FIXED	SPN Resources, LLC	1/1/1980		206	29.0440	-88.9669	2,756,202	145,047	
SP	77	SP078	C	FIXED	Chevron U.S.A. Inc.	1/1/1980		240	28.8222	-89.3950	2,620,786	61,825	
SP	49	SP049	C	FIXED	Maritech Resources, Inc.	1/1/1981		400	28.8784	-89.0765	2,722,359	84,130	
SP	58	SP078	D	WP	Chevron U.S.A. Inc.	1/1/1981		180	28.8392	-89.4126	2,615,023	67,890	
SP	60	SP061	F	FIXED	SPN Resources, LLC	1/1/1982		192	29.0640	-88.9553	2,759,741	152,382	
SP	67	SP061	A	FIXED	SPN Resources, LLC	1/1/1982		258	29.0548	-88.9366	2,765,784	149,151	
SP	37	SP027	E	FIXED	Hunt Oil Company	1/1/1983	8/10/2003	105	28.9480	-89.2510	2,666,048	108,364	
SP	60	SP061	G	FIXED	SPN Resources, LLC	1/1/1985		185	29.0568	-88.9643	2,756,937	149,683	
SP	93	SP089	B	FIXED	Exxon Mobil Corporation	1/1/1985		450	28.6696	-89.3935	2,622,194	6,346	
SP	89	SP089	B	FIXED	Marathon Oil Company	2/9/1985		456	28.6805	-89.3876	2,624,018	10,316	
ELENA													
SP	75	SP075	A	FIXED	GOM Shelf LLC	1/1/1986		356	28.8016	-89.3000	2,651,334	54,862	
SP	28	SP027	257(SL 1012)	WP	Energy Partners, Ltd.	1/1/1987		37	28.9873	-89.2466	2,667,213	122,866	
SP	62	SP062	D	FIXED	Apache Corporation	1/1/1987		325	29.0868	-88.7342	2,830,190	162,201	
SP	45	SP045	A	FIXED	GOM Shelf LLC	1/1/1989		189	28.8915	-89.2565	2,664,659	87,796	
SP	83	SP083	A	FIXED	Arena Offshore, LLC	1/1/1990		467	28.7833	-89.2422	2,669,952	48,542	
SP	52	SP052	A	FIXED	Apache Corporation	1/1/1991		531	28.8413	-89.1396	2,702,433	70,214	
SP	86	SP089	C	FIXED	Marathon Oil Company	3/27/1992		352	28.7183	-89.3931	2,622,023	24,051	
ANDREW													
SP	87	SP089	D	FIXED	Marathon Oil Company	3/19/1995		372	28.7200	-89.4308	2,609,929	24,466	
SP	47	SP049	A	FIXED	Samedan Oil Corporation	8/22/1995	5/8/2002	224	28.9125	-89.1430	2,700,825	96,100	
OPAL													
SP	27	SP027	11*A*	FIXED	Energy Partners, Ltd.	4/10/1996		82	28.9599	-89.2747	2,658,402	112,566	
SP	72	SP072	A	FIXED	W & T Offshore, Inc.	5/10/1996		260	28.9741	-89.0131	2,741,940	119,327	
GEORGES													
SP	89	SP089	MC674 #3	FIXED	Marathon Oil Company	12/27/1999		456					
SP	38	SP027	A	FIXED	Stone Energy Corporation	11/21/2001		111	28.9442	-89.2883	2,654,134	106,750	
LILI													
SP	89		E	FIXED	Proteus Oil Pipeline Company, LLC	8/23/2004		392	28.6974	-89.3959	2,621,246	16,420	
IVAN													
KATRINA													
RITA													

Index to "Structural Type" field:			
CAIS	Caisson	SPAR	SPAR Platform - floating production system
CT	Compliant tower	SSANC	Fixed anchors or mooring piles used to secure a structure to the seafloor
FIXED	Fixed Leg Platform	SSMNF	Subsea Manifold
FPSO	Floating production, storage, and offloading	SSTMP	Subsea templates
MOPU	Mobile Production Unit	TLP	Tension leg platform
MTLP	Mini Tension Leg Platform	UCOMP	Underwater completion or subsea caisson
SEMI	Semi Submersible (Column Stabilized Unit) Floating Production System	WP	Well Protector



Table P-6: Viosca Knoll Protraction Area: Platform History and Statistical Analysis (data from MMS, 2009)

VIOSCA KNOLL Platform Data - INSTALLED													
Searched by Area and Structure Installed Date Sorted by Installation Date													
Area Code	Block Number	Field	Structure Name	Struc Type	Operator	Install Date	Removal Date	Water Depth	Latitude	Longitude	Ptfm X Location	Ptfm Y Location	
VK	900	SP062	A	FIXED	Chevron U.S.A. Inc.	1/1/1975		340	29.0845	-88.7045	1,096,117	10,558,953	
ELOISE													
VK	899	SP062	B	FIXED	Chevron U.S.A. Inc.	1/1/1977	7/20/1990	395	29.0628	-88.7428	1,083,770	10,551,240	
FREDERIC													
ELENA													
VK	24	VK024	A	CAIS	El Paso Exploration & Production Managem	1/1/1988	4/24/2004	95	29.9479	-88.4844	1,170,438	10,871,878	
VK	32	VK032	S	CAIS	EOG Resources, Inc.	1/1/1988	9/19/2006	104	29.9411	-88.1067	1,289,986	10,868,070	
VK	32	VK032	3	CAIS	EOG Resources, Inc.	1/1/1988	9/18/2006	96	29.9656	-88.0861	1,296,599	10,876,930	
VK	74	VK074	2	CAIS	EOG Resources, Inc.	1/1/1988		107	29.9242	-88.1802	1,266,656	10,862,170	
VK	74	VK074	1	CAIS	EOG Resources, Inc.	1/1/1988	7/23/1988	109	29.9083	-88.2030	1,259,373	10,856,463	
VK	294	VK299	A	CAIS	Chevron U.S.A. Inc.	1/1/1988	3/20/2007	119	29.7010	-88.1827	1,265,050	10,781,034	
VK	156	VK156	A	CAIS	EOG Resources, Inc.	1/1/1990	1/3/1999	99	29.8155	-88.5209	1,158,223	10,823,910	
VK	22	MO990	A	CAIS	Chevron U.S.A. Inc.	1/1/1991		77	29.9730	-88.6042	1,132,629	10,881,519	
VK	27	VK027	A	CAIS	Chevron U.S.A. Inc.	1/1/1991	9/27/2004	102	29.9401	-88.3769	1,204,450	10,868,626	
VK	69	VK069	A	FIXED	Chevron U.S.A. Inc.	1/1/1991		102	29.9259	-88.4784	1,172,227	10,863,853	
ANDREW													
VK	204	VK203	3	CAIS	Energy Resource Technology, Inc.	1/1/1993		123	29.7961	-88.2887	1,231,783	10,815,960	
VK	203	VK204	A	FIXED	Energy Resource Technology, Inc.	6/19/1993		122	29.7815	-88.3331	1,217,640	10,810,819	
VK	204	VK204	C	WP	Energy Resource Technology, Inc.	6/23/1993		123	29.7789	-88.3079	1,225,608	10,809,777	
VK	203	VK204	B	WP	Energy Resource Technology, Inc.	6/25/1993		123	29.7867	-88.3492	1,212,555	10,812,748	
VK	31	VK031	A	FIXED	EOG Resources, Inc.	1/1/1994		103	29.9492	-88.1607	1,272,925	10,871,191	
VK	989	VK989	A-Pompano	FIXED	BP Exploration & Production Inc.	8/19/1994		1,290	28.9730	-88.6260	1,120,647	10,518,060	
VK	76	VK031	A	CAIS	El Paso Exploration & Production Managem	10/2/1994		105	29.9061	-88.1147	1,287,341	10,855,377	
VK	155		A	FIXED	TDC Energy Corporation	4/20/1995	9/29/2000	97	29.8385	-88.5620	1,145,330	-10,831,885	
VK	817	VK817	A	FIXED	Flextrend Development Company, L.L.C.	7/27/1995		671	29.1674	-88.4559	1,175,906	10,588,012	
OPAL													
VK	161		A	FIXED	Cronus Offshore, Inc.	7/27/1996	7/7/2007	139	29.8353	-88.2346	1,249,071	10,830,005	
VK	33	VK033	1	CAIS	El Paso Exploration & Production Managem	9/9/1996		105	29.9474	-88.0611	1,304,445	10,870,225	
VK	122	VK122	A(No.1)	CAIS	El Paso Exploration & Production Managem	9/29/1996	4/19/2001	110	29.8518	-88.0122	1,319,645	10,835,320	
VK	123	VK123	1	CAIS	El Paso Exploration & Production Managem	10/4/1996	5/6/2001	115	29.8607	-87.9560	1,337,490	10,838,404	
VK	117	VK117	#2	FIXED	PRS Offshore, L.P.	11/9/1996	6/12/1999	70	29.8911	-88.2362	1,248,810	10,850,300	
VK	124	VK124	A	CAIS	EOG Resources, Inc.	11/11/1996		103	29.8581	-87.9092	1,352,309	10,837,330	
VK	826		A-Neptune Spar	SPAR	Kerr-McGee Oil & Gas Corporation	11/19/1996		1,930	29.1635	-97.9878	132,529	10,585,025	
VK	35	VK035	1	FIXED	El Paso Exploration & Production Managem	1/25/1997	4/21/2001	115	29.9479	-87.9445	1,341,395	10,870,095	
VK	121	VK021	A	FIXED	El Paso Exploration & Production Managem	5/14/1997	6/30/2002	105	29.8863	-88.0467	1,308,830	10,847,975	
VK	956		A-Ram Powell	TLP	Shell Offshore Inc.	5/21/1997		3,216	29.0606	-88.0917	1,291,740	10,547,940	
VK	68	VK069	A	FIXED	Chevron U.S.A. Inc.	8/12/1997		99	29.9031	-88.4648	1,170,083	10,855,592	
VK	24	VK024	2	CAIS	Chevron U.S.A. Inc.	8/17/1997	3/27/1998	89	29.9681	-88.5238	1,158,055	10,879,416	
VK	209		A	FIXED	Newfield Exploration Company	12/1/1997	7/24/2002	110	29.8036	-88.0367	1,311,720	10,817,870	
VK	114	WILD	A	WP	Chevron U.S.A. Inc.	3/30/1998	7/14/2007	113	29.8532	-88.3959	1,198,035	10,837,120	
VK	780	VK780	A-Spirit	FIXED	Apache Corporation	7/3/1998		722	29.2372	-88.1084	1,287,028	10,612,194	
VK	251	MO990	A	CAIS	Chevron U.S.A. Inc.	7/5/1998		121	29.7458	-88.1583	1,272,962	10,797,214	
VK	70		1	CAIS	Chevron U.S.A. Inc.	7/30/1998	7/31/2001	105	29.8905	-88.4196	1,190,681	10,850,762	
GEORGES													
VK	915	VK915	A-Marlin TLP	TLP	BP Exploration & Production Inc.	7/27/1999		3,236	29.1076	-87.9436	1,339,179	10,564,590	
VK	734	VK734	A	FIXED	MOBIL OIL EXPLORATION & PRODUCINC	8/2/1999		322	29.2691	-88.1901	1,261,090	10,624,021	
VK	823	VK823	A (VIRGO)	FIXED	TOTAL E&P USA, INC.	9/17/1999		1,130	29.1819	-88.1677	1,267,895	10,592,265	
VK	786	VK786	A-Petronius CT	CT	Chevron U.S.A. Inc.	4/28/2000		1,754	29.2290	-87.7810	1,391,399	10,608,356	
VK	385	VK385	A	FIXED	El Paso E&P Company, L.P.	5/18/2000		130	29.5964	-88.0467	1,307,867	10,742,573	
VK	252	VK252	A	FIXED	Chevron U.S.A. Inc.	7/12/2000	11/21/2002	123	29.7606	-88.0953	1,292,979	10,802,394	
VK	340	WILD	A	FIXED	Chevron U.S.A. Inc.	11/1/2001		129	29.6365	-88.0921	1,293,572	10,757,282	
VK	113	WILD	A	FIXED	Coldren Resources LP	1/1/2002		104	29.8832	-88.4687	1,175,092	10,848,318	
LILI													
VK	384	VK384	A	WP	Chevron U.S.A. Inc.	10/14/2002		134	29.6139	-88.1007	1,290,750	10,749,086	
VK	213	WILD	A CAISSON #1	CAIS	Maritech Resources, Inc.	9/22/2003		131	29.7843	-87.8320	1,376,568	10,810,323	
IVAN													
VK	20	WILD	1	CAIS	Palace Operating Company	5/7/2005		59	29.9616	-88.6902	1,105,343	10,877,779	
KATRINA													
RITA													
VK	77	WILD	A	FIXED	Seneca Resources Corporation	7/23/2006		106	29.9261	-88.0553	1,306,230	10,862,458	
VK	432	WILD	A	FIXED	Seneca Resources Corporation	7/26/2006		124	29.5843	-87.8959	1,355,741	10,737,763	

Index to "Structural Type" field:			
CAIS	Caisson	SPAR	SPAR Platform - floating production system
CT	Compliant tower	SSANC	Fixed anchors or mooring piles used to secure a structure to the seafloor
FIXED	Fixed Leg Platform	SSMNF	Subsea Manifold
FPSO	Floating production, storage, and offloading	SSTMP	Subsea templates
MOPU	Mobile Production Unit	TLP	Tension leg platform
MTLP	Mini Tension Leg Platform	UCOMP	Underwater completion or subsea caisson
SEMI	Semi Submersible (Column Stabilized Unit) Floating Production System	WP	Well Protector



Table P-7: West Delta Protraction Area: Platform History and Statistical Analysis (data from MMS, 2009)

WEST DELTA Platform Data - INSTALLED													
Searched by Area and Structure Installed Date													
Sorted by Installation Date													
Area Code	Block Number	Field	Structure Name	Struc Type	Operator	Install Date	Removal Date	Water Depth	Latitude	Longitude	Ptfm X Location	Ptfm Y Location	
WD	29	WD030	A	FIXED	Anglo-Suisse Offshore Partners, LLC	1/1/1952		39	29.1408	-89.6083	2,550,722	176,561	
WD	29	WD030	C	FIXED	Anglo-Suisse Offshore Partners, LLC	1/1/1952		39	29.1297	-89.6052	2,551,787	172,538	
WD	29	WD030	G	FIXED	Chevron U.S.A. Inc.	1/1/1952	8/17/1997	37	29.1527	-89.6085	2,550,602	180,881	
WD	29	WD030	D	FIXED	Anglo-Suisse Offshore Partners, LLC	1/1/1952		39	29.1378	-89.5959	2,554,694	175,520	
WD	29	WD030	B	FIXED	Anglo-Suisse Offshore Partners, LLC	1/1/1952		38	29.1472	-89.6071	2,551,069	178,896	
WD	31	WD030	E-CMP	FIXED	Exxon Mobil Corporation	1/1/1954		50	29.1483	-89.6757	2,529,172	178,965	
WD	31	WD030	E-QTRS	FIXED	Exxon Mobil Corporation	1/1/1954		50	29.1483	-89.6760	2,529,072	178,965	
WD	31	WD030	E-DRL	FIXED	Exxon Mobil Corporation	1/1/1954		50	29.1485	-89.6759	2,529,101	179,045	
WD	58	WD058	A	FIXED	Samedan Oil Corporation	1/1/1954	12/31/1981	48	29.0117	-89.5237	2,578,468	130,033	
WD	29	WD030	F	FIXED	Anglo-Suisse Offshore Partners, LLC	1/1/1955		39	29.1424	-89.6106	2,549,987	177,152	
WD	30	WD030	G	FIXED	Exxon Mobil Corporation	1/1/1955	7/22/1994	39	29.1496	-89.6167	2,548,002	179,736	
WD	31	WD030	F	FIXED	Exxon Mobil Corporation	1/1/1955		47	29.1200	-89.6498	2,537,572	168,818	
WD	31	WD030	H	FIXED	Exxon Mobil Corporation	1/1/1955	9/29/2001	49	29.1540	-89.6651	2,532,522	181,112	
WD	45	WD030	A	FIXED	Nexen Petroleum U.S.A. Inc.	1/1/1955		58	29.1086	-89.6438	2,539,577	164,693	
WD	45	WD030	B	FIXED	Nexen Petroleum U.S.A. Inc.	1/1/1955		54	29.1069	-89.6174	2,548,011	164,195	
WD	29	WD030	H	FIXED	Anglo-Suisse Offshore Partners, LLC	1/1/1956		39	29.1427	-89.6113	2,549,750	177,259	
WD	29	WD030	I-QRT	FIXED	Anglo-Suisse Offshore Partners, LLC	1/1/1956		39	29.1408	-89.6080	2,550,822	176,561	
WD	29	WD030	E	FIXED	Anglo-Suisse Offshore Partners, LLC	1/1/1956		39	29.1396	-89.6105	2,550,027	176,136	
WD	30	WD030	J	FIXED	Exxon Mobil Corporation	1/1/1956		45	29.1161	-89.6194	2,547,322	167,518	
WD	31	WD030	L	FIXED	Exxon Mobil Corporation	1/1/1956		53	29.1401	-89.6720	2,530,375	176,018	
WD	45	WD030	C	WP	Nexen Petroleum U.S.A. Inc.	1/1/1956		53	29.1070	-89.6316	2,543,481	164,181	
WD	31	WD030	R	WP	Exxon Mobil Corporation	1/1/1957	12/31/1984	54	29.1166	-89.6641	2,533,022	167,498	
WD	31	WD030	N	FIXED	Exxon Mobil Corporation	1/1/1957		55	29.1324	-89.6637	2,533,070	173,260	
WD	32	WD030	Q	FIXED	Exxon Mobil Corporation	1/1/1957	6/26/2004	56	29.1287	-89.6794	2,528,092	171,818	
WD	44	WD030	D	FIXED	Nexen Petroleum U.S.A. Inc.	1/1/1957		49	29.1054	-89.6522	2,536,897	163,468	
WD	45	WD030	E	FIXED	Nexen Petroleum U.S.A. Inc.	1/1/1957		57	29.1068	-89.6383	2,541,335	164,055	
WD	54		TK BAT 3	FIXED	Palm Energy Offshore, L.L.C.	1/1/1957		9	0.0000	0.0000			
AUDREY													
WD	24	WD027	2	CAIS	Newfield Exploration Company	1/1/1958		30	29.1782	-89.5340	2,574,242	190,541	
WD	30	WD030	P	FIXED	Exxon Mobil Corporation	1/1/1958		43	29.1293	-89.6139	2,548,984	172,369	
WD	45	WD030	2	CAIS	Nexen Petroleum U.S.A. Inc.	1/1/1958	12/31/1983	50	29.1059	-89.6351	2,542,350	163,743	
WD	45	WD030	1	CAIS	Nexen Petroleum U.S.A. Inc.	1/1/1958	2/20/1989	50	29.1054	-89.6335	2,542,880	163,588	
WD	45	WD030	7	CAIS	Nexen Petroleum U.S.A. Inc.	1/1/1958		60	29.1045	-89.6355	2,542,222	163,219	
WD	24	WD027	1	CAIS	Chevron U.S.A. Inc.	1/1/1959	12/31/1985	30	29.1759	-89.5341	2,574,222	189,701	
WD	29	WD030	CB-REMOVED	WP	Chevron U.S.A. Inc.	1/1/1959	6/2/1997	44	29.1214	-89.6096	2,550,422	169,518	
WD	32	WD030	4	CAIS	Maritech Resources, Inc.	1/1/1959	1/7/2002	52	29.1466	-89.6873	2,525,479	178,318	
WD	45	WD030	F	FIXED	Nexen Petroleum U.S.A. Inc.	1/1/1959		53	29.0982	-89.6336	2,542,875	160,939	
WD	45	WD030	G	FIXED	Nexen Petroleum U.S.A. Inc.	1/1/1959		58	29.1103	-89.6409	2,540,472	165,338	
WD	29	WD030	7	CAIS	Anglo-Suisse Offshore Partners, LLC	1/1/1960		36	29.1525	-89.5960	2,554,586	180,883	
WD	32	WD030	6	CAIS	Maritech Resources, Inc.	1/1/1960	12/29/2001	64	29.1184	-89.6877	2,525,479	168,057	
WD	32	WD030	12	WP	Maritech Resources, Inc.	1/1/1960	12/24/2001	63	29.1381	-89.6960	2,522,747	175,176	
WD	32	WD030	4	WP	Maritech Resources, Inc.	1/1/1960	1/13/2002	61	29.1290	-89.7007	2,521,271	171,836	
WD	32	WD030	2	WP	Maritech Resources, Inc.	1/1/1960		68	29.1158	-89.7097	2,518,472	167,018	
WD	32	WD030	2	WP	Maritech Resources, Inc.	1/1/1960	1/10/2002	62	29.1309	-89.6917	2,524,159	172,557	
WD	32	WD030	1	WP	Maritech Resources, Inc.	1/1/1960	1/9/2002	62	29.1308	-89.6875	2,525,479	172,557	
WD	71	GI043	1	CAIS	Conoco Inc.	1/1/1960	12/31/1976	144	28.9650	-89.7751	2,498,338	111,892	
WD	71	GI043	B	WP	Conoco Inc.	1/1/1960	12/31/1978	145	28.9553	-89.7866	2,494,728	108,292	
ETHYL													
WD	29	WD030	CC	WP	Anglo-Suisse Offshore Partners, LLC	1/1/1961		44	29.1195	-89.6020	2,552,857	168,861	
WD	32	WD030	3	WP	Maritech Resources, Inc.	1/1/1961		57	29.1417	-89.6874	2,525,479	176,517	
WD	32	WD030	5	CAIS	Maritech Resources, Inc.	1/1/1961	12/22/2001	61	29.1234	-89.6877	2,525,479	169,857	
CARLA													
WD	23	WD027	3-PRD	FIXED	Newfield Exploration Company	1/1/1962		24	29.1780	-89.5518	2,568,554	190,353	
WD	23	WD027	S/POWER/PROD.	FIXED	Chevron U.S.A. Inc.	1/1/1962	9/8/1995	28	29.1912	-89.5770	2,560,432	195,030	
WD	23	WD027	3-PWR	FIXED	Newfield Exploration Company	1/1/1962		24	29.1784	-89.5525	2,568,328	190,496	
WD	23	WD027	3-CMP	FIXED	Newfield Exploration Company	1/1/1962		24	29.1787	-89.5533	2,568,072	190,608	
WD	23	WD027	1	CAIS	Chevron U.S.A. Inc.	1/1/1962	12/31/1985	30	29.1677	-89.5478	2,569,892	186,661	
WD	24	WD027	8	CAIS	Chevron U.S.A. Inc.	1/1/1962	12/31/1985	30	29.1801	-89.5399	2,572,342	191,192	
WD	24	WD027	4	CAIS	Chevron U.S.A. Inc.	1/1/1962	12/31/1985	30	29.1788	-89.5434	2,571,222	190,691	
WD	24	WD027	6	CAIS	Chevron U.S.A. Inc.	1/1/1962	12/31/1985	30	29.1780	-89.5372	2,573,222	190,441	
WD	24	WD027	3(Removed)	CAIS	Chevron U.S.A. Inc.	1/1/1962	9/16/1997	30	29.1751	-89.5439	2,571,074	189,354	
WD	24	WD027	5	CAIS	Chevron U.S.A. Inc.	1/1/1962	7/28/1995	30	29.1764	-89.5396	2,572,452	189,861	
WD	30	WD030	T	FIXED	Exxon Mobil Corporation	1/1/1962		50	29.1225	-89.6246	2,545,622	169,818	
WD	32	WD030	U	FIXED	Exxon Mobil Corporation	1/1/1962	8/24/1996	57	29.1251	-89.6801	2,527,895	170,514	
WD	32	WD030	S	FIXED	Exxon Mobil Corporation	1/1/1962		54	29.1462	-89.6785	2,528,271	178,183	
WD	32	WD030	A	FIXED	Maritech Resources, Inc.	1/1/1962		63	29.1285	-89.6903	2,524,613	171,723	
WD	41	WD041	FLR STACK	FIXED	Apache Corporation	1/1/1962	10/11/2002	87	29.0903	-89.7587	2,502,965	157,518	
WD	41	WD041	A	FIXED	Apache Corporation	1/1/1962		87	29.0929	-89.7586	2,502,965	158,441	
WD	45	WD030	CQ	FIXED	Nexen Petroleum U.S.A. Inc.	1/1/1962		53	29.1070	-89.6313	2,543,572	164,181	
WD	69	GI043	C	FIXED	GOM Shelf LLC	1/1/1962		121	28.9797	-89.8435	2,476,397	116,924	
WD	71	GI043	E	FIXED	GOM Shelf LLC	1/1/1962		137	28.9704	-89.7980	2,490,987	113,756	
WD	23	WD027	PWR	FIXED	Chevron U.S.A. Inc.	1/1/1963	9/8/1995	28	29.1912	-89.5769	2,560,472	195,030	
WD	23	WD027	4	CAIS	Newfield Exploration Company	1/1/1963		30	29.1853	-89.5626	2,565,072	192,961	
WD	23	WD027	FLARE	FIXED	Chevron U.S.A. Inc.	1/1/1963	8/7/1995	28	29.1912	-89.5769	2,560,472	195,031	
WD	23	WD027	JA	FIXED	Newfield Exploration Company	1/1/1963		24	29.1819	-89.5518	2,568,541	191,804	
WD	23	WD027	2	CAIS	Newfield Exploration Company	1/1/1963		30	29.1768	-89.5652	2,564,272	189,861	
WD	24	WD027	TEST-OIL	FIXED	Chevron U.S.A. Inc.	1/1/1963	7/28/1995	30	29.1778	-89.5412	2,571,922	190,361	
WD	29	WD030	CD	WP	Anglo-Suisse Offshore Partners, LLC	1/1/1963		42	29.1115	-89.6121	2,549,679	165,903	
WD	32	WD030	B	FIXED	Maritech Resources, Inc.	1/1/1963		60	29.1185	-89.6939	2,523,527	168,043	
WD	32	WD030	1	WP	Maritech Resources, Inc.	1/1/1963	1/3/2002	61	29.1311	-89.6992	2,521,767	172,601	
WD	70	GI043	D	FIXED	GOM Shelf LLC	1/1/1963		131	28.9696	-89.8195	2,484,107	113,373	
WD	73	WD073	A	FIXED	Exxon Mobil Corporation	1/1/1963		168	28.9463	-89.7063	2,520,428	105,392	
WD	99	WD117	A	FIXED	Exxon Mobil Corporation	1/1/1963		194	28.8315	-89.7956	2,492,444	63,258	
WD	23	WD027	6(Removed)	CAIS	Chevron U.S.A. Inc.	1/1/1964	9/18/1997	30	29.1833	-89.5557	2,567,262	192,261	
WD	23	WD027	7(Removed)	CAIS	Chevron U.S.A. Inc.	1/1/1964	9/17/1997	30	29.1817	-89.5496	2,569		

Table P-7 (continued): West Delta Protraction Area: Platform History and Statistical Analysis  
(data from MMS, 2009)

WEST DELTA Platform Data - INSTALLED													
Searched by Area and Structure Installed Date Sorted by Installation Date													
Area Code	Block Number	Field	Structure Name	Struc Type	Operator	Install Date	Removal Date	Water Depth	Latitude	Longitude	Ptfm X Location	Ptfm Y Location	
WD	32	WD030	18	WP	Maritech Resources, Inc.	1/1/1964	1/12/2002	55	29.1464	-89.6903	2,524,522	178,218	
WD	41	WD041	C	FIXED	Apache Corporation	1/1/1964	10/28/1994	83	29.1045	-89.7530	2,504,706	162,702	
WD	41	WD041	Qtrs	FIXED	Apache Corporation	1/1/1964		87	29.0929	-89.7585	2,503,022	158,441	
WD	41	WD041	AUX	FIXED	Apache Corporation	1/1/1964		87	29.0930	-89.7585	2,503,022	158,491	
WD	41	WD041	B	FIXED	Apache Corporation	1/1/1964		83	29.0994	-89.7679	2,499,967	160,769	
WD	73	WD073	C	FIXED	Exxon Mobil Corporation	1/1/1964		172	28.9420	-89.7156	2,517,500	103,763	
WD	73	WD073	QTRS	FIXED	Exxon Mobil Corporation	1/1/1964		168	28.9475	-89.7062	2,520,458	105,805	
WD	74	WD073	B	FIXED	Exxon Mobil Corporation	1/1/1964		180	28.9416	-89.6795	2,529,028	103,812	
WD	75	WD073	D	FIXED	Apache Corporation	1/1/1964		172	28.9598	-89.6632	2,534,145	110,478	
WD	90	WD073	A	FIXED	Apache Corporation	1/1/1964		180	28.9384	-89.6605	2,535,134	102,711	
WD	94	GI043	G	FIXED	BP America Production Company	1/1/1964		153	28.9336	-89.7791	2,497,215	100,457	
HILDA													
WD	30	WD030	5	CAIS	Exxon Mobil Corporation	1/1/1965	11/18/1988	35	29.1665	-89.6185	2,547,322	185,861	
WD	69	GI043	F	FIXED	Conoco Inc.	1/1/1965	9/29/1996	135	28.9520	-89.8356	2,479,071	106,911	
WD	70	GI043	I	FIXED	GOM Shelf LLC	1/1/1965		135	28.9521	-89.8230	2,483,079	107,000	
WD	70	GI043	H	FIXED	GOM Shelf LLC	1/1/1965		141	28.9448	-89.8098	2,487,331	104,403	
WD	73	WD073	D	FIXED	Exxon Mobil Corporation	1/1/1965		168	28.9475	-89.7064	2,520,388	105,805	
WD	74	WD073	F	FIXED	Exxon Mobil Corporation	1/1/1965		170	28.9523	-89.6837	2,527,640	107,667	
WD	93	GI043	E	FIXED	Exxon Mobil Corporation	1/1/1965		160	28.9376	-89.7616	2,502,798	101,992	
WD	103	WD105	A	FIXED	Apache Corporation	1/1/1965		223	28.8620	-89.6568	2,536,710	74,945	
WD	103	WD105	B	FIXED	Apache Corporation	1/1/1965		228	28.8655	-89.6441	2,540,777	76,294	
WD	104	WD105	C	FIXED	Apache Corporation	1/1/1965		228	28.8614	-89.6320	2,544,679	74,874	
WD	117	WD117	C	FIXED	Anglo-Suisse Offshore Partners, LLC	1/1/1965		214	28.8096	-89.7880	2,494,972	55,308	
WD	134	WD133	D	FIXED	KIRBY EXPLORATION COMPANY OF TEXAS	1/1/1965	1/20/1992	280	28.7344	-89.7352	2,512,282	28,208	
BETSY													
WD	29	WD030	23	CAIS	Anglo-Suisse Offshore Partners, LLC	1/1/1966		44	29.1191	-89.6018	2,552,910	168,715	
WD	40	WD041	A	FIXED	Apache Corporation	1/1/1966		83	29.0940	-89.7840	2,494,869	158,751	
WD	69	GI043	K	FIXED	GOM Shelf LLC	1/1/1966		134	28.9644	-89.8356	2,479,003	111,411	
WD	70	GI043	L	FIXED	GOM Shelf LLC	1/1/1966		135	28.9521	-89.8222	2,483,348	107,003	
WD	71	GI043	M	FIXED	GOM Shelf LLC	1/1/1966		136	28.9825	-89.7881	2,494,113	118,195	
WD	133	WD133	B	FIXED	Apache Corporation	1/1/1966		285	28.7315	-89.6930	2,525,812	27,359	
WD	23	WD027	12(Removed)	CAIS	Chevron U.S.A. Inc.	1/1/1967	9/18/1997	30	29.1783	-89.5572	2,566,822	190,461	
WD	23	WD027	14	CAIS	Chevron U.S.A. Inc.	1/1/1967	5/27/1997	30	29.1779	-89.5647	2,564,422	190,261	
WD	23	WD027	13(Removed)	CAIS	Chevron U.S.A. Inc.	1/1/1967	9/20/1997	30	29.1831	-89.5628	2,565,022	192,161	
WD	28	WD030	DA	CAIS	Anglo-Suisse Offshore Partners, LLC	1/1/1967		42	29.1287	-89.5695	2,563,184	172,372	
WD	28	WD030	33	WP	Anglo-Suisse Offshore Partners, LLC	1/1/1967		35	29.1399	-89.5791	2,560,037	176,374	
WD	31	WD030	3	CAIS	Exxon Mobil Corporation	1/1/1967	12/31/1978	48	29.1673	-89.6664	2,532,035	185,911	
WD	33	WD030	A	FIXED	ExxonMobil Oil Corporation	1/1/1967	12/31/1978	71	29.1159	-89.7157	2,516,572	167,018	
WD	42	WD041	Y	FIXED	Exxon Mobil Corporation	1/1/1967	8/1/1996	82	29.1000	-89.7375	2,509,677	161,149	
WD	70	GI043	N	FIXED	GOM Shelf LLC	1/1/1967		138	28.9427	-89.8248	2,482,547	103,568	
WD	71	GI043	O	FIXED	GOM Shelf LLC	1/1/1967		142	28.9641	-89.7839	2,495,527	111,519	
WD	96	GI043	R	FIXED	BP America Production Company	1/1/1967		148	28.8991	-89.8370	2,478,875	87,656	
WD	104	WD105	D	FIXED	Apache Corporation	1/1/1967		228	28.8649	-89.6073	2,552,543	76,246	
WD	133	WD133	E	FIXED	Apache Corporation	1/1/1967	6/2/1999	292	28.7222	-89.6866	2,527,923	24,001	
WD	23	WD027	16	CAIS	Newfield Exploration Company	1/1/1968		30	29.1838	-89.5571	2,566,822	192,461	
WD	23	WD027	15	CAIS	Newfield Exploration Company	1/1/1968		30	29.1800	-89.5575	2,566,722	191,061	
WD	35	WD035	A	FIXED	Walter Oil & Gas Corporation	1/1/1968		66	29.1375	-89.7921	2,492,053	174,512	
WD	42	WD041	X	FIXED	Exxon Mobil Corporation	1/1/1968	8/3/1996	83	29.1023	-89.7162	2,516,486	162,049	
WD	73	WD073	A-TWR	FIXED	Exxon Mobil Corporation	1/1/1968		168	28.9469	-89.7065	2,520,378	105,592	
WD	75	WD073	F	FIXED	Apache Corporation	1/1/1968		200	28.9686	-89.6553	2,536,628	113,734	
WD	90	WD073	B	FIXED	Apache Corporation	1/1/1968		180	28.9379	-89.6597	2,535,381	102,545	
WD	95	GI043	T	FIXED	BP America Production Company	1/1/1968	5/27/1995	150	28.9095	-89.8088	2,487,828	91,550	
WD	95	GI043	P	FIXED	BP America Production Company	1/1/1968	12/31/1979	145	28.9359	-89.8279	2,481,583	101,067	
WD	95	GI043	S	FIXED	BP America Production Company	1/1/1968		153	28.9058	-89.8207	2,484,049	90,163	
WD	32	WD030		FIXED	Exxon Mobil Corporation	1/1/1969	7/28/1996	54	29.1462	-89.6789	2,528,171	178,183	
WD	40	WD041	B	FIXED	Apache Corporation	1/1/1969		90	29.0693	-89.8055	2,488,105	149,671	
WD	79	WD079	C	FIXED	SPN Resources, LLC	1/1/1969		150	28.9483	-89.5182	2,580,592	107,009	
WD	89	WD073	C	FIXED	Eni Petroleum Co. Inc.	1/1/1969	8/17/1993	220	28.9270	-89.6168	2,549,178	98,792	
WD	117	WD117	E	FIXED	Anglo-Suisse Offshore Partners, LLC	1/1/1969		208	28.8135	-89.7846	2,496,050	56,753	
WD	117	WD117	D	FIXED	Anglo-Suisse Offshore Partners, LLC	1/1/1969		195	28.8189	-89.7899	2,494,318	58,684	
CAMILLE													
WD	29	WD030	27	CAIS	Chevron U.S.A. Inc.	1/1/1970	12/31/1976	35	29.1630	-89.6092	2,550,301	184,650	
WD	31	WD030	1	CAIS	Exxon Mobil Corporation	1/1/1970	11/14/1988	48	29.1588	-89.6711	2,530,584	182,811	
WD	32	WD030	D-QTR	FIXED	Maritech Resources, Inc.	1/1/1970		63	29.1285	-89.6906	2,524,513	171,723	
WD	45	WD030	H	FIXED	Nexen Petroleum U.S.A. Inc.	1/1/1970		53	29.1056	-89.6316	2,543,469	163,667	
WD	68	GI043	U	FIXED	GOM Shelf LLC	1/1/1970		111	29.0142	-89.8418	2,476,786	129,504	
WD	79	WD079	B	FIXED	SPN Resources, LLC	1/1/1970		132	28.9569	-89.5070	2,584,134	110,207	
WD	94	GI043	V	FIXED	GOM Shelf LLC	1/1/1970		156	28.9267	-89.7819	2,496,368	97,922	
WD	152	WD152	A	FIXED	Newfield Exploration Company	1/1/1970		373	28.5872	-89.6998	2,524,382	-25,151	
WD	32	WD030	E	FIXED	Maritech Resources, Inc.	1/1/1971		63	29.1490	-89.7087	2,518,622	179,086	
WD	35	WD035	B	FIXED	BP America Production Company	1/1/1971	10/6/1992	70	29.1252	-89.8006	2,489,414	170,027	
WD	36	WD035	2	WP	Gulf Oil Corporation	1/1/1971	12/31/1983	71	29.1248	-89.8137	2,485,222	169,818	
WD	80	WD079	D	FIXED	SPN Resources, LLC	1/1/1971		102	28.9706	-89.5004	2,586,162	115,225	
WD	28	WD030	10	CAIS	Anglo-Suisse Offshore Partners, LLC	1/1/1972		37	29.1364	-89.5547	2,567,872	175,218	
WD	64	WD064	A	WP	Belco Petroleum Corporation	1/1/1972	12/31/1980	118	29.0442	-89.7071	2,519,669	140,970	
WD	35	WD035	C	FIXED	Walter Oil & Gas Corporation	1/1/1973		66	29.1375	-89.7921	2,492,065	174,520	
WD	35	WD035	2	WP	Gulf Oil Corporation	1/1/1973	12/31/1983	37	29.1625	-89.8005	2,489,271	183,574	
WD	90	WD073	E	FIXED	Apache Corporation	1/1/1973		180	28.9384	-89.6602	2,535,228	102,711	
WD	95	GI043	X	FIXED	BP America Production Company	1/1/1973		153	28.9050	-89.8212	2,483,878	89,850	
WD	36	WD035	5	WP	Gulf Oil Corporation	1/1/1974	12/31/1983	71	29.1553	-89.8108	2,486,000	180,911	
WD	79	WD079	F	WP	SPN Resources, LLC	1/1/1974		90	28.9715	-89.5139	2,581,821	115,483	
WD	79	WD079	A	FIXED	SPN Resources, LLC	1/1/1974		90	28.9718	-89.5139	2,581,821	115,583	
WD	117	WD117	F	FIXED	Anglo-Suisse Offshore Partners, LLC	1/1/1974		200	28.8103	-89.7923	2,493,614	55,558	
CARMEN ELOISE													
WD	61	WD061	A	FIXED	Pioneer Natural Resources USA, Inc.	1/1/1978	9/7/2003	110	29.0175	-89.6306	2,544,278	131,634	
WD	71	GI043	Y	FIXED	GOM Shelf LLC	1/1/1978		149	28.9503	-89.7850	2,495,263	106,476	
WD	138	WD137	A	FIXED	TOTAL E&P USA, INC.	1/1/1978	4/14/1993	328	28.6914	-89.8077	2,489,253	12,261	
WD	34	WD035	2	WP	Forest Oil Corporation	1/1/1979		35	29.1617	-89.7523	2,504,641	183,506	
WD	117	WD117	G	FIXED	Anglo-Suisse Offshore Partners, LLC	1/1/1979		211	28.8048	-89.8018</			

WEST DELTA Platform Data - INSTALLED													
Searched by Area and Structure Installed Date Sorted by Installation Date													
Area Code	Block Number	Field	Structure Name	Struc Type	Operator	Install Date	Removal Date	Water Depth	Latitude	Longitude	Ptfm X Location	Ptfm Y Location	
WD	34	WD035	A	FIXED	Forest Oil Corporation	1/1/1980		50	29.1615	-89.7523	2,504,647	183,432	
WD	58	WD058	C	FIXED	Coldren Resources LP	1/1/1980		35	29.0041	-89.5232	2,578,678	127,284	
WD	63	WD064	A	FIXED	Walter Oil & Gas Corporation	1/1/1980	8/22/1997	125	29.0421	-89.6924	2,524,380	140,272	
WD	70	GI043	Z	FIXED	GOM Shelf LLC	1/1/1980		135	28.9488	-89.8261	2,482,098	105,758	
WD	109	WD109	A	FIXED	Chevron U.S.A. Inc.	1/1/1980		184	28.8340	-89.4532	2,602,078	65,808	
WD	28	WD030	11	CAIS	El Paso Production Company	1/1/1981	12/31/1985	40	29.1249	-89.5726	2,562,199	170,954	
WD	35	WD035	7	CAIS	BP America Production Company	1/1/1981	12/31/1985	70	29.1547	-89.8038	2,488,241	180,722	
WD	35	WD035	8	CAIS	Walter Oil & Gas Corporation	1/1/1982	9/25/2003	61	29.1542	-89.7833	2,494,782	180,647	
WD	58	WD058	D	FIXED	Palm Energy Offshore, L.L.C.	1/1/1982		70	29.0202	-89.5312	2,576,013	133,094	
WD	86	WD086	A	FIXED	SPN Resources, LLC	1/1/1982		143	28.9121	-89.5114	2,582,978	93,982	
WD	99	WD117	B	FIXED	Exxon Mobil Corporation	1/1/1982		200	28.8317	-89.7801	2,497,407	63,403	
WD	117	WD117	QRT	FIXED	Anglo-Suisse Offshore Partners, LLC	1/1/1982		214	28.8089	-89.7871	2,495,271	55,059	
WD	21	WD030	Z	FIXED	Exxon Mobil Corporation	1/1/1983		35	29.1768	-89.6139	2,548,743	189,643	
WD	67	WD067	A	FIXED	Conoco Inc.	1/1/1983	3/24/1991	100	29.0508	-89.8034	2,488,861	142,962	
WD	76	WD073	A	FIXED	BP America Production Company	1/1/1983	9/20/1996	180	28.9486	-89.6273	2,545,688	106,595	
WD	27	WD030	A	FIXED	Anglo-Suisse Offshore Partners, LLC	1/1/1984		39	29.1214	-89.5473	2,570,290	169,828	
WD	36	WD035	1	CAIS	Atlantic Richfield Company	1/1/1984	5/24/1992	73	29.1186	-89.8250	2,481,660	167,534	
WD	79	WD079	E	WP	SPN Resources, LLC	1/1/1984		90	29.8776	-89.5205	2,579,677	117,652	
WD	17	WD032	A	FIXED	Newfield Exploration Company	1/1/1985	10/22/2004	50					
WD	18	WD035	A	FIXED	Samedan Oil Corporation	1/1/1985	7/24/2000	30	29.1773	-89.7384	2,509,006	189,225	
ELENA													
WD	17	WD035	1	CAIS	Seneca Resources Corporation	1/1/1986	2/4/1999	47					
WD	18	WD035	3	CAIS	Samedan Oil Corporation	1/1/1986	11/28/1990	20	29.1779	-89.7374	2,509,322	189,450	
WD	18	WD035	5	CAIS	Samedan Oil Corporation	1/1/1986	5/24/1990	20	29.1768	-89.7409	2,508,222	189,061	
WD	50	WD050	4	CAIS	Signal Oil & Gas Company	1/1/1986		30	29.0615	-89.4770	2,593,117	148,390	
WD	50	WD050	3	CAIS	Signal Oil & Gas Company	1/1/1986		30	29.0603	-89.4724	2,594,574	147,970	
WD	75	WD073	G	WP	Apache Corporation	1/1/1986		190	28.9757	-89.6553	2,536,600	116,317	
WD	91	WD073	G	FIXED	Exxon Mobil Corporation	1/1/1986		180	28.9172	-89.6890	2,526,117	94,870	
WD	18	WD035	D	WP	Samedan Oil Corporation	1/1/1987	8/16/1999	20	29.1798	-89.7234	2,513,766	190,223	
WD	34	WD035	3	WP	Forest Oil Corporation	1/1/1987		55	29.1634	-89.7659	2,500,307	184,052	
WD	38	WD038	1	CAIS	Atlantic Richfield Company	1/1/1987	5/27/1992	78	29.1010	-89.8458	2,475,095	161,039	
WD	105	WD105	E	FIXED	Apache Corporation	1/1/1987		237	28.8513	-89.6011	2,554,616	71,350	
WD	33	WD035	E	CAIS	Samedan Oil Corporation	1/1/1988	11/25						

352

WEST DELTA Platform Data - INSTALLED													
Searched by Area and Structure Installed Date Sorted by Installation Date													
Area Code	Block Number	Field	Structure Name	Struc Type	Operator	Install Date	Removal Date	Water Depth	Latitude	Longitude	Ptfm X Location	Ptfm Y Location	
WD	21	WD030	BB	CAIS	Exxon Mobil Corporation	11/4/2004		36	29.1806	-89.6280	2,544,226	190,951	
WD	30	WD030	CC	FIXED	Exxon Mobil Corporation	2/1/2005		40	29.1541	-89.6185	2,547,408	181,341	
WD	133	WD133	F	FIXED	Newfield Exploration Company	8/8/2005		294	28.7114	-89.7018	2,523,088	19,984	
KATRINA													
RITA													
WD	64	WILD	C	FIXED	Peregrine Oil & Gas, LP	3/6/2006		142	29.0037	-89.7316	2,512,052	126,148	
WD	63	WD061	E	CAIS	Peregrine Oil & Gas, LP	5/17/2006		135	29.0302	-89.6945	2,523,794	135,958	
WD	117	WD117	H	FIXED	Anglo-Suisse Offshore Partners, LLC	6/20/2006		199	28.8172	-89.7985	2,491,586	58,039	
WD	68		JP	FIXED	Enterprise Field Services, LLC	7/15/2006		114	29.0013	-89.8418	2,476,855	124,786	
WD	64	WILD	D	FIXED	Peregrine Oil & Gas, LP	9/25/2006		140	28.9985	-89.7027	2,521,318	124,401	
WD	70	GD43	FF	FIXED	GOM Shelf LLC	4/23/2007		144	28.9503	-89.8045	2,489,027	106,393	

Index to "Structural Type" field:			
CAIS	Caisson	SPAR	SPAR Platform - floating production system
CT	Compliant tower	SSANC	Fixed anchors or mooring piles used to secure a structure to the seafloor
FIXED	Fixed Leg Platform	SSMNF	Subsea Manifold
FPSO	Floating production, storage, and offloading	SSTMP	Subsea templates
MOPU	Mobile Production Unit	TLP	Tension leg platform
MTLP	Mini Tension Leg Platform	UCOMP	Underwater completion or subsea caisson
SEMI	Semi Submersible (Column Stabilized Unit) Floating Production System	WP	Well Protector

## APPENDIX Q: DAILY MRDF PRODUCTION RATES AND MONETARY VALUE

Table Q-1: Daily production and monetary value, MRDF Validation Test Areas (data retrieved from PI/Dwights Database, 2009)

<b>Test Area 1</b>								
<u>Field name</u>	<u>Number of producing wells</u>	<u>Oil production per day (thousands of barrels)</u>	<u>Gas production per day (millions of ft<sup>3</sup>)</u>	<u>Oil price (\$/barrel)</u>	<u>Gas price (\$/MCF)</u>	<u>Oil value (daily production) (thousands)</u>	<u>Gas value (daily production) (thousands)</u>	<u>Total value (daily production) (thousands)</u>
MP 61	17	10.0	8.5	60	4.5	602	38	640
MP 73	26	3.4	3.4	60	4.5	205	15	220
MP 74	13	2.0	25.1	60	4.5	117	113	230
MP 139	1	0.0	0.5	60	4.5	0	2	2
MP 140	24	1.7	1.9	60	4.5	103	9	111
MP 62	1	0.0	1.2	60	4.5	1	5	6
MP 299	65	5.7	2.3	60	4.5	344	10	355
MP 129	4	0.9	0.5	60	4.5	56	2	58
	151	23.8	43.4			1,428	195	1,623
<b>Test Area 2</b>								
<u>Field name</u>	<u>Number of producing wells</u>	<u>Oil production per day (thousands of barrels)</u>	<u>Gas production per day (millions of ft<sup>3</sup>)</u>	<u>Oil price (\$/barrel)</u>	<u>Gas price (\$/MCF)</u>	<u>Oil value (daily production) (thousands)</u>	<u>Gas value (daily production) (thousands)</u>	<u>Total value (daily production) (thousands)</u>
MP 305	29	0.6	0.5	60	4.5	34	2	36
VK 817	7	0.1	1.7	60	4.5	3	8	11
	36	0.6	2.2			37	10	47
<b>Test Area 3</b>								
<u>Field name</u>	<u>Number of producing wells</u>	<u>Oil production per day (thousands of barrels)</u>	<u>Gas production per day (millions of ft<sup>3</sup>)</u>	<u>Oil price (\$/barrel)</u>	<u>Gas price (\$/MCF)</u>	<u>Oil value (daily production) (thousands)</u>	<u>Gas value (daily production) (thousands)</u>	<u>Total value (daily production) (thousands)</u>
SP 65	42	1.4	2.3	60	4.5	84	10	94
MC 20	14	4.2	6.9	60	4.5	250	31	281
	56	5.6	9.1			335	41	376
<b>Test Area 3</b>								
<u>Field name</u>	<u>Number of producing wells</u>	<u>Oil production per day (thousands of barrels)</u>	<u>Gas production per day (millions of ft<sup>3</sup>)</u>	<u>Oil price (\$/barrel)</u>	<u>Gas price (\$/MCF)</u>	<u>Oil value (daily production) (thousands)</u>	<u>Gas value (daily production) (thousands)</u>	<u>Total value (daily production) (thousands)</u>
SP 83	16	0.2	42.0	60	4.5	14	189	203
SP 27	327	0.7	1.0	60	4.5	45	4	49
MC 148	1	0.0	2.2	60	4.5	0	10	10
MC 194	12	2.0	8.3	60	4.5	119	37	156
	356	3.0	53.4			178	240	418
<b>TOTAL:</b>	<b>599</b>	<b>33.0</b>	<b>108.2</b>			<b>1,978</b>	<b>487</b>	<b>2,465</b>

## VITA

Walter Scott Guidroz was born in January 1958 in Morgan City, Louisiana, to Scott and Olive Guidroz. After attending public schools in Morgan City, the author entered Nicholls State University in Thibodaux, Louisiana, graduating with a Bachelor of Science degree in geology in May 1979. He then entered graduate school at the University of Mississippi in Oxford, Mississippi, graduating with a Master of Science degree in geology in August 1981.

The author then began his professional career with Amoco Production Company in New Orleans, Louisiana. Over the next ten years he worked a combination of geological and petrophysical job assignments, both onshore and offshore, within the Gulf of Mexico Basin. In August 1991, and after having moved to Houston, Texas in 1989, the author began work with Amoco Eurasia Petroleum Company to evaluate newly accessible oil and gas fields within the Soviet Union and, upon its dissolution, the Russian Federation. He next moved to Amoco's Brazil Program Team in 1997 to evaluate new opportunities created by the privatization of oil and gas properties owned by Petrobras, Brazil's state-sponsored petroleum company.

The author re-entered graduate school in August 1998 to complete an executive Master of Business Administration degree at The University of Texas at Austin. Upon graduating in May 2000, and after having received severance during the BP-Amoco merger in 1999, he began work as a credit risk manager with the Enron Corporation in Houston, Texas. This work involved evaluating and managing Enron's credit risk exposure associated with its online trading activities. However, in 2001 he returned to BP and his geological roots to work a series of geological, commercial, geohazard and managerial job roles.

The author re-entered graduate school (again) in August 2004, this time at Louisiana State University in Baton Rouge, Louisiana, to pursue a doctoral degree in the Department of Oceanography and Coastal Sciences while concurrently working at BP. No further degrees are anticipated.